

# Catalytic Activation and Functionalisation of Light Alkanes

## Advances and Challenges

Edited by

Eric G. Derouane, Jerzy Haber,  
Francisco Lemos, Fernando Ramôa Ribeiro  
and Michel Guisnet

NATO ASI Series

3. High Technology – Vol. 44

# Catalytic Activation and Functionalisation of Light Alkanes

Advances and Challenges

# NATO ASI Series

## Advanced Science Institutes Series

*A Series presenting the results of activities sponsored by the NATO Science Committee, which aims at the dissemination of advanced scientific and technological knowledge, with a view to strengthening links between scientific communities.*

The Series is published by an international board of publishers in conjunction with the NATO Scientific Affairs Division

**A Life Sciences**

Plenum Publishing Corporation  
London and New York

**B Physics**

**C Mathematical and Physical Sciences**

Kluwer Academic Publishers  
Dordrecht, Boston and London

**D Behavioural and Social Sciences**

**E Applied Sciences**

**F Computer and Systems Sciences**

Springer-Verlag

**G Ecological Sciences**

Berlin, Heidelberg, New York, London,  
Paris and Tokyo

**H Cell Biology**

**I Global Environmental Change**

### PARTNERSHIP SUB-SERIES

**1. Disarmament Technologies**

Kluwer Academic Publishers

**2. Environment**

Springer-Verlag / Kluwer Academic Publishers

**3. High Technology**

Kluwer Academic Publishers

**4. Science and Technology Policy**

Kluwer Academic Publishers

**5. Computer Networking**

Kluwer Academic Publishers

*The Partnership Sub-Series incorporates activities undertaken in collaboration with NATO's Cooperation Partners, the countries of the CIS and Central and Eastern Europe, in Priority Areas of concern to those countries.*

### NATO-PCO-DATA BASE

The electronic index to the NATO ASI Series provides full bibliographical references (with keywords and/or abstracts) to more than 50000 contributions from international scientists published in all sections of the NATO ASI Series.

Access to the NATO-PCO-DATA BASE is possible in two ways:

- via online FILE 128 (NATO-PCO-DATA BASE) hosted by ESRIN,  
Via Galileo Galilei, I-00044 Frascati, Italy.
- via CD-ROM "NATO-PCO-DATA BASE" with user-friendly retrieval software in English, French and German (© WTV GmbH and DATAWARE Technologies Inc. 1989).

The CD-ROM can be ordered through any member of the Board of Publishers or through NATO-PCO, Overijse, Belgium.



# Catalytic Activation and Functionalisation of Light Alkanes

## Advances and Challenges

edited by

**Eric G. Derouane**

Leverhulme Centre for Innovative Catalysis,  
University of Liverpool, U.K.

**Jerzy Haber**

Polish Academy of Sciences,  
Krakow, Poland

**Francisco Lemos**

Instituto Superior Técnico,  
Lisboa, Portugal

**Fernando Ramôa Ribeiro**

Instituto Superior Técnico,  
Lisboa, Portugal

and

**Michel Guisnet**

Université de Poitiers,  
Poitiers, France



Springer-Science+Business Media, B.V.



Proceedings of the NATO Advanced Study Institute on  
Advances and Challenges in the Catalytic Activation and Functionalisation of Light  
Alkanes  
Vilamoura, Portugal  
May 25–June 6, 1997

A C.I.P. Catalogue record for this book is available from the Library of Congress.

ISBN 978-90-481-4999-5

ISBN 978-94-017-0982-8 (eBook)

DOI 10.1007/978-94-017-0982-8

---

*Printed on acid-free paper*

---

All Rights Reserved

© 1998 Springer Science+Business Media Dordrecht

Originally published by Kluwer Academic Publishers in 1998

No part of the material protected by this copyright notice may be reproduced or utilized in any form or by any means, electronic or mechanical, including photocopying, recording or by any information storage and retrieval system, without written permission from the copyright owner.

## TABLE OF CONTENTS

PREFACE	ix
<b>SECTION 1 - LECTURES</b>	<b>1</b>
Upgrading of C1 and C2 Hydrocarbons <i>P.L. Villa and S. Rapagnà</i>	3
Transformation of Alkanes on Solid Acid and Bifunctional Catalysts <i>Avelino Corma and Agustín Martínez</i>	35
Activation of Light Alkanes: Past and Present <i>Ivan V. Kozhevnikov</i>	75
Superacid Catalysed Protolytic Activation, H/D Exchange and Oxidation of Small Alkanes <i>J. Sommer, J. Bukala, M. Hachoumy and R. Jost</i>	89
New Processes for Carbon-Carbon Bond Activation Catalysed by Oxyde Supported Surface Organometallic Complexes <i>Gerald P. Niccolai and Jean-Marie Basset</i>	111
Selective Oxidation of Light Alkanes <i>G.J. Hutchings</i>	125
Theoretical Basis of the Activation of C-H Bond <i>Jerzy Haber</i>	157
An Introduction to Molecular Heterogeneous Catalysis <i>C.R.A. Catlow, R.G. Bell, J.D. Gale, D.W. Lewis, D.C. Sayle and P.E. Sinclair</i>	189
Mono- and Binuclear Iron Complexes in Zeolites and Mesoporous Oxides as Biomimetic Alkan Oxidation Catalysts <i>P.P. Knops-Gerrits, A.-M. Van Bavel, G. Langouche and P.S. Jacobs</i>	215
Biocatalytic, Biomimetic and Suprabiotic Oxidation of Alkanes <i>R.A. Sheldon</i>	259
High Yield, Low Temperature Oxidation of Methane to Methanol <i>Roy A. Periana, Douglas J. Taube, Scott Gamble, Henry Taube and Hiroshi Fuji</i>	297
Functionalization of Light Alkanes Catalyzed by Heteropoly Compounds <i>Noritaka Mizuno and Makoto Misono</i>	311
Alkane Activation by Pseudo-Metals <i>G. Djéga-Mariadassou</i>	333

Molecular Chemistry of Alkane Activation: Formation and Reaction of  $\text{Ch}_x$  Species on Metal Surfaces

*F. Solymosi*

369

**SECTION 2 - COMMUNICATIONS**

**389**

The Effect of Acid Sites in Skeletal Isomerization of n-Butenes over Ferrierites and CoAlPO-11

*Jirí Cejka, Nadezda Zilková, Zdena Tvarozová and Blanka Wichterlová*

391

Oxidative Dehydrogenation of Propane on Large-Pore Zeolites

*Mirosław Derewinski, Joanna Krysciak, Zbigniew Olejniczak, Bogdan Sulikowski, Gema Bueno, Vicente Cortés Corberán and Rita Ximena Valenzuela*

397

Oxidative Coupling of Methane over Sodium-Manganese Catalysts in the Presence of HCl

*E.V. Shischak, M.S. Kazi, I.P. Dzikh, S.S. Abadjev and V.U. Shevchuk*

403

Mono- and Binuclear Iron Complexes in Zeolites, Clays and Mesoporous Oxides as Biomimetic Catalysts

*P.P. Knops-Gerrits and P.A. Jacobs*

413

Mixed  $\text{M}_2\text{O}_3\cdot\text{ZrO}_2\cdot\text{SO}_4^{2-}$  (M=Ga, In, Tl) Catalysts: Preparation, Characterisation and Catalytic Behaviour in Dehydroisomerisation of n-Hexane

*V. Parvulescu, S. Coman, P. Grange and V.I. Parvulescu*

417

The Selective Oxidation of n-Butane to Maleic Anhydride; Development of Silica- and Titania Supported V-P-O Catalysts

*Matthijs Ruitenbeek, R.A. Overbeek, D.C. Koningsberger and J.W. Geus*

423

The Effect of Cobalt Doping on the Structural Transformation Sequences Occurring during the Activation of Vanadium Phosphorus Oxide Catalysts

*S. Sajip, C. Rhodes, J.K. Bartley, A. Burrows, C.J. Kiely and C.J. Hutchings*

429

On the Active Sites for Selective Ammoxidation of Propane on Vanadium Containing Oxide Catalysts

*Horst Zanthoff*

435

Theoretical Modelling of Propane Partial Oxidation over Titanium Silicalites

*Georgi N. Vayssilov*

439

Chlorinated Alumina Catalyst for Isobutane / 2-Butene Alkylation: Influence of Added Noble Metals

*J.M. Goupil, G. Clet, F. Hemming-Maire, D. Cornet, G. Szabo, P. Nascimento and R. Loutaty*

447

**SECTION 3 - EC WORKSHOP****453**

Report of the Workshop on Challenges and Opportunities in Light  
Alkane Activation

*Jay A. Labinger and Graham J. Hutchings*

455

LIST OF PARTICIPANTS

467

SUBJECT INDEX

483

AUTHOR INDEX

489

## PREFACE

Catalysis plays an essential role in the petroleum, petrochemicals, and bulk and fine chemicals sectors. The major challenges for new and more flexible catalysis technology come from new and changing feedstocks, environmental considerations, and process economics. One of these challenges deals with the substitution of alkenes and aromatics, which are at the moment the basis for the production of petrochemicals, intermediates and fine chemicals with less expensive and readily available C<sub>1</sub>-C<sub>4</sub> alkanes.

Selective alkane activation, functionalisation and upgrading, and the direct use of alkanes as cheaper and more readily available raw materials, would provide an alternative and also greatly enhance the economy of processes based today on olefinic or aromatic intermediates. However, light alkanes cannot easily be activated, functionalised or converted selectively to more valuable or higher products because of the relative stability of their C-C and C-H bonds involved in such transformations, and the high temperatures usually necessary when conventional catalysts are used.

The issue is thus to identify and achieve novel catalytic mechanisms by which alkanes can be activated in mild conditions, functionalised, and reacted selectively, while ensuring satisfactory catalyst stability and life.

The basic understanding of reaction mechanisms and kinetics for alkane activation and functionalisation, and the rational utilization of this knowledge to design novel catalyst formulations with high activity, selectivity, and resistance to deactivation are amongst the essential keys to solving these challenges.

With these assertions in mind, an ASI bearing the title of this book was organized. This meeting took place in Vilamoura, Portugal, from May 25<sup>th</sup> to June 7<sup>th</sup>, 1997.

The present volume gathers all the lectures that were presented, as well as a selection of some of the communications. The response of the scientific community was very important, and the number of communications presented largely exceeded the possibilities of inclusion in this book; a significant amount of very good work has been left out due to the lack of space.

A particular characteristic of this book is that it embraces a very wide range of topics, going from homogeneous to heterogeneous approaches, with highly theoretical or experimental approaches. This large field of research, which was imparted to the ASI from the start, can be considered as one of its major achievements, and which we hope to be able to transport to this publication.

This should allow the researchers, both newcomers and senior ones, to become aware of topics from widely different lines of approach than their own, taking into consideration that all of them share a common interest: the upgrading of light alkanes.

The activation and functionalisation of light alkanes is, in fact, a very important issue and, simultaneously to the ASI, an EEC-funded workshop was held on the same subject. Its report, resulting from the discussions that took place during these days, both in a formal and in an informal manner, is included in this publication.

To everybody who attended the ASI, in particular to all the lecturers, as well as to those who coordinated and actively participated in the EEC workshop, we present our thanks. We also present a special thanks to all the people involved in the organization of this ASI, in particular to Profs. Filipe Freire, Maria Amélia Lemos, Isabel Santos Silva and Maria das Mercês Marques. Also to Pat Gibbs for her fine secretarial help.

Also, we wish to thank all the sponsors, namely the organizations who have shown interest and supported this event, the Luso-American Foundation for Development, the French Embassy in Lisbon, the Junta Nacional de Investigação Científica e Tecnológica, the EEC, through DG XII, and, last but not least, the NATO Scientific Affairs Division who took charge of most of the financial burden associated with this organization.

Eric Derouane

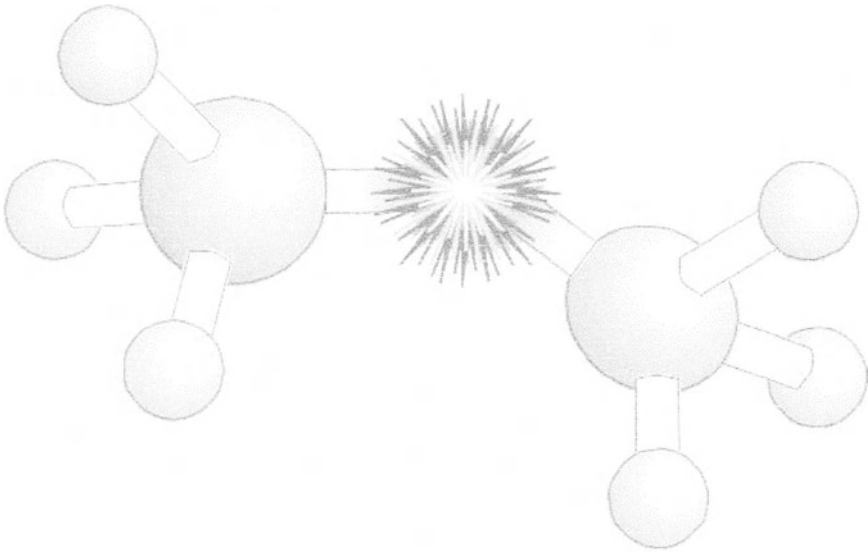
Jerzy Haber

Francisco Lemos

Fernando Ramôa Ribeiro

Michel Guisnet

# **SECTION 1**



# **LECTURES**

## UPGRADING OF C1 AND C2 HYDROCARBONS

P.L. VILLA AND S. RAPAGNÀ

*Dipartimento di Chimica, Ingegneria Chimica e Materiali  
Università di L'Aquila, 67100 L'Aquila, Italy*

### Abstract

Large scale natural gas reserves are often located far away from the area of utilization. This poses the problem of methane transformation into easily transportable products. After a brief overview of the reserves available, the direct conversion of methane to chloromethanes, hydrogen cyanide, carbon disulphide and acetylene with the present available technology is briefly described. The indirect transformation of methane via syngas manufacture to chemicals and fuels, such as ammonia, methanol and its derivatives, Fischer Tropsch products, “oxo-derivation” products, is outlined. The production of ethylene by steam cracking from different feedstocks, and its main applications in the production of polyethylenes, ethylene oxide, ethylene dichloride and ethylbenzene are summarized. Recent production data for some of the products are also given. Areas of research for the development of future technologies are discussed.

### 1. Introduction

The proven reserves of natural gas increase at a greater rate than those for oil [1], as shown in Figure 1. Indeed the gas/oil ratio of world proven reserves was 0.5 in 1970, 0.8 in 1982 and 0.98 in 1996. Very probably this ratio would



increase slightly further in favor of gas if, instead of proven reserves, the probable and possible reserves of gas and oil were considered\*.

Figure 2 shows the proved reserves of natural gas distribution around the world [1]. It is noteworthy that about 80% of the proven reserves are located in the CIS and OPEC areas and therefore often far from the main utilization zones.

Furthermore about 25% of the above reserves are located offshore.

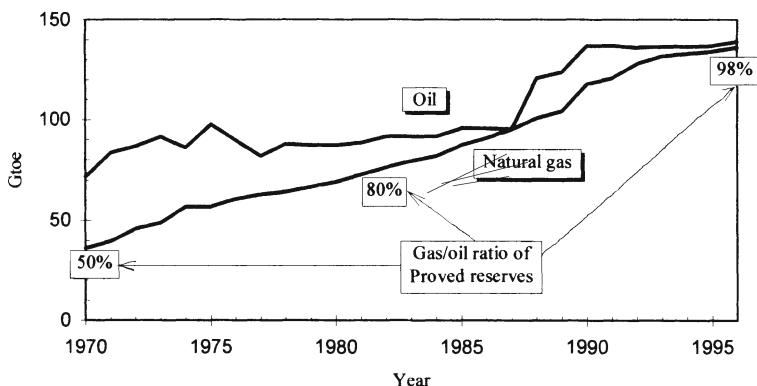


Figure 1. Proven world reserves of oil and natural gas (1000 m<sup>3</sup> of natural gas equal 0.85 toe; 1 ton of oil equal 7.33 barrels).

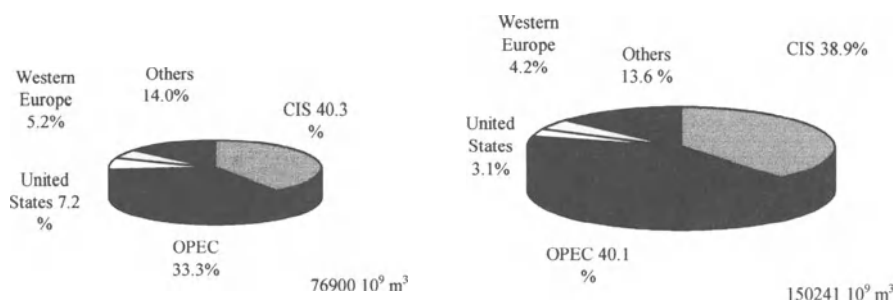


Figure 2. World natural gas proven reserves in 1980 and 1996.

\*Proven reserves refer to assessed reserves which can be used with the present technology and at the present market costs. Probable reserves are the reserves which may be used in the future with a slight improvement of the technology and not considering the market constraint. Possible reserves are the reserves that are likely to be found in the areas not already explored. For natural gas the proven, probable and possible reserves together, are estimated to be about twice the proven reserves, while for oil they are significantly less.

The cost of long distance transportation of gas is much higher than for oil [2], as reported in Figure 3, so as to render the utilization of natural gas on remotely located wells of little commercial interest, unless a transformation into liquid high value products is performed in situ.

This is one of the main reasons for which the ratio proven reserves/yearly consumption is much higher for natural gas than for oil as shown in Figure 4 [3]. Transportation cost from source to market may thus prevent its use, to such an extent that in the recent past (when natural gas associated with oil was obtained in regions like Middle East with restrictions on flaring it) it had a negative value related to the cost of repumping it into the well [4]. This explains why prices of natural gas differ so much around the world.

Oil and gas production for the year 1995 were 3.17 Gtoe ( $\sim 6.4 \cdot 10^7$  barrels daily) and 2.16 Gtoe ( $\sim 6.6 \cdot 10^9$  m<sup>3</sup> daily) respectively.

Pipeline transportation of compressed natural gas (CNG) competes with shipping of liquefied natural gas (LNG) only over very short transportation distances (3500 - 4000 km).

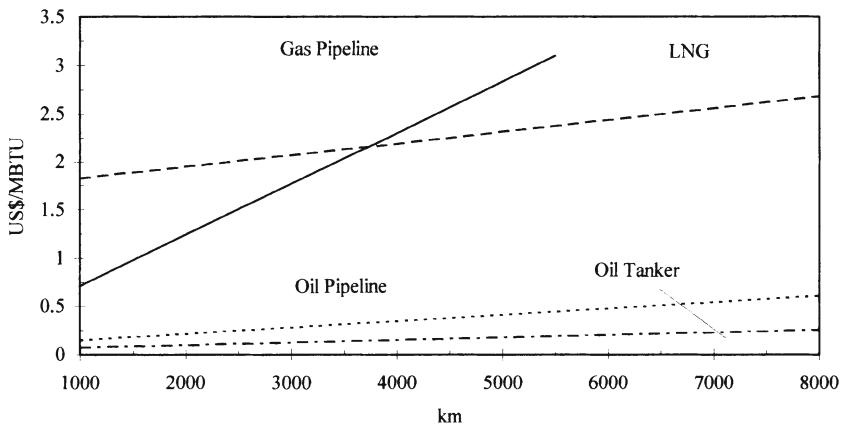


*Figure 3.* Cost to transport oil and natural gas.

It should also be considered that in remote areas such as Alaska, North West Africa, Northern Canada and central CIS, construction costs are higher than in industrialized areas because of the lack of regional infrastructure and skilled labor: in such conditions the best option is provided by processes that are not capital intensive, but rather raw material driven [5]: for example, plants for gas transformation in remote areas should preferably be not too complex.

In the past, the main use of natural gas has been for combustion to carbon dioxide and water for heating purposes and electricity generation in power stations. Indeed, natural gas combines high heating value, low sulphur content, and the largest H/C ratio - thereby giving rise to a reduction in greenhouse

effects. The production of electricity from methane can be obtained with higher efficiency by using fuel cells. Natural gas-fuelled Phosphoric Acid Fuel Cell (PAFC) technology for such applications is already available, with a 200 kW PAFC unit costing approximately US\$ 2500/kW; the unit operates at 40% electrical efficiency and 85% overall thermal efficiency (including heated water). The hydrogen rich gas fed to the unit should contain less than 1% by volume of CO [6].

The upgrading of natural gas into more valuable products is dependent on its composition. While natural gas produced in the Middle East and also the US contains significant amounts of  $C_2^+$  hydrocarbons (wet gas), in other parts of the world it consists almost entirely of methane (dry gas) as reported in Table 1 [2]. If wet gas is available, the separation of  $C_2^+$  hydrocarbons may easily lead to more profitable petrochemical intermediates such as olefins.

Methane, which is the main component of natural gas, is not easily transformed into other compounds because of its thermodynamic stability at temperatures below 825 °C [7] and because it displays four strong C-H bonds (of energy of 431kJ).

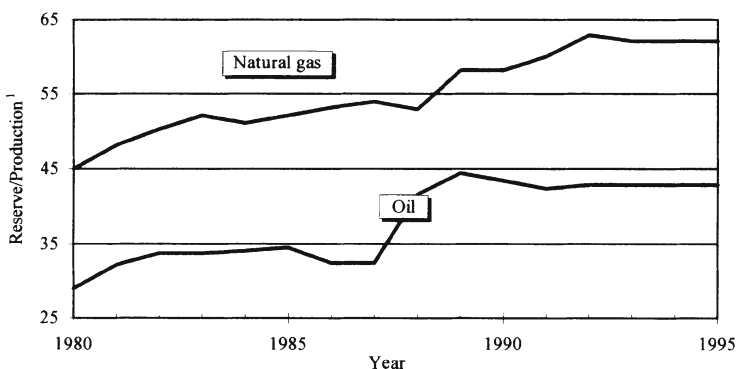


Figure 4. World Reserves/Production ratios

Table 1. Composition of natural gas from different areas.

	Methane	Ethane	Propane	Butanes	$C_5^+$	$N_2/He$	$H_2S$	$CO_2$
Holland	81.3	2.8	0.4	0.2		14.4		0.9
Italy	99.5	0.1				0.4		
UK	92.6	3.6	0.9	0.4	0.3	2.2		
Norway	90.9	5.9	1.1	1.1	1.1	0.6		1.5
Saudi Arabia	59.3	17.0	7.9	2.6	1.1	0.4	1.6	10.1
Iraq	55.7	21.9	6.5	3.9	1.2		7.3	3.0
Iran	76.1	11.1	6.1	2.2	1.1		0.3	3.1
USA	88.7	7.0	1.9	0.3		1.5		0.6

## 2. Direct conversion of methane.

The advances in the purification processes [8, 9] (for the elimination of sulphur, nitrogen, metals and chlorine containing compounds) allows for a more interesting use of natural gas in the synthesis of fuels and petrochemicals.

The transformations can be performed directly or indirectly, mainly via synthesis gas preparation. Methane may be transformed, employing well known technologies, into chloromethanes, HCN, CS<sub>2</sub> and C<sub>2</sub>H<sub>2</sub>. The direct conversion of methane is far less important than the indirect method because the world capacity of these compounds is of the order of only a few million tonnes.

### 2.1 CHLOROMETHANES.

Methane may be chlorinated directly with Cl<sub>2</sub>, or with HCl + air (oxichlorination): this latter reaction is exothermic and occurs by way of a radical chain mechanism [9, 10]. The main problem with this transformation arises from the difficulty of obtaining a distribution of products which exactly matches the market demand. Indeed, the consumption of CH<sub>3</sub>Cl, CH<sub>2</sub>Cl<sub>2</sub>, CHCl<sub>3</sub> and CCl<sub>4</sub> are very diverse and change with time. As the successive chlorination of CH<sub>3</sub>Cl is easier than the first chlorination of methane, the match with the market demand is approached by varying the CH<sub>4</sub>/Cl<sub>2</sub> ratio in the reactor, recycling the undesired chlorinated products, and eventually operating with more than one reactor if more deeply chlorinated products are required.

Methyl chloride demand is predicted to increase somewhat in the near future: it is mainly used in the production of silicones, methyl cellulose and butyl rubber.

Methylene chloride is mainly used for aerosols, paint strippers, metal degreasing and the production of polycarbonates. Its use is predicted to decline somewhat in the near future.

Chloroform is used for the production of polytetrafluoroethylene (PTFE) and chlorofluorocarbon CFC 22\*\*

The market for carbon tetrachloride is dominated by the manufacture of CFC 11 and CFC 12. Numerous studies started in the 80's have pointed out that CFCs are the main cause of the ozone hole in the atmosphere. As a result, the production of chlorofluorocarbons in the developed countries has been

---

\*\*The chlorofluorocarbons (CFC) are marked with two or three numbers that refer to the number of atoms present in the compound.. The first number is the number of carbon atoms minus one (the methane derivatives would have zero which is omitted), the second number is the number of hydrogens plus one, while the number of fluorines provide the third number. As an example CFC 11 and CFC 12 are CCl<sub>3</sub>F and CCl<sub>2</sub>F<sub>2</sub> respectively, while CFC 113 is CCl<sub>3</sub>CF<sub>3</sub>.

drastically reduced in recent years, and the market for carbon tetrachloride is expected to decrease substantially further in the near future.

The world capacity in 1994 of chloromethanes is reported in Table 2

*Table 2. World capacity of chloromethanes in 1994.*

World capacity in 1994	
	(metric tonnes)
CH <sub>3</sub> Cl	862000
CH <sub>2</sub> Cl <sub>2</sub>	738000
CHCl <sub>3</sub>	626000
CCl <sub>4</sub>	710000

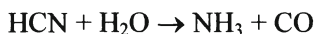
## 2.2 HYDROGEN CYANIDE, (HCN).

HCN is produced almost exclusively by the Andrussov process, and as a by-product of the propylene ammoxidation process for acrylonitrile. The Andrussov ammoxidation of methane [11] involves the reaction:



which is carried out catalytically at high temperature (1100 - 1150 °C), on a platinum/rhodium alloy gauze pad with a contact time of the order of a millisecond at a pressure of 0.2 MPa. A mixture of equal amounts of methane and ammonia with 75 vol % air is passed through the gauze in a similar way as in the reactor used for ammonia oxidation. The product gas contains some H<sub>2</sub> and CO, as well as unreacted NH<sub>3</sub> and a small amount of CH<sub>4</sub>, in addition the N<sub>2</sub> from the air. The yields based on methane and ammonia are roughly 88% and 70% respectively. The activity of the platinum pad passes through a maximum with time on stream because, in the first two or three days, the surface roughness is dramatically increased [11], thereby increasing the total surface area of the exposed metal. Thereafter the activity and selectivity decrease over a period of months.

Platinum losses in the Andrussov process are less severe than in the case of ammonia oxidation although the temperature of the gauze is some 250 °C higher: this is probably because the reducing atmosphere does not allow for the formation of volatile platinum oxide. The exit gases must be very rapidly quenched in order to avoid the very much favored homogeneous reaction:



Hydrogen cyanide is primarily used for adiponitrile synthesis with butadiene to produce nylon 6-6, and for the production of methyl methacrylate by reaction with acetone.

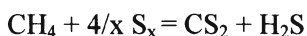
The consumption of methane for HCN production in USA in 1995 was  $663 \cdot 10^6 \text{ m}^3$ .

The capacity of HCN plants (synthetic + by-product) of USA + Japan + Western Europe is 1,100,000 tonnes.

### 2.3 CARBON DISULPHIDE, ( $\text{CS}_2$ ).

$\text{CS}_2$  is obtained mainly from the reaction between methane and sulphur [10]. However, alternative raw materials containing carbon and sulphur may also be considered. The mixed stream of methane and sulphur, with sulphur in slight excess, is fed to an adiabatic reactor operating with catalysts such as silica gel or  $\text{MgO}$ .

The reaction:



is carried out at a temperature of about  $650^\circ\text{C}$ . In calculating the heat of reaction one should remember that sulphur undergoes transformations with temperature to different allotropic forms:



The methane, that is at slightly less than the stoichiometric value, should be of high purity ( $>99\%$ ) in order to avoid unstable by-products which may be responsible for the formation of heavy tars. Carbon disulphide yields based on methane are  $90\div 95\%$ . The reactor effluent is cooled to  $130^\circ\text{C}$  and unreacted sulphur is separated and recycled. After absorption of  $\text{CS}_2$ , the off gas contains  $90\div 95\%$   $\text{H}_2\text{S}$  and passes to a Claus unit to produce sulphur for recycle. Both purification and handling of  $\text{CS}_2$  should be performed in controlled conditions in order to avoid explosion risks associated with the high volatility and high explosion limits of its mixture with air (1.25 % lower value, 50 % upper value by volume).

The  $\text{CS}_2$  is mainly used to produce  $\text{CCl}_4$ , rayon and cellophane. In 1993, the USA capacity was 100000 metric tonnes.

## 2.4 ACETYLENE.

Acetylene was the main building block in petrochemistry before the second world war. Therefore its production, although now rather limited, relies on well known technologies, involving, for example, the production of calcium carbide in an electrical oven which is then reacted with water under ambient conditions to give acetylene. Currently the main production route for acetylene (> 50%) is pyrolysis of methane.

Methane is a very stable compound requiring high temperatures for its transformation. At about 1200 °C the formation of radicals  $\text{CH}_3^\bullet$ ,  $\text{CH}_2^\bullet$  and  $\text{CH}^\bullet$  occurs which may be combined to give ethylene and acetylene. In all cases very short contact times and very rapid quenching are required in order to prevent the formation of soot and hydrogen which are the most stable products.

Several processes have been proposed, including the Huels and the Sachsse-Bartholomé processes.

The Huels process performs the pyrolysis of methane in a electrical arc at a temperature in the reaction zone of around 1250 °C. The quenching is realized with water.

In the Sachsse-Bartholomé process (BASF), which has found diffuse application in Europe and the USA, the high reaction temperature (1500 °C) is reached by feeding a mixture of methane and oxygen ( $\text{O}_2/\text{CH}_4=0.65$ ) to a burner. In addition to acetylene (8% by volume) a substantial amount of syngas is coproduced, together with a small amount of ethylene (1 % by volume).

All these processes are highly energy intensive and give low selectivity towards acetylene. For this reason acetylene production by pyrolysis is not expected to regain importance in the future [12].

The main applications of acetylene are for cutting and welding of metals, and for the production of vinyl acetate, vinyl chloride and acetylene black.

In 1993 the capacity of all plants producing acetylene was slightly in excess of 600,000 tons (excluding, due to the lack of data, the production of China).

In the last 30 years acetylene production has decreased by a factor of three, and further decreases are expected in the near future.

## 3. Areas of research for the direct conversion of methane.

It is clear that if the direct oxidation of methane to methanol or formaldehyde could be performed directly with high selectivities and yields, it could compare favorably with the indirect production via syngas due to it being less energy intensive and, as it would involve fewer transformations, less capital intensive. However, although several efforts have been made [13], the results are far from appealing from a commercial point of view. The reaction may be carried out

either in the homogeneous gas phase or over a catalyst: recent reviews make the point on both topics [14, 15].

It has been estimated [16] that, at 10 % conversion, the selectivity to methanol should be higher than 77% in order for it to be competitive with the indirect processes. It appears likely that efforts in this area will continue.

Also worthy of note is the process Catalytica [12] in which hydrogen is extracted at 180 °C with sulphuric acid to give  $\text{CH}_3\text{SO}_3\text{H}$  which may then be further hydrolyzed to methanol and dilute  $\text{H}_2\text{SO}_4$ .

### 3.1 OXIDATIVE COUPLING OF METHANE (OCM).

As we have previously seen, the pyrolysis of methane to higher hydrocarbons is not favored thermodynamically and requires operation at high temperature. The thermodynamic limitation may be removed if the pyrolysis is carried out in the presence of oxygen:



which is referred to as the oxidative coupling of methane to ethylene. Numerous papers have addressed this reaction since the first works of Mitchel/Waghorne and Keller/Bashin in the early 80's [17, 18]. The use of a catalyst in this reaction allows for lower temperatures than those necessary for the pyrolysis and therefore avoids the formation of carbon and aromatics. The outlet gas contains unreacted methane, ethane, ethylene, CO,  $\text{CO}_2$ ,  $\text{H}_2\text{O}$ , a small amount of  $\text{C}_3^+$  and hydrogen.

The reaction may be carried out in two reaction modes which operate with different catalytic systems and different plant schemes: the redox mode and the simultaneous mode.

In the redox mode (first proposed by Keller and Bhasin [18]) methane is oxidized with a reducible oxide such as  $\text{PbO}$ ,  $\text{Mn}_2\text{O}_3$ ,  $\text{SnO}_2$ ,  $\text{Pr}_6\text{O}_{11}$ . The implicit hypothesis which is made is that the lattice oxygen can give better yields in the  $\text{C}_2^+$  hydrocarbons, due to a better control of the deep oxidation to  $\text{CO}_2$  and  $\text{H}_2\text{O}$  in the homogeneous phase of the higher hydrocarbons obtained. Rather than a catalytic reaction, we are in the presence of a stoichiometric reaction between methane and metal oxide, with a separate regeneration with air of the oxide previously reduced by methane.

The reduced oxide can be continuously withdrawn from the coupling reactor and sent to a second reactor where it can be reoxidized with air. This operation mode (patented by Atlantic Richfield) is best performed transporting the oxide between two fluidised beds, in a similar way to FCC operation [19]. The best results were obtained with oxide of manganese or praseodymium doped with



alkali metals and supported on magnesia. For example, using  $\text{NaB}_2\text{Mg}_4\text{MnO}_x$  at 850 °C and atmospheric pressure, the methane conversion is 25% and the selectivity of  $\text{C}_2^+$  is between 72 and 74 %.

An alternative operation involves a cyclic mode in a single reactor [20] where the oxide is in contact alternatively with methane and air.

In the cofeed or simultaneous mode, the methane and oxygen are simultaneously fed to a refractory, basic and non reducible oxide. Among the numerous catalytic system taken in consideration, the most studied are the  $\text{Li}^+/\text{MgO}$  [21, 22] and the rare metal oxide systems.

According to Lunsford, a mixture of  $\text{Li}_2\text{O}-\text{MgO}$  (about 15% by wt of Li) heated to a temperature  $> 727$  °C and rapidly quenched in liquid nitrogen, gives EPR signals which show the presence of  $\text{Li}^+\text{O}^-$  species at high temperatures [23, 24]. Lunsford and co-workers [23, 25, 26, 27] have also shown that when  $\text{CH}_4$  and oxygen are fed to the  $\text{Li}/\text{MgO}$  system at 770 °C,  $\text{CH}_3^\bullet$  radicals are formed which are released in the gaseous phase and may be collected and measured downstream in solid argon for analysis with EPR. The trend of the  $\text{CH}_3^\bullet$  radical concentration versus Li contained in the oxide is very similar to the trend of the EPR signals for the  $\text{Li}^+\text{O}^-$  species as a function of the Li contained in the oxide. Similarly, a nice parallelism was found between the conversion of methane and the  $\text{Li}^+\text{O}^-$  species, measured as a function of the oxygen partial pressure.

The anion radical species  $\text{O}^-$  of the  $\text{Li}^+\text{O}^-$  couple would be responsible for the extraction of one hydrogen from the methane and the release in gas phase of the  $\text{CH}_3^\bullet$  radicals. The coupling of two  $\text{CH}_3^\bullet$  would give ethane and then ethylene.

Catalytic systems proposed for the oxidative coupling of methane are often unstable in operation due to the loss of components, such as the alkali metals and lead, in the gas phase. An even more severe drawback to overcome is the limited conversion and selectivity obtained per pass.

An economic evaluation [28] has shown that a yield in ethylene greater than 40 % for this reaction would be industrially viable. However, this goal is far from being reached, and much of the enthusiasm generated in the eighties for this reaction has evaporated.

Some hope for a revival of interest focuses on modifications of the process, such as those proposed by IFP and Snamprogetti [9, 29]. Both of these processes make use of a wet gas: the  $\text{C}_2^+$  fraction is firstly separated and then fed to the coupling reactor after the catalytic zone where the OCM reaction between  $\text{CH}_4$  and  $\text{O}_2$  has already occurred. It would thus be possible to utilize the heat produced by the OCM reaction to crack the ethane to ethylene, thereby reducing fractionation costs.

#### 4. Indirect conversion of methane.

The discovery of substantial reserves of natural gas has directed efforts towards the synthesis of useful products, mainly by means of indirect transformations. Indeed, it is possible, using a proven technology starting from natural gas, to manufacture synthesis gas from which many substances having applications as fuels or chemicals may be synthesized.

By synthesis gas (syngas) is understood a mixture of  $H_2$ , CO and eventually  $CO_2$ .

In the sixties and seventies, the relative abundance of liquid distillates obtained from oil made the use of virgin naphtha particularly relevant in Europe and Japan: now the favorite feedstock is methane.

The ideal feedstock depends to some extent on the final substance to be manufactured from the syngas. Syngas produced by steam reforming of methane has a  $H_2/CO$  ratio of typically 5-7 which is most suited for the production of pure hydrogen or ammonia. If methanol is the final desired product, the best stoichiometry for the syngas is a  $H_2/CO$  ratio of 2, which may be approached by steam reforming of methane or of virgin naphtha with  $CO_2$  recycle.

If the final product is gasoline, the best  $H_2/CO$  ratio is 1, which may be achieved in a competitive way by partial oxidation processes in which heavy oil can also be used as feedstock.

The world production of ammonia is based on steam reforming of natural gas and of hydrocarbons in general (77% and 85% of the total respectively). Steam reforming will also supply the marginal hydrogen supply necessary for hydrotreating operations in refineries.

Currently the most used technology for the production of syngas is the steam reforming of methane.

##### 4.1 STEAM REFORMING OF METHANE.

Steam reforming of methane is the simplest and most efficient way of manufacturing syngas for ammonia production, however several steps are necessary before the  $NH_3$  synthesis is performed, as shown in Figure 5 [30, 31].

In every case the most difficult step is the primary reforming of natural gas. In this step natural gas and steam react according to



the composition of the gas stream at the exit being near to the thermodynamic equilibrium.

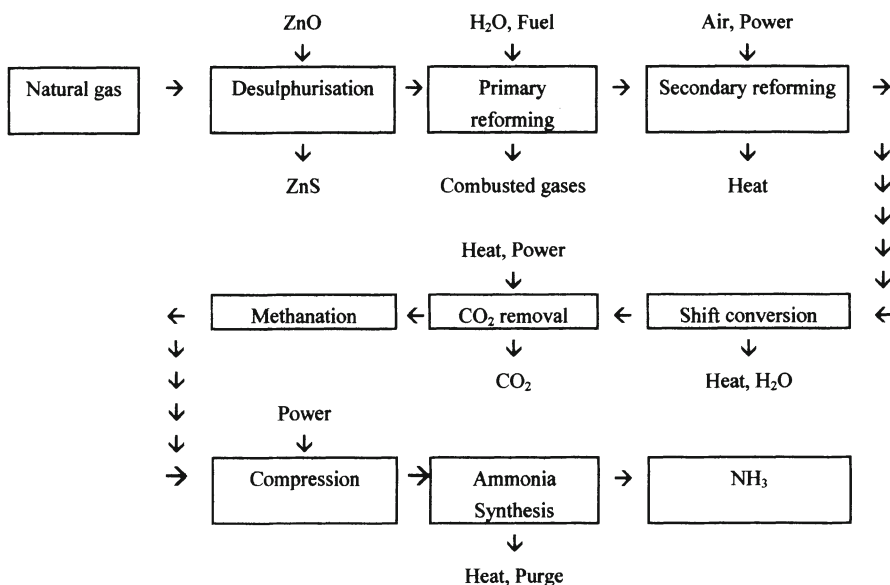


Figure 5. Synthesis of ammonia via natural gas steam reforming.

This transformation is performed at about 3.5 MPa; it requires a nickel catalyst (12 - 15 % by wt of Ni as NiO, on a  $\text{Al}_2\text{O}_3$ -CaO or  $\text{MgAl}_2\text{O}_4$  support [30]). The former reaction displays a  $\Delta G^\circ = 0$  at about 900 K: because of thermodynamic constraints, in order to obtain high conversion of methane it is necessary to operate at temperatures  $> 800^\circ\text{C}$ . A large excess of steam ( $\text{H}_2\text{O}/\text{CH}_4 = 3 - 3.5$  molar ratio) is necessary both to prevent carbon formation and to further increase methane conversion. The superficial contact time (based on feed gases at STP) is 0.5 - 1.5 s, which corresponds to residence times of several seconds.

To match these requirements, the reaction is typically performed in multitubular reactors that contain up to 1000 vertical tubes of high nickel chromium alloy steel, with internal diameters of  $\sim 120$  mm, wall thickness of 15 mm, and  $\sim 10$  m in height. The tubes are filled with catalyst and are fired externally; the exit temperature of the firing gas is about  $1000^\circ\text{C}$ , and maximum wall temperature of the tubes  $900^\circ\text{C}$ . The primary reformer is an expensive piece of equipment and rather complex to operate. Steam reforming requires careful operation and skilled technicians. Unskillful operation may lead to tube plugging and breaking. Catalyst breaking and sintering and carbon formation should be avoided. Furthermore the heat balance becomes acceptable

only because heat is recovered downstream of the primary reformer: only 40 % of the energy supplied is consumed by the reaction, 25 % is recovered as steam production, 10 % is recovered in the CO<sub>2</sub> separation section, leaving about 25 % that is lost with the flue gas [9]; according to Rostrup Nielsen [32] the total heat recovery may amount to 95%.

The severity of the primary reforming is also limited by the mechanical resistance of the tubes, which creep under stress at temperature > 1000 °C due to the combined conditions of high temperature, high thermal flux, and high partial pressure of steam. The tube cost is in the range of 15- 30 thousand dollars for a lifetime of the order of 10 years. There is a new generation of tubes, however, which can stand more severe conditions [32] (outlet gas temperature > 950 °C, wall temperature up to 1050 °C together with a reduced wall thickness). The exit gases contain significant amounts of unreacted methane ~ 9 - 10 % by volume on a dry basis, and a H<sub>2</sub>/CO ratio ~ 7, which may be suitable for ammonia production but not optimal for methanol synthesis and even worse for Fischer Tropsch synthesis.

The preparation of syngas requires other transformation steps which are indicated in Figure 5 and are well described in the available literature [8, 30, 32].

#### 4.2 OTHER METHODS OF SYNGAS PREPARATION.

A significant variation of conventional steam reforming is *heat exchange steam reforming*, which is based on the fact that the heat available in process gases leaving the oxygen-fired secondary reformer matches the heat required for primary reforming. It is therefore possible to use these hot gases in a heat exchange reformer thus avoiding the expensive primary reforming step. Small plants using heat exchange steam reforming are already operating [31].

Syngas may also be produced by gasification of any fossil feedstock, such as coal, oil residues and methane, following well established technologies. A comparison of natural gas reforming, heavy oil and coal gasification gives the following approximate figures based on European economic conditions [31]:

	Natural gas	Heavy oil	Coal
Energy Consumption	1.0	1.3	1.7
Investment cost	1.0	1.4	2.4
Production cost	1.0	1.2	1.7

It is likely that natural gas will be the preferred feedstock for ammonia production in Europe for at least 50 years, while in the long term coal may be expected to take over, together with heavy oil and gasification of waste materials.

The partial oxidation of methane with oxygen gives rise to high conversions to synthesis gas and is performed at temperatures of around 1400 °C at pressures up to 7 MPa in the absence of a catalyst (Shell and Texaco processes) with carbon efficiency > 95% and methane slip 1%. Carbon formation must be controlled and separated by water scrubbing. The use of oxygen instead of air implies an oxygen separation unit which features prominently in the economic evaluation. However partial oxidation allows for the manufacture of syngas with a molar ratio  $H_2/CO$  between 1.5 - 2 (Shell Gasification [33] and Texaco Processes) which is particularly suitable for Fischer-Tropsch synthesis.

#### 4.3 TRANSFORMATION OF SYNGAS TO FUELS AND CHEMICALS.

Syngas is a very versatile building block material. Figure 6 shows the main transformations performed with current proven technology.

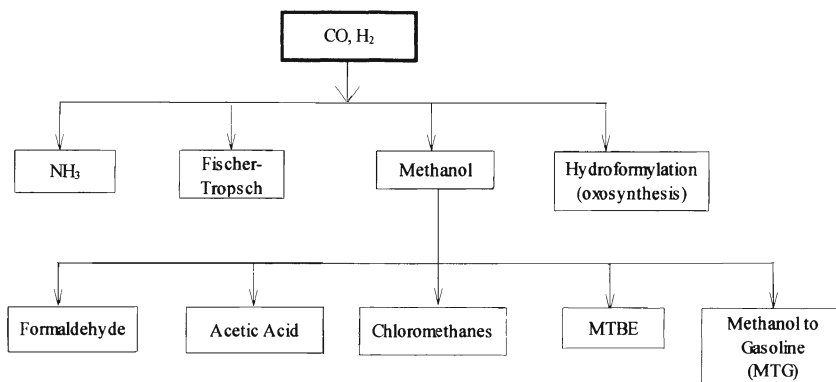
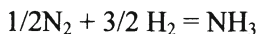


Figure 6. Main products obtained from syngas with available technology.

Although a detailed description of all these transformations is outside the scope of this work, a brief summary now follows.

##### 4.3.1 Ammonia.

Ammonia is mainly used in fertilizers and explosives as well as in intermediates for plastics, fibres and resins. It is obtained from:



$$\Delta H^\circ_{298} = - 45.7 \text{ kJ/mole}$$

$\Delta G^\circ = 0$  at about 473 K. This synthesis represented a milestone for the chemical industry and was the result of impressive research and development performed in Germany by Mittasch, Haber and Bosch; the first industrial plant was put into operation in 1913. The catalysts developed at the beginning of the

century are very similar to those used today in commercial plant and contain: Fe which during the operation is mainly reduced to the metallic state,  $\text{Al}_2\text{O}_3$  which controls the sintering of the Fe, and  $\text{K}_2\text{O}$  which acts mainly as an electron promoter, and other minor elements such as  $\text{MgO}$ ,  $\text{CaO}$  and  $\text{SiO}_2$ . The catalyst is obtained by fusion of a magnetite ore together with promoter precursors at around  $1500^\circ\text{C}$ ; a solid is then obtained by slow cooling in which aluminium oxide is in solid solution with iron oxide - and therefore in the best interspersed form to prevent the sintering of metallic iron during the operation. A ruthenium promoted magnetite type catalyst has also been proposed recently [34].

The mechanism of the reaction has been extensively studied and its elementary steps are now reasonably well known [35, 36].

Due to the fact that ammonia synthesis is performed in a temperature range that is thermodynamically unfavorable ( $350 - 550^\circ\text{C}$ ), operation under pressure is a necessity. The pressure used in the synthesis varied in the past between 10 and 100 MPa, and the most usual value being currently used is around 10 - 25 MPa. Different reactor types have been proposed which, in addition to withstanding the desired pressure, must be resistant to  $\text{H}_2$  at high temperatures and incorporate heat exchangers between the inlet and outlet gases. A significant improvement in design has come about with the use of radial reactors in which the pressure drop of the gas across the catalyst bed is significantly reduced, allowing for the use of smaller catalyst size, with resultant increase in catalyst efficiency [11].

Ammonia world-wide plant capacity is over 120 million tonnes per year (9).

#### **4.3.2 Fischer Tropsch synthesis**

Fischer and Tropsch in 1923 synthesized a liquid fuel from syngas utilizing alkalized iron turnings, at pressures of 10-15 MPa and temperatures in the  $400-450^\circ\text{C}$  range. This synthesis can now lead to a wide spectrum of products, such as gasoline, diesel oil, waxes, alcohols and olefins according to the reaction conditions. The main reaction is:



where  $n$  may vary between one and more than sixty, in accord with the Schultz-Flory distribution which takes into account chain growth and chain termination probabilities.

The catalysts used are mainly of two types: iron and cobalt based, both with alkali promoters. Iron is the preferred element and may be used in a variety of reactor types such as fixed bed, fluidised bed, circulating and slurry beds. The slurry bed is the most frequently used because the presence of a liquid phase

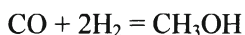
allows for a better control of the reaction temperature for this highly exothermic system.

Fischer-Tropsch synthesis from methane derived syngas is performed commercially in Malaysia (Shell Middle Distillate Synthesis process, SMDS) [33]. After the Fischer Tropsch synthesis this process performs a hydrocracking-hydroisomerization in order to improve the  $C_5^+$  yield and properties.

Sasol, in South Africa, have operated Fischer-Tropsch Synthesis for many years using coal as feedstock and making use of different reactor types.

#### 4.3.3 *Methanol synthesis*

Methanol is obtained from:



$$\Delta H_{298}^\circ = -91 \text{ kJ/mole}$$

and  $\Delta G^\circ = 0$  at about 140 °C. The synthesis became commercial in 1923 in Germany, the original catalyst being  $ZnO-Cr_2O_3$  oxides which are active at temperatures above 320 °C. The BASF process operated at about 30 - 40 MPa. Since the 60's the improved technology for purifying syngas from sulphur containing compounds has permitted the commercialization of copper based catalysts which at present consist of  $Cu/ZnO/Al_2O_3$  and are active in the 230 - 280 °C range, thereby permitting a lower operating pressure (5 - 10 MPa). The low pressure copper based catalyst has superseded the high pressure process and is used mainly in two commercial processes. The ICI process uses a quench type reactor in which fresh syngas is introduced at different depths of the catalyst bed. The Lurgi process operates with a multitubular reactor which allows for better temperature control: boiling water circulating on the shell side is used as the cooling agent. The methanol concentration at the reactor exit is only 3 - 7 % by volume, so that a substantial recycle ratio is required. Due to the fact that syngas produced from steam reforming has a  $H_2/CO$  ratio higher than the optimal value, some  $CO_2$  is always present in the feed gas and is recycled with  $H_2$  and  $CO$  to the reactor ( $CO$  8-10%,  $CO_2$  6-10% the rest being mainly  $H_2$ ). Methanol synthesis reactors with radial gas flow have also been proposed in recent years: these allow for a considerable reduction in reactor volume [11]. The world-wide methanol capacity and production in 1994 were  $26712 \cdot 10^3$  and  $22975 \cdot 10^3$  tonnes respectively.

##### 4.3.3.1 *Uses of methanol.*

Methanol is an important intermediate for the synthesis of both chemicals and fuels. Table 3 gives the world consumption of methanol for its various derivatives in 1994.



Table 3. Main use of methanol in 1994, in thousands metric tonnes.

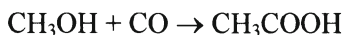
Formaldehyde	7500
MTBE	5500
CH <sub>3</sub> COOH	1560
Chloromethanes	780
Methylamines	650
Methylmethacrylate	640
Dimethyl terephthalate	630

The most important chemicals obtained from methanol are formaldehydes, acetic acid, chloromethanes and MTBE (which is used as a fuel additive).

- Formaldehyde may be produced by two different routes both at atmospheric pressure. The first route involves a methanol rich feed (about 50% methanol in air) and therefore operates above the higher explosion limit. This process currently uses silver catalyst, either as a silver wire gauze or silver crystals; the reaction is performed adiabatically at about 600 °C with a contact time of 0.01 seconds. The exit gases contain considerable amounts of hydrogen, carbon dioxide and water; the conversion per pass is lower than 70%, and the catalyst life depends on the purity of the methanol - varying from a few months up to two years. The presence of steam increases both conversion and catalyst life time.

The second route for formaldehyde production uses a methanol lean system (about 6-9 % methanol in air) and therefore operates below the lower explosion limit. The reaction is performed in a multitubular reactor employing a Fe<sub>2</sub>(MoO<sub>4</sub>)<sub>3</sub> based catalyst containing an excess of MoO<sub>3</sub> at a temperature in the range of 300-400 °C. Methanol conversion is in the 95-99% range, with good selectivity to formaldehyde (91-94%) so that only a single pass is necessary. The catalyst life time is of the order 6 - 12 months, depending on the temperature profile along the reactor tube and plant operating conditions.

- Acetic acid is currently produced mainly by carbonylation of methanol (58% of the world production):



$$\Delta H^\circ_{298} = -123 \text{ kJ/mole}$$



Monsanto performs this reaction using a rhodium complex in the homogeneous phase, at pressures between 1 - 4 MPa and temperatures of 150 - 200 °C. The low loss of rhodium achieved in the catalyst recycle has rendered the process commercially successful. BP Chemicals [37] have recently proposed a new catalytic system based on iridium compounds, promoted and stabilized by small quantities of rhenium. In 1991 the world capacity was about 5.4 million tonnes.

- Chloromethanes are also produced by reaction of methanol with HCl, as an alternative to the direct synthesis from methane reported above. Although methanol is more expensive than methane, this synthesis is competitive because HCl is used instead of Cl<sub>2</sub>, and because a better product distribution is achieved.



The reaction is performed preferentially in the gas phase, on an Al<sub>2</sub>O<sub>3</sub> catalyst in a fixed or fluidised bed at 300-350 °C, 0.3-0.6 MPa, with selectivity to CH<sub>3</sub>Cl of about 98%.

- Methyl Tert Butyl Ether (MTBE) was first produced commercially in 1973 by Snampromgetti/Anic. It now ranks in the first 50 commodities with a world production of 14 million tonnes in 1994.



MTBE is produced by passing isobutylene, with an excess of methanol, over cationic resins of the Amberlite type at 30 - 100 °C and 0.5 - 1.5 MPa. This product is used as an octane booster because of its high antiknocking properties, particularly when mixed with gasoline with which no phase separation occurs (Research Octane Number in the mix RON = 113-117, Motor Octane Number MON = 95-101). The increased market demand for MTBE has led to interest in both TAME (Tert-Amyl Methyl Ether) and ETBE ( Ethyl tert-Butyl Ether).

- In Mobil's Methanol to Gasoline process (MTG), methanol is dehydrated to obtain a gasoline mixture with a composition of 68% C<sub>5</sub>+, 20 % C<sub>4</sub> and about 10 % C<sub>3</sub> and less than 5% of C<sub>1</sub>-C<sub>2</sub> hydrocarbons. The unleaded gasoline obtained has a RON of 93-96.8 and contains no N or S compounds. The first commercial plant was started up in New Zealand in 1986 with a capacity of 600 thousand tonnes per year. The reaction is performed in fixed

beds operating with large recycle in order to control the temperature rise due to the highly exothermic reaction. Part of the methanol is converted to dimethylether in a prereactor to reduce the heat load on the main reactors. Zeolites ZSM-5 are used as catalyst in the main reactors. This process is currently not competitive in other parts of the world due to the rather low oil prices.

#### 4.3.4 Hydroformylation (oxosynthesis).

Hydroformylation, also called oxosynthesis, is the manufacture of aldehydes from olefins, carbon monoxide and hydrogen:



Hydroformylation is homogeneously catalyzed and performed at pressures between 20 and 35 MPa and temperatures around 100 - 150 °C, on Co, Rh or Ru complexes modified with amine or phosphine ligands.

A typical composition of the condensate obtained by hydroformylation of propylene using a cobalt based catalyst is: 80% C<sub>4</sub> aldehydes, 10-14% C<sub>4</sub> alcohols and butyl formates, with the normal/iso ratio between 3 and 4.

The first plant went into operation in 1945 for the manufacture of detergent alcohols with chain length between C<sub>12</sub> and C<sub>14</sub> [38].

In 1990 the total world capacity of hydroformylation products was over 7 million tonnes: approximately 74 % of the capacity corresponds to the C<sub>4</sub> aldehydes, 3-4 % to propionaldehyde and about 20 % to C<sub>9</sub>-C<sub>10</sub> aldehydes [9]. All these aldehydes are generally further hydrogenated to alcohols for the manufacture of solvent plastifiers and detergents.

1975 saw the first commercial plant working with a rhodium based catalyst for the hydroformylation of ethylene, and in 1976 a second plant for the hydroformylation of propylene was commissioned. Rhodium based catalysts allow for mild operating conditions (1.5 - 5 MPa, 60 - 120 °C) and display a normal/iso ratio of butylaldehyde of around 11. The success of rhodium based processes is also due to an easier separation of the catalyst from the liquid products, several options being possible in this respect.

The aldehydes so produced are used as intermediates for the production of alcohols, carboxylic acids and aldol condensation products. The hydrogenation to alcohols can be performed in principle in the hydroformylation reactor by using high temperatures. However, to increase the selectivity towards the normal alcohol, the hydrogenation is usually performed in a second reactor using nickel or copper catalysts. The world production of alcohols of "oxo derivation" was 5.1 million tonnes in 1991.

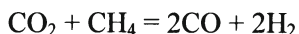
The economics of various natural gas processes that give rise to liquid products have recently been compared [39, 40, 41].

## 5. Areas of research for indirect conversion of methane.

### 5.1 FUTURE DEVELOPMENTS FOR SYNGAS PRODUCTION.

Syngas manufacture accounts for the most significant cost of the final product: in the 50 - 70 % range for fuel production, and around 70 % for alcohol synthesis. Therefore great efforts are currently being made to render the economics of the gas production more appealing.

- A significant example of process simplification is the autothermal reforming system (ATR) proposed by Topsoe [42]. By means of a newly designed burner which mixes the reagents more effectively, and a simple reactor which performs most of the transformations in a “combustion zone“, followed by a catalytic fixed bed for equilibration of the gas, it seems possible to use  $\text{H}_2\text{O}/\text{CH}_4$  ratios lower than 1.4 without causing soot formation. Autothermal reforming is a low investment process which produces syngas with a high  $\text{CO}/\text{H}_2$  ratio. It employs  $\text{O}_2/\text{CH}_4$  ratios in the range 0.55-0.6, and may become competitive if cheap oxygen is available: the resultant syngas can have  $\text{CO}/\text{H}_2$  molar ratios as high as 1 with methane slip less than 1 %.
- CO reforming, also called dry reforming, i. e. the manufacture of syngas by reaction with CO instead than  $\text{H}_2\text{O}$ , viz.



$$\Delta H_{298}^\circ = 247 \text{ kJ/mole}$$

could be another way to obtain syngas with low  $\text{H}_2/\text{CO}$  [43,44,32].

This reaction is slightly more endothermic than steam reforming and involves similar mechanisms. The risk of carbon formation in carbon dioxide reforming is higher than in steam reforming. Carbon formation seems to be kinetically prevented on metals like Rh or Ru, which however have a cost which is almost prohibitive. Topsoe has developed the SPARG process, which uses conventional steam reforming catalysts for combined  $\text{H}_2\text{O}/\text{CO}_2/\text{CH}_4$  reforming. Carbon-free reforming in this process is achieved by “ensemble control” involving sulphur poisoning: carbon formation and growth on conventional Ni-based catalysts requires an ensemble of 6 or 7 atoms, whereas  $\text{CH}_4$  reforming

requires an ensemble of 3 or 4 atoms. Although pure CO<sub>2</sub> reforming has yet to be performed industrially, combined H<sub>2</sub>O/CO<sub>2</sub>/CH<sub>4</sub> reforming has already been commercialized [44].

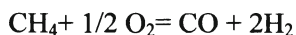
- Another effort directed at reducing the cost of syngas production, that involves both industrial and academic research, has led to the Catalytic Partial Oxidation process (CPO) where the use of catalyst seems to permit temperatures of about 800 °C instead of 1400 °C, and therefore a reduction in the consumption of oxygen, and product gas displaying a H<sub>2</sub>/CO ratio of 2 - favorable for methanol and Fischer Tropsch synthesis; this topic has been recently reviewed [45, 46].

This reaction can be performed using different types of reactor: packed bed, monolithic type and fluidised bed [47, 48, 49, 50]. Furthermore, the reactors turn out to be much simpler and smaller in volume than steam reforming reactors, and therefore particularly suited for operation in remote areas. The catalysts most frequently used are ruthenium, rhodium and nickel based. The very short contact times that appear necessary (10<sup>-2</sup>, 10<sup>-4</sup> s) could make the use of precious metal in the industrial operation affordable.

The best results for syngas production are obtained with undiluted gas. However, the use of undiluted oxygen and natural gas involves operation near to the flammability limits which are (at atmospheric pressure) 5.1 and 61 % of methane, while the stoichiometric value is 66.7 %. The limits become even further separated under pressure. This necessitates a detailed risk assessment prior to any experimental operation with undiluted gas [51].

The presence of temperature gradients make the determination of the intrinsic kinetics almost impossible and the reactor scale-up very difficult.

Whether CO and H<sub>2</sub> are primary products in certain cases is a much discussed question. This is an important point because it opens, at least in principle, the possibility of overcoming the thermodynamic constraints and performing the reaction



with high conversion and selectivity to syngas, using the stoichiometric amount of oxygen with no unwanted CO<sub>2</sub> and H<sub>2</sub>O. Recent results [52] obtained under transient conditions confirm the data of Hickman and Schmidt [53] and clearly show that CO and H<sub>2</sub> are primary products on catalyst system such as Y-stabilized zirconia, Ru supported on titania and metallic Rh and Pt .

## 5.2 METHANOL SYNTHESIS AT LOW PRESSURE AND TEMPERATURE.

At present syngas preparation and compression accounts for about 72% of the cost of manufacture of chemicals like methanol as shown in Figure 7 [54]. It would be profitable to develop an integrated process for syngas preparation and methanol synthesis at a lower global production cost of the final product [55].

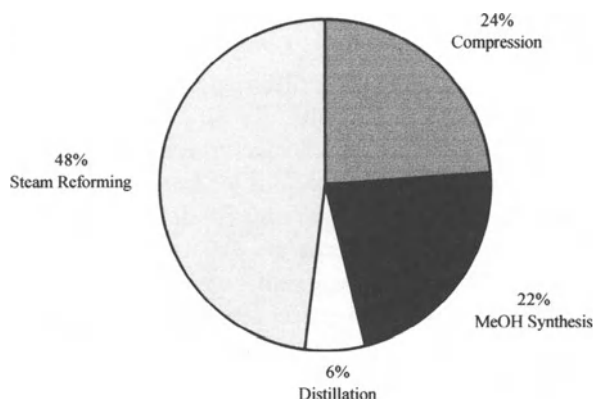


*Figure 7.* Share of costs for the manufacture of methanol

Methanol synthesis is currently carried out under thermodynamically unfavorable conditions (230 - 280 °C) and therefore with a conversion per pass in the 15-25 % range, even at pressures in the 5 - 10 MPa range. A significant recycling of the gas after methanol separation is therefore necessary. Catalysts working in the 80 - 120 °C temperature range could perform the synthesis of methanol at 1 - 5 Mpa of pressure and would allow for almost complete conversion per pass. Under these conditions the recycle of unreacted gas becomes unnecessary and the production of syngas containing N<sub>2</sub> could be performed economically by partial catalytic oxidation of CH<sub>4</sub> with air.

Mitsui Petrochemicals, Brookhaven National Labs and Shell have developed low temperature and pressure processes involving nickel based homogeneous catalysts which perform methanol synthesis in two steps via methyl-formate. This synthesis, however, involves the presence of Ni(CO)<sub>4</sub> which is volatile and very toxic.

## 6. Upgrading of C<sub>2</sub> hydrocarbons.

Before the second world war the main feedstock used for the most important chemical organic syntheses, particularly in Germany, was acetylene - manufactured mainly from calcium carbide and tars derived as by-products of the coke from coal process. After the 30's, the increased demand of gasoline and diesel oil, particularly in the USA, have pushed the refineries towards the thermal cracking of the heavy oil fractions. As a consequence, large fractions of light hydrocarbons were also available in that market.

Petrochemistry following the 50's has been dominated by the extensive use of light olefins as a feedstock. This has been possible because, during that period, several catalytic processes for the transformation of olefins were successfully developed.

Today, in addition to the thermocracking processes, which still find some application in oil refineries for the most difficult fractions to be dealt with, other processes have become important - such as FCC and hydrocracking which produce light gases which may be used for the production of ethylene.

The presence of significant C<sub>2</sub><sup>+</sup> hydrocarbons in some natural gas (see Table 1) enables this fraction to be used as a feedstock for the manufacture of light olefins. There are however, significant differences in the use of feedstock for olefin production between the USA on the one hand, and Europe and Japan on the other.

The large availability of ethane, propane and butane in the USA is due to two reasons: the oil market in USA is oriented mainly to the production of gasoline and diesel oil, and therefore makes extensively use of processes like FCC, hydrocracking and thermal cracking which produce large amounts of light gases. The *Liquefied Petroleum Gas* (LPG) so obtained accounts for about 25 % of ethylene production. The second reason is that in the USA the available natural gas is generally wet, so that it is easy to separate the C<sub>2</sub><sup>+</sup> fraction by absorption and stripping. Ethane obtained by wet gas separation accounts for about 40% of ethylene production in USA.

On the other hand, the oil market in Europe and Japan has been traditionally less oriented for the production of motor fuels with the result that smaller quantities of C<sub>2</sub><sup>+</sup> fractions have been available. For this reason virgin naphtha has been the most used feedstock for the production of ethylene in Europe and in Japan.

However, as a result of stringent environmental legislation and the increasing share of transportation fuels in the oil market (including that of Europe), refining strategies have become more complex and LPG and ethane are starting to become important feedstocks for olefins production also in Europe [56].

Ethylene is at present the feedstock for approximately 30 % of all petrochemicals.

## 6.1 ETHYLENE PRODUCTION.

Ethylene is the most important of the light olefins: the world yearly capacity was 82.6 million tonnes in 1996, and is expected to be 92.6 and 102.5 million tonnes in 1998 and 2000 respectively [57]. The Francis diagram [7] shows that olefins are thermodynamically unstable with respect to the elements at all temperatures. They become more stable than the corresponding paraffins at high temperatures: for example, ethylene is more stable than ethane at temperatures greater than about 800 °C. Most of the world production of ethylene (over 97%) is achieved by thermal cracking of hydrocarbons with steam (steam cracking). The feed is heated, mixed with steam and further heated to the incipient cracking temperature (500-600 °C depending on the type of feedstock), and then fed to a fired tubular reactor.

The transformation of paraffins into olefins is carried out at temperatures in the range 750 - 900 °C according to feedstock type, with a short residence time in the cracking zone (about 0.1 s), and low partial pressures of the hydrocarbons. The outlet total pressure is between 0.2 and 0.3 MPa, with a steam/hydrocarbon ratios in the ranges 0.25-0.6 and 0.4-0.75 for ethane and naphtha respectively [58, 59]. The presence of a significant amount of steam is necessary because it lowers the hydrocarbon partial pressure, reduces the partial pressure of aromatics, and therefore lowers the rate of coke formation.

Several types of reactor may be used depending on feedstock type. A typical reactor operating with virgin naphtha uses Cr-Ni coils 50 to 100 meters in length, internal diameter 60 - 120 mm [10] and 7-8.5 mm thick. In the cracking zone heat is transferred to the coil, mainly by radiation as the external temperature is in the range 1000 - 1200 °C.

The product distribution depends on the feedstock and process operating conditions: the wt % of ethylene on a dry basis may be 53 % starting from ethane and 34 % starting from virgin naphtha. The outlet gases must be rapidly quenched to 300 °C to avoid secondary reactions, compressed and purified with caustic soda to remove H<sub>2</sub>S and CO<sub>2</sub> and then carefully dried and separated by low temperature distillation.

Ethylene can be shipped over very long distances, but transportation of its derivatives, such as polyethylene, is preferred.

## 6.2 USES OF ETHYLENE.

As already stated, ethylene is the most important feedstock of all the petrochemicals. A very small amount is used for ripening fruits before delivery



for consumption. The main uses of ethylene in 1990 are reported in Table 4 [58].

*Table 4. Main products derived from ethylene world-wide (1990).*

Product	10 <sup>6</sup> tonnes
LDPE	16.4
LLDPE	7.2
HDPE	11.2
Ethylene oxide	8.2
Ethylene dichloride	10.1
Ethylbenzene	4.5
Ethanol	1.0
Linear olefins-alcohols	2.2
Vinyl acetate	1.2
Other	2.6

Table 3 shows the main use of ethylene to be for the manufacture of polyethylene. The polymer has a broad spectrum of properties according to its crystallinity, which is characterized mainly by density which ranges from 880 to 1000 kg/m<sup>3</sup> for the completely amorphous to the completely crystalline polymers respectively.

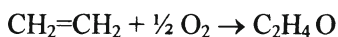
- Low Density Polyethylene (LDPE) is highly branched with density in the range 910 - 940 kg/m<sup>3</sup> and melting point in the range 105 - 115 °C. It is obtained by radical polymerization using O<sub>2</sub> or peroxides under high pressure (60 - 360 MPa) and temperature (about 350 °C). In this condition, the polyethylene produced is dissolved in the unreacted ethylene.
- High Density Polyethylene (HDPE) is a linear polyethylene of density 940 - 970 kg/m<sup>3</sup>, melting point 130 - 135 °C, with better mechanical properties than LDPE, that enables it to be injection moulded. Two different processes have been developed: Phillips Petroleum use Cr<sub>2</sub>O<sub>3</sub> supported on Silica at 50 - 300 °C and 0.1-20 MPa pressure. The second process uses Ziegler-Natta catalysts of aluminium alkyl and a slurry of TiCl<sub>4</sub> supported on magnesium oxide or carbonate, in a hydrocarbon diluent. Polymerization is performed at 65-90 °C, 1-3.5 MPa.
- Linear Low Density Polyethylene (LLDPE) is produced by Union Carbide, its density is in the range 920 - 945 kg/m<sup>3</sup>; it is mainly linear with short lateral branches, and is obtained by copolymerization with small quantities



of  $\alpha$ -olefins, such as 1-butene, 1-hexene or 1-octene, using a Ziegler-Natta catalyst.

- Ultra High Molecular Weight Polyethylene (UHMWPE) is characterized by a molecular weight between  $3 \cdot 10^6$  -  $6 \cdot 10^6$ , while typical values for other polyethylene are around 50000. It has a  $930 \text{ kg/m}^3$  density and melting point of  $135^\circ\text{C}$ . Polymerization is performed using Ziegler-Natta catalysts under different process conditions. The very high molecular weight imparts an exceptional combination of abrasion resistance, chemical inertness, toughness, low friction, and compatibility with foodstuff [59].
- Ethylene oxide itself is used as a disinfectant and sterilizing agent. About half the production of ethylene oxide is used for the manufacture of ethylene glycol which is mainly used as an antifreeze agent (for car radiators, etc.). Other uses include polyester fibre manufacture.

Ethylene oxide is currently obtained by direct oxidation of ethylene with oxygen or air, on metallic silver supported over  $\alpha$ -alumina, promoted with barium and cesium.



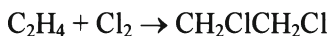
$$\Delta H^\circ_{298} = -105 \text{ kJ/mole}$$

The reaction is carried out in multitubular reactors containing several thousand tubes, 6-12 m long with internal diameter 20- 50 mm, packed with catalyst spheres or rings 3-10 mm in diameter. Typical selectivity is around 80%. The deep oxidation to  $\text{CO}_2$  and  $\text{H}_2\text{O}$ , accounting for the remaining 20 % selectivity, significantly increases the heat of reaction.

Two processes are utilized [38]. One, developed mainly by Scientific Design and UCC, operates with air, while the Shell process operates with oxygen. The total combustion is limited by the presence of some chlorine on the catalyst, which is the result of adding some dichloroethane or dichloropropane to the feed (1-10 ppm).

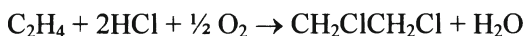
Overheating the catalyst should be avoided in order to prevent metallic silver deactivation. Operation with oxygen is preferred because it allows for limited conversion per pass (also less than 10%) and therefore an increased catalyst life time; in addition, equipment size with oxygen operation is considerably less than for air operation. The reaction is carried out in the  $250\text{-}270^\circ\text{C}$  range at about 1.2 MPa pressure, with a total yield of 65%.

- 1,2 dichloroethane (EDC) is used mainly for the production of vinylchloride - about 80%. The production involves either the addition of chlorine to ethylene,



$$\Delta H^\circ_{298} = -182 \text{ kJ/mole}$$

or oxichlorination:

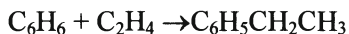


$$\Delta H^\circ_{298} = -240 \text{ kJ/mole}$$

The first reaction is carried out in the liquid phase using usually  $\text{FeCl}_3$  as catalyst and the same EDC produced as solvent. The reaction involves the electrophilic ionic mechanism, at temperatures of 40-70 °C, 0.4-0.5 MPa pressure. The selectivity to EDC can reach 98% based on  $\text{C}_2\text{H}_4$  and 99 % based on  $\text{Cl}_2$ . The presence of EDC in the liquid phase leads to a better temperature control as a result of the evaporation of part of the liquid. The reaction can, however, be carried out in gas phase at 90-130 °C.

The oxichlorination reaction is usually carried out in the gas phase at 220-240 °C, 0.2-0.4 MPa, using a  $\text{CuCl}_2$  catalyst containing activators and stabilizers, such as chlorides of rare earth and alkali metals supported on  $\text{Al}_2\text{O}_3$  or  $\text{SiO}_2$ . The conversion of both reagents is in the 95-99 % range, with a selectivity to EDC in the 93-96 % range. Fluidised bed reactors are often used for a better control of temperature.

- Ethylbenzene is used for the production of styrene. Most ethylbenzene is manufactured by alkylation of benzene with ethylene:



$$\Delta H^\circ_{298} = -106 \text{ kJ/mole}$$

The superfractionation of  $\text{C}_8$  aromatic cuts by distillation is now of minor importance.

The alkylation of benzene may be carried out in the liquid phase with a Friedel-Crafts catalyst, usually  $\text{AlCl}_3$ , at 100-140 °C, and 0.1-1 MPa. The control of the temperature is obtained by evaporation of benzene. The selectivity is enhanced by operating with limited benzene conversion (52-55%) and a high benzene/ethylene ratio. Higher ethylbenzenes are recycled to the reactor, where the transalkylation with benzene may occur.

Other types of process, operating in the gas phase and employing acidic catalysts, are operated in the USA. For example, the recent Mobil -Badger process which operates at 435-450 °C, with a modified ZMS-5 catalyst, at 1.4-2.8 MPa, gives a conversion of 85% with selectivity in ethylbenzene of 98%  $\text{C}_6\text{H}_6$  based, and 99%  $\text{C}_2\text{H}_4$  based.

## 7. Area of research for catalytic conversion of ethane to ethylene.

Although ethylene production by thermal steam cracking of hydrocarbons is a well established process, it requires high temperatures of operation, with attendant coke formation and a selectivity to ethylene which is not very high. If ethane is the feedstock, it would be interesting to develop catalytic process to transform it into ethylene.

Catalytic dehydrogenation of C<sub>10</sub>-C<sub>15</sub> alkanes to the corresponding alkenes has been practiced since the second world war for detergent production. More recently the catalytic dehydrogenation of isobutane to isobutene has been developed for MBTE production [60]. The catalytic dehydrogenation of propane to propylene, first developed by UOP in Thailand, is also used in commercial plant. Catalytic dehydrogenation of ethane to ethylene is not practiced and probably will not be practiced in the future. Indeed, by lowering the carbon number of the paraffin the thermodynamics of the reaction becomes the more and more unfavorable: higher temperatures of operation are necessary to reach the same conversion. Moreover, the enthalpy of formation per mole of the olefin from the corresponding paraffin is constant and around 125 kJ. This means that the heat of reaction, measured on a weight basis (kJ/kg) of olefin produced, increases on lowering the carbon number. It would therefore be desirable to develop catalysts for the selective oxidation of ethane to ethylene:



This reaction is not energy intensive and has the advantage of avoiding the necessity for frequent catalyst regeneration due to coke formation.

Albonetti et al. [61] have recently reviewed catalysts for selective oxidation of light paraffins.

## 8. Acknowledgements.

The authors are grateful for the financial support of the Consiglio Nazionale delle Ricerche (CNR): Contr. 96.01758.CT11.

## 9. References.

1. *Cedigaz*, July 1996.
2. Clerici, G. and Zennaro, R. (1997) Recent trends of research in natural gas utilization, *La Chimica e L'Industria*, February, 47-54.

3. International Energy Agency. Report on Natural Gas Transportation (1994) *OECD Paris*, Pag 3.
4. Parkyns, N. D., Warburton, C. I. and Wilson, J. D. (1993) Natural gas conversion to liquid fuels and chemicals: Where does it stand?, *Catalysis Today*, **18**, 385-442.
5. Axeldord, M. G., Gaffney A. M., Pitchai R. and Sofranko J. A. (1994) Natural Gas: Fuel or Feedstock, in H.E. Curry-Hyde and R.F Howe (eds.) *Natural Gas Conversion II*, Elsevier Science B.V., pp. 93-101
6. Cleghorn, S., Ren, X., Springer, T., Wilson, M., Zawodzinski, C., Zawodzinski, T. and Gottesfeld, S. (1996) Pem Fuel Cells for Transportation and Stationary Power Generation Applications, in T. N Veziroglu, C. J Winter, J. P Baselt and G Kreysa (eds.) *Hydrogen Energy Progress, Proceedings of the 11th World Hydrogen Energy Conference*, Stuttgart, 23-28 june, pp.1637-1646.
7. Francis A. W., (1928) The Free Energies of Some Hydrocarbons, *Industrial and Engineering Chemistry*, Vol. **20**, No.3, 277-282
8. Twigg, M. V. (1989) *Catalyst Handbook*, Wolfe Publishing Ltd, London.
9. Chaumette, P. (1996) Conversion chimique du gaz naturel, *Revue de L'Institut Francais du Petrole*, Vol. **51**, N° 5, October , 711-727.
10. Pasquon, I and Pregaglia, G.F., (1994) *Prodotti e Processi dell'Industria Chimica*, Città Studi Edizioni, Milano
11. Satterfield, C. N. (1991) *Heterogeneous Catalysis in Industrial Practice*, Mc Graw-Hill, Inc., New York.
12. Graeser, U., Keim, W., Petzny, W. J. und Weitkamp, J (1994) Perspektiven der Petrochemie, *DGMK- Tagungsbericht 9403*, 51-85
13. Fox III, J. M. (1993) The Different Catalytic Routes for Methane Valorization: An Assessment of Processes for Liquid Fuels, *Catal. Rev. - Sci. Eng.*, **35** (2), 169-212.
14. Foulds, G.A. and Gray, B.F. (1995) Homogeneous gas-phase partial oxidation of methane to methanol and formaldehyde *Fuel processing Technology* **42**, 129-150.
15. Hall, J.H., Hargreaves, S.J., Hutchings, G.J., Joyner, R.W., Taylor, S.H., (1995) Catalytic synthesis of methanol and formaldehyde by partial oxidation of methane *Fuel processing Technology* **42** 151-178)
16. Brown, M.J. and Parkyns, N.D. (1991) Progress in the partial oxidation of methane to methanol and formaldehyde, *Catalysis Today*, **8** (3), 305.
17. Mitchell, H. L. and Waghorne R. H., (1980) Process for the conversion of relatively low molecular weight hydrocarbons, to higher molecular weight hydrocarbons, catalyst-reagents for such use in such process, and the regeneration thereof, *US Patent, 4205194*, Exxon
18. Keller, G.E. and Bhasin M.M (1982) Synthesis of Ethylene via Oxidation Coupling of Methane, *Journal of Catalysis*, **73**, 9-19

19. Sofranko, J. A., Leonard, J. J. and Jones C.A. (1987) The oxidative conversion of methane to higher hydrocarbons, *Journal of Catalysis*, **103**, 302.
20. Jones, C.A., Leonard, J.J and Sofranko, J. A. (1987) The Oxidative Conversion of Methane to Higher Hydrocarbons over Alkali-Promoted Mn/SiO<sub>2</sub>, *Journal of Catalysis*, **103**, 311-319.
21. Lunsford, J.H. (1991) The catalytic conversion of methane to higher hydrocarbons, *Studies in Surface Science and Catalysis*, **61**, 3.
22. Lunsford, J.H. (1994) New Directions For the Catalytic Conversion of Methane. Final Report, November 1987-October 1993. *Report 94 N° GRI-94/0375; Order N° PB95-154183, NTIS*.
23. Discroll, D.J., Wilson, M., Wang, J.X. and Lunsford, J. (1985) Formation of Gas-Phase Methyl Radicals Over MgO, *J. Am. Chem. Soc.*, **107**, 58.
24. Ito, T. and Lunsford, J.H. (1985) Synthesis of ethylene and ethane by partial oxidation of methane over lithium-doped magnesium oxide, *Nature*, **314**, 721.
25. Campbell, K. D., Morales, E. and Lunsford, J.H. (1987) Gas-Phase Coupling of Methyl Radicals During the Catalytic Partial Oxidation of Methane, *J. Am. Chem. Soc.*, **109**, 7900
26. Campbell, K. D., Zhang, H. and Lunsford, J. H. (1988) Methane Activation by Lanthanide Oxide, *J. Phys. Chem.*, **92**, 750.
27. Campbell, K. D. and Lunsford, J.H. (1988) Contribution of Gas-phase Radical Coupling in the Catalytic Oxidation of Methane, *J. Phys. Chem.*, **92**, 5792
28. Fiels, S., Niruta, S. C. and McCarty, J.G. (1987) An Assessment of the catalytic Conversion of Natural Gas to liquids, *SRI International Project Report*, 6:9120-01-SQ.
29. D. Sanfilippo and S. Rossini, (1992) Procedimento integrato per produrre olefine da miscele gassose contenenti metano, *Italian Patent N° MI92A 02280*
30. Rostrup-Nielsen, J. R., (1984) Catalytic Steam Reforming, in *Catalysis Science and Technology*, Anderson J.R and Boudart M. (eds.) Vol.5, Springer-Verlag, Berlin 1-117
31. Production of Ammonia , Booklet No 1,(1996) *European Fertiliser Manufactures Association*, CU/E-96.22, 1-21
32. Rostrup -Nielsen ( 1993) Production of Synthesis gas Production of synthesis gas *Catalysis Today*, **18** 305-324
33. Van Wechem, V.M.H. (1994) Conversion of Natural Gas to Transportation Fuels via the Shell Middle Distillate Synthesis Process (SMDS), in H.E Curry-Hyde. and R.F Howe (eds.) *Natural Gas Conversion II*, Elsevier Science B.V., pp.43-71

34. Czuppon, T.A., Knez, S. A., Schneider, R.V. and Worobets, G, (1994), *Ammonia Plant Saf. Relat. Facil.*, **34**, 236
35. Ertl, G. Elementary Steps in Ammonia Synthesis, (1991), in J. R Jennings, (eds.) *Cap.3 in Catalytic Ammonia Synthesis: Fundamentals and Practice*, Ed. by. Plenum Press, New York
36. Stoltze, P. and Norskov, J. K., (1988) An Interpretation of the High Pressure Kinetics of Ammonia Synthesis Based on a Microscopic Model, *Journal of Catalysis*, **110**, 1-10.
37. Garland, C. S., Giles, M. F., Poole, A. D. and Sunley, J. G., (1996) Process for the production of a carboxylic acid, *US Patent 5,510,524*, 23<sup>rd</sup> april 1996.
38. Weissermel, K. and Arpe H.J (1993)., *Industrial Organic Chemistry* Second Edition, VCH, Weinheim.
39. Puskas, I., Natural gas to syncrude: Making the process pay off. *CHEMTECH*, december 1995, 43-49
40. Sundset, T., Sagge J. and Strom, T., (1994) Evaluation of natural gas based synthesis gas production technologie, *Catalysis Today*, **21**, 269-278.
41. Gradassi, M. J., and Green N. N., (1995) Economics of natural gas conversion processes; *Fuel Processing Technology* **42**, 65-83.
42. Christensen, T.S. and Primdahl I. L. (1994) Improve syngas Production Using Autothermal reforming, *Hydrocarbon Processing*, March, 39-46
43. Ashcroft, A.T., Cheetham A.K., Green, M.L.H. and Vernon P.D.F. (1991) Partial oxidation of methane to synthesis gas using carbon dioxide *Nature*. **352** 225-226
44. Edwards,J.H. and Maitra,A.M. The chemistry of methane reforming with carbon dioxide and its current and potential applications *Fuel Processing Tecnology* **42** (1995) 269-289
45. Tsang, S.C., Claridge, J.B., Green, M.L.H. (1995) Recent advances in the conversion of methane to synthesys gas *Catalysis Today* **23** 3-15
46. Bharadway, S.S., Schmidt,L.D. (1995) Catalytic partial oxidation of natural gas to syngas *Fuel Processing Technology* **42** 109-127 )
47. Choudhary, V. R., Rane, V. H. and Rajput, A. M. (1993) Selective Oxidation of Methane to CO and H<sub>2</sub> Over Unreduced NiO-Rare Earth Oxide Catalysts, *Catalysis Letters*, **22**, 289-297,
48. Hickman, D. A., Haupfear, E. A. and Schmidt, L.D. (1993) Synthesis gas Formation by Direct Oxidation of Methane over Rh Monoliths, *Catalysis Letters*, **17**, 223-237,
49. Santos, A., Menéndez, M. and Santamaria, J. (1994) Partial Oxidation of Methane to Carbon Monoxide and Hydrogen in a Fluidized Bed Reactor, *Catalysis Today*, **21**, 481-488,
50. Everett, B. M., Eisenbery, B. and Bauman, R.F. (1995) Advanced Gas Conversion Technology: A New Option for Natural Gas Development,

*First DOHA Conference on Natural Gas*, March 13-15, Doha - Qatar, Session 5/Paper No.21

51. Rapagnà, S., Villa, P.L., Bellavitis, F. and Munforti, C. (1997) Risk Assessment in the Catalytic Partial Combustion of Methane, *ECCEI - ICheaP-3*, May 4-7, Florence, 9/P93
52. Baerns, M., Blom, R., Marin, G.B., Mirodatos, C., van Ommen, J.G., Ross, J., Vasalos, I.A., and Verykios, X., (1996) Conversion of Natural Gas to Synthesis Gas and  $C_2^+$  Hydrocarbons, Summary Report on Contract N JOU2- CT92-0073 JOULE Programme 1/7/1996
53. Hickman, D.A. and Schmidt L.D. (1992) Synthesis Gas Formation by Direct Oxidation of Methane over Pt Monoliths, *Journal of Catalysis* **138**, 267-282
54. Wender, I., (1996) Reactions of synthesis gas, *Fuel Process. Technol.*, **48**, 189.
55. Marchionna, M., Lami, M. and Raspolli Galletti, A.M., (1997) Synthesizing methanol at lower temperatures, *CHEMTECH* April, 27-32
56. Courty, P. R. and Chauvel, A., (1996) Catalysis, the Turntable for a Clean Future, *Catalysis Today*, **29**, 3-15
57. Cornitius, T., (1997) Ethylene Stays Long Through 2001, *Chemical Week*, March 19, 41-45
58. Kirk Othmer, (1994), *Encyclopedia of Chemical Technology*, Fourth Edition, Vol. 9, John Wiley & Sons, New York, 877-915],
59. Ullmann's, (1987) *Encyclopedia of Industrial Chemistry*, Fifth, Edition, Volume A10, VCH, , 45-94
60. D. Sanfilippo, (1993) Dehydrogenation in a fluidized bed: an East-West collaboration, *CHEMTECH*, august, 35-39
61. Albonetti, S., Cavani, F. and Trifirò, F., (1996), Key Aspects of Catalyst Design for the Selective Oxidation of Paraffins, *Catal. Rev. - Sci. Eng.*, **38**, 413-438.



# TRANSFORMATION OF ALKANES ON SOLID ACID AND BIFUNCTIONAL CATALYSTS

AVELINO CORMA AND AGUSTÍN MARTÍNEZ  
*Instituto de Tecnología Química, UPV-CSIC*  
*Avda. de los Naranjos s/n. 46022 Valencia. Spain*

## 1. Introduction

The global energy demand of the different primary energy resources for the following years predicts that crude oil will continue to be the major energy resource of the future (Figure 1). However, a spectacular increase of natural gas demand is observed since the 1950's, and in due course is expected to grow at a similar rate within the next two decades. This fact has inspired the interest in developing new processes and technologies to convert natural gas into liquid hydrocarbons and more valuable products. Moreover, the lack of heteroatoms, metals and aromatic structures makes natural gas an ideal feedstock to produce clean fuel for the future [1]. Saturated hydrocarbons are the main components of natural gas and crude oil and therefore their transformation into high valued products is of prime importance. Owing to the relatively inertness of alkanes, their activation usually requires high temperatures and the use of a bifunctional catalyst, in which a hydrogenating-dehydrogenating component performs the initiation step and then the olefinic intermediates further transform into the final products on the acidic component.

Moreover, owing to environmental issues a major change is also taking place in the refining and petrochemical industry. The necessity of decreasing air pollutants from transportation fuels and the drive for cheaper feedstocks through the upgrading of less valuable oil components are forcing refiners to adapt the existing catalytic processes and catalysts and to design new ones in order to meet the new product specifications.

In this paper we will overview the different possibilities that can be envisaged for the catalytic transformation of alkanes and how new emerging catalytic technologies may help in adapting the actual refinery schemes to meet the demand for cleaner fuels. In the case of natural gas, the different routes of methane transformation will be considered. For refining and petrochemistry, the



conversion of LPG ( $C_2$ - $C_4$  alkanes) into aromatics, the skeletal isomerisation of n-butane into isobutane, the alkylation of isobutane with light olefins to produce high octane gasoline, and the upgrading of higher n-alkanes in gasoline and middle distillates through hydroisomerisation processes will also be reviewed.

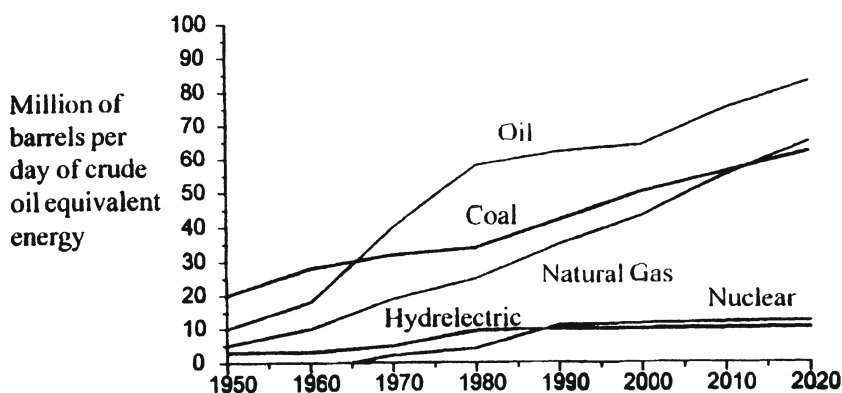


Figure 1. Global energy demand by primary energy type (1950 - 2020).

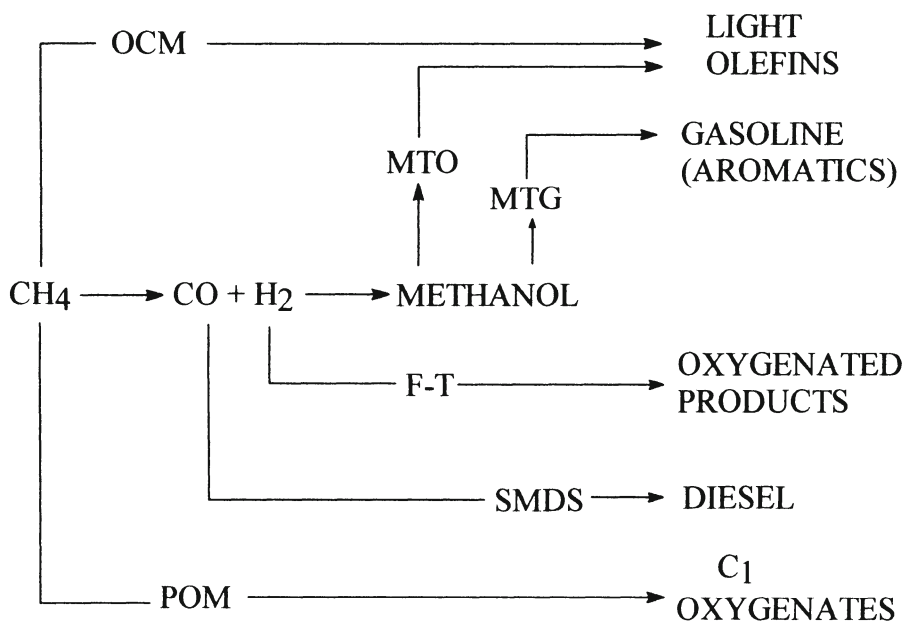


Figure 2. Catalytic processes for upgrading natural gas.

## 2. Transformation of alkanes

### 2.1 CATALYTIC CONVERSION OF METHANE

Different routes do exist for the catalytic transformation of methane, the main component of natural gas, into more valuable products. The main catalytic routes for upgrading natural gas are schematically presented in Figure 2. These can be classified into direct conversion processes and indirect routes, the latter going through the conversion of methane into synthesis gas. The most important processes will be briefly described below.

#### *2.1.1 Direct routes for methane conversion.*

The most studied process for the direct conversion of methane is the Oxidative Coupling of Methane (OCM). In this process methane is transformed into higher hydrocarbons, mainly ethylene, in the presence of oxygen at high temperatures, typically above 800°C [2-4]. Catalysts for OCM are usually based on metal oxides, in where oxygen species on the catalyst surface (lattice oxygen or adsorbed oxygen) react with methane to form methyl radicals, which then recombine in the gas phase leading to  $C_{2+}$  hydrocarbons. Total oxidation of either the methyl radicals and  $C_2$  hydrocarbons in the gas phase also occurs to a significant extent along with the surface catalytic reactions.  $C_{2+}$  yields obtained for most of the catalytic systems studied fall in the range of 15-25%. It has been shown [5] that unpromoted or promoted Li/MgO catalysts give the best results in long-test runs, achieving a stable yield of 15%  $C_{2+}$  at 1100°C, 1-2 bar pressure and using a 5-10  $CH_4/O_2$  ratio in the feed. However, from an economical point of view the key point will be to achieve very high selectivity at a reasonable conversion per pass. The results reported by Pereira et al. [6] using a new type of oxidative dehydrogenation catalyst may represent a step forward in this direction. The authors obtained nearly 100%  $C_{2+}$  selectivity at 10% methane conversion using a Ca-Ni-K oxide catalyst at low temperatures (< 610°C), but still the conversion is far from the target (> 35%) needed for commercialization.

Methane can also directly converted into methanol and formaldehyde by the Partial Oxidation (POM) process. The reaction can take place at relatively low temperatures (below 500°C) in an oxygen-deficient atmosphere in the absence of catalyst. However, much efforts have been devoted to direct the reaction catalitically, although the results obtained so far are not very promising. Among the different catalytic systems that have been studied for POM, it appears that vanadium and molybdenum oxides supported on silica are the most efficient [7]. However, high selectivities to the oxygenates could only be obtained when working at very low conversions (< 2-3%) per pass, and a sharp increase in the

selectivity to total oxidation products readily occurs as the conversion raises. This is easily explained from thermodynamic considerations owing to the much favorable conversion of methane into products of total oxidation, CO and CO<sub>2</sub>, if compared to the transformation into partial oxidation products (Table 1). Combining new selective catalyst formulations with optimized reactor designs that avoid overoxidation of the intermediate oxygenate products can be the key for improving the efficiency of the POM process in the future.

*Table 1.* Free energies and enthalpies (KJ mol<sup>-1</sup>) of the methane oxidation reactions.

REACTION	$\Delta G^0_{298}$	$\Delta H^0_{298}$
$\text{CH}_4 + \frac{1}{2} \text{O}_2 \rightleftharpoons \text{CH}_3\text{OH}$	-111.6	-126.2
$\text{CH}_4 + \text{O}_2 \rightleftharpoons \text{CH}_2\text{O} + \text{H}_2\text{O}$	-287.2	-282.6
$\text{CH}_4 + \frac{1}{2} \text{O}_2 \rightleftharpoons \frac{1}{2} \text{C}_2\text{H}_6 + \frac{1}{2} \text{H}_2\text{O}$	-64.0	-87.8
$\text{CH}_4 + \frac{1}{2} \text{O}_2 \rightleftharpoons \frac{1}{2} \text{C}_2\text{H}_4 + \text{H}_2\text{O}$	-143.4	-140.4
$\text{CH}_4 + 2 \text{O}_2 \rightleftharpoons \text{CO}_2 + 2 \text{H}_2\text{O}$	-800.0	-801.3
$\text{CH}_4 + 3/2 \text{O}_2 \rightleftharpoons \text{CO} + 2 \text{H}_2\text{O}$	-543.0	-518.7

### **2.1.2 Indirect conversion of methane via synthesis gas.**

Methane can be indirectly transformed into higher hydrocarbons by converting first natural gas into synthesis gas, CO+H<sub>2</sub>, via steam reforming at high temperatures, and subsequent transformation of syngas into hydrocarbons by low-temperature exothermic processes. One of them is based on the Fischer-Tropsch (F-T) synthesis [8], producing a mixture of straight-chain olefins and paraffins that obeys the Schulz-Flory (S-F) molecular weight distribution, together with some oxygenate products. The process has been commercialized by Sasol in South Africa using an Fe-based catalyst that produces the full range of products according to the Schulz-Flory distribution. Although the Sasol processed uses coal as the source of syngas, similar technology could be used for natural gas. New trends in F-T catalysts development are directed to overcome the S-F distribution. Some alteration of the S-F distribution has been obtained by using high-silica zeolite catalysts [9]. Some variations on the basic Fischer-Tropsch technology have been introduced in order to increase the yield of more valuable products, such as the production of gasoline range hydrocarbons, production of distillates, and the production of distillates and gasoline in combination with oligomerisation over a ZSM-5 catalyst in a two-step process [9].

Recently, the Shell Middle Distillate Synthesis (SMDS) process has been developed by Shell [10]. A diesel product with high cetane number is obtained

in a two-step process, in where a waxy product produced by F-T synthesis is selectively hydrocracked in the second reactor. Additionally, the synthetic gasoil produced by the SMDS process is poor in heteroatoms and aromatics and consequently it has many advantages from the environmental point of view.

Syngas can also be converted to valuable light olefins or gasoline via methanol by the Methanol-to-Olefins (MTO) and Methanol-to-Gasoline (MTG) processes developed by Mobil [11]. In the latter case, a substantial amount of light paraffins and aromatics are also formed in the presence of a ZSM-5 zeolite catalyst through cyclization of the olefins and hydrogen transfer reactions.

## 2.2 TRANSFORMATION OF SHORT-CHAIN $C_2$ - $C_4$ PARAFFINS

### 2.2.1 *Aromatization of $C_3$ - $C_4$ alkanes*

The Clean Air Act (CAA) amendments established in 1990 in USA contemplate a reduction of the gasoline volatility that will result in a removal of the n-butane stream from the gasoline pool. Moreover, an excess of  $C_2$ - $C_4$  alkanes will be expected from FCC units when operated for maximizing short olefins to be used in MTBE or alkylation units. This situation obviously will create an excess of LPG in the refinery, and therefore its transformation into liquid fuels or more valuable petrochemicals is of high interest.

$C_2$ - $C_4$  alkanes can be converted into aromatics (BTX) and  $H_2$  by using bifunctional catalysts. Csicsery showed in the 70's [12] that Pt,  $Cr_2O_3$ ,  $MnO_2$ ,  $V_2O_5$ ,  $WO_3$  and  $MoO_3$  supported on  $Al_2O_3$  were able to catalyze the dehydrocyclization of  $C_4$ - $C_5$  alkanes into aromatics, although the selectivities to aromatics were rather low and the catalysts rapidly deactivated with time on stream. A significant improvement in the process occurred in the 80's with the introduction of the medium pore MFI zeolite by Mobil and the development of the Cyclar process (BP-UOP) designed for  $C_3$ - $C_4$  aromatization using a Ga/H-ZSM-5 bifunctional catalyst [13, 14]. Besides Ga, Zn and Pt/ZSM-5 catalysts are also active for short alkane aromatization, although the former is the preferred metal. At the high reaction temperatures used ( $500^\circ C$ ) unwanted hydrogenolysis reactions occur in a larger extent on the Pt catalyst, whereas the main drawback associated with the use of Zn is its volatility at the reaction conditions, which still takes place to some extent even when the metal is incorporated into the zeolitic structure [15, 16]. Table 2 shows the effect of incorporation of Ga and Zn into H-ZSM-5 on product distribution during the conversion of propane at  $550^\circ C$  [17]. A sharp increase in conversion and aromatics yield is observed with the incorporation of Ga and Zn, and also the superiority of Ga with respect to Zn is clearly seen both in terms of conversion and selectivity under the same reaction conditions.

*Table 2.* Conversion of propane on H-ZSM-5 (Si/Al = 23), 1.8wt% Zn/H-ZSM-5, and 1.2 wt% Ga/H-ZSM-5 zeolites at 550°C, 101 Kpa C<sub>3</sub>, and W/F = 10.8 g h mol<sup>-1</sup>.

	Catalyst		
	H-ZSM-5	Zn-ZSM-5	Ga-ZSM-5
Conversion, %	56.3	72.5	85.5
Yield of aromatics, %	16.9	36.1	61.7
Product distribution, %			
CH <sub>4</sub> + C <sub>2</sub> H <sub>6</sub>	43.0	42.3	22.7
C <sub>2</sub> H <sub>4</sub> + C <sub>3</sub> H <sub>6</sub> + C <sub>4</sub> H <sub>8</sub>	21.8	7.0	4.4
C <sub>4</sub> H <sub>10</sub>	4.1	0.7	0.4
C <sub>5</sub> +	1.1	0.1	0.5
Aromatics	30.0	49.9	72.1
Aromatics Distribution, %			
Benzene	25.4	42.2	40.2
Toluene	46.2	36.8	40.7
C <sub>8</sub> alkylaromatics	26.0	14.1	12.6
C <sub>9</sub> +	2.4	6.9	6.5

However, in the case of the more refractory ethane Pt/H-ZSM-5 is the catalyst of choice owing to the higher dehydrogenation ability of the noble metal. In this case, and in order to avoid excessive hydrogenolysis at the high temperatures used, bimetallic PtMe/MFI catalysts are prepared (Me = Re, La, Ir, Cu or Ga). PdZn/ZSM-5 catalysts have also been studied for ethane aromatization, giving benzene as the major product in the aromatic fraction [18].

On these catalysts the reaction is thought to occur according to a classical bifunctional mechanism, provided a good balance between the metallic and acidic functions is achieved. In a first step, the alkane is dehydrogenated mainly on the metal sites (Ga, Zn, Pt), while oligomerisation of the olefins formed and cyclization of the oligomers will occur on the acidic sites of the zeolitic component. It is suggested that dienes are formed by further dehydrogenation of the oligomers on Ga sites before undergoing cyclization. Then, transformation of the cycloolefins into aromatics takes place on the metallic centers, probably

with the participation of the acid sites of the zeolite. A simplified reaction scheme for the aromatization of propane on Ga/H-ZSM-5 is proposed in Figure 3. Unfortunately, other competitive reactions, such as cracking on the acid sites and hydrogenolysis and hydrogenation of olefinic intermediates on the metallic centers can also take place during the aromatization process.

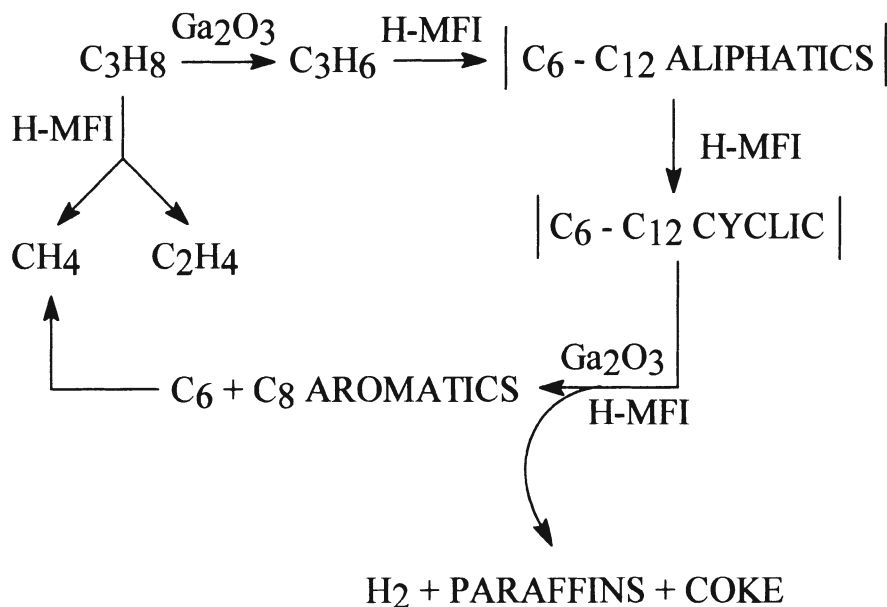


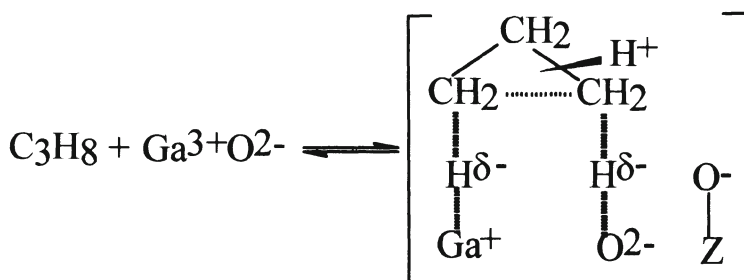
Figure 3. Reaction scheme for propane aromatization on Ga/ZSM-5 catalysts.

Although the reaction sequence is frequently rationalized on the basis of a classical bifunctional mechanism, with the participation of both acidic and metallic sites, the nature and location of the metal cations and their catalytic role during propane aromatization is still being questioned [13, 14]. It is recognized that both the metallic and acidic sites need to be in close proximity for achieving high aromatization selectivity. This is demonstrated in Table 3 by comparing the results obtained on a pure acidic H-ZSM-5 sample, a bifunctional Ga/ZSM-5 catalyst and a (Ga/ $\gamma$ - $\text{Al}_2\text{O}_3$ +MFI) disposed in a two beds configuration. Moreover, recent isotopic exchange experiments suggest that C-H bond activation occurs predominantly on Brönsted acid sites, and that the role of Ga (and Zn) sites at this stage is the removal of the H-atoms from the zeolite surface by recombinative desorption via the “reverse spillover” effect [19, 20].

*Table 3.* Influence of the proximity of the Ga and the acid sites for propane dehydrocyclization.

Catalyst	MFI	TWO BEDS	
		Ga/ $\gamma$ -Al <sub>2</sub> O <sub>3</sub> + MFI	Ga/MFI
Conversion, %	29	23	20
Selectivities, %			
C <sub>1</sub> - C <sub>3</sub>	52	51	25
C <sub>4</sub> - C <sub>6</sub>	8	15	3
BTX	39	33	65
C <sub>9+</sub>	1	1	7

The way of Ga incorporation (isomorphous substitution in the zeolite framework, ion exchange or wet impregnation) appears to have little effect on the final catalytic properties of Ga/H-ZSM-5 catalysts. Even similar results have been obtained when the catalyst is prepared by calcination of a physical mixture of Ga<sub>2</sub>O<sub>3</sub> and H-ZSM-5, especially if the mixture is previously molturated [21, 22]. This is not surprising taking into account that either in the Ga<sup>3+</sup>-exchanged sample and in the galloaluminosilicate highly dispersed extraframework Ga<sub>2</sub>O<sub>3</sub> species will be formed on the zeolite surface during calcination. These species are partially reduced during the pre-treatment of catalyst in H<sub>2</sub> or under the alkane stream at high temperatures, and appear to migrate into the zeolitic channels at cation exchange positions, probably via vapor-phase exchange of volatile Ga<sup>1+</sup> species with protonic sites [19]. Derouane et al. [23] proposed the following species as the active sites for the aromatization of propane on Ga/H-ZSM-5 catalysts:



As observed in Table 3 shown before, a large amount of benzene (about 45% of the aromatic fraction) is produced in the conversion of propane on Ga/H-ZSM-5 catalysts. Taking into account that the amount of benzene in the reformulated gasoline will be severely limited to less than 1%, maximization of C<sub>8</sub> alkylaromatics would be highly desired. For this purpose, the reaction conditions have to be optimized. The effect of reaction temperature on product



distribution is presented in Figure 4. It is seen that methane, ethane+ethylene, mainly formed by cracking and hydrogenolysis, and BTX yields increase with reaction temperature, whereas formation of  $C_7+C_8$  aliphatics,  $C_4-C_6$  and  $C_9+$  compounds is disfavored at high temperatures. However, looking at the distribution of the BTX fraction, it is seen that xylenes are the predominant compounds at low temperatures, showing a maximum at ca. 450°C, while the yield of benzene increases with temperature. Therefore, low reaction temperatures have to be used for maximization of xylenes, but under these conditions the dehydrogenation of propane is thermodynamically limited. In order to avoid this limitation, one may think in produce propene through oxidative dehydrogenation of propane. It has been shown that reacting a mixture of air and propane on a V/MgO catalyst mixed with Ga/ZSM-5 the reaction can be carried out at lower temperatures with higher yields of  $C_8$  alkylaromatics than the Ga/ZSM-5 catalyst alone [24]. However, the reaction was not enough selective and a significant amount of propane was lost as carbon oxides during the process.

After the introduction of the Cyclar process, other process have been developed for the aromatization of LPG: the M-2 forming by Mobil [25], which uses a pure acidic H-ZSM-5 catalyst and seems more appropriate for the production of high octane compounds from pyrolysis naphtha and paraffinic naphthas; and the Aroforming process developed by IFP and Salutec [26], which uses a shape-selective zeolite doped with metal oxides as catalyst, and gives a product distribution similar to that obtained in the Cyclar process.

### **2.2.2 Skeletal isomerisation of *n*-butane**

As stated before, reformulated gasoline has to accomplish, among other measures, a reduction in the Reid Vapor Pressure at levels below 8.1 psig. This will be fulfilled mainly by eliminating the volatile butanes from the gasoline pool, and consequently will produce an excess of *n*-butane availability in the refinery. One alternative to take profit of this product is its isomerisation into isobutane, which can be either used as co-feed in the alkylation units or be dehydrogenated into isobutene, a raw material used in the production of methyl-*tert*-butyl ether (MTBE).

The skeletal isomerisation of *n*-butane is a thermodynamically limited reaction, with higher concentrations of the isomer being obtained at lower temperatures. Moreover, as illustrated in Figure 5, the equilibrium concentration of isobutane is significantly lower than that of isopentane. Therefore, reaction temperatures as low as possible should be used in order to obtain high yields of isobutane.



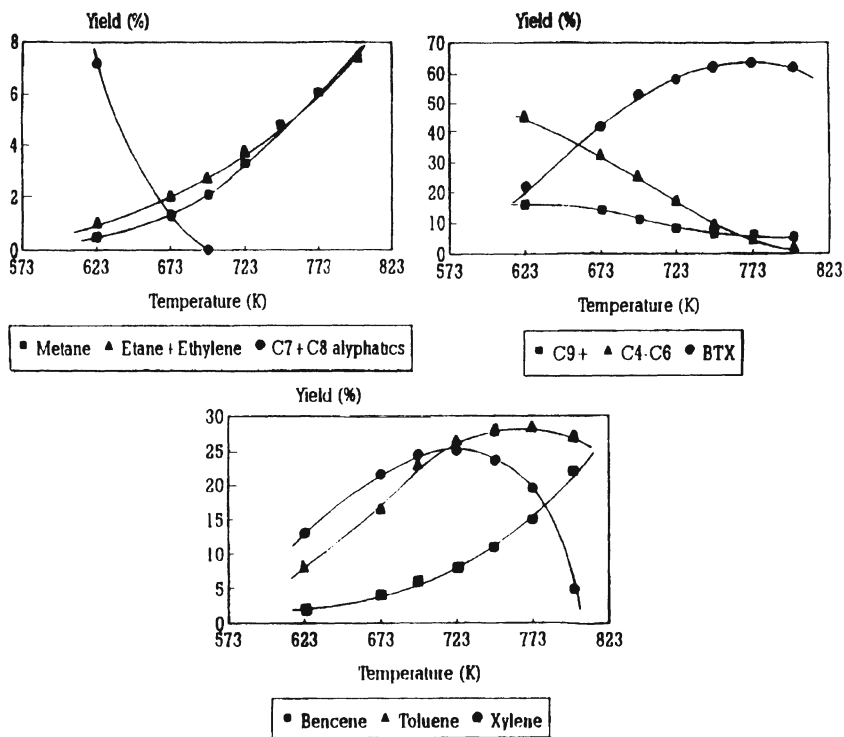


Figure 4. Influence of reaction temperature on product yields during the transformation of propene to aromatics ( $W/F = 32.6 \text{ g h mol}^{-1}$ ,  $P = 68.9 \text{ Kpa C}_3$ ).

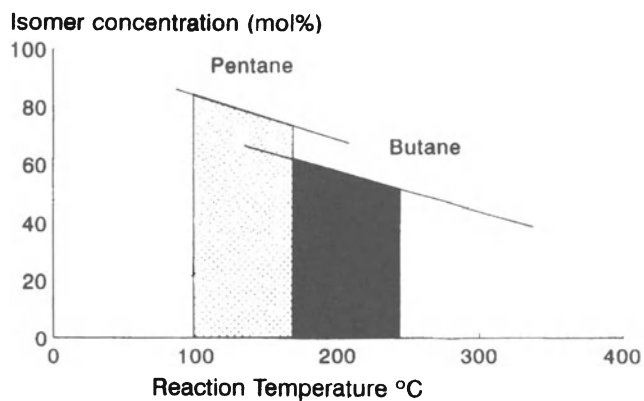
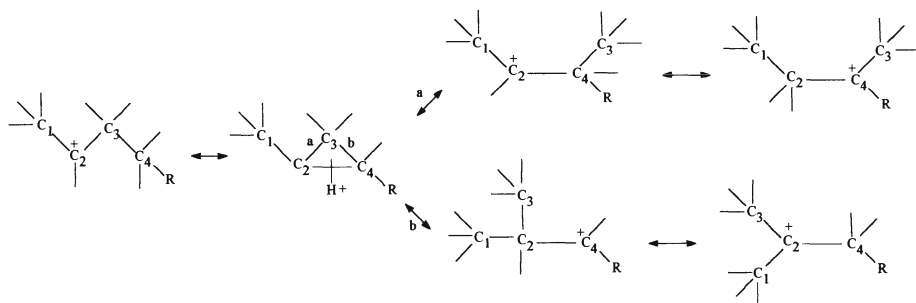
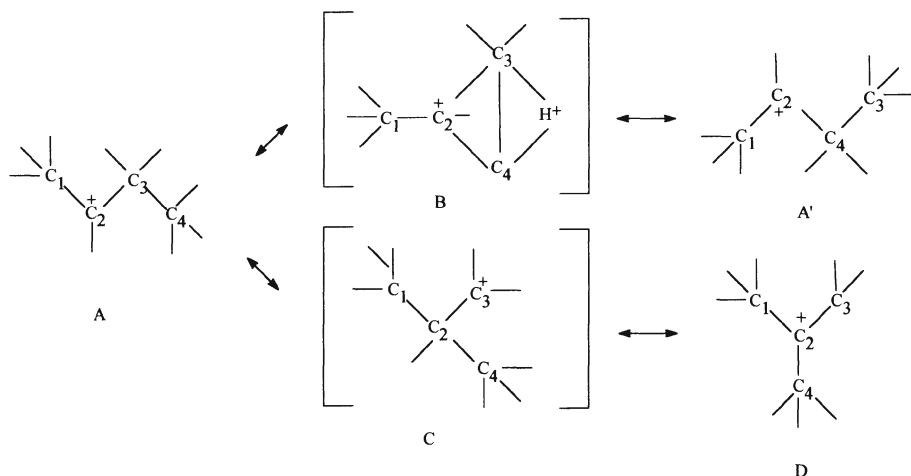


Figure 5. Equilibrium concentration of isomers for the isomerisation of  $n\text{-C}_4$  and  $n\text{-C}_5$  alkanes (comparison at same WHSV).

The mechanism of *n*-butane isomerisation is assumed to occur, by analogy with the reaction on liquid superacids, via the formation of carbenium ions. In the case of skeletal rearrangement of  $n\text{-C}_4^+$ , it is accepted that the reaction occurs via a protonated cyclopropane ring as intermediate, as proposed by Brouwer [27]. This is shown in the scheme below:



The opening of the cyclic intermediate at side **b** would lead to a primary carbenium ion, which after H-shift will form the *t*-butyl cation and branching rearrangement occurred. On the other hand, opening of the protonated cyclopropane at side **a** leads to a secondary *n*-butyl cation in which a terminal and a non-terminal carbon atoms have exchanged positions (C-scrambling reaction). However, recent theoretical calculations using *ab initio* methods [28] have shown that the protonated methyl-cyclopropane ring is not a common intermediate for these reactions, but it is a transition state for the C-scrambling reaction, while the isomerisation of *n*-butyl cation into *t*-butyl cation occurs through a primary carbenium ion. According to these calculations the authors proposed the following scheme for the transformation of  $n\text{-C}_4^+$  cations:



The activation energies obtained for these processes corresponded well with those obtained experimentally, about 8 and 20 Kcal/mol for the scrambling and direct isomerisation, respectively.

The process has been commercialized by several companies, such as UOP (Butamer process), ABB Lumus Crest, IFP and BP. In all cases the catalyst used is based on a noble metal, Pt, supported on a strongly acidic chlorinated alumina material. Such a strong acidity is required in order to stabilize the primary carbenium ion at relatively low reaction temperatures, and therefore under thermodynamically favorable conditions. These type of catalysts, however, suffer from serious drawbacks that makes their substitution by other solid acid catalysts highly desired. For instance, this catalyst shows a high sensitivity to small amounts of impurities that can be present in the feed, such as water, sulphur, oxygenates, and nitrogen, leading to an irreversible catalyst deactivation even in the presence of a few ppm of such compounds.

Zeolites are strong solid acids, and thus could be used in principle as catalysts for this reaction. When a large pore zeolite having strong Brönsted acid sites, such as mordenite, is used for the transformation of n-butane at 250°C, a high conversion is obtained at the beginning of the reaction (Table 4) but the catalyst rapidly deactivates with time on stream [29]. Moreover, the initial selectivity to isobutane was relatively low and C<sub>3</sub> and C<sub>5</sub> hydrocarbons were also formed in relatively large amounts. These results clearly suggested that isobutane is mainly formed through a dimerisation-cracking pathway involving the formation of branched C<sub>8</sub> carbenium ions as intermediates, which rapidly rearrange on the acid sites into more stable carbenium ions before they are cracked by  $\beta$ -scission into C<sub>3</sub>, C<sub>4</sub> and C<sub>5</sub> fragments, as shown in the Scheme 1.

Table 4. Isomerisation of n-butane on mordenite zeolite at 250°C and 1 atm.

Time on Stream (minutes)	5	20	25
Conversion (%)	60	22	15
Selectivities (%):			
Isobutane	49	65	74
C <sub>3</sub>	35	22	21
C <sub>5</sub>	16	13	5

Sulfated metal oxides, such as sulfated zirconia, were shown to be able to isomerize n-butane at temperatures below 100°C [30, 31]. Table 5 presents the results of n-butane isomerisation on a SO<sub>4</sub><sup>2-</sup>/ZrO<sub>2</sub> sample at 150 and 250°C

reaction temperature [29]. Two facts can be highlighted from this table: firstly, the initial selectivity to isobutane observed at short times on stream is relatively low and other reaction products ( $C_3$  and  $C_5$ ) are obtained besides isobutane, especially at higher reaction temperatures. Secondly, a significant decrease of isobutane yield is observed with time on stream. The first observation suggests that also in the case of sulfated metal oxides the isomerisation reaction can take place through a bimolecular mechanism involving the dimerisation of  $C_4$  and cracking of the  $C_8$  intermediates, as proposed in scheme 1. Experiments with  $^{13}C$  double-labeled n-butane on promoted and unpromoted sulfated zirconia catalysts further evidenced the importance of the bimolecular mechanism in the isomerisation of n-butane on sulfated metal oxides [32, 33].

Table 5. Isomerisation of n-butane on  $SO_4^{2-}/ZrO_2$  catalyst in  $N_2$  atmosphere.

Reaction Temperature (°C)	150			250		
Yield (%)	iC <sub>4</sub>	C <sub>3</sub>	C <sub>5</sub>	iC <sub>4</sub>	C <sub>3</sub>	C <sub>5</sub>
Time on Stream (min)						
5	24.7	7.5	1	36.5	8.6	4.2
20	17.9	0.7	0	23.9	2.2	1.2
35	15.5	0.6	0	19.6	1.4	0.8
50	14.4	0.5	0	16.8	1.1	0.7

Later on, it was reported that the activity and stability of sulfated zirconia could be enhanced by the incorporation of Fe and Mn [34] and even Pt [35, 36] to the catalyst. As an example, Table 6 shows the results of n-butane isomerisation obtained on a  $Pt/SO_4^{2-}/ZrO_2$  catalyst when the reaction is carried out in the presence of  $H_2$  as carrier gas. Much higher selectivities to isobutane and lower deactivation rates were observed for the Pt-promoted catalyst in comparison with an unpromoted SZ sample (Table 5). The beneficial effect of hydrogen on catalyst stability has been observed even for the Pt-free catalyst, provided the hydrogen pressure applied is high enough. This has been explained considering that  $H_2$  dissociates into  $H^+...H^-$  on the surface of unpromoted SZ, probably by interacting with the Lewis acid sites and thus creating new Brönsted acid sites available for the reaction [35]. However, it can also be considered that activated hydrogen can spill-over onto the catalyst surface and act as hydride transfer agent to facilitate the desorption of the adsorbed carbocation and regenerate the Brönsted acid site of the catalyst [37]. In this way, the positive effect of Pt in  $Pt/SO_4^{2-}/ZrO_2$  could be explained by facilitating the process of hydrogen activation on the catalytic surface, rather than acting as a dehydrogenating agent in the initiation step.

Table 6. Skeletal isomerisation of n-butane on a Pt/ SO<sub>4</sub><sup>2-</sup>/ZrO<sub>2</sub> catalyst in H<sub>2</sub> atmosphere.

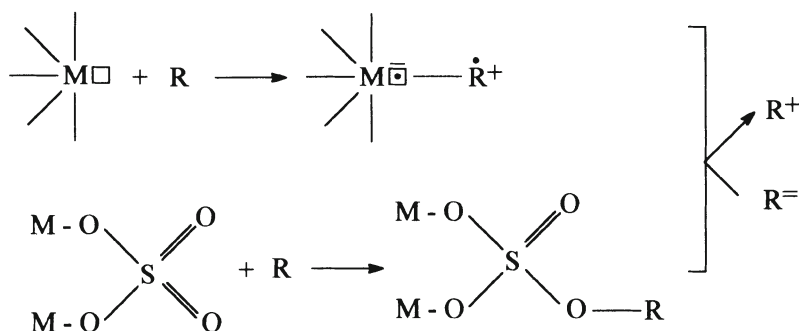
Sample	W/F (g.h.mol <sup>-1</sup> )	C <sub>4</sub> /H <sub>2</sub> (mol.mol <sup>-1</sup> )	Reaction Time (min)					
			5		35		65	
			X <sub>T</sub>	S <sub>i</sub>	X <sub>T</sub>	S <sub>i</sub>	X <sub>T</sub>	S <sub>i</sub>
Pt/SO <sub>4</sub> <sup>2-</sup> /ZrO <sub>2</sub>	36	5/1	33	88	25	91	24	92
	60	1/1	32	91	31	95	33	95
	1.3	1/3	33	100	37	100	37	100

Acid strengths of  $H_0 \leq -16$  as determined by Hammett indicators were reported for sulfated zirconia catalysts, and in that sense they have been usually considered as solid superacids. Nevertheless, there is no a general consensus on the origin of acidity and the nature of active sites in sulfated zirconia materials, and different opinions can be found in the literature, although it is generally accepted that both Brönsted and Lewis acid sites are needed to obtain catalytic

activity in n-butane isomerisation on SZ catalysts. Recently, the “superacidic” nature of these materials has been questioned on the bases of the following observations:

- i) Determination of acid strength by Hammett indicators in solids is meaningless [38].
- ii) Benzene is oxidized on sulfated zirconia at low temperatures [39].
- iii) Microcalorimetry and IR of  $\text{NH}_3$  adsorption indicated that only a small fraction of sites show initial heats of ammonia adsorption of 150-165 KJ/mol [40].
- iv) Proton NMR and acetonitrile adsorption show that Brönsted acid sites in sulfated zirconia are weaker than those present in ZSM-5 zeolite [41].
- v) The isomerisation of n-butane seems to occur by a bimolecular mechanism [32, 33].
- vi) The isomerisation reaction was seen to occur on Brönsted acid sites with heats of  $\text{NH}_3$  adsorption of 125-140 KJ/mol [40].
- vii) Sulfated zirconia catalysts promoted with Mn, Fe and Ni show enhanced activity for n-butane isomerisation with respect to unpromoted  $\text{SO}_4^{2-}/\text{ZrO}_2$ , but no significant changes in acid strength were observed [41, 42].

Besides these considerations, there are other evidences, such as the dominating role of Lewis acidity of SZ catalysts during n-butane isomerisation [43], and the fact that benzene forms radical cations [38], that strongly suggest that the high activity displayed by these materials is not related to “superacidity”, but to their ability to ionize molecules and to form radical cations on the surface. On these bases, the mechanism depicted in Scheme 2 can be proposed for the activation of saturated hydrocarbons on SZ catalysts.



*Scheme 2.* mechanism proposed for the activation of alkanes on SZ catalysts.

Both the physicochemical and catalytic properties of these materials are strongly dependent on the preparation conditions. A careful control and optimization of each preparation step is needed if maximum catalytic activity

wants to be obtained. Important parameters are for instance the pH of precipitation at which the zirconium hydroxide is obtained, the concentration of sulphate in the impregnation step, and the final calcination temperature at which the sulfated zirconium hydroxide is submitted [29]. All of these factors will influence the amount of tetragonal zirconia in the SZ catalyst, which seems to be an indispensable condition for obtaining catalytically active SZ samples.

Novel preparation methods for SZ, such as a sol-gel procedure [44, 45] and thermolysis of zirconium sulphate [46] have been recently reported. Moreover, very strong solid acids capable of activating short paraffins at relatively low temperatures have also been prepared by supporting  $\text{WO}_3$  or  $\text{MoO}_3$  on  $\text{ZrO}_2$  or sulfated zirconia [37].

### 2.2.3 Isobutane/butene alkylation

The gasoline produced from the alkylation of isobutane with light olefins (alkylate), usually butenes, has excellent antiknock properties (with typical values of 90-94 for both research, RON, and motor octane numbers, MON) and is mainly composed by unreactive branched paraffins with very low sulphur, aromatic and olefin contents. All this makes alkylation gasoline an ideal component of lead-free reformulated gasoline.

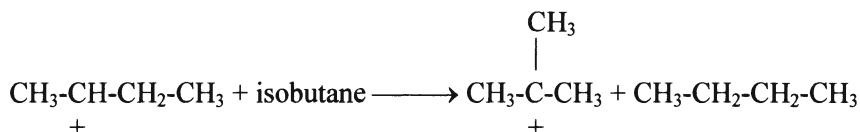
The reaction is accepted to occur through a carbenium ion mechanism, which in the case of isobutane/butene alkylation involves the following steps:

1) Protonation of the olefin:

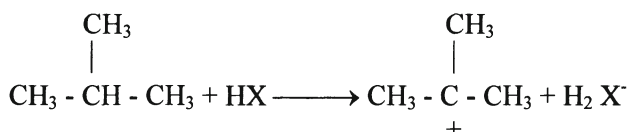


2) Formation of t-butyl cations:

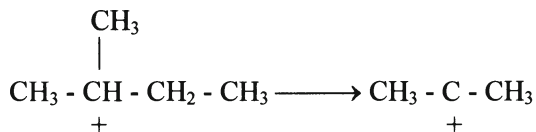
a) By hydride transfer from isobutane to *sec*-butyl cations:



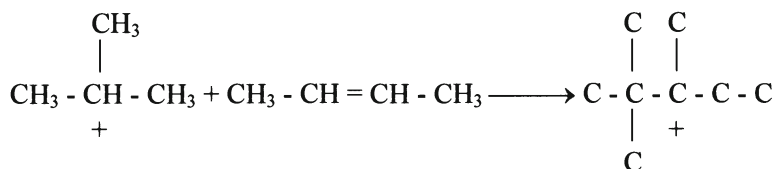
b) Hydride abstraction by the catalyst:



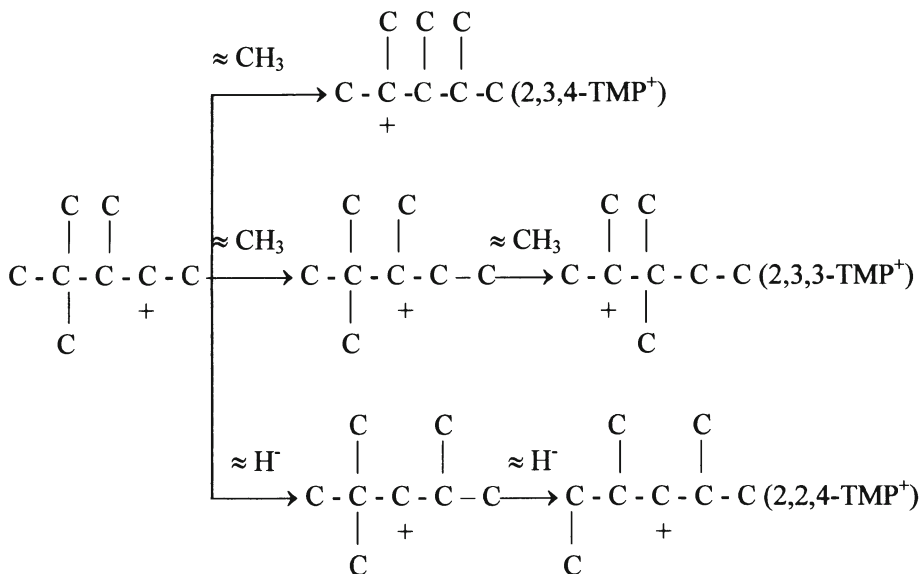
c) Branching isomerisation of the sec-butyl cation:



3) Alkylation step to give branched C8 carbenium ions, depending on the butene molecule used. In the case of 2-butene it will give 2,2,3-TMP<sup>+</sup> as primary product:

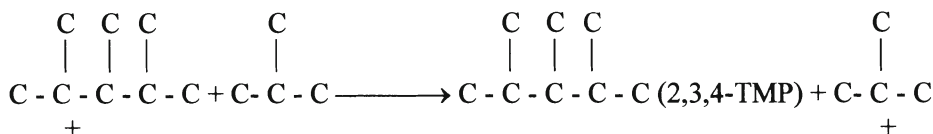


4) Isomerisation of C8 carbenium ions:





- 5) Desorption of the C8 isoparaffins by hydride transfer from an isobutane molecule to the C8 carbenium ions:



Besides the above reactions, other undesired reactions also take place, which in general tend to degrade the product and to decrease the quality of the alkylate. Among these are olefin oligomerisation and polymerization, cracking by  $\beta$ -scission of the oligomers to form light products (mainly C<sub>5</sub> - C<sub>7</sub> isoparaffins), and disproportionation of trimethylpentanes into C<sub>7</sub> and C<sub>9</sub> fragments. A simplified reaction scheme for the alkylation of isobutane with butenes and the main accompanying reactions is presented in Figure 6.

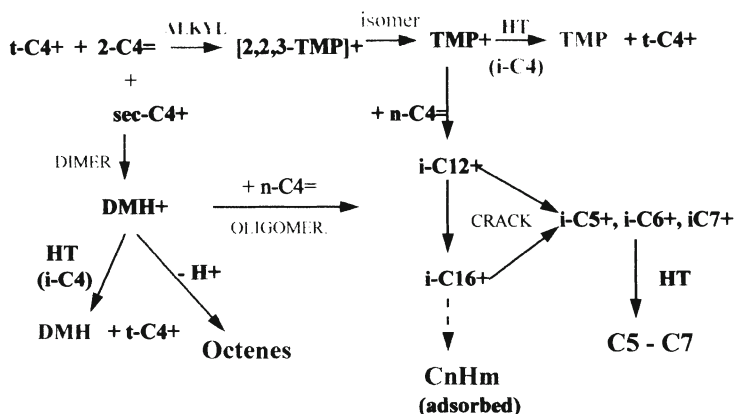


Figure 6. Reaction scheme for alkylation and accompanying reactions.

Unfortunately, the commercial process is carried out using harmful and environmentally dangerous liquid acids, HF and H<sub>2</sub>SO<sub>4</sub>, which are restraining the expected increase in alkylation capacity [47]. Particularly questioned is the construction of new alkylation plants based on HF, because of the high potential risk of acid release and the rapid formation of aerosol clouds extending over vast areas around the plant. In the last years, the risk of formation of aerosol from HF leaks has been reduced by using additives to HF, in combination with water spray mitigation. Nevertheless, the replacement of such liquid acids by safer and more environmentally acceptable solid acids is of much interest if a

higher contribution of isoparaffin alkylation to the reformulated gasoline pool is desired.

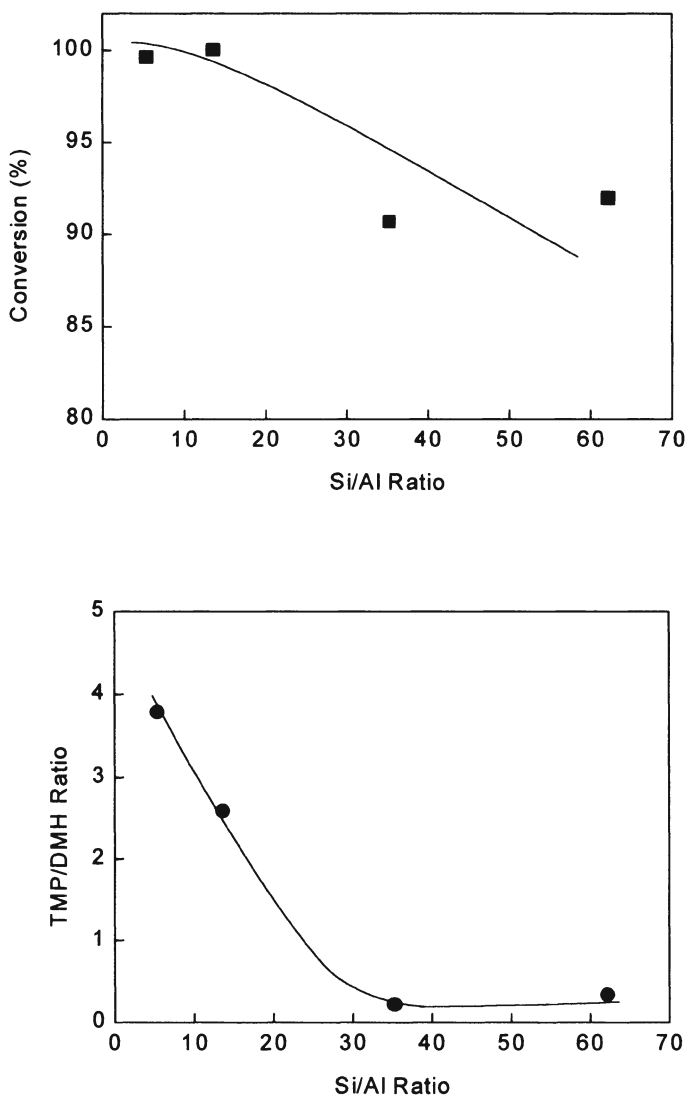


Figure 7. Initial 2-butene conversion and TMP/DMH ratio as a function of the framework Si/Al ratio of USY zeolites.

Acid zeolites, and particularly Y zeolite in the protonic form or exchanged with di- or trivalent cations, were firstly investigated as potential alkylation catalysts [48, 49]. The product distribution obtained with these catalysts presented some similarities with that obtained for liquid acids, suggesting that the general reaction mechanism presented above also operates in the case of solid acids. However, and owing to the particular adsorption properties of zeolites, dimerisation of the n-butenes was always an important competing reaction leading to the formation of dimethylhexanes (DMH) of lower octane number than the desired TMPs. The acidic and adsorption properties of zeolites can be modulated by varying the chemical composition, that is the framework Si/Al ratio. When a series of USY zeolites with different framework compositions were studied [50], a maximum in activity was observed for framework Si/Al ratios of about 6, but the TMP/DMH ratio in the products, which can be taken as a measure of the extent of alkylation versus dimerisation reactions, continuously increased when decreasing the framework Si/Al ratio, or what is equivalent, when increasing acid site density (Figure 7). This indicates that isobutane alkylation does not require strong acid sites to proceed on zeolites, but what is more important is to achieve a high concentration of acid sites in the pores that will favor a high hydrogen transfer capacity needed to desorb the primary  $\text{TMP}^+$  cations. Moreover, it has also been shown that extraframework Al species (EFAL) produced during steam dealumination of USY catalysts may also influence the activity, selectivity and stability of the zeolite [51].

Zeolites are active and selective alkylation catalysts during the initial stages of the reaction, but unfortunately their activity rapidly declines with time on stream (TOS) at the same time that the product distribution is shifted towards the formation of dimethylhexenes, indicating a change in the reaction pathway from isobutane alkylation to butene dimerisation. As an example, the evolution of the alkylate composition with TOS observed for a USY catalyst during isobutane/2-butene alkylation is shown in Figure 8.

Besides zeolite Y, the large pore high-silica zeolite Beta has also been studied for isobutane alkylation [52]. Samples synthesized with lower Si/Al ratios and having larger crystallites were observed to be more active and more stable towards deactivation (Figure 9), because they dealuminated to a lower extent and retained a higher concentration of Brönsted acid sites (and hence a higher hydrogen transfer capacity) after calcination. When compared to zeolite Y, zeolite Beta produces a lower concentration of TMPs in the  $\text{C}_8$  fraction, indicating that some limitations to the diffusion of the highly branched molecules could exist in the narrower pores of Beta.

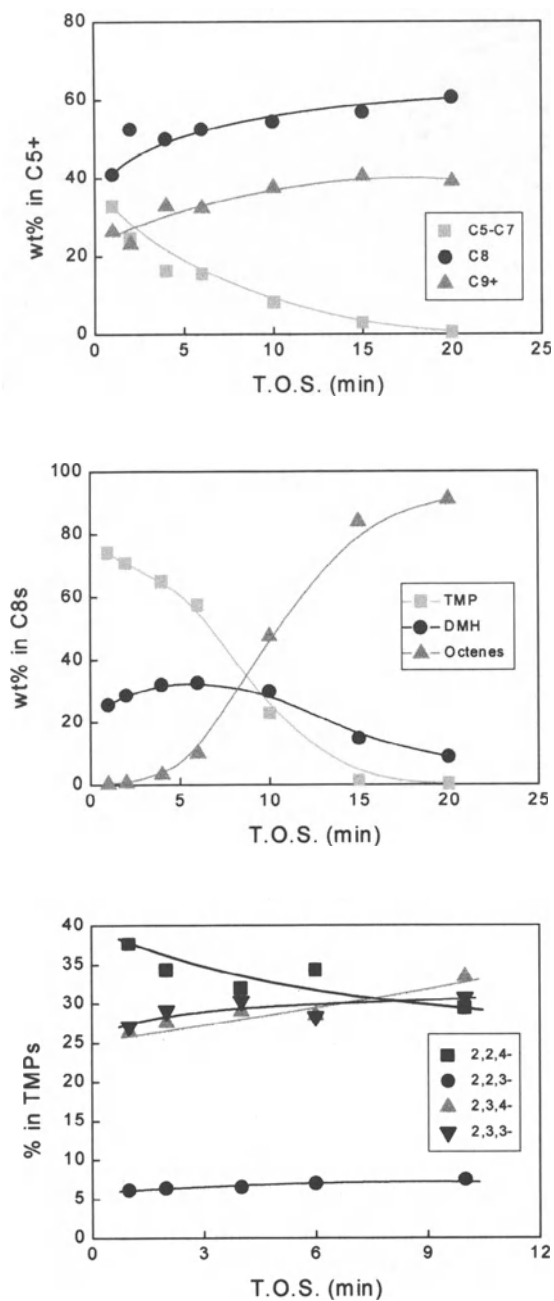


Figure 8. Change of the product distribution with time on stream (TOS) during isobutane/2-butene alkylation on a USY (Si/Al = 13.6) catalyst.

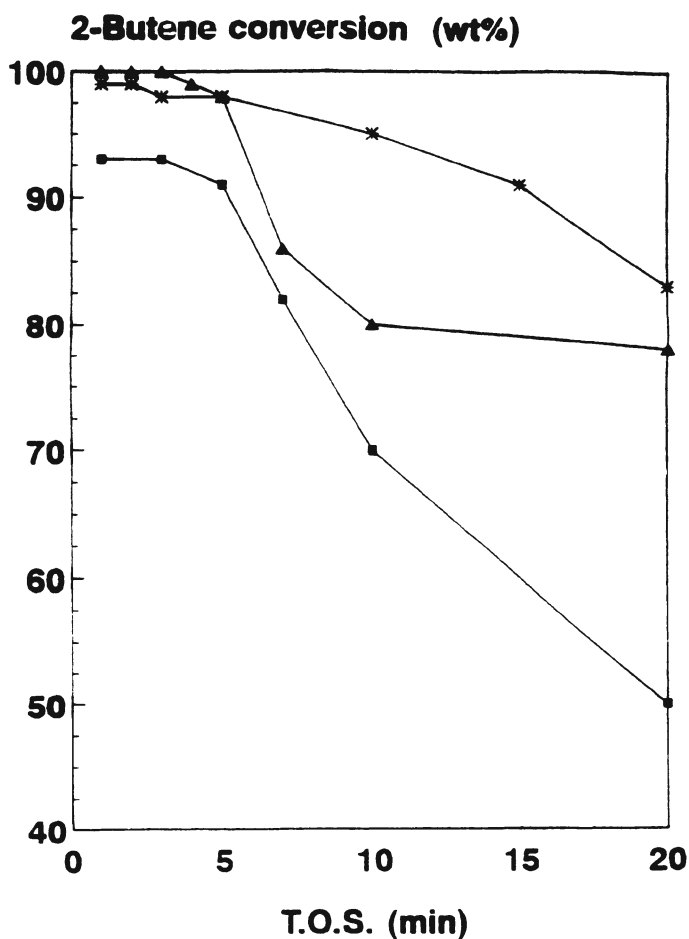


Figure 9. Deactivation trend of Beta zeolites with different Si/Al ratios and crystal sizes during isobutane/2-butene alkylation: (\*) Si/Al=14,  $\phi=0.35 \mu\text{m}$ ; (■) Si/Al=13,  $\phi=0.10 \mu\text{m}$ ; (▲) Si/Al=28,  $\phi=0.10 \mu\text{m}$ .

Recently, it has been reported [53, 54] that the combination of a Lewis acid, such as  $\text{BF}_3$ , with a large pore zeolite enhances the alkylation performance of the zeolite, especially if small amounts of water are added during the reaction [55]. The results presented in Table 7 show that better octane numbers are obtained with a  $\text{BF}_3$ /zeolite catalyst in comparison to HF in the case of alkylation of isobutane with 2-butene and isobutene [55].

Table 7. Alkylation of isobutane with different butene isomers on zeolite/BF<sub>3</sub> and HF catalysts.

	CATALYST					
	Zeolite/BF <sub>3</sub>			HF		
	1-C <sub>4</sub> =	2-C <sub>4</sub> =	i-C <sub>4</sub> =	1-C <sub>4</sub> =	2-C <sub>4</sub> =	i-C <sub>4</sub> =
Temperature (°C)	0	0	0	21	21	21
External i-C <sub>4</sub> /olefin ratio	10	10	10	12	12	12
Yields (g C <sub>5+</sub> /g olefin)	2.0			2.0		
Product Distribution (%):						
DMH	83.0	9.5	8.3	22.1	6.9	3.4
TMP	4.1	70.5	71.2	68.2	85.6	86.1
C <sub>9+</sub>	11.4	9.3	10.8	5.7	4.1	5.3
RON + O	72.0	99.7	99.6	94.0	99.0	98.0
MON + O	77.0	96.4	96.0	92.0	96.0	96.0

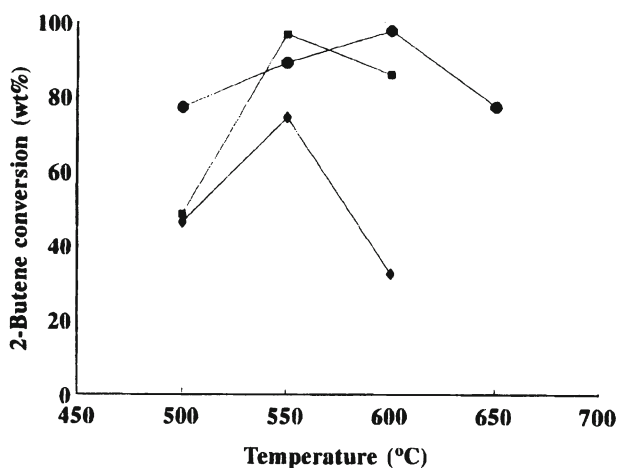


Figure 10. Initial 2-butene conversion as a function of calcination temperature of SO<sub>4</sub><sup>2-</sup>/ZrO<sub>2</sub> samples prepared from 1N H<sub>2</sub>SO<sub>4</sub> (●), 6 wt% (NH<sub>4</sub>)<sub>2</sub>SO<sub>4</sub> (◆), and 9 wt% (NH<sub>4</sub>)<sub>2</sub>SO<sub>4</sub> (■). Reaction conditions: 32°C, 2.5 MPa, I/O= 15, and olefin WHSV= 2 h<sup>-1</sup>.

As stated above, one of the main characteristics of alkylation on zeolites is the relatively high formation of less desired DMH, resulting from a selective adsorption of olefins in the zeolitic pores and their dimerisation on weak Brönsted acid sites. This has been tried to overcome by using other solid acids having a higher acid strength, such as sulphate-promoted metal oxides [56]. It has been shown that  $\text{SO}_4^{2-}/\text{ZrO}_2$  catalysts are very active and more selective to TMPs than zeolites at the beginning of the reaction, but lower reaction temperatures had to be used in order to avoid extensive cracking reactions on the very strong acid sites of these materials [57]. For these catalysts the preparation conditions, and particularly the temperature at which the sulfated hydroxide is calcined, need to be finely tuned if high activity and selectivity wants to be obtained [58]. This is shown in Figure 10, where the initial 2-butene conversion has been plotted against calcination temperature for three different sulfated zirconia catalysts prepared from different sulphate sources and sulphate concentrations [58]. Nevertheless, the activity of the catalysts rapidly declined after a few minutes on stream irrespective of the preparation and calcination conditions, as observed in Figure 11 [58]. We also tried to modify the acidic and catalytic properties of sulfated metal oxides by changing the nature of the metal cation [58]. The order of activity found corresponded well with the expected order of acid strength:  $\text{ZrO}_2 > \text{TiO}_2 \approx \text{SnO}_2 > \text{Fe}_2\text{O}_3 > \text{Al}_2\text{O}_3$ , but no significant differences in deactivation rate could be observed.

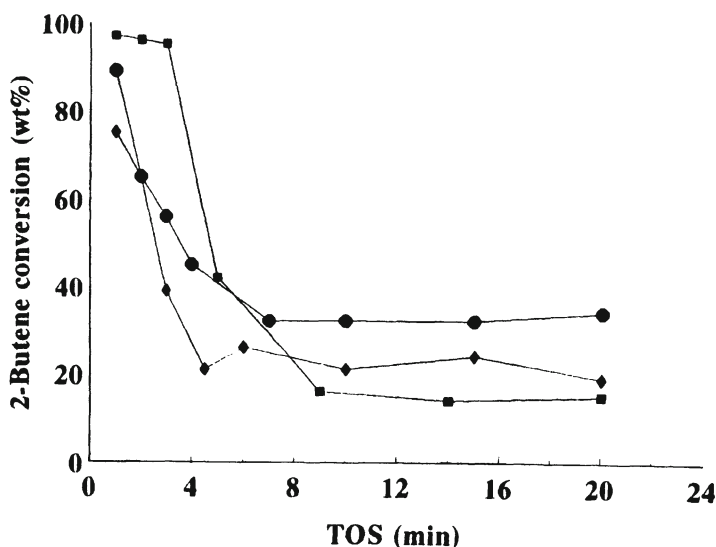
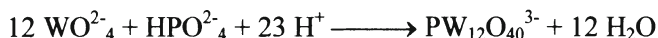
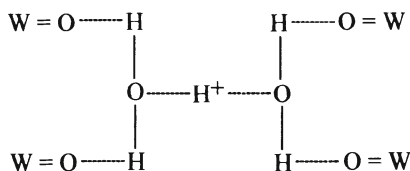


Figure 11. Decrease of 2-butene conversion with time on stream (TOS) for  $\text{SO}_4^{2-}/\text{ZrO}_2$  catalysts prepared from 1N  $\text{H}_2\text{SO}_4$  (●), 6 wt%  $(\text{NH}_4)_2\text{SO}_4$  (◆), and 9 wt%  $(\text{NH}_4)_2\text{SO}_4$  (■) and calcined at 550°C.

Recently, an interesting class of materials generically known as heteropoly compounds have also been investigated as solid alkylation catalysts [59, 60]. These are formed by the condensation of two or more oxoanions, as for instance:



In the solid state, protons are involved in the formation of the crystal structure of the heteropoly acid. For instance, in the case of the 12-tungstophosphoric acid (HPW) shown above, the terminal W=O sites are the preferred protonation sites, leading to the formation of  $\text{H}_5\text{O}_2^+$  species which are linking four neighboring heteropoly anions through hydrogen bonds, as represented below [61]:



In solid state, heteropoly acids behave as strong Brönsted acids, and in the case of HPW acid strengths higher than that of 100% sulphuric acid have been measured by Hammett indicators [62]. Unfortunately, solid heteropoly acids have very low surface areas (below 5 m<sup>2</sup>/g) which make them unfruitful as catalysts for acid-catalyzed heterogeneous reactions involving non-polar molecules, such as isobutane/butene alkylation. Hopefully, the surface area can be increased by partial exchange of the protons by larger monovalent cations, such as Cs<sup>+</sup>, K<sup>+</sup>, Rb<sup>+</sup>, and even NH<sub>4</sub><sup>+</sup> [63]. As observed in Table 8 [60], the final textural properties of the heteropoly salts depended on the nature of the exchanged cation but mainly on the degree of cation exchange (x). Larger surfaces areas are observed for values of x ≥ 2. Besides that, a significant microporosity developed for the high surface area compositions. When these catalysts were tested for isobutane/2-butene alkylation (Figure 12), a maximum in the activity was observed for degrees of proton substitution of x=2-2.5, depending on the nature of the cation [63]. As observed in Figure 12, the activity of the high surface area heteropoly salts was much higher than that of the parent HPW (x=0) under the same reaction conditions. This maximum in activity corresponded well with the expected maximum in surface acidity, which can be calculated in a first approximation as the product of the number of residual protons (3-x) by the surface area (Table 8). Moreover, results in Table 9



show that the most active compositions give a relatively high proportion of TMP in the  $C_8$  fraction, and that the product distribution depended on the nature of the exchanged cation [63], suggesting differences in acid strength of surface protons between the different salts. Nevertheless, the catalysts also suffered rapid deactivation with time, and as in the case of zeolites and sulfated metal oxides, dimerisation products (mainly dimethylhexenes) were predominant in the low activity period.

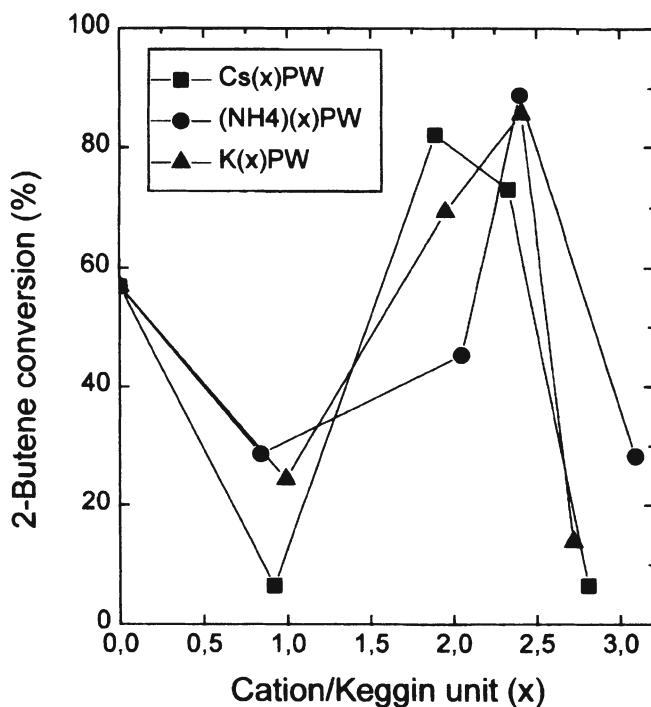


*Figure 12.* Initial 2-butene conversion as a function of cation content ( $x$ ) for the  $Cs^+$ ,  $K^+$ , and  $NH_4^+$  salts of 12-tungstophosphoric acid (HPW). Reaction conditions:  $80^\circ C$ , 2.5 MPa, I/O= 15 and olefin WHSV=  $1\ h^{-1}$ .

**Table 8.** Textural properties of Cs<sup>+</sup>, K<sup>+</sup>, and NH<sup>+</sup> salts of 12-tungstophosphoric acid (HPW) as a function of degree of cation exchange. Samples calcined at 300°C for 2 h before N<sub>2</sub> adsorption measurements.

Sample	S <sub>BET</sub> (m <sup>2</sup> /g)	V <sub>MICRO</sub> (cm <sup>3</sup> /g)	S <sub>MICRO</sub> (m <sup>2</sup> /g)	% S <sub>MICROPORE</sub>
Cs1	1	--	--	--
Cs2	62	0.0145	29	47
Cs2.5	79	0.0097	21	27
Cs3	46	0.0045	10	22
N1	5	0.0008	2	40
N1.5	13	0.0028	6	46
N2	29	0.0107	21	72
N2.5	56	0.0155	31	55
N3	56	0.0208	40	71
K1	9	0.0017	3	33
K2	28	0.0104	21	75
K2.5	51	0.0168	33	65
K3	44	0.0150	30	68

**Table 9.** Initial product distribution obtained during the alkylation of isobutane with 2-butene of heteropoly salts. Reaction conditions as in Figure 12.

Sample	HPW	Cs2PW	N2.5PW	K2.5PW
2-Butene conversion (%)	56.9	82.1	88.9	85.7
Product distribution (%):				
C <sub>5</sub> - C <sub>7</sub>	36.5	43.8	72.0	30.5
TMP	35.4	29.9	18.5	41.1
DMH	7.8	10.8	5.4	12.1
Octenes	13.2	2.9	1.0	2.3
C <sub>9+</sub>	7.1	12.6	3.1	14.0
TMP/DMH ratio	4.5	2.8	3.4	3.4

Another approach used to increase the number of surface protons in solid heteropoly acids has been to support them on high surface area carriers, silica

being the most often used [64]. In this case, critical points to control the acidic properties of the final catalysts are the extent of interaction of the heteropoly acid with the surface of support and the degree of acid dispersion, which depend on the nature of the support and the amount of supported acid [65]. As observed in Figure 13, a maximum of conversion during isobutane/2-butene alkylation is observed at acid loadings of about 40wt% for HPW/silica catalysts [66]. This maximum in activity occurs because at low acid loadings the HPW-support interaction becomes stronger making protons in the heteropoly acid to weaken even though the dispersion is high, and at high loadings large crystallites of HPW are formed on the silica surface, thus decreasing the number of accessible protons. When the composition of the alkylate product obtained on the HPW/silica catalysts is analyzed, a maximum in the concentration of the desired alkylation products, TMPs, is also observed at acid contents of ca. 40wt%. Besides silica, a high surface area mesoporous silica-alumina (MSA) and a silica MCM-41 materials were also used as supports for heteropolyacids [66]; however, they performed less efficiently than the HPW/silica catalysts for the isobutane alkylation reaction, despite higher acid dispersions were achieved

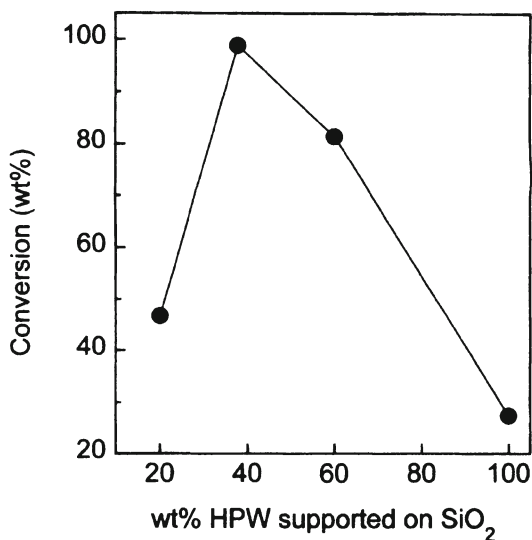


*Figure 13.* Initial activity for isobutane/2-butene alkylation of HPW/SiO<sub>2</sub> catalysts as a function of acid loading. Reaction conditions: 33°C, 2.5 MPa, I/O= 15 and olefin WHSV= 2 h<sup>-1</sup>.

with the former materials owing to their very high surface area. This is explained, in the case of the aluminosilicate MSA, by the presence of Brønsted acid sites in the support associated with tetrahedral Al which increases the interaction with the HPW molecules, and in the case of MCM-41 to partial blocking of the unidirectional mesoporous channels by small aggregates of HPW crystals. When compared to the high surface area heteropoly salts under the same reaction conditions, the HPW/silica catalyst with 40 wt% loading was much more active and deactivated at a lower rate, but still this catalyst deactivated faster than zeolites. Moreover, little has been addressed about the deactivation-regeneration of these materials, which can not be carried out by conventional calcination at high temperature in an oxidizing atmosphere because of decomposition of the heteropoly acid into the respective oxides readily occurs at temperatures above 300-350°C.

## 2.3 TRANSFORMATION OF LONG-CHAIN NORMAL PARAFFINS

### 2.3.1 Isomerisation of Light Straight Run (LSR) gasoline

In order to meet octane specifications in the lead-free reformulated gasoline the

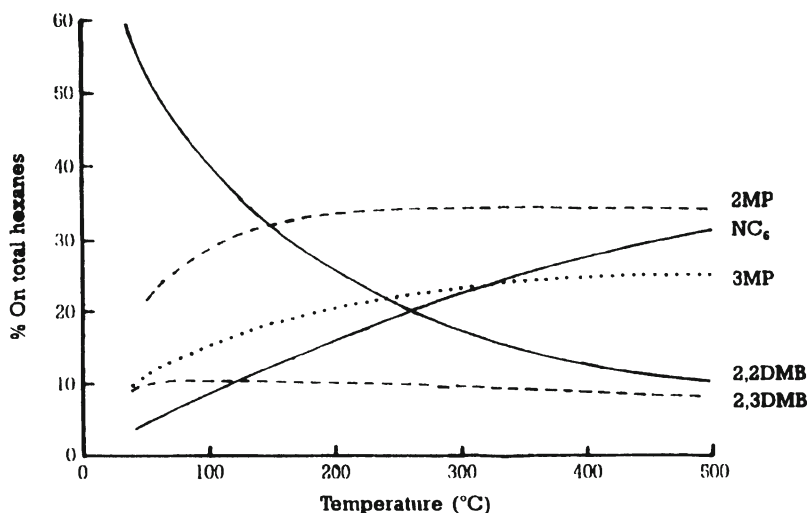


Figure 14. Thermodynamic equilibria for hexane hydroisomerization.

low octane LSR stream, which is mainly composed by n-pentane and n-hexane with an average octane number of 55-75, needs to be processed to increase its

octane rating before it could be added to the gasoline pool [67]. One attractive option is to isomerize the n-paraffins because of the much higher octane of the corresponding branched alkanes, as observed in Table 10. In the case of C<sub>6</sub>, a maximum concentration of the di-branched isomers should be achieved in order to maximize octane during LSR isomerisation. The isomerisation reaction is limited by thermodynamics, with low reaction temperatures favoring the formation of high octane isomerized products (Figure 14). By using chlorinated or fluorinated alumina containing a noble metal such as platinum LSR isomerisation can take place at temperatures as low as 150°C [68, 69]. However, these catalysts suffer from three main drawbacks: they are irreversibly deactivated by water, have low sulphur resistance, and need the continuous supply of fluorine or chlorine along with the feed, with the associated corrosion and contamination problems.

*Table 10.* Octane numbers of the C<sub>5</sub> - C<sub>7</sub> paraffins.

Hydrocarbon	RON	MON
i-pentane	92	90
n-pentane	62	62
2,2-dimethyl butane	92	93
2,3-dimethyl butane	101	94
2-methyl pentane	73	74
3-methyl pentane	75	74
n-hexane	25	26
2,2-dimethyl pentane	93	93
2,4-dimethyl pentane	83	82
2-methyl hexane	42	45
3-methyl hexane	52	56
n-heptane	0	0

Large pore zeolites containing a hydrogenating-dehydrogenating component, usually Pt, have been proposed as alternative catalysts, although due to their lower acidity higher reaction temperatures, in the order of 250°C, have to be used with the zeolite based catalysts. Table 11 shows the main characteristics of the LSR isomerisation processes using zeolite and chlorinated alumina based catalysts. Since the reaction requires the presence of strong Brönsted acid sites

to proceed at low temperatures, it is not surprising that mordenite, one of the most acidic zeolites, showed a good performance for LSR isomerisation.

*Table 11.* Characteristics of LSR isomerisation on zeolite and chlorinated alumina based catalysts.

	ZEOLITE	CHLORINATED ALUMINA
HCl Promotor	NO	YES
Reactor Temperature (°C)	250	150
RON-O		
Feed	70	70
Product	80	82
C5+ Yield	97	99
Cat Poisons		
Sulphur	NO	YES
H <sub>2</sub> O	NO	YES

In order to achieve high isomerisation activity and low coke tendency the acidity of the zeolite needs to be optimized. One important parameter for this is the framework Si/Al ratio. By increasing the framework Si/Al ratio the number of acid sites decreases but the acid strength of the remaining sites increases, up to a critical value for which all the framework Al atoms are isolated is achieved. According to theoretical calculations this is expected to occur at a Si/Al ratio of 9 in the case of mordenite [70]. However, results in Figure 15 show that when mordenite is dealuminated by different treatments, i.e. steam, acid, or acid+steam, the maximum activity for n-pentane isomerisation occurs at different Si/Al ratios depending on the particular dealumination procedure used [71]. The most effective procedure was the acid treatment followed by mild steaming leaving a small amount of extraframework Al (EFAL) on the zeolite. This clearly indicates that other parameters, besides the framework Si/Al ratio, influences the isomerisation activity of the zeolite. In fact, it has been shown in several zeolites that the presence of certain type of EFAL can have a synergetic effect on the Brönsted acid sites of the zeolite producing an increase of the acid strength [72, 73], and that this type of interaction can lead to an increase of the catalytic activity for hydrocarbon transformations. Thus, it should be possible to produce active isomerisation catalysts at higher Si/Al ratios, and hence with a lower coke tendency, by optimizing the amount and nature of the EFAL species left on the zeolite during dealumination. In the case of Pt/mordenite, an

optimum FAL/EFAL ratio of ca. 3 was found for the isomerisation of n-pentane at 250°C and 30 bar [71], as shown in Figure 16. A new LSR isomerisation process based on this modified mordenite catalyst, ISOPAR, has been commercialized by UOP. The catalyst has been shown to be particularly resistant to poisoning by sulphur and nitrogen containing compounds, and still worked efficiently in the presence of up to 4% benzene in the LSR stream.

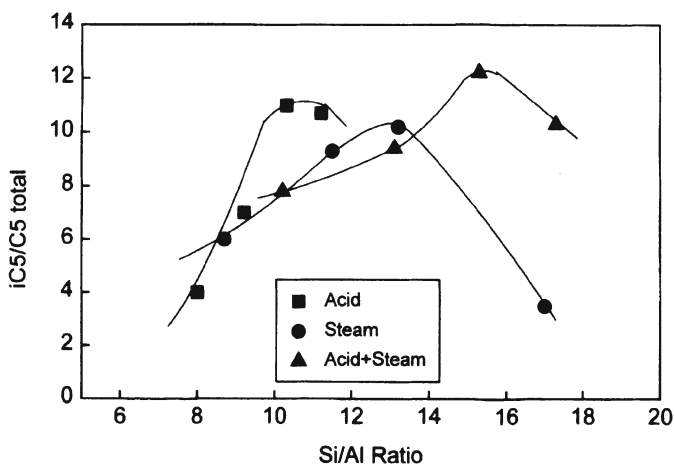


Figure 15. Influence of Si/Al ratio on the isomerisation activity of mordenite dealuminated by different procedures.

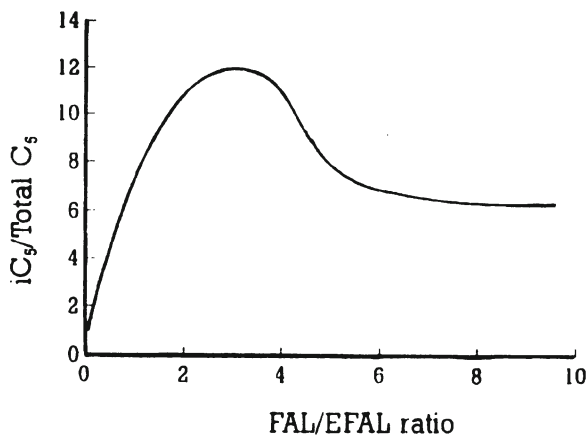


Figure 16. Influence of FAL/EFAL ratio on the activity for isomerisation of n-pentane on Pt/mordenite.

Zeolites other than mordenite have also been used for LSR isomerisation. Among them, beta and omega seems to give the most promising results. In the case of Pt/omega [74] the authors claimed a lower yield of gases than a Pt/mordenite at similar isomerisation conversions. On the other hand, the activity and isomerisation selectivity of Pt/Beta catalysts were seen to depend on the synthesis Si/Al ratio, and better results were reported for a sample with Si/Al ratio of 6.7 and 0.3 wt% Pt content [75]. This catalyst produced a higher amount of isomerized products and a higher proportion of the high octane dimethylhexanes than a reference Pt/mordenite catalyst, although no indication of the preparation procedure used for the latter sample was given.

Taking advantage of their higher acidity, bifunctional  $\text{Pt}/\text{SO}_4^{2-}\text{-ZrO}_2$  catalysts have also been applied for  $\text{C}_5/\text{C}_6$  isomerisation at low reaction temperatures. Selectivities of ca. 75% to *i*- $\text{C}_5$  in total  $\text{C}_5$  and of ca. 25% of 2,2-DMB in total  $\text{C}_6$  were reported for a  $\text{Pt}/\text{SO}_4^{2-}\text{-ZrO}_2$  catalyst during the isomerisation of a desulphurized light naphtha at 200°C and 30 bar, without appreciable decrease in the composition for nearly 1,000 hours on stream [76].

### 2.3.2 Naphtha isomerisation

Because of the limitation in the aromatics content, and particularly benzene, in reformulated gasolines, it could be of high interest to extend the isomerisation to larger *n*-paraffins present in the reformat feed and that are the precursors of BTX during naphtha reforming. However, this seems difficult to be achieved concurrently with  $\text{C}_5/\text{C}_6$  isomerisation, as the reactivity of the *n*-paraffin increases with chain length and thus isomerisation takes place at lower temperatures. Thus, at the typical temperatures used for LSR isomerisation the  $\text{C}_{7+}$  paraffins are rapidly cracked producing high yields of gases. The effect of the concentration of  $\text{C}_{7+}$  during the isomerisation of  $\text{C}_5/\text{C}_6$  on Pt/mordenite can be seen in Figure 17. Moreover, it has to be taken into account that in the case of  $\text{C}_7$  and larger *n*-paraffins only the multibranched isomers are interesting from the octane point of view, and that the cracking rate increases with the degree of branching of the hydrocarbon chain. Then, it is clear that isomerisation of *n*- $\text{C}_7$  and *n*- $\text{C}_8$  paraffins will require different reaction conditions and probably also different catalysts than those used for LSR isomerisation. In this case, zeolites with milder acidity and larger pores seems to be more adequate in order to avoid extensive cracking and allow the formation and diffusion of multibranched isomers. Table 12 shows the results obtained for *n*-octane isomerisation on different Pt/catalysts at a total conversion of 30% [77]. Higher isomerisation selectivities were observed for the HY and SAPO-11 as well as for the amorphous silica-alumina based catalysts, although the latter two were significantly less active. However, in all cases the concentration of the desired dimethylhexanes was relatively low, especially in the case of the medium pore



ZSM-5 and SAPO-11 catalysts. Better results have been obtained with a Pt/Beta catalyst [78]. Figure 18 shows the distribution of C<sub>8</sub> isomers formed during n-octane isomerisation on Pt/Beta as a function of conversion. A total isomerisation selectivity of 97% with a 21% selectivity to dimethylhexanes was obtained at 80% total conversion, but still the amount of multibranched isomers formed was not high enough to achieve a significant octane enhancement.

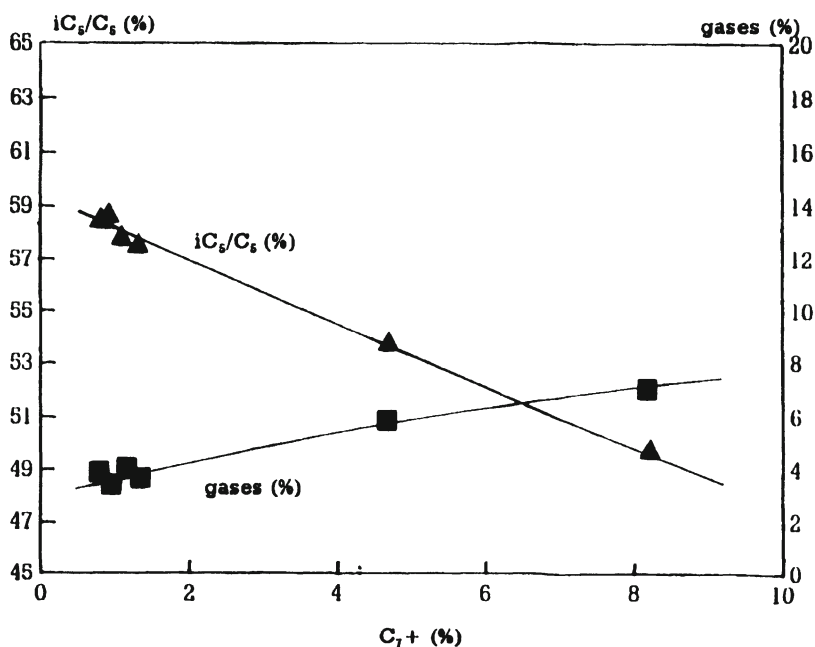


Figure 17. Isomerisation of LSR in the presence of C<sub>7+</sub> on a Pt/mordenite catalyst. Reaction conditions: 250°C, 30 bar, LHSV = 1 h<sup>-1</sup>, and H<sub>2</sub>/HC = 1.

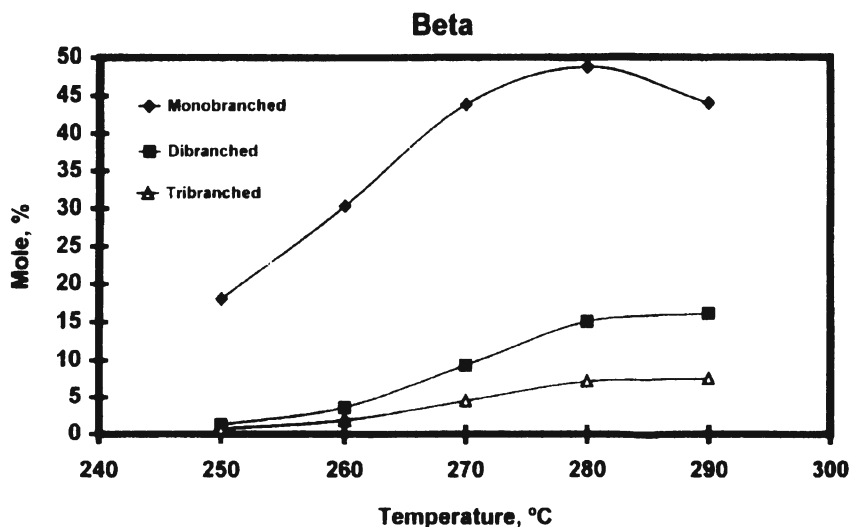


Figure 18. Distribution of isomers formed during the isomerisation of n-octane on Pt/Beta as a function of reaction temperature. Reaction conditions: 20 bar, 5.65 WHSV, 10 H<sub>2</sub>/n-C<sub>8</sub> ratio.

Table 12. Isomerisation of n-octane over Pt-catalysts at 1000 psig, 2.8 WSHV, 16 H<sub>2</sub>/HC ratio and 30% conversion.

Catalyst	SiO <sub>2</sub> -Al <sub>2</sub> O <sub>3</sub>	HY	ZSM-5	SAPO-5	SAPO-11
Temp., °C	371	257	260	304	331
iso-C <sub>8</sub> selectivity, wt%	96.4	96.8	56.6	49.3	94.8
2M-C <sub>7</sub> /3M-C <sub>7</sub>	0.67	0.71	1.54	0.46	1.07
C <sub>3</sub> +C <sub>5</sub> /C <sub>4</sub> , mol ratio	0.95	0.64	2.1	0.86	1.0
DM-C <sub>6</sub> selectivity, wt%	8.5	12	1.8	9.0	2.3

### 2.3.3 Isodewaxing

In the case of middle distillate fuels and lube oils, it is of high interest to improve the cold flow properties, such as viscosity, pour point, freezing point, etc. These properties depend upon the composition of the distillate and in the case of diesel the freezing point and pour point can be lowered by reducing the content of waxy linear paraffins. For lube oils, a low pour point high viscosity

index product is highly desired. This can be achieved by selective hydrocracking of the waxy n-paraffins into lighter components (*dewaxing*) while leaving the interesting hydrocarbons intact. Typical catalysts used for dewaxing are based on medium or large pore zeolites, such as mordenite, Ferrierite, ZSM-23, ZSM-5 or SAPO-11. Indeed, the medium pore ZSM-5 zeolite is the base of the Mobil's Distillate Dewaxing (MDDW) and Lube Dewaxing (MLDW) processes developed by Mobil [79]. However, if the content of waxes in the feed is high, catalytic dewaxing can be limited because of the large loss of product that occurs during the process. In that case, higher yields of valuable oil products can be achieved by the isomerisation of the long-chain normal paraffins (*isodewaxing*) on zeolite based bifunctional catalysts of the same type described above. The maximum isomerisation yields that can be obtained will depend not only on the structural characteristics of the zeolite used, but also on the nature of the n-paraffins present in the feed, as observed in Table 13. Recently, a new process so-called Isodewaxing has been commercialized by Chevron using a Pt/SAPO-11 catalyst [80]. Table 14 shows the comparison of Pt/SAPO-11 and Pt/SiO<sub>2</sub>-Al<sub>2</sub>O<sub>3</sub> catalysts for the isomerisation of n-hexadecane [81]. A higher isomerisation selectivity and lower pour point are obtained for Pt/SAPO-11. In this case, Pt/SAPO-11 produces a higher yield of monobranched isomers and a higher selectivity for branching at the center of the hydrocarbon chain (7- + 8-MC<sub>15</sub> isomers) which are need to obtain a high degree of pour point reduction. Moreover, it has also been shown that SAPO-11 is the only catalyst among different zeolites capable of isomerizing n-alkanes in the presence of iso-alkanes with minimum losses due to hydrocracking [82].

*Table 13.* Maximum isomerisation yield from n-paraffins as a function of hydrocarbon chain length.

Catalyst	Feed				
	n-C <sub>10</sub>	n-C <sub>12</sub>	n-C <sub>15</sub>	n-C <sub>16</sub>	n-C <sub>17</sub>
1% Pt/USY	52	---	---	50	47
0.5% Pt/HY	---	---	---	---	61
0.3% Pt/HY	56	---	---	---	57
0.75% Pt/ZSM-3	62	69	67	69	72
1% Pt/ZSM-20	52	---	---	---	50
1% Pt/Beta	63	---	---	---	51

*Table 14.* Isomerisation of n-hexadecane at 1000 psig, 3.1 WHSV, 30 H<sub>2</sub>/HC, and 96% conversion on Pt/SAPO-11 and Pt/SiO<sub>2</sub>-Al<sub>2</sub>O<sub>3</sub> catalysts.

CATALYST	Pt/SAPO-11	Pt/SiO <sub>2</sub> -Al <sub>2</sub> O <sub>3</sub>
Temperature, °C	340	360
Isomerisation Selectivity, wt%	85	64
C <sub>16</sub> Product Composition, wt%		
7- + 8-MC <sub>15</sub>	22.9	6.1
6M-C <sub>15</sub>	7.1	3.2
5M-C <sub>15</sub>	7.5	3.1
4M-C <sub>15</sub>	8.1	3.2
3M-C <sub>15</sub>	7.7	3.3
2M-C <sub>15</sub>	4.7	6.0
n-C <sub>16</sub>	29.8	37.8
Other C <sub>16</sub>	12.2	34.6
Pour Point, °C	-51	-28

### 3. References

1. I.E. Maxwell and J.E. Naber, Catal. Lett. 12, 105 (1992).
2. G.E. Keller and M.M. Bhasin, J. Catal. 73, 9 (1982).
3. W. Hinsen and M Baerns,, Chem. Ztg. 107, 223 (1983).
4. J. Lunsford, Catal. Today 6, 235 (1990).
5. I. Pasquon, Plenary Lecture at EUROPACAT-1, Montpellier, France, September 12-17, 1993.
6. P. Pereira, S.H. Lee, G.A. Somorjai and H. Heineman, Catal. Lett. 6, 255 (1990).
7. A. Parmaliana, F. Arena, F. Frusteri, D. Micelli and V. Sokolovskii, Catal. Today 24, 231 (1995).
8. M.A. Vannice, Catal. Rev.-Sci. Eng. 14, 153 (1976).
9. J.M. Fox III, Catal. Rev.-Sci. Eng. 35, 169 (1993).
10. J. Eilers, S.A. Posthuma and S.T. Sie, AIChE Spring National Meeting, Orlando, Florida, 18-22 March (1990).
11. C.D.Chang, Stud. Surf. Sci. and Catal. 61, 393 (1991).

12. S.M. Csicsery, J. Catal. 17, 205 (1970); *ibid* 17, 217 (1970); *ibid* 17, 315 (1970); *ibid* 17, 322 (1970); *ibid* 18, 30 (1970).
13. Y. Ono, Catal. Rev.-Sci. Eng. 34, 179 (1992).
14. G. Giannetto, R. Monque and R. Galiasso, Catal. Rev.-Sci. Eng. 36, 271 (1994).
15. P. Chu and F.G. Dwyer, ACS Symp. Ser. 218, 59 (1983).
16. T. Inui, J. Jap. Petrol. Inst. 33, 198 (1990).
17. M. Shibata, H. Kitagawa, Y. Sendoda, Y. Ono, Proc. 7th Int. Conf. Zeol., Tokyo, p. 717, 1986.
18. Y. Ono, H. Nakatani, H. Kitagawa and E. Suzuki, Stud. Surf. and Catal. 44, 279 (1989).
19. J.A. Biscardi and E. Iglesia, Catal. Today 31, 207 (1996).
20. I. Nakamura and K. Fujimoto, Catal. Today 31, 335 (1996).
21. G.L. Price, J. Catal. 130, 611 (1991).
22. K.M. Dooley, C. Chang, G.L. Price, Appl. Catal. 84, 117 (1992).
23. E.G. Derouane, S.B. Abdul Amid, I. Ivanova, N. Blom and P.-E. Hojlund-Nielsen, J. Mol. Catal. 86, 371 (1994).
24. A. Corma, J.M. López-Nieto, N. Paredes, Appl. Catal. A:General 97, 159 (1993).
25. N.Y. Chen and T.Y. Yan, Ind. Eng. Chem. Proc. Des. Dev. 35, 151 (1986).
26. L. Mank, A. Minkinen and J. Shaddick, Hydrocarbon Tech. Int., 69 (1992).
27. D.M. Brouwer and H. Hogeveen, Prog. Phys. Org. Chem. 9, 179 (1972).
28. M. Boronat, P. Viruela and A. Corma, Appl. Catal. A:General 146, 207 (1996).
29. A. Corma, V. Fornés, J.M. López-Nieto and M.I. Juan-Rajadell, Appl. Catal. A:General 116, 151 (1994).
30. M. Hino and K. Arata, J. Amer. Chem. Soc. 101, 6439 (1979).
31. M. Hino and K. Arata, Chem. Lett., 482 (1979).
32. V. Adeeva, G.D. Lei and W.M.H. Sachtler, Appl. Catal. A:General 118, L11 (1994).
33. V. Adeeva, G.D. Lei and W.M.H. Sachtler, Catal. Lett. 33, 135 (1995).
34. C.-Y. Hsu, C.R. Heimbuch, C.T. Armes and B.C. Gates, J. Chem. Soc. Chem. Commun., 1645 (1992).
35. K. Ebitani, J. Konishi and H. Hattori, J. Catal. 130, 257 (1991).
36. K. Ebitani, H.H. Konno, T. Tanaka and H. Hattori, J. Catal. 143, 322 (1993).
37. A. Corma, Chem. Rev. 95, 559 (1995).
38. G. Genciu and D. Farcasiu, J. Mol. Catal. A:Chemical 109, 273 (1996).
39. A. Jatia, C. Chang, J.D. Macleod, T. Okubo and M.E. Davis, Catal. Lett. 25, 21 (1994).

40. K.B. Forgash, G. Yaluris, M.R. Gonzalez, P. Ouraipryvan, D.A. Ward, E.L. Ko and J.A. Dumesic, *Catal. Lett.* 32, 241 (1995).
41. V. Adeeva, J.W. Dehaan, J. Janchen, G.D. Lei, V. Schunemann, L.J.M. Vandeven, W.M.H. Sachtler and R.A. van Santen, *J. Catal.* 151, 364 (1995).
42. M.A. Coelho, D.E. Resasco, E.C. Dikabwe and R.L. White, *Catal. Lett.* 32, 253 (1995).
43. F. Pinna, M. Signoretto, G. Strukul, G. Cerrato and C. Morterra, *Catal. Lett.* 26, 339 (1994).
44. D. Tichit, B. Coq, H. Armendariz and F. Figueras, *Catal. Lett.* 38, 109 (1996).
45. C. Morterra, G. Cerrato, S. Di Ciero, M. Signoretto, F. Pinna and G. Strukul, *J. Catal.* 165, 172 (1997).
46. E. Escalona Platero, M. Peñarroya Mentrut, C. Otero Arean and A. Zecchina, *J. Catal.* 162, 268 (1996).
47. A. Corma and A. Martínez, *Catal. Rev.-Sci. Eng.* 35, 483 (1993).
48. F.W. Kirsch, J.D. Potts and D.S.J. Barmby, *J. Catal.* 27, 142 (1972).
49. T.J. Huang and S. Yurchak, *ACS Symp. Ser.* 55, 75 (1977).
50. A. Corma, A. Martínez and C. Martínez, *J. Catal.* 146, 185 (1994).
51. A. Corma, A. Martínez and C. Martínez, *Appl. Catal. A:General* 134, 169 (1996).
52. A. Corma, V. Gómez and A. Martínez, *Appl. Catal.* 119, 83 (1994).
53. T.J. Huang, *US Patent* 4,384,161 (1988).
54. J.E. Child, A. Huss Jr., C.R. Kennedy, D.O. Marler and S.A. Tabak, *US Patent* 5,012,033 (1991).
55. T.S. Chou, A. Huss Jr., C.R. Kennedy and R.S. Kurtas, *World Patent* 90/00533 (1990).
56. A. Corma, M.I. Juan-Rajadell, J.M. López-Nieto, A. Martínez and C. Martínez, *Appl. Catal.* 111, 175 (1994).
57. A. Corma, A. Martínez and C. Martínez, *J. Catal.* 149, 52 (1994).
58. A. Corma, A. Martínez and C. Martínez, *Appl. Catal. A:General* 144, 249 (1996).
59. T. Okuhara, M. Yamashita, K. Na and M. Misono, *Chem. Lett.* 8, 1451 (1994).
60. A. Corma, A. Martínez and C. Martínez, *J. Catal.* 164, 422 (1996).
61. G.M. Brown, M.R. Noe-Spirlet, W.R. Bushing and H.A. Levy, *Acta Crystallogr. B* 33, 1038 (1977).
62. H. Hayashi and J.B. Moffat, *J. Catal.* 77, 473 (1982).
63. G.B. McGarvey and J.B. Moffat, *J. Catal.* 130, 483 (1991).
64. I. V. Kozhevnikov, *Catal. Rev. Sci. Eng.*, 37, 311 (1995).
65. K. Nowinska, R. Fiedorow and J. Adamiec, *J. Chem. Soc. Faraday Trans.* 87, 749 (1991).
66. A. Corma, A. Martínez and P. Martínez-Escolano, to be published.

67. G.H. Unzelman, *Oil and Gas J.*, April 9, 43 (1990).
68. G. Bour, C.P. Schwoerer and G.F. Asselin, *Oil and Gas J.* 68, 43 (1970).
69. K.J. Ware and A.H. Richardson, *Hydrocarbon Processing* 51, 11 (1972).
70. D. Barthomeuf, *Mater. Chem. Phys.* 17, 49 (1987).
71. A. Corma, J. Frontela and J. Lázaro, US Patent 5,057,471 (1991).
72. C. Mirodatos and D. Barthomeuf, *J. Chem. Soc., Chem. Commun.* 39 (1981).
73. A. Corma, *Stud. Surf. Sci. and Catal.* 49, 49 (1990).
74. F. Fajula, M. Boulet, B. Coq, V. Rajaofanona, F. Figueras and T. Des Courières, 10th ICC, Budapest (1992).
75. L.-J. Len, L.-Y. Hou, B. Chan-Kang, Ch. Li, S. Tzywu and J.-Ch. Wu, *Appl. Catal* 69, 49 (1991).
76. T. Hosoi, T. Shimidzu, S. Itoh, S. Baba, H. Takaoka, T. Imai and N. Yokoyama, *Prep. ACS, Div. Petr. Chem.* 33, 562 (1988).
77. S. J. Miller, *Microp. Mater.* 2, 439 (1994).
78. A. Corma, A. Chica, unpublished results.
79. J.J. Wise, J.R. Katzer and Y.N. Chen, *Am. Chem. Soc.* 173 An. Mtg., NY, April (1986).
80. S. J. Miller, M.A. Shippey and G.M. Masada, NPRA Natl., Fuels and Lubr. Mtg., Paper FL-92-109 (1992).
81. S.J. Miller, *Stud. Surf. Sci. and Catal.* 84, 2319 (1994).
82. R.J. Taylor and R.H. Petty, *Appl. Catal. A: General* 119, 121 (1994).

# ACTIVATION OF LIGHT ALKANES: PAST AND PRESENT

IVAN V. KOZHEVNIKOV

*The Leverhulme Center for Innovative Catalysis, Department of Chemistry, The University of Liverpool, Liverpool L69 7ZD, UK*

Results on catalytic activation and functionalisation of light alkanes by soluble metal complexes in homogeneous solutions are reviewed. Under discussion are H/D exchange, oxidation, carbonylation, and carboxylation of light alkanes catalyzed by a range of metal complex systems including Pt(II), Pt(IV), Pd(II), Rh(III), Hg(II), Ziegler-Natta catalysts, and polyoxometalates.

## 1. Introduction

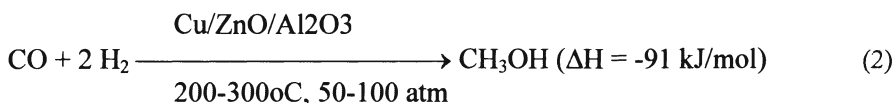
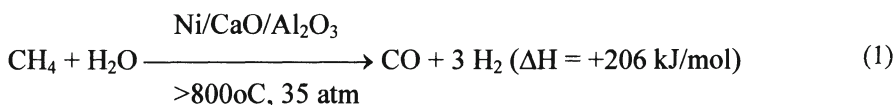
The problem of activation and functionalisation of alkanes, in particular light alkanes, by metal complexes emerged in the end of 1960s, shortly after the metal-complex activation of other small molecules, such as dihydrogen, carbon monoxide, alkenes, and dinitrogen, had made a tremendous progress [1-3].

The present paper attempts to highlight achievements in the field of catalytic activation and functionalisation of light alkanes, especially methane, by soluble metal complexes in homogeneous solution. The term "activation" is used to describe a chemical process where a substitution of a stronger  $sp^3$  C-H bond in alkanes occurs to form a weaker metal-carbon bond. "Functionalisation" is used to refer to a process where the metal-carbon bond is replaced by any bond except a C-H bond [2,4]. Several reviews on the alkane activation by metal complexes have been published [2,3,5-10].

The selective functionalisation of methane is one of the greatest challenges to the catalyst scientist. Methane - the primary component of natural gas (Table 1) - is an abundant resource that could serve not only as an efficient fuel source but also as chemical feedstock. The world reserves of natural gas are comparable to those of petroleum. However, in contrast to petroleum, the current use of methane is relatively small. If methane could be used efficiently, it could replace projected dwindling petroleum reserves in the 21st century. Efficient utilization of methane is challenging because its largest reserves are in remote places, and the low boiling point of methane ( $-164^\circ\text{C}$ ) makes this gas too expensive to transport. A solution to this problem could be the conversion of



methane to methanol or another useful liquid product at the remote site. Such processes have been developed, but current technology based on the high-temperature ( $>800^{\circ}\text{C}$ ), energy-intensive conversion of methane and water to carbon monoxide and hydrogen (Eqs 1 and 2) [11] is uneconomical. It has been estimated that a high-selectivity ( $>85\%$ ), high-conversion ( $>30\%$ ) process for the oxidation of methane to methanol with dioxygen as the terminal oxidant could provide the basis for an economical functionalisation of methane [4].



Methane is a very unreactive molecule. This is demonstrated by the high C-H bond strength (439 kJ/mol), high ionization potential (12.5 eV), low proton affinity (4.4 eV), and low acidity ( $\text{pK}_a = 48$ ) of the molecule. Methane can be made to react by using very reactive species generated under very forcing conditions or with very reactive reagents such as strong oxidants, radicals, carbenes, superacids, etc. [2,3]. However, under these conditions the initial (and more useful) products of reaction are more reactive than methane and selective reactions of methane in high yield are very difficult. Thus reactions with oxygen are possible but require temperatures above  $700^{\circ}\text{C}$ . Under these conditions, only low selectivities ( $<30\%$ ) to methanol have been reported at methane conversions above 10%, giving ca. 3% overall yields [4 and references therein].

*Table 1.* Typical compositions of natural gas [11]

Component	North Sea	Qatar	Netherlands	Pakistan
$\text{CH}_4$	94.85	76.6	81.4	93.48
$\text{C}_2\text{H}_6$	3.90	12.59	2.9	0.93
$\text{C}_3\text{H}_8$	0.15	2.38	0.4	0.24
$\text{C}_4^+$	0.08	0.34	0.1	0.51
$\text{CO}_2$	0.20	6.18	1.0	0.23
$\text{N}_2$	0.79	0.24	14.2	4.02
S	4 ppm	1.02 ppm	1 ppm	-

## 2. Thermodynamic Considerations

Alkanes are among the least reactive of organic compounds. However, the bond strength of the C-H bond in the least reactive alkane, methane, (439 kJ/mol) is lower than that in the quite reactive arene, benzene (455 kJ/mol). On the other hand, catalytic hydrogenations proceed readily under mild conditions although the H-H bond strength in dihydrogen (435 kJ/mol) is similar to that in methane.

The nature of the problem of alkane activation becomes clearer if we consider the simple oxidative addition of either methane or dihydrogen to a metal complex,  $L_nM$  (Eqs 3 and 4) [7].



As the bond strengths of dihydrogen and of the C-H bond in methane are similar, reaction (4) differs from reaction (3) in that two M-H bonds are formed rather than one M-H bond and one M-CH<sub>3</sub> bond. The energies of metal-hydrogen bonds are in general greater than those of metal-alkyl bonds by 60-120 kJ/mol [2,7,12], so a given metal ion is more likely to react with dihydrogen rather than with alkanes.

In alkane activation both thermodynamic and kinetic factors must be considered. Activation of relatively open dihydrogen must be more favored sterically than alkane activation where the carbon atom will have three other atoms attached, which will hinder approach of any activator [2,3,7].

## 3. Alkane Oxidation

### 3.1 ACTIVATION BY PLATINUM COMPLEXES

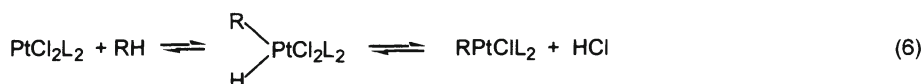
Shilov et al. pioneered the field of alkane activation by metal complexes discovering the hydrogen/deuterium exchange of methane and ethane catalyzed by Pt(II) chloride complexes in solution in 1969 [2], shortly after Garnett and Hodges found H/D exchange of arenes in this system [13]. The reaction proceeds homogeneously in aqueous acetic acid at 90-120°C. Detailed kinetic studies showed that there is a complex series of equilibria present in these

solutions, and the complexes  $\text{PtCl}_3\text{L}^-$ ,  $\text{PtCl}_2\text{L}_2$ , and  $\text{PtClL}_3^+$  are all active in H/D exchange. The rate increases in the order of alkanes  $\text{CH}_4 < \text{C}_2\text{H}_6 < \text{C}_3\text{H}_8$ . Steric factors play an important role: isolated methyl groups are the most active while tertiary C-H bond is not active at all.

The exchange is suggested to proceed via the reversible addition of the alkane RH to a Pt(II), e.g.,  $\text{PtCl}_2\text{L}_2$ :

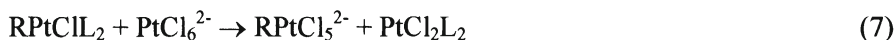


This is probably an oxidative addition of RH followed by reductive elimination of HCl.



In the early 1980s, Bergman, Graham and others directly observed and studied in detail the oxidative addition of light alkanes to transition metal centers to form hydrido(alkyl)metal complexes in stoichiometric reactions (for a review, see [10]).

Addition of Pt(IV) allows oxidation of the alkanes to yield both alkyl chlorides and alcohols. The oxidation is suggested to proceed via the formation an alkyl platinum(IV) intermediate, which was indeed observed by  $^1\text{H}$  NMR spectroscopy [2b].



In the presence of dioxygen as a terminal oxidant and a cocatalyst such as  $\text{CuCl}_2$ , quinone or heteropoly acid, the reaction can be made catalytic with respect to platinum, but the catalyst turnover number is small [2b].

The apparently simple reaction of alkanes with platinum(II) chloride complexes in aqueous acetic acid remains intriguing because it does not require the forcing conditions often needed for other activation reactions (see below).

Labinger and Bercaw [8,14] have extended this reaction to the hydroxylation of functionalised systems, e.g., the oxidation of ethanol to ethylene glycol, and have investigated the mechanism of the process. Thus evidence has been obtained that the alkane oxidation in the Pt(II)/Pt(IV) system may proceed by nucleophilic cleavage of the Pt-C bond in an alkyl-Pt(II) complex to form alkanol and Pt(0) followed by reoxidation of Pt(0) to Pt(II) by Pt(IV) [8].

### 3.2 ALKANE ACTIVATION IN STRONGLY ACIDIC MEDIA

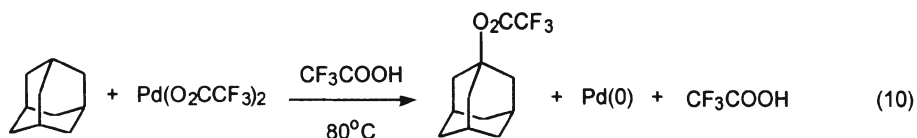
Rudakov et al. [3 and references therein] were first to study the activation of alkanes by metal complexes in strongly acidic media, in particular in concentrated  $\text{H}_2\text{SO}_4$ . A number of efficient homogeneous oxidation reactions of alkanes with metal complexes, such as Pd(II), Pt(II), Pt(IV), Hg(II), Ru(IV), Mn(III), etc., were found in 80-96%  $\text{H}_2\text{SO}_4$  at the temperature below  $100^\circ\text{C}$ , and their kinetics and mechanism were studied in detail. These studies showed that Brönsted acid catalysis plays important role in metal-mediated activation of alkanes, greatly enhancing the activity of metal complexes. More recently, several efficient activating systems have been developed with the use of strongly acidic media (see below).

### 3.3 ACTIVATION BY PALLADIUM COMPLEXES

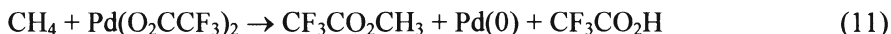
Palladium(II) complexes are a particularly attractive choice for oxidative functionalisation of alkanes for the following reasons [3, 15]: 1) Pd(II) is a powerful electrophile and a good two-electron oxidant, thus avoiding the formation of free radicals; 2) Pd(0) is readily reoxidized to Pd(II) by dioxygen using different cooxidants (e.g., Cu(II), heteropoly acids, etc.), which has been utilized in a number of Pd(II) catalyzed oxidation processes (e.g., the Wacker process). It should be noted, however, that the reoxidation of Pd(0) by  $\text{O}_2$  could be very difficult under forcing conditions often required for alkane activation.

Rudakov et al. [3] reported that Pd(II) can activate alkanes when present in strongly acidic media. Thus Pd(II) sulphate in 85-93% sulphuric acid, Pd(II) trifluoroacetate in trifluoroacetic acid, and Pd(II) phosphate in a 1:1  $\text{H}_3\text{PO}_4/\text{BF}_3$  medium all oxidize alkanes at the temperature  $<100^\circ\text{C}$ , Pd(II) being reduced to Pd(0). The activity of Pd(II) increases with the acidity of the media. Cyclohexane is dehydrogenated to cyclohexene and then to benzene. The reactivity of alkane C-H bonds is in the order of their strengths tertiary > secondary > primary, differing from that for the activation by platinum complexes. The reactions are first-order in both Pd(II) and alkane.

Sen et al. reported that heating adamantane with  $\text{Pd}(\text{O}_2\text{CCF}_3)_2$  in  $\text{CF}_3\text{CO}_2\text{H}$  at  $80^\circ\text{C}$  resulted in the precipitation of Pd metal and the formation of 1-adamantyl trifluoroacetate in >50% yield [15].

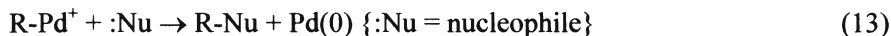


More significantly, methane (at 60 atm) was oxidized to methyl trifluoroacetate in >60% yield based on Pd(II) under the same conditions.



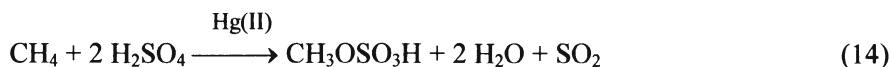
Since the ester can be readily hydrolyzed to the corresponding alcohol, this reaction provides a potential route for the conversion of methane to methanol. However, there has been some concern about the reproducibility of this work. Thus later Periana et al. [4] although confirmed this reaction, but found the yield to be only 5% on palladium.

The reaction is believed to proceed via the electrophilic substitution of hydrogen by Pd(II) in the alkane (Eq 12) followed by nucleophilic attack (Eq 13). If step (12) is reversible, the incorporation of deuterium into the starting alkane may be expected in the presence of  $\text{CF}_3\text{CO}_2\text{D}$ . However, no deuterium incorporation into adamantane was observed during its oxidation, indicating that the subsequent nucleophilic attack was fast [15].

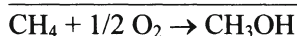
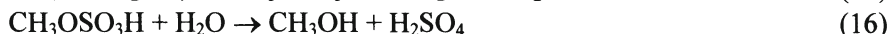
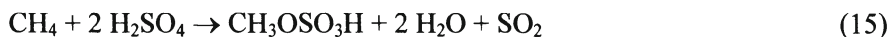


### 3.4 ACTIVATION BY MERCURY COMPLEXES

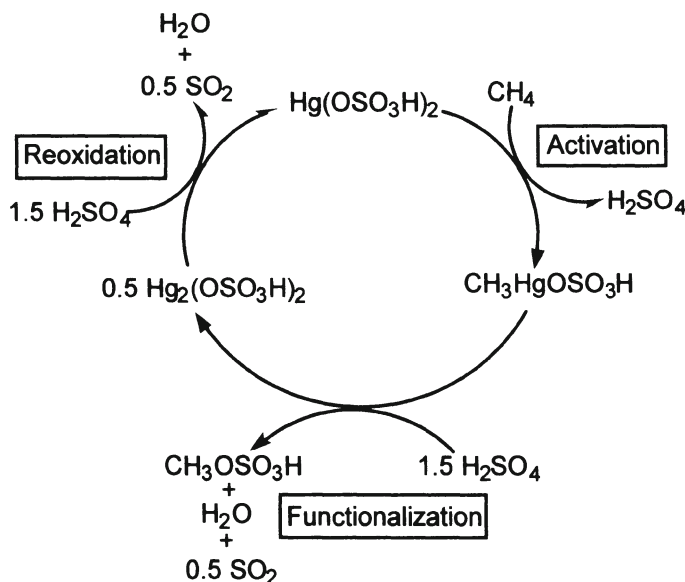
Periana et al. [4] reported a homogeneous system for the selective catalytic oxidation of methane to methanol via methyl bisulphate. The net reaction catalyzed by mercuric ions, Hg(II), is the oxidation of methane by concentrated sulphuric acid to produce methyl bisulphate, water, and sulphur dioxide.



The reaction is quite efficient and achieves 85% selectivity to methyl bisulphate (43% yield) at a methane conversion of 50% and Hg(II) turnover frequency of  $10^{-3} \text{ s}^{-1}$ . Separate hydrolysis of methyl bisulphate and reoxidation of the sulphur dioxide with air provides a potential route for the oxidation of methane to methanol with dioxygen (Eqs 15-17).



The primary steps of the Hg(II)-catalyzed reaction were individually examined and the essential elements of the mechanism were identified (Scheme 1) [4]. The Hg(II) ion reacts with methane by an electrophilic displacement mechanism to produce an observable species,  $\text{CH}_3\text{HgOSO}_3\text{H}$ . Under the reaction conditions, this species readily decomposes to  $\text{CH}_3\text{OSO}_3\text{H}$  and the reduced mercurous species,  $\text{Hg}_2^{2+}$ . The catalytic cycle is completed by the reoxidation of  $\text{Hg}_2^{2+}$  with  $\text{H}_2\text{SO}_4$  to regenerate Hg(II) and form by-products  $\text{SO}_2$  and  $\text{H}_2\text{O}$ . Thallium(III), palladium(II), and the cations of platinum and gold also oxidize methane to methyl bisulphate in sulphuric acid.



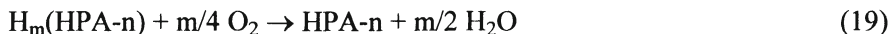
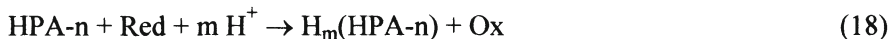
**Scheme 1**

Apparently, the difficulty in separating methyl bisulphate from concentrated sulphuric acid will be a problem in scaling-up such process. In addition, there is a serious concern about environmental impact of mercury. Nevertheless, the Hg(II)-sulphuric acid system provides important example of efficient catalytic system for selective low-temperature oxidation of methane to methanol. The knowledge gained from this study should be useful in guiding the development of more practical systems.

### 3.5 ALKANE OXIDATION BY POLYOXOMETALATES

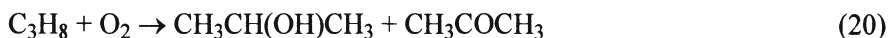
Catalysis by polyoxometalates (POMs) is a relatively new field emerged in the early 1970s [16,17]. In the last two decades, several new acid-type and oxidation processes based on catalysis by POMs have been commercialized [17]. Among a wide variety of POMs, the Keggin - having heteropolyanions  $[XM_{12}O_{40}]^{x-8}$  where X is the central atom ( $P^{5+}$ ,  $Si^{4+}$ , etc.),  $x$  is its oxidation state, and M is the polyatom ( $Mo^{6+}$ ,  $W^{6+}$ ,  $V^{5+}$ , etc.) - are the most stable and easily available; these and related POMs are the most important for catalysis. Multicomponent POMs are considered as robust inorganic metalloporphyrin analogues [17,18]. Several reviews on catalysis by POM in the liquid-phase oxidation have been published [16-20].

Mixed-addenda polyanions  $[PMo_{12-n}V_nO_{40}]^{(3+n)-}$  ( $n = 2-6$ ) are efficient and versatile catalysts for oxidation by  $O_2$ . These are the reversibly acting oxidants under mild conditions [16,20]. Generally, reactions catalyzed by HPA- $n$  proceed via a stepwise redox mechanism represented by Eqs. (18) and (19):



This mechanism includes stoichiometric oxidation of the substrate (Red) by HPA- $n$  followed by reoxidation of the reduced form of the oxidant,  $H_m(HPA-n)$ , with dioxygen, where  $H_m[HPA-n] = H_m[PMo_{12-n}^{6+}V_{n-m}^{5+}V_m^{4+}]^{(3+n)-}$ ,  $m \leq n$ .

Geletii and Shilov [2] used HPA-6 as a cocatalyst for the oxidation of light alkanes by  $O_2$  under mild conditions in the presence of Pt(II). More recently Ellis et al. [21] have oxidized alkanes by  $O_2$  with HPA- $n$  as a one-component catalyst. For example, propane is oxidized in an AcOH- $H_2O$  solution in the presence of HPA- $n$  at  $150^\circ C$  to a mixture of isopropanol and acetone in 42% and 52% selectivity, respectively (Eq 20).



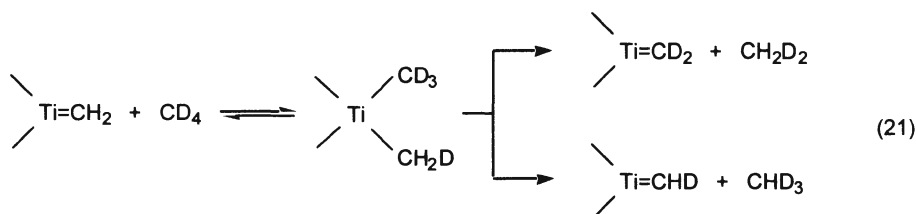
The mixed-addenda HPA-n are more efficient catalysts than the all-molybdenum heteropolyanions.

Other types of POMs are also active in light alkane oxidation, e.g., a trisubstituted Keggin anion  $[\text{PW}_9\text{Fe}_2\text{NiO}_{37}]^{7-}$  [22]. As shown by Mizuno et al., [23] this polyanion also catalyses the oxidation of cycloalkanes such as cyclohexane and adamantane.

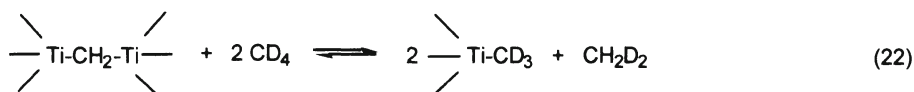
Neumann et al. [24] reported that a new  $\text{Ru}^{3+}$ -substituted sandwich POM,  $[(\text{WZnRu}_2)(\text{OH})(\text{H}_2\text{O})(\text{ZnW}_9\text{O}_{34})_2]^{11-}$ , catalyses the hydroxylation of adamantane by  $\text{O}_2$ . The hydroxylation takes place almost exclusively at the tertiary carbon positions to form 1-adamantanol, suggesting a non-radical pathway.

#### 4. Activation by Ziegler-Natta Catalyst Systems

Grigoryan et al. [5] reported a series of novel reactions of alkanes with Ziegler-Natta catalytic systems in hydrocarbon media. For example,  $\text{CD}_4$  was shown to be capable of exchanging deuterium atoms with the hydrogen of methyl groups in such systems as  $\text{TiCl}_4 + \text{AlMe}_2\text{Cl}$ ,  $(\eta^5\text{-C}_5\text{H}_5)_2\text{TiCl}_2 + \text{AlMe}_2\text{Cl}$  and  $\text{VCl}_3 + \text{AlMe}_2\text{Cl}$  in heptane solution at 20-50°C and methane pressure of 0.3-4 atm. The products were found to be  $\text{CHD}_3$ ,  $\text{CH}_2\text{D}_2$ , and  $\text{CH}_4$ . The authors suggested carbene complex as an intermediate (Eq 21):

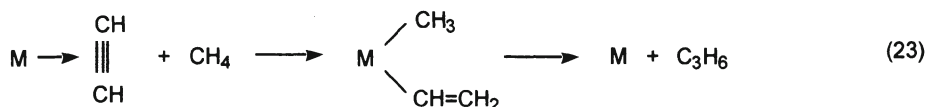


or binuclear complex (Eq 22):





Another interesting reaction is the addition of methane to a multiple bond [5]. Thus, in the system  $\text{Ti}(\text{OBu})_4 + \text{AlEt}_3$  in benzene, methane adds to ethylene to form propane, though with a rather small yield. Subsequently, the addition of methane to acetylene to form propene was observed for the complexes of iron, nickel, and platinum. A possible mechanism of this reaction is the recombination of alkyl groups in the coordination sphere of the metal, e.g., for acetylene:

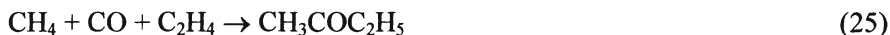


## 5. Reactions with Carbon Monoxide

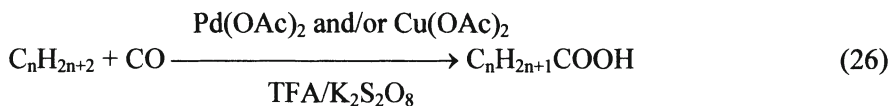
Enikolopyan and Grigoryan found the carbonylation of methane to acetaldehyde under non-oxidative conditions in the Ziegler-Natta system  $\text{Cp}_2\text{TiCl}_2 + \text{AlMe}_2\text{Cl}$  in benzene or toluene at 20-50°C and high pressure (1500-3000 atm) [25].



In the presence of ethylene the formation of methyl ethyl ketone was observed.



Fujiwara et al. [26,27] have demonstrated the efficient oxidative carboxylations of methane, ethane and other alkanes with CO using  $\text{Pd}(\text{OAc})_2/\text{Cu}(\text{OAc})_2$  or  $\text{Cu}(\text{OAc})_2$  catalyst systems and potassium peroxodisulfate as a terminal oxidant in TFA solution at 80°C.



The reaction of ethane is catalyzed best by  $\text{Pd}(\text{OAc})_2/\text{Cu}(\text{OAc})_2$  to give propionic acid in 7600% yield based on palladium. The reaction proceeds

probably via electrophilic substitution. In contrast, the carboxylation of methane is catalyzed best by  $\text{Cu}(\text{OAc})_2$  alone to give acetic acid in 11130% yield based on copper. In the methane case, a radical mechanism is suggested [32].

Recently, Sen et al. [28,29] reported that  $\text{RhCl}_3$ , in the presence of several equivalents of  $\text{Cl}^-$  and  $\text{I}^-$  ions, catalyses the direct formation of methanol and acetic acid from methane, CO, and  $\text{O}_2$  (1:0.2:1.1) at 80-85°C and 3000 psi in 6:1 mixture of perfluorobutyric acid and water.



The approximate turnover rate is  $3 \text{ h}^{-1}$  based on Rh. Formic acid is the only significant by-product observed. It is possible to direct the process to form either methanol or acetic acid by a simple change in the solvent system. As expected, ethane is more reactive than methane, and under similar reaction conditions forms methanol, ethanol, and acetic acid at a turnover rate  $7.5 \text{ h}^{-1}$  based on Rh. Surprisingly, product alcohols are less reactive than starting alkanes. Another important feature is that for ethane and higher alkanes products derived from C-C cleavage dominated over those derived from C-H cleavage. Unfortunately, no mention was made of the yield of oxygenated products based on alkane and CO consumed. It is believed that this reaction proceeds via a Rh-alkyl complex, though little direct mechanistic information is available.

## 6. Conclusion

Extensive knowledge of C-H bond activation has been obtained during the past 20 years. But a significant number of questions remain to be answered in order to move from relatively fundamental to more practical goals. We need a better understanding of the factors that control the rate, selectivity, and stereochemistry of C-H bond activation and of the nature and role of metal-alkane complexes. It still remains a puzzle why some metals are capable of activating alkanes and why some are not. On the other hand, we require better insight into the effect of ligands on alkane activation processes.

Exploratory goals include the search for new types of C-H activating systems. More detailed knowledge of the relationship between homogeneous, heterogeneous, and biological catalysis for alkane functionalisation will guide the search for more efficient activating systems. Investigation of new ligands that could convert nonreactive metals into reactive ones will be fruitful. Of particular interest are oxidatively resistant ligands such as polyoxometalates which are considered as robust analogs of metalloporphyrins. As this field

continues to expand, no doubt that progress will be made in the development of reliable catalysts for alkane functionalisation (e.g., methane-to-methanol process) that can be employed on a large scale.

## 7. References

1. Halpern, J. *Disc. Faraday Soc.* 1968, 46, 7.
2. Shilov, A.E. *Activation of Saturated Hydrocarbons by Transition Metal Complexes*, Reidel: Dordrecht, 1984. (b) Shilov, A.E. In *Activation and Functionalisation of Alkanes*, Hill, C.L., Ed.; Wiley-Interscience: New York, 1989; p. 1.
3. Rudakov, E.S. *Reactions of Alkanes with Oxidants, Metal Complexes, and Radicals in Solution*, (in Russian), Naukova Dumka: Kiev, 1985.
4. Periana, R.A.; Taube, D.J.; Evitt, E.R.; Löffler, D.G.; Wentreck, P.R.; Voss, G.; Masuda, T. *Science* 1993, 259, 340.
5. Grigoryan, E.A. *Russ. Chem. Rev.* 1984, 53, 210.
6. Jones, W.D. In *Activation and Functionalisation of Alkanes*, Hill, C.L., Ed.; Wiley-Interscience: New York, 1989; p. 111.
7. Chipperfield, J.R. *Stud. Inorg. Chem.* 1991, 11, 147.
8. Labinger, J.A.; Herring, A.M.; Bercaw, J.E. *Adv. Chem. Ser.* 1992, 230, 221.
9. Barton, D.H.R.; Doller, D. *Acc. Chem. Res.* 1992, 25, 504.
10. Arndtsen, B.A.; Bergman, R.G.; Mobley, T.A.; Peterson, T.H. *Acc. Chem. Res.* 1995, 28, 154.
11. *Catalyst Handbook*, 2nd Ed., Twigg, M.V., Ed.; Wolfe: London, 1989.
12. Labinger, J.A.; Bercaw, J.E. *Organometallics* 1988, 7, 926.
13. Garnett, J.L.; Hodges, R.J. *J. Am. Chem. Soc.* 1967, 89, 4546.
14. Stahl, S.S.; Labinger, J.A.; Bercaw, J.E. *J. Am. Chem. Soc.* 1996, 118, 5961.
15. Sen, A. *Acc. Chem. Res.* 1988, 21, 421.
16. Kozhevnikov, I.V.; Matveev, K.I. *Appl. Catal.* 1983, 5, 135.
17. Okuhara, T.; Mizuno, N.; Misono, M. *Adv. Catal.* 1996, 41, 113.
18. Hill, C.L.; Prosser-McCarthy, C.M. *Coord. Chem. Rev.* 1995, 143, 407.
19. Kozhevnikov, I.V. *Catal. Rev. Sci. Eng.* 1995, 37, 311.
20. Kozhevnikov, I.V. *J. Mol. Catal. A*, 1997, 117, 151.
21. Ellis, P.E.; Lyons, J.E.; Myers, H.K.; Suld, G.; Langdale, W.A. *Eur. Patent* 301,723, 1989.
22. Lyons, J.E.; Ellis, P.E.; Durante, V.A. In *Stud. Surf. Sci. Catal.*, Elsevier: Amsterdam, 1991; p. 99.
23. Mizuno, N.; Hirose, T.; Tateishi, M.; Iwamoto, M. *J. Mol. Catal.* 1994, 88, L125.

24. Neumann, R.; Khenkin, A.M.; Dahan, M. *Angew. Chem. Int. Ed. Engl.* 1995, 34, 1587.
25. Enikolopyan, N.S.; Menchikova, G.N.; Grigoryan, E.A. *Dokl. Akad. Nauk. SSSR* 1986, 291, 11.
26. Fujiwara, Y.; Takaki, K.; Watanabe, J.; Uchida, Y.; Taniguchi, H. *Chem. Lett.* 1989, 1687.
27. Nakata, K.; Yamaoka, Y.; Miyata, T.; Taniguchi, Y.; Takaki, K.; Fujiwara, Y. *J. Organometal. Chem.* 1994, 473, 329.
28. Lin, M.; Sen, A. *Nature* 1994, 368, 613.
29. Lin, M.; Hogan, T.E.; Sen, A. *J. Am. Chem. Soc.* 1996, 118, 4574.

# SUPERACID CATALYSED PROTOLYTIC ACTIVATION, H/D EXCHANGE AND OXIDATION OF SMALL ALKANES.

J. SOMMER\*, J. BUKALA, M. HACHOUMY AND R. JOST

*\*Laboratoire de Physico-Chimie des Hydrocarbures,  
Centre de Recherches Chimie, Université Louis Pasteur,  
1, rue Blaise Pascal, 67008 Strasbourg, France*

## Abstract.

The behavior of propane, butane and isobutane toward the HF(DF)-SbF<sub>5</sub> superacid in the presence of carbon monoxide is described. The initially formed reactive carbenium ions are converted into stable oxocarbenium ions, limiting in this way drastically the hydride transfer step. The deuterium distribution, in the recovered (apparently unreacted) alkane, shows in all cases that the reversible protonation of all  $\sigma$ -bonds is very fast in comparison of the competitive protolytic cleavage. The extent of the isotope exchange is related with the  $\sigma$ -basicity of the C-H bonds and not with the reactivity of the  $\sigma$ -bond towards protolytic cleavage.

The product distribution, based on the amount of Hydrogen and smaller alkanes recovered in the gas phase and the alkyl esters recovered by ethanolysis of the superacid phase allows the estimation of the relative importance of the competitive activation pathways. The change in product distribution which is tied to the HF/SbF<sub>5</sub> ratio suggests that two activation reactions compete: in HF containing up to 20 mol % SbF<sub>5</sub>, ionization occurs by protolysis of C-H and C-C bonds with formation of a smaller alkane and a smaller carbenium ion. At higher SbF<sub>5</sub> concentrations the protolytic activation is accompanied increasingly by reduction of SbF<sub>5</sub>. In the absence of HF, the alkane is directly oxidized by SbF<sub>5</sub> with production of SbF<sub>3</sub>.

## 1. Introduction

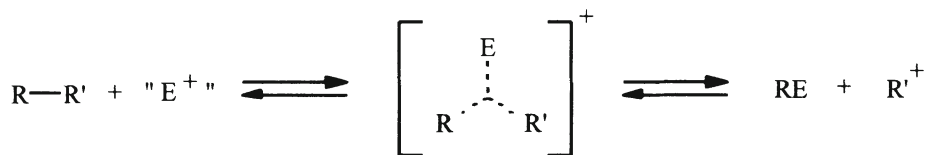
Acid-catalyzed hydrocarbon conversions, such as catalytic cracking, isomerisation and alkylation, are large-scale industrial processes using solid or

liquid strong acids, such as H-Zeolites, chlorinated aluminas, sulphuric acid and hydrogen fluoride [1 – 3]. The chemical inertness of the starting material is overcome by strong acidity and high temperature. Solid and liquid superacid catalyzed isomerization of C<sub>4</sub>-C<sub>6</sub> alkanes has been studied extensively in the last decades [4, 5]. In part, this interest arises from the industrial importance of the branched isomers in processes yielding high octane gasoline. Due to environmental pressure, the branched isomers are also essential for preparing octane boosters such as MTBE (Methyl, tertiobutylether) and TAME (t-amyl, methylether) which shall replace aromatics and lead additives [6].

The advantage of superacids is the low temperatures at which alkanes can be activated, as the branched isomers are thermodynamically favored when temperature is lowered. That saturated hydrocarbons do react at room temperature and below with various superacidic media has been known since the late 1960's when both Hogeveen [7] and Olah [8] and his group published their pioneering work on isobutane ionization.

This discovery incited Olah's group to study the reactivity of all the other alkanes from C<sub>4</sub> to C<sub>9</sub> in superacid media [9]. Olah, recognizing the importance of these reactions, proposed and developed the concept of  $\sigma$ -basicity in a landmark paper that appeared in *Angewandte Chemie* in 1973 [10].

The concept describes the ability of a  $\sigma$ -bond to share its bonded electron pair with an electrophile to form a hypercoordinated [11], carbonium ion transition state (eventually also a reaction intermediate when the structure is stabilized).



R, R' = alkyl, H. "E<sup>+</sup>" = H<sup>+</sup>, Br<sup>+</sup>, NO<sup>2+</sup>, OH<sup>+</sup>, etc..

*Scheme 1.* The  $\sigma$ -basicity concept.

This unifying concept rationalizes all acid-catalyzed hydrocarbon conversions including, electrophilic substitution, Wagner-Meerwein rearrangements,  $\beta$ -scission as well as inter and intramolecular hydride transfers. It was extremely useful in extending the carbocation concept from the classical trivalent carbenium ion to the pentacoordinated carbonium ions. The importance

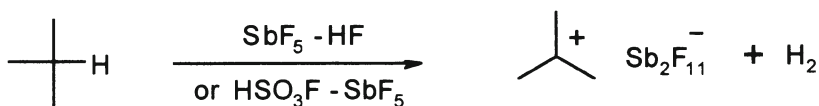
of this concept as well as the cation chemistry in superacid media was recognized by the Nobel Prize Award to Olah in 1994 [12].

A major drawback with acid-catalyzed hydrocarbon chemistry resides in the lack of selectivity due to the inertness of the starting material in comparison with the high reactivity of the cationic intermediates. This leads to competitive intra and intermolecular hydride transfer associated with skeletal rearrangement, and cracking reactions.

On the basis of our work on alkane activation in the presence of carbon monoxide [13] we try in this review to illustrate the factors governing the selectivity in protolytic activation of small alkanes in superacidic media using propane, butane and isobutane as model compounds.

## 2. General schemes concerning the reactivity of alkanes in superacidic media

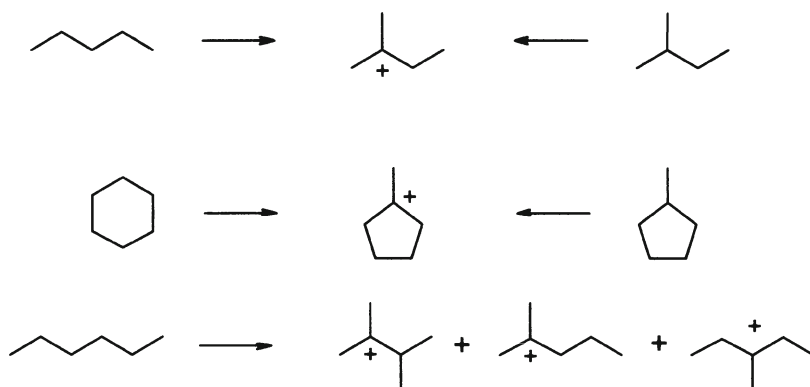
In comparison with other acids, the advantage of superacid systems is the stability of the carbenium ion intermediates, which can be generated in these media. Due to the extremely low basicity of the conjugate bases of the superacid, carbenium ions do not deprotonate. For this reason, the NMR spectrum of the solution of the t-butyl ion obtained from isobutane, tertio-butanol or other precursors, can be observed even after several days at room temperature.



*Scheme 2.* Formation of the stable t-butyl ion from isobutane.

As we will see below, isobutane is a special model for mechanistic studies, as the reactivity of the tertiary CH bond is by far and away the highest in comparison with the C-C and the primary C-H bonds.

For other ions, when possible, skeletal isomerization occurs yielding the thermodynamically most stable carbenium ion. n-Pentane and isopentane ionized under the same conditions lead to the t-amyl ion. Cyclohexane and methyl cyclopentane give both the methylcyclopentyl cation, whereas the ionization of n-hexane gives the three isomeric t-hexyl ions (Scheme 3).

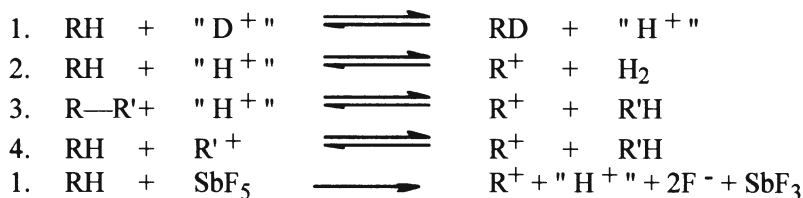


*Scheme 3.* Formation of the most stable tertiary ions in superacid media.

On the basis of the carbenium ion distribution observed when  $C_3$ - $C_9$  alkanes were reacted with  $HSO_3F$ - $SbF_5$  on  $HF$ - $SbF_5$  superacids, Olah and his group rated the reactivity of the various  $\sigma$ -bonds in the following sequence [9]:



In the course of these studies a large variety of competitive reactions have been described (scheme 3) and discussed which can be summarized in the following scheme.



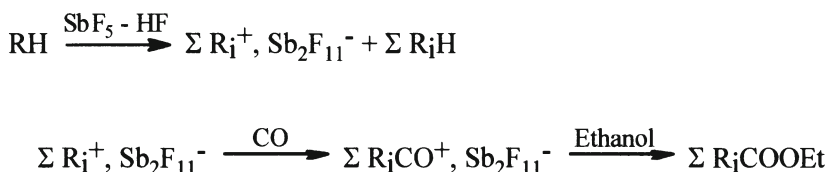
*Scheme 4.* Competitive reactions for alkanes in superacids.

When ionization occurs via C-C bond protolysis, a smaller alkane and a smaller carbenium ion are produced. Both the alkane and carbenium ions can in turn reenter the reaction system generating new alkanes and carbenium ions. As most of these reactions can occur on any of the various C-C and C-H  $\sigma$ -bonds, the picture is generally too complex to allow quantitative studies.

However when the carbenium ions are formed in the presence of carbon monoxide, they show a very high affinity for this nucleophile. This results in the



formation of much more stable oxocarbenium ions which are rather inactive towards hydride transfers from the alkane. Further, the oxocarbenium ions can also be trapped by quenching the superacid in excess ethanol and, since the resulting esters can be analyzed by G.C., a quantitative study becomes possible.<sup>13</sup> (Scheme 5).



*Scheme 5.* Ionization in the presence of carbon monoxide.

We have experienced a satisfactory balance in product distribution for a quantitative determination of all products and reagents, by using the rather simple experimental set up schematized as in figure 1. It comprises essentially a kel-F reactor, a recirculation pump and a gas collector. The gaseous mixture (alkane/CO) at atmospheric pressure is bubbled at a rate of 220 mL.h<sup>-1</sup> through the HF-SbF<sub>5</sub> solution in the Kel-F reactor below room temperature. The cations initially formed in the superacid solution react with carbon monoxide and form stable oxocarbenium ions. The superacid solution is then quenched in ethanol followed by G.C. analysis of the resulting esters. The alkanes and hydrogen coming out of the reactor are collected in the isobaric flask from which they can be analyzed by G.C., M.S. or NMR.

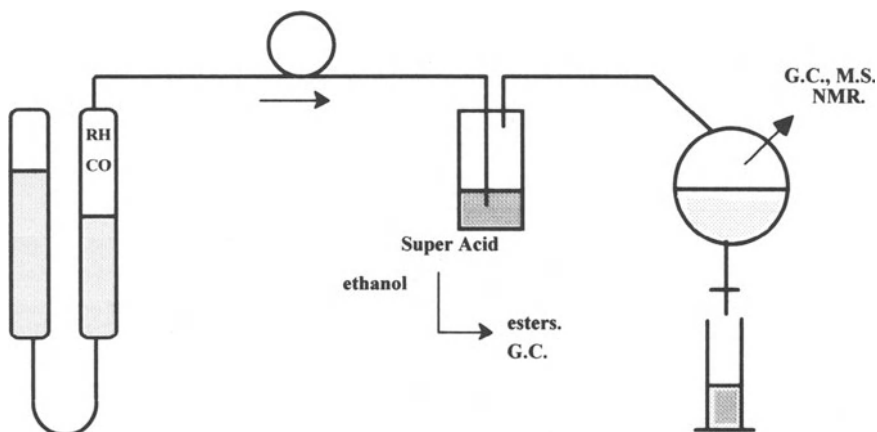


*Figure 1.* Experimental set-up for activation of alkanes in the presence of carbon monoxide.

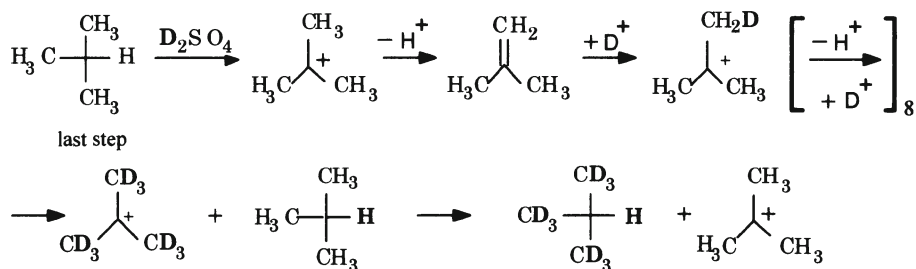
The complete material balance obtained for the products distributed over the acid and gaseous phases is very useful to establish the initial competitive reaction pathways.

### 3. The protolytic pathways : (Reversible protonation of C<sub>3</sub>-C<sub>4</sub> alkanes in competition with protolytic ionization)

Protolysis of alkanes starts always with the reversible protonation step (reaction 1 in scheme 3) which produces a carbonium ion intermediate or transition state in which the 2 electrons of the protonated  $\sigma$ -bond are shared between three nuclei : the electrophile and the two nuclei (C or H) bound by the  $\sigma$ -bond.

The direct hydron exchange, taking place at this point, between the C-H bond of an alkane and the superacid, constitutes the simplest example of electrophilic substitution and has been described by Olah in the late sixties [14] and also by the group at Shell [15]. Due to the occurrence of side reactions (as described on Scheme 4), only a few quantitative studies have been reported.

These reports, in excellent agreement with the formation of carbonium ion intermediates in superacid media contrast markedly with the H/D exchange observed earlier by Stevenson and Otvos [16], who found that, in D<sub>2</sub>SO<sub>4</sub>, isobutane readily exchanged all 9 primary protons for deuterons but not the methine proton. In this case, the exchange could be rationalized by a carbenium ion mechanism, including successive deprotonation and reprotonation followed by a hydride transfer step (scheme 6).



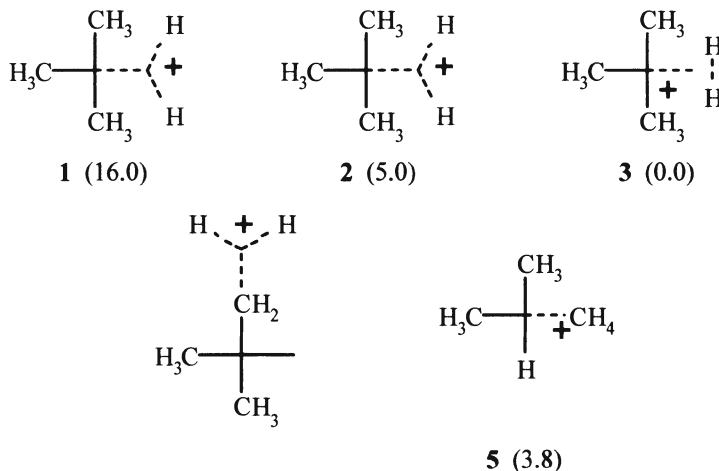
*Scheme 6.* Deuteration of isobutane in D<sub>2</sub>SO<sub>4</sub>.

The same regiospecificity in H/D exchange on the positions vicinal to the branching has recently been reported by us [17] for isoalkanes contacted with D<sub>2</sub>O-exchanged solid acids, such as zeolites or sulfated zirconia.

The structure of small carbonium ions (C<sub>1</sub>-C<sub>4</sub>) has been investigated by various theoretical ab initio methods and the true nature of the intermediate or transition state as well the reaction path leading to it is still under discussion [18 – 20].

For methane the protonation pathway proposed by Van Santen [18] (protonation at the carbon) is at odds with the model suggested by O'Malley [19] (protonation on the  $\sigma$ -bond). For isobutane the DFT calculations of Mota and colleagues [20] seem to indicate that the tertiary-C-H protonated alkane 2 is less stable than the corresponding  $H_2$  complex of t-butyl cation, 3.

The calculated relative energies of protonated isobutane <sup>20</sup> have been represented in Scheme 7.



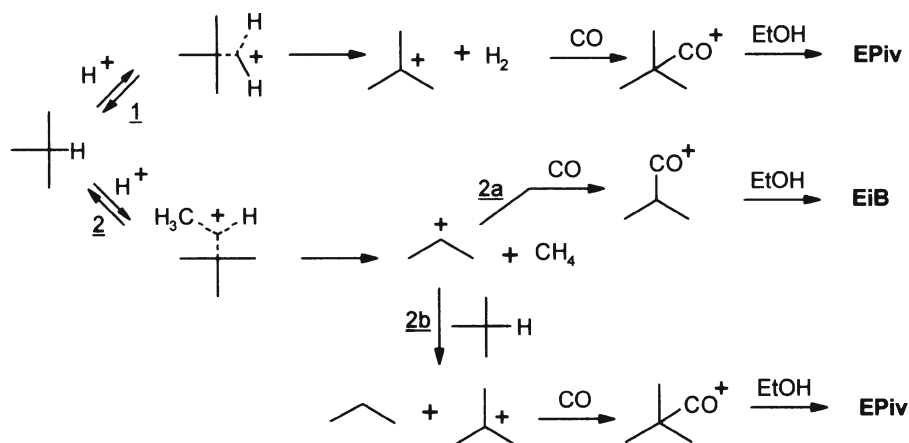
*Scheme 7.* Relative energies in  $\text{kcal mol}^{-1}$  of  $i\text{-C}_4\text{H}_{11}^+$ .

As will be seen below, these results are not fully in accord with our experimental findings concerning isobutane protolysis vs H/D exchange which show preferential protonation/cleavage of the tertiary C-H bond.

#### 4. Protolytic ionization of isobutane

Among small alkanes, isobutane has received special attention due to simple structure and product distribution. It is, for this reason, a good model, very useful for comparison of the initial steps of activation.

When an isobutane/carbon monoxide mixture (ratio 1:3) is bubbled during 1 hour at a rate of 220 mL/hour, through  $\text{HF-SbF}_5$  at  $-10^\circ\text{C}$ , the formation of the various gaseous products as well as the ethylesters obtained by quenching the oxocarbenium ions in the liquid phase, can be rationalized by the pathways presented in Scheme 8.



*Scheme 8.* Protolytic ionization of isobutane in the presence of carbon monoxide.

The product distribution shows that the main pathway for ionization involves protolytic cleavage (path 1) of the tertiary C-H bond, producing the t-butyl ion, which is titrated as ethylpivalate, and a stoichiometric amount of hydrogen. Some ethylpivalate is also formed as a by-product (path 2b) when the carbon-carbon bond is cleaved with formation of methane and propyl cation. The secondary cation, even in the presence of carbon monoxide will, in part, ionize isobutane by hydride transfer as shown by the small amount of propane detected in the gas phase. In accord with a purely protolytic activation of isobutane in this superacid medium no precipitate of  $\text{SbF}_3$  was noticed.

On basis of the product distribution, we assigned the relative rates of pathways 1 and 2 as being in the order 18:1 [21]. This order confirms all earlier reports on the high reactivity of the tertiary C-H bond. The relative rates of pathways 2a and 2b which are here roughly in the order of 1:5 are very much dependent on the CO/hydrocarbon ratio which controls the competitive hydride transfer or carbonylation of the propyl cation.

On the other hand as the reaction proceeds,  $\text{SbF}_5$  is used up in the formation of the large  $(\text{SbF}_5)_n\text{F}^-$  anions which stabilize the oxocarbenium ions in solution. For this reason the conversion of isobutane will be dependant on the concentration of  $\text{SbF}_5$ .

In order to assess the importance of  $\text{SbF}_5$  in the ionization process, we have measured the conversion of isobutane under the same experimental conditions, in the presence of CO but in HF containing various initial concentrations of  $\text{SbF}_5$ . The time dependence of the conversion is illustrated in figure 2.

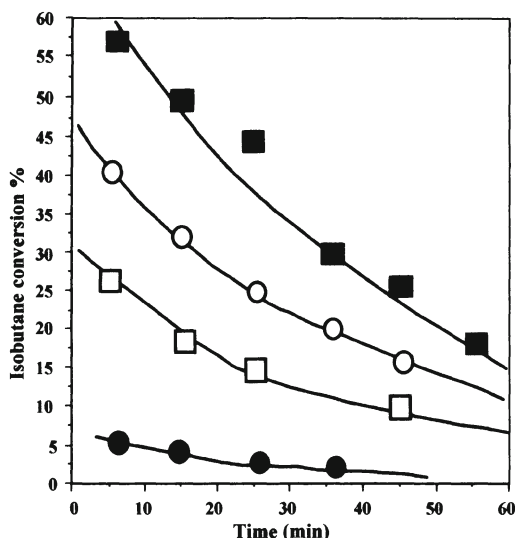


Figure 2. Isobutane conversion vs time on stream in HF-SbF<sub>5</sub> with varying initial concentrations : ■ 1.3, ○ 18.3, □ 16.0, ● 10.8 mol% SbF<sub>5</sub>.

It shows that conversion of isobutane in HF does depend on the concentration of SbF<sub>5</sub> which not only governs the acidity of the medium but also allows for the stabilization of the resultant cations.

In the concentration range of 10 to 22 mol % SbF<sub>5</sub> in HF the anions are essentially SbF<sub>6</sub><sup>-</sup> and Sb<sub>2</sub>F<sub>11</sub><sup>-</sup> in slow equilibrium.<sup>22</sup>



As the reaction proceeds, the superacidic species H<sub>3</sub>F<sub>2</sub><sup>+</sup> is progressively replaced by the carbenium (or oxocarbenium ion), HF is generated, and the acidity decreases accordingly (reaction 3). For this reason the slope of the curves decreases progressively.



When the average conversion of isobutane (based on the formation of ethylpivalate during the 1 hour experiment), is plotted as a function of the concentration of SbF<sub>5</sub> in HF, a steady and strong increase of conversion is noted when the concentration of the Lewis acid increases (Figure 3).

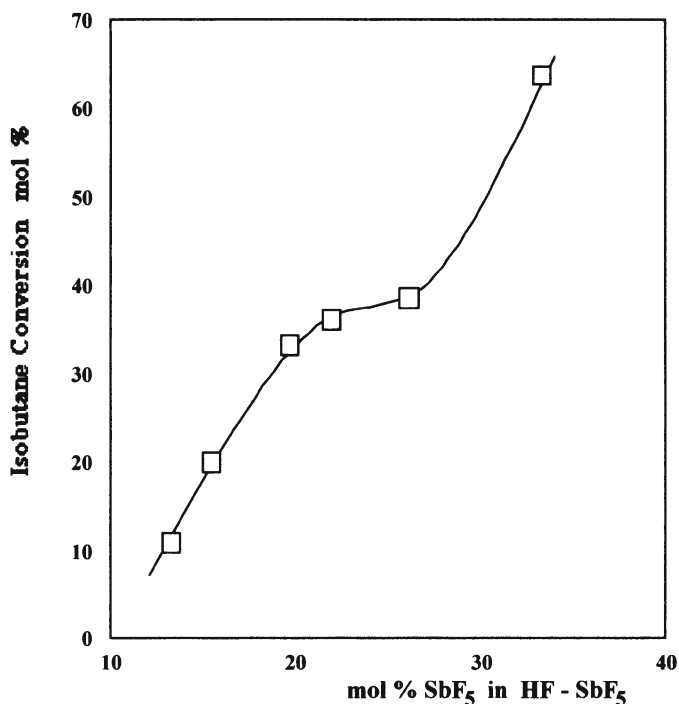


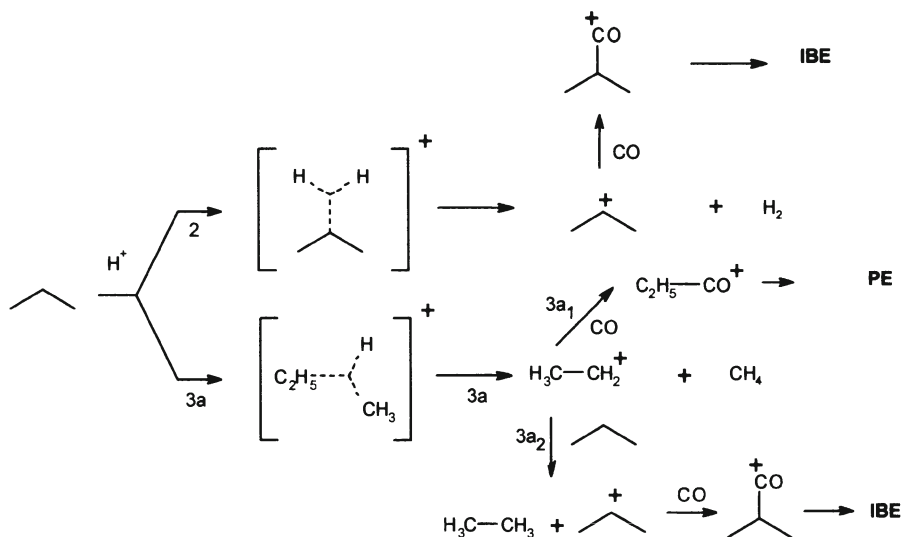
Figure 3. Dependence of the conversion of isobutane on SbF<sub>5</sub> concentration in HF ( 1 hour experiment).

## 5. Protolytic ionization of propane

Propane has no tertiary hydrogen and as the primary hydrogens are quite unreactive towards protolysis, the reaction scheme for protolysis should involve only secondary C-H bond and C-C bond protolysis. This is also what is observed when propane/CO mixture (1:3 molar ratio) is bubbled through HF:SbF<sub>5</sub> at 0°C. Analysis of the product distribution is in accord with scheme 9.

Besides hydrogen, methane and ethane, only propionic acid ethylester (PE) and isobutyric ethylesters (IBE) were observed (1:3 molar ratio). The ratio of these two esters can be drastically changed by changing the CO/C<sub>3</sub>H<sub>8</sub> ratio. When more than 50% of propane is present in the initial mixture, activation of propane occurs selectively by hydride transfer to the initially formed ethyl cation (pathway 3a). In this way isobutyryl ethyl ester can be obtained with more than 98% selectivity albeit at the expense of sacrificing one mole of propane/per

ester for the indirect activation step. Isobutyryl esters are potential starting material for methacrylic esters, important monomers for polymethacrylates.



*Scheme 9.* Protolytic activation of propane in the presence of CO in HF-SbF<sub>5</sub>.

The industrial interest in this route is at the origin of our studies of the mechanistic aspects of alkane activation in the presence of carbon monoxide [23].

A high selectivity of the reaction towards production of isobutyryl ethyl ester can also be obtained when superelectrophiles such as halocarbonyl [24] or halomethyl cations [25], are produced in the superacid medium. In this case the electrophilic attack occurs preferentially on the C-H bond despite the presence of a large excess of superacid.

Superelectrophiles have been defined by Olah [26] as "electrophiles that are further interacting with a strong Lewis or Brönsted acid". A series of these electrophiles possessing a lone pair available for Hydrogen bonding or protosolvation: COBr<sup>+</sup>, CCl<sub>3</sub><sup>+</sup>, CO, HNO<sup>+</sup> have shown a strong increase in activity in the presence of strong protic acids.

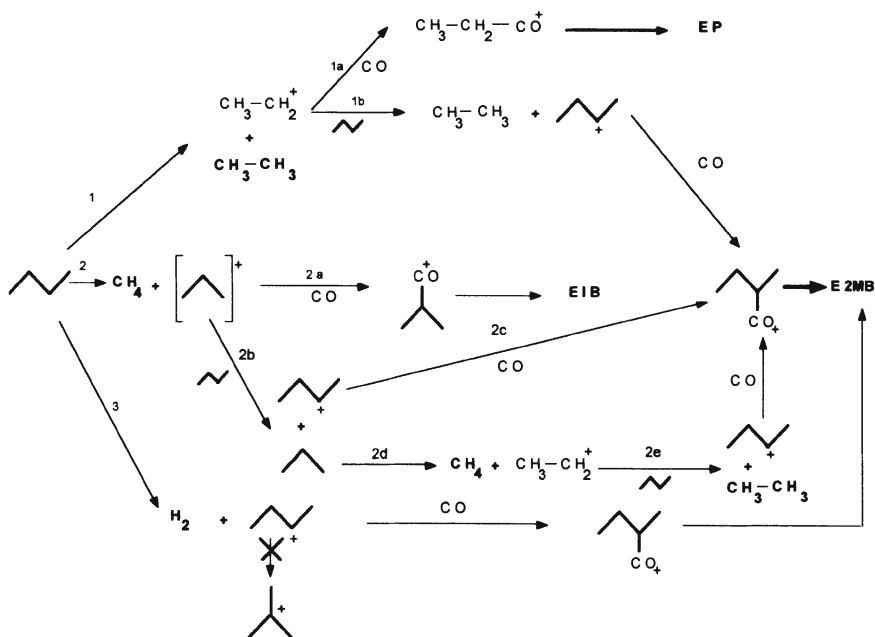
## 6. Protolytic ionization of n-butane.

Solid and liquid superacid-catalyzed isomerization of n-butane to 2-methylpropane (isobutane) has been studied extensively over the last few decades [4, 27, 28]. In part, this interest arises from the industrial importance of

the branched isomer in isobutane/butene alkylation processes yielding high octane-rated branched alkanes.

Olah has shown that n-butane was efficiently isomerized by the  $\text{HSO}_3\text{F}\text{-HF}$  (5%) superacid at room temperature. However Brouwer [29] found that, in the strong  $\text{HF}\text{-SbF}_5$ , despite substantial  $^{13}\text{C}$  label scrambling in recovered n-butane, no isomerization was observed.

When a mixture of butane/ $\text{CO}$  (3:1 molar ratio) is bubbled through  $\text{HF}\text{:SbF}_5$  (4:1 molar ratio) the product distribution between acid and gas phase is reflected in Scheme 10 .



*Scheme 10.* Protolytic activation of n-butane in the presence of CO in  $\text{HF}\text{-SbF}_5$ .

As no isobutane, and no pivalic acid ethyl ester was detected, it shows that the secondary butyl cation is very efficiently trapped by carbon monoxide under these conditions [30]. Estimations based on a detailed analysis of the product distribution are in accord with the relative rates between pathways 1, 2 and 3 as 15: 9: 1. Protolysis of a secondary C-H bond is always a minor activation step when a C-C bond can be cleaved. The production of the ethyl ester of 2-methylbutyric acid E2MB is essentially the result of indirect activation of n-butane by hydride transfer. The primary ions generated by C-C bond cleavage prove to be strong hydride abstractors despite the presence of CO when carbon monoxide is not in large excess and under pressure.



In the experiments at 0°C with a CO:RH ratio of 3 the relative rates of carbonylation (1a) versus hydride transfer (1b) to the ethyl cation was estimated to be of the order of 5 to 1. The ratio of carbonylation vs hydride transfer to the propyl cation (paths 2a or 2b) was estimated to be 9 to 1 under the same conditions. It was interesting to notice that when CO was absent during the activation step, but was added to the superacid mixture after 1 hour reaction with n-butane, a very high selectivity in pivalic acid ethyl ester was obtained. This shows that in the absence of CO, the secondary butyl ion rearranges rapidly into the tertiary ion. However as no isobutane was detected it seems that the hydride transfer from butane to the t-butyl ion is very slow under these conditions.

For higher alkanes the number of available pathways increases rapidly and the carbocation/alkane system becomes very complex. The investigation should however be possible by running the reaction under substantial pressure of CO. The hydride transfer steps could probably be avoided completely due to higher efficiency in trapping the primary ions.

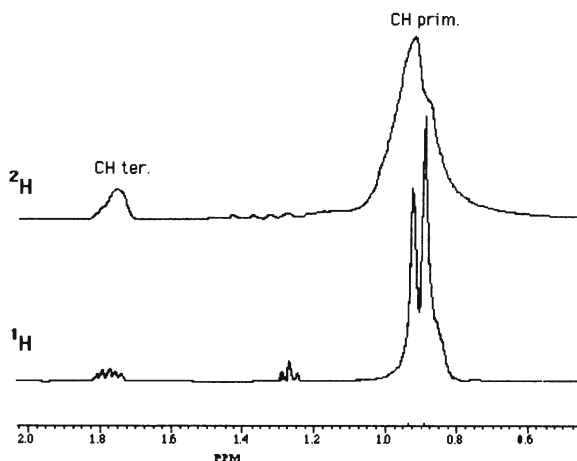


Figure 4.  $^1\text{H}$  and  $^2\text{H}$  NMR Spectra of isobutane after H/D exchange in  $\text{DF-SbF}_5$  at  $-10^\circ$  (GSHV = 250).

## 7. The reversibility of alkane protonation. Protium-Deuterium exchange between $\text{DF-SbF}_5$ and alkanes in competition with ionization.

When deuterated superacids were used, in the studies described above, it was possible to monitor the rate of reversible protonation which occurred in competition with the protolysis reaction. As often, the use of isotopic tracers is a

powerful tool for experimental determination of reaction mechanisms. It helps to show that apparently unreacted starting material has in fact undergone important transformations which, due to degenerate equilibria, can not be observed in the absence of isotopic markers.

We used this technique in the case of *n*- and isobutane activation by DF-SbF<sub>5</sub>.

a) Reversible protonation of isobutane in DF-SbF<sub>5</sub>.

When a mixture of isobutane and carbon monoxide (molar ratio RH/CO 1:3) is bubbled through 1 mL of DF-SbF<sub>5</sub> (molar ratio 7:1) during 30 minutes at a rate of 4 mL/min., the <sup>1</sup>H and <sup>2</sup>H NMR spectra (Fig.4) of the recovered isobutane (approximately 95% of the starting material) show that both the primary and the tertiary hydrogens have been exchanged for deuterons (7.4 atom % of the hydrogens in the methyl groups and 17.4 atom % of the methine). These values, which are average values for 30 minute experiments, are in line with the relative  $\sigma$ -basicity of the tertiary and primary C-H bonds.

It is interesting to note that the difference in exchange rates is rather small in comparison with the relative energies needed to ionize these two bonds. Conversion of isobutane during this time on stream, as based on hydrogen production and pivaloyl ester formation is only 4%.

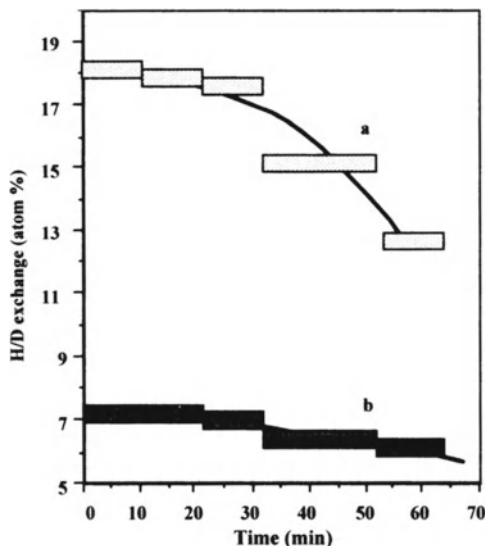
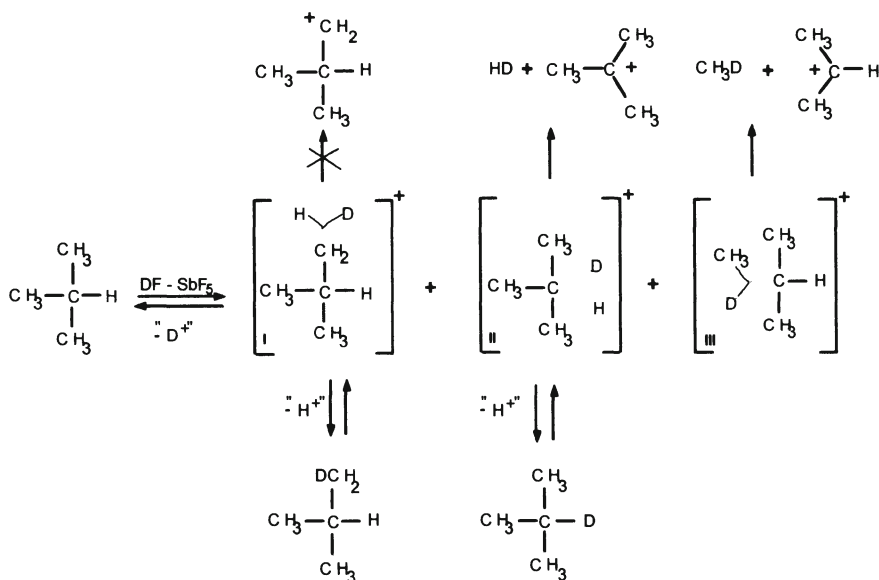


Figure 5. H/D exchange observed on the tertiary (a) and primary (b) protons of isobutane vs. time on stream in HF containing 10.8 mole % SbF<sub>5</sub>

If we compare the exchange rate of the tertiary C-H bond with the ionization rate normalized to 1 mole of isobutane we notice that, on this very reactive bond, H/D exchange is approximately 4-5 times faster than cleavage. If we take into account the total exchange for 1 mole of isobutane including the exchange of the 9 primary hydrogens ( $7.7 \times 9$ ) we notice that the total H/D exchange on isobutane amounts to 0.87 hydrogens exchanged in comparison with 0.04 mol ionized. That is a ratio of 22 to 1 for H/D exchange in comparison with ionization.

In order to check the time dependence of the exchange process, we ran a series of experiments under the same conditions as above except that isobutane was trapped at 10 minute intervals and analyzed for H/D exchange by NMR. The results plotted in Figure 5 show that the exchange rate decreases slowly with time on stream, for both primary and tertiary hydrogens. Considering the large excess of DF used in the experiment, the observed change can be rationalized by a slow decrease in acidity due to ion complexation, as described above.

The competitive protonation and ionization of isobutane in DF-SbF<sub>5</sub> can be described by the following scheme (scheme 11) :

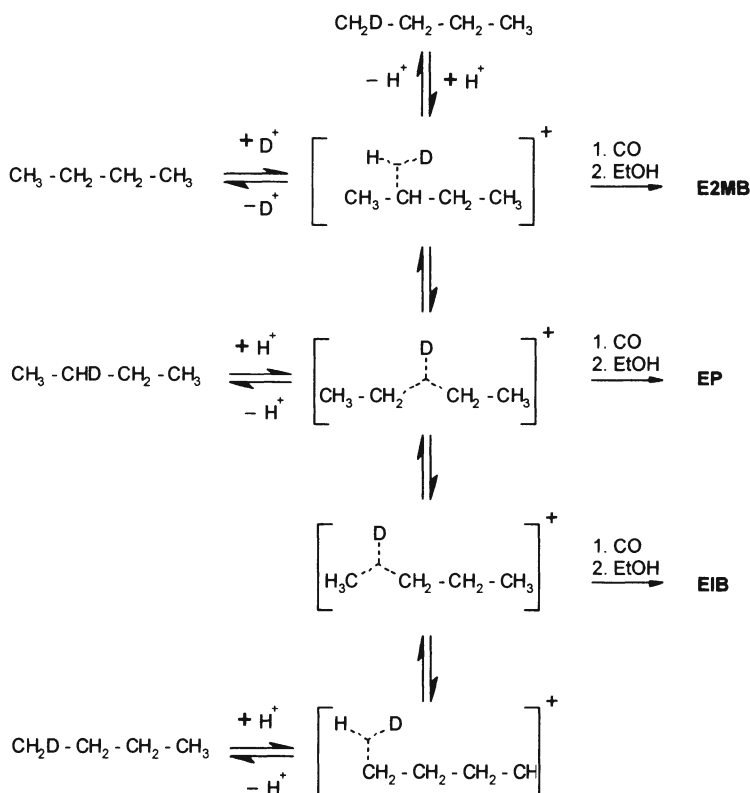


*Scheme 11.* H/D exchange vs ionization of isobutane in DF-SbF<sub>5</sub>.

Isobutane is reversibly protonated on the various sigma-bonds forming the three isomeric carbonium ions in equilibrium. The relative concentration of these pentavalent reaction intermediates depends only on the relative sigma-

basicity of the proton-accepting bond and does not reflect the ability of that bond to undergo protolytic cleavage. The fate of the carbonium ions depends on the relative energies required for the available reaction pathways : namely, deprotonation or cleavage to form a trivalent carbenium ion and a neutral species (in this case HD or deuteromethane). For this reason, ion I will only exchange protium for deuterium and ion II will give the stable t-butyl ion in competition with H/D exchange. Unfortunately, reversible protonation of C-C bonds (ion III) cannot be detected by this technique but, in accord with the higher energy needed for the formation of the 2-propylium ion in comparison with the tertiary ion, protolytic cleavage of the C-C bond is a pathway of minor importance as shown by the product distribution.

b) Reversible protonation of n-butane in DF-SbF<sub>5</sub>.



*Scheme 12.* H/D exchange vs ionization of n-butane in DF-SbF<sub>5</sub>.

When the n-butane/CO mixture (3:1 molar ratio) is bubbled at 0°C through DF-SbF<sub>5</sub> (8:1 molar ratio) at 220 mL/hour, the apparent conversion based on

recovered n-butane after 30 minutes time on stream is 15 mol %. Analysis of the recovered alkane by  $^1\text{H}$  and  $^2\text{H}$  NMR shows that 39 atom % of the methylene protons and 29 atom % of the methyl protons were exchanged for deuterium. If we take in account that n-butane has 4 secondary hydrons and 6 primary hydrons we must multiply these figures by 4 and 6 respectively in order to estimate the total amount of deuterium which entered 1 mole of n-butane. This amounts to 3.30 mole of protons exchanged in 30 minutes on stream whereas only 0.15 mol of butane were ionized. The average ratio of exchange over ionization is thus in the order of 20 to 1. Here also we notice that the rate of exchange of the secondary hydrons is faster than the primary hydrons in accord with their relative basicity. The general scheme of n-butane activation in  $\text{DF-SbF}_5$  can be presented as in Scheme 12.

### 8. Oxidative ionization of alkanes in $\text{SbF}_5$ based superacids.

In our studies on isobutane activation by  $\text{HF-SbF}_5$  we have found that the conversion of isobutane (based on recovered unreacted alkane after 1 hour) increased steadily with increasing concentration of  $\text{SbF}_5$  (Fig. 3, Fig. 6a).

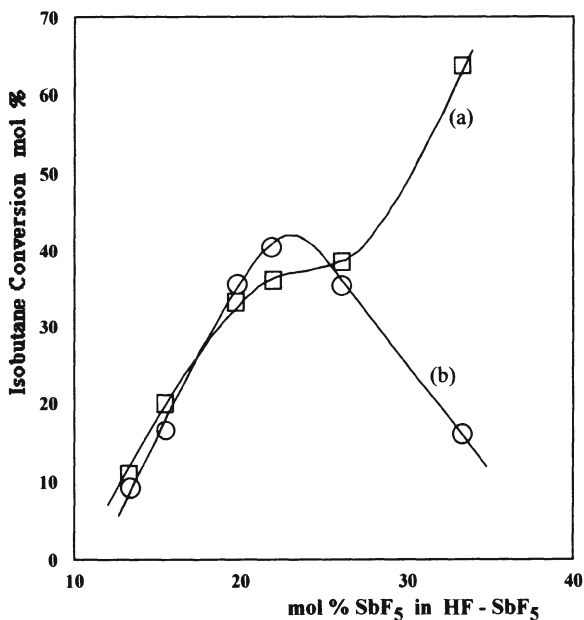


Figure 6. Isobutane conversion as based on ethylpivalate production (a) compared with hydrogen production (b).

When however, under the same conditions, the amount of  $H_2$  is measured as a function of  $SbF_5$  concentration and compared with the production of ethyl pivalate, a very different result is observed (Fig. 6b). Up to 20-25 mol %  $SbF_5$  in HF, in accord with the protolytic ionization, hydrogen production reflects roughly the conversion as based on pivalic ester production. For concentrations higher than 25 mol %  $SbF_5$  a drastic change in hydrogen production is noticed which decreases rapidly with increasing concentration in  $SbF_5$ . Simultaneously a white precipitate identified as  $SbF_3$  is produced.  $SbF_5$  is increasingly participating in the ionization with production of HF as suggested earlier by Olah.



*Scheme 13.*  $SbF_5$  reduction by a protonated alkane.

$^{19}\text{F}$  NMR studies [31] of the HF- $SbF_5$  system show that for  $SbF_5$  concentrations > 20 mol %, besides  $(\text{SbF}_5)_n\text{F}^-$  ( $n=1-4$ ) anions, a small amount of uncomplexed  $SbF_5$  was present in the superacid solution. This amount increased with increasing  $SbF_5$  concentrations.

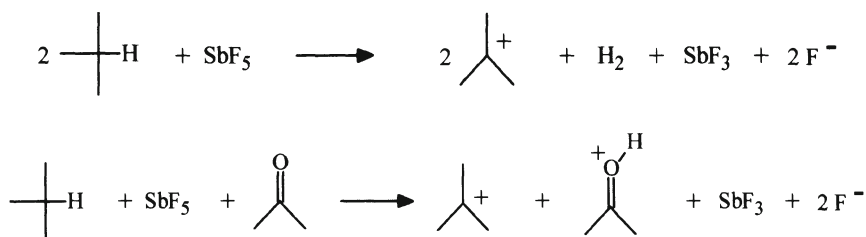
On the other hand we have shown that the upper limit of acidity of the HF- $SbF_5$  system was already reached with 20 mol %  $SbF_5$  [32].

The participation of  $SbF_5$  in the activation of isobutane was a very controversial topic for decades at the origin of which was mainly the non-stoichiometric production of hydrogen accompanying the formation of the t-butyl ion. We notice here that the reaction is stoichiometric as long as the concentration of  $SbF_5$  is low enough to act only as Lewis superacid enhancing the acidity of HF by complexation of the fluorinated conjugated bases. At higher concentrations  $SbF_5$  can participate in the activation process even without protonic assistance as we have demonstrated some years ago by using a proton trap [33].

We compared the two following experiments:

- (i) when isobutane was mixed at low temperature ( $<-30^\circ\text{C}$ ) with  $SbF_5$  in  $\text{SO}_2\text{ClF}$  solution, a stoichiometric amount of hydrogen was collected.
- (ii) when under the same experimental conditions excess acetone was added before addition of isobutane (molar ratio 3:1 isobutane), no hydrogen was produced and the  $^1\text{H}$  NMR spectrum showed the complete ionization of isobutane to the t-butyl-ion and the corresponding amount of protonated acetone.

These reactions can be written as :



The oxidation of the alkane occurs selectively on the tertiary C-H bond and generates an equivalent amount of protons and t butyl-cations. Formally the oxidoreduction process is best represented as :



In the presence of acetone the proton generated by the oxidation process is trapped by the carbonyl group and no hydrogen is formed. In the absence of acetone, the proton will attack the strongest base present, i.e. the alkane, on the tertiary C-H bond in agreement with the  $\sigma$ -bond reactivity sequence and protolytic ionization of the alkane does occur. This explains why in many cases the stoichiometric amount of hydrogen was not found.

## 9. Conclusion.

The behavior of small alkanes in liquid superacids is typical of an acid-base reaction. The first step is the reversible protonation of the alkane as shown by isotopic exchange when deuterated acids are used. It is shown that the reversible protonation is very fast in comparison with protolysis. It is essentially related to the basicity of the  $\sigma$ -bond and not to the further reactivity of the protonated  $\sigma$ -bond. The fate of the isomeric protonated alkanes which are formed in this process is kinetically controlled. It depends essentially on the energy needed to reach the next step which is the protolytic cleavage of the protonated  $\sigma$ -bond.

The use of carbon monoxide as trapping agent for the initially formed carbenium ions is a very good technique for studying the reactivity of each  $\sigma$ -bond and also to understand the mechanism of the protolytic cleavage.

## 10. References

1. Pines, H. (1981) *The Chemistry of Catalytic Hydrocarbon Conversion*; Academic Press: New York.
2. Olah, G.A. and Molnar, A. (1995) *Hydrocarbon Chemistry*, J.Wiley, New York.
3. Corma, A. (1995) *Chem. Rev.* 95, 559.
4. Olah, G.A., Prakash, S.K., and Sommer, J. (1985) *Superacids*, J. Wiley, New York.
5. a) Yamagushi, T. (1990) *Applied Catal.*, 1, 61. b) Song, K. and Sayari, A. (1996) *Catal. Rev. Sci. Eng.*, 38, 329.
6. Chaumette, and Torck, B. (1994) *Rev. Inst. Français du Pétrole*, 49, 641.
7. Hogeveen, H. and Bickel, G.F. (1967) *J. Chem. Soc., Chem. Commun.* 635.
8. Olah, G.; Schlosberg, R.H. (1968) *J. Am. Chem. Soc.* 90, 2726.
9. Olah, G.A., Halpern, Y., Shen, J., and Mo, Y.K. (1971) *J. Am. Chem. Soc.* 93, 1251.
10. Olah, G.A. (1973) *Angew. Chem. Int. Ed.* 12, 173.
11. Olah, G.A., Prakash, S.K., William, R.E., Field I.D., and Wade, K. (1987) *HyperCarbon Chemistry*, Wiley Interscience, New York.
12. In october 1994 the Swedish Royal Academy of Sciences awarded the Nobel Price to George Olah (USC, Los Angeles) for his contribution to carbocation chemistry.
13. Sommer, J. and Bukala, J. (1993) *Acc. Chem. Res.* 26, 370.
14. Olah, G.A., Klopman, G., and Schlosberg, R.H. (1969) *J. Am. Chem. Soc.* 91, 3261.
15. Hogeveen, H. and Gaasbeck, C.J. (1968) *Rec. Trav. Chim. Pays-Bas*, 97, 319.
16. (a) Otvos, J.W., Stevenson, D.P., Wagner, C.D., and Beeck, O. (1951) *J. Am. Chem. Soc.* 73, 5741-5746. (b) Stevenson, D.P., Wagner, C.D., Beeck, O., and Otvos, J.W. (1952) *J. Am. Chem. Soc.* 74, 3269-3282.
17. (a) Sommer, J., Hachoumy, M., Garin, F., and Barthomeuf, D. (1994) *J. Am. Chem. Soc.* 116, 5491. (b) Sommer, J., Hachoumy, M., Garin, F., Barthomeuf, D., and Vadrine, J. (1995) *J. Am. Chem. Soc.* 117, 1135.
18. (a) Kramer, G.J., Van Santen, R.A., Emeis, C.A., and Novak, A.K. (1993) *Nature*, 363. (b) Kazanski, V.B., Fresh, M.V., and Van Santen, R.A. (1994) *Catal. Lett.* 28, 211. (c) Blaskowski, S.R., Nascimento, M.A.C., and Van Santen, R.A. (1996) *J. Phys Chem.* 100, 3463. (d) Lercher, J.A., Van Santen, R.A., and Vinek, H. (1995) *Catalysis Letters* 31, 440. (e) Kramer, G.J. and VanSanten, R.A. (1995) *J. Am. Chem. Soc.* 117, 1766.
19. (a) Collins, S.J. and O'Malley, P.J. (1995) *Chem. Phys. Letters* 246, 555. (b) Collins, S.J. and O'Malley, P.J. (1996) *J. Chem. Soc., Faraday Trans.*, 92, 4347.



20. (a) Mota, C.J.A., Esteves, P.M., and de Amorim, M.B. (1996) *J. Phys. Chem.* 100 , 12418. (b) Mota, C.J.A., Esteves, P.M., Ramirez-Solis, A. and Hernandez-Lamonedá, R. (1997) *J. Am. Chem. Soc.* 119, in press.
21. Sommer, J., Hachoumy, M., Jost R., and Bukala, J.. (1997) *J. Am. Chem. Soc.*, 119, 3274.
22. Gillespie, R.J. and Peel, T.E. (1972) *Adv. Phys. Org. Chem.* 9, 1.
23. (a) Delavarenne, S., Fauconet, M., Simon, M., and Sommer, J. *Eur. Pat.* 270398, October 22, 1987. (b) Delavarenne, S. et al. *Eur. Pat.* 272945, October 22, 1987.
24. (a) Delavarenne, S., Simon, M., Fauconet, M., and Sommer, J. (1989) *J. Am. Chem. Soc.* 111, 383. (b) Bukala, J., Sommer, J., and Culmann, J.-C. (1992) *J. Chem. Soc. Chem. Commun.*, 481.
25. Sommer, J., Culmann, J.-C., and Simon, M. (1990) *J. Chem. Soc. Chem. Commun.*, 4057.
26. Olah, G.A. (1993) *Angew. Chem., Int. Ed. Engl.*, 32, 767.
27. Olah, G.A., Farooq, A., Husain, A., Ding, N., Trivedi, N.J., and Olah, J.A. (1991) *Catal. Letters*, 10, 239.
28. Gonzalez M.R., Fogash, K.B., Koba, J.M., and Dumesic, J.A. (1997) *Catalysis Today*, 33, 303.
29. Brouwer, D.M. (1968) *Rec. Trav. Chim. Pays-Bas*, 87, 1435.
30. Sommer, J., Hachoumy, M., and Bukala, J. (1996) *Rev. Chem.Intermed.*, 22, 753.
31. a) Jost, R., and Sommer, J.; unpublished results. b) Fauconet, M. (1987) PhD Thesis, Univ. Louis Pasteur, Strasbourg (France).
32. a) Touiti, D., Jost, R., and Sommer, J. (1986) *J. Chem. Soc. Perkin II*, 1793. b) Jost, R., and Sommer, J. (1988) *Rev. Chem.Intermed.*, 9, 171 .
33. Culmann, J.-C. and Sommer, J. (1990) *J. Am. Chem. Soc.* 112, 4057.

# NEW PROCESSES FOR CARBON-CARBON BOND ACTIVATION CATALYSED BY OXIDE SUPPORTED SURFACE ORGANOMETALLIC COMPLEXES

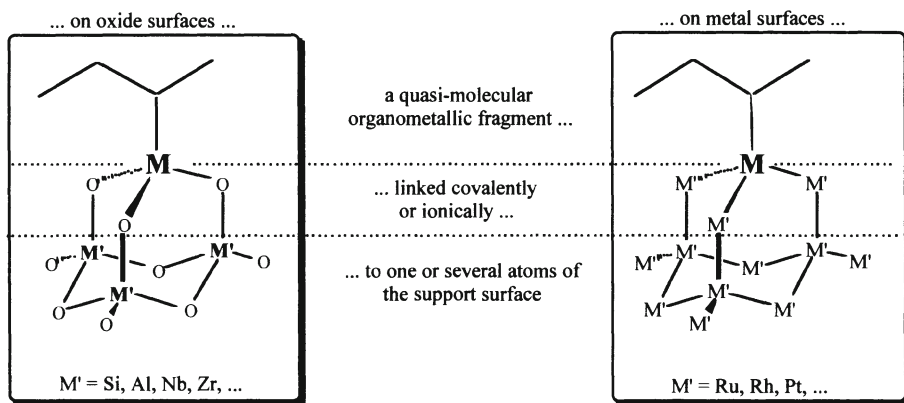
GERALD P. NICCOLAI AND JEAN-MARIE BASSET  
*Laboratoire de Chimie Organométallique de Surface*  
43, boulevard du 11 novembre 1918  
69616 Villeurbanne cédex FRANCE

## 1. Introduction to Surface Organometallic Chemistry

The expanding field surface organometallic chemistry (referred to as SOMC, or by its French acronym, COMS) offers new possibilities to heterogeneous catalysis. The basic philosophy of this new area of heterogeneous catalysis is based on the concept that the supported catalyst is a kind of molecular entity. Ideally, one ceases to speak of "the immobilization of a catalyst" or of "the modification of a surface" but rather one considers the entire continuum - support, metal, and ligands - as a quasi-molecular species responding to both the fundamental rules derived from organometallic chemistry and to the rules of surface science. Surface organometallic chemistry preserves some of the advantages of traditional supported catalysis such as the ease of separation of the catalyst from the substrate/product and the heightened stability with respect to homogeneous analogs. As with traditional techniques, one can vary such parameters as the surface area, porosity, and electrophilicity of the support, and the identity of the metal. Surface organometallic chemistry offers much more precise control of other metal-centered factors such as the oxidation state and coordination geometry of the catalytic site. The stoichiometric nature of COMS synthesis often leads to catalytic systems with very high percentages of relatively well defined active catalytic sites.

The surface organometallic complex is represented schematically below. An organometallic fragment, bearing one or many "traditional" ligands is bound to the surface "ligand" by one or several ionic or covalent bonds. Given this construct, one has a number of parameters available when considering the type of system best adapted to a particular catalytic application, notably, the choice of metal (identity, oxidation state), ligands (number, basicity, lability, hapticity), the type of ligand-surface bond (ionic, dative, covalent, van der Waals) and the surface (a metal surface, an amorphous or crystalline inorganic oxide, a zeolite).

### Schematic Model of Surface Supported Organometallic Complex



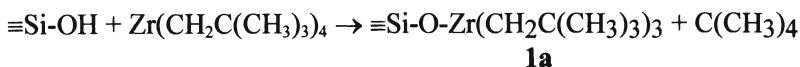
Surface organometallic chemistry has the subject of a number of reviews.[1 - 5]. In this report we wish to concentrate on the catalytic activation of alkane carbon-carbon bonds by oxide supported early transition metal hydride complexes. Specifically, oxide supported group 4 hydride complexes have been shown to be catalysts for the low temperature catalytic hydrogenolysis of alkanes, a reaction for which we have conducted some mechanistic studies and for which we suggest an initial application, the hydrogenolytic degradation of polyolefins to lighter alkanes. A second major reaction expanded here is the alkanes metathesis (or disproportionation) reaction catalyzed by silica supported tantalum(III) hydride. This reaction permits the conversion of  $C_n$  alkanes in the absence of hydrogen to  $C_{n-i}$  and  $C_{n+i}$  alkanes.

#### 1.1 SILICA SUPPORTED GROUP 4 METAL HYDRIDE COMPLEXES: HYDROGENOLYSIS AND ISOMERISATION OF ALKANES

The utility of surface organometallic chemistry is to be seen in our recent work on the low temperature hydrogenolysis of alkanes by silica supported zirconium hydride. A simple organometallic reaction was used to produce an initial surface organometallic complex, which was then cleanly transformed to a second complex. This complex, a sterically unhindered zirconium monohydride, was strongly bound to the surface by several zirconium-oxygen bonds, and thus could not undergo intermolecular decomposition. The result was a highly reactive complex capable of the room temperature activation of alkane carbon-hydrogen bonds and low temperature activation of alkane carbon-carbon bonds.

### 1.1.1 Synthesis and Characterization

Sublimation of  $\text{Zr}(\text{CH}_2\text{C}(\text{CH}_3)_3)_4$  silica partially dehydroxylated at  $500^\circ\text{C}$  ( $\text{silica}_{(500)}$ ) results in the electrophilic cleavage of an Zr-C bond by surface protons, with formation of a grafted species described as  $\equiv\text{Si-O-Zr}(\text{CH}_2\text{C}(\text{CH}_3)_3)_3$  (**1a**) [6]

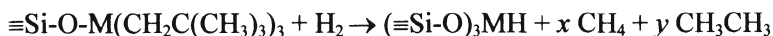


Thus the intensity of the  $\nu(\text{OH})$  vibration at  $3747\text{ cm}^{-1}$  attributed to isolated surface silanols disappears during the reaction, and  $\nu(\text{C-H})$ ,  $\delta(\text{CH}_2)$  and  $\delta(\text{CH}_3)$  bands appear which are stable to prolonged exposure to dynamic vacuum. The surface species has also been characterized by  $^{13}\text{C}$  CP-MAS NMR (33.9 ppm,  $\text{CH}_2\text{C}(\text{CH}_3)_3$ ) and elemental analysis, which shows that during the reaction exactly one equivalent of neopentane is evolved and that, on the surface, 3 alkyl groups remain after grafting. This stoichiometry was confirmed by a number of other chemical assays, for example, reaction of the surface complex with oxygen and extraction of the resultant complex with HCl leads to the formation of three equivalents of neopentanol.

EXAFS analysis [7] of **1a** showed that surface zirconium atoms are surrounded by, on average, 3.2 carbon atoms at  $2.219(4)\text{ \AA}$  and 1.1 oxygen atom at  $1.956(3)$ , further confirming our structural assignment.

Analogous methods have been used to synthesize and characterize  $\equiv\text{Si-O-Hf}(\text{CH}_2\text{C}(\text{CH}_3)_3)_3$  [**8**] **1b** and  $\equiv\text{Si-O-Ti}(\text{CH}_2\text{C}(\text{CH}_3)_3)_3$  [**9**] **1c**.

The reaction of these species with dry hydrogen (450 torr,  $150^\circ\text{C}$ ) leads to hydrogenolysis of the M-C bonds with formation of a surface supported hydride species,  $(\equiv\text{SiO})_3\text{MH}$  [**2a**,  $\text{M}=\text{Zr}$ , **2b**,  $\text{M}=\text{Hf}$ , **2c**,  $\text{M}=\text{Ti}$ , with simultaneous formation of a surface  $>\text{SiH}_2$  fragments, methane and ethane. [7 - 10] This



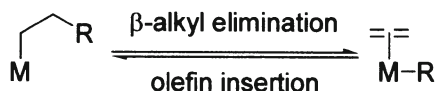
reaction can be followed by infrared: the  $\nu(\text{C-H})$ ,  $\delta(\text{CH}_2)$  and  $\delta(\text{CH}_3)$  bands disappear of bands associated with the surface  $\text{SiH}_2$  groups ( $2263$  and  $2196\text{ cm}^{-1}$ ) and M-H groups (**2a**,  $1625\text{ cm}^{-1}$ , **2a**,  $1701\text{ cm}^{-1}$ , **2c**,  $1795\text{ cm}^{-1}$ ) are observed. In the case of zirconium, **2a**, the hydride ligand has been observed in the  $^1\text{H}$  NMR ( $\delta$  10) and EXAFS has shown that the zirconium is coordinated to three oxygens at a distance of  $1.945(3)\text{ \AA}$  [7]. Again, a large number of chemical test reactions have been used together with elemental analysis to confirm the stoichiometry of one hydride per metal.

### 1.1.2 Zirconium and Hafnium Hydrides: Hydrogenolysis

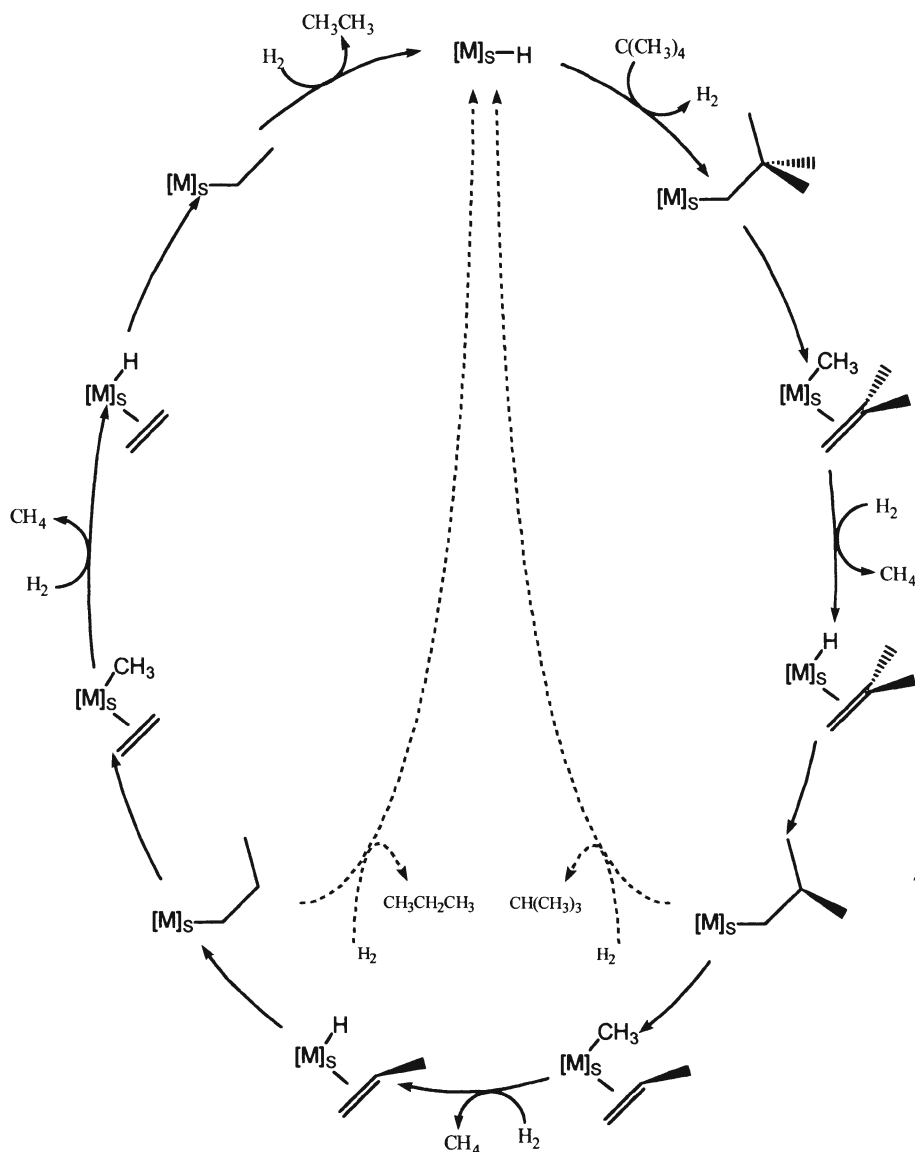
It is perhaps not surprising that the surface hydride complexes **2** are capable of the low temperature activation of simple alkane carbon-carbon bonds. The grafted hydrides ( $\equiv\text{SiO}$ )<sub>3</sub>MH have a formal valence electron count of eight and are thus expected to be very electrophilic. We consider that the silica surface occupies one half of the coordination sphere of the metal (i.e. has a cone angle of 180 °), but the other coordination hemisphere bears only the hydride ligand and thus should be sterically very accessible to reactants. These properties are undoubtedly responsible for the extraordinary reactivity of the zirconium hydride complex toward the inactivated C-H bonds of CH<sub>4</sub> (100°C), propane and cyclooctane (25°C) [11]. The reaction is believed to be one of  $\sigma$ -bond metathesis, well known in homogeneous chemistry. The further observation of catalytic cleavage of carbon-carbon bonds, at room temperature in the case of hafnium, was certainly unexpected.

Indeed, the reaction was first observed in the synthesis of **2a**. As mentioned above, when **1a** is heated under dry hydrogen to 150 °C for three hours, **2a** is formed together with nine equivalents of methane and three equivalents of ethane. The formation of methane and ethane rather than neopentane was a clear evidence of hydrogenolysis under the synthetic conditions. The hydrogenolysis of neopentane, isobutane, and n-butane catalyzed by **2a** [12] and **2b** [13] has since been thoroughly studied. It was observed that the reaction of neopentane occurred by step-wise formation of at first isobutane and methane, then conversion of the former to a second equivalent of methane and propane which is further converted to ethane and a third equivalent of methane. The carbon-carbon bond of ethane cannot be cleaved by  $\beta$ -methyl elimination because a surface metal-ethyl fragment has no methyl group in the  $\beta$ -position.

The  $\beta$ -alkyl elimination step can be considered as analogous to the more familiar  $\beta$ -hydride elimination in which a carbon-carbon bond is broken instead of a carbon-hydrogen bond. Note that this reaction is the microscopic reverse of the propagation step in the mechanism of the Ziegler-Natta polymerization of olefins.



The  $\beta$ -alkyl elimination reaction has been indicated in a number of studies of aluminum alkyls [14] in high-valent early transition metal systems [15] and low-valent late transition metal systems [16]. In particular, Horton directly observed the reaction at temperatures well below room temperature. The reaction step is of great interest due evidence that under certain conditions it

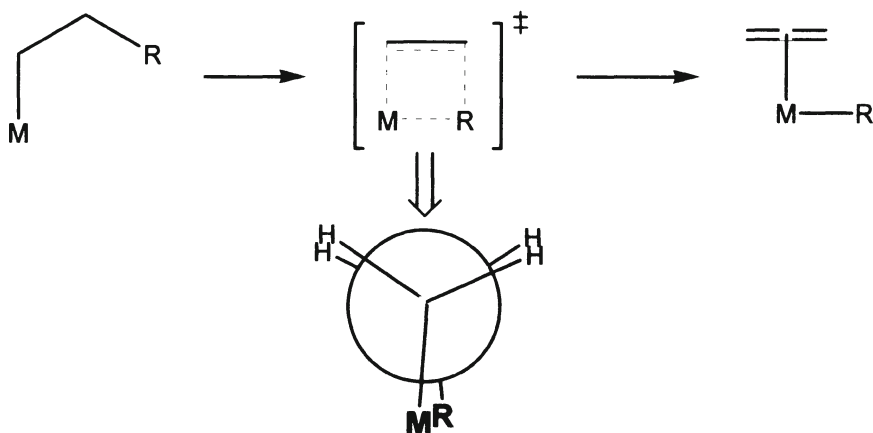


It was thus logical to attempt the hydrogenolytic degradation of polymers catalyzed by surface supported group 4 metal hydrides. In particular, it was found that a silica-alumina supported analog of **1a** was capable of polymerizing ethylene and propylene [18]. Furthermore, when the resultant polymer/surface

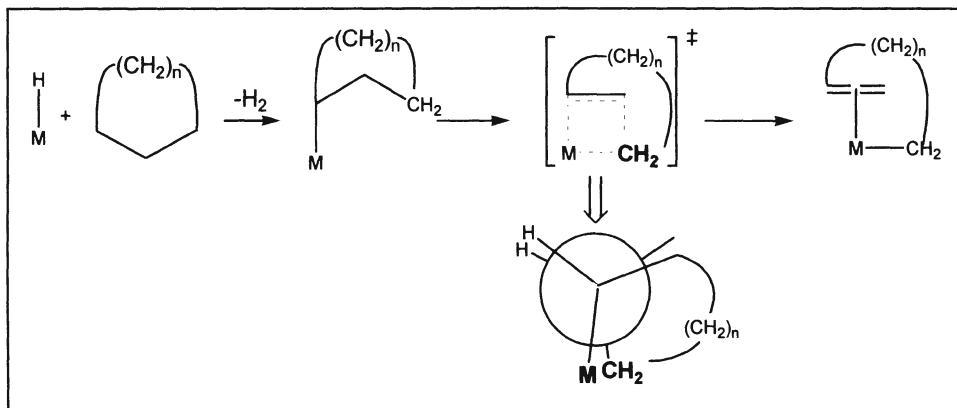
complex was heated under hydrogen, the polymer was converted to light alkanes and the zirconium was converted to a hydride of the type  $(\equiv\text{SiO})_3\text{ZrH}$ . The latter was also an active catalyst for the polymerization of olefins. The hydride supported on silica-alumina was prepared directly from  $1\mathbf{a}\bullet\text{SiO}_2\text{-Al}_2\text{O}_3$  and this latter hydride was used for the hydrogenolytic degradation of polymers [19].

Initially, for reasons of catalyst stability we studied only polymers that would melt below 200 °C, essentially polyethylenes, polypropylenes, and polystyrenes. This serious limitation could be resolved if we could find a solvent for these polymers that was not in and of itself reactive toward the catalyst/hydrogen mixture. It was from a study of purely mechanistic interest that we found the solution to this problem.

During our studies of the hydrogenolysis of n-butane, particularly catalyzed by  $2\mathbf{b}$ , we found that the carbon-carbon cleavage step could involve the transfer of ethyl groups, thus  $\beta$ -alkyl elimination. If one considers that this mechanism, like the  $\beta$ -hydride elimination reaction, passes through a four-center intermediate in which the metal-C( $\alpha$ ) and C( $\beta$ )-C( $\gamma$ ) bonds are broken in a concerted manner, the reaction must pass through an intermediate where the



four atoms involved are coplanar. Now, given a cycloalkyl-metal fragment, it is clear that the accessibility of this intermediate will be determined by the size of the cycloalkyl ring, that is by the length of the carbon chain connecting the  $\alpha$ -carbon to the nominal  $\gamma$ -carbon. Examination of simple ball-and-stick structural models makes it clear that cyclopentyl- and cyclohexyl-metal fragments should not undergo this bond breaking reaction whereas cyclooctyl-metal fragments certainly should. The cycloheptyl-metal model can be easily manipulated into a



configuration in which the  $M-C(\alpha)-C(\beta)-C(\gamma)$  torsion angle is less than 10 degrees but not planar, thus we considered this case borderline.

Indeed, it was found that, in effect the carbon-carbon bonds of cyclopentane and cyclohexane were not cleaved when heated in the presence of **2a** or **2b**, neither in the presence nor the absence of hydrogen [8, 20]. Cycloheptane and cyclooctane reacted to form linear  $C_n$  and lower alkanes as well as cyclohexanes and substituted cyclohexanes. Thus we knew that the solvent must be composed only of  $C_5$  or  $C_6$  cycles, but also should have a low vapor pressure to permit the use of simple glass reactors. The solvent chosen was the mixture cis-/trans-decalin and the results were satisfactory [19].

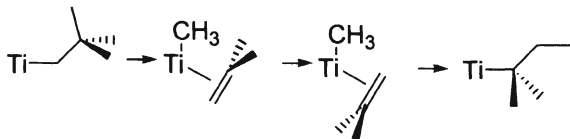
### 1.1.3 Titanium Hydride: Hydroisomerisation

It was noted that during the formation of **2c** methane and ethane were not formed in a 3:1 ratio, but rather in a 1:1 ratio. Detailed studies on the hydrogenolysis of neopentane and isobutane catalyzed by **2c** have permitted us to demonstrate that this result was due to the isomerization of neopentane during the hydrogenolysis cycle [9].

In the case of neopentane, at low conversion methane, isobutane, and n-butane are primary products. Although isopentane was not observed, the presence and importance of n-butane early in the reaction was a clear indication of carbon skeletal rearrangement prior to the formation of products. Furthermore, propane and ethane were initially formed in a 1:1 ratio which can also be considered as the signature of the isomerization of surface neopentyl fragments to isopentyl fragments prior to product formation. A similar result was obtained in the reaction of isobutane with hydrogen at 150 °C. Ethane was clearly a primary product, the implication being that the initially formed surface isobutyl fragment has rearranged to an n-butyl fragment. In this case, the  $C_4$  isomerization product n-butane was observed in significant quantities and the selectivity for this product increased at lower conversion, suggesting that it is indeed a primary product (although a minor one).



The skeletal alkane isomerization is not difficult to explain. Following an initial step of C-H bond activation the surface alkyl fragment can undergo  $\beta$ -methyl elimination. In the case of titanium, the intermediate metal-alkyl-olefin complex persists long enough (relative to olefin rotation) to undergo reinsertion of the rotated olefin into the metal-carbon bond. This isomerization step is illustrated for the neopentyl fragment.



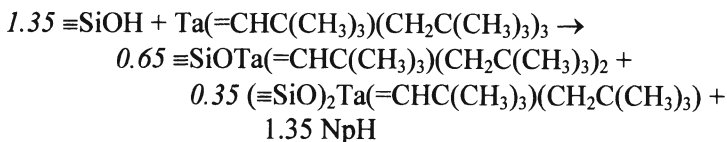
Thus the remarkable activity of these surface complexes with respect to carbon-carbon bonds is thus more interesting given the possibility of light hydrocarbon isomerization at very mild temperatures.

## 1.2 SILICA SUPPORTED TANTALUM METAL HYDRIDE : ALKANE METATHESIS

An analogous chemistry has been studied for complexes of tantalum leading to a number of surprising new reactions. We were able to synthesize and characterize the first clearly defined surface organometallic carbene complex. This synthesis was accompanied by the observation of a new grafting mechanism involving the addition of surface silanols across a tantalum carbon double bond. A tantalum hydride derived from the surface carbene products has been fully characterized and has been shown to catalyze the metathesis or disproportionation of simple alkanes.

### 1.2.1 Synthesis and Characterization

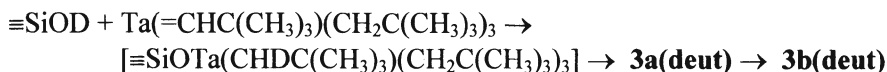
The carbene,  $\text{Ta}(=\text{CHC}(\text{CH}_3)_3)(\text{CH}_2\text{C}(\text{CH}_3)_3)_3$  was sublimed on to the surface of a silica<sub>(500)</sub> leading to a mixture of two carbenes, one bound by one siloxy ligand to the silica surface,  $\equiv\text{SiOTa}(=\text{CHC}(\text{CH}_3)_3)(\text{CH}_2\text{C}(\text{CH}_3)_3)_2$ , **3a**, and the other bound by two siloxy ligands,  $(\equiv\text{SiO})_2\text{Ta}(=\text{CHC}(\text{CH}_3)_3)(\text{CH}_2\text{C}(\text{CH}_3)_3)$ , **3b**, in a



ratio of 2:1 [21]. These are the first examples of fully and well characterized surface supported carbene species. In the infrared, the results are essentially

identical to those observed for the group 4 metals. It was necessary to develop a series of chemical tests in order to confirm the stoichiometry of the complex mixture. The average Ta/C<sub>5</sub> stoichiometry is derived, as for the group 4 metals, by a series of chemical assays (hydrolysis, hydrogenolysis, partial oxidation). The pseudo-Wittig reaction between **3** and acetone lead to the formation of exactly one equivalent of the expected olefin, (CH<sub>3</sub>)<sub>2</sub>C=CHC(CH<sub>3</sub>)<sub>3</sub>, suggesting that on average there was one carbene per tantalum.

When the reaction of Ta(=CHC(CH<sub>3</sub>)<sub>3</sub>)(CH<sub>2</sub>C(CH<sub>3</sub>)<sub>3</sub>)<sub>3</sub> was performed on a deuterated silica, deuterium was incorporated in the resulting surface complex (**3d**). This observation was confirmed by 1) the presence of neopentane-d<sup>1</sup> and neopentane-d<sup>2</sup> among the gaseous products of the reaction 2) the presence of neopentane-d<sup>3</sup> among the products of deuterolysis 3) the partial deuteration of the olefin product of the reaction of the surface complex with acetone. Statistical modeling of the isotopic distributions of these reaction products permit the suggestion of a mechanism of grafting in which the initial step is the addition of the silanol SiO-D bond across the tantalum-carbon double bond followed by α-hydride(deutride) elimination leading to the surface carbene products.



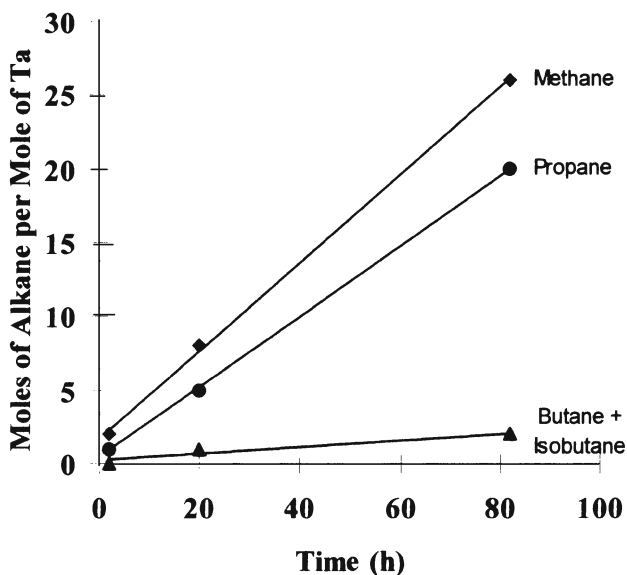
The reaction of the mixture **3** with dry hydrogen at 200 °C for three hours leads to the formation of silica supported tantalum(III) hydride, (≡SiO)<sub>2</sub>TaH, **4** [22]. In the infrared spectrum, the disappearance of the bands associated with the ν(C-H), δ(CH<sub>2</sub>) and δ(CH<sub>3</sub>) bands of complex **3** is accompanied by the appearance of ν(Si-H) bands at 2215 and 2270 cm<sup>-1</sup> and ν(Ta-H) bands around 1800 cm<sup>-1</sup>. These assignments were confirmed by reversible deuteration of TaH with deuterium gas. Further characterization was accomplished by EXAFS, KOH titration of silanes, and various chemical reactions (deuterolysis, reaction with CH<sub>3</sub>I, reaction with hydrocarbons, reaction with ketones).

### 1.2.2 Tantalum Hydride: Alkane Metathesis

Paraffins, particularly methane and light alkanes, constitute an abundant yet low-value feedstock. Light alkanes would be very valuable if they could be easily transformed to higher molecular weight hydrocarbons. We have recently reported such a conversion which we have called "alkane metathesis" by analogy with the olefin metathesis reaction [23]. By this thermoneutral reaction, carbon-carbon and carbon-hydrogen bonds seem to be reversibly broken and formed allowing one to unselectively isomerize C<sub>n</sub> alkanes to C<sub>n+</sub> and C<sub>n-</sub> alkanes.

The difference between the catalytic action of the tantalum system and the groups 4 hydrides is clearly demonstrated by the reactivity vis-a-vis ethane. When ethane is heated to 150 °C in the presence of **4** (800 mol CH<sub>3</sub>CH<sub>3</sub>/mol Ta) one notes the apparition of principally methane and propane but also traces of n-butane and isobutane (n/iso = 4).

### Metathesis of Ethane at 150 °C



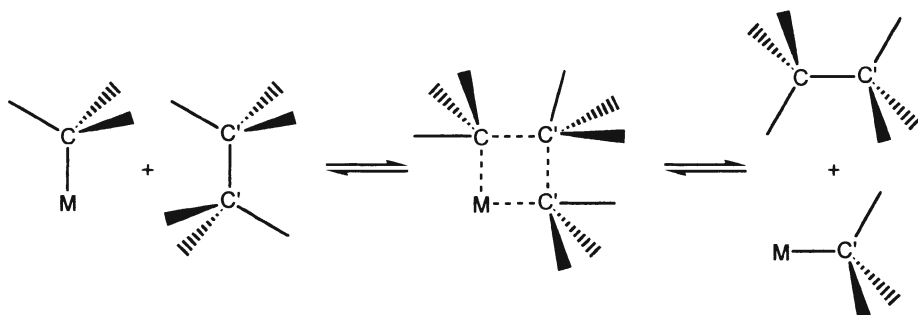
The experiment was repeated with <sup>13</sup>C-monolabeled ethane. Nonlabelled, monolabelled, dilabelled, and trilabelled propane were all observed (5:44:43:8) which clearly demonstrates the cleavage of the <sup>12</sup>C-<sup>13</sup>C bond of ethane and redistribution of the <sup>13</sup>C atoms into the propane product.

When higher alkanes were submitted to the same treatment, several higher and lower homologues were produced due to the presence of a larger number of different C-H and C-C bonds in the substrate. For example, the metathesis of propane yielded mainly n-butane and isobutane (n/iso = 4) together with ethane but also produced both higher and lower homologues. This suggests that the transfer of methyl fragments is more facile than the transfer of longer chains. Secondary reactions would account for some but not all of the higher and lower homologues.

Notable exceptions to this reaction are methane and neopentane. The exception of methane is particularly disappointing given the extraordinary efforts made in the field of methane homologation. In this case it may be

attributed to the low concentration of methane at the oxide surface at the low (<1 atm) pressures studied. The case of neopentane is perhaps related to steric factors.

During the reaction, in situ infrared spectroscopy shows no **4** is present but rather surface tantalum-alkyl. Our first speculative mechanistic hypothesis for this reaction involves a reaction step analogous to that of  $\sigma$ -bond metathetic C-C bond activation in which the alkane C-C bond directly approaches a surface C-C bond and transfer takes place via a four-center intermediate.



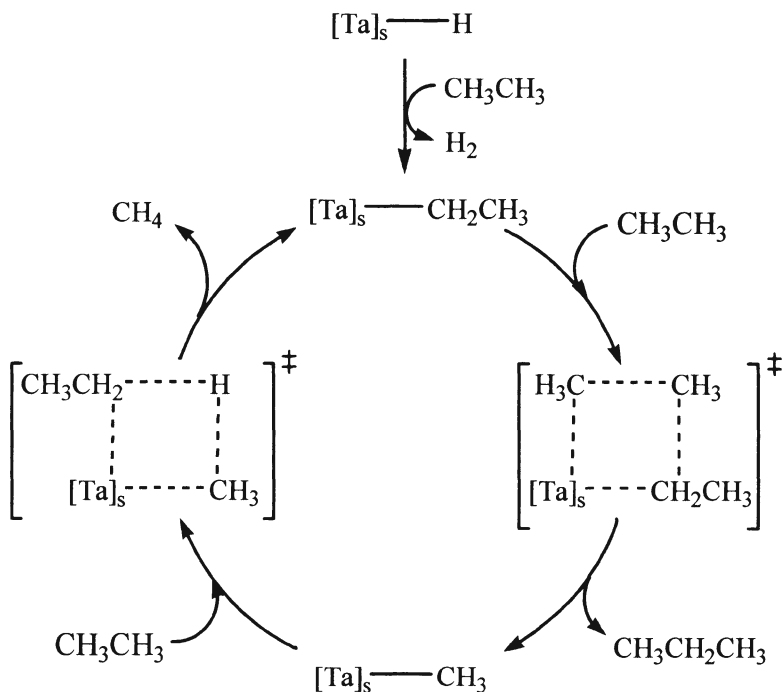
Given the possibility of such an intermediate step we write a propagation mechanism in which **4** reacts with an alkane (ethane shown in scheme) to produce the active species. A carbon-carbon bond of an incoming substrate molecule is then cleaved simultaneously with the formation of a new tantalum-carbon bond via a four center  $\sigma$ -bond metathesis intermediate. A second molecule of substrate approaches, this time presenting a carbon-hydrogen bond leading to the generation of a new alkane (methane in this case) and the original metal-alkyl intermediate.

Several other mechanisms of carbon-carbon bond cleavage are under consideration. The reaction could proceed by an oxidative addition of an alkane C-C bond of a metal alkyl followed by reductive elimination of a new alkane. From an initial metal-alkyl fragment, carbene deinsertion could cleave the carbon-carbon bond, followed by  $\sigma$ -metathesis leading to the lower alkane and an alkyl-metal-carbene species, then carbene insertion into the metal-alkyl bond and  $\sigma$ -metathesis leading to the heavier alkane and regenerating the initial metal-alkyl species.

The importance of steric considerations in product distribution is also demonstrated in the metathesis of isobutane. The initial C-H bond activation reaction step can produce either a surface isobutyl fragment or a surface tert-butyl fragment. Second step  $\sigma$ -bond metathesis from a tert-butyl intermediate would produce neopentane, a product which is not observed. Substantial amounts of isopentane is however observed, implying that either the C-H bond

activation step or the carbon-carbon bond cleavage step is hindered by the crowding around the tertiary carbon of isobutane.

Preliminary studies indicate that this reaction may also be possible with titanium, tungsten and chromium surface hydride complexes.



### 1.3 CONCLUSIONS

We have reported that surface supported early transition metal hydride complexes catalyze a variety of carbon-carbon bond cleavage reactions under very moderate conditions of temperature and pressure. It is the high electrophilicity together with the coordinative unsaturation of these complexes that permits this remarkable reactivity, and stable complexes having these properties are easily synthesized by surface organometallic chemistry.

Future studies on these and related complexes will seek to discover new reactions, applications of known reaction, methods of catalyst regeneration, and new catalysts stable with respect to heteroatom substituted substrates.

## 2. References

1. Basset, J.-M.; Candy, J.-P.; Choplin, A.; Didillon, B.; Quignard, F.; Theolier, A. in *Perspectives in Catalysis*; Thomas, J. A. and Zamaraev, K. I.; eds.; Blackwell Scientific: Oxford, 1992, pp 125-145.
2. Scott, S. L.; Basset, J.-M. *J. Mol. Catal.* **1994**, *86*, 5-22.
3. Basset, J.-M.; Candy, J.-P.; Choplin, A.; Nedez, C.; Quignard, F.; Santini, C. C.; Theolier, A. *Materials Chemistry and Physics* **1991**, *29*, 5.
4. Scott, S. L.; Basset, J.-M.; Quignard, F.; Niccolai, G. P.; Santini, C.; Lecuyer, C.; Choplin, A. *New J. Chem.* **1994**, *18*, 115-122.
5. Basset, J.-M., Niccolai, G. P. "Molecularly Defined Organometallic Complexes" in *Applied Homogeneous Catalysis by Organometallic Complexes*, Cornils, B. and Herrmann, W. A. eds.; VCH: Weinheim 1996.
6. Quignard, F.; Lecuyer, C.; Bougault, C.; Lefebvre, F.; Choplin, A.; Olivier, D.; Basset, J. M. *Inorg. Chem.* **1992**, *31*, 928-30.
7. Corker, J.; Lefebvre, F.; Lecuyer, C.; Dufaud, V.; Quignard, F.; Choplin, A.; Evans, J.; Basset, J.-M. *Science* **1996**, *271*(5251), 966-9.
8. S. Reyes, Doctoral Thesis, Universidad Centrale de Venezuela, 1996.
9. Rosier, C.; Niccolai, G. P.; Basset, J.-M., manuscript submitted.
10. a) Quignard, F.; Choplin, A.; Basset, J. M. *J. Chem. Soc., Chem. Comm.* **1991**, 1589-1590. b) d' Ornelas, L.; Reyes, S.; Quignard, F.; Choplin, A.; Basset, J. M. *Chem. Lett.* **1993**, 1931-4.
11. a) Quignard, F.; Lecuyer, C.; Choplin, A.; Olivier, D.; Basset, J.-M. *J. Mol. Catal.* **1992**, *74*, 353-363. b.) Niccolai, G. P.; Basset, J.-M. *Appl. Catal. A: General* **1996**, *146*, 145-156.
12. Lecuyer, C.; Quignard, F.; Choplin, A.; Olivier, D., Basset, J.-M. *Angew. Chem., Int. Ed. Eng.* **1991**, *30*, 1660-1661.
13. d' Ornelas, L.; Reyes, S.; Quignard, F.; Choplin, A.; Basset, J. M. *Chem. Lett.* 1993, 1931-4.
14. a) Bent, B. E.; Nuzzo, R. G.; Dubois, L. H. *J. Am. Chem. Soc.* **1989**, *111*, 1634. b) Fehlner, T. P. *Chemtracts: Anal., Phys., Inorg. Chem.* **1990**, *2*, 45.
15. a) Yang, X.; Jia, L.; Marks, T. J. *J. Am. Chem. Soc.* **1993**, *115*, 3392. b) J. E. Bercaw, *Pure Appl. Chem.* **1990**, *62*, 1151. c) Watson, P. L.; Roe, D. C. *J. Am. Chem. Soc.* **1982**, *104*, 6471. d) Horton, A. D. *Organometallics* **1996**, *15*, 2675.
16. a) McNeill, K.; Andersen, R. A.; Bergman R. G. *J. Am. Chem. Soc.* **1995**, *117*, 3625-3626. b) Thomson, S. K.; Young, G. B. *Organometallics* **1989**, *8*, 2068.
17. a) Rossi, A.; Odian, G.; Zhang, J. *Macromolecules* **1995**, *28*, 1739. b) Resconi, L.; Piemontesi, F.; Franscisoni, G.; Abis, L.; Fiorani, T. *J. Am. Chem. Soc.* **1992**, *114*, 1025. c) Yamazaki, H. *Organomet. News* **1992** 114, and references therein.

18. Dufaud, V.; Anierte, C.; Lucas, C.; Basset, J.-M., manuscript submitted.
19. Dufaud, V.; Basset, J.-M., FR 2736646 A1 970117; FR 95-8552 950713.
20. Reyes, S.; Bastide, F.; Niccolai, G. P.; Basset, J.-M., manuscript submitted.
21. Dufaud, V.; Niccolai, G. P.; Thivolle-Cazat, J.; Basset, J. M. *J. Am. Chem. Soc.* **1995**, *117*, 4288-94.
22. Vidal, V.; Théolier, A.; Thivolle-Cazat, J.; Basset, J.-M.; Corker, J. *J. Am. Chem. Soc.* **1996**, *118*, 4595-4602.
23. Vidal, V.; Théolier, A. Thivolle-Cazat, J.; Basset, J.-M. *Science* **1997**, *276*, 99-102.

# SELECTIVE OXIDATION OF LIGHT ALKANES

G.J. HUTCHINGS

*Leverhulme Centre for Innovative Catalysis, Department of Chemistry, University of Liverpool, Liverpool, L69 3BX, UK.*

## 1. Abstract

The main features concerning the selective activation of light alkanes are described and discussed for heterogeneous catalysts based on oxides and phosphates. These key features are then exemplified using the oxidation of alkanes over vanadium phosphate catalysts, in particular for the oxidation of butane to maleic anhydride. In the final part of the paper a simplified approach for the design of novel catalyst systems, based on D/H and  $^{18}\text{O}_2/^{16}\text{O}_2$  exchange reactions, is described and exemplified.

## 2. Introduction

Heterogeneous catalysts are extensively used for the synthesis of petrochemicals, bulk and effect chemicals. The feedstocks for these processes are mainly based on oil and natural gas. In particular the chemical industry utilises alkenes, derived from naphtha cracking, as basic building blocks for the synthesis of a number of effect chemicals. A number processes have been commercialized using the oxidation of  $\text{C}_2\text{-C}_4$  alkenes (e.g.  $\text{Bi}_2\text{MoO}_6$  for the production of acrolein and acrylonitrile from propene,  $\text{Ag}/\alpha\text{-Al}_2\text{O}_3$  for the oxidation of ethene to ethene oxide, molybdates for the production of butadiene from butene and  $\text{V}_2\text{O}_5/\text{MoO}_3$  for the production of maleic anhydride from butene). In contrast, light alkanes, although readily available as either LPG or natural gas liquids, are little used and, to date, the only commercial process is based on the production of maleic anhydride from butane using vanadium phosphate catalysts. The activation of light alkanes is considered to be more difficult than the corresponding alkene and consequently there has been only limited success in attempting to utilize the more economic alkane feedstocks.



However, with the widespread availability of light alkanes at fuel value there is a clear opportunity to upgrade these materials and to use them as basic building blocks for the production of effect chemicals.

Selective oxidation of hydrocarbons provides a facile way of functionalising light alkanes to enable them to be used as chemical intermediates or final products. It is an important unit operation in the chemical industry and there is an ever increasing need for the identification of novel improved catalysts. Three factors are important for heterogeneous oxidation catalysts: activity, selectivity and lifetime. Of these it is selectivity to the desired product that is of crucial importance since the production of non-desired by-products is costly both in terms of feedstock costs but also in terms of disposal charges. There is therefore a significant commercial need to design improved oxidation catalysts that can be use relatively inexpensive and readily available light alkane feedstocks. To date, there has been a considerable research effort expended at the identification of selective catalysts for the oxidation of butane as the conversion of this alkane to maleic anhydride is operated industrially.

During the period 1984-1994 significant research was aimed at the partial oxidation of methane. One of the early observations concerning methane activation was that virtually all oxides were active for the oxidative coupling of methane to methanol [1]. It was soon recognized [2] that methane was activated on the surface of the oxide to form methyl radicals which were released into the gas phase where they either coupled directly to form ethane or reacted with oxygen, or hydroxyl radicals, to form oxygenated intermediates which lead mainly to the formation of carbon oxides. Homogeneous gas phase reactions are found to dominate the oxidation of methane. As the number of carbon atoms in the alkane increase the effect of gas phase reactions decreases and is largely absent for  $\geq C_4$  alkanes. One of the main consequences of homogeneous gas phase oxidation reactions is that they tend to be a source of non-selective oxidation, and therefore control or management of such gas phase reactions is the key when utilizing lower carbon number hydrocarbons. For this reason many studies have concentrated on the oxidation of butane as homogeneous gas phase reactions do not pose a significant problem. Most studies have concentrated on the use of vanadium phosphate since this is the preferred industrial catalyst. In view of this emphasis in the literature on methane and butane oxidation, these two reactions will be utilised to make the key points concerning the design and preparation of selective lower alkane oxidation catalysts.

## 2.1 OXIDES AS CATALYSTS FOR OXIDATION REACTIONS

Oxides are used extensively as catalysts for a number of classes of oxidation reactions and key examples are given in Table 1. Each of the catalysts listed in

Table 1 have been studied in detail and these studies have led to a number of key features being identified.

*Table 1. Oxides as oxidation catalysts*

Process	Reaction	Catalyst
Total Oxidation	$\text{CO} \rightarrow \text{CO}_2$	$\text{CuMn}_2\text{O}_4$
Selective Oxidation	methane $\rightarrow$ ethane propene $\rightarrow$ acrolein butane $\rightarrow$ maleic anhydride benzene $\rightarrow$ phenol	Li/MgO $\text{Bi}_2\text{MoO}_6$ $(\text{VO})_2\text{P}_2\text{O}_7$ TS-1
Oxidative Dehydrogenation	butenes $\rightarrow$ butadiene	$\text{Bi}_2\text{MoO}_6$
Non Oxidative Dehydrogenation	propane $\rightarrow$ benzene	$\text{Ga}_2\text{O}_3/\text{H-ZSM-5}$

## 2.2 FEATURES OF OXIDES AS CATALYSTS FOR THE SELECTIVE OXIDATION OF HYDROCARBONS

In general there are four main features that can be identified from the preceding studies, however, none of these features serve as general rules.

*Importance of specific compounds* has been recognized in many studies. In particular in the oxidation of propene to acrolein a range of specific compounds (e.g.  $\text{BiMo}_2\text{O}_6$ ,  $\text{FeSbO}_4$  and  $\text{USb}_3\text{O}_{10}$ ) have all been found to be particularly effective. In contrast, tin antimony oxide catalysts are equally effective and no compounds have been found in this catalyst system.

*Importance of specific crystallographic planes* has been observed in many studies. For example in the oxidation of methane over MgO catalysts the morphology of the oxide has been found to be particularly important [3].

*Presence of cation/anion vacancies, optimal concentration of the active oxidation species* is well recognized in the catalyst systems effective for the oxidation and ammoxidation of propene and recent studies are starting to recognise the importance of this feature in vanadium phosphate catalysts.

*Acid/base properties* are most important particularly with respect to adsorption/desorption and reactant activation. Although most studied in zeolites,

the interplay of Brønsted and Lewis acidity is widely recognized as being important in many catalyzed reactions.

These main features of oxides as oxidation catalysts together with the importance of catalyst preparation methodology will now be exemplified using the oxidation of butane with vanadium phosphate catalysts.

### 3. Vanadium Phosphate Catalysts

Vanadium phosphate catalysts represent one of the best studied heterogeneous catalyst systems for the selective oxidation of alkanes. Well over one thousand papers and patents have addressed this subject since it was first observed that these materials were catalysts for the oxidation of butane to maleic anhydride [4]. Early research concentrated on refining the method of preparation [5,6] or the identification of catalyst promoters [7]. It was recognized, very early on, that the most effective catalysts were prepared from precursors comprising a single compound ( $\text{VOHPO}_4 \cdot 0.5\text{H}_2\text{O}$ ) which were transformed *in situ* in the reactor in the presence of butane/air to a final catalyst that comprised mainly  $(\text{VO})_2\text{P}_2\text{O}_7$  [8,9]. Recently, considerable effort has been applied in order to gain an understanding of the nature of the active site for these catalysts. To some extent this has been aided by the use of improved *in situ* spectroscopic and electron microscopy techniques. It is generally recognized that the preparation method used for an oxide catalyst can be crucial in governing the final catalytic performance that can be achieved. In this respect it is often considered that there are two important steps in the preparation of an active oxide catalyst, namely the synthesis of the precursor and its transformation to the final catalyst using a calcination procedure. Both of these preparative steps must be carefully controlled if the optimum performance is to be achieved. This is also the case for vanadium oxide catalysts and research has concentrated on the following two areas:

- (i) the control of the morphology of the initial  $\text{VOHPO}_4 \cdot 0.5\text{H}_2\text{O}$  precursor.
- (ii) the transformation of the precursor to the final catalysts.

These are both crucial aspects of the preparation of active catalysts and the studies involving vanadium phosphorus catalysts can be viewed as being of general significance for other oxide catalysts. However, the control of precursor morphology is especially important for vanadium phosphate catalysts since the precursor/ final catalyst transformation is considered to be topotactic [8,10] and hence final catalyst morphology can be readily controlled at the precursor stage.

### 3.1 CATALYST STRUCTURE/ACTIVITY RELATIONSHIP FOR VANADIUM PHOSPHATE CATALYSTS

One of the most fascinating aspects of oxide catalysts is that there are many different methods by which they can be prepared. For example  $\text{WO}_3/\text{Al}_2\text{O}_3$  catalysts can be prepared either by incipient wetness impregnation or by adsorption from a tungstate solution [11],  $\text{MgO}$  can be prepared by burning  $\text{Mg}$  or by thermal decomposition of the hydroxide, carbonate or basic carbonate [12]. Vanadium phosphate catalysts are no exception and the precursor hemihydrate compound,  $\text{VOHPO}_4 \cdot 0.5\text{H}_2\text{O}$ , can be prepared by an extensive range of methods [7-10,13,14]. Most preparations use  $\text{V}_2\text{O}_5$  and  $\text{H}_3\text{PO}_4$  as reagents. The initial methods for the preparation of high activity catalysts utilised  $\text{HCl}$  as a reducing agent using either water or isobutanol as solvents [5,6]. This early research established that the transformation of the hemihydrate precursor to the final catalyst was best carried out *in situ* in the reactor using the butane/air reaction mixture. The process was recognized as a dehydration and water loss was observed to occur at two temperatures, *ca.* 360-400 and 460-500 °C. It is now known that the transformation of the hemihydrate only involves the higher temperature water loss and the lower temperature process was associated with the decomposition of  $\text{VO}(\text{H}_2\text{PO}_4)_2$  which is an impurity present at *ca.* 10% by mass. Removal of this impurity by water extraction gave improved catalytic performance [15] and this procedure is now standard in many preparations used today. An interesting observation made for catalysts prepared using  $\text{HCl}$  is that the catalyst performance is mainly a function of surface area and that within experimental error the specific activity of the catalysts is constant even when a range of additives are also included [15].

The morphology of vanadium phosphate catalysts has been investigated for catalysts prepared using three distinctly different methods [16]. The first, denoted VPA, is the standard aqueous  $\text{HCl}$  method followed by a water extraction step [16,17]; the second, denoted VPO, was prepared by the reaction of  $\text{V}_2\text{O}_5$  with  $\text{H}_3\text{PO}_4$  in isobutanol followed by a water extraction step [16,17]; the third, denoted VPD, was prepared by the reaction of  $\text{VOPO}_4 \cdot 2\text{H}_2\text{O}$  with isobutanol [16,17]. It is clear that the three methods produce very different final structures and the control of morphology and the effect on catalyst activity is shown in the next section.

#### **3.1.1 Preparation of VPD Catalysts from $\text{VOPO}_4 \cdot 2\text{H}_2\text{O}$**

The reduction of  $\text{VOPO}_4 \cdot 2\text{H}_2\text{O}$  has been studied using a wide range of alcohols. Initially, a series of primary and secondary alcohols were studied and the products were characterized using powder X-ray diffraction and typical results for primary and secondary alcohols are given in Figure 1. It is apparent that use of a primary alcohol as the reducing agent leads to the formation of

VOHPO<sub>4</sub>.0.5H<sub>2</sub>O crystals for which the [220] reflection is virtually the only feature of the diffraction pattern. In contrast, secondary alcohols lead to the formation of VOPO<sub>4</sub>.0.5H<sub>2</sub>O for which the [001] reflection is the dominant feature of the diffraction pattern, but it is clear that many other diffraction lines are also present and the diffraction pattern is similar to that observed for VOHPO<sub>4</sub>.0.5H<sub>2</sub>O prepared by a variety of methods [8,18]. These results indicate that the VOHPO<sub>4</sub>.0.5H<sub>2</sub>O prepared using primary and secondary alcohols exhibit distinctly different morphologies, which has been confirmed by scanning electron microscopy [16]. Typically the precursor prepared from a primary alcohol is made up of thin platelets (~1 μm in diameter and 60 nm in thickness) densely packed to form 'rose like' cluster. The surface areas of VOHPO<sub>4</sub>.0.5H<sub>2</sub>O prepared by using primary alcohols can be in the range 30-45 m<sup>2</sup>g<sup>-1</sup> and therefore represents a preparative route to a high area catalyst. The precursors prepared using secondary alcohols typically consist of discrete randomly orientated platelets whose lateral dimensions are typically 2-4 μm and thicknesses are typically 200 nm. The surface areas of VOHPO<sub>4</sub>.0.5H<sub>2</sub>O prepared using secondary alcohols were much lower, typically in the range 5-10 m<sup>2</sup>g<sup>-1</sup>.

Subsequently, a wide range of C<sub>4</sub>-C<sub>12</sub> alcohols were investigated for the reduction of VOPO<sub>4</sub>.2H<sub>2</sub>O and the results of these studies are given in Table 2. It is apparent that the use of most alcohols give VOHPO<sub>4</sub>.0.5H<sub>2</sub>O as the product. However, 3-octanol as reducing agent leads to exclusive formation of VO(H<sub>2</sub>PO<sub>4</sub>)<sub>2</sub> and in this special case VOHPO<sub>4</sub>.0.5H<sub>2</sub>O was only observed as a minor impurity in some preparations. Previously VO(H<sub>2</sub>PO<sub>4</sub>)<sub>2</sub> has been prepared in pure form via V<sub>2</sub>O<sub>4</sub> [19] however, this new method based on the reaction of VOPO<sub>4</sub>.2H<sub>2</sub>O with 3-octanol represents a novel and simple preparative route to this material.

### 3.1.2 Comparison of VPA, VPO and VPD Catalysts

The catalytic performance of a VPD type catalyst prepared from the precursor derived from the reduction of VOPO<sub>4</sub>.2H<sub>2</sub>O with a primary alcohol (isobutanol) has been compared with catalysts derived from two other VOHPO<sub>4</sub>.0.5H<sub>2</sub>O precursors prepared either (i) using aqueous HCl as a reducing agent for V<sub>2</sub>O<sub>5</sub> [16] denoted VPA and (ii) using isobutanol as solvent and reducing agent for V<sub>2</sub>O<sub>5</sub> denoted VPO [16]. The catalytic data obtained after 72h time on line are given in Table 3 and at this stage the catalytic performance of all the materials had stabilized. It is clear that the material derived from VOPO<sub>4</sub>.2H<sub>2</sub>O is considerably more active and selective to maleic anhydride when compared with the other catalysts. However, this difference in activity is largely due to the enhanced surface area of this catalyst, which results from the high surface area of the precursor being retained on activation, and all three catalysts display virtually the same specific activity of *ca.* 1.2x10<sup>-5</sup> mol

$\text{MA m}^{-2}\text{h}^{-1}$ . It is therefore apparent that the distribution of active sites is similar for these catalysts. The advantage gained by using the preparative route based on the reduction of  $\text{VOPO}_4 \cdot 2\text{H}_2\text{O}$  with a primary alcohol, is that it provides a simple and reliable method for the preparation of a high area catalyst.

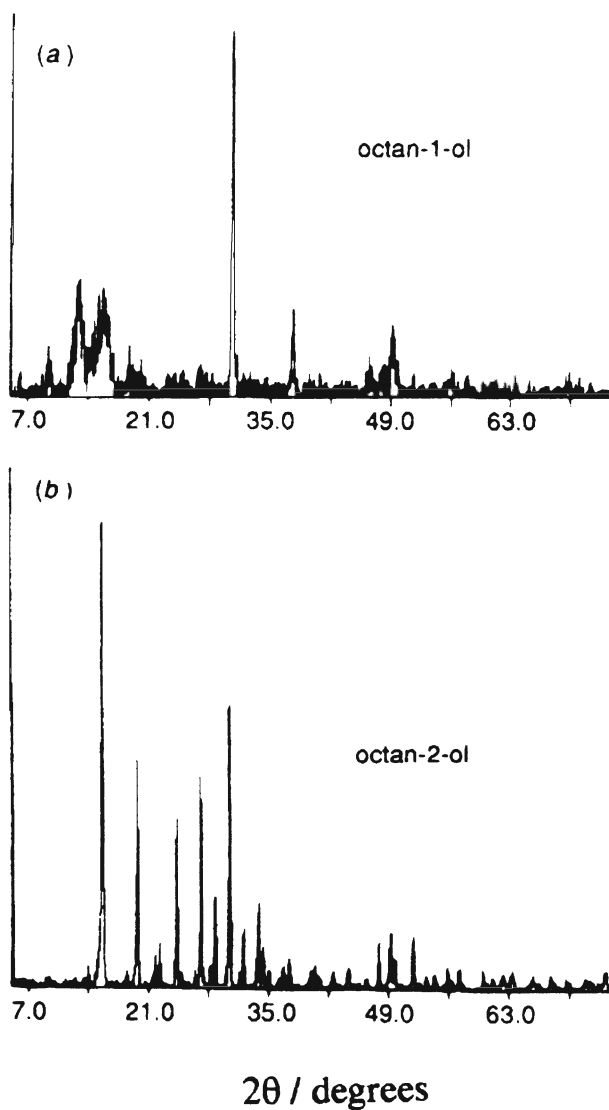


*Figure 1.* Powder X-ray diffraction patterns for  $\text{VOHPO}_4 \cdot 0.5\text{H}_2\text{O}$  prepared by the reaction of  $\text{VOPO}_4 \cdot 2\text{H}_2\text{O}$  with (a) a primary alcohol and (b) a secondary alcohol.

*Table 2.* Product types derived from the reaction of  $\text{VOPO}_4 \cdot 2\text{H}_2\text{O}$  with various alcohols [12]<sup>a</sup>

Alcohol	Product Type <sup>b</sup>
2 methyl 1 propanol	1
butanol	1
2 butanol	2
butenol	2
1 pentanol	1
2 pentanol	2
3 pentanol	2
1 hexanol	1
2 hexanol	2
3 hexanol	2
1 heptanol	1
2 heptanol	2
3 heptanol	2
1 octanol	1
2 octanol	2
3 octanol	3
1 nonanol	1
2 nonanol	2
3 nonanol	2
1 decanol	1
2 decanol	2
3 decanol	2

<sup>a</sup> reaction under reflux, 20h

<sup>b</sup> Type 1 as figure 1a (high surface area rosette structures).

Type 2 as figure 1b (lower surface area hemihydrate platelets).

Type 3  $\text{VO}(\text{H}_2\text{PO}_4)_2$

### 3.1.3 Characterization of VPA, VPO and VPD Catalysts

A detailed study of the microstructure of the catalysts has been carried out using transmission electron microscopy (TEM) and high resolution electron microscopy (HREM) and representative micrographs are shown in Figure 2. A standard TEM and HREM atlas of VPO pure phases has been compiled to enable the identification of the phases present in catalyst samples. The VPA catalyst was found to contain a complex microstructure in which at least four



**a****b**

*Figure 2a.* TEM micrograph of activated VPA; (a)  $\delta$ -VOPO<sub>4</sub>, (b) (VO)<sub>2</sub>P<sub>2</sub>O<sub>7</sub>.



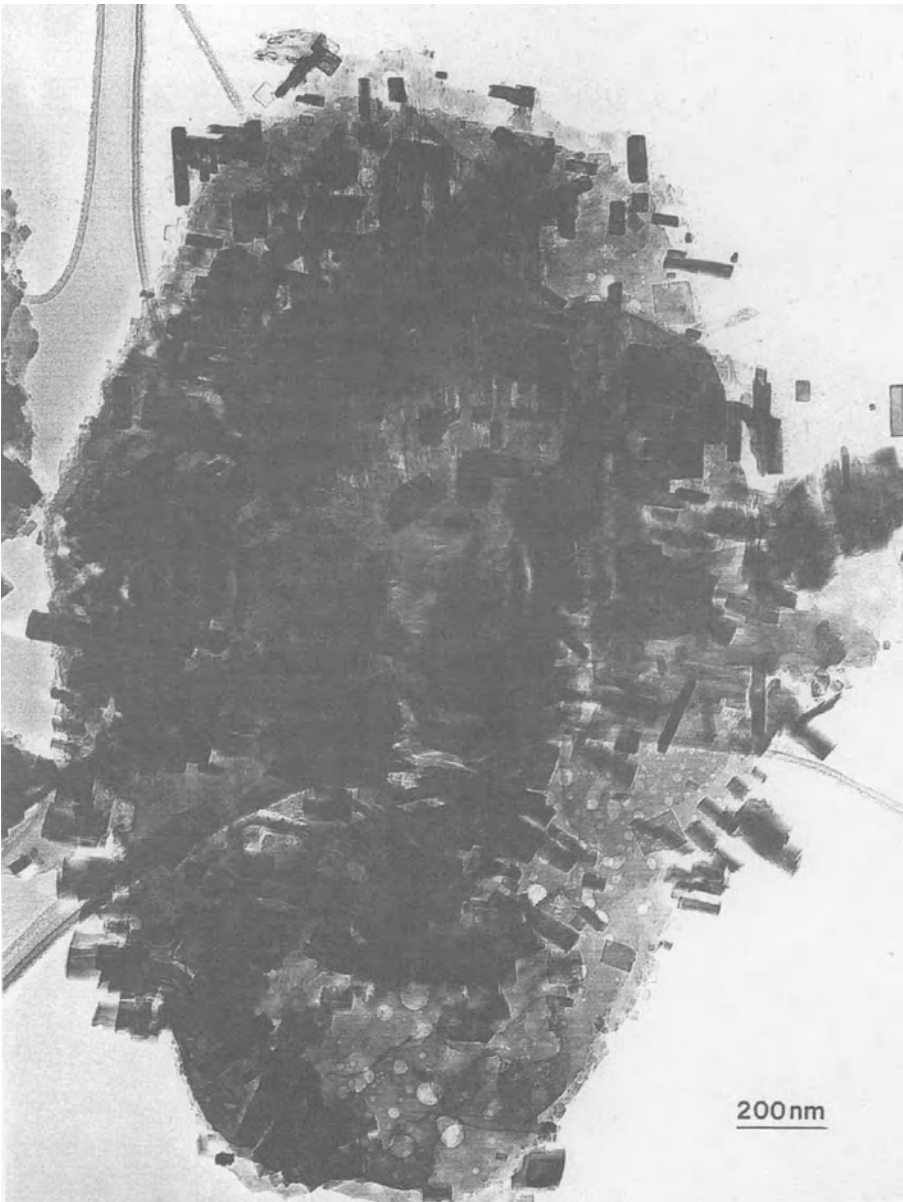


*Figure 2b.* TEM micrograph of activated VPO.



Figure 2c. TEM micrographs of activated VPD.

distinct phases were identified. The majority phase (*ca.* 80 vol %) was  $\alpha_{II}$ -VOPO<sub>4</sub> present as 1  $\mu$  diameter platelets, and lesser amounts of  $\delta$ -VOPO<sub>4</sub> (10 vol %), (VO)<sub>2</sub>P<sub>2</sub>O<sub>7</sub> (5 vol %) and  $\gamma$ -VOPO<sub>4</sub> (5 vol %) were also present. For the VPO catalyst, three distinct morphologies are observed. The major component is oblong (VO)<sub>2</sub>P<sub>2</sub>O<sub>7</sub> crystallites that preferentially expose (100), (021) and (012) faces, together with  $\delta$ -VOPO<sub>4</sub> (20 vol %) and large plate-like grains 1-2  $\mu$  in diameter of an amorphous 'disorganized' (VO)<sub>2</sub>P<sub>2</sub>O<sub>7</sub>. TEM investigation of the VPD final catalyst showed that the material comprised isolated platelets of  $\alpha_{II}$ -VOPO<sub>4</sub> (3-4 vol %) with the (001) plane preferentially exposed together with the majority of the material being rosette-type agglomerates of (VO)<sub>2</sub>P<sub>2</sub>O<sub>7</sub> (>95 vol %) that preferentially expose the (100) crystal plane. In VPD there was some evidence that a minor fraction of the initial hemihydrate phase (<1 vol %) remained untransformed.

These materials can only be considered to be partially transformed as they have only been activated for 72 h, but it is clear that a range of very different morphologies are displayed by the three preparations. It is therefore interesting to observe that the intrinsic activity for the formation of maleic anhydride is almost the same for the three materials (Table 3). In particular, the VPD catalyst comprises a much higher proportion of (VO)<sub>2</sub>P<sub>2</sub>O<sub>7</sub> that preferentially expose the (100) crystal plane (>95 vol %) when compared with the VPO material (<80 vol %), however, the specific activities are almost the same. This leads us to the conclusion that the active sites for the activation of butane and the formation of maleic anhydride can be formed on a broad range of phases.

Table 3. Butane conversion to maleic anhydride for VPA, VPO and VPD catalysts

Catalyst	BET area m <sup>2</sup> g <sup>-1</sup>		conv %	selectivity /%			intrinsic activity 10 <sup>-5</sup> mol m <sup>-2</sup> h <sup>-1</sup>
	precursor			MA	CO	CO <sub>2</sub>	
	activated						
VPA	3	4	11	51	41	7	1.24
VPO	11	14	27	52	34	14	1.35
VPD	32	43	62	64	21	14	1.19

### 3.2 SPECTROSCOPIC AND ELECTRON MICROSCOPY STUDIES OF THE PRECURSOR TO FINAL CATALYST TRANSFORMATION

The transformation of the catalyst precursor to the final catalyst is a crucial aspect of catalyst preparation but there are very few systems for which this has

been given much attention. This transformation in VPO catalysts has been studied using two complimentary techniques; namely, *in situ* laser Raman spectroscopy (LRS) and TEM. The LRS studies were carried out in a specially designed cell [20] in which the vanadium phosphate catalyst is heated in flowing butane/air and the laser Raman spectra were recorded as a function of temperature and activation time. The VPA catalyst was used since no interference from fluorescence was encountered with this material. With VPO type materials the presence of the organic solvent leads to interference by fluorescence at temperatures below 350 °C and the transformation process is less easily followed. At 25 °C the spectrum of  $\text{VOHPO}_4 \cdot 0.5\text{H}_2\text{O}$  was well defined (Figure 3) and on heating no significant changes in the spectra were recorded up to 340 °C, although the intensity of the Raman scattering decreased and non-selective butane conversion was apparent at 234 °C. At 370 °C the material became disorganized and a large number of VPO compounds were observed to be present in this complex structure  $\{(\text{VO})_2\text{P}_2\text{O}_7$   $\alpha_{\text{II}}$ - and other  $\text{VOPO}_4$  and non transformed  $\text{VOHPO}_4 \cdot 0.5\text{H}_2\text{O}\}$ . Subsequent heating at 394 °C for 20 h leads to a gradual crystallisation of the catalyst and the catalyst performance improved (Figure 4) and the final material comprised a mixture of  $(\text{VO})_2\text{P}_2\text{O}_7$ ,  $\alpha_{\text{II}}$ - $\text{VOPO}_4$   $\delta$ - $\text{VOPO}_4$  and  $\gamma$ - $\text{VOPO}_4$ , which is in agreement with the TEM characterisation of this material [16]. The appearance of the V(V) phases was correlated with the onset of maleic anhydride formation and the high degree of disorder is observed only when maleic anhydride is first produced. Detailed studies using the pure VPO compounds observed at this stage of the transformation [21] showed that these materials did not exhibit a loss of Raman scattering due to disorder when examined under identical conditions. This was the first observation that this transformation process was not a simple process in which one structure recrystallises into another. Experiments in which maleic anhydride was added to the butane/air pretreatment gases showed that the structural disorder occurred at a lower temperature and hence it was concluded [20] that maleic anhydride plays an important role in the establishment of the active catalyst surface.

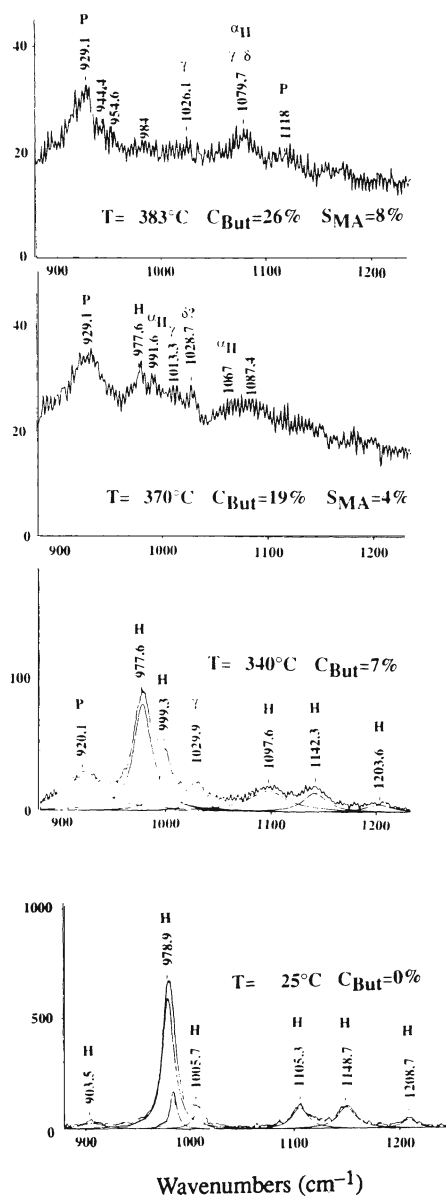


Figure 3. *in situ* Laser Raman spectra and catalytic performance data obtained during the activation of VPA in 1.5% butane/air. Key: H,  $\text{VOHPO}_4 \cdot 0.5\text{H}_2\text{O}$ ; P,  $(\text{VO})_2\text{P}_2\text{O}_7$ ;  $\alpha_{11}$ ,  $\alpha_{11}\text{-VOPO}_4$ ;  $\gamma$ ,  $\gamma\text{-VOPO}_4$ ;  $\delta$ ,  $\delta\text{-VOPO}_4$ .

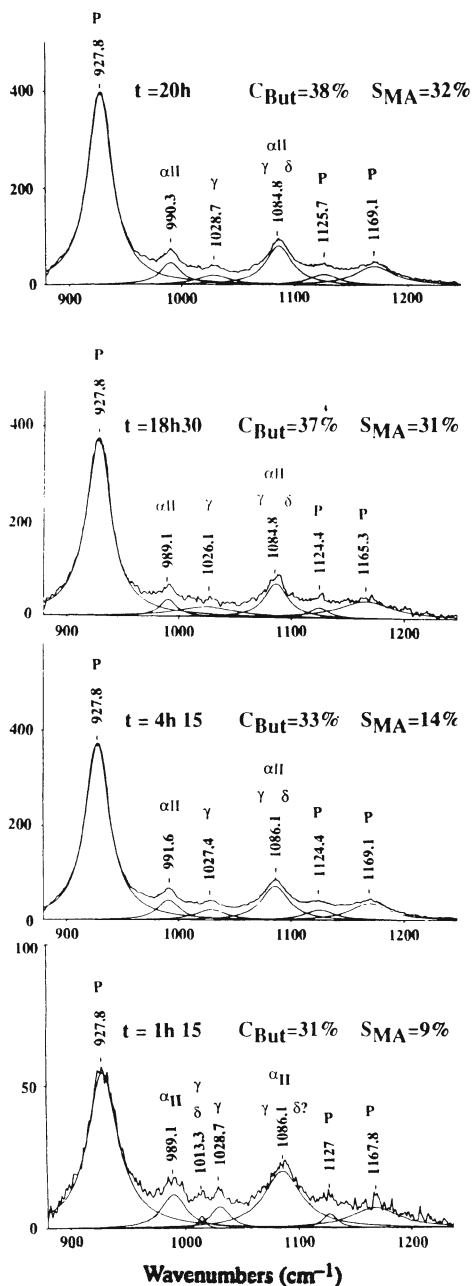


Figure 4. *in situ* Laser Raman spectra and catalytic performance data obtained during the activation of VPA in 1.5% butane/air at 394 °C. Key as in Figure 3.

*Table 4.* Butane conversion to maleic anhydride as a function of increasing activation time

Catalyst	time on stream/ h	BET area $\text{m}^2\text{g}^{-1}$	conv %	selectivity /%			intrinsic activity $10^{-8} \text{ mol cm}^{-2}$
				MA	CO	CO <sub>2</sub>	
VPO-0.1	0.1	10.5	22	34	47	17	0.43
VPO-8	8	7.6	26	48	36	15	0.99
VPO-84	84	14.8	55	66	20	12	1.48
VPO-132	132	19.4	65	69	19	11	1.39

The hemihydrate to final catalyst transformation has also been characterized in a detailed TEM study [22]. In these experiments the VPO precursor was selected for investigation, four separate experiments were carried out using the same reaction mixture in a standard laboratory microreactor ( $\text{n-C}_4\text{H}_{10}/\text{O}_2/\text{He}$  : 1.6/18/80.4) and flow conditions ( $2.4 \text{ l.h}^{-1}$  with  $\text{GSHV}=1500\text{h}^{-1}$ ). The temperature was ramped from room temperature to  $400^\circ\text{C}$  at a constant rate of  $0.5^\circ\text{C.min}^{-1}$ . Although the initial treatment was identical for all four experiments, the time on stream at  $400^\circ\text{C}$  was systematically varied ; namely 0.1h., 8h., 84h. and 132h. The four 'activated' catalysts are denoted VPO-0.1, VPO-8, VPO-84 and VPO-132 respectively. The catalytic performance data for the four samples activated for different time periods are summarized in Table 4. The n-butane conversion increases from 22 to 65% with increasing activation time. We also observe a decrease in the selectivity for CO and CO<sub>2</sub>. It is particularly noticeable that the selectivity to CO decreases very rapidly in the first 10 hours. When the variation in surface areas is taken into account, it is apparent that the intrinsic activity for maleic anhydride production increases steadily with time on stream up to 84 hours and then tends to level off as the catalyst becomes stabilized. The catalysts were quenched after these different activation times by cooling the reactor rapidly with reactants being present and were then examined using TEM. The VPO precursor comprised rhomboid shaped platelets with thicknesses between  $0.03 - 0.1\mu$  as shown by TEM (Figure 5). Selected area diffraction patterns taken normal to one of these platelets

confirmed that the major and minor axes of the rhomboid correspond to the [100] and [010] directions of the  $\text{VOHPO}_4 \cdot 0.5\text{H}_2\text{O}$  crystal structure respectively.

Low magnification transmission electron micrographs of typical crystallites from the VPO-0.1, VPO-8, VPO-84 and VPO-132 samples are shown in Figures 6(a), (b), (c) and (d) respectively. It is clear from the sequence of micrographs that the characteristic rhomboid platelet morphology of the hemihydrate is retained to varying extents in all the specimens. The VPO-0.1 sample (Figure 6(a)) shows a number of subtle changes from the crystalline hemihydrate platelet. Firstly a number circular features, which are probably internal voids, have appeared. Secondly, isolated patches of the platelet show very characteristic fissures which seem to be crystallographic in origin because they tend to align along the minor axis of the rhomboid platelet. As the activation time increases to 8 hours (VPO-8; Figure 6(b)) the density of circular features has increased markedly and a distinct dark fringe about 25nm thick is beginning to form along the periphery of the platelet. The fringe appears darker than the centre of the platelet due to diffraction contrast, implying that well crystallised material is nucleating at the platelet rim. The material in the interior of the platelet is much more disordered in character and is very sensitive to electron beam damage. As activation progresses further (VPO-84; Figure 6(c)) the crystalline fringe at the periphery is now continuous and has coarsened to a thickness of 50-70 nm. Detailed higher magnification studies confirmed that this periphery comprised small crystallites of the pyrophosphate. Furthermore large holes in the interior of the platelet of up to 300 nm in diameter are now apparent. The residual interior material remains rather disordered and beam sensitive. Finally, the VPO-132 sample in Figure 6(d) shows the 'end-state' where in addition to the well crystallised rim, the material in the interior of what remains of the platelet appears more crystalline in character. When the samples were analysed at higher magnification (Figure 7) it is apparent that the rim of the platelet consists small crystallites each around 50-100 nm in size. When these are investigated using HREM, analysis of the fringe spacings and intersection angles confirmed that the image (Figure 7b) was the [100] projection of the  $(\text{VO})_2\text{P}_2\text{O}_7$  phase. Selected area diffraction patterns of the VPO-0.1 sample confirmed the coexistence of  $\text{VOHPO}_4 \cdot 0.5\text{H}_2\text{O}$ ,  $(\text{VO})_2\text{P}_2\text{O}_7$  and  $\delta\text{-VOPO}_4$ . Furthermore these studies showed that the relative orientations of all three phases are epitaxially related. For instance, the epitaxial orientation relationship between  $\text{VOHPO}_4 \cdot 0.5\text{H}_2\text{O}$  and  $(\text{VO})_2\text{P}_2\text{O}_7$  is;  $[001]^{\text{hemi}} // [100]^{\text{pyro}}$  and  $[010]^{\text{hemi}} // [010]^{\text{pyro}}$ . This orientation relationship has been reported previously [22] in terms of the topotactic transformation that can occur between  $\text{VOHPO}_4 \cdot 0.5\text{H}_2\text{O}$  and  $(\text{VO})_2\text{P}_2\text{O}_7$ . However, these studies also indicate that a further topotactic transformation occurs  $[001]^{\text{hemi}} // [100]^{\text{delta}}$  and  $[010]^{\text{hemi}} // [001]^{\text{delta}}$ .



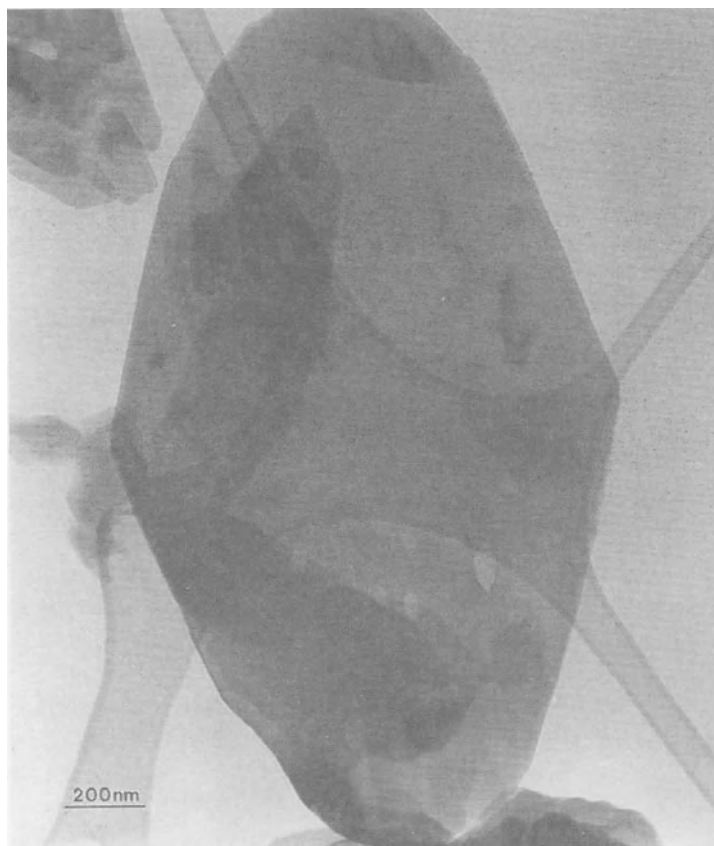


*Figure 5.* Bright field transmission electron micrograph image of  $\text{VOHPO}_4 \cdot 0.5\text{H}_2\text{O}$



*Figure 6a.* Bright field transmission electron micrographs of platelet morphologies in VPO-0.1 activated catalyst.

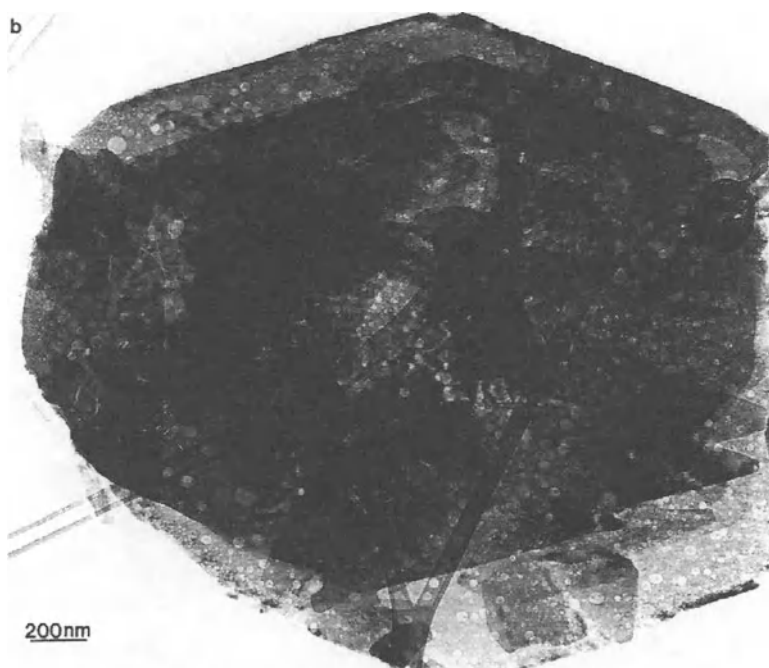


*Figure 6b.* Bright field transmission electron micrographs of platelet morphologies in VPO-8 activated catalyst.

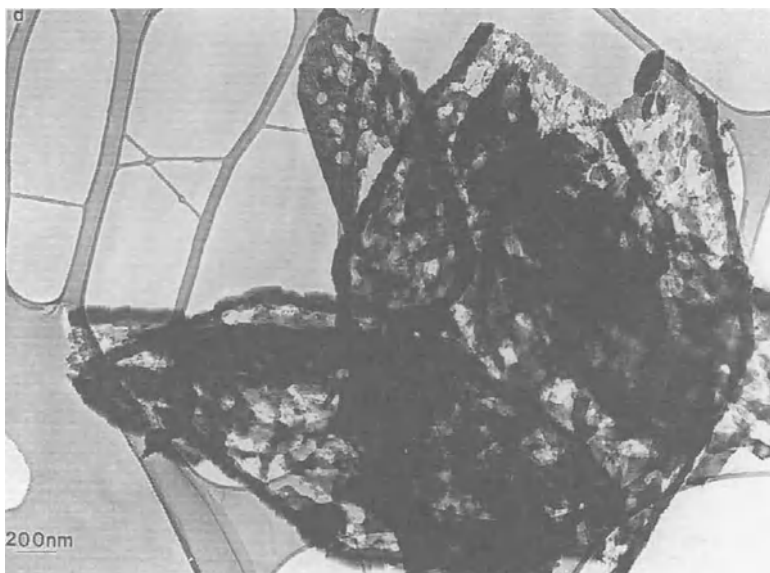


*Figure 6c.* Bright field transmission electron micrographs of platelet morphologies in VPO-84 activated catalyst.

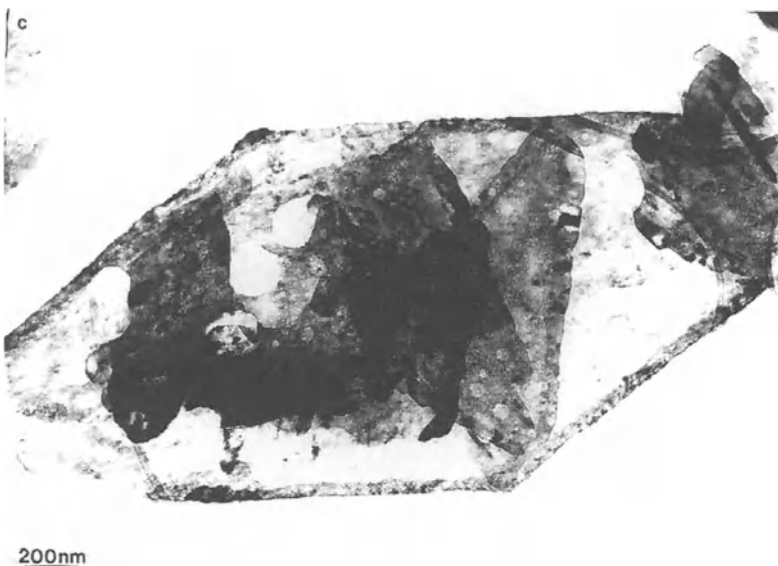


*Figure 6d.* Bright field transmission electron micrographs of platelet morphologies in VPO-132 activated catalyst.

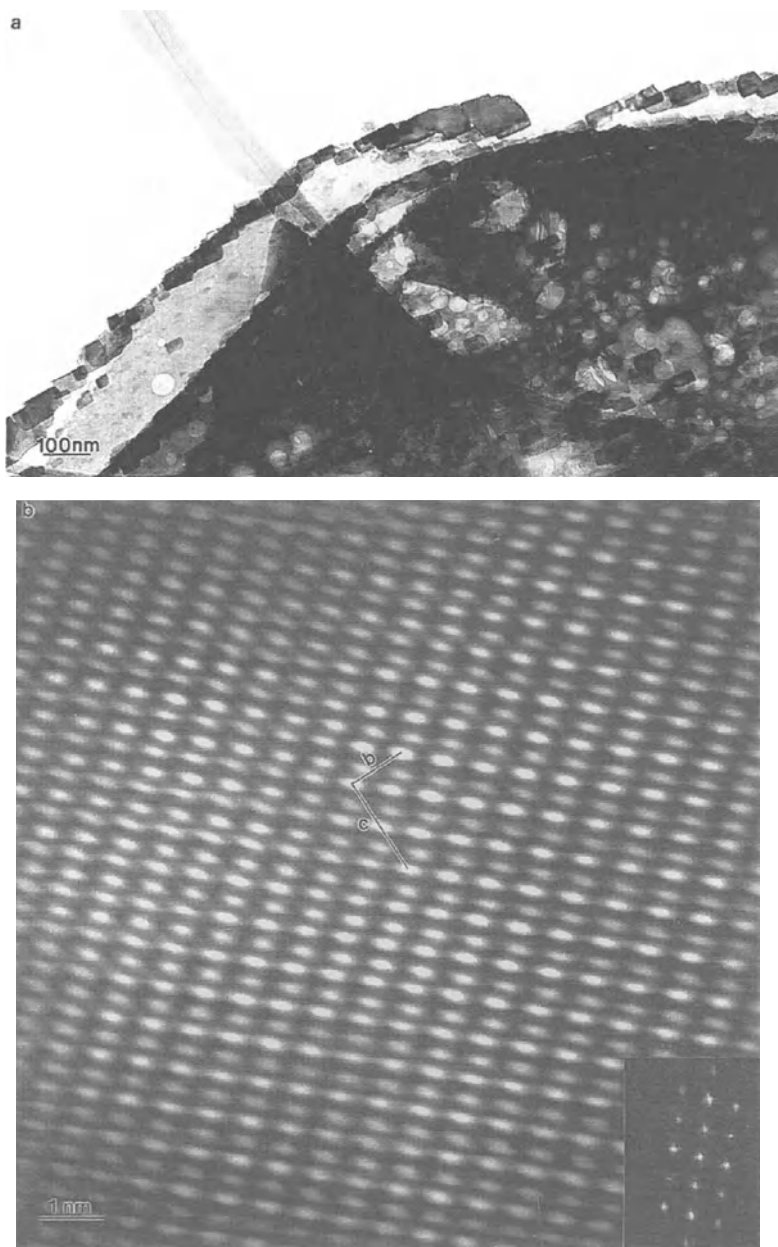


**Figure 7** (a) Bright field micrograph showing a string of  $(VO)_2P_2O_7$  crystallites at the edge of the VPO-84 platelet; (b) HREM image obtained from one of the crystals of the type shown in Figure 7a which is characteristic of the  $[100]$  projection of  $(VO)_2P_2O_7$ .

Dark field imaging experiments were used to confirm that initially crystalline pyrophosphate forms at the rim of the platelet, whereas the interior seems to consist of very disordered hemihydrate phase in which discrete domains of  $\delta\text{-VOPO}_4$  have nucleated. These domains of  $\delta\text{-VOPO}_4$  and the residual hemihydrate material subsequently appear to progressively convert to the pyrophosphate phase with increasing time on stream. Simultaneously the pyrophosphate phase which forms topotactically at the edge of the platelet gradually coarsens and thickens.

Under the particular butane/air transformation conditions used in these studies, two routes by which the hemihydrate phase can convert to the pyrophosphate phase are observed. At the edge of the platelet a direct topotactic transformation between  $\text{VOHPO}_4 \cdot 0.5\text{H}_2\text{O}$  and  $(\text{VO})_2\text{P}_2\text{O}_7$  occurs. In the interior of the platelet the transformation between the two phases can occur indirectly via an intermediate  $\delta\text{-VOPO}_4$  phase. As these two types of transformation can apparently occur side by side, it is highly likely that small changes in the transformation conditions or the precursor morphology may critically affect the proportion of direct to indirect transformation occurring. This may go some way to explaining why catalyst samples that have been prepared via different routes and which have not been fully equilibrated show considerably different relative proportions of crystalline  $\text{VOPO}_4$ , crystalline  $(\text{VO})_2\text{P}_2\text{O}_7$  and disordered mixed  $\text{V}^{4+}\text{-V}^{5+}$  phases, as is the case in our VPA, VPO and VPD catalysts.

The TEM studies therefore confirm the observations made in the *in situ* LRS studies, i.e. that after a very short exposure to butane/air at  $>370^\circ\text{C}$  the hemihydrate precursor is transformed into a largely amorphous material which gradually crystallises into  $(\text{VO})_2\text{P}_2\text{O}_7$  and  $\text{VOPO}_4$  phases. These studies also confirm that the catalyst activity/selectivity are stabilized after a relatively short time ( $<100$  h) when a mixture of V(IV) and V(V) phases are present, although structural changes continue to occur for much longer time periods.

### 3.3 COMMENTS ON THE NATURE OF THE ACTIVE SITE OF VANADIUM PHOSPHATE CATALYSTS

The key results from these studies can be summarized as follows:

- (a) the observation of similar specific activity for the VPA, VPO and VPD catalysts indicates that the active site can be formed on a wide range of vanadium phosphorus containing phases.
- (b) the detailed *in situ* LRS and TEM studies show that the hemihydrate to final catalyst transformation is complex and that after a short exposure to butane air at temperatures  $>370^\circ\text{C}$  the hemihydrate is transformed to a mainly disordered material. At the onset of maleic anhydride formation there is a complex mixture of phases present including  $(\text{VO})_2\text{P}_2\text{O}_7$  and  $\text{VOPO}_4$  phases.

From these studies it is possible to suggest that the active centre for butane activation and maleic anhydride formation comprise a  $V^{4+}/V^{5+}$  couple that is well dispersed on the surface of a range of VPO phases, which for well equilibrated catalysts will be  $(VO)_2P_2O_7$ . Further evidence in support of this has been obtained from the study of promoted catalysts. Detailed studies with  $Co^{2+}$  promoted VPO and VPD catalysts show that the activity for maleic anhydride formation is a function of the concentration of the V(V) phases present [23]. It is possible that the active site could be at a defect site as indicated in the studies of Gai and Kourtakos [24] or alternatively it is possible that a contact synergy between well dispersed microcrystalline  $VOPO_4$  phases (i.e. non detectable by XRD) and well crystalline  $(VO)_2P_2O_7$  may also play a role. Recent studies have also confirmed the importance of V(V) phases. Coulston *et al.* [25] have used time resolved *in situ* X-ray absorption spectroscopy and have shown that when either  $\alpha_1$ - $VOPO_4/SiO_2$  or  $(VO)_2P_2O_7/SiO_2$  catalysts are exposed to butane, the rate of maleic anhydride formation is correlated with the decay in the concentration of the  $V^{5+}$  species in the catalyst. This supports the hypothesis that V(V) is important for the selective activation of butane to maleic anhydride. However, the exact nature of the active sites (dispersed  $V^{5+}$  or small  $VOPO_4$  domains with a limited size and crystallinity on the  $(VO)_2P_2O_7$  matrix) is still a matter of debate.

It should be remembered that vanadium phosphorus catalysts, when used in industry, contain additives to stabilize the phosphorus content during the extended use in the reactor or to enhance catalyst activity and selectivity [7]. However, it can be expected that the work described on the unpromoted formulation will have relevance to the nature of the active site for the promoted industrial formulations.

#### 4. Design of Improved Oxidation Catalysts

The design of catalysts has in many cases either been as a result of a chance observation or have resulted from extensive catalyst screening programmes. Often both have been involved. It has long been recognized that it is necessary to consider novel design approaches for the selection of novel catalyst formulations. In this section an approach developed at the Leverhulme Centre for Innovative Catalysis is described and exemplified for the oxidation of methane to methanol as a test reaction, however, it is considered that this approach can have general applicability.

The direct partial oxidation of methane to methanol would offer considerable economic advantages over the current two stage process, by-passing the costly steam reforming step. Such a process would also facilitate the utilization of the vast natural gas reserves which are often located in remote and inhospitable



areas. It is therefore not surprising that the partial oxidation of methane to methanol has received considerable research attention and although appearing a relatively simple transformation the development of efficient catalysts has met with little success [26]. One of the major challenges encountered with methane oxidation in many heterogeneous systems is the high temperatures required to activate the methane molecule, the use of such temperatures often leads to the production of deep oxidation products which are more stable compared to methanol. This may not be such an important problem with higher carbon number alkanes but it is still the general principle that the C-H bond is required to be activated for an alkane to be oxidized selectively.

Recent research [27] has demonstrated that a novel approach for the scientific design of new methane partial oxidation catalysts can be utilised. This approach has studied the activation of methane and oxygen on single metal oxides and the stability of the methanol over the same oxides. By studying these interactions the suitability of single oxides for inclusion as components in methane oxidation catalysts can be assessed.

Initially, a ranking order was produced for the stability of methanol over a range of over thirty candidate oxides, this was based on the temperature at which 30% of the methanol feed was converted to carbon oxides [27], this is illustrated in Figure 8.

The majority of oxides tested totally combusted methanol below 400°C. Over the oxide  $\text{Sb}_2\text{O}_3$  methanol showed exceptional stability as only 3% methanol conversion was exhibited at 500 °C. The oxides  $\text{MoO}_3$ ,  $\text{Nb}_2\text{O}_5$ ,  $\text{Ta}_2\text{O}_5$  and  $\text{WO}_3$  all showed high methanol conversion, however, the major reaction products were formaldehyde and dimethylether which are desirable by-products from a methane partial oxidation process.

The exchange of  $^{18}\text{O}_2/^{16}\text{O}_2$  isotopes with oxide surfaces have been extensively studied by Winter [28] and Boreskov [29] and the general agreement between the two data sets is excellent. These results can be used to give a relative ranking order for the activation of oxygen on the oxide surfaces and this is shown in Figure 9.

Comparison of the methanol stability results with the surface oxygen exchange activity of the oxides showed that a correlation was evident [27]. This correlation, albeit weak, can be expected to be important for the ultimate design of methane partial oxidation catalysts.

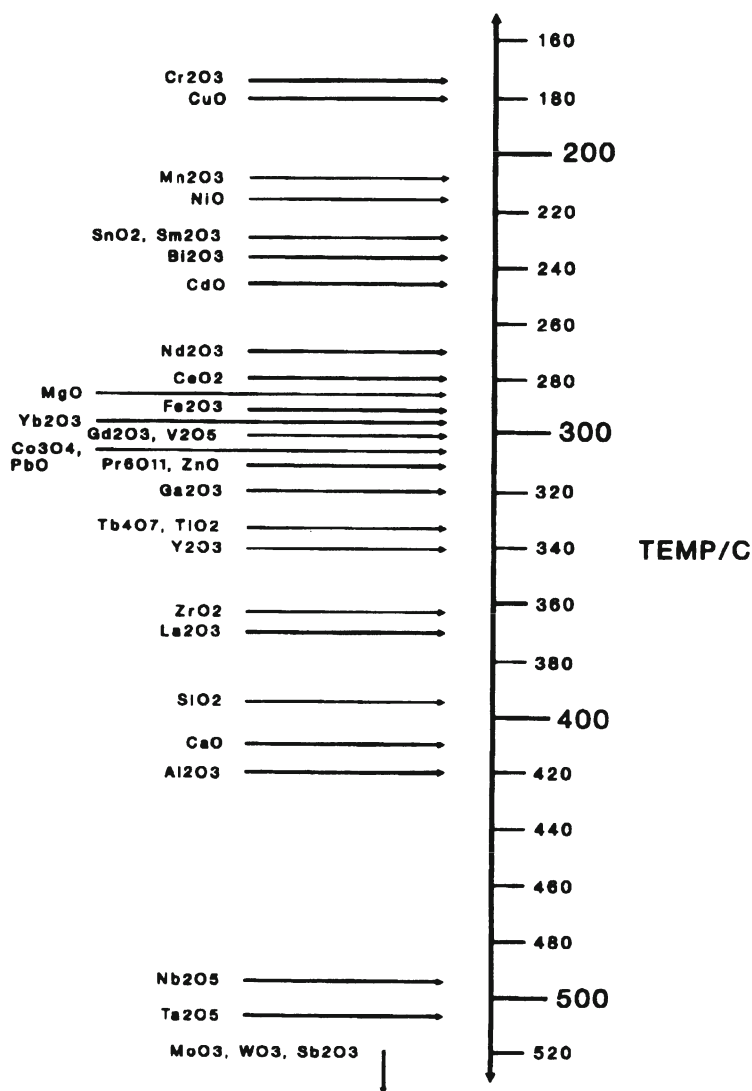


*Figure 8.* Ranking for methanol stability based on the temperature at which 30% methanol feed was converted to carbon oxides. [Experiments were carried out in a conventional liquid feed microreactor with a fused silica reactor tube. Reaction conditions: methanol/oxygen/helium feed ratio 1/4/12, gas hourly space velocity (GHSV) 12,000 h<sup>-1</sup>, temperature 100°C to 500°C at atmospheric pressure. Product analysis was performed on-line using a Varian GC-MS system.]



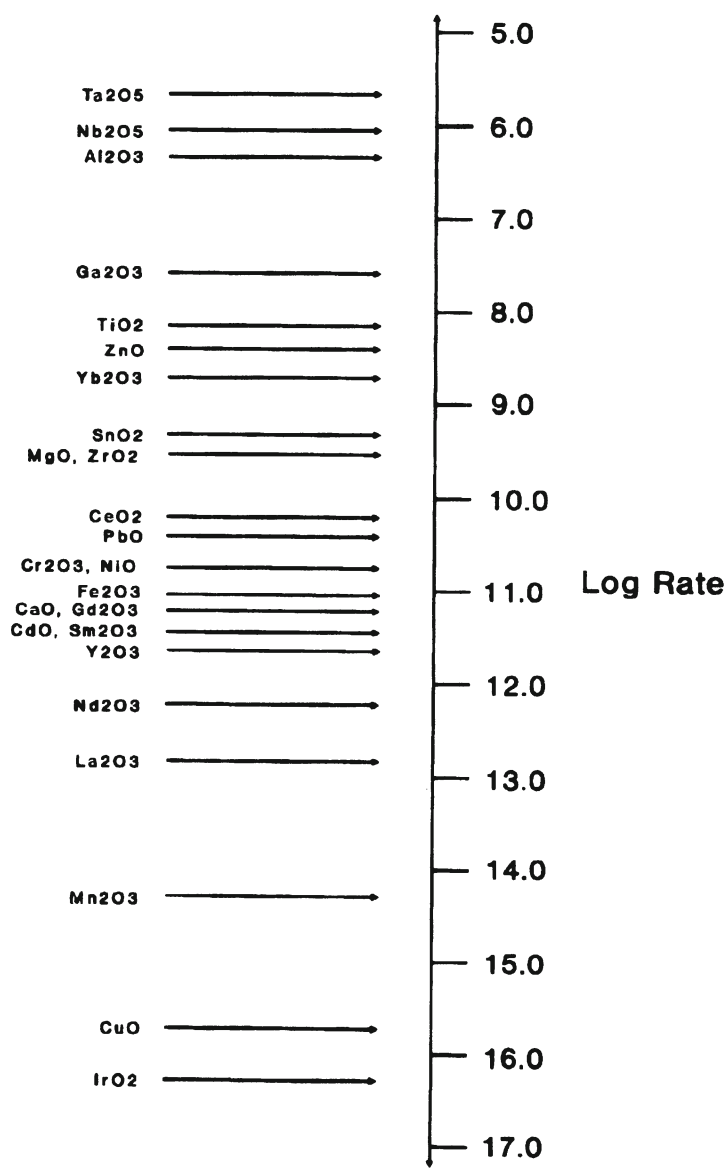
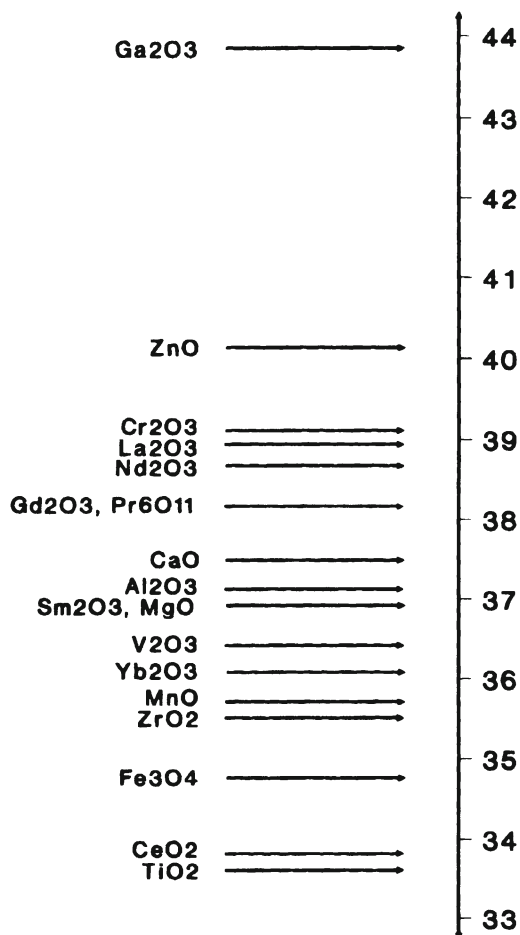


Figure 9. Relative ranking order for the exchange of <sup>18</sup>O<sub>2</sub>/<sup>16</sup>O<sub>2</sub> isotopes with oxide surfaces normalised at 500 °C (Winter [28] and Boreskov [29]).



*Figure 10.* Methane/deuterium surface area normalised exchange rates at 500 °C. [A low dead volume isotope pulsing reactor was used for methane/deuterium exchange studies. Under normal operation methane and hydrogen (1/1) were passed over the catalyst at 700 h<sup>-1</sup>. The hydrogen supply was then switched to deuterium and the exchange reaction monitored].

The pattern of activity for the activation of methane at 500 °C normalised for surface area effects is shown in Figure 10. The most active catalyst by a considerable margin was Ga<sub>2</sub>O<sub>3</sub> which showed an exchange rate several orders of magnitude greater than any other oxide. ZnO also showed high activity for the exchange reaction. It is interesting to note that these two oxides are recognized for their high activity in other processes involving hydrocarbon

activation [30]. For all the oxides included in Figure 10 the exchange process took place in a step wise manner.  $\text{CH}_3\text{D}$  was the primary product whilst traces of  $\text{CH}_2\text{D}_2$  were detected at higher rates of exchange. The oxides  $\text{MoO}_3$ ,  $\text{Nb}_2\text{O}_5$ ,  $\text{Ta}_2\text{O}_5$  and  $\text{WO}_3$  were all reduced under reaction conditions and were inactive or showed very low activity for the exchange reaction.

A correlation was noted between the exchange activity and the ionic radii of the lanthanide sesquioxides. It has been established that the basicity of the lanthanide oxides decreased in a gradual manner as the 3+ metal ionic radius decreased [31]. Thus the relationship observed indicates that the exchange rates were related to the strength of basic sites on the oxide surface and is consistent with methane activation by the abstraction of  $\text{H}^+$  to form a surface methyl anion.

These initial results were then used as a guide for the selection of suitable methane oxidation catalyst components.  $\text{Ga}_2\text{O}_3$  was selected for the ability to activate methane whilst  $\text{MoO}_3$  was selected for two reasons. Firstly, the major product from methanol oxidation was formaldehyde, produced with 97% selectivity at 500 °C, the balance of products were carbon oxides. Secondly, the mechanism of oxygen exchange identified by Winter [28] was of R3 type. This type of mechanism involved exchange with the whole of the lattice oxygen, not merely the surface layer indicating that the mobility of oxygen throughout the oxide lattice was a facile process and this high mobility was considered important for the design of a catalyst for C-H bond activation. The catalytic activity for methane partial oxidation was studied in a silica lined stainless steel microreactor maintained at 15 bar pressure. The reactant feed consisted of methane/oxygen/helium in the ratio 23/2/5 and experiments were conducted at a constant gas hourly space velocity of ca. 5,000  $\text{h}^{-1}$ . at this stage no special method of catalyst preparation was utilised and either samples of the pure oxides obtained commercially or a physical mixture of the two oxides were used. The results of methane oxidation studies are shown in Table 5 for  $\text{Ga}_2\text{O}_3/\text{MoO}_3$ ,  $\text{Ga}_2\text{O}_3$ ,  $\text{MoO}_3$  and the reactor tube packed with quartz chips.

*Table 5. Results of methane oxidation studies.*

Catalyst	$\text{CH}_4$ Conv/%	Selectivity/%				Relative Per Pass $\text{CH}_3\text{OH}$ Yield
		$\text{CH}_3\text{OH}$	$\text{CO}$	$\text{CO}_2$	$\text{C}_2\text{H}_6$	
Quartz Chips	0.1	-	-	100	-	-
$\text{Ga}_2\text{O}_3$	1.5	3	27	68	2	5
$\text{MoO}_3$	0.3	13	69	18	-	4
$\text{Ga}_2\text{O}_3/\text{MoO}_3$	3.0	22	50	27	1	66

$\text{CH}_4/\text{O}_2/\text{He} = 23/3/5$ , 15 bar, GHSV = 5000  $\text{h}^{-1}$ , temperature 455 °C

The simple physical mixture of  $\text{Ga}_2\text{O}_3/\text{MoO}_3$ , when utilised as a catalyst, produced the highest maximum yield of methanol. Comparison with the activity of the empty reactor tube showed that methanol yields were higher in the absence of any packing, indicating that homogeneous gas phase reactions were important for methanol production. However, it was that the catalytic activity should be considered against the homogeneous methane oxidation activity of the quartz chips bed. This comparison provides a more valid comparison as residence time in the heated zone of the reactor and the heat transfer throughout the catalyst bed will be similar, although the pore volumes may differ slightly. The methanol yields over  $\text{MoO}_3$  and  $\text{Ga}_2\text{O}_3$  were very low in contrast to the dual oxide catalyst. Comparison of the methane oxidation results for  $\text{MoO}_3$  and  $\text{Ga}_2\text{O}_3$  shows that  $\text{MoO}_3$  is more selective for methanol production whilst  $\text{Ga}_2\text{O}_3$  is more active, showing a higher methane conversion. These observations are consistent with the high activity for methane activation over  $\text{Ga}_2\text{O}_3$  and the oxygen exchange mechanism and the selective oxidation function exhibited by  $\text{MoO}_3$  during methanol oxidation studies. The physical mixture of  $\text{Ga}_2\text{O}_3$  and  $\text{MoO}_3$  combined the beneficial aspects of both oxides for methane partial oxidation. These were the high activity of  $\text{Ga}_2\text{O}_3$  and the selective oxidation function of  $\text{MoO}_3$ . The increased yield of methanol obtained with physical mixture of  $\text{Ga}_2\text{O}_3$  and  $\text{MoO}_3$  compared to the homogeneous gas phase reaction in the quartz chips reactor suggests that there was the development of a co-operative effect between the two phases. Such an effect can be envisaged by considering the bifunctional nature of the catalyst. The surface of  $\text{Ga}_2\text{O}_3$  could provide the methane activation function to produce a surface methyl activated species. Such a species would be surface mobile and able to migrate to sites on the  $\text{MoO}_3$  phase responsible for oxygen insertion leading to methanol formation. The intimate mixture of the two component oxides provides many phase boundaries at which methanol may be formed. For  $\text{MoO}_3$  containing catalysts, surface  $\text{M}=\text{O}$  species have been proposed as active sites for the partial oxidation of methane to formaldehyde at atmospheric pressure [32]. Similar  $\text{M}=\text{O}$  sites have also been proposed as important for other selective oxidation reactions [33]. The migration of the surface methyl species to this site could lead to the insertion of oxygen forming a surface methoxy species. The desorption of this species to the gas phase may then be a relatively facile process as the diffusion of oxygen throughout the  $\text{MoO}_3$  lattice to regenerate the surface  $\text{M}=\text{O}$  site would be rapid [28]. The regeneration of such surface sites by bulk lattice oxygen has been previously proposed for selective methane oxidation on  $\text{MoO}_3$  [32]. The production of methanol from a methoxy precursor has also previously been proposed as an important mechanistic step [35, 36]. The production of methanol from the methoxy species may take place either via the release of the methoxy radical to the gas phase followed by hydrogen abstraction from another source, usually methane. Methanol may also be formed

from a surface reaction of the methoxy group with a supply of surface hydrogen, possible from surface hydroxyl groups, followed by desorption of the product.

Co-operative, or synergistic, effects in catalysis have often been attributed to the formation of a new phase which is more active or selective than the individual phases [37]. However, this is not the case in the example cited above since characterisation of the  $\text{Ga}_2\text{O}_3/\text{MoO}_3$  catalyst by powder X-ray diffraction and X-ray photoelectron spectroscopy before and after use did not reveal any evidence for the formation of a new mixed oxide phase.

It is considered that the relatively simple approach outlined above can be used to design novel selective oxidation catalysts. This is clearly an initial step in the catalyst design process since once an active formulation is identified using this approach it is necessary that the optimum preparation procedure for the catalyst as well as promoters identified are identified .

## 5. Acknowledgements

Many colleagues have been involved with the work on butane and methane oxidation reviewed in this paper. The studies on vanadium phosphate catalysts has involved a long standing collaboration with Chris Kiely and Jean-Claude Volta. The studies on methane oxidation were carried out in collaboration with Justin Hargreaves, Richard Joyner and Stuart Taylor.

## 6. References

1. Hutchings, G.J., Scurrrell, M.S. and Woodhouse, J.R. (1989) *Chem. Soc. Rev* **18**, 251.
2. Hutchings, G.J. and Scurrrell, M.S. (1992) *Direct Methane Conversion by Oxidative Processes, Fundamental and Engineering Aspects*, Van Nostrand Reinhold, New York, 200.
3. Hargreaves, J.S.J., Hutchings, G.J., Joyner R.W. and Kiely, C.J. (1992) *J. Catal.* **135**, 576.
4. R.L. Bergman and N.W. Frisch, US Patent 3293268 (1966), assigned to Princeton Chemical Research.
5. Harrison, J.P. *US Patent* 3985775 (1976), assigned to Chevron Research Co.
6. Schneider, R.A. *US Patent* 3864280 (1975), 4043943 (1977) assigned to Chevron Chemical Research.
7. Hutchings, G.J. (1991) *Appl. Catal.* **72**, 1.

8. Johnson, J.W., Johnson, D.C., Johnson, A.J. and Brady, J.F. (1984) *J. Am. Chem. Soc.* **106**, 8123.
9. Horowitz, H.S., Blackstone, C.M., Sleight, A.W. and Truffer, G. (1988) *Appl. Catal.*, **38**, 193.
10. E. Bordes, (1988) *Catal Today* **3**, 163.
11. Maitra, A.M., Cant, N.W. and Trimm, D.L. (1966) *Appl. Catal.*, **27**, 9.
12. Hargreaves, J.S.J., Hutchings, G.J., Joyner, R.W. and Kiely, C.J. (1992) *J. Catal.*, **135**, 576.
13. Ellison, I.J., Hutchings, G.J., Sananes, M.T. and Volta, J.C. (1994) *J. Chem. Soc., Chem. Commun.* 1093; Sananes, M.T., Hutchings, G.J. and Volta, J.C. (1995) *J. Chem. Soc., Chem. Commun.* 243.
14. Hutchings, G.J., Sananes, M.T., Sajip, S., Kiely, C.J., Burrows, A., Ellison I.J. and Volta, J.C. (1997) *Catal. Today*, **33**, 161.
15. G.J. Hutchings and R. Higgins, *J. Catal.*, **162** (1996) 153.
16. Kiely, C.J., Burrows, A., Sajip, S., Hutchings, G.J., Sananes, M.T., Tuel A. and Volta, J.C. (1996) *J. Catal.* **162**, 31.
17. Hutchings, G.J., Olier, R., Sananes, M.T. and Volta, J.C. (1994) *Stud. Surf. Sci. Catal.*, **82**, 213.
18. Centi, G. ed., 'Vanadyl Pyrophosphate Catalysts', *Catal. Today*, Vol. 16, Part 1, Elsevier, Amsterdam, 1993.
19. Bordes, E. (1987) *Catal. Today* **1**, 499.
20. Hutchings, G.J., Desmartin-Chomel, A., Olier, R. and Volta, J.C. (1994) *Nature (London)*, **368**, 41.
21. Ben Abdelouahab, F., Olier, R., Guilhaume, N., Lefebvre, F. and Volta, J.C. (1992) *J. Catal.*, **134**, 151.
22. Kiely, C.J., Burrows, A., Hutchings, G.J., Bere, K.E., Volta, J.C., Tuel, A. and Abon, M. (1997) *J. Chem. Soc., Faraday Disc.*, in press.
23. Hutchings, G.J., Sananes, M.T. and Volta, J.C. (1997) *J. Catal.*, in press
24. Gai, P.L. and Kourtakakis, K. (1995) *Science* **267**, 661.
25. Coulston, G.W., Bare, S.R., Kung, H., Birkeland, K., Bethke, G.K., Harlow, R., Herron, N. and Lee, P.L. (1997) *Science* **275**, 191.
26. Hall, T.J., Hutchings, G.J., Hargreaves, J.S.J., Joyner, R.W. and Taylor, S.H. (1995) *Fuel Processing Technology* **42**, 151.
27. Taylor, S.H., Hargreaves, J.S.J., Hutchings, G.J. and Joyner, R.W. (1995) *Appl. Catal.*, **126**, 287.
28. Winter, E.R.S. (1968) *J. Phys. Chem. (A)* 2889.
29. Boreskov, G.K. (1966) *Disc. Faraday Soc.* **41**, 263.
30. Guisnet, M., Gnep, N.S. and Alario, F. (1992) *Appl. Catal.*, **89**, 1.
31. Moeller, T. and Kremers, H.E. (1945) *Chem. Rev.*, **37**, 97.
32. Smith, M.R. and Ozkan, U.S. (1993) *J. Catal.*, **141**, 124.
33. Kung, H.H. (1989) *Stud. Surf. Sci. Catal.*, **45**, 169.

34. Liu, H.F., Liu, R.S., Liew, K.Y., Johnson, R.E. and Lunsford, J.H. (1984) *J. Am. Chem. Soc.* **106**, 4117.
35. Spencer, N.D., Pereira, C.J. and Grasselli, R.K. (1990) *J. Catal.* **126**, 546.
36. Weng, L.T. and Delmon, B. (1992) *Appl. Catal.. A.* **81**, 141.

# THEORETICAL BASIS OF THE ACTIVATION OF C-H BOND

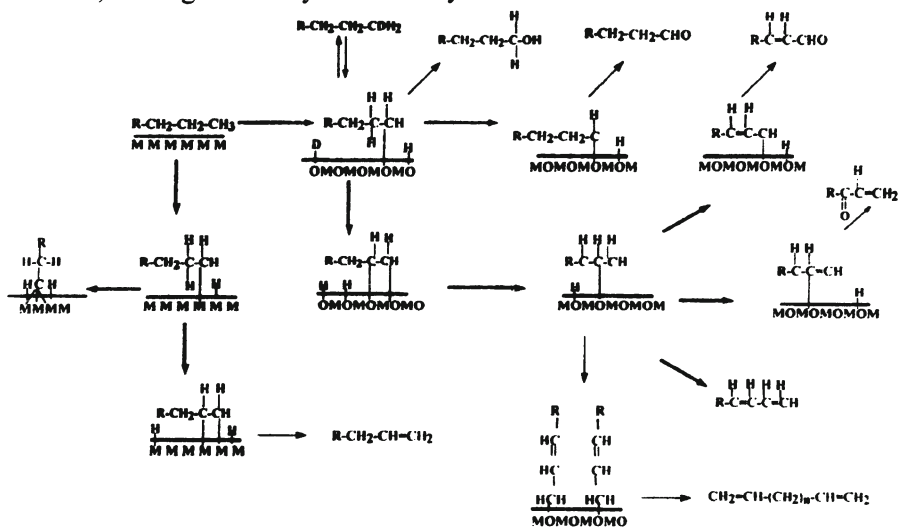
JERZY HABER

*Institute of Catalysis and Surface Chemistry  
Polish Academy of Sciences, Krakow, Poland*

## 1. Introduction

Activation of the C-H bond is the first step of the majority of transformations of hydrocarbon molecules and therefore it is the basis of petrochemical industry. Among others, all processes of selective oxidation of hydrocarbons, which are the main route for functionalisation of hydrocarbon molecules, start with activation of the C-H bond. However, in this case, the activation of C-H bonds must be usually repeated several times before the given reactant transforms into the desired product, because reactions of selective oxidation form a network of parallel and consecutive elementary steps of hydrogen abstraction and oxygen addition [1]. As an example, Fig.1 shows the network of reactions which may take place when a hydrocarbon molecule interacts at the surface of a solid catalyst. When the solid is a metal, interaction with the surface may result in the abstraction of hydrogen and formation of a surface alkyl, adsorbed hydrogen atoms recombining to desorb. If deuterium is simultaneously introduced, isotopic exchange takes place. The surface alkyl may further react in two directions. Either further hydrogen atoms are abstracted from the  $\alpha$  carbon atom of the alkyl group and alkylidyne species are formed, as observed experimentally at the surface of several metals, e.g. Pt [2], or the second hydrogen atom is abstracted from the  $\beta$  carbon atom of the alkyl group and a bridging surface species appears, which desorbs as an olefin molecule. Different reaction networks develop at oxide surfaces. Activation of the C-H bond may result in the formation of a surface alkoxy-species, which is an intermediate of several different reaction pathways. When deuterium is passed over, isotopic exchange is observed similarly as in the case of metals. The alkoxy species may pick up a proton and desorb as an alcohol, the overall process being equivalent to the insertion of oxygen into the terminal C-H bond. The alkoxy species may also lose the second hydrogen atom, either from the  $\alpha$  carbon atom with the formation of a precursor of an aldehyde, which may then desorb, or from the  $\beta$





In all these transformations only the participation of nucleophilic oxygen has been taken into account. Many oxides contain surface vacancies that form F-centers, which may play the role of sites for activation of oxygen molecules to various reactive moieties of electrophilic character. Moreover, nonstoichiometric transition metal oxides are in dynamic equilibrium with the gas phase and the surface may be populated with transient electrophilic oxygen moieties, as discussed below. At higher temperatures these moieties may

perform an electrophilic attack on any of the intermediates of the hydrocarbon reaction network, resulting in oxygenolysis (electrophilic oxidation), at lower temperatures in the liquid phase they may react with the  $\pi$ -electron system of the hydrocarbon molecule, which leads to the formation of dioxirane metallocycle and finally in epoxidation. Further complication arises, when the surface contains also OH groups which show Brönsted acid properties. Their protons may form hydrogen bonds with the  $\pi$ -bonds of the olefins, and when the acid properties are strong enough, the transfer of a proton from the surface to the olefin molecule may take place, resulting in the formation of a carbocation. This may start a whole network of reactions proceeding by a carbocation mechanism, e.g. isomerization, transalkylation, cracking etc.

The complexity of the reaction network in selective oxidation of a hydrocarbon molecule is the reason why the activation of hydrocarbon molecules represents this elementary step of the selective oxidation, which is particularly challenging for both physical chemists and chemical engineers. It is so because it must be achieved in the presence of many constraints:

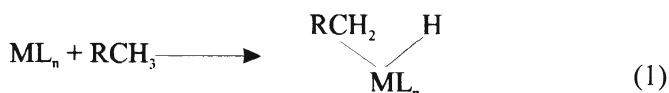
- in hydrocarbon oxidation processes thermodynamics favors the ultimate formation of carbon dioxide and water, therefore all products of partial oxidation are derived by kinetic control of the reaction;
- the catalyst must strictly control the relative rates, accelerating the series of consecutive elementary steps leading from the given reactants to the desired product and hindering those, in which unwanted by products are formed;
- the C-H bonds in the initial reactant are usually stronger than those in the intermediate products (Table 1), which makes these intermediates prone to rapid further oxidation and renders the first C-H bond activation rate determining.

*Table 1. C-H bond energies in hydrocarbons and their derivatives*

Bond	Energy kcal/mol	Bond	Energy kcal/mol
CH <sub>3</sub> -H	102	H <sub>2</sub> C=CH-CH <sub>3</sub>	109
C <sub>2</sub> H <sub>5</sub> -H	97	H <sub>2</sub> C=CHCH <sub>3</sub> -CH <sub>3</sub>	62
n-C <sub>3</sub> H <sub>7</sub> -H	97	C <sub>6</sub> H <sub>5</sub> -CH <sub>3</sub>	89
iso-C <sub>3</sub> H <sub>7</sub> -H	94	C <sub>6</sub> H <sub>5</sub> CH <sub>2</sub> -CH <sub>3</sub>	63
tert-C <sub>4</sub> H <sub>9</sub> -H	91	C-O	85.5
H <sub>2</sub> C=CH-H	122	C--O (aldehyde)	176
H <sub>2</sub> C=CHCH <sub>2</sub> -H	77	C=O (ketone)	179
C <sub>6</sub> H <sub>5</sub> -H	102	C-O (CO <sub>2</sub> )	255.8
C <sub>6</sub> H <sub>5</sub> CH <sub>2</sub> -H	78	O-H	110.6
CH <sub>3</sub> -CH <sub>3</sub>	84	O <sub>2</sub>	118
n-C <sub>3</sub> H <sub>7</sub> -CH <sub>3</sub>	79		
iso-C <sub>3</sub> H <sub>7</sub> -CH <sub>3</sub>	75		

## 2. Activation of C-H Bond by Transition Metal Complexes

A large number of organometallic complexes are known to activate the C-H bond in alkanes and enter in the reaction of oxidative addition:



The driving force is the energy gained from the formation of strong metal-hydride and metal-carbon bonds, which compensates for the energy used in the C-H bond breaking, at least in the case of third row transition metals [3]. Experiments on the oxidative addition and reductive elimination of alkanes from transition metal complexes showed that the reaction proceeds through the formation of alkane complexes as reaction intermediates. There are several ways of coordinating the alkane molecule to a transition metal [4]. They are shown in figure 2. The alkane can be bound in an end-on fashion through one, two or three hydrogen atoms, forming  $\eta^1$ ,  $\eta^2\text{-H,H}$  and  $\eta^3\text{-H,H,H}$  complexes respectively. In the  $\eta^2\text{-H,H}$  and  $\eta^3\text{-H,H,H}$  structures the metal is in direct contact with the carbon atom. Thus, the  $\eta^2\text{-H,H}$  description is equivalent to the coordination of two C-H  $\sigma$ -bonds to the metal atom, and the  $\eta^3\text{-H,H,H}$  description – to the coordination of three C-H  $\sigma$ -bonds. The alkane may also bind side-on through a single C-H  $\sigma$ -bond,  $\eta^2\text{-C,H}$ . These  $\sigma$ -complexes may be defined as complexes, in which the donor is a  $\sigma$ -bond, and include the dihydrogen complexes. They differ from those, in which the donor is an atom with a lone pair or a  $\pi$ -bond. Agnostic complexes represent the class of  $\sigma$ -complexes in which the donor is a C-H bond of a ligand already bound to the metal – an intramolecular C-H-M interaction.

Two processes may take place on the interaction of the C-H bond with organometallic complex. Electrons of the C-H bond may become donated to the empty metal orbital of a  $\sigma$  symmetry and simultaneously back donation from the filled metal orbitals of  $\pi$ -symmetry to the antibonding C-H orbital may take place. In the first case the hydrocarbon molecule forms a complex with the metal centre, but further reaction requires usually a considerable activation energy. In the second case oxidative addition of the hydrocarbon molecule to the metal centre takes place, often without any activation energy. The two situations are represented in figure 3. Which of them is realized depends on the mutual positions of the C-H and transition metal complex orbitals on the energy

scale and on the electron population of the latter. Two further parameters must be taken into account. When the metal centre has a high spin configuration ground state and the dissociation complex lies on the low-spin surface, the latter

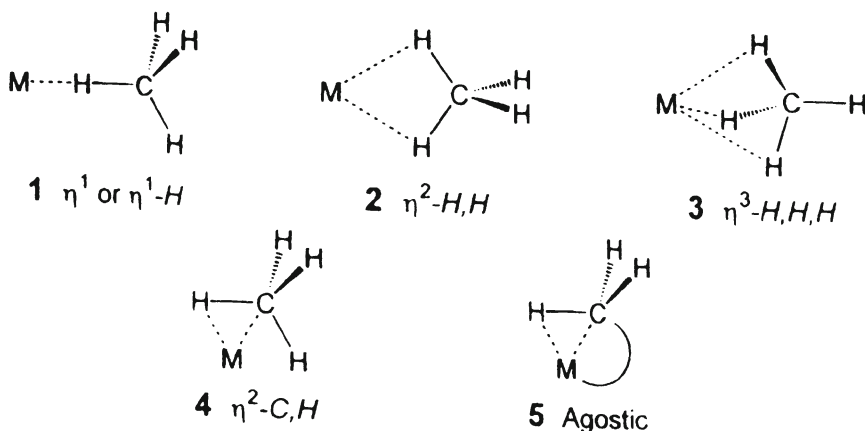


Figure 2. The modes of coordination of methane to metal atoms (adapted from ref. 4).

may be reached only through the preceding spin transition, which requires an activation energy. Moreover, in the case of electronic configuration involving the outermost 5 electrons, repulsive interaction operates between the metal centre and the hydrocarbon molecule and the hydrocarbon-metal complex is unstable, but the insertion product has substantial stability.

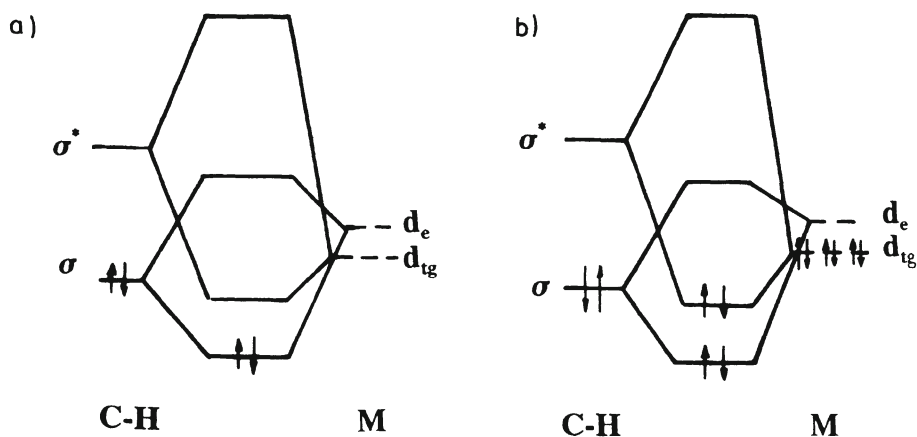
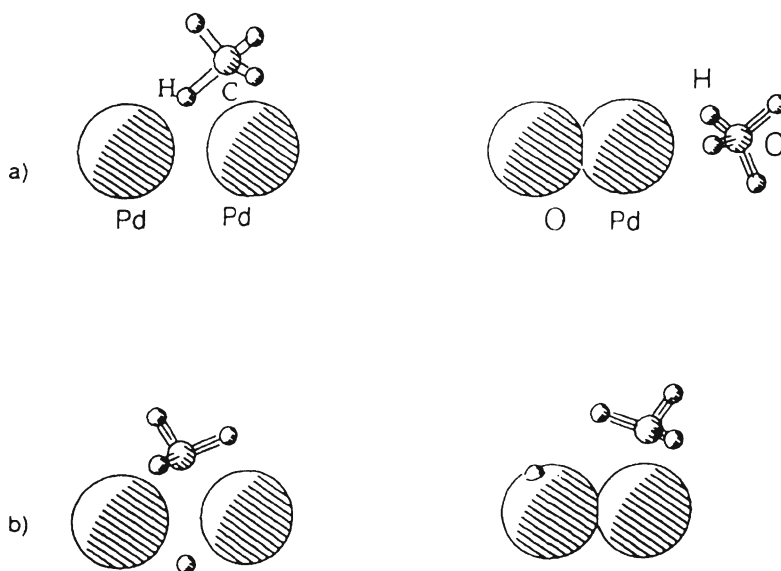


Figure 3. Orbital correlation diagram of the interaction of C-H bond in a hydrocarbon molecule with a transition metal complex.

### 3. Activation or the C-H Bond by Diatomic Molecules M-M and M-O

Interesting information concerning the importance of different factors operating in C-H bond activation by transition metals was obtained by applying the DFT to the calculation of the reaction pathway of C-H bond scission in  $\text{CH}_4$  molecule on its approach to diatomic molecules M-M and M-O, where M was V, Mo, Rh and Pd [5]. Figure 4 shows the optimal geometries of the system composed of methane and diatomic molecules in the adsorb state (a) and after cleavage of the C-H bond (b) for the case of palladium dimer (left panel) and palladium oxide (right panel).



*Figure 4.* Geometry of methane interaction with palladium dimer (left panel) and PdO molecule (right panel). a - adsorbed methane b - adsorbed methyl and hydrogen after C-H bond scission (after ref.. 5)

In the case of Pd O no energy minimum was found for the approach towards oxygen, whereas stable adsorption complexes were formed for positions collinear to Pd-O axis and bridging, between palladium and oxygen (not shown in Fig. 4), the first being lower by 13 Kcal. Starting from the bridging position and stretching the C-H bond a transition state was reached on the pathway to the cleavage of the C-H bond. Next stable structure was the product of the C-H bond scission with hydrogen forming the OH group and the methyl forming a bond with palladium (right part of Fig. 4b). The stability of the dissociated system with respect to the adsorbed state was 35 kcal/mol and the activation energy 25 kcal/mol.

Different behavior was observed in the case of  $\text{Pd}_2$  dimer. Detailed calculations revealed that methane adsorbs strongly in the bridging position, with the Pd-C distance equal to 2.2 Å and bonding energy equal to 25.7 kcal/mol. It may be noticed that hydrogen is bonded within the coordination spheres of both metal atoms, whereas carbon is bonded by one Pd atom. On stretching the C-H distance the transition state is reached at 1.48 Å, from which the hydrogen atom migrates almost freely around the palladium dimer. The stability of the system with respect to the adsorbed state amounts to only 11 kcal/mol. Apparently on Pd dimer adsorption is strong, but bonding of the dissociated parts is weak. The activation of the C-H bond by adsorption is much more pronounced on  $\text{Pd}_2$ , where it undergoes 23% stretch, compared to 2% on PdO. The reason of bond destabilization is different in both cases: on Pd-O the withdrawal of bonding electrons from methane weakens the bond, whereas on  $\text{Pd}_2$  the back-donation of electrons to the antibonding orbital of methane has a strong influence on the C-H bond strength. In both cases substantial decrease in bond polarization adds to the effect, again more profoundly on palladium dimer. On the contrary, the stabilization effect after C-H bond dissociation is much stronger on Pd-O, where the hydrogen forms a very strong, polarized bond with oxygen, whereas negatively charged hydrogen atom moves almost freely in the entire subspace of palladium dimer and the recombination reaction is very probable. The adsorbed methyl moiety acquires overall positive charge, but the carbon atom is much more negative and bonds are highly polarized.

Figures 5 and 6 show the analyses of the evolution of the density of states graphs along the methane dissociation paths on Pd-O and Pd-Pd clusters respectively. The graphs have been constructed relative to the Fermi level, with total density of states depicted by the solid line, and partial contributions marked with appropriate symbols (Pd and O for PdO and Pd and C for  $\text{Pd}_2$ ). The Fermi level lies within partially populated states. In the case of PdO the overall shape of the spectrum does not change significantly after adsorption of methane. The additional feature due to carbon is shifted from 5 e V in the initial state (a) to around 6 e V below the Fermi level (b), indicating a weak interaction. In the transition state the bonding of methane is even weaker, carbon peak shifting almost to its original position of free molecule. After final C-H bond scission the Fermi level shifts to the energy gap, because in the case of an isolated molecule, at variance with a solid, the formation of bonds entails the appearance of an energy gap. Now the shape of the spectrum changes completely, new features appear in the spectrum due to the formation of strong bonds between carbon and palladium, and between hydrogen and oxygen. One can clearly distinguish the C-Pd and H-O bonding orbitals in the lower part of the spectrum and the corresponding antibonding orbitals in its upper part. They have been marked in Fig. 5d.

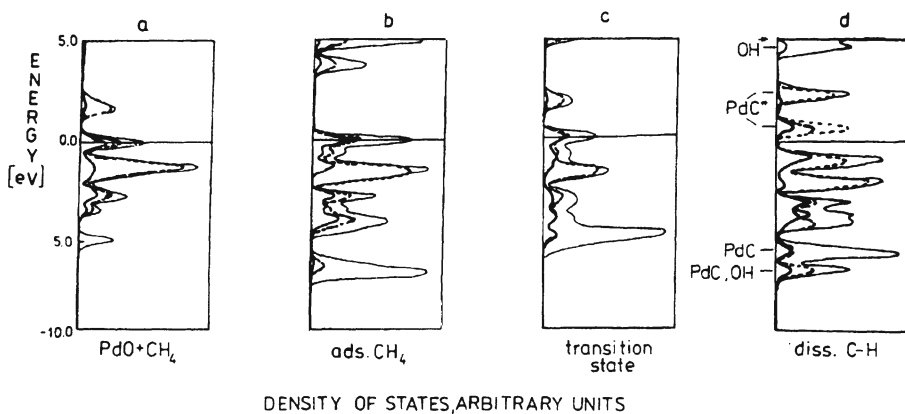


**Figure 5.** Evolution of Density of States along methane dissociation pathway on PdO. — total DOS, ---- Pd contribution, - O contribution (after ref. 5)

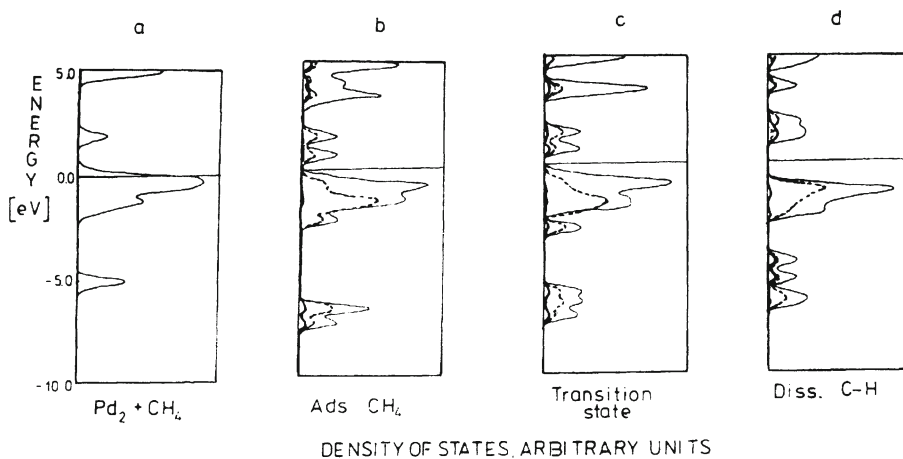


**Figure 6.** Evolution of density of states along methane dissociation pathway on Pd dimer. total DOS, --- Pd<sub>1</sub> contribution, - C contribution (after ref. 5)

The case of palladium dimer is different. Here already methane adsorption of methane (Fig. 6b) is strong enough to shift the Fermi level to the energy gap. In addition, bonding states with large carbon contribution are split and shifted down by 2 eV. In transition state (c) the system remains still strongly bonded and finally the dissociated system (d) generates a spectrum with large energy gap and well developed shapes below 5 eV representing the bonding orbitals of methyl and hydrogen with Pd atoms. Corresponding antibonding orbits lie very high and are not visible in the figure.



Open-shell rhodium oxide behaves very much alike open shell palladium oxide, showing comparable preliminary collinear adsorption and activation. Rhodium dimer, however, does not create the conditions for such a strong adsorption of methane as palladium dimer, at least in low-energy high-spin state. Methane molecule binds weakly in collinear position, and no sizeable stretching of the C-H bond, comparable to Pd<sub>2</sub>, is observed. In the case of palladium atom with closed-shell d<sup>10</sup> electronic structure no 5s electrons, which could be responsible for repulsive interactions, are present, and the adsorption complex is therefore relatively stable, but the dissociation product is not. Rhodium atom has the open-shell electronic d<sup>8</sup>s<sup>1</sup> configuration and due to the presence of 5s electrons generating repulsion, the adsorption complex is unstable, but the dissociation product has substantial stability. In the case of Pd<sub>2</sub> dimers all reaction intermediates lie on the same spin surface, thus both the adsorption complex and the dissociation product are stable. For rhodium dimer in its high-spin ground state the adsorption complex lies on a low-spin surface and may be reached only via spin-transition, which is responsible for a high activation energy. The same is true for palladium oxide molecule.

*Table 2.* Properties of adsorption complexes of methane with PdO, Rh<sub>2</sub> and Pd<sub>2</sub>

	Adsorption position	Adsorption energy (kcal/mol)	$\Delta Q$ (methane cluster)	Activation energy (Kcal/mol)	$\nu\text{C-H}$ (cm <sup>-1</sup> )
PdO	collinear on Pd	19.2	-0.20	spin trans.	2754
Rh <sub>2</sub>	collinear on Rh	11.0	-0.25	spin trans	2826
Pd <sub>2</sub>	bridging	25.7	+0.10	2.0	1903

Table 2 summarizes the most important properties of the interacting systems and makes evident the unique position of the palladium dimer. Only in this case the bridging position is preferred for adsorption, resulting in donation of electrons to the hydrocarbon molecule. At the same time it is the strongest adsorption among the studied systems. Other systems withdraw electrons from the adsorbed hydrocarbon molecule without any back donation. On Pd<sub>2</sub> the elongation of the C-H bond, as indicated by the decrease of its frequency of vibration, is greatest, and hence the activation energy for final scission of the bond is very small. Rh<sub>2</sub> and PdO provide reaction pathways with substantial barrier. In addition to the very strong interaction with Pd<sub>2</sub> already the adsorbed complex has a proper low-spin state, whereas on PdO and Rh<sub>2</sub> weak adsorption leads to high spin and a preceding spin transition to low spin (triplet-singlet for PdO or quintet-triplet for Rh<sub>2</sub>) is required, which adds to the reaction barrier. Finally, the calculated frequencies for the carbon-hydrogen stretching vibrations



in adsorption complexes, given in Table 2, reflect the trends: in each case weakening of the bond is visible (in free methane the DFT calculated frequency amounts to  $2994\text{ cm}^{-1}$ ) but on palladium dimer the effect is remarkably large.

The electronic structure of a transition metal atom may be controlled by the selection of appropriate ligands. It may be thus expected that also the reactivity of the organometallic transition metal complexes with hydrocarbon molecules will be modified by the nature of the ligands. To this end the behavior of a rhodium dimer, described above, may be compared with properties of rhodium complexes. As an example, *ab initio* calculations of the activation of the C-H bond on cyclopentadienylcarbonylrhodium may be quoted [6,7]. A following reaction sequence involving formation of a weakly bound intermediate has been proposed:



The geometries of the reactants, products, intermediates and transition states of this reaction have been calculated by using the second order Moller-Plesset (MP2) perturbation theory. Figure 7 shows the potential energy profiles of the reaction of  $\text{CpRh}(\text{CO})$  with  $\text{CH}_4$  and for comparison also with  $\text{H}_2$ . At gas-phase collisionless conditions the oxidative addition reaction of H-H and  $\text{CH}_3$ -H bonds to  $\text{CpRh}(\text{CO})$  takes place without a barrier. The ease of oxidative addition reaction, of H-H and  $\text{CH}_3$ -H bonds to  $\text{CpRh}(\text{CO})$  takes place without a barrier. The ease of oxidative addition reaction, i.e. the existence of an activation barrier and its height were found to be correlated to the Rh-H and Rh-R bond strength, which were calculated to be 65.0 and 59.3 kcal/mol, respectively, as compared to the cleaved R-H bond strength amounting to 108 kcal/mol. The exothermicity, equal to the Rh-R plus Rh-H bond energy minus R-H bond energy, is 16 kcal/mol for the oxidative addition of  $\text{CH}_4$  and 31 kcal/mol for oxidative addition of  $\text{H}_2$ . The orbital correlation diagram for the oxidative addition of the C-H  $\sigma$ -bond to an organic complex of a transition metal with vacant coordination sites is shown in figure 8. The highest occupied orbitals are the metal based  $d_{z^2}$  and the metal-based  $(m+1)a''(d_{yz})$  orbital, and the lowest empty orbital is the metal based  $(n+2)a'(d_{xy})$  orbital. Interaction of the HOMO of the complex with the C-H  $\sigma$ -bond results in the donation of the C-H bond electrons to the metal orbitals and the back donation of the metal electrons to the anti-bonding C-H orbital, which results in the cleavage of the C-H bond. Comparison of the potential energy surfaces of reaction (2) for  $\text{H}_2$  and  $\text{CH}_4$  molecules shows that, in spite of the similarity of the H-H and H- $\text{CH}_3$  bond strengths, the H-H bond in the hydrogen molecule is activated without a barrier, whereas the C-H bond in methane has a small activation barrier of 5.5 kcal/mol calculated relative to the intermediate complex  $(\text{RH})\dots\text{RhCp}(\text{CO})$ . This

difference in the behavior of the activation of H-H and C-H bonds can be explained in terms of the directionality of the  $\text{CH}_3$  orbital compared to the H orbital, as suggested by Siegbahn et al. [8]. Due to the spherical nature of the H orbital, the Rh-H bond can start to form simultaneously to the weakening of the H-H bond so that there is no barrier for the cleavage of the H-H bond. In contrast, because of the directionality of the  $\text{CH}_3$  unpaired orbital the C-H bond must be broken before the new Rh- $\text{CH}_3$  is formed, thus leading to a barrier for the reaction. In solution or in the gas phase, when collisional energy equilibration is faster than the reaction itself, the reaction should be considered to start from the intermediate complex. In such conditions the ease of oxidative addition reaction is essentially determined by the bond strength binding the intermediate complex. Thus, it would be very difficult to activate R-H bonds of molecules that have a strong Lewis base character.

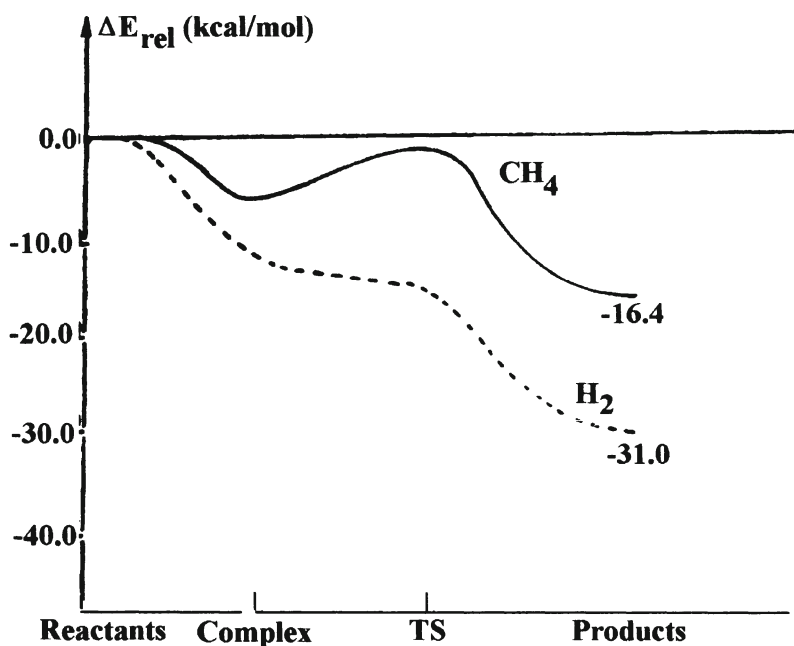


Figure 7. The potential energy profiles of the reaction of  $\text{CpRh(CO)}$  with  $\text{H}_2$  and  $\text{CH}_4$  (after ref. 7).

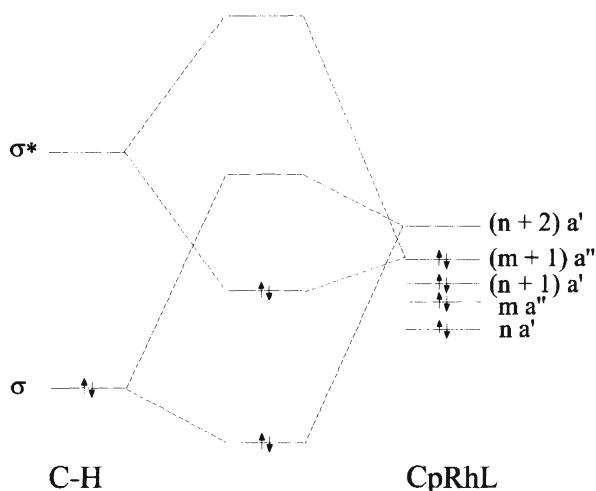


Figure 8. Orbital correlation diagram of the Rh complex with methane.

#### 4. Activation of C-H Bond by Oxy-anions

The situation changes when the interaction of the C-H bond with an oxyanion of a transition metal is considered. Oxy-anions of a number of transition metals, deposited on different supports, are known to be active and selective catalysts in partial oxidation of hydrocarbons. The system of supported  $\text{VO}_x$  is particularly interesting because of its excellent catalytic properties in oxidation of olefins and alkylaromatics. Extensive studies of the type of  $\text{VO}_x$  species present at the surface of such supports as  $\text{TiO}_2$  or  $\text{Al}_2\text{O}_3$ , carried out with the help of different techniques (Raman and IR spectroscopies, EXAFS, DRIFT) led to the conclusion [9] that at very small surface coverages the surface is covered by isolated  $\text{VO}_4$  tetrahedra, three oxygen atoms being common with the support, which neutralizes three negative charges of the free  $\text{VO}_4^{3-}$  anion, existing in aqueous solutions. Thus, calculations basing on the INDO method, using the ZINDO programme have been carried out [10] of the changes of the potential energy, bond order indices and Mulliken population on approaching a propene molecule to the  $\text{VO}_4$  tetrahedron with three oxygen linked to hydrogen atoms to neutralize the charge and mimic the interaction with the solid. Two ways of approach of propene along the trigonal axis of the  $\text{VO}_4\text{H}_3$  moiety were considered: (1) - the  $\eta^3\text{-H,H,H}$  situation of the methyl group of propene in respect to the vanadyl oxygen, and (2) - the  $\eta^3\text{-H,H,H}$  situation in respect to the central vanadium cation of the moiety (Fig.9). Only repulsive interactions were found to operate in case (2) so we shall limit our discussion to case (1).

Calculations indicate that the highest occupied orbital of the moiety is the lone pair orbital of oxygen atoms, and the lowest empty orbital - the d-orbitals of vanadium. Thus, an orbital correlation diagram of the interaction of the C-H bond of the methyl group of propene with the  $\text{VO}_4\text{H}_3$  moiety can be constructed as shown in Fig.10. The energy level of the C-H  $\sigma$ -bond lies below the energy levels of the oxygen lone pair electrons. The C-H bond electrons are donated to the bonding orbital formed as the result of the interaction of the methyl group of propene with the  $\text{VO}_4\text{H}_3$  moiety. The antibonding  $\sigma^*$  C-H orbital interacts also with the p-orbitals of oxygen ions and the oxygen lone pair electrons are back-donated to this antibonding  $\sigma^*$  orbital, the C-H bond being cleaved. Calculations of the total energy showed that on approaching propene, attractive interaction begins to operate at the distance of about 2.0 Å and an energy minimum is then attained, corresponding to the formation of a carbon-oxygen bond and abstraction of one hydrogen atom from the methyl group, hydrogen becoming bonded to the same oxygen atom. As there are oxygen lone electron pair orbitals, which are used for the formation of molecular orbitals, both carbon and hydrogen atom become bonded to this oxygen. This is equivalent to the insertion of oxygen into the C-H bond at variance with the case of low-valence transition metal complexes, when it is the metal atom, which is inserted into the C-H bond in the course of the oxidative addition. It should be however taken into account that the sum of the C-O and H-O bond energies is higher than the sum of C-V and H-O bond energies making the first pathway preferred. When now oxygen atom is allowed to move freely, the precursor of an alcohol molecule moves away of the complex. It may be thus supposed that interaction of a hydrocarbon molecule with an isolated surface  $\text{VO}_4$  species will result in the formation of an alcohol.

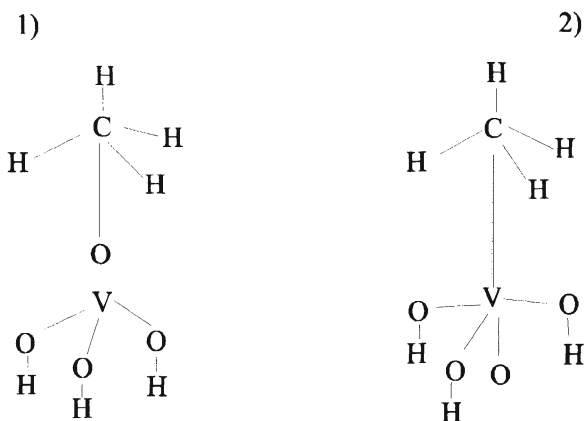


Figure 9. Pathways of approach of propene molecule to a  $\text{VO}_4\text{H}_3$  cluster.

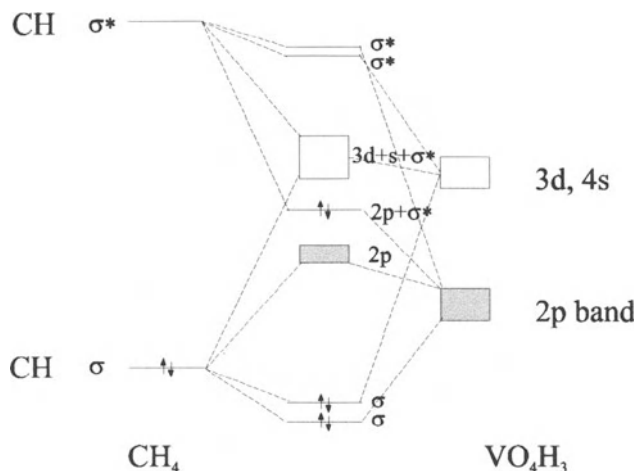


Figure 10. Orbital correlation diagram of the interaction of a methyl group of propene with  $\text{VO}_4\text{H}_3$  cluster.

## 5. Activation of C-H Bond by Oxides

Activation of C-H bonds in hydrocarbon molecules on oxide catalysts has been analysed on the basis of quantum chemical calculations using different methods. The ASD-ED-MO (Atom Superposition and Electron Delocalisation Molecular Orbital) approach [11] led to the conclusion that on oxide catalysts the oxidative addition of the C-H bond to the metal cation requires a very high activation energy because the antibonding orbital, which must accept two electrons, lies very high. When a hole appears in this orbital, the reaction becomes more facile.

Interesting conclusions on the molecular mechanism of the activation of C-H bond at oxide surfaces may be drawn from the results of semiempirical quantum chemical calculations of the interactions developing on approach of a hydrocarbon molecule to different clusters taken as models of  $\text{V}_2\text{O}_5$  catalysts [12]. Calculations showed [13] that a cluster cut off from the surface of  $\text{V}_2\text{O}_5$  in such a way that it contains 10 vanadium atoms arranged in two corner linked zig-zag ribbons of edge-linked vanadium-oxygen square pyramids (Fig. 11B) well represents the properties of  $\text{V}_2\text{O}_5$  surface. It contains three kinds of oxygen atoms present in the structure: the vanadyl oxygen O (I) atoms, which form only one double bond with vanadium atoms, the bridging oxygen O (II) atoms which form two bonds and bridging oxygen atoms O (III) which form three bonds with vanadium atoms. In order to simulate the embedding of the cluster in the oxide lattice and to neutralize the charge of the cluster appropriate number of hydrogen atoms has been added to terminal oxygen atoms. Calculations with

such a large cluster are however time-consuming, therefore very often simplified model of two corner-linked vanadium-oxygen square pyramids (Fig.11A) is used to obtain some basic qualitative answers.

Figure 12 presents the pathway of approach of the propene molecule to the cluster  $V_2O_9H_8$ [10]. Positions of all atoms of the propene molecule and all oxygen atoms in the plane of the cluster have been optimized, positions of vanadium atoms, vanadyl oxygen atoms and hydrogen atoms saturating the cluster have been kept frozen. The pathway directed towards the bridging oxygen atom from side opposite to vanadyl oxygens turned out to be energetically most favorable. The arrangements of the electronic structure are summarized in Table 3. On approaching the propene molecule to the cluster repulsion is at first observed and as its result the bridging oxygen is shifted beneath the plane of the cluster. This is manifested by the increase of the total energy of the system, representing the activation barrier with a maximum at 1.6 Å. Simultaneously, the propene molecule becomes tilted and rotated so that the double bond be positioned above the vanadium atom, however, no bond is being formed between this atom and the  $\pi$ -bond of propene. On further approach, at the distance of 1.55 Å, the C(1)-O(5) bond is formed, one hydrogen atom from the methyl group being pushed along the carbon chain to the C(2) atom with the appropriate rearrangement of electrons. As seen from Table 3, the C-O bond order at 1.55 Å is 1.082, but no H-O bonds are yet formed. Simultaneously, the bond between the bridging oxygen O(5) and the vanadium atom V(1) is so weakened that its order becomes 0.16 and it is elongated to about 2.4 Å. Then the hydrogen atom is split from the C(2) atom and the double bond between the C(2) and C(3) atoms is restored so that the system is composed of hydrocarbon fragment, linked to the bridging oxygen atom O(5) and hydrogen atom H(2) bound to the terminal oxygen O(11), as indicated by the O(11)-H(2) bond order of 0.912. An electron is injected onto the vanadium d-orbitals. The formation of the latter bond results in the destabilization of the bond between the bridging oxygen atom O(5) and the second vanadium atom V(2). Now, practically without any activation barrier, abstraction of the second hydrogen atom from C(1) carbon atom takes place with the formation of O(9)-H(3) bond, as indicated by its bond order of 0.761 at 1.4 Å. The system now can be considered as composed of a precursor of acrolein molecule, with  $R_{Co}=1.248$  Å (bond order 1.832) and  $R_{C(2)-C(3)}=1.335$  Å (bond order 1.938). It is still weakly bonded to the cluster, as indicated by the small values of the bond order between its oxygen O(5) and the two vanadium atoms, which amount to 0.113 and 0.309 respectively. Thus, at variance with the reaction at one vanadium-oxygen polyhedron, where both parts of the cleaved C-H bond become attached to the same oxygen atom with the formation of an alcohol molecule, here the two parts of the C-H bond: hydrogen atom and the allyl group become linked to

two different oxygen atoms and the allyl group, after losing the second hydrogen atom, transforms into the aldehyde molecule.

A series of calculations repeated with different parts of the cluster frozen and only some oxygen atoms allowed to optimize their positions showed that the direction of the reaction pathway depends on the possibility of relaxation of oxygen atoms in the cluster. A conclusion may be thus formulated that one of the decisive factors determining the direction of the reaction of propene at the oxide surface is the availability of mobile oxygen atoms at this surface and the possibility of its easy reconstruction.

Table 3. Bond distances and bond order indexes (in parenthesis) for selected reaction coordinates  $R_{C-O}$  on approach of propene molecule to  $V_2O_9H_8$  cluster.

$R_{C-O}$ (Å)	$V_1-O_5$	$V_2-O_5$	$V_2-O_9$	$V_2-O_{11}$	$C_1-O_5$	$O_9-H_3$	$O_{11}-H_2$
$\infty$	1.89 (1.11)	1.89 (1.11)	1.89 (1.11)	1.89 (1.11)			
3.0	1.93 (1.15)	1.93 (1.15)	2.05 (1.01)	2.05 (1.01)	2.88 (0.00)	3.32 (0.00)	3.32 (0.00)
1.6	1.95 (1.04)	1.96 (1.01)	2.08 (0.97)	2.03 (1.02)	2.35 (0.01)	2.69 (0.00)	2.44 (0.00)
1.55	2.45 (0.16)	2.01 (0.86)	2.08 (0.98)	2.02 (1.06)	1.35 (1.08)	2.60 (0.00)	1.47 (0.00)
1.5	2.00 (0.97)	2.28 (0.34)	2.16 (0.86)	2.34 (0.29)	1.37 (0.97)	2.65 (0.00)	1.01 (0.91)
1.4	2.47 (0.16)	2.66 (0.11)	2.29 (0.42)	2.29 (0.35)	1.28 (1.67)	1.05 (0.76)	1.00 (0.91)
Optimum	2.65 (0.11)	2.36 (0.31)	2.31 (0.38)	2.29 (0.49)	1.25 (1.83)	1.05 (0.90)	1.04 (0.72)

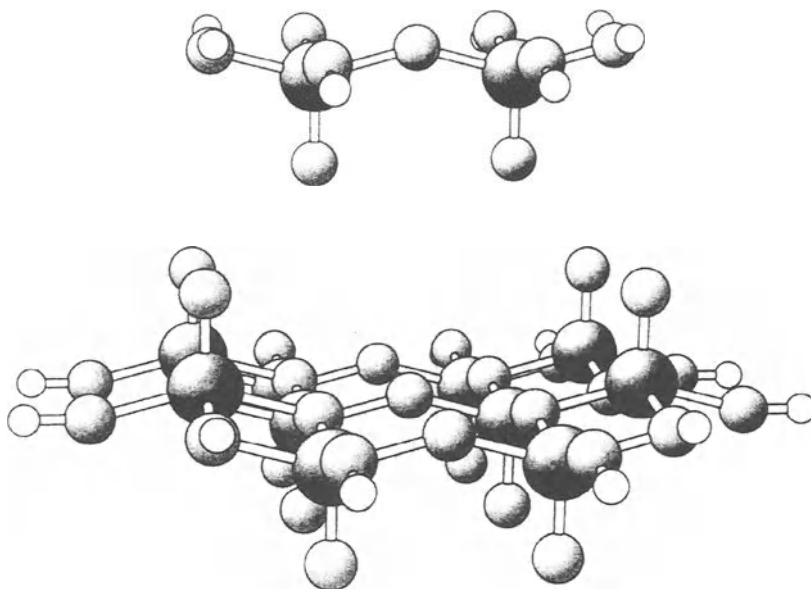


Figure 11. Cluster models of the  $V_2O_5$  catalysts: A)  $V_2O_9H_8$ , B)  $V_{10}O_{31}H_{12}$

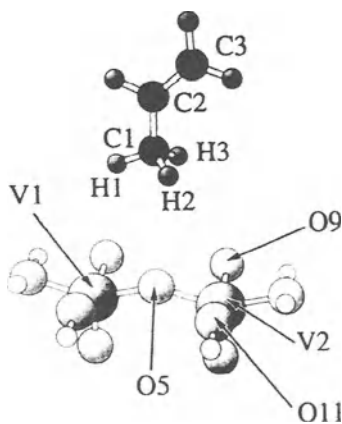
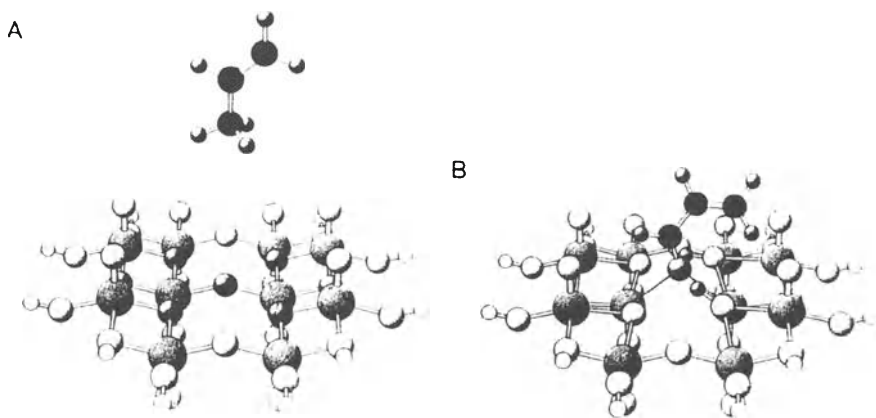


Figure 12. Direction of approach of propene molecule to  $V_2O_9H_8$  cluster.

These results were confirmed by calculations of the interaction of propene with clusters  $V_{10}O_{31}H_{12}$ . When propene molecule is placed at the distance of 2.6 Å above the bridging oxygen atom of the cluster (Fig. 13A) end-on, with the methyl group facing cluster, and all its atoms, as well as oxygen atoms of the cluster, are allowed to "move" freely and "find" the positions corresponding to



the minimum of potential energy, one of the C-H bonds in the methyl group of propene is cleaved and the hydrogen atom migrates to one of the adjacent bridging oxygen atoms, whereas the allyl group becomes linked to the bridging oxygen atom forming an alkoxy group. It then loses the second hydrogen atom, which forms a second OH group with another oxygen atom of the cluster the alkoxy group transforming into adsorbed acrolein.. Simultaneously, the oxygen atoms are lifted above the plane of the cluster. The initial and final state of these interactions are illustrated in Fig. 13A and B. It may be seen that similarly as in the case of the cluster, composed of two square pyramids, both parts of the cleaved C-H bond bind to surface oxygen atoms. Similar mechanism [12,14] operates in the case of a toluene molecule approached end-on with the methyl group pointing to the bridging oxygen O(II) of the  $V_{10}O_{31}H_{12}$ . At first the bond is formed between the carbon atom of the methyl group of toluene and the bridging oxygen O(II) of the cluster, which is pulled out above the surface of the cluster. Simultaneously the two hydrogen atoms of the methyl group consecutively move to oxygen atoms O(III), which are also raised above the surface of the cluster and the molecule of benzaldehyde is formed. The bonds between its oxygen atom and the vanadium atoms of the cluster are so weak that the molecule may be considered as weakly chemisorbed at the surface. The consecutive steps of the interaction of a toluene molecule with the cluster are shown in Fig. 14.



*Figure 13.* Interaction of propene with the  $V_{10}O_{31}H_{12}$  cluster, A - initial state, B - final state (after ref. 10).

Ab Initio Hartree-Fock calculations of the electronic structure of vanadium oxide clusters revealed [15] that a strong negative electrostatic potential, generated by oxide ions, stretches above its surface. As the hydrocarbon molecule is also surrounded by a negative electrostatic potential, repulsive

forces operate. Once the energy barrier arising from this repulsive is overcome, attractive interactions may develop. The HOMO of the cluster are oxygen p-orbitals which form a band. Well above this band lie the LUMO of the cluster, composed mainly of the d orbitals of vanadium, which may be considered to practically form a band of non-bonding levels. The HOMO of the hydrocarbon molecule which should be considered when this molecule approaches the cluster with its methyl group, is the complex pC and sH orbital of the methyl group. Its energy corresponds to the energy of the HOMO of the cluster. The LUMO of the hydrocarbon molecule is the corresponding antibonding orbital. A mechanism of the activation of the C-H bond and formation of a C-O bond may be envisaged, in which the incoming hydrocarbon molecule, under the influence of the electrostatic field, becomes first polarized so that a positive charge appears on carbon atom of the methyl group (Fig. 15). Then a bond is formed between this carbon atom and oxygen atom of the cluster through interaction of the HOMO of the cluster, which is the lone electron pair orbital of oxygen atoms and the LUMO of the hydrocarbon molecule, which is the  $\sigma^*$  antibonding C-H orbital of the methyl group. The C-H bond becomes cleaved and both parts are linked to oxygen ions. In the next step the second hydrogen atom from the same carbon atom or from adjacent one is transferred to oxygen atom of the cluster, and electrons are injected onto the vanadium empty orbitals. Oxidation or oxidative dehydrogenation takes place.

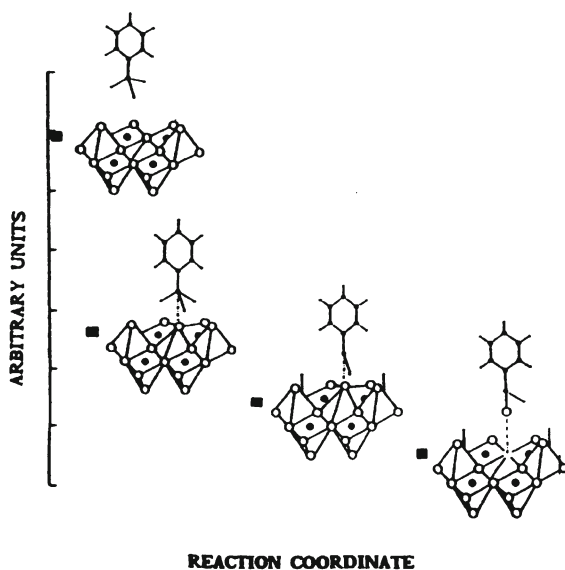
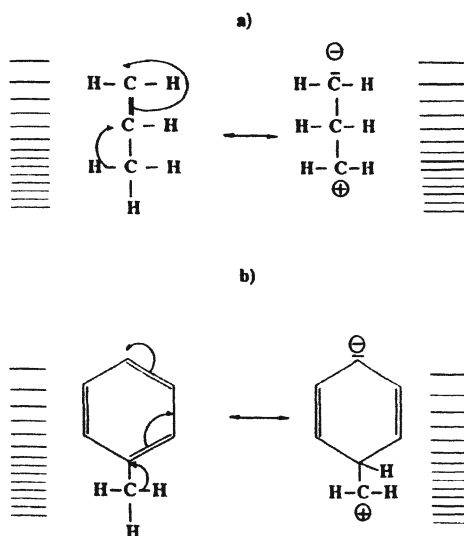


Figure 14. The sequence of elementary steps in the oxidation of toluene (after ref. 11).



*Figure 15.* Polarization of propene (a) and toluene (b) molecules in the electrostatic field at the surface of an oxide cluster.

The process of injection of electrons from species, adsorbed at the surface, into the energy bands of the solid is governed by the relative positions of the energy levels of the redox system in the reduced and oxidized state relative to the band gap of the solid, the density of states and the position of the Fermi level in the solid and the orbital overlap. It should be also remembered that bending of energy bands at the surface may take place due to the appearance of the surface charge.

## 6. Oxidation of Butane

Oxidation of n-butane to maleic anhydride is the only process of selective oxidation of a paraffin applied on a large industrial scale [16, 17]. It is the 14 electron oxidative transformation, in which 6 hydrogen atoms are abstracted from and 3 oxygen atoms are attached to the hydrocarbon molecule. Analysis of Fig. 1 leads to the conclusion that the reaction pathway from butane to maleic anhydride may lead through following elementary steps:

n-butane  $\rightarrow$  butenes  
 butene -2  $\rightarrow$  butadiene  
 butadiene  $\rightarrow$  2,5 dihydrofuran  
 2,5 dihydrofuran  $\rightarrow$  furan  
 furan  $\rightarrow$  maleic anhydride

oxidative dehydrogenation  
 oxidative allylic dehydrogenation  
 1,4 oxygen addition  
 oxidative dehydrogenation  
 oxygen addition

Experiments show that the initial rate of butenes oxidation is several tens times higher than that of butane. Therefore it has been concluded that the transformation of butane into butenes is rate determining. However, the most striking feature of the oxidation of butane to maleic anhydride is that no intermediates are observed among the reaction products. Several explanations have been suggested. The absence of intermediates may be due to kinetic reasons: if in the series of consecutive transformations all steps show much higher rate than the first one, the concentrations of intermediate products may be very small and difficult to detect. However, the compounds formed as intermediates are known to react along several different pathways, giving various products. Indeed, in the oxidation of butenes, butadiene and furan, at the same conditions as those used for the oxidation of n-butane, maleic anhydride is formed with much lower selectivity, whereas the oxidation of butane is remarkably selective. High selectivity and absence of intermediate products may be also explained by assuming that the rate of desorption of the intermediates is very small. Thus, the rake mechanism, usually assumed in the case of selective oxidation processes, does not operate in the oxidation of butane, in the course of which all the transformations take place in the chemisorbed state [18]. Finally, the characteristic features of the oxidation of butane may be explained by assuming that it is proceeding by a concerted mechanism.

The only catalytic system found to be active and selective in butane to maleic anhydride oxidation is V-P-O. A large number of studies attribute catalytic activity and selectivity to the presence of the bulk crystalline phase of vanadyl pyrophosphate  $(VO)_2P_2O_7$  [19]. It is now generally accepted that it is the (100) crystal plane of vanadyl pyrophosphate which exposes the active sites of the reaction. These sites are composed of two edge-linked vanadium-oxygen square pyramids with trans orientation of vanadyl groups, surrounded by phosphate groups corner-linking the dimeric vanadium square pyramids into sheets, and sheets into tridimensional lattice by formation of pyrophosphate bonds [20]. Schematic representation of such composite active site is shown in Fig. 16. Some data published recently seem to indicate that the active phase is an amorphous vanadium phosphate of P/V ratio around 2, supported on vanadyl pyrophosphate [21]. This raises the question as to whether the long range order is really necessary for the catalyst to be active and selective or the short range order is sufficient for the transformation of the molecule to take place.

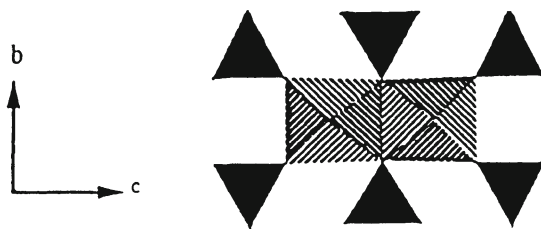


Figure 16. Schematic representation of the elementary unit of the  $(VO)_2P_2O_7$

Some time ago a mechanism of n-butane oxidation was proposed [22], in which four dimers delineated by pyrophosphate groups, sticking out above the surface, were assumed to be composite active site. In the model, these dimeric sites undergo a cycle, in which the oxidation state of vanadium ions of the dimer is changed from  $V^{IV}$ - $V^{IV}$  in the initial vanadium pyrophosphate to  $V^{IV}$ - $V^V$  (one electron oxidation to state  $S_3$ ) and to  $V^V$ - $V^V$  (two-electron oxidation to state  $S_2$ ) after adsorption of oxygen to  $V^{III}$ - $V^{III}$  (state  $S_0$ ) after interaction with butane and finally back to  $V^{IV}$ - $V^{IV}$  after reoxidation with oxygen (Fig.17). The

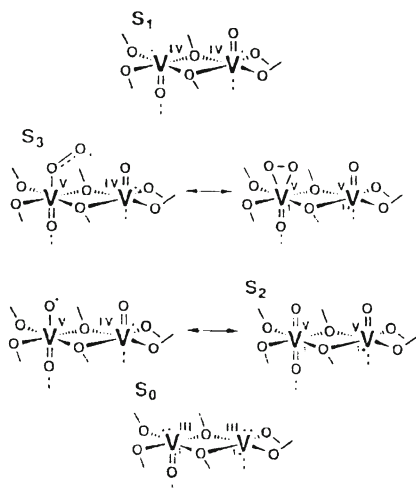


Figure 17. Schematic representation of the structure of the dimeric active site in the various dynamic states that it can assume in the course of n-butane oxidation (after ref. 22)

initial activation of butane occurs by hydrogen abstraction from a methylene group to give a surface bound hydroperoxy group and the adjacent vanadyl

group interacts with the alkyl radical to form a surface bound alkoxy group. The hydroperoxy group can abstract the second hydrogen either from the  $\alpha$  or  $\beta$  position of the alkoxy group to form water and either of the two surface species shown in Fig.18: 2-butanone adsorbed on active site in the state S1 or 2-butene adsorbed on active site in the state S2. Butene becomes then oxidized to 1,3-butadiene which interacts with oxygen of the vanadyl group to give furan, and by reaction with adsorbed molecular oxygen to maleic anhydride. On the basis of comparison of the reaction of n-butane with molecular oxygen and with  $N_2O$  the authors claimed that only molecular efficiently and with high selectivity oxidizes n-butane to maleic anhydride, what they considered as supporting the above mechanism. On the other hand it has been found [20] that the oxidation of n-butane in a riser-type reactor occurs with high selectivity in the absence of molecular oxygen, yielding maleic anhydride with a selectivity higher than that obtained in the presence of oxygen.

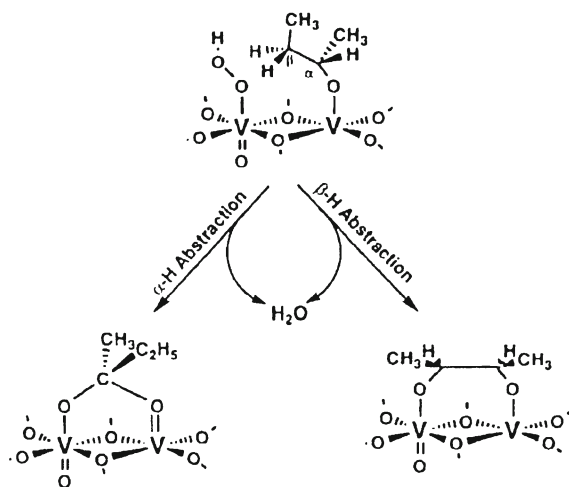
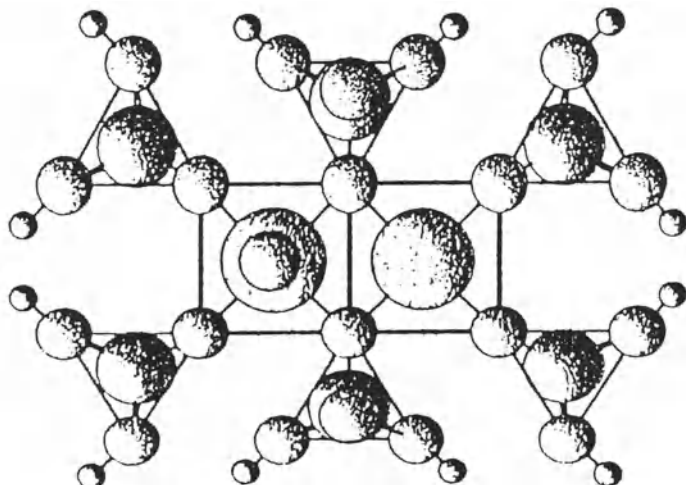


Figure 18. Surface species generated by the interaction of n-butane with the active site in state S3 (after ref. 22)

In order to obtain more detailed information on the molecular mechanism of this reaction an attempt was undertaken to model on the basis of quantum chemical calculations the interaction of butane molecule on its approach to the cluster of the composition  $(VO_4)_2(PO_3)_6 H_{12}$  taken as a model of an elementary structural unit of the (100) crystal plane of vanadyl pyrophosphate, in which the terminal oxygen atoms at the edges were saturated by hydrogen atoms to mimic the embedding of the cluster in the lattice of the solid catalyst (Fig.19). The calculations were carried out by means of the INDO method using the

ZINDO programme. The butane molecule was approached to the cluster with the carbon atoms plane parallel or perpendicular to the basic plane of the cluster, in the latter case the terminal methyl groups pointing to the cluster along the common edge of the two vanadyl-oxygen square pyramids. In this way local minima located along the pathway of the approach or in its vicinity were identified [23].



*Figure 19.* Cluster model used to mimic the active site of the catalyst surface (after ref. 12)

When butane molecule is approached to the cluster, represented by the model show in Fig. 19, along the perpendicular reaction pathway, the two surface oxygen atoms of  $\text{PO}_4$  tetrahedra become inserted into the C-H bonds of C1 and C4 carbon atoms, forming terminal C-OH groups. Simultaneously, the terminal carbon and hydrogen atoms interact with the oxygen atom of the vanadyl group, which results in splitting the C-H bonds and formation of an oxygen bridge between the two carbon atoms, (Fig.20). The possible molecular mechanism of such concerted reaction is show in Fig. 21. A question may be raised at this point as to whether the presence of phosphate groups plays any role in the formation of the C-O-C bridge. In order to answer this question, the calculation has been repeated for an analogous system, in which the phosphorus atoms were substituted by vanadium atoms. It turned out that in such case the terminal C-OH groups are formed similarly as on vanadyl pyrophosphate unit, but no formation of the C-O-C bridge takes place. It may be thus concluded that the arrangement of vanadium-oxygen square pyramids surrounded by corner-linked phosphate groups shows a unique property of forming the C-O-C bridge.



The calculations carried out with a cluster  $V_{10}O_{28}$ , cut off from the real structure of  $V_2O_5$  gave the same result of formation of only terminal C-OH groups confirming the conclusion that the ability to form C-O-C bridge seems to be connected with the simultaneous presence of both V-O and P-O polyhedra linked together through corners. It is interesting that recent "in situ" studies in HREM [19] revealed that on exposure of vanadium pyrophosphate to butane at 400 °C shear planes are formed by removal of oxygen atoms from the phosphate groups bridging the vanadium-oxygen square pyramid dimers.

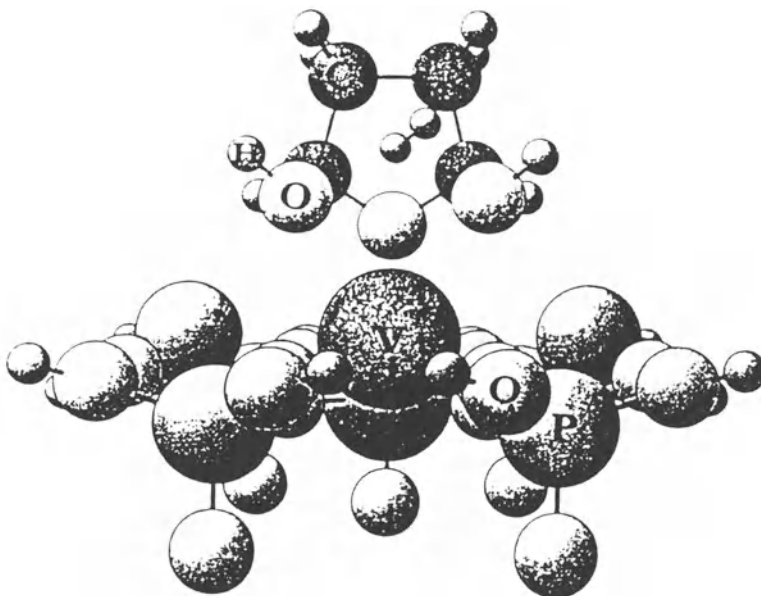


*Figure 20.* Precursor of maleic anhydride formed as the result of the perpendicular approach of butane molecule to the cluster of fig. 19 (after ref. 12)

When only two adjacent oxygen atoms at phosphorus and vanadium are present at the surface, a geminal dialcohol is formed because only one carbon atom becomes activated in such a way that it is able to form a bond with vanadyl oxygen. The presence of additional surface oxygen atoms in the phosphate groups located further away does not influence the course of the reaction. Apparently, the given reaction pathway on the potential energy hypersurface seems to be dependent mainly on the nearest surrounding.

These examples illustrate the critical importance of the presence of three surface oxygen atoms in an appropriate sequence P-O, V=O, P-O, for the formation of the oxygen bridge between terminal carbon atoms of butane molecule. It is noteworthy that all three oxygen atoms required to transform



butane into maleic anhydride may become incorporated in the first step of the reaction by a concerted transformation. The question remains as to how the four hydrogen atoms are removed from this intermediate in the next step or steps of the reaction to give the molecule of maleic anhydride.

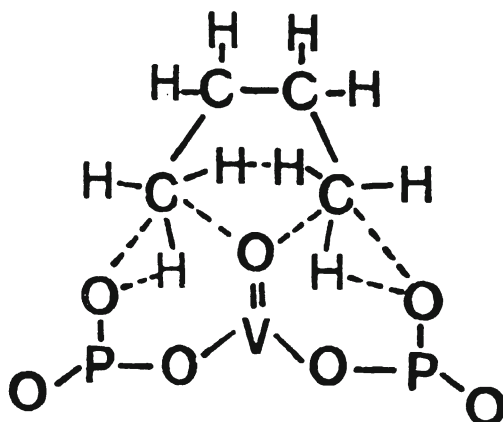


*Figure 21.* Transition complex of the reaction leading to the formation of a precursor of maleic anhydride, represented in Fig. 20 (after ref. 12).

## 7. Perspectives or C-H Bond Activation

As mentioned in the introduction, many different steps of the selective oxidation of a hydrocarbon molecule require an activation of the C-H bond. One of the most important steps is the activation of alkanes for their oxidative dehydrogenation. Since lower alkanes are now in large surplus, their price is steadily decreasing, whereas the demand for olefins continues to grow steadily, due primarily to an increase in demand of propene and isobutene. The demand for propene increases because of the rapid growth in the market for polypropylene. Isobutene is the conventional feedstock for the production of methyl-tert-butyl ether (MTBE), an important additive to gasoline, whose demand grows rapidly. Propene and iso-butene are obtained conventionally by steam cracking. As demand continues to grow, dehydrogenation of propane and iso-butane are expected to become an increasingly important source of olefins.

Non-oxidative catalytic dehydrogenation faces a number of technical challenges, including thermodynamic limitations, high endothermicity and the deposition of coke on the catalyst. Most of these challenges can be avoided by using oxidative dehydrogenation. The introduction of a hydrogen acceptor into

a dehydrogenation reaction medium shifts the thermodynamic equilibrium making the reaction virtually irreversible, even at lower temperatures.

The dehydrogenation reaction of a hydrocarbon molecule may be expressed by the formula



The equilibrium constant,  $K_p$  for this dehydrogenation reaction is calculated using the formula

$$-RT \ln K_p = \Delta G^0_{\text{C}_n\text{H}_{2n}} - \Delta G^0_{\text{C}_n\text{H}_{2n+2}} \quad (4)$$

Paraffins are more stable than olefins, because the Gibbs free energies of formation ( $\Delta G^0$ ) of paraffins at low temperatures are lower than those of the corresponding olefins.

However, the  $\Delta G^0$  values of paraffins increase with temperature much more rapidly than those of olefins. At higher temperatures, therefore, olefins become more stable than paraffins and dehydrogenation is favored. The temperature, at which  $\Delta G^0$  for the above reaction is zero ( $K_p = 1$ ) is the inversion temperature.

When a hydrogen acceptor (A) is introduced into the system, the dehydrogenation becomes an oxidative dehydrogenation. Equation (3) is replaced with equation (5):



The equilibrium constant is given by the equation:

$$-RT \ln K_p = \Delta G^0_{\text{C}_n\text{H}_{2n}} + 2\Delta G^0_{\text{HA}} - \Delta G^0_{\text{C}_n\text{H}_{2n+2}} \quad (6)$$

If A is a strong hydrogen acceptor, the Gibbs free energy of formation of HA ( $\Delta G^0_{\text{HA}}$ ) has a high negative value and  $K_p$  has a high positive value. Hence the equilibrium of reaction (5) shifts sufficiently far to the right that the reaction may be considered to be irreversible, even at relatively low temperatures.

Many different molecules function as hydrogen acceptors. Such molecules include:

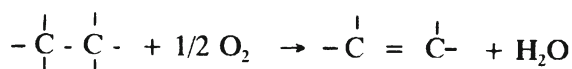
- oxygen and compounds that release oxygen on decomposition,
- halogens,
- sulphur compounds, such as sulphur dioxide, hydrogen sulphide and carbon sulfoxides.

These accepts form with hydrogen forms simple compounds, such as water, hydroiodic acid, hydrobromic acid, hydrochloric acid and hydrogen sulphide are characterized by negative values of the Gibbs free energy of formation over

almost the entire temperature range for the dehydrogenation reaction. The most commonly used hydrogen acceptor is oxygen. The Gibbs free energy of formation of water (228.7 kJ/mol at room temperature) is considerably greater than the change of Gibbs free energy usually associated with dehydrogenation (87 kJ/mol<sup>-1</sup>). This high value of the Gibbs free energy of formation accounts for the irreversibility of oxidative dehydrogenation over a broad range of temperatures. The high heat of formation of water (243 kJ/mol) not only compensates for the energy loss due to the abstraction of hydrogen, but also makes the dehydrogenation reaction strongly exothermic.

Any oxygen present in the reaction medium may attack and may be incorporated into the hydrocarbon molecule, which results in the formation of oxygenated products (partial oxidation) and, finally, in the total combustion of the molecule. All these processes are accompanied by large negative changes in Gibbs free energy. The most thermodynamically stable products are carbon dioxide and water, which should always be formed preferentially. Therefore, the main challenge is to activate C-H bonds in the presence of gas phase oxygen but incorporated into the hydrocarbon molecule. The catalyst should be tailored to significantly accelerate the abstraction of hydrogen from the hydrocarbon molecule and to minimize both the nucleophilic addition of oxygen to this molecule and the electrophilic attack of oxygen molecules on the C-C bonds.

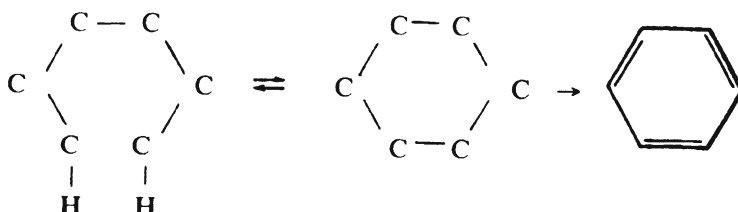
The oxidative dehydrogenation may be intramolecular or intermolecular. The intramolecular oxydehydrogenation occurs when the two C-H bonds split are on adjacent carbon atoms and a  $\pi$  bond is formed:



Typical intramolecular oxidative dehydrogenation reactions include:

- oxidative dehydrogenation of a C<sub>4</sub> mixture to butadiene,
- oxidative dehydrogenation of ethylbenzene to styrene,
- oxidative dehydrogenation of propane to propene,
- oxidative dehydrogenation of isopentene to isoprene.

When the two C-H bonds that are split belong to nonadjacent carbon atoms, a cyclane is formed. The cyclane dehydrogenates to an aromatic ring whenever possible:



In the first step, which is oxidative dehydrocyclisation, a  $\sigma$  carbon-carbon bond is formed. This first step cannot usually be separated from the second step, which is the aromatization. For example, hexane reacts to form cyclohexane, cyclohexene and eventually benzene.

Oxidative dehydrogenation can also be applied to hydrocarbon molecules that contain functional groups. This opens many new perspectives for the synthesis of fine chemicals. Many other possibilities emerge from intermolecular oxidative dehydrogenation (dehydrocondensation). The simplest example is dehydrodimerization, in which hydrogen atoms are abstracted from two hydrocarbon molecules and a  $\sigma$  bond is formed between two  $\alpha$  carbon atoms. With alkyl benzenes this bond may be formed either between the carbon atoms of the ring or between the carbon atoms of the alkyl groups. The reaction may be described by the general equation:



The most studied example is coupling of methane to form ethane and ethylene. Many catalysts have been tested, among them lithium-doped magnesium oxide, lead oxides, chromium oxides supported on titanium oxide. Another typical example is the dimerization of isobutene to xylene using oxides of tin and bismuth. Bond formation between alkyl group carbons is illustrated by the formation of dibenzyl and stilbene. A separate group of reactions called oxidative dehydroheterocyclization may be represented by the equation



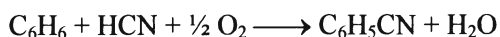
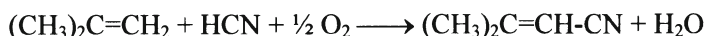
The heterocycle is formed using an oxygen atom and two carbon atoms of the hydrocarbon from which hydrogen is abstracted. An example is the formation of furan from n-butene and butadiene in the presence of oxygen.

Oxidative coupling reactions, which are very interesting synthetic reactions, include oxidative alkylation reactions that combine dehydrogenation and dehydration. Oxidative coupling reactions may be represented by the schemes:

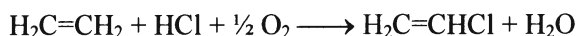


A good example of oxidative alkylation is the synthesis of isoprene by the alkylation of isobutene with methanol in the presence of oxygen. The reaction uses oxides of tungsten and tellurium or uranium and molybdenum as catalysts.

Another interesting oxidative reaction is the oxidative dehydrovinylation of benzene with ethylene. Styrene is obtained when catalysts of platinum group metals supported on active carbon are used. Among the oxidative coupling reactions oxidative cyanation and oxidative chlorination have gained considerable importance. Oxidative cyanation offers an easy route to nitriles:



Oxidative chlorination is used to obtain chlorides of hydrocarbons, as demonstrated in the one-step production of vinyl chloride:



## 8. References

1. Haber, J., 1996, Selectivity in Heterogeneous Oxidation of Hydrocarbons. in B.K. Warren and S.T. Oyama (eds) Heterogeneous Hydrocarbon Oxidation. ACS Symp. Series 638 American Chemical Society, Washington, p.20
2. Van Hove, M.A., Samorjai, G.A., 1994, Adsorption and adsorbate induced restructuring: a LEED perspective, Surf. Sci. 299/300, 487.
3. Stoutland, P.O., Bergman, R.G., Nolan S.O., Hoff, C.D., 1988, Polyhedron 7, 1429.
4. Hall, C., Perutz, R.N., (1996), Transition Metal Alkane Complexes. Chem.Rev., 96, 3125.
5. Broclawik, E., (1997), Density Functional Theory in Catalysis: Activation and Reactivity of a Hydrocarbon Molecule on a Metallic Active Site, Adv. Quantum Chem. (in print).
6. Schultz, R.H., Bengali, A.A., Tauber, M.J., Weiller, B.H., Wasserman, E.P., Kyle, K.R., Moore, C.B., Bergman, R.G., (1994), IR Flash Kinetic Spectroscopy of C-H Bond Activation of Cyclohexane-d<sub>0</sub> and d<sub>12</sub> by CpRh(CO)<sub>2</sub> in Liquid Rare Gases, J. Am. Chem. Soc. 116, 7369.

7. Musaev, D.G., Morokuma, K., 1995, Ab Initio Molecular Orbital Study of the Mechanism of H-H, C-H, N-H, O-H, and Si-H P Activation on Transient Cyclopentadienylcarbonylrhodium, *J. Am. Chem. Soc.* 117, 799.
8. Blomberg, M.R.A., Siegbahn, P.E.M., Svenson, M., 1991, *J. Phys. Chem.* 95, 4313.
9. Deo, G., Wachs, I., Haber, J., 1994, Supported Vanadium Oxide Catalysts: Molecular Structural Characterization and Reactivity Properties. *Critical Rev. Surf. Chem.* 4, 141.
10. Haber, J., Witko, M., Tokarz, R., 1997, Molecular Mechanism of the Catalytic Activation of Hydrocarbons in Oxidation Processes, (in print).
11. Anderson, A.B., 1990, Structure and Electronic Factors in Heterogeneous Catalysis: C=C, C=CO and C-H Activation Processes on Metals and Oxides, in J. Moffat (ed) *Theoretical Aspects of Heterogeneous Catalysis*, Van Nostrand Reinhold, New York, p. 431.
12. Haber, J., Witko, M., 1995, Quantum-chemical modelling of hydrocarbon oxidation on vanadium-based catalysts, 23,311.
13. Witko, M., Tokarz, R., Haber, J., 1997 Vanadium Oxide. II. Quantum-chemical Modelling, *Appl. Catal.* 157.
14. Haber, J., Tokarz, R., Witko, M., 1994, Quantum-chemical description of the of alkylaromatic molecules on vanadium oxide catalysts, *Stud. Surf. Sci. Catal.* 82, 739.
15. Witko, M., 1996, *Catal. Today* 32, 89.
16. Cavani, F., Trifiro, F., 1992, *Appl. Catal. A: General*, 88, 115.
17. Centi, G., Trifiro, F., Ebner, K.J.R., Franchetti, V.M., 1988, *Chem. Rev.* 88, 55.
18. Cavani, F., Trifiro, F., 1997, An Analysis of the Aspects that Affect the Selective Oxidation of C1-C5 Paraffins, *Proc. Memorial Boreskov Conference*, Boreskov Institute of Catalysis, Novosibirsk, p. 100.
19. Centi, G. *Catal. Today* 1993, 16, 1.
20. Cavani, F., Trifiro, F., 1994, in *Selective Oxidation of C4 Paraffins*, in *Catalysis, Specialist Periodical Reports*, Royal Society of Chemistry, London, vol. 11, p.224.
21. Szakacs, C., Wolf, H., Mink, G., Bertoli, L., Wustnek, N., Lucke, B., Seeboth, H., 1987, *Catal. Today* 1, 27.
22. Agaskar, P. A., DeCaul, L., Grasselli, R. K., 1994, A Molecular Level Mechanism of n-Butane Oxidation to Maleic Anhydride over Vanadyl Pyrophosphate, *Catal. Lett.* 23, 339.
23. Haber, J., Tokarz, R., Witko, M., 1996, Mechanism of Selective Oxidation of Butane to Maleic Anhydride on Vanadyl Pyrophosphate Catalysts: QuantumChemical Description, in B.K. Warren and S.T. Oyama (eds) *Heterogeneous Hydrocarbon Oxidation ACS Symposium Series 638*, American Chemical Society, Washington, p.249.8

# AN INTRODUCTION TO MOLECULAR HETEROGENEOUS CATALYSIS

C.R.A. CATLOW, R.G. BELL, J.D. GALE, D.W. LEWIS,  
D.C. SAYLE, P.E. SINCLAIR

*Davy Faraday Laboratory, The Royal Institution of Great Britain,  
21 Albemarle Street, London W1X 4BS, UK*

## 1. Introduction

Computer modelling is now an indispensable tool in modelling complex systems in both physical and biological sciences. Catalysis is proving to be an increasingly fruitful field for the application of these techniques, with notable recent contributions to the elucidation of structures — both local and long range — of complex microporous materials[1, 2, 3]; to the modelling of sorption and diffusion in catalytic systems[4, 5, 6]; to the understanding of reaction mechanisms[7, 8, 9] and to the modelling[10, 11, 12] and design[13] of templates for the synthesis of specific microporous architectures. These and other recent studies clearly demonstrate the rôle of computational methods in developing models which are of direct relevance to real catalytic systems and problems.

As the field has been extensively reviewed in recent years, both by ourselves[14, 15, 16] and others[17, 18], the account presented in this article does not attempt to be comprehensive. Rather, we aim to illustrate the present status and scope of atomistic modelling in catalysis by providing a number of illustrations from our own recent work. Our account includes a discussion of the modelling of reaction mechanisms, as we see the development of improved procedures for modelling reactivity as perhaps the key challenge to the field at present; and, as we will show, there has been substantial progress in modelling reactions in microporous solids. Modelling of structural properties of catalytic materials and of molecular sorption and diffusion remains, nevertheless, an active area, as illustrated in earlier sections of the article where we describe recently developed models for mesoporous silicates and discuss the important recent developments, referred to above, in the computational design of



templates. First, however, we summarise both the rôles of computer modelling in catalytic studies and the main techniques that are now available to the field.

## 2. Aims and Methodologies

The overall objective of the application of atomistic computer modelling techniques in catalysis is, as we have discussed elsewhere[15] to contribute to our understanding of catalysts and catalysis at the molecular level. Such an understanding requires models first of structures of, for example, microporous catalysts and the surfaces of catalytic oxide materials, but more importantly, the local structure of defects and impurities that commonly provide the active sites in catalysts. Secondly, we need models of the sorption and diffusion of molecules within the micropores and on surfaces. Finally, as already emphasised, we need to develop models of mechanistic processes in catalytic reactions.

Modelling of the structural properties and of sorption and diffusion is best achieved by methods based on interatomic potentials (which may be referred to as "forcefield" techniques). *Energy Minimisation* (EM) methods have been used with great effect to *model the structures and energies* of complex inorganic solids, for example, microporous materials[1, 2, 3, 19]. Moreover, by combining minimisation techniques with other procedures such as simulated annealing[16, 20, 21, 22] and genetic algorithm[22] methods which can effectively generate approximate models (which may then be refined by minimisation techniques), these methods have become increasingly predictive, as in the recent work of Akporiaye *et al.*[23] which successfully solved the structure of a complex microporous solid UiO-7. The field of structure modelling and prediction has been extensively discussed elsewhere[3, 16, 20], to which we refer the reader. In this article we give, as noted, one example in section 3 of a recent application to a highly complex problem, namely the development of atomistic models for mesoporous silicate systems.

Modelling of *local structures* can also be effected by minimisation procedures. Good examples are provided by the work of Lewis *et al.* on the local environment of ferric iron in the Fe ZSM-5 catalyst[24]. A recent application to the topical Cu ZSM-5 system will follow in section 5.

*Surface modelling* has developed rapidly in recent years using standard minimisation procedures, adapted to the 2-dimensional periodicity of surface structures. It is now possible to develop detailed models of the surfaces of complex catalytic materials, including microporous solids. A recent review is available in reference 25.

The modelling of *sorption and diffusion* of molecules on (and in) catalytic materials is now well developed. *Molecular dynamics* (MD) methods[4, 5, 26,]



have been used extensively to model, for example, hydrocarbon diffusion in zeolites. The method is restricted to relatively rapid diffusion processes; modelling of slower diffusers can, however, be effected by methods based on transition state theory[27]. *Monte Carlo* (MC) methods have been extensively used in modelling sorption. Work of Yashonath *et al.*[28] demonstrated the efficacy of standard canonical MC methods for studying the temperature dependence of sorption in zeolites. Freeman *et al.*[29] have shown the value of a procedure which blends MC, MD and EM techniques for locating low energy sites for sorbed molecules in microporous solids. Our ability to model the sorption of larger alkane molecules in zeolites has been greatly advanced by the configurational bias MC methods used by Smit and coworkers[6]. In addition, standard Grand Canonical Monte Carlo methods[30, 31] are being used increasingly to simulate sorption isotherms; and "Kinetic Monte Carlo" methods may be used to model diffusion processes[32]. The procedures in this field are, in general, now well developed and the main need is for the refinement of the interatomic potentials which, of course, ultimately determine the reliability of calculations.

A related and highly topical field concerns the interaction of template molecules with microporous hosts — a crucial factor controlling the synthesis of these materials. As noted, this topic has been extensively explored in recent years using a range of simulation techniques, and has now reached the stage that computational methods can be used to predict templates for specific microporous structures. A recent example is given in section 4.

Interatomic potential based methods can therefore be used with great effect to investigate the structural and physical chemistry of catalytic materials. Investigation of reactivity requires, of course, the use of methods that model bond breaking and bond making, *i.e.* quantum mechanical techniques. A powerful battery of such methodologies are now available, including *Hartree Fock* (HF)[33, 34] (and post Hartree Fock) methods and *Density Functional Theory* (DFT) techniques[35]. Moreover, these methods can be applied to clusters (embedded whenever possible in a representation of the surrounding lattice) to represent the active site of the catalyst interacting with a molecule; or to periodic arrays of active site/molecule complexes. Examples of both approaches, with greater details of the techniques employed, will follow later in this article, which will emphasise applications to catalysis in microporous materials. The following sections, however, describe a range of simulation studies based on the use of interatomic potentials.

### 3. Modelling of Structures

Since the discovery of the first ordered mesoporous molecular sieves with pore diameters in the range 25–100 Å, there has been a phenomenal growth in research into these fascinating materials, with a wide range of different structures and compositions having been reported, as well as a variety of catalytic applications.

In many cases the short-range structure of the new mesopores is not well understood. In particular, the original MCM-41 phases[36, 37], prepared by liquid crystal templating, form highly regular hexagonal arrays of pores, and were initially reported to have pore walls as thin as *ca.* 2 T-atoms width. However, there was no evidence for any short range order, and it has been generally accepted that the pore walls consist largely of amorphous silica, a conclusion which is supported by the presence of a high concentration of terminal silanol groups. It is, nevertheless, reasonable to suppose that there exists some degree of ordering of SiO<sub>4</sub> tetrahedra.

In attempting to model the properties of these materials, we have followed two approaches: first, we have designed regular "zeolitic mesopore" model structures in which, as in conventional zeolites, each T atom is connected to four others by an oxygen bridge. Secondly, we have used a completely amorphous silica surface, still containing 4-coordinated T atoms, but replete with terminal SiOH groups. Each model has been subjected to energy minimisation calculations, and a number of properties of the material simulated from the optimised models.

#### 3.1 MODELS

As first postulated by Smith and Dytrych[38], it is possible to construct an infinite series of hexagonal zeolite structures with uniform channels of  $6n$  T atoms, where  $n = 2$  represents the AFI structure and, as it transpired,  $n = 3$  is equivalent to the topology of VFI. We have extended this series to obtain structures with effective pore diameters of greater than 25 Å, and have examined 30-, 36- and 42-ringed structures. Each framework was constructed from SiO<sub>4</sub> tetrahedra and subjected to full energy minimisation. The principal features of the optimised structures are summarised as follows:

Table 1. Structural data for hypothetical "Zeolitic Mesopores"

T atoms in ring	$a/\text{\AA}$	$c/\text{\AA}$	Free diameter/ $\text{\AA}$	Space group
30	27.96	8.36	21.0	$P62m$
36	32.40	8.51	25.3	$P6/mcc$
42	37.03	8.36	30.0	$P62m$

Table 2. "Zeolitic Mesopores": relative stabilities

Material	Lattice energy ( $\text{kJmol}^{-1}/\text{SiO}_2$ )
Quartz	0
Silicalite	11
30-ring	24
36-ring	27
42-ring	26

Like all siliceous zeolites, the "zeolitic mesopores" are metastable with respect to quartz. The relative lattice energies (around  $25 \text{ kJmol}^{-1}$  less stable than quartz) compare well with reported thermodynamic data[39].

Amorphous mesopore models (see Figures 1 and 2), were based on the silica glass structures modelled by Vessal *et al.*[40] using molecular dynamics techniques. The shape of the hexagonal mesopore was excised from the bulk silica structure, with the pore wall thickness set at about 2  $\text{SiO}_4$  tetrahedra and the  $a$  repeat distance at  $37.03 \text{\AA}$ , and with any resulting dangling bonds satisfied by OH groups or protons (such that there were no Si-H bonds). The amorphous model was then optimised by energy minimisation. As in the case of the "zeolitic mesopore" structure, the amorphous model was fully periodic.

### 3.2 COMPUTATIONAL METHODS

Energy minimisations were carried out using both *GULP*[41] and *Discover*[42], using respectively the Sanders *et al.*[43] and *cff91\_czeo*[44] forcefields. Grand Canonical Monte Carlo calculations of  $\text{N}_2$  adsorption were carried out using the *Sorption* module of *InsightII*, using the *cff91\_czeo* atomic charges for the framework, and *Universal Forcefield* potential parameters.

### 3.3 SIMULATIONS

Powder X-ray diffraction patterns and total Si–O radial distribution functions, for both the amorphous model and the 42–ring zeolitic model, are shown in Figures 1 and 2. It may be seen that, in the case of the XRD patterns, there is little difference between the two models with the patterns in both cases being dominated by the four lowest angle  $hk0$  reflections. From the Si–O RDFs, there also appears to be little difference between the two models, at least at the resolution that might be expected from experimental techniques such as WAXS or Si XANES, with the gross features of the spectra being located in similar spatial ranges. This would indicate that none of these techniques could be used to determine unambiguously the short range structure of MCM-41.

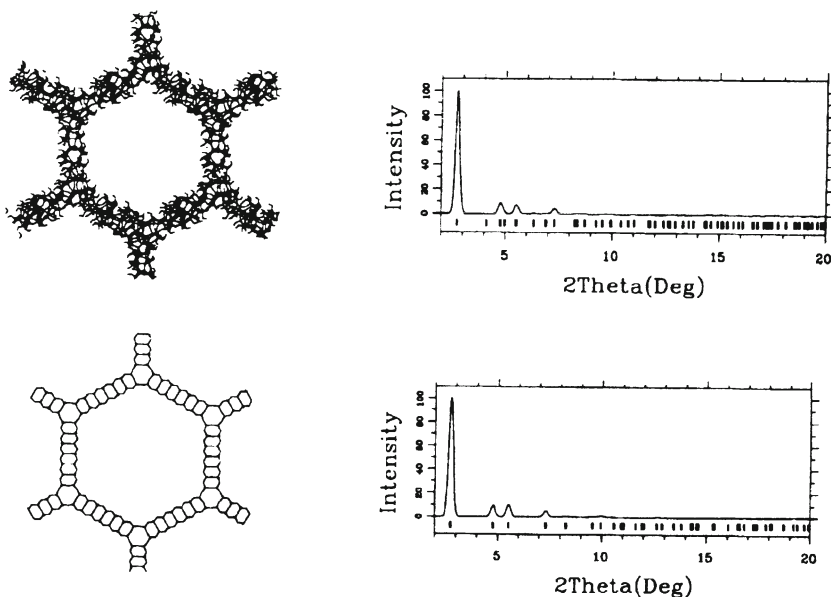


*Figure 1.* Simulated powder XRD patterns for "Zeolitic" and disordered mesopore models.

Current work on the simulation of  $N_2$  adsorption isotherms[45] suggests, however, that the nitrogen adsorption properties of the mesoporous materials are strongly influenced by the concentration of surface hydrogens.

The work summarised above demonstrates our ability to develop detailed structural models at the atomic level for highly complex catalytic systems. Their refinement will require further interaction and comparison with experimental structural and physical data.

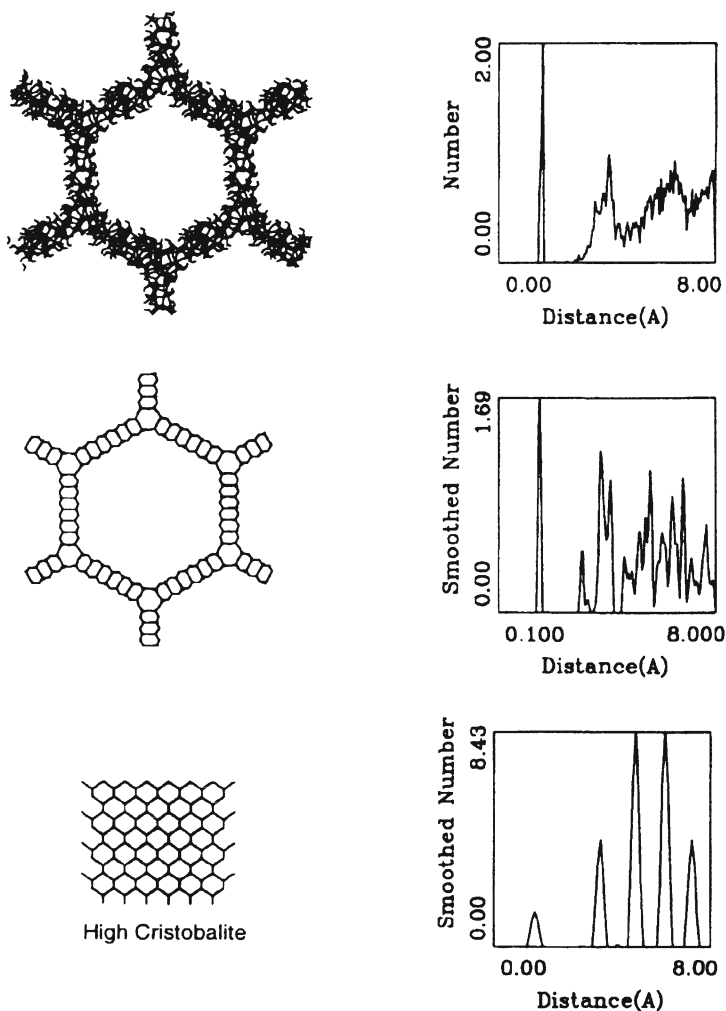


Figure 2. Total Si-O RDFs for ordered and disordered mesopore models compared with high cristobalite.

#### 4. Designing Templates for the Synthesis of Microporous Materials

The ability to synthesise catalytically active microporous materials with pre-determined structural and chemical properties can be considered one of the ultimate challenges for the zeolite chemist. The processes of self-assembly of these crystalline materials from their constituent atoms is not only complex but

also extremely difficult to characterise under hydrothermal synthesis conditions. One profitable avenue for obtaining materials with particular pore topologies is the use of organic bases which act as structure directing agents or templates[46, 47]. These molecules are encapsulated within the inorganic framework and their size and shape is reflected to a certain degree in the resultant pore structure of the framework.

A number of new materials have been synthesised by judicious and rational selection of a suitable template molecule[48]. We recently published[13] a methodology for the automated design of such molecules, which generates suitable candidates for templating for the synthesis of a target structure. We describe here our recent application of this methodology to design a template which would allow the synthesis of a particular structure with pre-determined properties[49, 50].

Chabazitic structured microporous materials (CHA structure code), both aluminosilicate and aluminophosphate based, are effective catalysts for converting light olefins to methanol. However, the synthesis is limited to a narrow range of compositions — a relatively high concentration of aliovalent metal substitution is required — and by contamination with other competitively formed microporous phases. We therefore set out to design a new template which would form a cobalt containing aluminophosphate with the CHA structure which would avoid these problems.

Small amine templates are present at a concentration of two molecules per unit cell in typical CHA syntheses and the need closely to pack the templates results in the likelihood of other phases, where template organisation is less critical, also being formed[51]. Such a template concentration also results in high metal concentrations in the aliovalent metal (e.g. Co) being required to neutralise the cationic (under synthesis conditions) nature of the template. Thus we determined that the ideal template would be present as a single molecule per unit cell (occupying the entire cage of the CHA structure). Similarly, we would wish that the resulting molecule be suitable for modification so that a variation in the charge on the template could be made, allowing different metal concentrations to be obtained.

We applied our ZEBEDDE code to design such a template for the CHA structure. The method[13, 49] computationally grows molecules from a starting seed molecule by adding molecular fragments from a library and manipulating the resultant molecule, so that the final molecule generated is a close van der Waals match to the microporous host. Of the 20 or so candidate structures generated in our simulations[49] many were similar in geometry to that found for the two triethylamine molecules found to template the formation of CHA. These molecules could be considered as two tertiary alkyl fragments linked across the two halves of the cage. Although such molecules are, as far as their void filling properties are concerned, likely to be reasonable templates, their

flexibility may be a disadvantage. However, another template grown was dicyclohexane; Figure 3a shows the growth of the molecule from seed. This molecule was grown from an ethane molecule with the ability of the code to form rings from linear alkyl chains encouraged. The cyclic nature of the molecule makes it much more rigid than the branched amines, but also its symmetry is such that the non-bonding interactions with the framework (a reasonable measure of the templating effect) would be the same irrespective of the available orientations in the cage. However, the aqueous environment of the synthesis makes the molecule unsuitable. Nevertheless, by appropriate atomic substitution, we can generate a more suitable template. Given the success of syntheses which have an effective charge of 2- on the framework per unit cell, we modified dicyclohexane to form 4-piperidino piperidine, ensuring, by energy minimisation, that its fit inside the cage was still suitable (Figure 3b). We also note that this material is commercially available.

A subsequent synthesis programme using 4-piperidino piperidine as a template, resulted in the formation of a  $\text{CoAlPO}_4$  material, designated DAF-5[50], which had a framework composition of  $\text{Co}_{0.28}\text{Al}_{0.72}\text{PO}_4$ ; a material with a di-protonated 4-piperidino piperidine template compensated for by two  $\text{Co(II)}$  atoms per unit cell would have a composition of  $\text{Co}_{0.25}\text{Al}_{0.75}\text{PO}_4$ . The material was formed rapidly (<4 hours at  $165^\circ\text{C}$ ) and with no contamination from other microporous phases. Subsequent single crystal synchrotron radiation X-ray diffraction studies located the statically disordered template within the cage at positions close to those predicted[52]. We believe that similar syntheses using 4-cyclohexyl piperidine, and given a suitable non-polar environment, dicyclohexane, would also result in the formation of a CHA structured material.

This application of *de novo* molecular design demonstrates again the potential of this new method for designing new templates for the synthesis of microporous materials. Future work will consider structures formed only as minerals and also structures that are currently hypothetical.

## 5. Copper Clusters in Cu-zeolite-Y - A direct structural comparison with the NO decomposition catalyst, Cu-ZSM-5

The discovery by Iwamoto and co-workers[53] that the zeolite, Cu-ZSM-5, can, when ion exchanged with copper, catalyse the decomposition of NO at high conversion, has stimulated much interest in these systems[54–60], with special attention being paid to their potential in vehicle exhaust catalysis[61]. In contrast to Cu-ZSM-5, the Cu-zeolite-Y system exhibits much inferior activity for NO decomposition[62]. In a previous study[63] we identified models for the active site in Cu-ZSM-5 and suggested they comprise  $\text{Cu(II)-OH-Cu(I)}$  species, strongly anchored to the zeolite wall *via* framework aluminium. Here



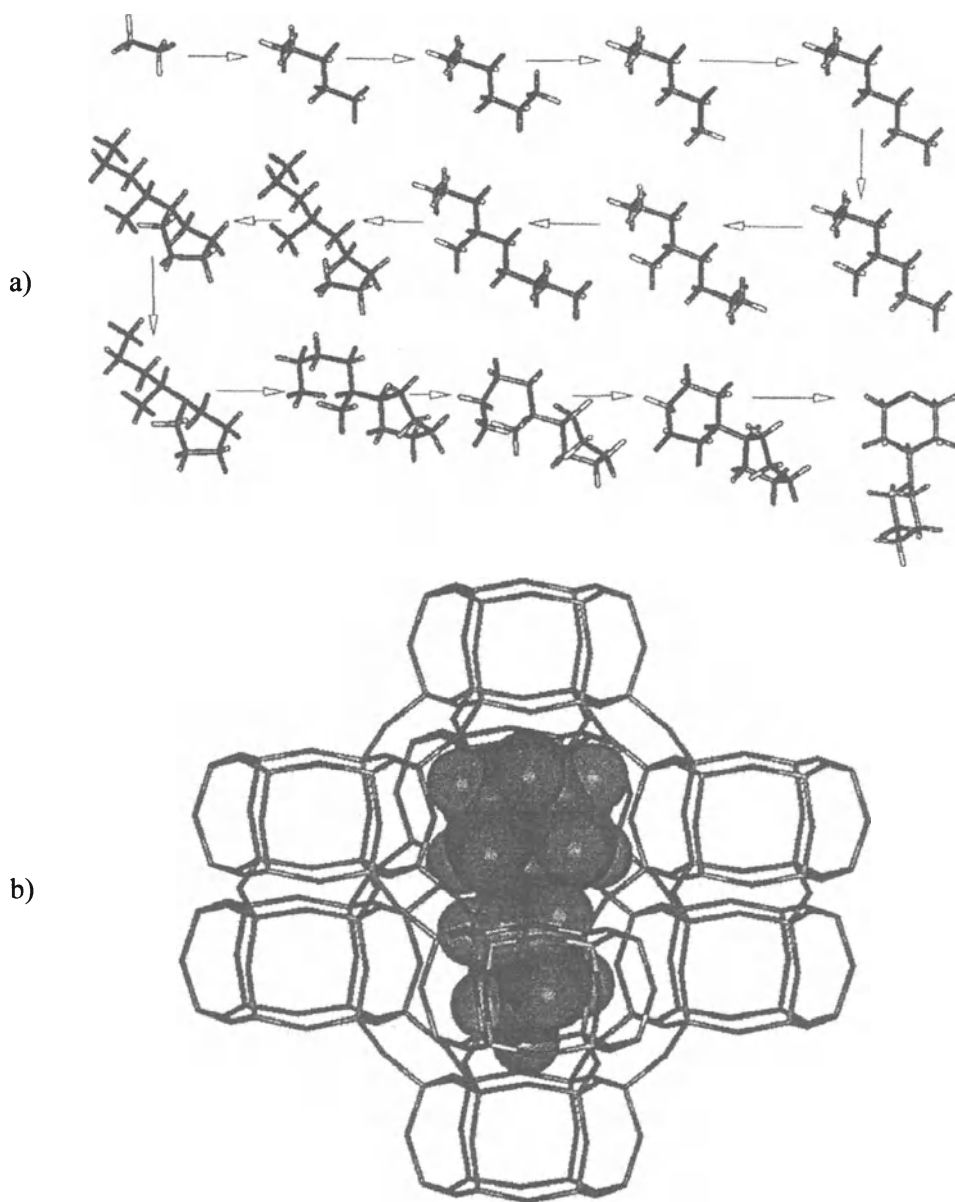


*Figure 3. (a) The stages by which dicyclohexane, which was then modified to give 4-piperidino piperidine, was grown from an ethane seed in a unit cell of CHA using ZEBEDDE[49]. Note that the molecule is orientated to illustrate best the growth process rather than its true position in the CHA cage. (b) Energy minimised location of 4-piperidino piperidine in the CHA cage.*



we highlight recent work on a direct structural comparison of the copper species in Cu-ZSM-5 and Cu-zeolite-Y, which may help rationalise the much reduced activity of Cu-zeolite-Y compared with Cu-ZSM-5, and which amplifies our understanding of the active site in this system.

Our approach is based on the use of static lattice methodologies, the details of which are given elsewhere[64, 65]. The methods are based on the calculation and minimisation of the lattice energy of the system using the GULP program[41]. By system we are referring to the zeolite framework and, in this case, additional extra-framework species added. During the minimisation, the positions of the framework and extra-framework ions are varied until a minimum energy configuration is achieved. The potential parameters used in this study are all presented in reference[63].

The siting of isolated copper species, Cu(I) and Cu(II) in zeolite-Y has been documented experimentally[55] and therefore as a useful test of our potential model we investigated the location of these ions within zeolite-Y. Isolated Cu(I) and Cu(II) were randomly introduced into the purely siliceous form of the zeolite lattice at infinite dilution and directed to low energy configurations by energy minimisation. Cu(I) and Cu(II) species were observed to occupy sites IIG and IC (Figure 4) with equal preference. The energy difference between the copper species located in these sites and the IA site was calculated to be 100 kJmol<sup>-1</sup> and 80 kJmol<sup>-1</sup> for Cu(II) and Cu(I) respectively. Clearly, such a high energy difference prohibits copper from occupying the IA site. Our findings are consistent with experimental results[55] and, moreover, demonstrate the ability of our potential model to describe accurately the behaviour of copper species within zeolite host lattices.

To enable a direct comparison to be made between the copper species in Cu-ZSM-5 and Cu-zeolite-Y, our model for the Cu-zeolite-Y system is based on a Si/Al ratio and copper exchange commensurate with that of the active Cu-ZSM-5 system considered previously: Si/Al=12 and 150% copper exchange, where 100% exchange represents 1 Cu(I) or 0.5 Cu(II) ions per framework aluminium[63]. For a unit cell of zeolite-Y containing 96 T-sites, the Si/Al ratio of 12 is achieved by replacing 8 silicon species by aluminium. To accommodate a 150% exchange, 4 Cu(I) and 4 Cu(II) ions were introduced and the charge imbalance of overexchange, restored by introducing 4 OH species. To model this system trial structures were constructed, by replacing, at random, 8 of the 96 T-sites with aluminium ions. The 4Cu(II), 4Cu(I), 4OH<sup>-</sup> extra-framework species are introduced into the zeolite, again randomly, with the only constraint imposed being a simple proximity criterion to prevent excessive steric overlap; potentially overlapping extra-framework species are rejected and a further random insertion applied. 1000 'trial structures' were obtained and the energy of each system calculated. Full energy minimisation was then applied to

those 30 systems with the lowest energy. The procedure should generate all low energy extra-framework copper configurations.

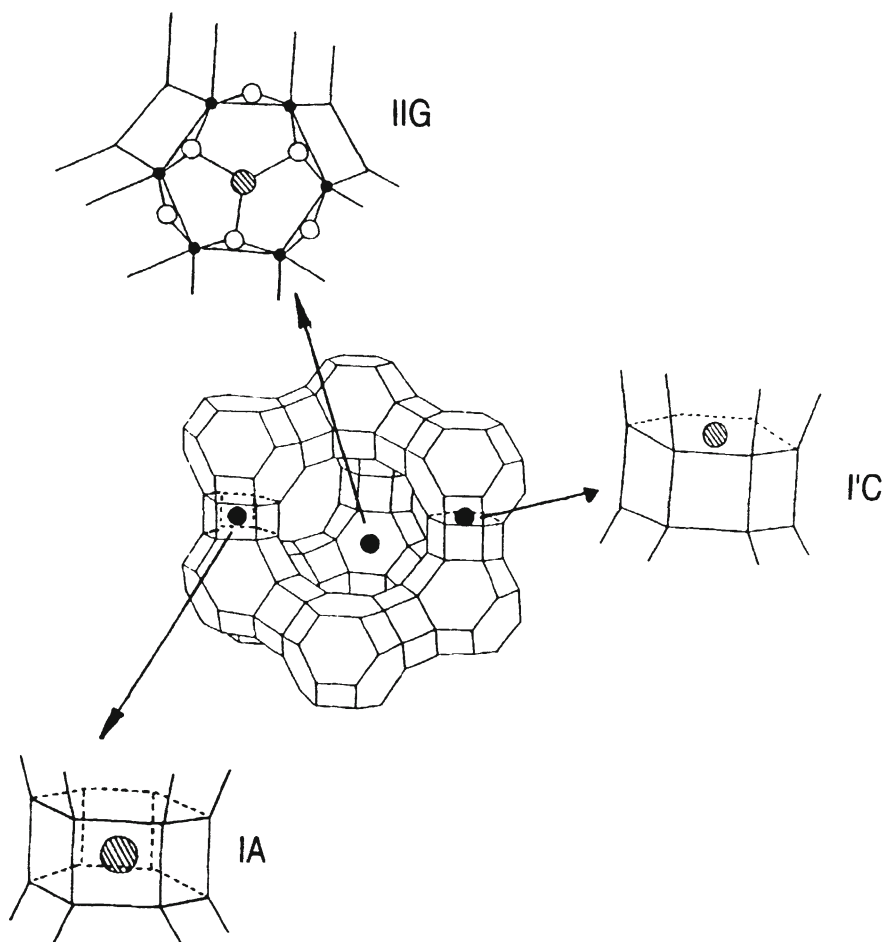


*Figure 4.* Schematic of the zeolite-Y structure illustrating the exchangeable cation sites, IIG I'C and IA.

Out of 30 systems considered for full energy minimisation, 5 systems were successfully converged with the remaining 25 systems suffering a collapse of the zeolite-Y host lattice under energy minimisation. The high failure rate is attributed to the low density of this highly porous material (12.7 T sites per  $1000\text{\AA}^3$ ). We do not consider this problem to be attributable to the minimisation method or potential model as zeolites are, of course, metastable with respect to quartz.

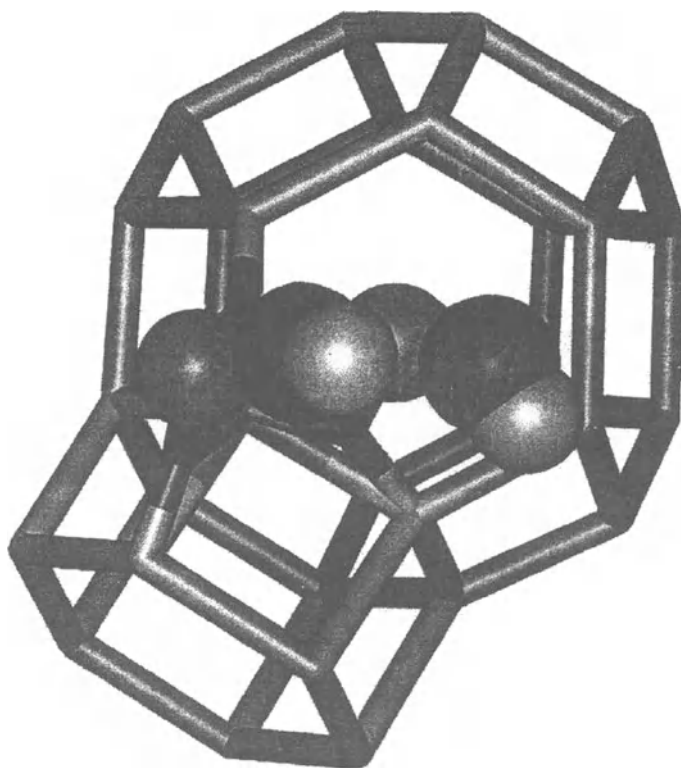


*Figure 5.* Schematic of the Cu(II)–OH–Cu(II)–OH cluster in zeolite–Y. The silicon ions of the zeolite are represented by vertices of the sticks, the copper species by light grey spheres and the hydroxyl groups by the interconnecting dark and light spheres respectively.

As noted, our proposed model for the active site in Cu–ZSM–5 [11], comprises a copper pair, bridged by a hydroxyl group, specifically Cu(II)–OH–Cu(I). If zeolite Y had been unable to stabilise these pairs, it might have explained its low activity with respect to NO decomposition. However, three copper pairs were identified which suggests that simple pairing of the copper species is not a sufficient criterion for high activity and the requirements for an effective active site are more complex. Closer inspection of the copper clusters in zeolite–Y revealed the clusters comprise two hydroxyl groups associated with each copper pair whereas the active site proposed for the Cu–ZSM–5 system contained only a *single* hydroxyl group bridging the copper pair. The extra hydroxyl group is likely to interfere with the NO decomposition and may, in part, explain the inferior activity of Cu–zeolite–Y. Figure 5 illustrates the structure of a Cu(II)–OH–Cu(II)–OH cluster within the zeolite–Y host zeolite;

we also note that this cluster is anchored to the zeolite wall *via* framework aluminium.

Our results emphasise the rôle of computer modelling in generating detailed structure models for the active sites in complex systems. In conjunction with a simple static lattice approach, the application of quantum mechanical calculations to this problem will help resolve the reaction mechanisms and will be the subject of a future study. In the following section we illustrate the application of quantum mechanical techniques to the study of titanium silicates.

## **6. Modelling of Active Sites b: Ti(IV) active sites in Ti-silicate partial oxidation catalysts**

Ti(IV) silicates have attracted a great deal of attention since Enichem's report of the production of highly efficient, selective partial oxidation catalysts by the incorporation of Ti(IV) into the framework of silicate molecular sieves with the MFI and MEL structure, the so called TS-1 and TS-2 materials[66]. Since then a large number of aluminosilicates, aluminophosphates (AlPOs), and silicoaluminophosphates (SAPOs) framework materials have been reported in which Ti(IV) has been incorporated into the zeolite framework; for more information the reader is referred to one of the excellent reviews on the subject[67, 68, 69]. Thus, environmentally safe liquid-phase partial oxidations of a large range of industrially important organic materials has now been reported over Ti(IV) silicates using sacrificial oxidants such as H<sub>2</sub>O<sub>2</sub> or tert-butyl hydrogen peroxide in a number of different solvents[67, 68, 69].

Much of the early work concerning the characterisation of these materials revolved around the question of the nature of the Ti(IV) centre incorporated into the material in terms of its location (framework or extraframework), in terms of its coordination (4 to 6) and in terms of its local structure, in particular the question of whether Ti=O species are present. The first question has been studied by a number of authors[70, 71, 72] and depends essentially on the material involved and the synthesis method. It is clear, however, that only Ti(IV) incorporated into the framework of the molecular sieve is active for partial oxidation catalysis.

The second question, that of the coordination number of the Ti(IV) centre, has been more difficult to solve due to the problem of poorly synthesised materials and the presence of adsorbates which can coordinate to Ti(IV) making spectroscopic characterisation more difficult. Recent theoretical work[73] has, however, indicated that in silicates, Ti(IV) in a four coordinated framework site is energetically preferred to 5 and 6 coordinated framework sites, for example, those in JDFL-1[74] and ETS-10[75] respectively. In addition we have recently published density functional theory calculations concerning the question of

Ti(IV) coordination in the presence of coordinating solvents, *e.g.*, water[76]. In this study we used clusters containing 4 silicate tetrahedral units, 4T clusters, with the central Si replaced by Ti and with all dangling bonds being terminated by hydrogen atoms to model the Ti(IV) site. Figure 6 shows the results of the geometry optimisations for the three commonly accepted forms of Ti in silicate frameworks, *i.e.*, with four bridges to the framework  $\text{Ti}(\text{OSi})_4$ , with three bridges to the framework and one hydroxyl,  $\text{TiOH}$ , and with two bridges to the framework and two hydroxyls,  $\text{Ti}(\text{OH})_2$ . The diagram shows the energy changes for the interconversion of these species (hydrolysis), neglecting intermolecular hydrogen bonding that would occur between the fragments in a real system, and the effect of hydrating the four coordinate complexes. It is immediately clear that in all cases, addition of water will result in expansion of the Ti(IV) coordination shell exothermically, *i.e.*, only in the case of dehydrated materials will Ti(IV) show 4 coordination and only in the case of fully hydrated materials will Ti(IV) show 6 coordination with all other conditions giving rise to a mixture of 4 and 6. This result goes some way to explaining the early difficulty experienced in characterising these materials and is also in full agreement with recent experimental results on the careful loading of TS-1 with small doses of water and ammonia[77].

The final question, that of the chemical nature of the Ti(IV) centre in silicates is still under debate and is known to depend on the method of Ti(IV) incorporation into the material[78]. One interesting development however comes as a result of recent density functional theory calculations on the formation of  $\text{Ti}=\text{O}$  species from  $\text{TiOH}$  complexes in the presence of a single water molecule[79]. These calculation suggest that in the absence of water, formation of  $\text{Ti}=\text{O}$  is highly unlikely but in the presence of even a single water molecule,  $\text{Ti}=\text{O}$  may become *kinetically* accessible. Work on this problem continues.

## 7. Reaction mechanisms in zeolites

Zeolites are amongst some of the most important heterogeneous catalysts in use commercially today, combining acid-base catalysis due to the presence of Brönsted acid sites with shape selectivity resulting from the microporous environment[80]. Despite this, there is still a great deal of uncertainty concerning the mechanisms of many of the processes which are known to occur and the way in which the zeolite accelerates them. While much information has been obtained from experimental techniques, including infra-red spectroscopy and Magic Angle Spinning NMR[81], there is presently a need for models and reaction pathways to aid in their interpretation. Here theoretical methods are playing a major rôle in the field of microporous materials.

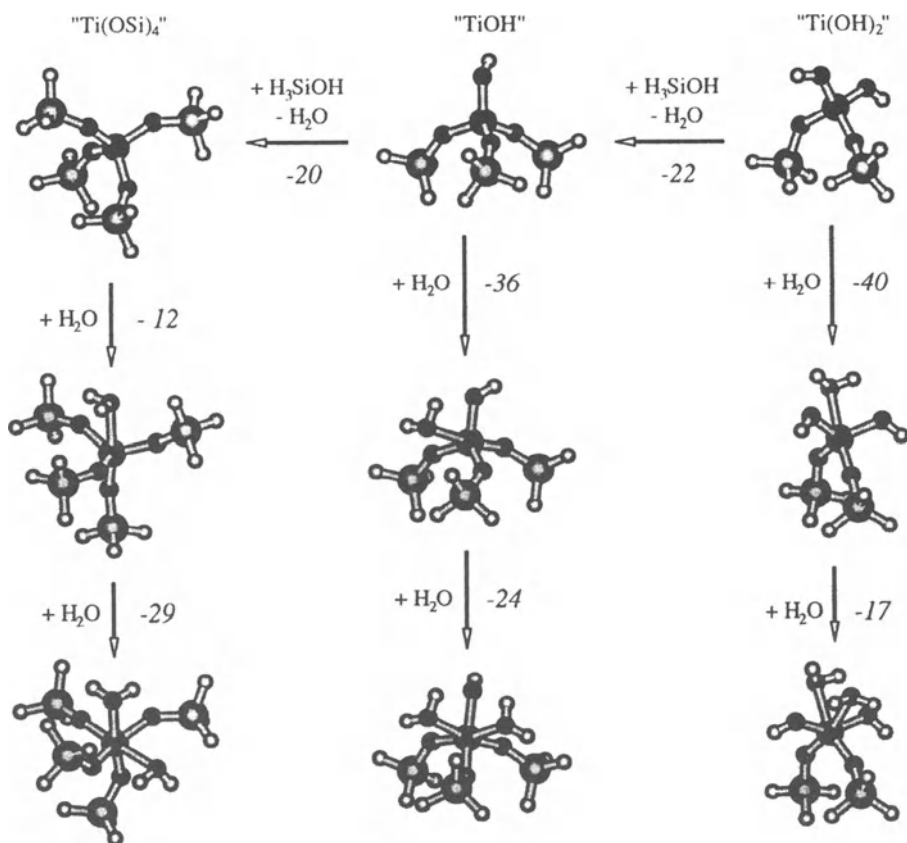


*Figure 6.* DFT (Becke-Perdew) optimized structures of Ti(IV)-silicate clusters showing the calculated energy changes for partial hydrolysis of the Ti-O-Si bonds (top row) and for the coordination of one and two water molecules (down each column). For further details see reference 76.

Perhaps the most studied of all reactions to date has been the conversion of methanol to gasoline[82], as one of commercial importance and academic interest. It has been known for a long time that methanol is readily condensed to form dimethyl ether over many zeolites and under the appropriate conditions it can proceed to form hydrocarbons in the gasoline fraction. However, the mechanism for the process is as yet unclear with various intermediates being postulated including framework bound methoxy- species, carbenes and ylides[83, 84]. In this section we illustrate how computational methods are having a significant impact on this particular problem.

Much of the early debate in this area centred around the nature of the adsorbed state of methanol when interacting with a Brönsted acid site and the



question of whether the proton was transferred to form an ion pair complex. It was believed that the formation of methoxonium would allow facile nucleophilic substitution to occur at carbon, thus leading to the formation of the first observed product, dimethyl ether.

There have been several quantum mechanical studies to determine whether methanol is present as a neutral molecule or ion pair complex in zeolites[85, 86]. The original studies all used the cluster method in which a gas phase model was cut from the zeolite framework with dangling bonds being saturated by hydrogen. Typically it was only feasible to include three tetrahedral units in the representation of the zeolite.

Although the size of model that can be handled is rapidly increasing, it still falls a long way short of accurately representing both the electrostatic potential and geometric constraints of the full framework. While it is possible to improve matters by using an embedding scheme[87], the alternative approach of using periodic boundary conditions is now feasible for the study of intermediates and the greater simplicity often outweighs the extra computational cost.

The use of the planewaves [88] to represent the valence wavefunction, with non-local pseudopotentials replacing the core electrons and nuclei, has become an exciting development in the study of zeolite chemistry. In this way it has become possible not only to study intermediates by energy minimisation, but also the dynamics of adsorbates over a few picoseconds.

Cluster calculations predicted that the ion pair complex of methanol is actually a transition state, rather than a minimum. However, through the use of planewave methods it has been possible to study the behaviour of methanol in specific framework topologies. In static calculations it was found that methanol formed only a neutral complex in open cavities, such as that found in the sodalite structure, but within the confines of the eight-ring of chabazite the methoxonium ion was the local minimum[89, 90]. Haase *et al.*[91] have extended this by including the effect of dynamics and found that the proton resides predominately on the framework at room temperature for a single molecule of methanol in chabazite. A variety of other zeolites have been studied and it is becoming apparent that the proton is highly mobile and whether it coordinates mainly to methanol or the framework depends strongly on the zeolite concerned and the concentration of methanol[93].

Beyond the study of the initial adsorption complex of methanol, we have used planewave methods to examine which postulated intermediates of the methanol to gasoline reaction are feasible within the aluminosilicate environment of chabazite — a known catalyst[93]. Two pathways (Figure 7) have been proposed for the initial formation of dimethyl ether involving either the coordination of a  $\text{CH}_3^+$  species to the framework ( $\text{CH}_3$ -Zeolite) instead of a proton or *via* the direct condensation of two methanols. These calculations have demonstrated that the pathway for the latter route lies consistently lower in

energy as can be seen from the energy profile (Figure 8). As part of this study the conversion of intermediates into possible reactive species, namely carbenes and ylides, was considered. However, no evidence of any local minima for either species could be found.

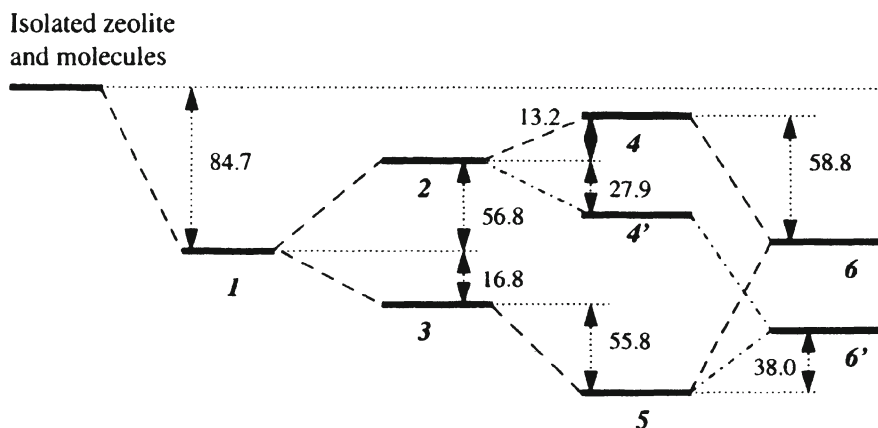


Figure 7. Schematic illustration of two possible pathways for the formation of dimethyl ether. The complexes shown are (1) methoxonium cation, (2) framework methoxy-species with water, (3) methoxonium cation with a second methanol adsorbed prior to nucleophilic attack, (4) framework methoxy-species with methanol coordinated, (5) protonated dimethyl ether hydrogen bonded to water which is in turn coordinated to the aluminium defect and (6) dimethyl ether adsorbed at an acid site.

Although periodic boundary condition methods are highly advantageous for the study of minima, cluster models still have an important part to play, particularly in the location of transition states where the dominant contribution to the barrier is just the local change of bonding. In addition, a major advantage of using the cluster approximation is that standard *molecular* quantum chemistry packages can be employed together with the wealth of experience that has been built up over the years concerning calculations on finite systems. Of particular importance to the study of reactive phenomena is the efficient calculation of (analytical) second derivatives of the energy of the system with respect to the nuclear coordinates, the Hessian matrix. The ability to obtain this Hessian matrix (currently extremely difficult using periodic density functional theory methods) is crucial if efficient geometry search algorithms (based on a quadratic expansion of the energy) are to be applied to the optimisation of the saddle point structures.



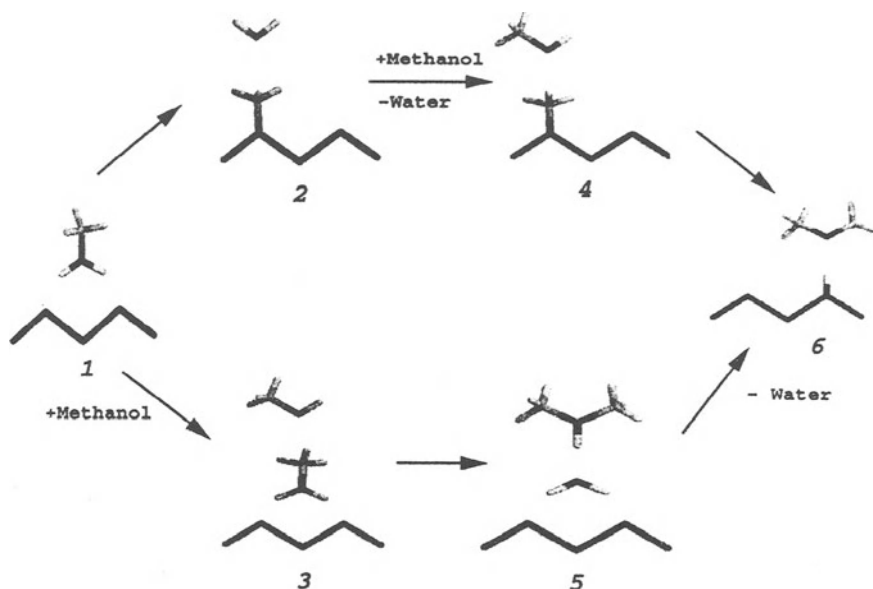
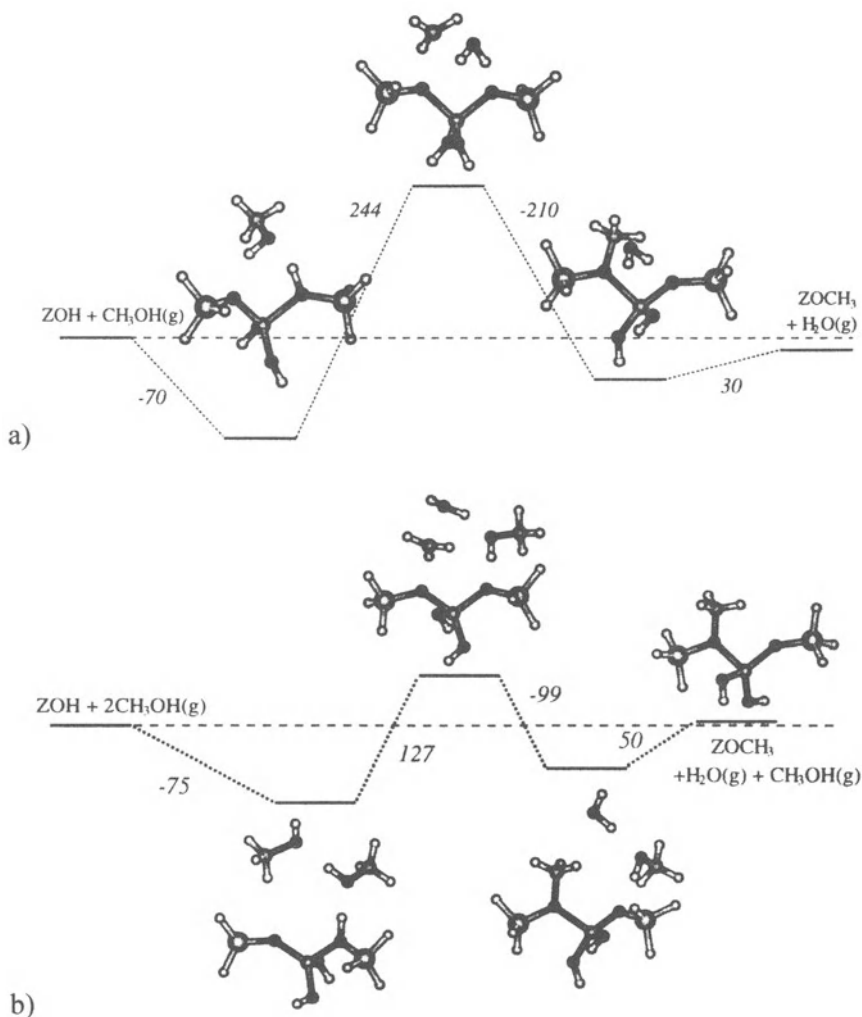


Figure 8. Energy profile for pathways for the formation of dimethyl ether from methanol. Numbers in italics refer to the complexes referred to in Figure 7 - configurations 4' and 6' are the same as 4 and 6, respectively, except with water coordinated to the complexes. All energies are in  $\text{kJmol}^{-1}$

As previously noted, cluster methods have shown problems in unambiguously characterising the mode of methanol adsorption at Brönsted acid sites in zeolites. However, the subsequent transformation of the primary reactants, methanol and/or dimethyl ether has now been studied in some detail. In agreement with the *thermodynamic* predictions of the periodic density functional study shown in Figure 7 and Figure 8, Blaskowski and van Santen[7] have reported density functional theory calculations on hydrogen terminated three tetrahedral unit clusters (3T units) and have concluded that dimethyl ether forming from direct condensation of two methanol molecules aided by the Brönsted proton is *kinetically* favoured over methylation of an adsorbed methanol molecule by a framework bound methoxy,  $\text{CH}_3\text{-O}(\text{Zeolite})$ .

In addition to the possibility of forming dimethyl ether,  $\text{CH}_3\text{-O}(\text{Zeolite})$  species have been implicated in the process of hydrocarbon formation from methanol and/or dimethyl ether[83, 94, 95]. It is thus of importance to know how these species can form from dimethyl ether, methanol, water and/or a combination of these basic constituents in the reaction mixture. Figures 9 and 10 show four pathways for the formation of  $\text{CH}_3\text{-O}(\text{Zeolite})$  from Figure 9(a) one methanol molecule[8], Figure 9(b) two methanol molecules[96], Figure 10(a) one dimethyl ether molecule and Figure 10(b) one dimethyl ether and one



**Figure 9.** Calculated pathways (within the cluster approximation) for the formation of  $\text{CH}_3\text{-O(Zeolite)}$  from a) one methanol molecule [95], b) two methanol molecules [96]. Energies are in  $\text{kJmol}^{-1}$ . See text for more details.

water molecule. With the exception of Figure 10(b) which was calculated using Hartree-Fock geometries and second order Möller-Plesset corrected energies with a 4T cluster, all calculations were performed using density functional theory methods[97] on a 3T cluster. Two things are immediately apparent: first, that "two is better than one" indicating the importance of polar solvents in the process and second, that the activation energies are such that at 673K, the temperature at which hydrocarbons are formed, all of these transformations will

be active. This latter point is, at least partially, responsible for the difficulties that have been encountered in experimentally probing the mechanism: too many processes are occurring simultaneously.

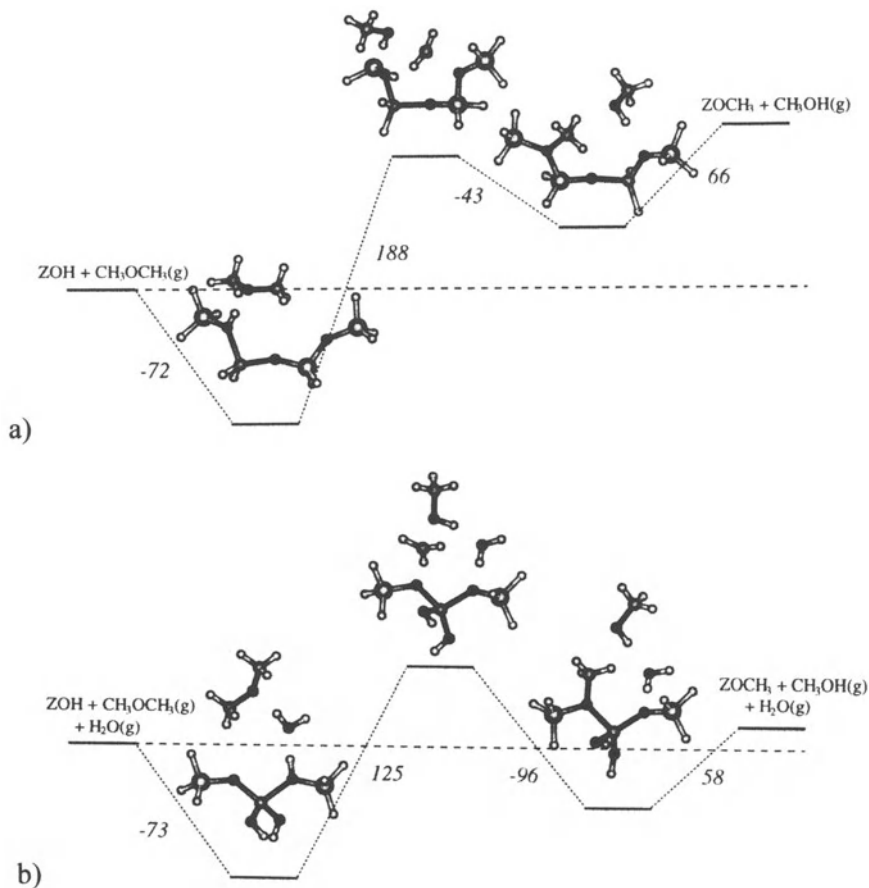


**Figure 10.** Calculated pathways (within the cluster approximation) for the formation of  $\text{CH}_3\text{-O(Zeolite)}$  from a) one dimethyl ether molecule and b) one dimethyl ether and one water molecule. Energies are in  $\text{kJmol}^{-1}$ . See text for more details.

Finally, transition states for the formation of framework stabilised carbenes have been located using 3T clusters models[96]. Kinetically, formation of this species is within the experimental bounds of the activation energies for the methanol to gasoline process over zeolite H-ZSM-5[98]. However, given the result that this species does not appear to be significant in the periodic density functional theory calculations mentioned above, it is not clear whether framework carbene species are an artifact of the cluster methodology or due to

the difficulties in searching configuration space in the periodic calculations. Work is currently in progress to shed more light on this important question.

## 8. Summary

The recent case studies described above illustrate, we hope, the rôle of computational techniques in investigating central problems in contemporary catalytic studies. As noted in the Introduction, the greatest challenge in the field is now to develop methods for modelling reaction pathways with "chemical" accuracy. Recent developments promise that this goal is achievable with extensions of current methodologies.

## Acknowledgements

We are grateful to Sir John Meurig Thomas, Drs G. Sankar, R. Oldroyd, T. Maschmeyer, M.-A. Perrin and P. Nortier for their contributions to the work described in this chapter. We would like to thank EPSRC and Rhône Poulenc for financial support. J.D. Gale is grateful to the Royal Society for a University Research Fellowship and D.W. Lewis to the Oppenheimer Trust of the University of Cambridge for a Fellowship.

## References

1. Wright, P.A., Natarajan, S., Thomas, J.M., Bell, R.G., Gai-Boyes, P.L., Jones, R.H., Chen, J., (1992) *Angew. Chem. Intl. Ed. Engl.*, **31**, 1472.
2. Wright, P.A., Jones, R.H., Natarajan, S., Bell, R.G., Chen, J., Hursthouse, M.B., Thomas, J.M., (1993) *J. Chem. Soc., Chem. Commun.*, 663.
3. Freeman, C.M., Newsam, J.M. in *Computer Modelling in Inorganic Crystallography*, Ed. C.R.A. Catlow, Academic Press, London, 1997.
4. Demontis, P., Suffriti, S.B., in *Modelling of structure and reactivity in zeolites*, Ed. Catlow, C.R.A., (Academic Press Limited, London) 1992.
5. Hernandez, E., Catlow, C.R.A., (1995) *Proc.R.Soc.Lond.A*, **448**, 143-160.
6. Smit, B., (1995) *J. Phys. Chem.*, **99**, 5597.
7. Blaskowski, S.R., van Santen, R.A., (1997) *J. Phys. Chem. B*, **101**, 2292.
8. Sinclair, P.E., Catlow, C.R.A., (1997) *JCS Faraday Trans.*, **92**, 2099.
9. Sinclair, P.E., Catlow, C.R.A., (1997) *J. Chem. Soc., Faraday Trans.*, **93**(2), 333-345.
10. Lewis, D.W., Freeman, C.M., Catlow, C.R.A., (1995) *J.Phys.Chem.*, **99**(28), 11194-11202.

11. Bell, R.G., Lewis, D.W., Voigt, P., Freeman, C.M., Thomas, J.M., Catlow, C.R.A., in *Zeolites and Related Microporous Materials: State of the Art 1994*. Proceedings of the 10th International Zeolite Conference, Garmish-Partenkirchen, Germany, July 17-22, 1994. (Eds. Weitkamp, J., Karge, H.G., Pfeifer, H. Hölderich, W., Studies in Surface Science and Catalysis, Vol. 84, 1994, Elsevier Science B.V.)
12. Shen, V., Watanabe, K., Bell, A.T., (1997) *J. Phys. Chem. B*, **101**(12), 2207.
13. Lewis, D.W., Catlow, C.R.A., Thomas, J.M., Willock, D.J., Hutchings, G.J., (1996) *Nature*, **382**(6592), 604-606.
14. Catlow, C.R.A., Bell, R.G., Gale, J.D., Lewis, D.W. in "Zeolites: A Refined Tool for Designing Catalytic Sites", Proceedings of the International Zeolite Symposium, Quebec, Canada, eds L. Bonneviot and S. Kaliaguine, Elsevier Science B.V., Amsterdam, 1995, and (1995) *Studies in Surface Science and Catalysis*, **97**, 87-100.
15. Catlow, C.R.A., Ackermann, L., Bell, R.G., Gay, D.H., Holt, S., Lewis, D.W., Nygren, M.A., Sastre, G., Sayle, D.C., Sinclair, P.E., (1997) *J. Mol. Catal., A, Chemical* **115**(3), 431-448.
16. Catlow, C.R.A., in 'Handbook of Heterogeneous Catalysis', ed. H. Knözinger, VCH, Weinheim, Germany, 1997.
17. Sauer, J., *Struc. Surf. Sci. Catal.*, (1994) **84**, 2039.
18. van Santen, R.A., Kramer, G.J., (1995) *Chem. Rev.*, **95**(3), 637.
19. Jackson, R.A.; Catlow, C.R.A. (1988) *Molecular Simulation*, **1**, 207-224.
20. Schoen, J.C., Jansen, M., *Angew. Chem. Int. Ed., Engl.*, (1996) **35**, 1286.
21. Freeman, C.M., Newsam, J.M., Catlow, C.R.A., Levine, S.M., (1993) *J. Chem Soc., J. Mater. Chem.*, **3**, 53.
22. Bush, T.S., Catlow, C.R.A., Battle, P.D., (1995) *J. Chem. Soc., J. Mater. Chem.*, **5**(8) 1269-1272.
23. Akporiaye, D.E., Fjellrag, H., Lillerud, K.P., (1996) *J. Phys. Chem.*, **100**, 16641.
24. Lewis, D.W., Carr, S., Sankar, G., and Catlow, C.R.A., (1995) *J. Phys. Chem.* **99**, 2377-2383.
25. Catlow, C.R.A., Gay, D.H., Nygren, M.A., Sayle, D.C., in 'Chemisorption and Reactivity on Supported Clusters and Thin Films', Proceedings of NATO ASI, 1996, p. 479-521, Eds. R.M. Lambert, G. Pacchioni, Kluwer Academic Publishers, The Netherlands, 1997.
26. Allen, M.P., and Tildesley, D.J., 'Computer Simulation of Liquids', Oxford University Press, 1987.
27. June, R.L., Bell, A.T., Theodorou, D.N., (1991) *J. Phys. Chem.*, **95**, 8866.
28. Yashonath, S., Thomas, J.M., Nowak, A.K., and Cheetham, A.K., (1998) *Nature*, **331**, 601.

29. Freeman, Clive M.; Catlow, C. Richard A.; Thomas, John M.; Brøde, Stefan, (1991) *Chem. Phys. Letts.* **186**,137.
30. Goodbody, S.J., Watanabe, K., Macgowan, D., Walton, J.P.R.B., Quirke, N., (1991) *J. Chem. Soc., Faraday Trans.*, **87**(13), 1951.
31. Smit, B., (1995) *Mol. Phys.*, **85**,153.
32. Auerbach, A.M., Henson, N.J., Cheetham, A.K., Metiu, H.I., (1995) *J. Phys. Chem.*, **99**, 10600.
33. Dovesi, R., Roetti, C., Freyria-Fava, C., Aprà, E., Saunders, V.R., Harrison, N.M., p. 203 in 'New methods for modelling processes within solids and at their surfaces', Eds. Catlow, C.R.A., Stoneham, A.M.; Sir John Meurig Thomas, The Royal Society Oxford University Press 1993.
34. Harrison, N. in 'Computer Modelling in Inorganic Crystallography', Ed. C.R.A. Catlow, Academic Press, London, 1997.
35. Wimmer, E. in 'New Trends in Materials Chemistry', eds. C.R.A. Catlow, A.K. Cheetham, Kluwer Academic Press, The Netherlands, 1997.
36. Kresge, C.T., Leonowicz, M.E., Roth, W.J., Vartuli, J.C., Beck, J.S., (1992) *Nature*, **359**, 710.
37. Beck, J.S., Vartuli, J.C., Roth, W.J., Leoniwicz, M.E., Kresge, C.T., Schmitt, K.D., Chu, C.T-W., Olsen, D.H., Sheppard, E.W., McCullen, S.B., Higgins, J.B., Schlenker, J.L., (1992) *J. Am. Chem. Soc.*, **114**, 10834.
38. Smith, J.V., Dytrych, W.J., (1984) *Nature*, **309**, 607.
39. Navrotsky, A., Petrovic, I., Hu, Y.T., Chen, C.Y., Davis, M.E., (1995) *Microporous Materials*, **4**, 95.
40. Vessal, B., Amini, M., Fincham, D., (1993) *J. Non-Cryst. Solids*, **159**, 184.
41. Gale, J.D., *J. Chem. Soc., Faraday Trans.*, (1997) **93**(4), 629.
42. *InsightII* v. 400; *Discover* 95.0, Molecular Simulations Inc., San Diego (1996).
43. Sanders, M.J., Leslie, M., Catlow, C.R.A., (1984) *J. Chem. Soc., Chem. Commun.*, 1273.
44. Hill, J.R., Sauer, J., (1994) *J. Phys. Chem.*, **98**, 1238.
45. Bell, R.G. — to be published
46. Davis, M.E., Lobo, R.F., (1992) *Chem. Mater.*, **4**, 759.
47. Lok, B.M., Cannan, T.R., Messina, C.A., (1983) *Zeolites*, **3**, 282.
48. For example a) Zones, S.I., Santilli, D.S., in R. von Ballmoos, J.B. Higgins, M.M.J. Treacy (eds) *Proceedings of the 9th International Zeolites Conference*, Butterworth-Heinemann, USA (1992) pp 171; b) Wright, P.A., Jones, R.H., Natarajan, S., Bell, R.G., Chen, J., Hursthouse, M.B., Thomas, J.M. (1993) *J. Chem. Soc., Chem. Commun.*, 633; c) Schmitt, K.D., Kennedy, G.J., (1994) *Zeolites*, **14**, 635; d) Lobo, R.F., Davis, M.E., (1995) *J. Am. Chem. Soc.*, **117**, 3766.
49. Willock, D.J., Lewis, D.W., Catlow, C.R.A., Hutchings, G.J., Thomas, J.M., (1997) *J. Molec. Catal. A*, **119**, 415.

50. Lewis, D.W., Sankar, G., Wyles, J., Thomas, J.M., Catlow, C.R.A., Willock, D.J., *Angew. Chemie*, in press.
51. Lewis, D.W., Catlow, C.R.A., Thomas, J.M., (1996) *Chem. Mater.*, **8**, 1112.
52. Sankar, G., Wyles, J., Jones, R.H., Thomas, J.M., Lewis, D.W., Catlow, C.R.A., Clegg, W., Coles, S.J., Teat, S.J., submitted.
53. Iwamoto, M., Yokoo, S., Saskai, S., Kagawa, S., (1981) *J. Chem. Soc., Faraday Trans. 1* **77**, 1629
54. Shelef, M., (1992) *Catalysis Letters*, **15**, 305 and references cited therein.
55. Schoonheydt, R.A., (1993) *Catal. Rev. -Sci. Eng.*, **35**, 129.
56. Liu, D.J., Robota, H.J., (1993) *Catalysis Letters*, **21**, 291.
57. Ansell, G.P., Diwell, A.F., Golunski, S.E., Hayes, J.W., Rajaram, R.R., Truex, T.J., Walker, A.P., (1993) *Applied Catalysis B: Environmental*, **2**, 81.
58. Hall, W.K., Valyon, J., (1992) *Catalysis Letters* **15**, 311.
59. Spoto, G., Bordiga, S., Scarano, D., Zecchina A., (1992) *Catalysis Letters*, **13**, 39.
60. Moretti G., (1994) *Catalysis Letters*, **28**, 143.
61. Truex, T.J., Searles, R.A., Sun D.C., (1992) *Platinum Metals Rev.*, **36**, 2
62. Li, Y., Hall K., (1991) *J. Catal.* **129**, 202.
63. Sayle, D.C., Catlow, C.R.A., Gale, J.D., Perrin, M.-A., Nortier, P., (1997) *J. Phys. Chem. A*, **101**, 3331.
64. C.R.A. Catlow, ed., "Modelling of Structure and Reactivity in Zeolites" (Academic Press, London, 1992).
65. Catlow, C.R.A., Gay, D.H., Ackermann, L., Bell, R.G., Holt, S., Lewis, D.W., Nygren, M.A., Sastre, G., Sayle, D.C., Sinclair, P.E., (1997) *J. Mol. Cat. A: Chemical*, **115**, 431.
66. Taramasso, M., Perego, G., Notari, B.; US Patent 4410501, 1983.
67. Notari, B., (1996) *Advances in Catalysis*, **41**, 253.
68. Notari, B., (1993) *Catalysis Today*, **18**, 163.
69. Arends, I.W.C.E., Sheldon, R.A., Wallau, M., Schuchardt, U., (1994) *Angewante Chemie*, **36**, 1145.
70. A. Jentys, A., Catlow, C.R.A., (1993) *Catt. Lett.*, **22**, 251.
71. Trong On, D., Biittar, A. Sayari, A., Kaliaguine, S., Bonnevot, L., (1992) *Catt. Lett.*, **16** 85.
72. Blasco, T., Cambor, M.A., Corma, A., Perez-Pariente, J., (1993) *J. Am. Chem. Soc.*, **115**, 11806.
73. A.J.M. de Man, A.J.M., Sauer, J., (1996) *J. Phys. Chem*, **100**, 5025.
74. Roberts, M.A., Sankar, G., Thomas, J.M., Jones, R.H., Du, H., Chen, J., Pang, W., Xu, R., (1996) *Nature*, **381**, 401.
75. Anderson, M.W., Terasaki, O., Ohsuna, T., Malley, P.J.O., Philippou, A., Mackay, S.P., Ferreira, A., Rocha, J., Lidin, S., (1995) *Phil. Mag. B*, **71**, 813.



76. Sinclair, P.E., Sankar, G., Catlow, C.R.A., Thomas, J.M., Maschmeyer, T., (1997) *J. Phys. Chem*, **101**, 4232.
77. Bordiga, S., Coluccia, S., Lamberti, C., Marchese, L., Zecchina, A., Boscherini, F., Buffa, F., Genomi, F., Leofanti, G., Petrini, G., Vlaic, G., (1994) *J. Phys. Chem*, **98**, 4125.
78. T. Blasco, A. Corma, M.T. Navarro, J. Perez-Pariente, (1995) *J. Catal.*, **156**, 65.
79. Sinclair, P.E., Catlow, C.R.A., *Chem. Comm.*, in press.
80. Thomas, J.M., (1990) *Phil. Trans. R. Soc. London A*, **333**, 173.
81. Mirth, G., Lercher, J.A., Anderson, M.W., Klinowski, J., (1990) *JCS Faraday Trans.*, **86**, 3039.
82. Meisel, S.L., McCulloch, J.P., Lechthaler, C.H., Weisz, P.B., (1976) *Chem. Tech.*, **6**, 86.
83. Forester, T.R., Howe, R.F., (1987) *J. Am. Chem. Soc.*, **109**, 5076.
84. Chang, C.D., Silvestri, A., (1977) *J. Catal.*, **47**, 249.
85. Sauer, J., Kölmel, C., Haase, F., Ahlrichs, R., in Proc. 9th Inter. Zeolite Conf. (Montreal, Canada), Vol II, eds. R. von Ballmoos *et al.* (Butterworth-Heinemann, London), 679 (1993)
86. Gale, J.D., Catlow, C.R.A., Carruthers, J.R., (1993) *Chem. Phys. Lett.*, **216**, 155.
87. Greatbanks, S.P., Hillier, I.H., Burton, N.A., Sherwood, P., (1996) *J. Chem. Phys.*, **105**, 3770.
88. Payne, M.C., Teter, M.P., Allan, D.C., Arias, T.A., Joannopoulos, J.D., (1992) *Rev. Mod. Phys.*, **64**, 1045.
89. Nusterer, E., Blöchl, P.E., Schwarz, K., (1996) *Angew. Chem. Int. Ed.*, **35**, 175.
90. Shah, R., Gale, J.D., Payne, M.C., (1996) *J. Phys. Chem.*, **100**, 11688.
91. Haase, F., Sauer J., Hutter, J., (1997) *Chem. Phys. Lett.*, **266**, 397.
92. Stich, I., Gale, J.D., Terakura, K., Payne, M.C., (submitted)
93. Shah, R., Gale, J.D., Payne, M.C., (1997) *J. Phys. Chem. B*, **101**, 4787.
94. Bronnimann, C.E., Maciel, G.E., (1986) *J. Am. Chem. Soc.*, **108**, 7154.
95. Hutchings, G.J., Hunter, R., (1990) *Catalysis Today*, **6**, 279.
96. Sinclair, P.E., Catlow, C.R.A., (1997) *J. Phys. Chem. B*, **101**, 295.
97. DGAUSS 3.0, a Density Functional Theory electronic structure code from Cray Research Inc; Andzelm, J., Wimmer, E., (1992) *J. Phys. Chem.*, **96**, 1280. A DZVP basis was used on all atoms with an A1 auxiliary basis. 'Medium' integration grid quality was employed.
98. Jayamurthy, M., Vasudevan, S., (1996), *Catal. Lett.*, **36**, 111.



# MONO- AND BINUCLEAR IRON COMPLEXES IN ZEOLITES AND MESOPOROUS OXIDES AS BIOMIMETIC ALKANE OXIDATION CATALYSTS

P.P. KNOPS-GERRITS<sup>+</sup>, A.-M. VAN BAVEL<sup>§</sup>,  
G. LANGOUCHE<sup>§</sup> AND P.A. JACOBS<sup>+</sup>

<sup>+</sup>*Centrum voor Oppervlaktechemie en Katalyse, Kardinaal Mercierlaan 92,*

<sup>§</sup>*Instituut voor Kern- en Stralingsfysica, Celestijnenlaan 200D,  
KU Leuven, B-3001 Heverlee, Belgium.*

## 1. Introduction

Many enzymes [1-10] successfully catalyse the oxidation of alkanes, even the most inert ones such as methane. The precise architecture of their active site allows such catalytic properties. Such an active site contains a dinuclear iron core, in which  $\mu_2$ -O or  $\mu_2$ -OH bridging is observed. The environment in which the active site is embedded e.g. the protecting protein matrix, adds to the substrate specificity of the enzyme. Apart from the dinuclear iron active site, proximal functions such as catalytic initiators e.g. tyrosyl-radicals, help to establish long range, proton coupled electron transfer chains. Furthermore the interactions between enzymatic subunits add to the complexity of these systems.

For enzymes [1-10] such as methane mono-oxygenase (MMO) limited substrate binding requirements exist, whereas for enzymes such as ribonucleotide reductase (RR), the substrate binding is more complex and the distances between the necessary functions of the enzyme may add up to 3,5 nm. The presence of clefts with cysteine groups and binding sites for allosteric effectors furthermore increase the complexity of this latter system. There remain enigmatic differences in the reactivity between the active sites in methane monooxygenase, ribonucleotide reductase and hemerythrin, an oxygen binding enzyme.

The variety in metallo-proteins that catalyse oxidation of organic substrates with dioxygen and iron in mono- or polynuclear form, is staggering. They are exemplified by the heme- [1-2] and iron-sulfur [3] proteins, dioxygen transport

[4-5], oxidation of methane to methanol [6-7], reduction of ribonucleotides to deoxyribo-nucleotides [8], acid phosphatase activity [9] and iron storage [10] proteins. They show the biological versatility of oxo-bridged di- or poly-iron cores [11-30]. Oxygen transfer is possible from the  $[\text{Fe}_2(\text{OH})(\text{RCOO})_2]$  and  $[\text{Fe}_2\text{O}(\text{RCOO})_2]$  cores in homogeneous methane monooxygenase mimics [17-20]. For Cytochrome P-450 and their mimics a lot of research emphasis has been put on the study of mononuclear iron oxo chemistry [65-67].

The occlusion of these active sites in micro- or mesoporous oxide hosts, respectively, is an important current interest. The occlusion in mesoporous oxides contributes to the "second generation" enzyme mimics, that due to their size, allow the presence of long-range electron transfer chains. The spectroscopic and catalytic fate of the complexes in such oxide structures is studied here. In the past much emphasis has been directed towards the understanding of the catalytic and spectroscopic features of mononuclear iron complexes in microporous oxides, the "first generation" enzyme mimics. The "Ship-in-a-Bottle" approach proves an interesting approach to synthesise such metal complexes in zeolites and microporous materials [43-57]. Early examples include iron phthalocyanines (FePc) inside Y zeolites [44] or FePc as template for zeolite X synthesis [45]. Topological variation and cation variation as a means to change the reactivity was achieved for bipyridine complexes of manganese in EMT, Y and X zeolites in their Na form and Li, Na, K, Cs pre-ion exchanged Y zeolites [46-50]. Both manganese and iron porphyrino-silicas are interesting new materials [51]. Iron based inorganic catalysts for alkane activation are based on sodalite or 5A zeolites [49-50]. Occluded iron complexes tend to be interesting for the biomimetic functionalisation of alkanes.

The aim of this paper is the heterogenisation of iron, iron oxo, iron  $\mu$ -hydroxo and iron peroxo chemistry and to rationalise the behaviour of such chemistry on micro- and mesoporous supports. Ferrous iron in FeNa-Y zeolites is complexed with bipyridine, phenantroline and bipyrimidine [52] and the tetradentate  $\text{N}_4$  ligands [53] such as  $\text{N,N}'$ -bis(2-pyridinecarboxamide)-1,2/3-R (with R= ethane (bpen), propane (bppn), benzene (bpb) and cyclohexane (bpch)). The latter are functional models of iron porphyrins in cytochrome P-450. Ferric iron in binuclear heptapodate coordinated iron(III)-complexes are immobilised on the mesoporous oxide MCM-41. The ligands of the type :  $\text{N,N,N}',\text{N}'$ -tetrakis(2-benzimidazolylmethyl)-2-hydroxy-1,3-diamino propane (HPTB) and  $\text{N,N,N}',\text{N}'$ -Tetrakis(2-pyridylmethyl)-2-hydroxy-1,3-diamino-propane (HPTP) are used for this purpose. The resulting iron complexes contain  $[\text{Fe}_2(\text{HPTP})(\mu\text{-OH})]^{4+}$  (1) and  $[\text{Fe}_2(\text{HPTB})(\mu\text{-OH})]^{4+}$  (2) cores in the mesoporous oxide. Their heterogenisation on clays and their catalytic properties are of current interest [54-55].

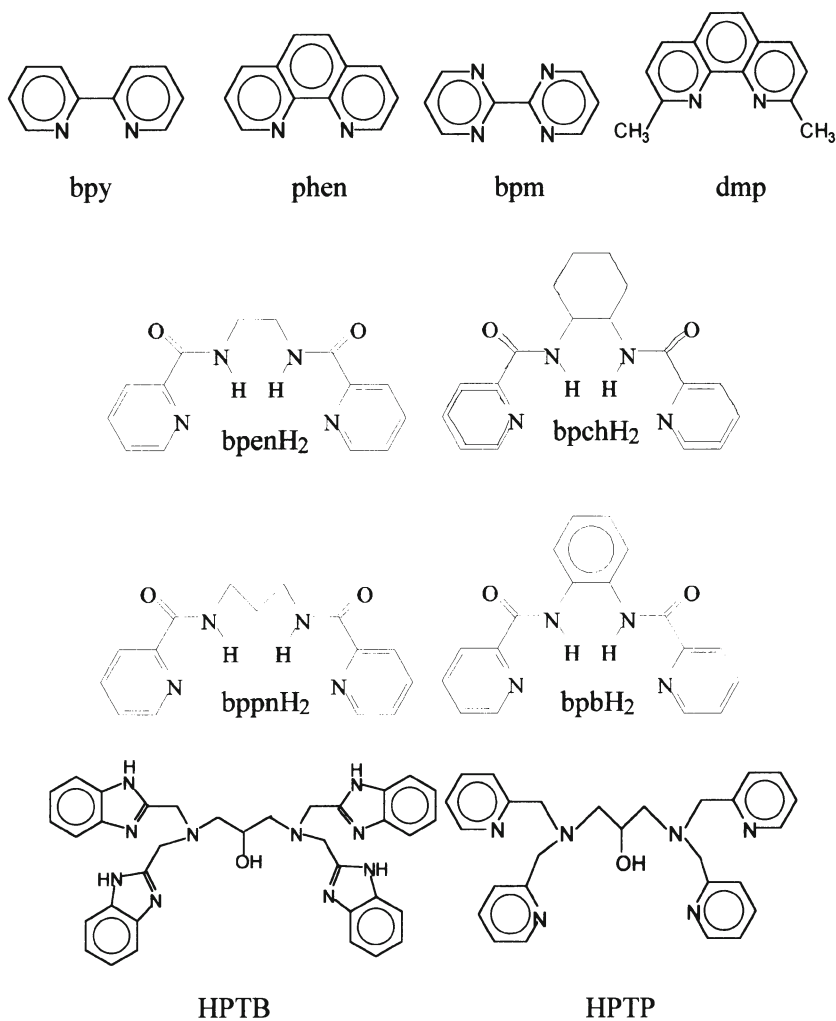


*Figure 1. Organic ligands used in for iron complexation in oxide supports.*

## 2. Experimental

### 2.1 MATERIALS

NaY samples with a Si/Al ratio of 2.47 are obtained from Zeocat; pyridine-2-carboxylic acid (picolinic acid, 99%, ALDRICH), 1,2-diaminoethane (99%, ALDRICH), 1,3-diaminopropane (99%, ALDRICH), 1,2-diaminocyclohexene (99%, ALDRICH), 1,2-diaminobenzene (99%, ALDRICH), dichloromethane (99%, ACROS), cyclohexane (99%, ACROS), cyclohexanol (99%, ACROS), adamantane (99%, ACROS), hydrogen peroxyde (30% solution in water, ACROS) and *t*BHP (70% solution in di-*tert*-butyl-peroxyde, ACROS) are used.

### 2.2 SYNTHESIS

The ligands N,N'-bis (2-pyridinecarboxamide)-1,2/3-R (R = ethane, propane, cyclohexene, benzene) are synthesised as described [37-39]. The synthesis occurs through a triphenylphosphine intermediate, that allows fast dehydration allowing a complete synthesis in 24 hours. N,N'-bis (2-pyridinecarboxamide)-1,2-ethane (bpenH<sub>2</sub>); melting point (mp) 190 °C; N,N'-bis(2-pyridine carboxamide)-1,3-propane (bp1,3pnH<sub>2</sub>); mp 91 °C; N,N'-bis (2-pyridinecarboxamide)-1,2-propane (bp1,2pnH<sub>2</sub>); mp 73 °C; N,N'-bis (2-pyridinecarboxamide)-1,2-benzene (bpbH<sub>2</sub>); mp 167 °C; N,N'-bis (2-pyridinecarboxamide)-1,2-cyclohexane (bpchH<sub>2</sub>); mp 193 °C; (melting points are determined on recrystallised ligands in a capillary on an Electrothermal Melting Point Apparatus). The purity of all complexes is higher than 99 % as based on <sup>1</sup>H-NMR-spectra recorded on a Bruker AMX 300 (pulstime 1 μs, 12 scans with 1s repetition time). <sup>1</sup>H-NMR are recorded in D<sub>2</sub>O (HOD at 4,8 ppm). The bands at 7.44 ppm (H5), 7.84 ppm (H4), 7.89 ppm (H3) and 8.48 ppm (H6) are pyridine protons. N-H protons are invisible because of deuteration to N-D in D<sub>2</sub>O. In bpenH<sub>2</sub> the ethane group shows a band at 3,33 ppm, in bpnH<sub>2</sub> the propane group gives bands at 2,03 and 3,04 ppm from -CH<sub>2</sub>- and N-CH<sub>2</sub>- groups respectively, in bpchH<sub>2</sub> the cyclohexane group gives coupled bands between 1,29 and 2,14 ppm from -CH<sub>2</sub>- and at 3.27 and 3.61 ppm for N-CH<sub>2</sub>- groups. <sup>1</sup>H-NMR for Bpb are recorded in C<sub>6</sub>D<sub>6</sub> shows superposition of benzene and pyridine protons between 7.82 and 8.22 ppm.

A series of iron bis- and tris-complexes Fe(bpy)<sub>n</sub>-NaY, Fe(phen)<sub>n</sub>-NaY and Fe(bpm)<sub>n</sub>-NaY (n=2,3) are synthesised in NaY faujasites zeolites according to an Fe for Na-exchange in zeolite Y (from Zeocat, Si:Al-ratio of 2.47), in which oxidation of Fe<sup>2+</sup> to Fe<sup>3+</sup> can occur, followed by ligand (L) addition in a L : Fe = 2 : 1-ratio.

10 g of NaY zeolite was ion exchanged with 1,89 g of  $\text{FeSO}_4 \cdot 7\text{H}_2\text{O}$  in 2.5 liter water for 4 h. The exchange was done under a nitrogen flow at pH 4 to avoid oxidation to  $\text{Fe}^{\text{III}}$ . After exchange the light-blue sample is washed till sulphate-free and dried for 4 hours at RT. Subsequently, the sample is heated under a flow of nitrogen to 200 °C at a rate 1 °C per minute. This sample is denoted as  $\text{Fe}^{\text{II}}\text{Y}$  and contains 1 ferrous iron per supercage.

$\text{Fe}^{\text{II}}(\text{bpy})_2^{2+}\text{-Y}$ : An  $\text{Fe}^{\text{II}}(\text{bpy})_2^{2+}\text{-Y}$  sample is made under  $\text{N}_2$ -atmosphere by adding bpy in a bpy : Fe ratio of 2:1. Complexation for 4 days at 90 °C gives a red sample. A soxhlet extraction with dichloromethane is performed to remove the excess of free bpy.

$\text{Fe}^{\text{II}}(\text{phen})_2^{2+}\text{-Y}$ : An  $\text{Fe}^{\text{II}}(\text{phen})_2^{2+}\text{-Y}$  sample is made under  $\text{N}_2$ -atmosphere by adding bpy in a bpy : Fe ratio of 2:1. Complexation for 4 days at 130 °C gives an orange sample.

$\text{Fe}^{\text{II}}(\text{bpm})_2^{2+}\text{-Y}$ : An  $\text{Fe}^{\text{II}}(\text{bpm})_2^{2+}\text{-Y}$  sample is made under  $\text{N}_2$ -atmosphere by adding bpy in a bpm : Fe ratio of 2:1. Complexation for 4 days at 130 °C gives a brown-orange sample.

$\text{Fe}(\text{bpen})\text{-NaY}$ : To the dried  $\text{Fe}^{\text{II}}\text{-NaY}$  zeolite under  $\text{N}_2$ -atmosphere bp-1,2-en (MW = 270 mp = 192-193 °C) is added in a 1:1 metal to ligand ratio. After complexation for 4 days at 205 °C the sample is brown.

$\text{Fe}(\text{bppn})\text{-NaY}$ : To the dried  $\text{Fe}^{\text{II}}\text{-NaY}$  zeolite bp-1,3-pn (MW = 284 mp = 95 °C) is added in a 1:1 metal to ligand ratio. After complexation for 4 days at 120 °C the sample is yellow-brown.

$\text{Fe}(\text{bpb})\text{-NaY}$ : The  $\text{bpbH}_2$  (MW = 318 mp = 175 °C) is added in a 1:1 metal to ligand ratio. After complexation for 4 days at 190 °C the sample is grey.

$\text{Fe}(\text{bpch})\text{-NaY}$ : To the dried  $\text{Fe}^{\text{II}}\text{-NaY}$  zeolite bpch $\text{H}_2$  (MW = 324 mp = 201 °C) is added in a 1:1 metal to ligand ratio. After complexation for 4 days at 205 °C the sample is yellow-brown.

For all samples a Soxhlet-extraction with dichloromethane is performed to remove the excess of ligand.

### 2.2.1 $[\text{Fe}_2(\text{HPTB})(\text{OH})(\text{NO}_3)_2](\text{NO}_3)_2$

*N,N,N',N'*-tetrakis(2-benzimidazolylmethyl)-2-hydroxy-1,3-diaminopropane (HPTB) is prepared by crushing o-phenylenediamine or 1,2-diaminobenzene (10.55 g, 0.097 mol) and mixing it to 2-hydroxy-1,3-diaminopropanetetra-acetic acid (5.0 g, 0.016 mmol, formed from the diamine and chloroacetic acid). The mixture is heated to 170-180 °C for 1 hour, till gas formation stops. After cooling the red glassy structure is diluted with HCl (150 ml, 4 M), and a blue precipitate is formed. After filtration the precipitate is washed several times with acetone, dissolved in water and neutralised with a diluted ammonia solution. The white precipitate is recrystallised in acetone, crushed to a fine powder and dried under vacuum. To an ethanolic solution of  $\text{Fe}(\text{NO}_3)_3 \cdot 6\text{H}_2\text{O}$

(0.31 g) the HL (0.30 g) is added. The precipitated binuclear iron complex is then collected.

### 2.2.2 $[Fe_2(HPTP)(OH)(NO_3)_2](ClO_4)_2$

The synthesis of *N,N,N',N'*-tetrakis(2-pyridylmethyl)-2-hydroxy-1,3-diaminopropane  $H(HPTP)^*$  as perchlorate is performed from *p*-chloropicoline and 2-hydroxy-1,3-diaminopropane as described [40-41]. As in the previous synthesis,  $Fe(NO_3)_3 \cdot 6H_2O$  (0.31 g) and  $H(HPTP)(ClO_4)_2$  (0.28 g) are solved in ethanol. The complex formed is washed with acetonitrile/diethylether and recrystallised in diethylether.

### 2.2.3 $[Fe_2(HPTB)(OH)(NO_3)_2]^{2+}$ - or $[Fe_2(HPTP)(OH)(NO_3)_2]^{2+}$ - MCM41

In the MCM-41 complex impregnation procedure, to 1 g of mesoporous MCM-41 0.02 g or 0.1 g of complex is added in 20 ml  $CH_3CN$ . Using a 2 or 10 weight % iron complex loading, only 0.1 or 0.2-0.3 weight % iron is detected on MCM-41. The MCM-41 was prepared according to the recipe of Beck *et al.* [31]. The mixture is first refluxed in  $CH_3CN$  at 85°C for 35 h to immobilise the cationic complexes and in  $CH_2Cl_2$  at 45°C for 4 h to remove possible decomposition products.

## 2.3 SPECTROSCOPY

The ESCA surface-concentration [32] is performed on a SSX 100/206 (Xprobe) from FISIONS. An  $AlK\alpha$  monochromatised X-ray source ( $h\nu=1486.6$  eV) was used. The spot size is 600  $\mu m$  corresponding to an area of 0.493  $mm^2$ . An  $Fe_2O_3$  standard shows  $^2p_{1/2}$  line at 724.3 eV and a  $^2p_{3/2}$  line at 710.7 eV. The values obtained for the ferrous organic complexes within the zeolites are in close proximity of this of the  $K_4Fe(CN)_6$  complexes with values for the  $^2p_{1/2}$  line at 721.7 eV and a  $^2p_{3/2}$  line at 708.3 eV. The  $Fe_2O_3$  standard shows the  $^2p_{1/2}$  and  $^2p_{3/2}$  lines at 724.3 eV and 710.7 eV, respectively. The values obtained for the ferric organic complexes within the supports are in close proximity of those of  $K_3Fe(CN)_6$  with the  $^2p_{3/2}$  line at 710.2 eV.

The FT-IR spectra were recorded on a Nicolet F-730 spectrometer.

The Diffuse Reflectance Spectroscopy (DRS) spectra were recorded on a Cary-5 spectrophotometer with a  $BaSO_4$  integration-sphere in the UV-VIS-NIR region.

Mössbauer spectra [33] are recorded on a vertical constant acceleration drive in transmission geometry with a 28mCi  $^{57}Co(Rh)$  source. Isomer shift data are expressed relative to  $SNP(Na_2Fe(CN)_5(NO) \cdot H_2O)$  which has an isomer shift  $\delta=+0.2649$  mm/s relative to the natural iron standard  $\alpha-Fe$ .

Magnetic experiments were performed with a MPMS Squid magnetometer from Quantum Design at field strengths between 0.1 and 0.8 T and at

temperatures between 30 and 400K. Molecular modelling was done with the program Hyperchem 3.0 for Windows (Hypercube, Inc.).

### 3. RESULTS AND DISCUSSION

#### 3.1 MONONUCLEAR BIDENTATE COORDINATED Fe COMPLEXES IN THE ZEOLITE LATTICE

##### *3.1.1 Siting and Complexation of the Complexes*

XRD allows to determine the localisation of the Fe-complexes in NaY [43], more specifically from the relative peak intensities of the 331, 311 and 220 reflections. In NaY the intensities follow the order  $I_{331} > I_{220} > I_{311}$ , pointing to a random distribution of the cations within the zeolite lattice. For  $\text{Fe}(\text{bpy})_2\text{-Y}$ ,  $\text{Fe}(\text{phen})_2\text{-Y}$  and  $\text{Fe}(\text{bpm})_2\text{-Y}$  the intensities follow the order  $I_{331} > I_{311} > I_{220}$ , suggesting that the location of cations changes from position II or III to position I and I' as a result of the redistribution of  $\text{Na}^+$  to sodalite cages and hexagonal prisms.

The spectroscopic study of a number of Fe-diimine-complexes in NaY reveals the influence of the nature of the ligands and of the ligand over metal stoichiometry on their spin-states. A rationalisation of analogies and differences of such isolated, zeolite occluded complexes with those of pure or mixed-crystal complexes is given. The implication of cooling  $[\text{Fe}(\text{bpm})_2]^{2+}\text{-NaY}$  to liquid helium temperatures on geometrical deformation of the complex within the zeolite is discussed as well.

Comparison of CA and XPS Si/Al ratios of the parent NaY sample shows that the zeolite crystal rims are depleted in Al. Tables 3.1.1-3. indicate that within the accuracy of the XPS measurements, after cation exchange of  $\text{Fe}^{2+}$  for  $\text{Na}^+$  and consecutive complexation, a decrease of the  $\text{Na}^+$  concentration at the surface is seen. The Fe/Na ratio shows that the concentration of divalent iron in the crystal rim is enhanced upon complexation. Moreover, the Si/Al ratio of the zeolite is higher for the  $\text{FeL}_2\text{NaY}$  compared with the dried  $\text{FeNaY}$ . When large amounts of ferric iron are exchanged on the zeolite or formed by oxidation, dealumination occurs [42]. When compared for  $\text{FeL}_2\text{NaY}$  and  $\text{FeNaY}$ , the  $\text{Fe}/(\text{Si}+\text{Al})$  ratio is higher for the latter, meaning that due to the easy migration of bidentate ligands the Fe complexes must be homogeneously distributed across the crystals, whereas there is an accumulation of uncomplexed Fe ions on the  $\text{FeNaY}$  surface. The lower Fe/N ratio with respect to the synthesis Fe/N stoichiometry points to presence of residual free Fe.



*Table 3.1.1. XPS analysis of representative ferrous iron complexes in zeolite Y.*

Ligand	Fe	Na	Si	Al	Si /Al	Fe/Na	Fe/(Si+Al)
bpy	0.34	0.49	21.60	3.98	5.43	0.69	0.0126
phen	0.40	0.57	21.24	3.53	6.02	0.68	0.0140
bpm	0.54	0.69	20.95	4.92	4.26	0.78	0.0200
Y	1.09	2.18	19.93	5.25	3.80	0.50	0.0433

*Table 3.1.2. XPS analysis of representative ferrous iron complexes in zeolite Y.*

Ligand	Fe	N	C	Fe/N
bpy	0.34	3.66	22.11	0.1097
phen	0.40	3.31	20.56	0.1391
bpm	0.54	4.00	20.03	0.1266
Y	1.09	2.65	20.24	0.4113

*Table 3.1.3. XPS binding energies and peak-widths of the asymmetric Fe <sup>2</sup>p<sub>3/2</sub> peak .*

Ligand	Fe(eV)	Width	Fe(eV)	Width	Fe(eV)	Width
bpy	708.51	2.29	711.08	3.02	714.96	3.63
phen	708.90	2.47	711.29	2.65	714.58	3.55
bpm	709.87	2.88	712.52	2.93	715.53	2.92
Y	710.18	3.08	713.18	3.12	715.84	2.98

With respect to the parent Fe<sup>II</sup>Y, for all samples with encapsulated complexes the total Fe concentration remains unchanged. A decrease in the Na<sup>+</sup> concentration is observed at the surface pointing to Na<sup>+</sup> removal from the crystal rims. All this indicates that the distribution of Fe<sup>II</sup> complexes over the crystals is governed by the framework Al distribution. In any case, preferential adsorption of complexes at the external surface of the crystals can be excluded.

The binding energies of the iron [32] complexes within the zeolites are obtained from decomposed XPS spectra as shown in Table 3.1.3.. They correspond well with the oxidation state and the covalency of the binding of K<sub>4</sub>Fe(CN)<sub>6</sub>. The peaks are asymmetric and satellite peaks are seen. Compared with the bpy and phen complexes the Fe <sup>2</sup>p<sub>3/2</sub> binding energies of the bpm complexes are higher by about 1 to 1.5 eV.

### **3.1.2 Reflectance spectroscopy on mononuclear bidentate coordinated Fe complexes**

DRS on Fe<sup>2+</sup>(L)<sub>2</sub>-Y shows MLCT (Fe(d) → L(π\*)) and LMCT (lattice oxygen O<sub>L</sub> → Fe(d)) bands (Fig 3.1.1. and Table 3.1.4.). LMCT bands are very low in intensity, indicating that only a minor fraction of [Fe(bpy)<sub>2</sub>]<sup>3+</sup> is present. The



complexes have an octahedral coordination with a  $d^6 (t_{2g})^4 (e_g)^2$  ground state. The red colour of  $[\text{Fe}(\text{bpy})_2]^{2+}$ -Y, the orange colour of  $[\text{Fe}(\text{phen})_2]^{2+}$ -Y and the salmon-pink colour of  $[\text{Fe}(\text{bpm})_2]^{2+}$ -Y is caused by a MLCT around 500 nm. The MLCT transition bands appear as the empty  $\pi^*$  orbitals of 2,2'-bipyridine can form a bond with the filled  $t_{2g}$  orbitals of the metal ion. The stability of this binding results from the  $t_{2g} \rightarrow \pi^*$  backbonding. The MLCT consists of two bands. The first and second band correspond to a  $d \rightarrow \pi^*$  electron transfer from the metal to the lowest and higher anti-bonding orbitals of the ligand, respectively. For  $[\text{Fe}(\text{bpy})_2]^{2+}$ -Y these are situated at 528 and 470 nm, respectively. The frequency difference between both bands corresponds to the energy difference between the two lowest  $\pi^*$  levels in the diimine ligand. A LMCT is observed at 400 nm ( $\pi \rightarrow e_g$ ). Intra-ligand transitions ( $\pi \rightarrow \pi^*$ ) occur between 200 and 300 nm. A shoulder at 600 nm for  $[\text{Fe}(\text{bpy})_2]^{n+}$ -Y points to the presence of an extra LMCT, possibly attributable to an  $\text{Fe}^{3+}$  complex species. From DRS a clear difference can be made between bis and tris-coordination in Fe-complexes with three bpy or two bpy ligands and two halogen atoms in an octahedral coordination [34]. Since the stabilisation energy of  $\text{Fe}^{2+}(\text{bpy})_n$ -complexes is tris-coordination is hard to circumvent, only a limited amount of bis-, mono- and uncoordinated  $\text{Fe}^{2+}$  ion is seen.

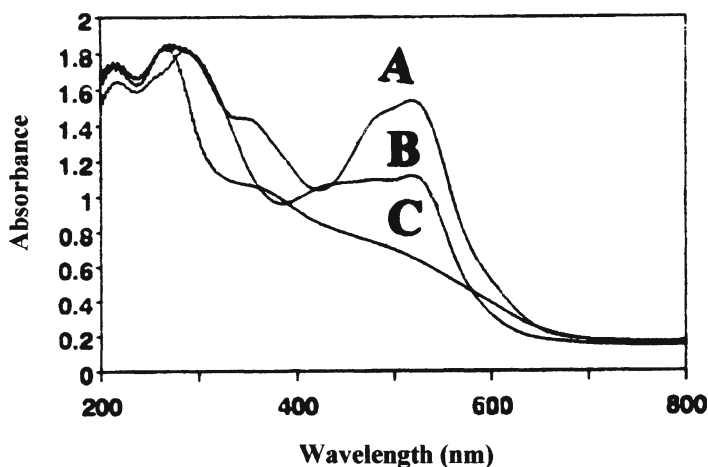


Figure 3.1.1. DRS spectra of  $\text{Fe}^{2+}(\text{bpy})_2$ -Y (a),  $\text{Fe}^{2+}(\text{phen})_2$ -Y (b) &  $\text{Fe}^{2+}(\text{bpm})_2$ -Y (c).

**Table 3.1.4.** DRS frequencies (nm) and assignments for the  $\text{Fe}^{2+}(\text{L})_2(\text{L}')_2$  and  $\text{Fe}^{2+}(\text{L})_n\text{-NaY}$  complexes.

	$\pi \rightarrow \pi^*$	LMCT $\pi \rightarrow e_g^*$	MLCT $t_{2g} \rightarrow \pi$
$\text{Fe}(\text{bpy})_3\text{-Y}$	208, 240, 298	-, 393, 347	532, 478
$\text{Fe}(\text{phen})_2\text{-Y}$	210, 263	430, 367, 332	530, 481
$\text{Fe}(\text{bpm})_2\text{-Y}$	209, 258	414, 349	569, 498

### 3.1.3 Mössbauer Characterisation

The Mössbauer spectra of  $^{57}\text{Fe}(\text{bpy})_n\text{-NaY}$ , recorded at 293 K, are shown in Figure 3.1.3. An analysis with four quadrupole doublets is made as shown in Table 3.1.5.

It should be stressed that in the determination of the relative intensities of the different components no account was made for the f-fraction of the MS-atom in its local environment. Available literature data make assignments of the different components tedious due to the inconsistencies between the different references.

The Mössbauer parameters  $\delta$  (IS) and  $\Delta$  (QS) of the quadrupole doublets QS3 and QS4 (Table 3.1.5.) show the presence of  $\text{Fe}^{2+}$  in a high spin-state. Both resonances can be ascribed to free  $\text{Fe}^{\text{II}}$  uncoordinated with bpy-ligand, interacting with water.

For weakly coordinating ligands such as water, a high spin-state  $\text{Fe}^{2+}$  is expected to be present. Possibly the free  $\text{Fe}^{2+}$  is present in the sodalite cages and the hexagonal prisms, explaining the two types of sites. This is in accordance with the results of Rees and Morice on uncomplexed  $\text{Fe}^{2+}$  in NaY. They ascribe a QS-component with  $\delta = +1.22$  mm/s and  $\Delta = 2.44$  mm/s to free  $\text{Fe}^{2+}$  [42].

**Table 3.1.5.** Mössbauer parameters, spin-state and assignment of the observed components of  $^{57}\text{Fe}(\text{bpy})_2\text{-NaY}$  (at RT with an isomeric shift relative to  $\alpha\text{-Fe}$ ).

	$\delta$ [mm/s]	$\Delta$ [mm/s]	$\Gamma$ [mm/s]	relat. int. [%]	spin	assignment
QS1	+0.20(2)	0.32(5)	0.28(2)	58	Fe(II), LS	tris, Fe(II)
QS2	+0.37(2)	0.91(5)	0.50(2)	30	Fe(II), HS	supercage bis, Fe(II)
QS3	+0.73(2)	2.21(5)	0.22(2)	3	Fe(II), HS	supercage free Fe(II)
QS4	+0.89(2)	2.60(5)	0.36(2)	9	Fe(II), HS	free Fe(II)

This assignment is also in agreement with the XPS data, in which the Fe/N ratio indicates the presence of residual free  $\text{Fe}^{2+}$ .

The component QS2 is attributed to high spin, bis-complexed Fe(II), e.g.  $[\text{Fe}(\text{bpy})_2]^{2+}$  in the supercage of the zeolite. As for homogeneous  $[\text{Fe}(\text{bpy})_2]^{2+}$  complexes at 293 K high spin-characteristics are expected. Rees *et al.* assigned comparable components to Fe, covalently bound with lattice-oxygen-atoms [42]. A deviation of the parameters in our complexes could point to another covalent environment for  $\text{Fe}^{2+}$ . In their study of  $[\text{Fe}(\text{bpy})_3]^{2+}$ , Lunsford *et al.* observed two quadrupolar components : (1)  $\text{QS}_{\text{L1}}$  ( $\delta_{\text{L1}} = +0.37$  mm/s (relative to  $\alpha\text{-Fe}$ ) and  $\Delta_{\text{L1}} = 0.34$  mm/s, 88 %), that is ascribed to low spin tris-complexed Fe(II), and (2)  $\text{QS}_{\text{L2}}$  ( $\delta_{\text{L2}} = +0.48$  mm/s (relative to  $\alpha\text{-Fe}$ ) and  $\Delta_{\text{L2}} = 1.25$  mm/s, 12 %), associated to low-spin  $\text{Fe}^{2+}$  in the hexagonal prisms of the zeolite [43]. This last component is comparable to our QS2. The isomeric shift is also in favour of a low spin  $\text{Fe}^{2+}$  assignment. Gütlich, however discards such assignment, because  $\text{Fe}^{2+}$  at 293K is expected in a high spin-state [33]. We assign QS2 to  $[\text{Fe}(\text{bpy})_2]^{2+}$ . QS1 is dominantly present and has low spin characteristics. We assign QS1 to  $[\text{Fe}(\text{bpy})_3]^{2+}$ . By the high stabilisation energy of Fe(bpy) complexes the tris-coordination can in fact hardly be avoided, moreover this assignment is in good agreement with the observations of Lunsford *et al.* for  $\text{QS}_{\text{L1}}$ . Alternatively, it should be possible to keep bis-complexes in a low spin-state through steric constraints in certain topologies with smaller cages compared to NaY, in which only short Fe-N-bond lengths can be accommodated and thus no high spin-states can be realised.

The Mössbauer spectrum of  $\text{Fe}(\text{phen})_n\text{-NaY}$  recorded at 293 K is shown in Figure 3.1.2. An analysis of the results is shown in Table 3.1.6.

*Table 3.1.6.* Mössbauer parameters, spin-state and assignment of the observed components of  $^{57}\text{Fe}(\text{phen})_2\text{-NaY}$  (at 293 K, the isomeric shift relative to  $\alpha\text{-Fe}$ ).

	$\delta$ [mm/s]	$\Delta$ [mm/s]	$\Gamma$ [mm/s]	relat. int. [%]	spin	assignment
QS1	+0.20(2)	0.82(5)	0.49(2)	55	Fe(II), LS	tris, Fe(II) supercage
QS2	+0.49(2)	0.92(5)	0.34(2)	21	Fe(II), HS	bis, Fe(II) supercage
QS3	+0.90(2)	2.55(5)	0.42(2)	13	Fe(II), HS	free Fe(II)
QS4	+0.93(2)	1.96(5)	0.33(2)	11	Fe(II), HS	free Fe(II)

The assignment is similar to that of the bpy sample, the larger quadrupolar split for QS1 illustrating the influence of the ligand-environment on the  $\Delta$  (QS) of the low spin-components. An explanation can be found in the possibility for bpy to rotate around the axis of the  $\text{C}_2\text{-C}_2'$ -bond, in which the octahedral coordination is preserved. In the phen-complex the possibility of ligand

deformation is absent. In comparison with the bpy-complex a slight decrease in concentration of the low spin, tris-complexes is observed.

The Mössbauer spectrum of  $^{57}\text{Fe}(\text{bpm})_2\text{-NaY}$ , recorded at 293 K is shown in Figure 3.1.2. In analogy to the interpretation of the  $\text{Fe}(\text{bpy})_n\text{-NaY}$  and  $\text{Fe}(\text{phen})_n\text{-NaY}$  complexes in Table 3.1.7. an analysis is proposed with 4 QS resonances.

*Table 3.1.7. Mössbauer parameters, spin-state and assignment of the observed components of  $^{57}\text{Fe}(\text{bpm})_2\text{-NaY}$  at 293 K. (isomeric shift relative to  $\alpha\text{-Fe}$ ).*

	$\delta$ [mm/s]	$\Delta$ [mm/s]	$\Gamma$ [mm/s]	relat. int. [%]	spin	assignment
QS1	+0.02(2)	0.77(5)	0.34(2)	29.5	Fe(II), LS	tris, Fe(II)
QS2	+0.43(2)	0.69(5)	0.60(2)	40	Fe(II), HS	supercage bis, Fe(II)
QS3	+0.97(2)	2.30(5)	0.32(2)	8.5	Fe(II), HS	supercage free Fe(II)
QS4	+1.18(2)	2.37(5)	0.30(2)	22	Fe(II), HS	free Fe(II)

The relative abundance of low spin tris-coordinated  $\text{Fe}^{2+}$  in  $\text{Fe}(\text{bpm})_n\text{-NaY}$  has decreased with  $\sim 25\%$  in comparison with  $\text{Fe}(\text{bpy})_n\text{-NaY}$  and  $\text{Fe}(\text{phen})_n\text{-NaY}$ . As a result of the presence of 4 N-atoms in the bpm ligand, of which two coordinate with iron, the electrostatic repulsion between the negatively charged N-atoms leads to a strong destabilisation of the ligand energy levels. This is confirmed by the observation of a less intense MLCT-band for bpm compared with bpy. Additional coordination of a third ligand is thus less favoured. The dominance of high spin complexes makes this sample interesting for temperature dependant measurements, in view of the occurrence of potential high spin  $\rightarrow$  low spin-transitions of complexed Fe, this is however not observed, as high spin characteristics are maintained over the entire temperature regime.

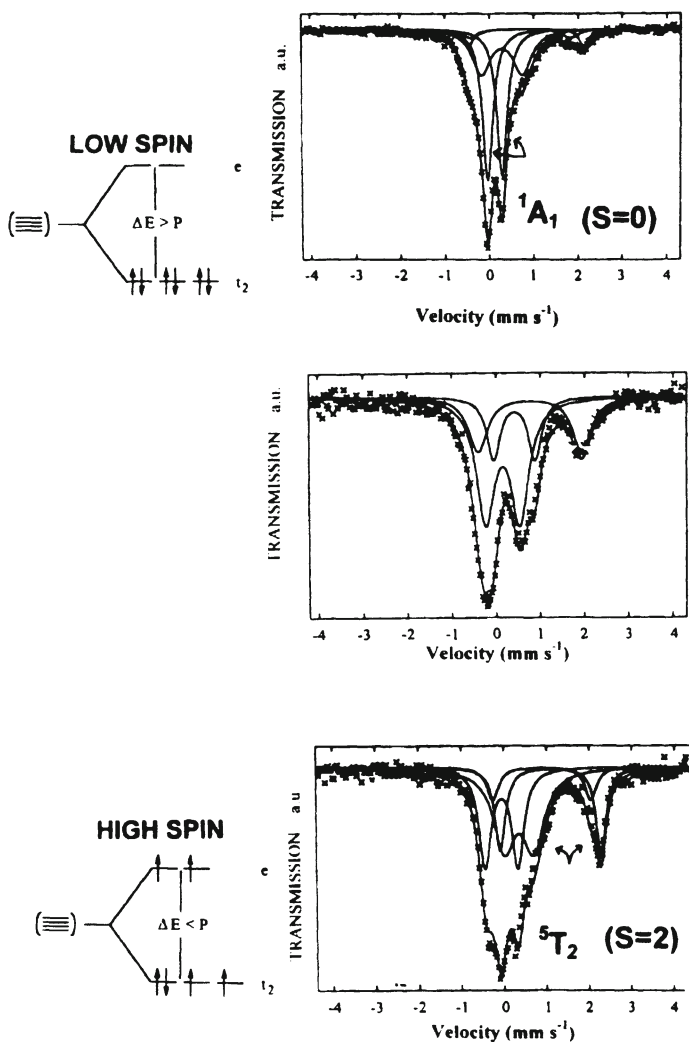


Figure 3.1.2. Mössbauer spectrum of  $^{57}\text{Fe}(\text{bpy})_n\text{-NaY}$  (Top),  $^{57}\text{Fe}(\text{phen})_n\text{-NaY}$  (Middle) and  $^{57}\text{Fe}(\text{bpm})_n\text{-NaY}$  (bottom) recorded at 293K.

### 3.1.4 Magnetic Characterisation

The amount of high-spin  $\text{Fe}^{2+}$  has also been determined for  $\text{Fe}(\text{bpy})_3\text{-Y}$  and  $\text{Fe}(\text{bpm})_2\text{-Y}$  by a SQUID measurement (Fig 3.1.3.). The diamagnetic effect of the zeolite is eliminated by cooling the sample, thus allowing to determine the paramagnetism of  $\text{Fe}^{2+}$ . The plot of the magnetisation  $M$  against  $1/T$  initially yields a straight line. From the Curie-Weiss plot, a value of 0.801 and 2.699  $\text{cm}^3\text{mol}^{-1}\text{K}$  was calculated for  $\chi_M T$  of the respective samples. The high value for the molar susceptibility,  $\chi_M$ , is in agreement with the percentage of high spin complexed species as derived from Mössbauer spectroscopy. The value of the magnetic moment,  $\mu$ , can be calculated with the help of to the assigned percentages for the different spin states as determined by Mössbauer spectroscopy. As such the values of  $\mu$  obtained are 0.0 for 58 %, 2.1 for 30 % and 5.2 for 12 % for  $[\text{Fe}(\text{bpy})_3]^{2+}\text{-Y}$  and 2.0 for 29.5% and 5.2 for 70.5%.

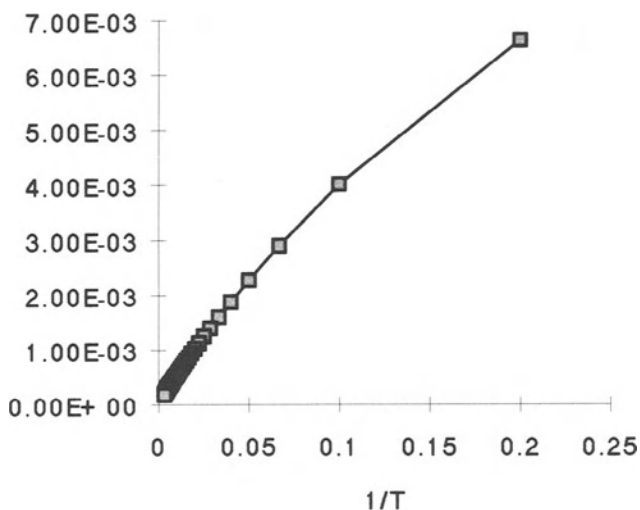


Figure 3.1.3. SQUID plot of magnetisation,  $M$ , against  $1/T$  for  $[\text{Fe}(\text{bpm})_2]^{2+}\text{-NaY}$ .

$[\text{Fe}(\text{bpm})_2]^{2+}\text{-Y}$  is a characteristic sample with complexes containing high-spin  $\text{Fe}^{\text{II}}$  (5.0-5.5) since the  $\mu$  of 5.2 is at the lower limit of that of high-spin  $\text{Fe}^{\text{III}}$  (5.2-6.0). Comparing Mössbauer and magnetic data for the  $[\text{Fe}(\text{bpy})_3]^{2+}\text{-Y}$  sample with 88% of low-spin tris-complexed iron and 12 % high-spin bis-complexed iron very low  $\mu$  values are obtained. The inconsistency may originate from errors on the f-fractions in Mössbauer spectroscopy and mass determination for the samples used in SQUID.

### 3.2 MONONUCLEAR TETRADENTATE COORDINATED Fe COMPLEXES IN THE ZEOLITE LATTICE

#### 3.2.1 Complex Distribution in the zeolite lattice

Comparison of CA and XPS after complexation of the  $\text{Fe}^{\text{II}}$  with tetradentate ligands and thorough washing of the samples does not affect the  $\text{Fe}^{\text{II}}$  concentration in the crystal rims ( $\text{Fe}/(\text{Si}+\text{Al})$  ratios), the concentration is slightly higher than this for the bidentate coordinated iron complexes given in 3.1.1.. Si/Al ratios of the parent NaY sample shows that the zeolite crystal rims are depleted in Al. Table 3.2.1. indicates that within the accuracy of the XPS measurements, the ion exchange with  $\text{Fe}^{\text{II}}$  and its subsequent complexation does not cause further crystal rim dealumination, the Fe concentration remains unchanged, while the Na content decreases (Fe/Na ratios) and thus analogous explanations as in 3.1.1. can be envisaged. The binding energies for the tetradentate ferrous iron complexes within the zeolites again correspond well with these of other ferrous organic complexes such as  $\text{K}_4\text{Fe}(\text{CN})_6$ .

Table 3.2.1. XPS analysis of representative ferrous iron complexes in zeolite Y.

Ligand	Fe	Na	Si	Al	Si/Al	Fe/Na	Fe/(Si+Al)
bpenH <sub>2</sub>	1.11	0.79	19.66	5.32	3.70	1.41	0.044
bpchH <sub>2</sub>	0.99	1.36	20.03	4.85	4.13	0.73	0.040
Y	1.09	2.18	19.93	5.25	3.80	0.50	0.043

Table 3.2.2. XPS binding energies and peak-widths of the asymmetric Fe 2p<sub>3/2</sub> peak.

Ligand	Fe (eV)	Width	Fe (eV)	Width	Fe (eV)	Width
bpenH <sub>2</sub>	709.54	3.00	712.14	2.81	714.82	3.13
bpchH <sub>2</sub>	709.98	2.94	712.46	2.73	715.21	3.36
Y	710.18	3.08	713.18	3.12	715.84	2.98

Table 3.2.3. XPS analysis of representative ferrous iron complexes in zeolite Y.

Ligand	Fe	N	C	Fe/N
bpenH <sub>2</sub>	1.11	4.43	23.02	0.251
bpchH <sub>2</sub>	0.99	2.35	25.20	0.421
Y	1.09	2.65	20.24	0.411

### 3.2.2 Reflectance spectroscopy on Fe complexes in Y zeolite

As complexation of amide ligands with zeolitic iron results in ligand deprotonation, square-pyramidal complexes can be formed as with the usual inorganic anions [45,46]: iron will be above the square plane formed by the 4 N ligating atoms while water or a lattice oxygen will function as a weak fifth axial ligand. DRS spectra of the zeolite immobilised amide complexes (Table 3.2.4.) are characterised by a broad region of  $\pi \rightarrow \pi^*$  absorption bands that are relatively insensitive to complexation. The intensity of the LMCT bands decreases in the order:  $\text{Fe}(\text{bpen})\text{Y} > \text{Fe}(\text{bppn}^*)\text{Y} > \text{Fe}(\text{bpchH}_2)\text{Y} > \text{Fe}(\text{bpbH}_2)\text{Y}$  expressing the decreasing extent of lattice oxygens or water stabilisation of ferrous complexes as well as the increasing MLCT interactions from iron to ligand nitrogen. Molecular modelling indicates that all ligands except  $\text{bpbH}_2$  should migrate easily in the zeolite structure and coordination should to a great extent be determined by the flexibility of the ligand. For  $\text{Fe}^{\text{II}}(\text{bpen})\text{Y}$  the MLCT band at 480 nm is absent, whereas it is the sole band for *high spin*  $\text{Fe}(\text{bpenH}_2)\text{Cl}_2 \cdot 0.5\text{H}_2\text{O}$  [46]. This is another indication that points to complete ligand deprotonation in zeolite Y occluded complexes. In such cases important MLCT bands appear around 574 and 402 nm, analogous with deprotonated homogeneous complexes. Indeed for *low spin*  $\text{Cu}(\text{bpen})\text{H}_2\text{O}$ , and for diamagnetic  $\text{Ni}(\text{bpen})\cdot\text{H}_2\text{O}$  MLCT bands are at 580 and 400 nm, respectively [46]. For polynuclear iron complexes such as  $\text{Fe}_2(\text{bpenH}_2)_3$  an additional band at 850 nm is present, which in the zeolite is always absent. Thus the DRS spectra firmly indicate that only mononuclear complexes with deprotonated ligands are formed in the supercage.

Table 3.2.4. DRS assignments (nm) of zeolite Y encaged tetradentate iron complexes.

Species	$\pi \rightarrow \pi^*$	LMCT	MLCT
$\text{Fe}(\text{bpen})\text{Y}$	301, 261, 211	402, 340	574
$\text{Fe}(\text{bppn})\text{Y}$	315, 264, 210	422, 339	562
$\text{Fe}(\text{bpch})\text{Y}$	303, 264, 215	392, 316	570
$\text{Fe}(\text{bpb})\text{Y}$	290, 272, 235	396	625, 573

### 3.2.3 Mössbauer Characterisation

Bush and co-workers showed that coordination of iron(II) by macrocyclic quadridentates in a cyclic planar configuration allows control of spin-pairing through the field-strength of axial ligands [35]. As for the complexes reported here (Fig. 3.2.1.) no axial coordination is apparent and only high-spin species are expected. The Mössbauer spectra and the deconvoluted data of Table 3.2.5. show that most of the iron (quadrupole doublet QS1) is present as coordinated



high spin ferrous iron. Coordination with a tetradentate ligand should involve an all-*trans* complex. *cis*-Geometry, in which the lattice exerts the *cis*-coordinating influence, forms an alternative to stabilise high spin complexes at room temperature. Lattice oxygen and/or adsorbed water will coordinate only via a weak ligand field. The quadrupole doublet QS2 has been attributed earlier either to high spin ferric or low spin more than six-fold coordinated ferrous iron, and therefore assigned to iron in hexagonal prisms [43]. Quadrupole doublet QS3 results from loosely held ferrous high spin iron ion, that corresponds to free ferrous iron, possibly located in supercage sites.

Table 3.2.5. Mössbauer spectral data of zeolite encaged complexes.

Species	$\delta$ mm/s	$\Delta$ mm/s	$\Gamma$ mm/s	Rel. Int. %	$\Delta$	spin	assignment
Fe(bpen)Y	0.15	0.85	0.55	70	QS1	II, HS	complexed Fe <sup>II</sup>
	0.44	1.01	0.37	20	QS2	II	hexagonal prism Fe <sup>II</sup>
	0.85	2.70	0.42	10	QS3	II, HS	free Fe <sup>II</sup>
Fe(bppn*)Y	0.17	0.77	0.59	66	QS1	II, HS	complexed Fe <sup>II</sup>
	0.44	1.14	0.38	9	QS2	II	hexagonal prism Fe <sup>II</sup>
	0.83	2.55	0.48	25	QS3	II, HS	free Fe <sup>II</sup>
Fe(bpch)Y	0.23	0.72	0.52	89	QS1	II, HS	complexed Fe <sup>II</sup>
	0.45	0.92	0.26	6	QS2	II	hexagonal prism Fe <sup>II</sup>
	0.97	2.58	0.47	12	QS3	II, HS	free Fe <sup>II</sup>
Fe(bpb)Y	0.24	0.74	0.52	71	QS1	II, HS	complexed Fe <sup>II</sup>
	0.84	2.18	0.41	18	QS3	II, HS	Fe <sup>II</sup> (see text)
	1.22	2.14	0.46	11	QS4	II, HS	free Fe <sup>II</sup>

$\delta$ , IS = isomeric shift,  $\Delta$ , QS = quadrupole splitting,  $\Gamma$  = full width of spectral line at half maximum; HS = high spin; data relative to  $\alpha$ -Fe .

Quadrupole doublet QS4 only appears for the bpb ligand with high spin Fe<sup>II</sup>. It can be assigned to free Fe<sup>II</sup> in oligomers loosely bound to the external surface. Molecular graphics predicts a difficult access of bpbH<sub>2</sub> to the zeolite cages. Summarizing, the Mössbauer data indicate that at least 70 % of Fe<sup>II</sup> is complexed with the tetradentate ligands in a high spin state. Most uncoordinated iron remains in the hexagonal prisms. Some 10 % of the iron is present as free Fe<sup>II</sup>, possibly located in supercage sites.

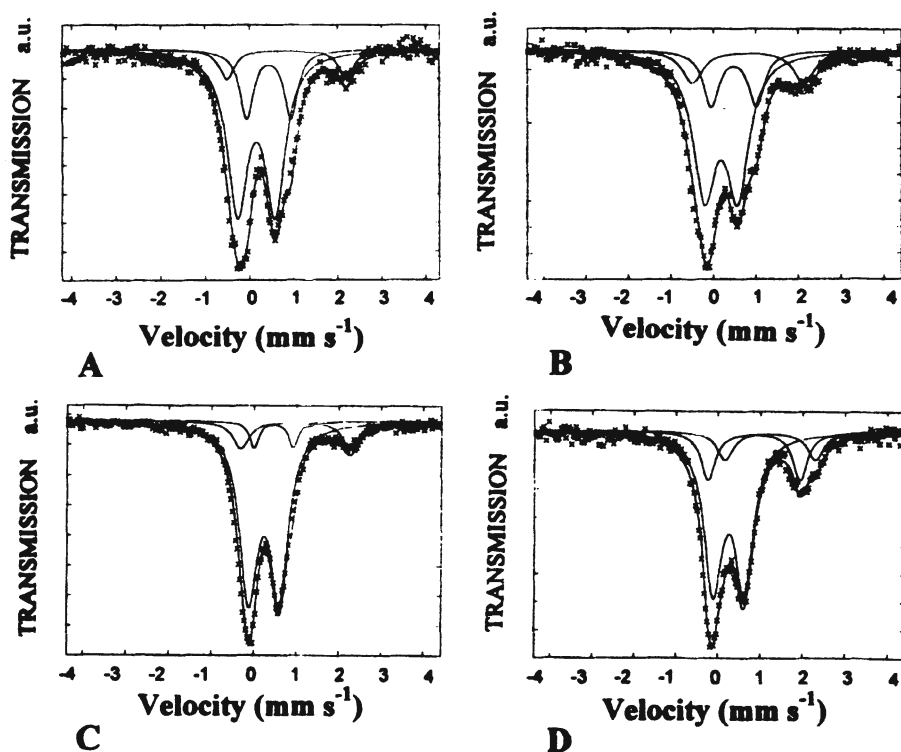


Figure 3.2.1. Mössbauer spectra of a. Fe(bpen)-Y, b. Fe(bppn\*)-Y, c. Fe(bpch)-Y, and d. Fe(bpb)-Y.

(Reprinted from Ref. [53], p. 816, with kind permission of Elsevier Science - NL, Sara Burgerhartstraat 25, 1055 KV Amsterdam, The Netherlands)

### 3.2.4 Magnetic Characterisation of the Iron

The amount of high-spin  $\text{Fe}^{\text{II}}$  has also been determined for Fe(bpen)Y by a SQUID measurement (Fig. 3.2.2.). The diamagnetic effect of the zeolite is eliminated by cooling of the sample, thus allowing to determine the paramagnetism of  $\text{Fe}^{2+}$ . The plot of the magnetisation  $M$  against  $1/T$  yields a straight line.

From the Curie-Weiss plot, a value of  $3.11681 \text{ cm}^3 \text{ mol}^{-1} \text{ K}$  was calculated for  $\chi_M T$ . The high value for the molar susceptibility,  $\chi_M$ , is in agreement with the 70 % of high spin complexed species as derived from Mössbauer spectroscopy. The value of the magnetic moment,  $\mu$ , thus obtained is 5.01, characteristic of high-spin  $\text{Fe}^{\text{II}}$  (5.0-5.5) and differs from that of high-spin  $\text{Fe}^{\text{III}}$  (5.2-6.0).

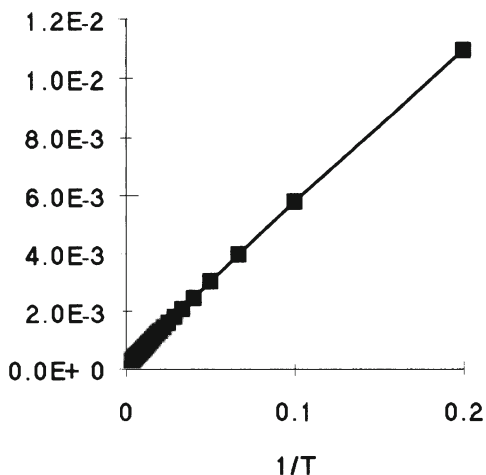


Figure 3.2.2. SQUID plot of magnetisation,  $M$ , against  $1/T$  for sample  $\text{Fe}(\text{bpen})\text{-NaY}$ .

(Reprinted from Ref. [53], p. 817, with kind permission of Elsevier Science - NL, Sara Burgerhartstraat 25, 1055 KV Amsterdam, The Netherlands)

### 3.3 BINUCLEAR HEPTADENTATE COORDINATED Fe COMPLEXES IN THE MESOPOROUS OXIDE

#### 3.3.1 Complex distribution in the mesoporous oxide

The XPS surface-concentration, is calibrated with an  $\text{Fe}_2\text{O}_3$  standard. The values obtained for the organic complexes within the supports are in close proximity of those of  $\text{K}_3\text{Fe}(\text{CN})_6$ . Table 3.3.1-3. show the concentrations and binding energies of the pure and the lattice exchanged / impregnated complexes. The use of supports complicates the static charge binding energy referencing, as this is a problem for non-conducting materials. As a positive charge forms at the surface when its atoms lose electrons in the photo-emission process, a retarding electric field is created, that shifts the kinetic energy of the photoelectron peaks. To correct for this charge accumulation several references can be used : the  $\text{C}_{1s}$  line at 285 eV of adventitious carbon, the  $\text{O}_{1s}$  at 530.0 eV for metallic oxides, and at 534.6 eV for metalloid oxides; the  $\text{Fe } 2p_{3/2}$  at 707.7 eV for metallic iron and at 711.1 eV for oxidized iron. Gold decoration or flood gun static charge neutralisation may be used as well. In this work the  $\text{Si}_{2p}$  line was chosen at 103.5 eV for  $\text{SiO}_2$  in MCM-41.

Table 3.3.1. XPS concentrations (%) of the heterogenised iron complexes.

Sample	Fe	C 1	C 2	C 3	C 4	O 1 / 2	N 1 / 2	Cl 1 / 2
HPTB/Fe	1.63	43.80	19.55	2.41		0.59/14.15	14.08/3.50	0.29/-
HPTP/Fe	2.10	57.69	1.64			0.50/22.32	9.15/1.43	0.73/4.4 0
HPTB/Fe 2%/MCM41	0.07	6.08	1.63	1.10		57.49	0.29/0.30	
HPTP/Fe 2%/MCM41	0.07	4.03	2.26	0.66	4.36	51.39	0.86	
HPTB/Fe 10%/MCM41	0.17	6.22	2.67	0.68	2.62	52.30	1.27	
HPTP/Fe 10%/MCM41	0.25	4.79	3.96	1.58	0.84	56.50	1.07	

Table 3.3.2. XPS concentrations (%) of iron in complexes and ions in the support.

Sample	Fe / Si	Si
HPTB/Fe 2%/MCM41	0.21	32.66
HPTP/Fe 2%/MCM41	0.26	26.93
HPTB/Fe 10%/MCM41	0.59	28.92
HPTP/Fe 10%/MCM41	0.86	29.03

Table 3.3.3. XPS binding energies.

Sample	Fe <sub>2p3</sub>	C <sub>1s</sub> 1&2	C <sub>1s</sub> 3&4	O <sub>1s</sub>	Si <sub>2p</sub>	N <sub>1s</sub> 1&2	Cl <sub>2p3/2</sub>
HPTB/Fe	711.07	284.73	291.59	530.02		399.86	198.75
		286.23		532.20		406.69	
HPTP/Fe	710.61	285.00		529.11		399.51	198.08
		292.18		531.72		406.54	207.12
HPTB/Fe 2%	709.14	284.24	286.82	532.72	103.50	398.98	
MCM-41	711.03	285.74				400.73	
HPTP/Fe 2%	710.82	284.72	287.76	532.69	103.50	399.78	
MCM-41		286.22	292.04				
HPTB/Fe 10%	709.32	284.40	287.49	532.70	103.50	400.00	
MCM-41	711.48	285.90	292.01				
HPTP/Fe 10%	709.12	284.23	287.09	532.68	103.50	399.90	
MCM-41	711.07	285.73	292.04				

The maximal surface coverage with iron for these complexes is 1 % in the mesoporous oxides. Due to the high fraction of the organic part in the weight of the complex the fraction of iron in the overall product is rather low.

For a given amount of complex added, the method of preparation of the samples largely determines the amount of complex heterogenised. When the complex is added during preparation as a co-template, almost no residual iron could be found in the final mesoporous oxide. Upon impregnation of increasing amounts, followed by soxhlet extraction initially no complex is retained. Using a high amount of complex results in the retention of salt occlusions. When intermediate amounts are used the nitrate and perchlorate anions all disappear and the complexes are retained possibly via electrostatic interactions. Thus using 2 weight % of complex only 0.1 weight % iron is detected on MCM-41. Using 10 weight % of complex generally 0.2 to 0.3 weight % iron is found for the  $[\text{Fe}_2(\text{HPTB})(\text{OH})]^{4+}$  and  $[\text{Fe}_2(\text{HPTP})(\text{OH})]^{4+}$  complexes on MCM-41 samples.

Slightly higher binding energies are seen for iron in the  $[\text{Fe}_2(\text{HPTB})(\text{OH})(\text{NO}_3)_2](\text{NO}_3)_2$  complexes compared with the  $[\text{Fe}_2(\text{HPTP})(\text{OH})(\text{NO}_3)_2](\text{ClO}_4)_2$  complexes. Upon heterogenisation in MCM-41 no significant reduction of the iron binding energy is observed.

In organic ligands nitrogen present in general gives a signal at a BE of 400 eV. For the pure  $[\text{Fe}_2(\text{HPTP})(\text{OH})(\text{NO}_3)_2](\text{ClO}_4)_2$  and  $[\text{Fe}_2(\text{HPTB})(\text{OH})(\text{NO}_3)_2](\text{NO}_3)_2$  complexes the bands at 407 eV are in agreement with the occurrence of nitrate-bridging groups. They were also detected for the supported complexes, albeit at much lower concentrations. The  $[\text{Fe}_2(\text{HPTP})(\text{OH})(\text{NO}_3)_2](\text{ClO}_4)_2$  shows the 207.12 eV band related to the presence of perchlorate ions.

On the mesoporous support MCM-41, without or with different loadings of the  $[\text{Fe}_2(\text{HPTP})(\mu\text{-OH})]^{4+}$  or  $[\text{Fe}_2(\text{HPTB})(\mu\text{-OH})]^{4+}$  complexes, either after synthesis via co-templating as well as impregnation, unchanged spacings of the hexagonal channels are observed in XRD, and calculated to be around 2.97-3.04 nm.

### 3.3.2 Reflectance Spectroscopy on Fe complexes in MCM-41

With DRS in the UV-Vis region, d-d,  $\pi$ - $\pi^*$  transitions, and charge transfer between metal and ligand such as MLCT and LMCT can be probed. The spectrum of  $[\text{Fe}_2(\text{HPTB})(\text{OH})(\text{NO}_3)_2](\text{NO}_3)_2$  shows  $\lambda_{\text{max}}$  at 340 nm, due to the benzimidazole-iron charge transfer [52]. The spectrum of  $[\text{Fe}_2(\text{HPTP})(\text{OH})(\text{NO}_3)_2](\text{ClO}_4)_2$  (B) shows  $\lambda_{\text{max}}$  at 290 nm, of a pyridyl-iron charge transfer [49]. Maxima occur at 340 and 500 nm for  $[\text{Fe}_2(\text{HPTB})(\text{OH})(\text{NO}_3)_2](\text{NO}_3)_2$  and at 355 nm and 490 nm with a shoulder at 600 nm for the  $[\text{Fe}_2(\text{HPTP})(\text{OH})(\text{NO}_3)_2](\text{ClO}_4)_2$  complexes (Figure 3.3.1.). From 300-400 nm

oxo $\rightarrow$ Fe CT transitions are seen and for the bent Fe-O-Fe geometries three  $\pi$ -derived transitions of oxo  $p_x$ ,  $p_y$ ,  $p_z$  to Fe  $d_{xz}$ ,  $d_{yz}$  and  $d_{x'z}$  are expected. In the 440-510 nm region pairs of absorption bands due to the bent Fe-O-Fe with 10-fold lower intensity are seen if carboxylato, carbonato or phosphato-bridges are present.

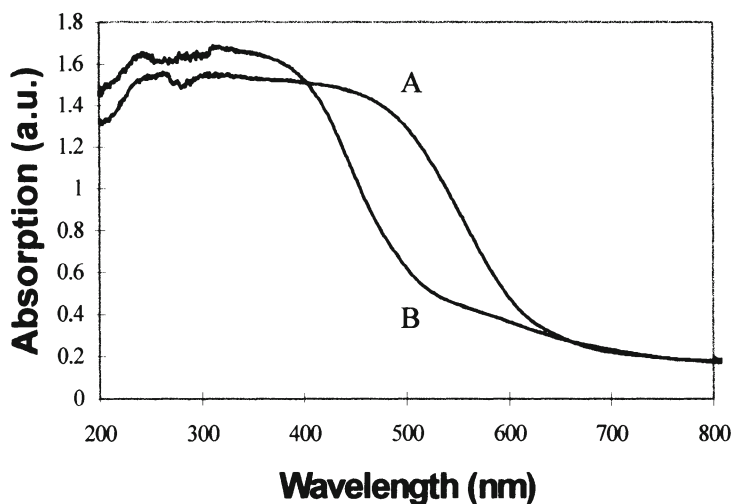


Figure 3.3.1. DRS-spectra of  $[\text{Fe}_2(\text{HPTB})(\text{OH})(\text{NO}_3)_2](\text{NO}_3)_2$  (A) and  $[\text{Fe}_2(\text{HPTP})(\text{OH})(\text{NO}_3)_2](\text{ClO}_4)_2$  (B).

Peroxo $\rightarrow$ Fe CT absorption arise at 470 nm upon addition of  $\text{H}_2\text{O}_2$  to dinuclear iron complexes in methanol. Easy formation of the 1:1 adduct of  $[\text{Fe}_2(\text{HPTB})(\text{OH})(\text{NO}_3)_2](\text{NO}_3)_2$  and catechol or  $\text{H}_2\text{O}_2$  may be analogous to interaction of the reduced complex with oxygen. The new shoulder shows a decrease in absorption in time. When *t*-butylhydro-peroxide is sorbed on the pure complexes an absorption shoulder around 600 nm arises (Figure 3.3.2.), assigned to the “blue species” of the peroxide-Fe charge transfer. The oxygen adduct of the binuclear Fe(II) complexes is formally analogous to the peroxide adduct of the Fe(III) complex e.g., oxy-hemerythrin as a two electron transfer occurs. For oxy-hemocyanin and oxy-tyrosinase analogous species developed with a blue color. A partial charge redistribution can occur after peroxide $\rightarrow$ Fe interaction. Concomitant changes in the ligand iron distances lead to changes in the coordination of benzimidazole or pyridine with Fe. Thus  $[\text{Fe}_2(\text{HPTB})(\text{OH})(\text{NO}_3)_2](\text{NO}_3)_2$  has a different stability compared to  $[\text{Fe}_2(\text{HPTB})(\text{H}_2\text{O}_2)(\text{NO}_3)_2](\text{NO}_3)_2$ .

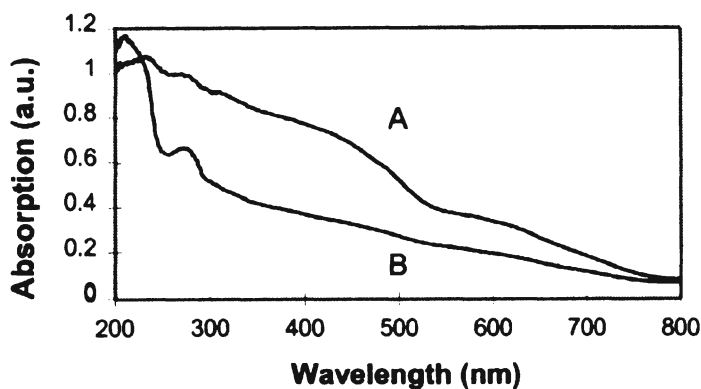


Figure 3.3.2.  $[\text{Fe}_2(\text{HPTP})(\text{OH})(\text{NO}_3)_2](\text{ClO}_4)_2$  to which *t*BHP is added after A. 15 and B. 30 minutes.

DRS-spectra of  $[\text{Fe}_2(\text{HPTB})(\text{OH})(\text{NO}_3)_2](\text{NO}_3)_2$  are shifted to higher wavelengths compared to the supported complexes. The 'support' dilutes species and the removal of the charge-compensating anions affects their symmetry.

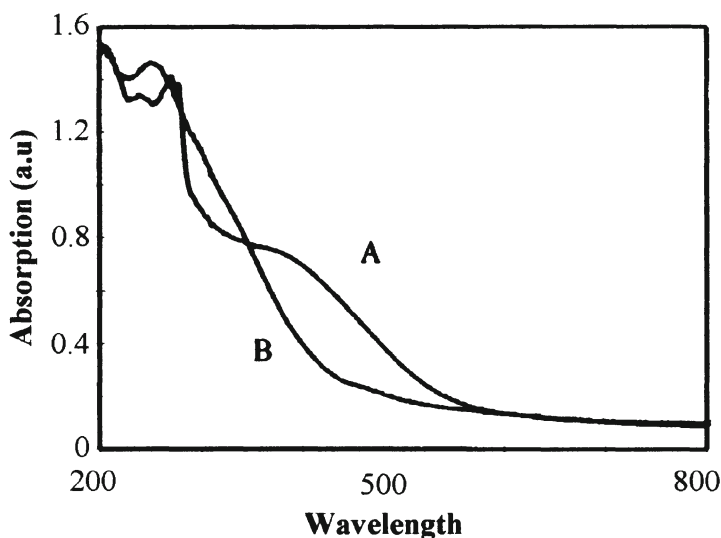
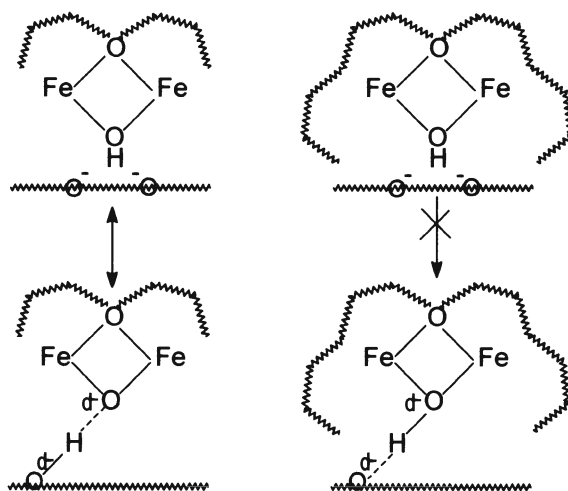


Figure 3.3.3. Effect of MCM-41 heterogenisation on the UV-Visible adsorption of both (A) HPTB/Fe and (B) HPTP/Fe complexes.

### 3.3.3 Mössbauer Spectroscopy

The original and decomposed Mössbauer spectra of  $[\text{Fe}_2(\text{HPTB})(\mu\text{-OH})(\text{NO}_3)_2](\text{ClO}_4)_2$  and  $[\text{Fe}_2(\text{HPTB})(\mu\text{-OH})(\text{NO}_3)_2](\text{NO}_3)_2$  prior to and after heterogenisation in MCM-41 are reported in Figures 3.3.4. and in Tables 3.3.4. For diiron complexes Mössbauer spectroscopy allows to assess (1) oxidation and spin states of the iron atoms, (2) diamagnetism and ferromagnetism of the ground state for diferric and mixed-valent oxidation levels respectively, (3) valence (de)localisation in the solid state for mixed-valence complexes [33]. Isomer shifts (IS,  $\delta$  [mm/s] relative to metallic iron at 300 K) in the range 0.35–0.60 mm/s are characteristic of 5- or 6-coordinate high-spin diferric  $\mu$ -hydroxo complexes. Tetrahedral high-spin ferric iron has lower IS in the range of 0.22 mm/s [33]. For isolated ferric iron with  $S = 5/2$  IS values of 0.34 mm/s are seen. In diferric complexes the quadrupole splitting for  $\mu$ -oxo complexes and  $\mu$ -hydroxo complexes is larger than 1 mm/s in the former and lower than 1 mm/s in the latter case.

The reduction in electric field gradient, indicated by the smaller QS in the hydroxo-bridged complexes may be due to the lengthening of the Fe–O bond upon deprotonation of the hydroxo bridge (Scheme 3.3.1.). This seems a general trend for both di- and tribridged complexes [21–24]. The QS however is also sensitive to changes in the coordination sphere (Scheme 3.3.2.).

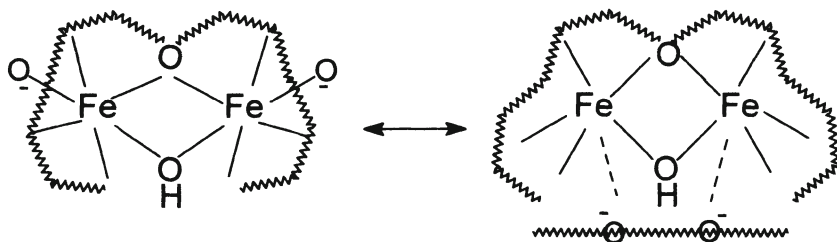


*Scheme 3.3.1.* Representation of the H-bond interaction of  $[\text{Fe}_2(\text{HPTB})(\mu\text{-OH})]^{4+}$  with oxide surfaces and the lack of interaction as a result of shielding of Fe with HPTB in  $[\text{Fe}_2(\text{HPTB})(\mu\text{-OH})]^{4+}$  as inferred from FT-Raman and Mössbauer data.



In  $[\text{Fe}_2(\text{HPTB})(\mu\text{-OH})(\text{NO}_3)](\text{NO}_3)_2$  (2) all of the iron (quadrupole doublet QS1) is present as coordinated high spin ferric iron as can be seen in Table 3.3.4. and Fig. 3.3.4. The value of 0.32 mm/s for the IS is rather low, although such values are also encountered for other ferric model systems. The value of 0.65 mm/s for the QS points to  $\mu$ -hydroxo-type complexation. From the variable-temperature  $^{57}\text{Fe}$  Mössbauer characteristics there is no evidence for changes in the localised electronic structure as the temperature is increased from 4.2 to 293 K.

After heterogenisation of  $[\text{Fe}_2(\text{HPTB})(\mu\text{-OH})]^{4+}$  in MCM-41 (Tables 3.3.4. and Fig. 3.3.4.), 96 % of the species have a comparable IS of 0.25 mm/s with QS of 0.91 mm/s. The interaction of silanol or bridge hydroxyls with the  $\mu$ -oxo bridge may lead to H-bonding, and an increased QS. Alternatively 5- compared to 6- coordinated dinuclear centers may show significantly higher QS, as the less symmetrical trigonal-bipyramidal Fe(III) site has a higher QS compared to the more symmetrical octahedral Fe(III) site. This explanation may be more likely because removal of charge compensating  $\text{NO}_3^-$  groups, reduces the coordination sphere symmetry around the Fe(III) core (Scheme 3.3.2.) . The observed increase of the line-width from 0.42 mm/s for perfectly equivalent iron sites to the value of 0.88 mm/s is also indicative of a decrease in degree of equivalence of the two iron atoms.



*Scheme 3.3.2.* Schematic representation of the changes in coordination geometry of  $[\text{Fe}_2(\text{HPTR})(\mu\text{-OH})]^{4+}$  with the oxygen anions of nitrates (left) and with an oxide surface (right) as inferred from FT-Raman and Mössbauer data.

A slight increase of the QS with temperature decrease is typical for high-spin Fe(III) systems due to changes in the Boltzmann populations of the low-lying electronic states that form as a consequence of spin-orbit and low-symmetry crystal field perturbations. The other 4 % of the species have an IS of 0.02 mm/s and QS of 0.33 mm/s due to low-spin Fe(III) as described by Lunsford *et al.* [43] for species bound with aromatic rings via  $\pi$ -bonding.

For  $[\text{Fe}_2(\text{HPTP})(\mu\text{-OH})(\text{NO}_3)](\text{ClO}_4)_2$  the iron speciation is more complex as shown in Table 3.3.4. and Fig. 3.3.4. Although the two isomer shifts of 0.29 and

0.30 mm/s are almost identical, the values of the quadrupole splitting shows that 55% of the complexes are  $\mu$ -O bridging and 45% are  $\mu$ -OH bridging.

Upon heterogenisation of  $[\text{Fe}_2(\text{HPTP})(\mu\text{-OH})]^{4+}$  in MCM-41 a clear change in speciation is encountered. In MCM-41 only 46 % of the iron is complexed in a way intermediate between  $\mu$ -O and  $\mu$ -OH bridging, due to the lattice H-bonded ( $\mu$ -OH) bridging. The other 54% has a reduced IS of 0.08 mm/s and a QS of 0.36 mm/s can be assigned to low-spin Fe(III) [43] for species  $\pi$ -bound to aromatic rings.

*Table 3.3.4. Mössbauer parameters at 4.2K of  $[\text{Fe}_2(\text{HPTB})(\mu\text{-OH})(\text{NO}_3)_2](\text{ClO}_4)_2$  and of  $[\text{Fe}_2(\text{HPTB})(\mu\text{-OH})(\text{NO}_3)_2]^{2+}$  - MCM-41 and  $[\text{Fe}_2(\text{HPTP})(\mu\text{-OH})(\text{NO}_3)_2](\text{NO}_3)_2$  and of  $[\text{Fe}_2(\text{HPTP})(\mu\text{-OH})(\text{NO}_3)_2]^{2+}$  - MCM-41;  $\delta$  relative to  $\alpha$ -Fe;*

Support	Parameters		
none <b>HPTB</b> <b>Fe</b>	$\delta$ [mm/s]	0.2996(17)	
	$\Delta$ [mm/s]	0.6940(29)	
	$\Gamma$ [mm/s]	0.5109(49)	
	rel. int. [%]	100	
MCM-41 <b>HPTB</b> <b>Fe</b>	$\delta$ [mm/s]	0.2508(5)	0.0168(50)
	$\Delta$ [mm/s]	0.907(16)	0.327(84)
	$\Gamma$ [mm/s]	0.701(22)	0.350(-)
	rel. int. [%]	96	4
none <b>HPTP</b> <b>Fe</b>	$\delta$ [mm/s]	0.3088(1)	0.2988(1)
	$\Delta$ [mm/s]	0.42(1)	1.38(2)
	$\Gamma$ [mm/s]	0.34(1)	0.84(3)
	rel. int. [%]	45.5	54.5
MCM-41 <b>HPTP</b> <b>Fe</b>	$\delta$ [mm/s]	0.2588(1)	0.0788(1)
	$\Delta$ [mm/s]	0.96(1)	0.36(2)
	$\Gamma$ [mm/s]	0.39(2)	0.66(6)
	rel. int. [%]	46	54

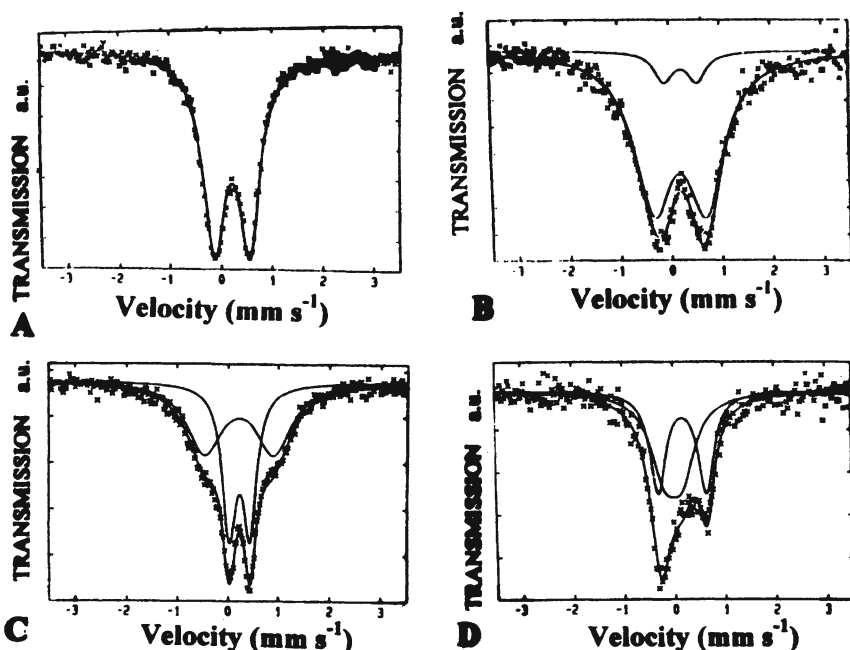


Figure 3.3.4. Mössbauer spectra of  $[\text{Fe}_2(\text{HPTB})(\mu\text{-OH})(\text{NO}_3)_2](\text{NO}_3)_2$  (A) versus  $[\text{Fe}_2(\text{HPTB})(\mu\text{-OH})]^{4+}$ -MCM-41 (B) and  $[\text{Fe}_2(\text{HPTP})(\mu\text{-OH})(\text{NO}_3)_2](\text{ClO}_4)_2$  (C) versus  $[\text{Fe}_2(\text{HPTP})(\mu\text{-OH})]^{4+}$ -MCM-41 (D) all at 4 K with  $\delta$  [mm/s] relative to metallic Fe for which  $\delta_{\text{me-Fe}} = \delta_{\alpha\text{-Fe}} - 0.0888$  [mm/s].

## 4. Oxidation Catalysis

### 4.1 ALKANE VERSUS PEROXIDE REACTIVITY

Cytochrome P-450 and its mononuclear iron oxo chemistry [1-2, 44-45, 51, 53, 65-68] and Methane Mono-Oxygenase and its dinuclear iron oxo or peroxo chemistry [6-7, 11-30, 54-57, 69-75] show considerable differences in reactivity compared to the chemistry encountered in solutions containing mononuclear iron, such as the aqueous Fenton chemistry [58-59] and the GIF chemistry in organic solvents [60-61]. These differences result from the complex interplay of homogeneous and heterogeneous mechanisms, radical and oxo- mechanisms, and the different geometric and electronic implications of the design of the active site [25-27].

Partial oxidation can be exothermic [68], however, the direct attack of oxygen on cyclohexane is endothermic by 47 kcal/mol. The heats of combustion for alkanes are generally about 105 kcal/mol for each mole of oxygen or 52 kcal/g-atom of O consumed. Partial oxidation shows more variation, e.g. for ethane to acetic acid, acetaldehyde, ethanol and ethylhydroperoxide the exothermicity decreases from 70, 49, 40 to 19 kcal/mol. The hydrogen over carbon ratio determines the overall dissociation energy of the hydrocarbon bond. As this ratio is the highest for methane, the dissociation energy will also be the highest in this case. Thus the highest CH bond energies are seen for methane and aromatics, respectively 102 kcal/mol for the CH bond in benzene and methane, around 97 to 94 kcal/mol for the CH bond in ethane, 91 kcal/mol for the tertiary CH in iso-butane and 85 kcal/mol for the CH in the methyl group of toluene.

Sawyer *et al.* [66] and Tolman *et al.* [68] both described the differences in reactivity of hydroperoxides and oxygen depending on their unique bond energies (e.g. H-OOH, 90 kcal/mol ; HO-OH, 51 kcal/mol ; H-OO*t*Bu, 91 kcal/mol ; HO-O*t*Bu, 47 kcal/mol, CH<sub>3</sub>O-OH 43 kcal/mol, CH<sub>3</sub>O-OCH<sub>3</sub> 36 kcal/mol ) which allow low energy rearrangements to give  $^{\circ}\text{OOR}$ ,  $^{\circ}\text{OR}$ ,  $^{\circ}\text{OOH}$ ,  $^{\circ}\text{OH}$  and  $^{\circ}\text{O}^{\circ}$  radicals that are important as they are more easily activated. It is remarkable that the  $^{\circ}\text{OO-H}$  bond energy in a peroxyradical is as low as 47 kcal/mol. Thus the extent of heterolysis versus homolysis of *t*BuOOH and H<sub>2</sub>O<sub>2</sub> can be compared to study the mechanism. The oxidation of organic substrates by triplet oxygen in the ground state of oxygen inhibits its reactivity. Singlet oxygen formation with dinuclear iron complexes has been postulated.

Autoxidation of organic substances [63] is significantly faster after addition of peroxides as initiators. Their build up via initiation and propagation is rather slow starting from alkanes. Due to the lower thermodynamic stability of peroxides compared to alkanes it is important to assess their way of decomposition. As all carbon radicals combine with oxygen, peroxy radicals are formed in propagation reactions. These can abstract hydrogen and carry the chain or combine with other peroxy-radicals and terminate to yield dialkylperoxides and oxygen. Induced decomposition of peroxides may follow an organic or heavy metal catalysed pathway. In the cyclic transition states encountered in thermal peroxide decomposition at relatively lower temperatures often a non-radical pathway is favoured as radical-inhibitors do not affect these reactions.

As the rate of termination [64] defines the chain carrying species in catalysis and secondary and primary peroxy radicals terminate chains more rapidly than tertiary ones even in reactions with *t*BuOOH and hydrogen peroxide cyclohexyl hydroperoxides and secondary adamantyl peroxides will be very important.

## 4.2 OXIDATION CATALYSIS WITH MONONUCLEAR FERROUS IRON COMPLEXES

The knowledge from the organisation of iron in enzymes prompts us to study the geometrical implications on radicalar versus oxo-chemistry [63-64]. Iron decomposes  $\text{H}_2\text{O}_2$  with generation of molecular oxygen, with correspondingly low alkane oxidation capability. By complexation of the iron by the zeolite lattice or mesoporous oxide oxygen atoms this behaviour is only slightly moderated as shown in the oxidation of cyclohexane [53-55]. On the other hand, ligation of zeolitic iron by organic ligands has a pronounced effect on its redox behaviour and its electrophilicity, thus modifying Fenton- or Barton type chemistry and promoting (heme type) oxo or (non-heme type) mono-oxygenase chemistry.

### 4.2.1 Oxo-Chemistry versus Organic Peroxide Generation

The reaction between the reactive iron complex intermediate in oxo-type chemistry involves either  $\text{Fe}^{\text{IV}}\text{O}$  or  $\text{Fe}^{\text{V}}\text{O}$  and the alkane and leads to the generation of an alcohol molecule via an oxygen rebound mechanism. An  $\text{Fe}^{\text{III}}\text{OOH}$  and an alkane, on the other hand via a free radical chain mechanism generate alkyl radical intermediates. In the case of cyclohexane this cyclohexyl radical traps oxygen and the formed cyclohexylperoxy radical easily abstracts hydrogen to form CHHP ( $\text{C}_6\text{H}_{11}\text{OOH}$ ) and carry the chain. The presence of CHHP [60-68] can be demonstrated by  $^{13}\text{C}$  NMR [60] and via phosphine decomposition [63]. Reactions under Nitrogen or Argon flow have a reduced activity, as oxygen formed via decomposition pathways is removed efficiently.

The cyclohexane conversion decreases from 26 % for oxidation with iron complexes with tetradentate ligands, with  $\text{Fe}(\text{bppn}^*)\text{-Y}$  as most active catalyst, to only 9 % for zeolite ligated iron in  $\text{FeY}$  (Table 4.1.1.). The selectivity for the CHHP varies from 68 % with  $\text{Fe}^{\text{II}}\text{Y}$  to 37 % with  $\text{Fe}(\text{bpb})\text{-Y}$ .  $\text{Fe}(\text{bpy})_2\text{-Y}$  and  $\text{Fe}(\text{phen})_2\text{-Y}$  show the highest CHHP yields. Thus bidentate ligands tend to favor *cis*-bis ligand chelation, thus allowing the formation of *cis*- $\text{Fe}(\text{OH})(\text{OOH})$  active sites, whereas the function of the tetradentate ligands is clearly to avoid such *cis* coordination and to stabilise the higher oxidation states such as  $\text{Fe}^{\text{IV}}\text{O}$  and to decrease the radical chain pathways involved.

The ketone/alcohol ratio can change over time. As long as  $\text{H}_2\text{O}_2$  is present, the  $\text{L}_2\text{Fe}(\text{OH})(\text{OOH})$  generates the CHHP that is consequently decomposed. On Lewis acid ferric sites the direct dehydration to the ketone is known to occur. In acetonitrile  $\text{FeY}$  shows a pronounced ketone formation with a cyclohexanone/ol ratio of 1.9. The pure radicalar termination would result in a ratio around 1.0. As  $\text{H}_2\text{O}_2$  is depleted, organic radicals may reduce the ferric iron resulting in the presence of more ferrous iron. This ferrous iron can react as a reductant with the CHHP leading to hydroxyl anions and alkoxy radicals. The latter radicals

abstract hydrogen and form alcohols. The disproportionation takes over and more alcohol is formed. The ketone/alcohol ratio increases in time for Fe(bpR)-Y, as here the alcohol is directly formed from the cyclohexane and the ketone is consequently formed from the direct oxidation of cyclohexanol.

*Table 4.1.1. Cyclohexane oxidation <sup>a</sup>.*

catalyst	Conversion (%)	Selectivity ( % )		
		cyclohexanol	cyclohexanone	CHHP
Fe <sup>II</sup> Y	9	11	21	68
Fe(bpy) <sub>2</sub> Y	22	3	3	94
Fe(phen) <sub>2</sub> Y	15	7	6	87
Fe(bpch)Y	10	21	28	51
Fe(bpb)Y	15	27	36	37
Fe(bpen)Y	22	28	30	42
Fe(bppn*)Y	26	17	20	63

<sup>a</sup> Reaction conditions: 0.05 g of catalyst (0.035 mmol complex), 0.2 g of cyclohexane (2.5 mmol) in 2 g of acetonitrile as solvent and 2 g of H<sub>2</sub>O<sub>2</sub> (30 % in water, 25 mmol) as oxidant; reaction time of 24 h at 293 K.

#### **4.2.2 Organic Peroxide Decomposition**

Both the temperature and the solvents have a significant influence on the CHHP decomposition [63]. Thermal CHHP decomposition may favor homolytic O-O bond cleavage, leading to ketone and alcohol in identical amounts. In table 4.2.1. it is clear that at 293 K both FeY and the blank reaction are inactive deperoxidation catalysts. In a polar solvent such as acetonitrile the presence of ketone and alcohol points to the intermolecular heterolytic reaction between CHHP and an alcohol can lead to ketone and water, regenerating an alcohol; cyclohexanol can also be formed from reaction between CHHP and cyclohexane (Fig.4.2.1.).

From CHHP, cyclohexanol and cyclohexanone can be formed by metal ions, e.g. Haber-Weiss type decomposition. This occurs with metals such as Mn<sup>2+</sup> and Co<sup>2+</sup> to generally yields a ketone/alcohol ratio of 0.5. With Fe<sup>2+</sup>, Fenton type chemistry occurs with peroxides as will be further discussed, the ferrous iron splits and reduces the peroxide yielding a hydroxyl anion and a hydroxy radical [68], the ferric iron can be involved in the intramolecular heterolytic

reaction with intramolecular oxido-reduction. In the ideal case pure ketone and no byproducts are formed (Fig.4.2.2.).

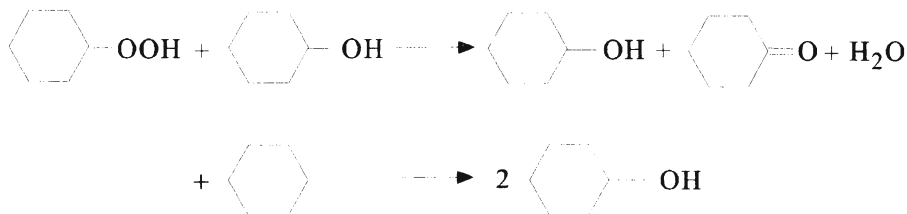


Figure 4.2.1. The heterolytic intermolecular decomposition.

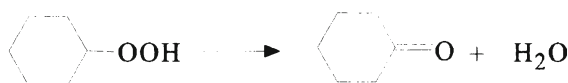


Figure 4.2.2. The heterolytic intramolecular decomposition.

An example of the latter heterolytic intramolecular decomposition is seen in the presence of Brönsted or Lewis acid sites (Fig.4.2.3.). High ketone ratios can be caused by the zeolite Brönsted acidity at elevated temperatures or Lewis acids such as  $\text{Fe}^{\text{III}}\text{OH}$  formed from  $\text{Fe}^{\text{II}}$  after homolytic splitting of  $\text{H}_2\text{O}_2$ . In a subsequent attack between  $\text{Fe}^{\text{III}}\text{OH}$  and CHHP ketone is formed by abstraction of  $\text{H}_2\text{O}$ .

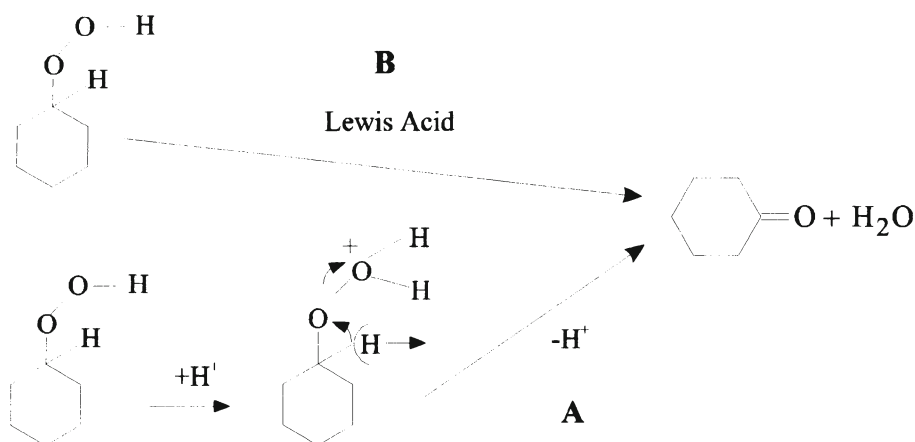


Figure 4.2.3. Lewis and Brönsted acid catalysed ketonisation scheme.

Table 4.2.1. Decomposition of CHHP to cyclohexanol / cyclohexanone <sup>a</sup>.

Catalyst	CHHP (%)	cyclohexanol / one ratio
none	0	-
FeY	0	-
Fe(bppn)Y	7	0.35
Fe(bpy) <sub>2</sub> <sup>2+</sup> Y	12	0.90
FePcY	30	0.35

<sup>a</sup> Reaction conditions: 0.05 g of catalyst in 2 g of oxidative mixture, 60 h at 293 K.

In the direct decomposition of CHHP shown in Table 4.2.1. the Fe(bpR)-Y complexes show preferential ketone formation. This ratio is analogous to this of Fe(Pc)-Y, thus the tetradentate ligands allow a stabilisation of the iron as Fe<sup>IV</sup>O. In the direct oxidation of cyclohexanol, Fe(bppn)-Y gives a much higher conversion to cyclohexanone than Fe(bpy)<sub>2</sub><sup>2+</sup>-Y. Such reactivity is reminiscent of the Cytochrome P-450 hydroxylation with an oxygen rebound mechanism, showing consecutive oxidation.

#### 4.2.3 Adamantane oxidation

Oxidation of adamantane, with 12 secondary and 4 tertiary carbon atoms, by random attack would lead to a C<sup>2</sup>/C<sup>3</sup> ratio of 3. Radical reactions involving free radicals show a C<sup>2</sup>/C<sup>3</sup> ratio between 0.05 and 0.15 [62]. In Table 4.2.3. for Fe<sup>II</sup>-Y the C<sup>2</sup>/C<sup>3</sup> ratio is closest to the expected C<sup>2</sup>/C<sup>3</sup> ratio for radical reactions. Catalysts in which higher oxidation states Fe<sup>IV-V</sup> take part, give higher C<sup>2</sup>/C<sup>3</sup> ratios. The value of 0.30 for Fe(bpen)-Y indicates that these tetradentate iron complexed catalysts do not only follow an oxo mechanism, but that the uncomplexed Fe<sup>II</sup> and possibly also part of the seems involved in radical reactions involving the Fe<sup>III</sup>OH and *t* butoxy- radicals. The blank reaction with FeY involves purely radical reactions with decreased C<sup>2</sup>/C<sup>3</sup> ratios. The *t*BuO radicals can abstract hydrogen and form *t*BuOH. observed in complete absence of radical intermediates. Chlorinated products (1-Cl, 2-Cl) are only present in negligible amounts.

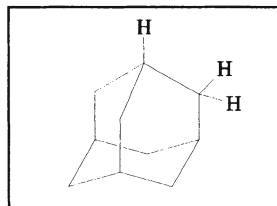




Table 4.2.3. Oxidation of adamantane <sup>a</sup>.

Catalyst	conv. (%)	adam- antan- 1-ol	adam- antan- 2-one	adam- antan- 2-ol	others	C <sup>2o</sup> /C <sup>3o</sup>
Fe <sup>II</sup> -Y	0.04	0.01	<0.001			0.05
Fe(bpen)Y	7	2.60	0.230	0.26	0.60	0.30
Fe(pic) <sub>2</sub> Y	5	1.44	0.235	0.18	0.03	0.28

<sup>a</sup> Reaction conditions: yields expressed as mol product per mol iron; 0.1 g adamantane (0.75 mmol) and 0.8 g *t*BHP (7.5 mmol) in 3 g CH<sub>2</sub>Cl<sub>2</sub>, for 24 h at 293 K.

### 4.3 ALKANE OXIDATION CATALYSIS WITH DINUCLEAR FERRIC IRON COMPLEXES

#### 4.3.1 Ketonisation versus Organic Peroxide Generation

Both electronic and geometric effects affect the mechanism and activation of intermediates in alkane oxygenation on dinuclear iron cores [69-75]. Cyclohexane oxidations by [Fe<sub>2</sub>(HPTP)(OH)(NO<sub>3</sub>)<sub>2</sub>](ClO<sub>4</sub>)<sub>2</sub> complexes are performed at low substrate conversions around 2-5 %. The use of MeCN as a solvent increases the reaction rate. In general the combined coordination of peroxides and oxygen effect the oxidation of the alkane to the alkylhydroperoxide, the coordination of peroxides alone is sufficient for the subsequent decomposition pathways to yield alcohols and ketones.

In the *t*BHP oxidation in the presence of oxygen the formation of cyclohexylhydroperoxide (CHHP) and cyclohexyl-*t*-butylperoxide (CHBP) points to a radical process. CHHP results from oxygen uptake in the propagation, followed by hydrogen abstraction from cyclohexane. CHBP is reminiscent of the mixed peroxide intermediates observed in GIF chemistry prior to the peroxide decomposition by pyridines. Decomposition products of organic peroxides are generally demonstrated with phosphines. As such triphenylfosfine-oxide and cyclohexanol are formed from CHHP and triphenylfosfine.

The homogeneous dinuclear iron(III) complexes catalyse a rather complete deperoxidation, when they are deposited at a high concentration they show an analogous behaviour, possibly due to the surface associated complexes, or complexes returning into solution during catalysis. When they are loaded into MCM-41 at the 2% level, they are isolated and remain associated with their host as the supernatant remains colourless.

In the cyclic transition states encountered in metal catalysed peroxide decomposition, the metal peroxo complexes are the active species. This requires the intimate presence of the bound and free peroxides, which is more difficult to achieve within a host-guest system with a tight fit.

The very significant difference with the homogeneous case cannot be solely the result of conversion differences. Inherently the stabilisation of the complexes on the mesoporous support decreases complex destruction, thus inhibiting the leakage of iron(III) in solution, yielding reduced iron that can be involved in Fenton chemistry. At very low loadings and after very long extraction times the complexes are however thought to open up.

Furthermore the extent to which intermolecular reactions can occur within the mesoporous oxides is fairly limited, due to the difficulty to accommodate the intermolecular transition state. Thus the difference in the product distribution can be due to the involvement of an intramolecular transition state within the mesoporous oxides.

Table 4.3.1. Cyclohexane oxidation with *t*-butylhydroperoxide at 293 K <sup>a</sup>

	Conv. (%)	Select. <i>c</i> HHP	(%) <i>c</i> H <sub>2</sub> BP*	<i>c</i> hexanol	<i>c</i> hexanone
HPTB/Fe	6.43	3.6	5.4	33.4	57.5
HPTB/Fe 10% /MCM41	5.82	8.4	10.5	30.1	51.2
HPTB/Fe 2% /MCM41	1.80	72.5	27.4	0	0
HPTP/Fe	5.19	8.7	5.4	38.8	47.0
HPTP/Fe 10% /MCM41	4.93	12.9	9.8	34.6	42.6
HPTP/Fe 2% /MCM41	1.40	79.8	20.2	0	0

0.1mmol HPTP/Fe or HPTB/Fe (either pure or MCM-41), 0.2 g cyclohexane (2.4 mmol) and 1.8 g *t*-butylhydroperoxide (16 mmol) in 2 g MeCN, 24h;

\* *t*-butylperoxy-cyclohexane.

All complexes properly heterogenised in mesoporous oxides show similar activity. This probably points to the existence of extra-granular diffusion and/or the enhanced stability of the peroxo-adducts on supports. The difference in product selectivity among the mesoporous oxides, is merely a conversion effect.

In solution the cyclohexanone/ol ratio is 1.72 and 1.21 for [Fe<sub>2</sub>(HPTB)(OH)(NO<sub>3</sub>)<sub>2</sub>](NO<sub>3</sub>)<sub>2</sub> and [Fe<sub>2</sub>(HPTP)(OH)(NO<sub>3</sub>)<sub>2</sub>](ClO<sub>4</sub>)<sub>2</sub>, respectively. The fact that the HPTB ligand better shields the reactive intermediates compared to HPTP may indicate that in such a “cryptating complex-lattice cage environment” in which ketonisation is favoured.

Furthermore the higher binding energy of the  $[\text{Fe}_2(\text{HPTB})(\text{OH})(\text{NO}_3)_2](\text{NO}_3)_2$  compared to the  $[\text{Fe}_2(\text{HPTP})(\text{OH})(\text{NO}_3)_2](\text{ClO}_4)_2$  complex correlates well with the higher Peroxide/Alcohol+Ketone and the higher Ketone/Alcohol ratio.

In the presence of ascorbic acid as radical scavenger, supplying the necessary electrons for transfer of free radicals into anions, a complete lack of oxidation of cyclohexane is apparent, pointing to the radical nature of the oxidation (table 4.3.3.).

*Table 4.3.2. Cyclohexane oxidation in absence and presence\* of ascorbic acid.*

	Conv.(%)	Selectivity (%)		
		chexanol	chexanone	cHHP
HPTP/Fe	7.4	31.2	60.3	3.4
HPTP/Fe*	+/- 0	+/- 0	+/- 0	+/- 0
HPTB/Fe	6.2	37.1	49.8	8.9
HPTB/Fe*	+/- 0	+/- 0	+/- 0	+/- 0

0.1mmol HPTP/B/Fe, 0.2 g cyclohexane (2.4 mmol), (\*) of 0.15 mmol ascorbic acid and 2 g  $\text{H}_2\text{O}_2$  (30% soln. in  $\text{H}_2\text{O}$ , 16 mmol) in 2 g MeCN, 24h at 293K.

#### **4.3.2 Organic Peroxide Decomposition**

Cyclohexylhydroperoxide (cHHP) can be completely decomposed by  $[\text{Fe}_2(\text{HPTP})(\mu\text{-OH})(\text{NO}_3)_2](\text{ClO}_4)_2$  and  $[\text{Fe}_2(\text{HPTB})(\mu\text{-OH})(\text{NO}_3)_2](\text{ClO}_4)_2$  complexes into a cyclohexanol/one mixture at 323 K, whereas in blank conditions only 8.3% conversion is seen (Table 4.3.3.). Lowering the temperature to 293 K lowers the activity of the pure complexes, and suppresses any blank activity. Upon heterogenisation a severe drop in deperoxidation activity is seen. The stabilisation of (organic) peroxide adducts by supported diiron complexes has been previously described. The  $[\text{Fe}_2(\text{HPTP})(\mu\text{-OH})]$  complex seems to stabilise peroxides better than the related  $[\text{Fe}_2(\text{HPTB})(\mu\text{-OH})]$  complexes. The latter show more intramolecular peroxide decomposition at low complex loading on MCM-41. This results in the observation of pure ketone as the intramolecular peroxide decomposition prevails.

Table 4.3.3. Conversion of cyclohexylhydroperoxyde (cCHHP).

Catalyst	cHHP (%)	CHol / CHone	CHHP (%)	CHol / CHone
	293 K	293 K	323 K	323 K
none	0.0	-	8.3	1.00
HPTP/Fe	28.4	0.35	100.0	-
HPTP/Fe 2% /MCM41	0.0	-	12.9	0.81
HPTB/Fe	23.5	0.41	100.0	-
HPTB/Fe 2% /MCM41	1.4	pure ketone	11.2	pure ketone

0.02 g HPTB/Fe or HPTP/Fe; 0.02 g HPTR/Fe/MMT or 0.05 g HPTR/Fe/HMS of catalyst in 5 g of oxidative mixture, 24 h at 293 K or 323 K.

The direct oxidation of cyclohexanol to cyclohexanone (Table 4.3.4.) in presence of  $[\text{Fe}_2(\text{HPTR})(\mu\text{-OH})]$  complexes is fast, in contrast with that of mononuclear iron complexes or in absence of catalyst. The  $[\text{Fe}_2(\text{HPTP})(\mu\text{-OH})]$  complexes are more active than the  $[\text{Fe}_2(\text{HPTB})(\mu\text{-OH})]$  complexes. Cyclohexanone is thus not only formed through CHHP decomposition, but also by a rapid consecutive cyclohexanol oxidation .

Table 4.3.4. Cyclohexanol oxidation.

	Cyclohexanol (%)	Cyclohexanone (%)
no catalyst	82	18
HPTP/Fe	30	70
HPTB/Fe	46	54

\* 0.1 mmol HPTPorB/Fe, 0.2 g cyclohexanol (98 % purity), 0.1 g chlorobenzene and 1.8 g *t*-butylhydroperoxide (16 mmol) in 2 g MeCN, 24 h at 293 K.

#### 4.3.3 Adamantane oxidation

For phase-separation reasons, the adamantane oxidation was studied in dichloromethane with an 80% solution of *t*BHP in di-*tert*-butylhydroperoxide. The  $\text{C}^{2\circ}/\text{C}^{3\circ}$ -ratio is known to depend on the oxygen concentration in solution if a radical process is involved. The catalytic activity, selectivity and  $\text{C}^{2\circ}/\text{C}^{3\circ}$  ratio are compared in Table 4.2.6. For the  $[\text{Fe}_2(\text{HPTP})(\mu\text{-OH})]$  complex the major oxidation product is adamantan-1-ol, for  $[\text{Fe}_2(\text{HPTP})(\mu\text{-OH})]$ -MCM41 the situation is comparable and the co-occurrence of small amounts of alkylperoxides that are stabilised on MCM41 are seen. For both pure

[Fe<sub>2</sub>(HPTB)(μ-OH)] complex and [Fe<sub>2</sub>(HPTB)(μ-OH)]-MCM the major oxidation products are the adamantan-1-ol and the adamantanyl-1-OO*t*Bu, as the latter compound is stabilised on this complex.

Table 4.3.5. Adamantane oxidation

	Conv.(%)	C <sup>2o</sup> /C <sup>3o</sup>
HPTB/Fe	7.5	0.14
HPTB/Fe 2% /MCM-41	3.2	0.20
HPTP/Fe	7	0.19
HPTP/Fe 2% /MCM-41	0.2	0.48

In Table 4.3.5. it is seen that both the [Fe<sub>2</sub>(HPTR)(μ-OH)] complexes as well as their MCM41 heterogenised counterparts have C<sup>2o</sup>/C<sup>3o</sup> ratios close to these of radical reactions. Regarding the C<sup>2o</sup>/C<sup>3o</sup> ratios these catalysts compare well with these of other complexes with established non-heme iron monooxygenase activity [69-70]. For the [Fe<sub>2</sub>(HPTB)(μ-OH)] complexes the chemistry is closer to the radical chemistry, whereas for the [Fe<sub>2</sub>(HPTP)(μ-OH)] complexes the chemistry is closer to the oxo-type chemistry. For secondary versus tertiary peroxy-radicals a much faster termination reaction is observed. Thus marked difference is observed in the absence and the presence of an α-hydrogen.

Table 4.3.6. Adamantane oxidation (Product selectivities, %).

%	1-ol	2-ol	2-one	1-Cl	2-Cl	1-ol-2-one	1-OO <i>t</i> Bu
HPTB/Fe	40.4	6.7	4.5	2.1	0.8	1.5	44.0
HPTB/Fe 2%/MCM	25.9	6.8	4.28	10.5	5.6	0	46.9
HPTP/Fe	67.3	13.2	9.8	9.8	0	2.0	4.5
HPTP/Fe 2%/MCM	44.8	16.5	16.1	22.6	0	0	0

0.05 mmol HPTR/Fe, 0.2 g adamantane (1.47 mmol) and 1.8 g *t*BHP (16 mmol) in 4 g CH<sub>2</sub>Cl<sub>2</sub>, for 24 h at 293 K.

The hetero-bimolecular tert-adamantylperoxy and tert-butylperoxy radicals will terminate more easily than the homo-bimolecular tertiary adamantylperoxy radical termination, thus leading to more tert-adamantyl-peroxy-tert-butyl adduct. Adamantyl-hydroperoxide easily disproportionates on the dinuclear iron site to adamantanol or -one mixtures. Fish *et al.* [72-75] have stated that for some binuclear MMO mimicks the reaction is free of free radical coupling

products. Que *et al.* [25-30] have demonstrated such free radical coupling products using the mononuclear Fe complexes with *t*BHP.

Tertiary peroxy radicals are known to rearrange via two main pathways [64], either via the binuclear recombination to give two RO<sup>•</sup> alkoxy radicals and oxygen or the direct dimerisation of the two alkylperoxy radicals to the ROOR dimer and oxygen. The main pathways starting from the RO<sup>•</sup> alkoxy radicals are the binuclear recombination to the ROOR dimer. The *tert*-adamantylperoxy-*tert*-butyl adducts observed in the adamantane oxidation clearly indicate the co-occurrence of radicalar reactions.

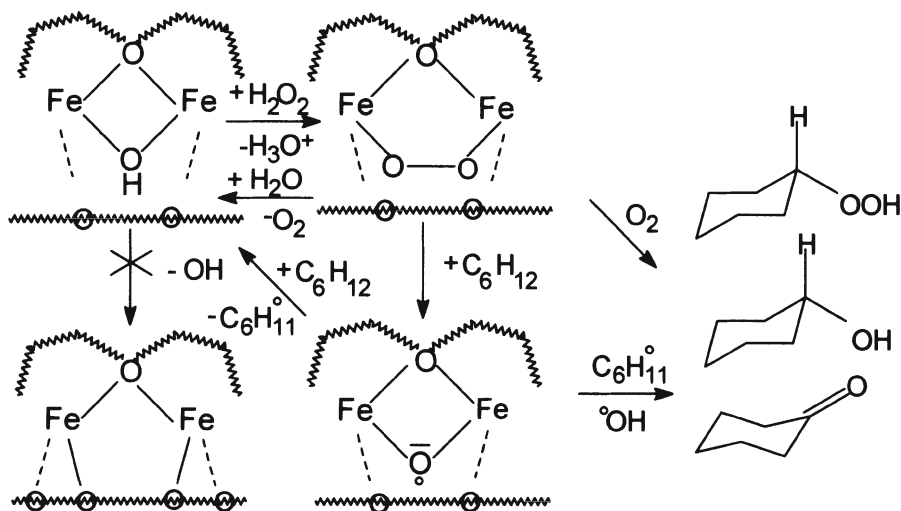


Figure 4.4.  $[\text{Fe}_2(\text{HPTR})(\mu\text{-OH})]^{2+}$  complexes interacting with peroxides e.g. hydrogen peroxide or *t*butyl hydroperoxide are thought to react via a  $\mu$ -peroxo intermediate that can either generate oxygen (catalase activity) or react with alkanes (mono-oxygenation).

(Reprinted from Ref. [55], p. 7-10, with kind permission of Elsevier Science - NL, Sara Burgerhartstraat 25, 1055 KV Amsterdam, The Netherlands)

## 5. Conclusion

The choice of the transition metal ion largely determines the spectroscopic properties and catalytic possibilities of the supramolecular systems. The coordinative stability of complexes of iron is very high. The higher oxidation states are more substitution inert than the lower ones. The catalytic implications of this choice are considerable, either two electron changes are seen as for oxo-chemistry with iron. One electron changes in radical or peroxo- chemistry are also seen for iron.

The choice of the ligand to coordinate the TMI in the lattice affects the stability of the resulting complexes and the relative coordination of these with the lattice. Lattices in general coordinate in a polydentate fashion. The ligands chosen in this work coordinate in a bi-, tetra- or hepta-dentate fashion. The strength of complexation of the ligand, described by their position in the spectro-chemical series, affects the degree of iron complexation and thus its competition with lattice coordination. Aromatic ligands were selected due to their stability towards oxidation, diimines such as 2,2'-bipyridine, 2,6,2',6'-bipyrimidine and 1,10-phenantroline are the most stable and allow a wide variety of coordinative geometries, depending on the choice of the TMI complexed within the zeolite lattice. For catalytic purposes coordinatively unsaturated environments, with bis complexation is preferred.

The deprotonation of amides and alcohol groups on aromatic ligands in the presence of iron affects the complex coordination geometry. For the tetradentate *N,N'*-bis-(2-pyridinecarboxamide)-1,2-alkane ligand deprotonation is complete for iron complexes. The stoichiometry of ligand coordination is influenced by the crystal field stabilisation energy, which is extremely high for iron. These effects of coordination are observed in Mössbauer and diffuse reflectance spectroscopy in the different complexes.

The heptapodate *N,N,N',N'*-tetrakis(2-*R*-methyl)-2-hydroxy-1,3-diaminopropane ligands with *R* = benzimidazolyl (HPTB) and *R* = pyridyl (HPTP), allow the coordination of two iron molecules to generate a dinuclear reaction center that can selectively bind peroxides and oxygen in case of Fe<sup>III</sup> and Fe<sup>II</sup> coordination, respectively.  $[\text{Fe}_2(\text{HPTP})(\mu\text{-OH})]^{4+}$  and  $[\text{Fe}_2(\text{HPTB})(\mu\text{-OH})]^{4+}$  complex cores show no accessibility to 12 MR pores of faujasite zeolites and need larger mesoporous supports for their inclusion. They can be retained in the mesoporous oxides such as MCM-41. The difference with the salts  $[\text{Fe}_2(\text{HPTP})(\mu\text{-OH})(\text{NO}_3)_2](\text{ClO}_4)_2$  and  $[\text{Fe}_2(\text{HPTB})(\mu\text{-OH})(\text{NO}_3)_2](\text{NO}_3)_2$  are the changes in the coordination geometry due to substitution or removal of the charge compensating anions, the variation in the extent of H-bridging of hydroxo- or oxo- groups of complexes to support oxo- or hydroxo-groups, the stabilisation of the complex guest by a better fit in the mesoporous oxide support host, the selective binding of peroxides on the diferric sites and the stable association of organic peroxides on supports and the stabilisation of the complexes against self-oxidation.

The lattice topology, the degree of hydration, the cation and TMI loading, the temperature, the degree of TMI accessibility and the choice of the ligand all affect the extent of complex formation. The compositional, steric and electrostatic properties of the host-lattice affect the geometry, oxidation state (to which the concept of nuclearity is intimately linked) and less obviously also the spin state of the TMI-guest that is accommodated. The latter effects of



cryptation as a direct means to change the spin states of TMI's in such hosts remains a challenge.

The cyclohexane and adamantane oxidation and the cyclohexylhydroperoxide deperoxidation chemistry are described and compared for all these systems. Mechanistic aspects on alkane activation may vary from radicalar Fenton chemistry to "Groves"-type oxo catalysis. Purely radicalar  $\text{Fe}^{\text{III}}\text{-OOH}$  decomposition is encountered for the bidentate diimine complexes, whereas a combination of radicalar and "oxo"-type  $\text{Fe}^{\text{IV}}=\text{O}$  species are active in  $\text{N,N}'\text{-bis-(2-pyridine-carboxamide)-1,2-alkane}$  complexes. Within zeolites in general the radicalar chemistry is defavored. Still another intermediate is seen for the  $[\text{Fe}_2(\text{HPTP})(\mu\text{-OH})]^{4+}$  methane monooxygenase mimics for which  $\text{Fe-O}^\circ\text{-Fe}$  radicals are formed out of an  $\text{Fe-OO-Fe}$  intermediate, whereas singlet oxygen can also be directly liberated from the active site, and be responsible for the observed product distribution. The radicalar propagation and termination chemistry in combination with the steric nature of the active site determine the complex chemistry observed. The intermolecular reactions are sterically hindered in the NaY and MCM-41 supported reactions as a tight fit of the host-guest system will favour intramolecular deperoxidation at the active site. Catalytic results after appropriate heterogenisation more closely match this observed for the enzymatic activity.

## Acknowledgments

The authors acknowledge IUAP-PAI sponsoring from the Belgian Federal Government. PPKG and AMVB are grateful to the Belgian National Fund for Scientific Research (NFWO) for a research grant as post-doctoral and doctoral research assistant respectively.

## References

1. Dolphin, D.(Ed.) *Porphyrins* 1978-1979, Academic Press, New York.
2. Momenteau, M., Reed, C.A., (1994), *Chem. Rev.*, 94, 659.
3. Lovenberg, W.(Ed.) *Iron-Sulfur Proteins*, (1973-1977), Academic Press, New York.
4. Reem, R.C., Solomon, E.I., *J. Am. Chem. Soc.*, (1987), 109, 1216.
5. Stenkamp, R.E., (1994), *Chem. Rev.*, 94, 715.
6. Stassinopoulos, A., Cardonna, J.P., (1990), *J. Am. Chem. Soc.*, 112, 7071.
7. Stassinopoulos, A., Schulte, G., Papaefthymiou, G.C., Cardonna, J.P., (1991), *J. Am. Chem. Soc.*, 113, 8686.



8. Sturgeon, B.E., Burdi, D., Chen, S., Huynh, B.H., Edmondson, D.E., Stubbe, J., Hoffman, B.M., (1996), *J. Am. Chem. Soc.*, 118, 7551.
9. Antaniatis, B.C., Aisen, P., (1983), *Adv.Inorg.Biochem.*, 5, 111.
10. Theil, E.C., (1987), *Annu.Rev.Biochem.*, 56, 289.
11. Murray, K.S., (1974), *Coord.Chem.Rev.*, 12, 1.
12. Lippard, S.J., (1988), *Angew.Chem.Int.Ed.Engl.*, 27, 344.
13. Armstrong, W.H., Lippard, S.J., (1983), *J.Am.Chem.Soc.*, 105, 4837.
14. Armstrong, W.H., Lippard, S.J., (1984), *J.Am.Chem.Soc.*, 106, 4632.
15. Armstrong, W.H., Lippard, S.J., (1985), *Inorg.Chem.*, 24, 981.
16. Armstrong, W.H., Spool, A., Papaefthymiou, G.C, Frankel, R.B., Lippard, S.J., *J.Am.Chem.Soc.*, 1984, 106, 3653.
17. Feng, X., Bott, S.G., Lippard, S.J., (1989), *J.Am.Chem.Soc.*, 111, 8046.
18. Rozenzweig, A.C., Frederick, C.A., Lippard, S.J., Nordlund, P., (1993), *Nature*, 366, 537.
19. Liu, K.E., Wang, D., Huynh, B.H., Edmondson, D.E., Salofoglou, A., Lippard, S.J., (1994), *J.Am.Chem.Soc.*, 116, 7465.
20. Liu, K.E., Valentine, A.M., Qiu, D., Edmondson, D.E., Appelman, E.H., Spiro, T.G., Lippard, S.J., (1995), *J.Am.Chem.Soc.*, 117, 4997.
21. Kurtz, D. M. jr., Shriver, D.F., Klotz, I. M., (1977), *Coord. Chem. Rev.*, 24, 145.
22. Klotz, I. M., Kurtz, D. M., (1984), *Acc.Chem. Res.*, 17, 16.
23. Kurtz, D. M., (1990), *Chem. Rev.*, 90, 585.
24. Klotz, I. M., Kurtz, D. M., (1994), *Chem. Rev.*, 94, 567.
25. Que, jr., L., (1983), *Coord. Chem. Rev.*, 50, 73.
26. Brennan, B. A., Chen, Q., Garcia, C.J., True, A.E., O'Connor, C.J., Que Jr., L., (1991), *Inorg.Chem.*, 30, 1937.
27. Leising, R.A., Brennan, B.A., Que, Jr., L., Fox, B.G., Münck, E., (1991), *J. Am. Chem.Soc.*, 113, 3988.
28. Dong, Y., Fujii, H., Hendrich, M.P., Leising, R.A., Pan, G., Randall, C.R., Wilkinson, E.C., Zang, Y., Que Jr., L., Fox, B.G., Kauffmann, K., Münck, E., (1995), *J.Am.Chem.Soc.*, 117, 2778.
29. Dong, Y., S.Yan, V.G.Young Jr., L.Que Jr., (1996), *Angew.Chem.*, 108, 6, 674.
30. Shu, L., Nesheim, J.C., Kaufmann, K., Munck, E., Lipscomb, J.E., Que, L., (1997), *Science*, 275, 515.
31. Beck, J.S., Vartuli, J.C., Roth, W.J., Leonowicz, M.E., Kresge, C.T., Schmitt, K.D., Chu, C.T.W., Olson, D.H., Sheppard, E.W., McCullen, S.B., Higgins, J.B. and Schlenker, J.L., (1992), *J. Am. Chem. Soc.*, 114, 10834.
32. Briggs, D., Sheah, M.P., (1983), *Practical Surface Analysis by Auger and X-ray photo-electron spectroscopy*, Wiley, London.

33. Gütlich, P., Link, R., Trautwein, A., "Mössbauer spectroscopy and transition metal chemistry", *Inorg.Chem.Concepts*, M.Becke, et al., Series eds., 3, 1978, Springer-Verlag, Berlin.
34. McWhinnie, W.R., Miller, J.D., (1963), *J.Inorg.Nucl.Chem*, 26, 15.
35. Goedken, V.L., Merrel, P.H., Bush, D.H., (1972), *J.Am.Chem.Soc.*, 94, 3397.
36. Leung, W.H., Ma, J.X., Yam, V., Che, C., Poon, C.K., (1991), *J.Chem.Soc., Dalton Trans.*, 1071.
37. Chapman, R.L., Vagg, R.S., (1979), *Inorganica Chimica Acta*, 33, 227.
38. Barnes, D.J., Chapman, R.L., Stephens, F., Vagg, R.S., (1981), *Inorganica Chimica Acta*, 51, 155.
39. Mulqi, M., Stephens, F.S., Vagg, R.S., (1981), *Inorganica Chimica Acta*, 52, 73.
40. Toftlund, H., (1981), *Acta Chem. Scand.*, 35A, 575.
41. Nishida, Y., Nasu, M., Akamatsu, T., (1992), *J.Chem.Soc., Chem.Comm.*, 93.
42. Morice, J.A., Rees, L.V.C., (1967), *Trans. Faraday Soc.*, 64, 1388.
43. Quayle, W., Peeters, G., De Roy, G., Vansant, E., Lunsford, J.H., (1982), *Inorg.Chem.*, 21, 2226.
44. Herron, N., Stucky, G.D., Tolman, C.A., (1986), *J.Chem.Soc., Chem.Comm.*, 1521.
45. Balkus, K.J., Kowalak, S., Ly, K.T., Hargis, D.C., (1991), in "Zeolite Chemistry and Catalysis", Jacobs, P.A. et al., Eds., Elsevier, Amsterdam, 93.
46. Knops-Gerrits, P.P., De Vos, D., Thibault-Starzyk, F., Jacobs, P.A., (1994), *Nature*, 369, 543.
47. Knops-Gerrits, P.P., De Schryver, F., Van Mingroot, H., Van der Auweraer, M., Jacobs, P.A., (1996), *Chem.Eur.J.*, 2, 592.
48. Knops-Gerrits, P.P., Toufar, H., Jacobs, P.A., (1996), *Stud.Surf.sci.Catal.*, 105, 1109.
49. Knops-Gerrits, P.P., L'Abbé, M., Jacobs, P.A., (1997), *Stud.Surf.Sci.Catal.*, in press.
50. Knops-Gerrits, P.P., De Vos, D., Jacobs, P.A., *J.Molec.Catal*, 117 (1-3), 1997, 57.
51. Battioni, P., Cardin, E., Louloudi, M., Schöllhorn, B., Spyroulias, G.A., Mansuy, D., Traylor, T.G., (1996), *J.Chem.Soc., Chem.Comm.*, 2037.
52. Knops-Gerrits, P.P., Van Bavel, A.-M., Langouche, G., L'Abbé, M., Jacobs, P.A., ECME 96, *Third European Conference on Molecular Electronics*, 1996, Leuven.
53. Knops-Gerrits, P.P., L'Abbé, M., Leung, W.H., Van Bavel, A.-M., Langouche, G., Bruynseraede, Y., Jacobs, P.A., *Stud.Surf.Sci.Catal.*, 101, 1996, 811-820.

54. Weiss, A., Dick, S., (1994), *Zeitschrift fur Naturforschung*, 49b, 1051.
55. Knops-Gerrits, P.P., Dick, S., Weiss, A., Genet, M., Rouxhet, P., Li, X.Y., Jacobs, P.A., *Stud.Surf.Sci.Catal.*, in press 1997.
56. Lyons, J.E., Ellis, P.E., Durante, V.A., in "*Struct.-Act. and Sel. Relat. in Het. Catal.*" , Grasselli, R.K., Sleight, A.W., Eds., Elsevier, Amsterdam, 99, 1991.
57. Herron, N., Tolman, C.A., (1987), *J.Am.Chem.Soc.*, 109, 2837.
58. Merz, J.H., Waters, W.A., (1947), *Discuss. Faraday Soc.*, 2, 179 ; Waters, W.A., (1959), "*Vistas in free radical chemistry*", Int.Ser.Monographs Org.Chem., Barton, D.H.R., Doering, W., Ser.Eds., Pergamon Press,.
59. Barton, D.H.R., Csuhai, E., Doller, D., Belavoine, G., (1990), *J.Chem.Soc., Chem.Comm.*, 1787;
60. Barton, D.H.R., Doller, D., (1992), *Acc.Chem.Res.*, 25, 504.
61. Sheldon, R.A., Kochi, J.K. (1981) *Metal-Catalyzed Oxidations of Organic Compounds*, Academic Press., New York;
62. Ingold, K.U., (1961), *J.Chem.Soc.*, 563.
63. Traylor, T.G., Russell, C.A., (1965), *J.Am.Chem.Soc.*, 110,
64. Beck, W., Schruierer, E., (1962), *Ber.Deutch.Chem.Ges.*, 95, 3048.
65. Sheldon, R.A., (1997), NATO ASI Advances and Challenges in the Catalytic Activation and Functionalisation of Light Alkanes, this volume.
66. Sobrowiak, A., Tung, H.C., Sawyer,D.T., (1992), *Progr.Inorg.Chem.*, 40, 291.
67. Groves, J.T., McClusky, G.A., (1976), *J.Am.Chem.Soc.*, 98, 859.
68. Hill, C.L., "*Activation and Functionalisation of Alkanes*", Wiley, New York, (1989), Chapter X : Tolman, C.A., Druliner,J.D., Nappa, M.J., Herron, N., p.303.
69. Steinmann, A.A., (1992), *Mendeleev Commun.*, 155.
70. Gritsenko, O.N., Nesterenko, G.N., Steinmann, A.A., (1995), *Russ.Chem.Bull.*, N12.
71. Kitajima, N., Fukui, H., Moro-oka, Y., (1988), *J.Chem.Soc., Chem.Comm.*, 485.
72. Vincent, J.B., Huffman J.C., Christou, G., Li, Q, Nanny, M.A., Hendrickson, D.N., Oberhausen, K.J., Fong, R.H., Fish, R.H., (1988), *J.Am.Chem.Soc.*, 110, 6898.
73. Fish, R.H., Konings, M.S., Oberhausen, K.J., Fong, R.H., Yu, W.M., Christou, G., Vincent, J.B., Coggin, D.K., Buchanan, R.M., (1991), *Inorg.Chem.*, 30, 15, 3002.
74. Fish, R.H., Oberhausen, K.J., Chen, S., Richardson, J.F., Pierce, W., Buchanan, R.M., (1993), *Catal.Lett.*, 110, 6898.
75. Rabion, A., Buchanan, R.M., Seris, J.L., Fish, R.H., (1997), *J.Mol.Catal.*, 116, 43.

# BIOCATALYTIC, BIOMIMETIC AND SUPRABIOTIC OXIDATION OF ALKANES

R.A. SHELDON

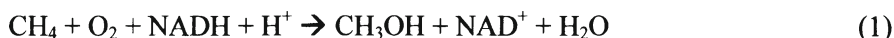
*Laboratory for Organic Chemistry and Catalysis  
Delft University of Technology, Julianalaan 136  
2628 BL Delft, The Netherlands*

## 1. Introduction

The controlled partial oxidation of hydrocarbons (alkanes, alkenes and aromatics) is the single most important technology for converting petrochemical feedstocks to industrial organic chemicals [1-4]. For economic reasons, these processes predominantly involve the use of molecular oxygen (dioxygen) as the primary oxidant. The success of these processes depends largely on the use of transition metal catalysts to promote both the rate of reaction and the selectivity to partial oxidation products. Both gas phase and liquid phase oxidations, employing heterogeneous and homogeneous catalysts, respectively, are practical industrially (Table 1). A cursory examination of Table 1 reveals that alkane oxidations, generally speaking, tend to give lower selectivities than alkenes or alkylaromatics. However, there is a marked trend towards substitution, where possible, of olefin and aromatic feedstocks by cheaper alkanes. Particularly desirable targets include the use of propane as the feedstock for acrylonitrile and acrylic acid, ethane for acetic acid and n-pentane for phthalic anhydride. The direct conversion of methane to methanol, rather than via synthesis gas, is also a highly attractive goal. Hence, there is considerable industrial interest in developing more selective methods for the oxidation of (lower) alkanes with dioxygen.

A possible source of inspiration for developing selective catalysts for alkane oxidation is the wide variety of biological systems that mediate the selective oxidation of alkanes, at ambient temperature and pressure, by employing metalloenzymes, appropriately known as oxygenases. For example, the methane monooxygenase (MMO) found in methanotrophic bacteria mediates the oxidation of methane, thereby circumventing the atmospheric egress of nearly 1 billion tons of this greenhouse gas annually [5]. The first step involves the

selective oxidation of the unreactive C-H bond of methane. Two reducing equivalents of a nicotinamide adenine dinucleotide (NADH) cofactor are utilized to cleave the O-O bond of dioxygen, one oxygen atom being incorporated into the substrate and the other affording water (Reaction 1).



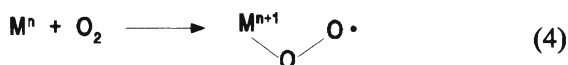
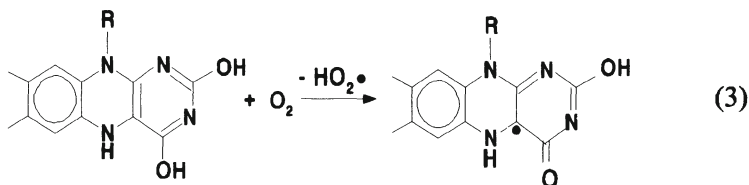
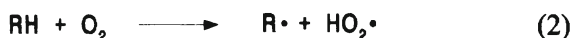
NAD = nicotine adenine dinucleotide

*Table 1. Catalytic Oxidation Processes.*

Product	Raw Materials	Catalyst	Conv. (%)	Sel. (%)
<b>Gas Phase</b>				
Formaldehyde	Methanol/air	Ag	95	98
		MoO <sub>3</sub> /Fe <sub>2</sub> O <sub>3</sub>	95 - 99	91 - 94
Ethylene oxide	Ethylene/oxygen	Ag	15	85
Acrolein	Propylene/air	MoO <sub>3</sub> /Bi <sub>2</sub> O <sub>3</sub>	>90	80 - 85
Acrylic Acid	Propylene/air	Mixed oxide Mo	>95	90 - 95
Acrylonitrile	Propylene/NH <sub>3</sub> /air	MoO <sub>3</sub> /Bi <sub>2</sub> O <sub>3</sub>	>99	75 - 80
Methacrolein	Isobutene/air	Mixed oxide Mo	>97	85 - 90
Methacrylic acid	Methacrolein/air	Mixed oxide Mo	70 - 75	80 - 90
Maleic anhydride	Benzene/air	V <sub>2</sub> O <sub>5</sub>	98	75
	n-Butane/air	V <sub>2</sub> O <sub>5</sub> /P <sub>2</sub> O <sub>5</sub>	75 - 90	67 - 72
Phthalic anhydride	o-Xylene/air	V <sub>2</sub> O <sub>5</sub> /P <sub>2</sub> O <sub>5</sub>	99	84
<b>Liquid Phase</b>				
Propylene Oxide	Propylene/RO <sub>2</sub> H	Mo <sup>IV</sup> or Ti <sup>IV</sup> /SiO <sub>2</sub>	ca. 10	ca. 95
Acetic acid	n-Butane/air	Co/Mn	10 - 20	ca. 40
		Co/Mn	100	95 - 97
Acetaldehyde	Ethylene/air	Pd/Cu	>95	>95
Cyclohexanone/ol	Cyclohexane/air	Co	<10	80 - 85
Terephthalic acid	p-Xylene/air	Co/Mn/Br	>95	>95
Benzoic acid	Toluene/air	Co	ca. 30	ca. 90
Phenol	Cumene/air	none	30-50	85 - 95
	Benzoic acid/H <sub>2</sub> O	Cu	>90	85 - 90

## 2. Structure and Reactivity of Dioxygen

The existence of life in an aerobic environment depends on the low kinetic reactivity of dioxygen in its reactions with organic compounds which are highly exothermic. The origin of this low reactivity is the triplet ground state of dioxygen which means that reactions with organic molecules with singlet ground states are spin forbidden. This barrier can be circumvented by exciting the  $O_2$  molecule to one of its singlet states or via a free radical pathway. Thus, reaction of a singlet molecule with  $^3O_2$  to afford two free radicals (doublets) is spin-allowed (Reaction 2). However, this reaction is highly endothermic (up to  $50 \text{ kcal.mol}^{-1}$ ) and is observed at moderate temperatures only with very reactive substrates, that afford resonance stabilized radicals (Reaction 3). Nature takes advantage of this property of reduced flavins in the activation of  $^3O_2$  by flavin-dependent oxygenases (see later). Alternatively, this spin conservation obstacle can be overcome by combining  $^3O_2$  with a paramagnetic transition metal ion (Reaction 4).



The half-filled antibonding molecular orbitals of  $^3O_2$  can accommodate two extra electrons. Addition of one electron affords the superoxide anion,  $O_2^{\cdot-}$ , and two-electron reduction gives the peroxide ion,  $O_2^{2-}$ . Hence, reaction of  $^3O_2$  with a transition metal ion leads via one-electron transfer to the superoxo metal complex. This can lead to the subsequent formation of a variety of active oxygen species (Figure 1) that may play a role in (bio)catalytic oxidations involving metal ions.

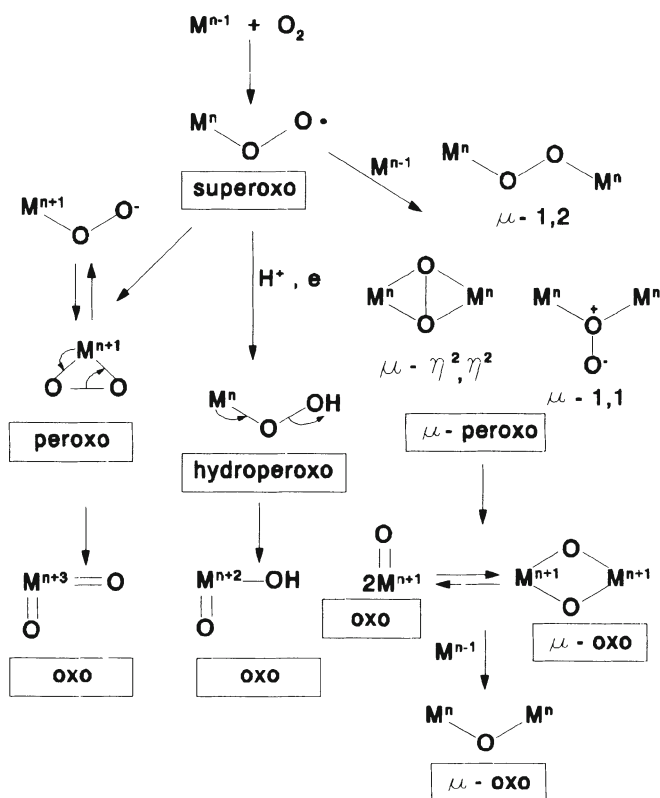


*Figure 1. Metal-oxygen species.*

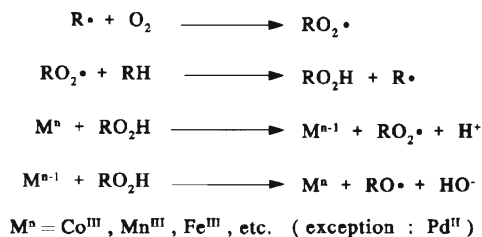
### 3. Oxidation Mechanisms

Liquid phase oxidations with dioxygen generally involve a free radical chain autoxidation mechanism (Figure 2). Variable valence transition metal ions, e.g. Co and Mn, catalyze this process by generating chain-initiating radicals, under mild conditions, in one-electron transfer reactions with traces of RO<sub>2</sub>H or, in some cases, with the substrate, RH. Hence, most liquid phase processes involve catalysis by Co and/or Mn salts (see Table 1). Gas phase oxidations, in contrast, generally involve the so-called Mars-van Krevelen mechanism [6] in which the substrate undergoes oxidation by an oxometal species ( $V^V = O$  or  $Mo^{VI} = O$ ) followed by regeneration with dioxygen. The palladium catalyzed oxidation of olefins in the liquid phase (Wacker process) involves oxidation of the substrate by Pd<sup>II</sup> followed by copper-promoted reoxidation of Pd<sup>0</sup> with O<sub>2</sub> and can be viewed as a special case of the Mars-van Krevelen mechanism. How do we account for the marked difference between gas and liquid phase oxidations? In

the liquid phase with relatively high concentrations of RH autoxidation chain lengths are long and it is, hence, difficult to compete with the ubiquitous free radical autoxidation. In the gas phase, on the other hand, concentrations of RH are much lower and chain processes are less favorable. Free radical autoxidation is a largely indiscriminate process giving high selectivities only with molecules containing one reactive position and giving a stable product, e.g. toluene to benzoic acid.

There is a great need, therefore, for catalysts that are able to compete with free radical chain autoxidation in the liquid phase, i.e. a Mars-van Krevelen mechanism in the liquid phase. As we shall see later oxygenases appear to have this capability of simulating gas phase conditions at ambient temperature in the liquid phase.

#### LIQUID PHASE (free radical chain autoxidation)



#### GAS PHASE (Mars van Krevelen Mechanism)

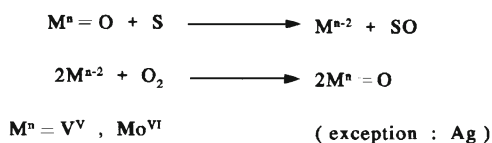


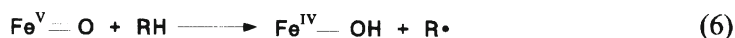
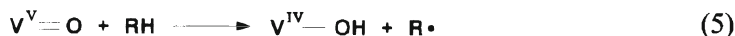
Figure 2. Mechanisms of catalytic oxidations with O<sub>2</sub>.

## 4. Substrate Activation vs Oxygen Activation

Whether a Mars-van Krevelen type mechanism is referred to, in the case of an alkane substrate, as alkane activation or oxygen activation appears to depend on which step is the initial one. In the oxidation of n-butane, in the presence of a vanadium phosphate catalyst, the initial, rate-limiting step appears to be [7] hydrogen abstraction by oxovanadium(V) (Reaction 5) and this is generally referred to as alkane activation. Similarly, alkane oxidations mediated by iron-dependent monooxygenases are generally believed (see later) to involve hydrogen abstraction by a formally oxoiron(V) species (Reaction 6) as the key step. In this case, however, the catalyst is added as an iron(III) complex (i.e.

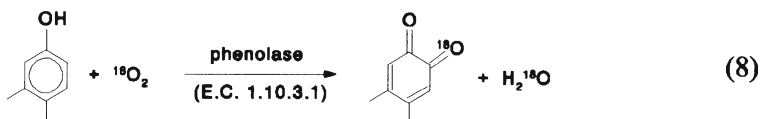
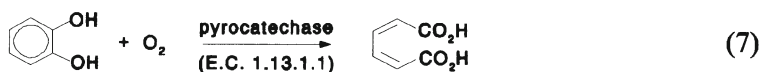


resting enzyme) and reaction (6) is not rate-limiting. Hence, the conversion is considered to be an example of dioxygen activation.



## 5. Oxygenases: Discovery and Classification

Prior to 1955 it was generally believed that the sole function of dioxygen in enzymatic oxidations was as an electron acceptor, forming water or hydrogen peroxide. In that year Hayaishi [8] and Mason [9] independently demonstrated the incorporation of dioxygen into the organic substrate in reactions (7) and (8), respectively.



Enzymes that incorporate oxygen atoms from dioxygen in such reactions were designated as oxygenases by Hayaishi [10]. It is now recognized that oxygenases are widely distributed in plants, animals and microorganisms where they play essential metabolic roles.

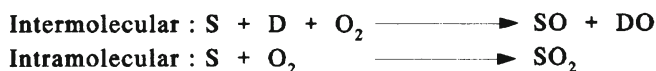
Oxygenases are further classified into monooxygenases and dioxygenases, depending on whether one or both oxygen atoms of dioxygen are incorporated into the substrate (Figure 3).

Monooxygenases require two reducing equivalents (two electrons and two protons) to reduce the second oxygen atom to water. These can come from an external reducing agent (the cofactor) or the substrate itself and are designated external and internal monooxygenases, respectively. Similarly, dioxygenases are either intra- or intermolecular depending on whether both oxygen atoms are incorporated into the substrate or one into the substrate and the other into an additional cofactor. It should be emphasized that the terms mono- and dioxygenase describe only the stoichiometry of the transformation and say nothing about its mechanism.

### Monooxygenase



### Dioxygenase



$S, SH_2$  = substrate ;  $D, DH_2$  = cofactor

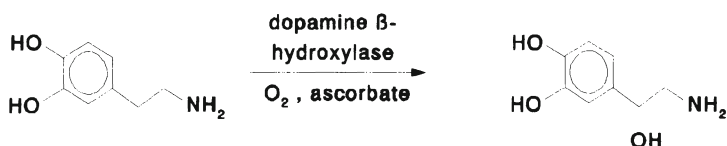
*Figure 3. Mono- and dioxygenases.*

Oxygenases can also be divided into four general classes on the basis of the cofactor or prosthetic group that is involved: enzymes that utilize flavin, copper, heme-iron and non-heme-iron centers. Flavin dependent monooxygenases catalyze the oxidation of relatively reactive substrates, e.g. the hydroxylation of 4-hydroxybenzoate to 3,4-dihydroxybenzoate, by involving a flavin hydroperoxide as the active oxidant. They are not important in the context of alkane oxidation and will not be considered further. Similarly, copper-dependent mono- and dioxygenases mediate the oxidation of electron-rich aromatics (Figure 4). There is one possible exception: a methane monooxygenase which is thought to contain a trinuclear copper cluster in the active site [11].

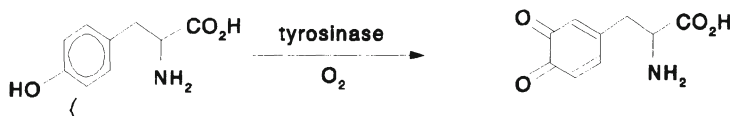
In the context of oxidation of simple alkanes iron-dependent oxygenases are by far the most important. They can be broadly divided into three types depending on the nature of the iron-containing prosthetic group: heme, non-heme mononuclear, and non-heme binuclear iron. The best known and most well-studied are the heme-dependent oxygenases, typified by cytochrome P450 [12-14]. More recently attention has been focused on binuclear non-heme oxygenases [15-17]. This interest stems from the fact that one example of this group, methane monooxygenase (MMO) [18-20] is able to mediate the oxidation of a broad range of substrates, including methane, at ambient temperature. Similarly, interest in mononuclear non-heme oxygenases is rapidly growing [16, 17, 21, 22] because of their amazingly diverse catalytic properties, from lipid oxidation to penicillin biosynthesis. A key requirement for understanding the mechanism of dioxygen and/or substrate activation in these systems is an intricate knowledge of the three dimensional structure of the active site. Hence, the availability of high resolution X-ray structures of several

of these enzymes (see Figure 5 for examples) represents a significant advance in this respect.

### External monooxygenase (binuclear Cu)



### Internal monooxygenase (binuclear Cu)



### Intramolecular dioxygenase (mononuclear Cu)

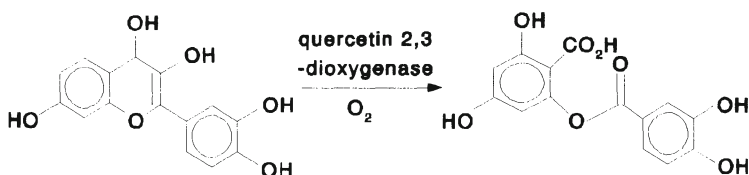


*Figure 4.* Copper dependent oxygenases.

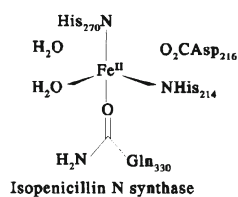
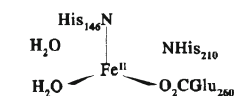
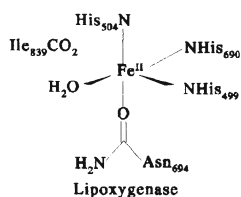
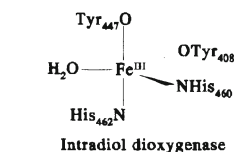
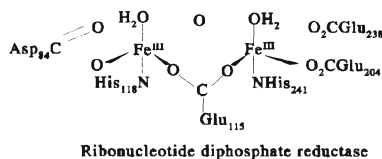
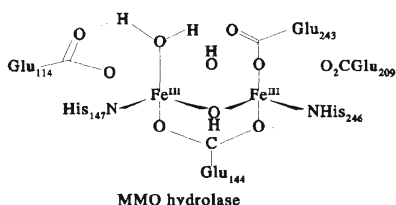
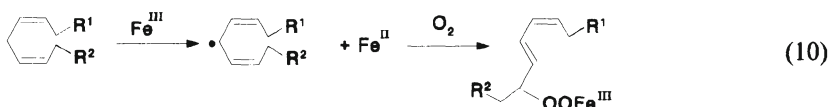
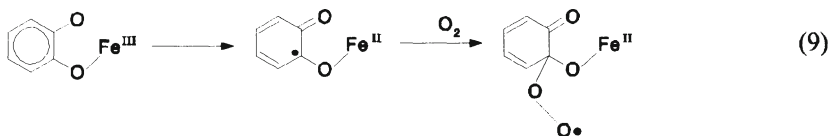
**Mononuclear non-heme****Binuclear non-heme**

Figure 5. Active site structures of iron-dependent oxygenases.

## 6. Iron-dependent Oxygenases: Mechanisms of Dioxygen Activation

As noted above oxidations mediated by (iron-dependent) oxygenases generally involve activation of dioxygen rather than the substrate. Substrate activation is observed only with very reactive molecules which undergo facile one electron oxidation, e.g. catechols (intradiol dioxygenase) and linoleic acid (lipoxygenase) [16, 22]. In both cases the key step is one-electron oxidation of the bound substrate by  $\text{Fe(III)}$  reactions (9 and 10). Interestingly, the resting state of lipoxygenase contains  $\text{Fe(II)}$ , which means that the reaction is initiated by reaction with traces of  $\text{RO}_2\text{H}$  derived from classical free radical autoxidation of linoleic acid.

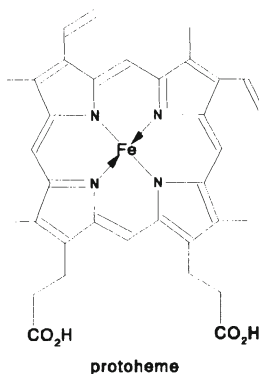


With less reactive substrates a stronger oxidant than Fe(III) is required and in many cases high valent oxoiron species have been invoked as the active oxidant. In heme-containing oxygenases the high oxidation state of iron is stabilized by delocalization of electrons from the porphyrin ring which forms a radical cation. In non-heme oxygenases, a second iron centre or a tyrosine residue in the protein assumes the stabilizing role of the porphyrin.

## 6.1 CYTOCHROME P450

Cytochrome P450-dependent monooxygenases are widely distributed in living organisms where they catalyze highly regio- and stereoselective oxidations of endogenous molecules, e.g. steroids and fatty acids, involved in metabolic processes. A second role of cytochrome P450 enzymes is to mediate the oxidation, and subsequent elimination from the organism, of exogenous compounds, e.g. drugs, pesticides, etc. In this case they are generally less substrate specific and less regio- and stereoselective. More than 450 different cytochrome P450 enzymes are known and more than 100 of these have been cloned and sequenced [12, 13].

All of these enzymes contain iron protoporphyrin IX (protoheme) as the prosthetic group:



In their resting iron(III) state they exist in two forms which are in equilibrium: a hexacoordinate low-spin iron complex with two axial ligands - cysteinate and an OH-containing ligand ( $\text{H}_2\text{O}$  or an alcohol moiety of a protein amino acid) - and a pentacoordinate high-spin iron complex with cysteinate as the sole axial ligand. Binding of the substrate in the hydrophobic active site, close to the heme, leads to a shift of the equilibrium towards the pentacoordinate complex (Figure 6). The latter is reduced by the cofactor to give a high-spin iron(II) complex which has an accessible coordination site for binding dioxygen, leading to a relatively stable low-spin complex which may be described as  $\text{Fe(II)O}_2$  or  $\text{Fe(III)-O-O}\cdot$ . In either resonance structure the complex

is diamagnetic; there are no unpaired electrons in  $\text{Fe(II)O}_2$  and in  $\text{Fe(III)-O}_2\cdot$  the two unpaired electrons are spin-coupled. The active oxidant in the P450 catalytic cycle is derived from one electron reduction of the superoxo complex. This active species is so short-lived that it has not been detected by any spectroscopic technique. It is generally believed to be a high-valent oxoiron species, formed by heterolysis of a  $\text{Fe(III)O-OH}$  complex, which is facilitated by the electron-donating cysteinyl axial ligand. Formally, it is an oxoiron(V) species but it is usually represented as oxoiron(IV) coordinated to a porphyrin radical cation, analogous to compound (I) of peroxidases.

Alternatively, the oxoiron oxidant can be formed directly from the resting iron(III) state by reaction with a single oxygen donor such as  $\text{H}_2\text{O}_2$ ,  $\text{RO}_2\text{H}$ ,  $\text{NaOCl}$ , etc. (the so-called peroxide shunt), thus circumventing the need for a stoichiometric cofactor.

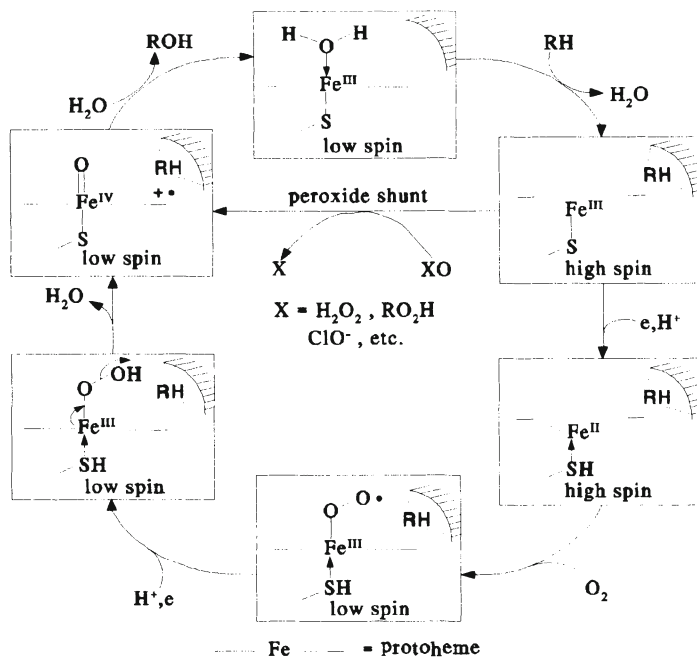


Figure 6. Catalytic Cycle of cytochrome P450.

The active oxidant reacts with most organic compounds, e.g. hydroxylation of aliphatic and aromatic C-H bonds and epoxidations of double bonds. The precise mechanism of hydroxylation of aliphatic C-H bonds is still controversial [12]. The most generally accepted mechanism, so-called oxygen rebound, involves initial hydrogen abstraction by the oxoiron species followed by rapid

transfer of the OH ligand to the radical, R· (Figure 7). On the other hand, evidence has also been presented in favour of carbocation or alkyliron intermediates [12].

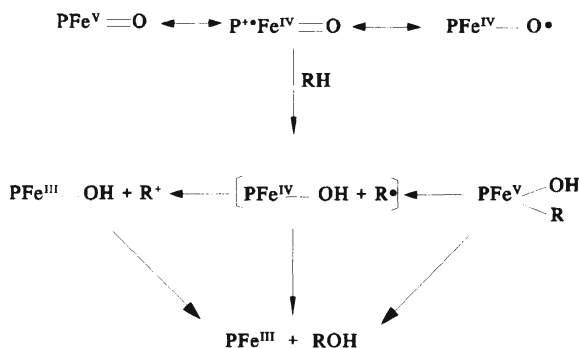
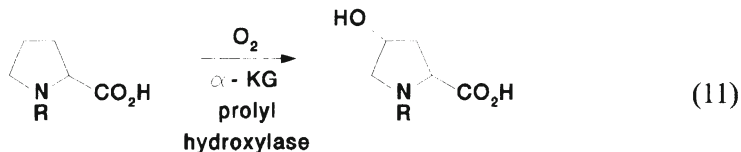


Figure 7. Mechanism of Alkane hydroxylation by cytochrome P450.

The relative reactivities of C-H bonds towards cytochrome P450 follow that expected for homolytic hydrogen abstraction, i.e.  $3^{\circ} > 2^{\circ} > 1^{\circ}$ .

## 6.2 NON-HEME IRON OXYGENASES

As noted earlier non-heme iron-dependent oxygenases can be divided into two groups: mononuclear and binuclear. The mononuclear class comprises a diverse group of oxygenases including lipoxygenase and catechol dioxygenases (see earlier) [16, 17, 21, 22]. The  $\alpha$ -ketoacid-dependent enzymes are of interest in the context of alkane activation as they mediate the oxidation of unactivated C-H bonds [21, 22], e.g. the hydroxylation of proline residues (Reaction 11).



A molecule of  $\alpha$ -ketoglutarate ( $\alpha$ -KG) is consumed in the process with concomitant formation of succinic acid and  $\text{CO}_2$ . A mechanism has been proposed [21, 22] which involves the intermediacy of an iron(II) percarboxylate which undergoes heterolysis to an oxoiron(IV) species (Figure 8).

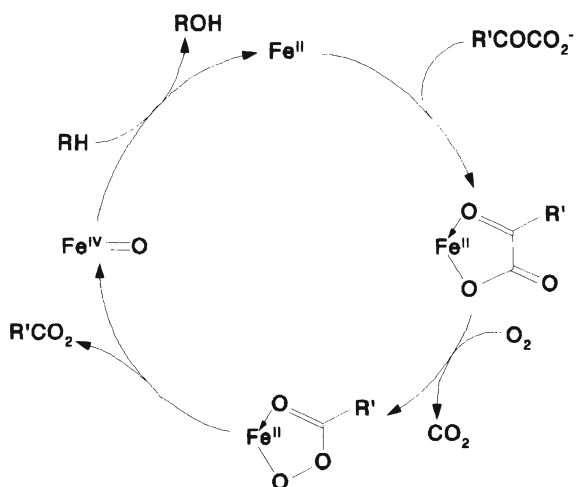


Figure 8. Proposed mechanism for  $\alpha$ -ketoacid-dependent hydroxylases.

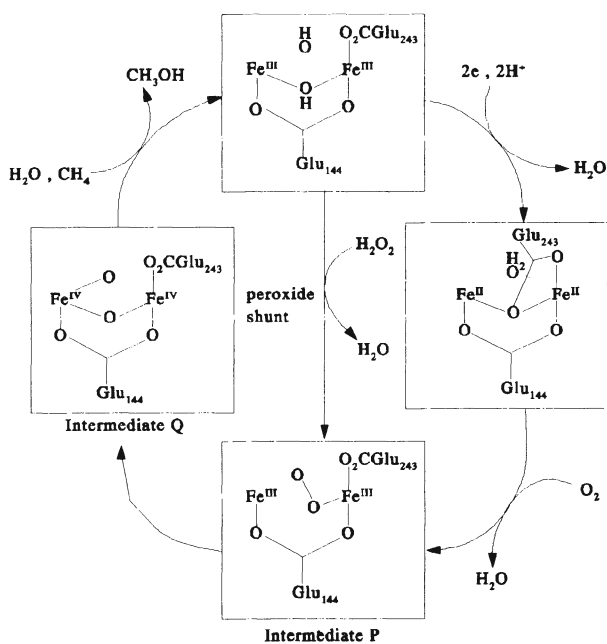


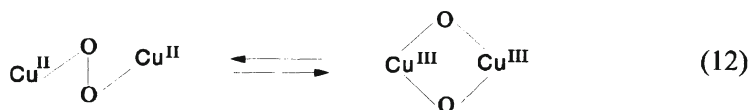
Figure 9. Catalytic cycle of methanemonooxygenase (MMO).



Several features of MMO-mediated hydroxylation are well-understood. The reduced diiron(II) form of the enzyme reacts with dioxygen leading to the formation of a  $\mu$ -1,2-peroxodiiron(III) species [24] designated as intermediate P. This subsequently undergoes O-O bond homolysis to afford the active oxidant, intermediate Q, which has been designated as a bis( $\mu$ -oxo)diiron(IV) species  $\text{Fe}_2(\text{IV})\text{O}_2$  on the basis of Mössbauer and EXAFS analysis [20]. Reaction of intermediate Q with methane, affording methanol, returns MMO to the resting diiron(III) state (Figure 9).

Analogous to cytochrome P450 a peroxide shunt pathway is also possible albeit less effective and, as would be expected for a binuclear pathway, only feasible with  $\text{H}_2\text{O}_2$ . As noted earlier, the oxidant in heme enzymes is an oxoiron(IV)porphyrin radical cation. In MMO the two oxidizing equivalents are stored in the diiron(IV) moiety, i.e. the second iron centre plays the role of the porphyrin ligand in storing the second oxidizing equivalent, with the two oxo bridges stabilizing the diiron(IV) oxidation state. The mononuclear nature of cytochrome P450 requires heterolytic cleavage of the O-O bond to avoid formation of highly reactive OH radicals. Consequently nature has developed an elaborate push-pull mechanism to promote O-O heterolysis.

Binuclear iron enzymes, in contrast, can readily achieve the diiron(IV) state by homolysis of the O-O bond in the  $\mu$ -peroxodiiron(III) species. Interestingly, an analogous, reversible O-O bond homolysis has recently been observed with a model  $\mu$ -peroxo copper II complex [25]:



The mechanistic details of the hydroxylation step of MMO are, just as with cytochrome P450, a matter of debate [15-18]. It is generally thought to involve an 'oxygen rebound' type mechanism (see earlier). An intriguing alternative, which is not available to heme enzymes, involves electrophilic attack on the C-H bond by one of the oxoiron moieties simultaneous with nucleophilic assistance by the second oxoiron in removing hydrogen (Figure 10). An interesting aspect of this proposal [26] is that it would require a precise alignment in the active site and, hence, could explain the high activity with methane.

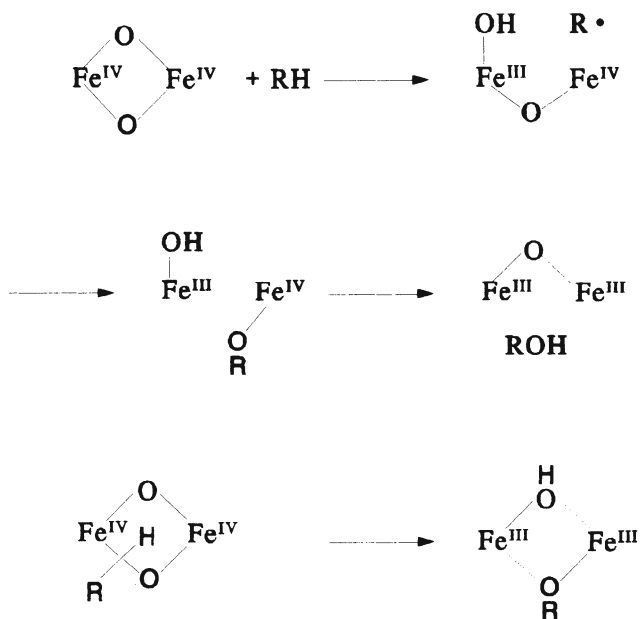


Figure 10. Mechanism of hydroxylation by MMO.

## 7. Biomimetic Oxidations of Alkanes

The ability of oxygenases to catalyze the chemo-, regio- and stereoselective oxidation of hydrocarbons including unactivated alkanes stimulated extensive studies of model systems with the goal of emulating this desirable activity [27]. As we have pointed out elsewhere [28], an interesting historical quirk is the fact that the first oxygenase model system, Udenfriend's reagent, was reported in 1954 [29], one year prior to the discovery of the enzymes that it emulates. Udenfriend and coworkers found that a mixture of Fe(II), EDTA, ascorbic acid and  $\text{O}_2$  is able to hydroxylate aromatic rings at neutral pH and under mild conditions. Subsequently, it was shown that the ascorbic acid could be replaced by other sacrificial reductants [30, 31], notably hydrazobenzene, 2-mercapto-benzoic acid, 2-mercaptoethanol,  $\text{H}_2$ /colloidal platinum, metallic zinc, and even metallic iron powder.

Before discussing model systems it is worthwhile to consider the inherent limitations of the biological catalysts which they attempt to emulate. As outlined in the preceding section, a characteristic feature of the iron-dependent monooxygenases is the need for stoichiometric quantities of a sacrificial reductant, as shown in reaction 1 for methane hydroxylation. *In vivo* this function is fulfilled by the NAD(P)H cofactor which is continuously

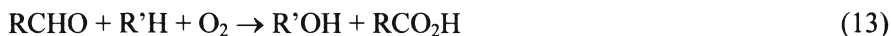
regenerated by intracellular biosynthesis. In the context of developing an economically viable process for the *in vitro* hydroxylation of light alkanes the need for a sacrificial reductant is prohibitive. Virtually all stoichiometric reductants that can be envisaged, including  $H_2$ , would not be economically viable (but see later). Another inherent limitation, of the heme-dependent monooxygenases, is the instability of the porphyrin ring towards oxidative degradation under the reaction conditions. In principle, this problem can be addressed in biomimetic systems by modifying the porphyrin ring (see later) or replacing it altogether. Moreover, we note that the abundant element, iron, forms the basis of biological catalysts for alkane hydroxylation while in the laboratory less abundant elements, e.g. ruthenium, with superior properties are available. Obviating the need for the sacrificial reductant, the porphyrin ligand and even the iron leads to the concept of suprabiotic catalysis (see later). However, as was noted earlier nature has developed elaborate mechanisms for avoiding the formation of highly indiscriminate  $HO\cdot$  radicals in monooxygenase-mediated oxidations. This characteristic feature also needs to be emulated by biomimetic systems in order to be viable.

## 7.1 CYTOCHROME P450 MIMICS

The most extensively studied mimics of monooxygenases have involved the use of metalloporphyrins, i.e. mimics of cytochrome P450 [32, 33]. In the 1970s several groups, e.g. those of Collman, Baldwin, Traylor and Momenteau [34] performed elegant studies of model systems for the oxygen transport hemoproteins, hemoglobin and myoglobin. A primary aim of these studies was to prevent further reaction of the iron-dioxygen complex, which is needed for oxygen activation. At about the same time other authors, notably Hrycay and coworkers [35] demonstrated that liver microsomal cytochrome P450 catalyzes the hydroxylation of hydrocarbons using a variety of single oxygen donors, e.g.  $H_2O_2$ ,  $RO_2H$ ,  $NaClO_2$  and  $NaIO_4$  as the primary oxidant. This pathway, which later became known as the 'peroxide shunt' (see earlier), provided a means for circumventing the need for a sacrificial reductant in such systems.

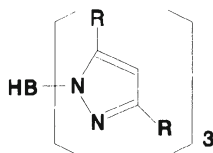
In 1979 Groves and coworkers [36] were the first to translate these results to a model system. They described the use of iron(III) meso-tetraphenylporphyrin (TPP) chloride in combination with iodosylbenzene as the oxygen donor for the epoxidation of olefins and the hydroxylation of alkanes. Following this seminal study metalloporphyrin-catalyzed oxidations, utilizing a variety of oxygen donors such as  $H_2O_2$ ,  $RO_2H$  and  $RCO_3H$ , were extensively investigated [32, 33]. These studies have provided valuable insights into the mechanism of cytochrome P450-mediated hydroxylations of hydrocarbons. However, in the context of light alkane oxidation, they all suffer from the limitation of requiring an expensive primary oxidant. In fact these systems do not really obviate the

need for a sacrificial reductant they merely convert this to an extramural activity, e.g. the production of  $\text{H}_2\text{O}_2$  by reduction of  $\text{O}_2$ . Similarly, in cooxidations of alkanes with aldehydes [37] the aldehyde plays the role of sacrificial reductant (Reaction 13). In the context of light alkane oxidation this is also not economically viable.

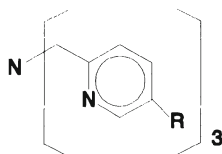


## 7.2 MMO MIMICS

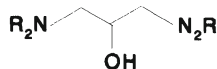
As noted in section 6.2 the hydroxylase enzyme of MMO contains a dinuclear  $\mu$ -oxoiron(III) complex in the active site. Recently much attention has been focused on developing models for this interesting enzyme [38-43]. Ligand design is more complicated than with cytochrome P450 models. In the enzymes the ligands consist largely of monodentate amino acid residues. In model complexes monodentate ligands undergo facile exchange and, hence, multidentate ligands have been used to mimic the active site. Prominent among these are the tripodal ligands, hydrotris (3,5-diisopropyl-1-pyrazolyl)borate (I) [39, 40, 42] and tris-(2-pyridylmethyl)methane (II) [41, 43], and the dinucleating ligand with a 2-hydroxypropane backbone (III) [41, 42].



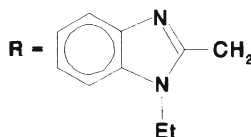
(I) ( $\text{R} = \text{i-Pr}$ )



(II) ( $\text{R} = \text{H}, \text{Et}$ )



(III)



Dinuclear iron complexes of ligands (I)-(III) have been shown to mimic various features of the proposed catalytic cycle of MMO hydroxylase (see earlier). For example, a  $\mu$ -oxodiiron complex of I ( $\text{R}=\text{H}$ ) catalyzed the hydroxylation of cyclohexane and adamantane with  $\text{O}_2$  in the presence of acetic acid and Zn powder as sacrificial reductant [39, 40]. A mononuclear iron(II) carboxylate complex of I ( $\text{R}=\text{i-Pr}$ ) reacted with  $\text{O}_2$  at temperatures below  $-50^\circ\text{C}$  to afford a  $\mu$ -1,2-peroxo complex (Figure 11) with bridging carboxylates [42]. Similarly, a diiron(II) complex of (III) formed a  $\mu$ -1,2-peroxo complex on exposure to  $\text{O}_2$  at  $-60^\circ\text{C}$  [41, 43]. Reaction of a  $\mu$ -oxodiiron(III) complex of II

(R=Et) with  $\text{H}_2\text{O}_2$  [41] gave a  $\mu$ -dioxodiiron complex (Figure 11) containing a formal Fe(III)/Fe(IV) oxidation state, i.e. one oxidation equivalent lower than intermediate Q in the MMO cycle.

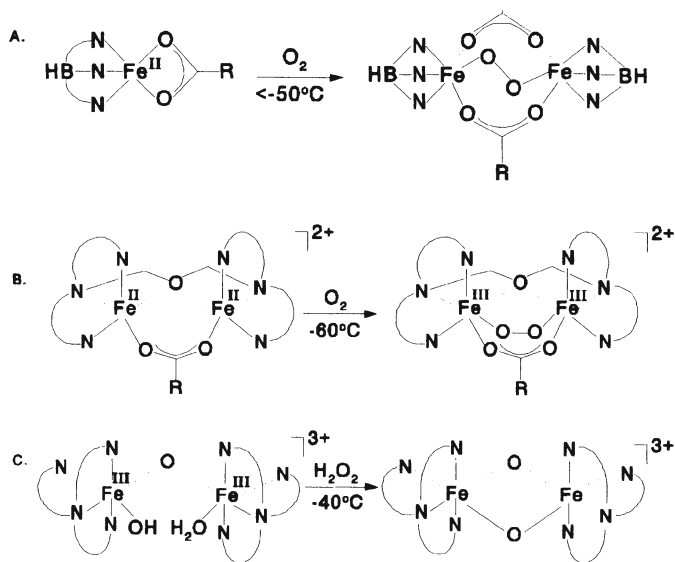


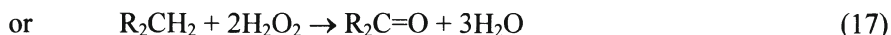
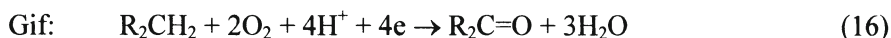
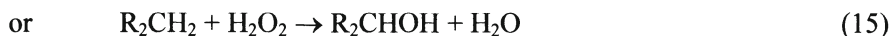
Figure 11. Reaction of iron complexes of ligands I(A) and III(B) with  $\text{O}_2$  and of II(C) with  $\text{H}_2\text{O}_2$ .

We note, however, that although various  $\mu$ -peroxo and  $\mu$ -oxo diiron species have now been isolated and characterized none of these complexes have actually been shown to hydroxylate an alkane.

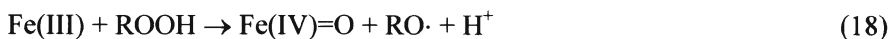
### 7.3 GIF CHEMISTRY

The so-called 'Gif' family of systems, developed by Barton and colleagues [44, 45], occupy a special position in the biomimetic alkane functionalization arena. The initial system reported in 1983 [46] consisted of iron(II) and dioxygen in pyridine solvent in combination with zinc or iron powder and acetic acid as sources of electrons and protons, respectively. This system was shown to selectively oxidize alkanes to give the corresponding ketones directly, rather than further oxidation of an initially formed alcohol. Further evolution followed a similar path to the cytochrome P450 models and culminated in a system comprising picolinic acid or related ligands in combination with iron(III) and  $\text{H}_2\text{O}_2$  or  $\text{RO}_2\text{H}$  as a single oxygen donor [47, 48].

Although the Gif systems have several features in common with MMO, e.g. carboxylate and heterocyclic nitrogen ligands in a putative dinuclear iron complex, they appear to be fundamentally different, affording the ketone and alcohol as the major product, respectively (Reactions 14-17).



The mechanism of Gif chemistry has been extensively discussed in the literature and is still the subject of intense debate [49, 50]. With alkyl hydroperoxides as the oxidant there is very convincing evidence that the key step in the Gif and related MMO model systems (see Section 7.2) is hydrogen abstraction from the alkane by an alkoxy radical [51, 52]. When an iron(III) complex is used, alkoxy radical formation is assumed to involve homolysis of an initially formed alkylperoxoiron(III) complex (Reaction 18). The oxoiron(IV) species formed in Reaction 18 is not kinetically competitive with  $\text{RO}\cdot$  and it was suggested that its principal fate is to oxidize  $\text{RO}_2\text{H}$ , thus returning the catalyst to its original trivalent state (Reaction 19).



Oxidation of the alkane substrate occurs via a conventional free radical autooxidation mechanism in which the  $\text{O}_2$  is derived from termination of  $\text{RO}_2\cdot$  radicals.

The situation is less clear when  $\text{H}_2\text{O}_2$  is the terminal oxidant and Barton distinguishes two different pathways - an  $\text{Fe(II)/Fe(IV)}$  and an  $\text{Fe(III)/Fe(V)}$  manifold (see Figure 12) - depending on the oxidation state in which the iron is introduced [47, 48, 50]. Both pathways are proposed to involve formation of a high-valent alkyliron species. In the  $\text{Fe(II)/Fe(IV)}$  manifold an unstable alkyliron(IV) species is assumed to undergo facile homolytic scission to afford

an alkyl radical. The putative alkyliron(V) intermediate in the Fe(III)/Fe(V) manifold, in contrast, is more stable and affords the ketone product without the intermediacy of an alkyl radical. No explanation was offered for the higher stability of alkyliron(V) compared to alkyliron(IV).

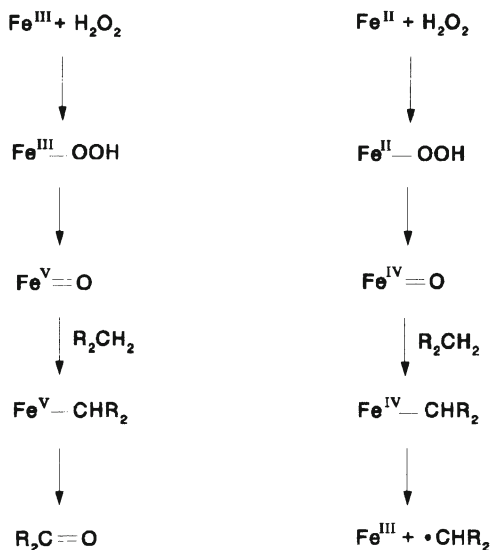


Figure 12.  $\text{Fe}^{\text{III}} / \text{Fe}^{\text{V}}$  and  $\text{Fe}^{\text{II}} / \text{Fe}^{\text{IV}}$  manifolds in Gif chemistry

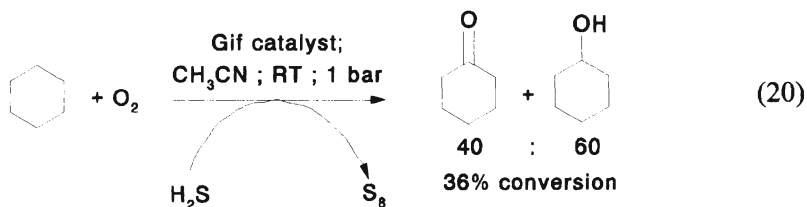
The key step in which the alkyliron(V) species is formed is proposed to involve reaction of a dimeric  $\mu$ -peroxo-oxoiron(V) intermediate with the alkane substrate (Figure 13) [53].

Alkane oxidations with iron(II),  $\text{O}_2$  and a source of electrons and protons are mechanistically equivalent to iron(III) with  $\text{H}_2\text{O}_2$ . i.e. both systems proceed via a  $\mu$ -peroxoiron(III) complex. Although they afford different products (see above) it is noteworthy that Gif systems afford the same  $\text{C}^3/\text{C}^2$  oxidation ratio (3:1 per hydrogen atom) as observed with MMO *in vivo* [54].

Irrespective of the mechanism all of the model systems described above suffer from the inherent disadvantage of requiring a sacrificial reductant or a relatively expensive oxygen donor, neither of which is economically viable for the oxidation of lower alkanes.





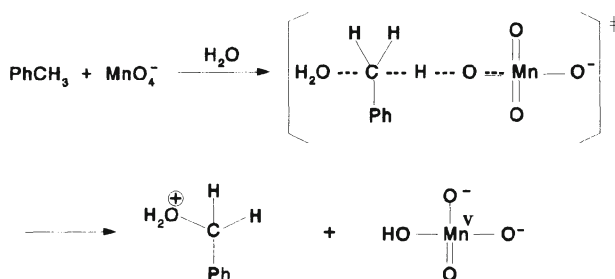


Gif catalyst =  $\text{FeCl}_3$  / picolinic acid / t-butylpyridine

cyclohexane :  $\text{FeCl}_3$  : pic : t-Bupy  
 20 : 1 : 4 : 15

Finally, it is worth emphasizing that reactions with biomimetic systems are generally performed in organic solvents while the enzymes they are intended to emulate operate in aqueous media. This difference may not be trivial: oxidation of toluene with  $\text{MnO}_4^-$  was shown [57] to involve hydrogen atom transfer in non-polar solvents and hydride transfer in water (Figure 14).

$\text{H}_2\text{O}$  solvent (hydride transfer)



$\text{PhCH}_3$  solvent (hydrogen atom transfer)

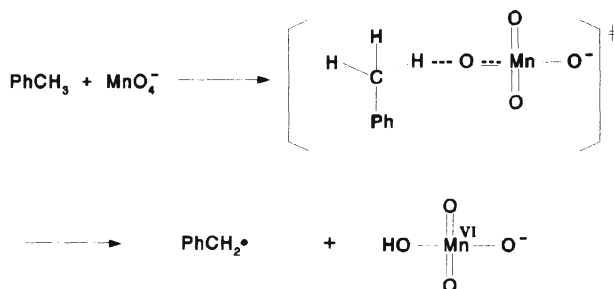
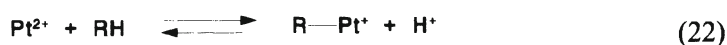
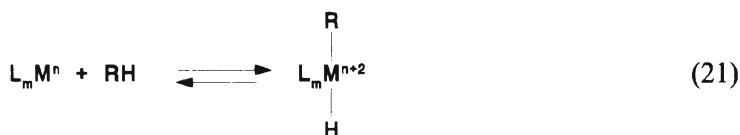


Figure 14. Hydride vs hydrogen atom transfer in oxidation of toluene by  $\text{MnO}_4^-$ .

## 8. The Quest for Suprabiotic Oxidation Catalysis

As noted above a fundamental shortcoming of biological and biomimetic catalysts for alkane oxidation with  $O_2$  is the requirement for a sacrificial reductant. Hence, there is a need for suprabiotic catalysis which circumvents this shortcoming of natural catalysts, i.e. for a Mars-van Krevelen type mechanism in the liquid phase.

The *in vitro* oxidation of alkanes is not limited to the use of the same redox metals (iron and copper) or ligands (porphyrins and amino acids) that are the active constituents of monooxygenases. However, in this section we shall limit ourselves to a discussion of systems that involve analogous oxometal species as the active oxidant. A detailed discussion of systems that involve C-H activation by oxidative addition to low-valent metal centres (Reaction 21) [58, 59] or electrophilic activation [60, 61] by late transition metal ions such as platinum(II) (Reaction 22) is beyond the scope of this review.



In the former case the presence of low-valent metal species is incompatible with oxidizing agents such as  $O_2$  and, hence, these systems are not useful for catalytic oxidation. In the latter case the reactions have been generally performed in strongly acidic media. There are two reasons for this: (a) the conjugate bases of strong acids are weakly coordinating, thereby enhancing the electrophilic character (redox potential) of the metal ion and (b) esterification of the alcohol product by the strong acid (e.g. trifluoroacetic acid) protects it from further oxidation. One impressive achievement in this area is worthy of mention: the Hg(II)-catalyzed oxidation of methane to methyl sulfate described by Catalytica scientists [62]. The sulfuric acid serves two purposes: it is the terminal oxidant and it protects the methanol product as the sulfate ester.

Shilov and colleagues were the first to show that simple platinum(II) complexes, such as  $PtCl_4^{2-}$ , can activate alkanes under mild conditions in water [60]. Nevertheless, this system is not compatible with the use of  $O_2$  as the terminal oxidant. Sen and colleagues have reported [63-65] the oxidation of methane and ethane with  $O_2$  in the presence of Pd- [64] or Rh-based [65] catalysts and carbon monoxide as sacrificial reductant. These systems probably involve the initial formation of hydrogen in the water-gas shift reaction. The noble metal subsequently catalyzes the formation of  $H_2O_2$  from  $H_2$  and  $O_2$  and the final step involves metal-catalyzed oxidation of the alkane by  $H_2O_2$ .

possibly via intermediate hydroxyl radicals. As with the biomimetic systems the requirement for a sacrificial reductant is an obvious drawback.

In a series of publications in the period 1989-1993, Lyons and Ellis [66, 67] showed that iron complexes of perhalogenated porphyrins, such as octabromotetrakis-(pentafluorophenyl)porphyrinato iron(III) chloride  $[\text{Fe}(\text{TFPPBr}_8)\text{Cl}]$ , are remarkably active catalysts for the hydroxylation of light alkanes by  $\text{O}_2$ , under mild conditions. For example, isobutane afforded tert-butanol with > 90% selectivity and turnover numbers exceeding 13000 at 25 °C. Propane required more forcing conditions (125 °C and 70 bar air) and gave a mixture of isopropanol and acetone with a turnover number of > 400.

Lyons and Ellis suggested [66, 67] that the active oxidant is an oxoiron(IV)porphyrin produced via homolysis of a  $\mu$ -peroxoiron(III) dimer, the latter being formed by reaction of the iron(II) porphyrin with  $\text{O}_2$ . As shown in Figure 15 this would constitute an example of suprabiotic oxidation catalysis, i.e. there is no requirement for a sacrificial reductant. The increased activity of perhalogenated porphyrin complexes is rationalized on the basis of the electron-withdrawing halogen substituents increasing the electrophilic character (i.e. redox potential) of the oxoiron(IV) intermediate. Secondly, by removing electron density from the ring the porphyrin ligand becomes less susceptible to oxidative degradation by reaction with oxoiron(IV). Moreover, it was suggested [66, 67] that, with perhalogenated porphyrin ligands, formation of an unreactive  $\mu$ -oxoiron(III) species, by reaction of the oxoiron(IV) with iron(II), was less favourable as a result of steric and electronic effects.

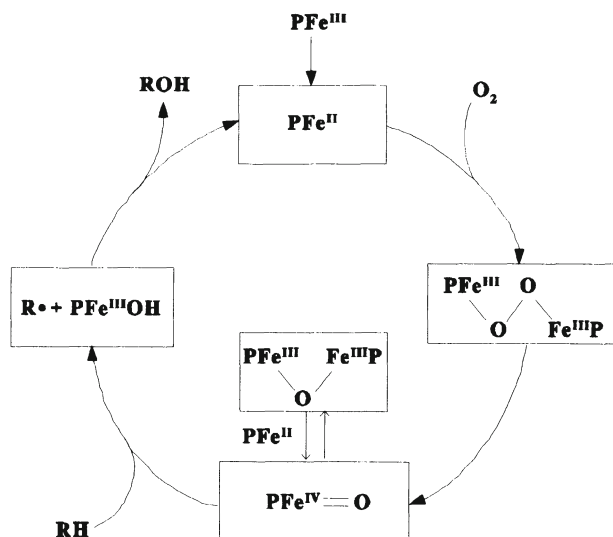
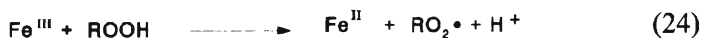
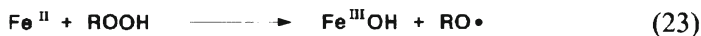


Figure 15. Proposed mechanism for alkane hydroxylation by  $\text{O}_2$  catalysed by  $\text{Fe}(\text{TFPPBr}_8)\text{Cl}$  [66, 67].

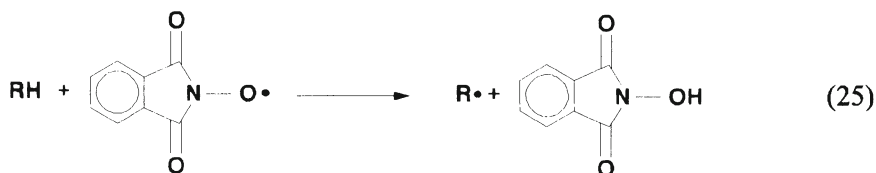
More recently, Labinger and colleagues [68-70] provided convincing evidence, from mechanistic studies and computer modelling of the kinetics, that these systems involve a classical free radical chain autoxidation pathway. Apparently, iron perhalogenated porphyrin complexes are extraordinarily active catalysts for the homolytic decomposition of  $\text{RO}_2\text{H}$  into chain initiating radicals via Reactions 23 and 24.



Similar conclusions were reached regarding the oxidation of cyclohexene catalyzed by electronegative iron salen complexes [71]. Hence, this is yet another example where C-H bond cleavage is effected by metal-free species ( $\text{HO}\cdot$ ,  $\text{RO}\cdot$ ,  $\text{RO}_2\cdot$ ) and the role of the catalyst is limited to promoting the generation of these active species. It was suggested [70] that the main consequence of using a perhalogenated porphyrin ligand is to accelerate the slower of the two catalytic steps, the oxidation of  $\text{RO}_2\text{H}$  by  $\text{Fe}(\text{III})$  (Reaction 24). One may ask the question: does it really matter what the mechanism is? The answer is yes. Free radical autoxidation is a favourable process for tertiary C-H bonds but not for secondary or primary C-H bonds. The high termination rate of secondary and primary alkylperoxy radicals leads to short chain lengths and low selectivities, i.e. inefficient oxidations for linear alkanes.

Similarly, the hydroxylation of methane with  $\text{H}_2\text{O}_2$  in the presence of a sterically hindered ruthenium complex of 2,9-dimethyl-1,10-phenanthroline complex (75 °C and 4 bar  $\text{CH}_4$ ) [72] probably involves the initial formation of hydroxyl radicals by ruthenium-mediated homolytic decomposition of  $\text{H}_2\text{O}_2$ . Likewise, the oxidation of cyclohexane by TBHP catalyzed by dinuclear iron complexes in aqueous micelles, as MMO models, were shown to involve intermediate tert-butoxy radicals [73].

Ishii and coworkers [74, 75] recently reported yet another novel system for the oxidation of (cyclo)alkanes with  $\text{O}_2$ . It comprises a combination of  $\text{Co}(\text{acac})_2$  and N-hydroxyphthalimide (NHPI) as the catalyst. However, here again the reaction involves a free radical autoxidation pathway in which hydrogen abstraction by a phthalimide-N-oxyl radical (Reaction 25) is a key step. Hence, one would not expect this system to be suitable for light alkane oxidation. Nevertheless, we note that n-octane was oxidized to a mixture of octanols and octanones under relatively mild conditions (100 °C, 1 bar  $\text{O}_2$  in acetic acid).



## 9. Redox Molecular Sieves as Catalysts for Alkane Oxidations

Another approach to designing oxidation catalysts with unique activities is to incorporate redox metal ions into the framework or cavities of zeolites and related molecular sieves [76, 77]. Confinement of a redox active centre in the constrained environment of a molecular sieve can be expected to endow the material with unique catalytic activity as a result of strong electrostatic interactions between acidic and basic sites on the internal surface and the substrate or reaction intermediate. Such interactions can be likened with those involving acidic carboxyl and basic amino groups of amino acid residues in the active sites of redox enzymes (see earlier). Moreover, the superstructure of the molecular sieve can impose an unusual (high energy) geometry at a metal site thus enhancing its redox potential. In bioinorganic chemistry this is referred to as the entatic state [78] and it is generally believed to play a major role in determining the activity of (redox) metalloenzymes by modifying the redox potential of the central metal atom.

In this context it is worth noting the suggestion of Dewar that the high rates of enzymatic processes are due to the exclusion of solvent molecules from the active site, such that the reaction takes place under quasi gas phase conditions [79]. Similar conditions are achieved in the micropores and cavities of molecular sieves. Moreover, by an appropriate choice of pore size and hydrophobicity one is able, just as with enzymes, to influence which molecules have ready access to the active site on the basis of size and/or hydrophobic/hydrophilic character. Hence, tailor-made catalysts can, in principle, be designed which distinctly resemble redox enzymes where the protein mantle plays a similar role. It is perhaps not surprising, therefore, that such materials have been referred to as 'mineral enzymes' or 'zeozymes' [80].

Two important variables in the design of a redox molecular sieve with a particular metal are the nature of the molecular sieve (pore size, hydrophobicity and acidity) and the method of confinement. Zeolites and zeotypes are crystalline oxides comprising corner sharing  $\text{TO}_4$  tetrahedra ( $\text{T} = \text{Si}, \text{Al}, \text{P}$ , etc.) and consisting of a regular pore system with diameters of molecular dimensions, hence the term molecular sieve. Zeolites refers to aluminosilicates ( $\text{T} = \text{Si}$  and  $\text{Al}$ ) and zeotypes to molecular sieves having analogous structures but different elemental compositions, e.g. silicalites ( $\text{T} = \text{Si}$ ), aluminophosphates ( $\text{AlPOs}$ ;  $\text{T}$

= Al, P) and silicoaluminophosphates (SAPOs; T = Si, Al and P). Molecular sieves are categorized into small pore (< 4 Å), medium pore (4-6 Å), large pore (6-8 Å), extralarge pore (8-14 Å) and mesoporous (15-100 Å).

If we exclude simple ion exchange from our discussion we can distinguish three types of redox molecular sieves on the basis of the method of confinement: (a) framework substitution, (b) encapsulation and (c) grafting or tethering of metal complexes to the internal surface.

## 9.1 FRAMEWORK-SUBSTITUTED REDOX MOLECULAR SIEVES

Framework substitution can be achieved by hydrothermal synthesis or post-synthesis modification of molecular sieves [76, 77]. The oxidation of alkanes catalyzed by framework-substituted redox molecular sieves can be divided into two types [76, 77]: those involving early transition metals (Ti, V) in combination with  $\text{H}_2\text{O}_2$  and those involving later transition metals (Co, Mn, Cr) in combination with  $\text{O}_2$ . The former are not of interest in the context of light alkane oxidation for reasons of economic viability. On the other hand, alkane oxidations with  $\text{O}_2$  catalyzed by cobalt- [81] and chromium-substituted [82] aluminophosphates, for example, almost certainly involve classical free radical autoxidation pathways and are, for reasons outlined earlier, unsuitable for light alkane oxidation. Moreover, extensive leaching of the metal ion is observed [81] in acetic acid as solvent and probably even in the neat hydrocarbon, e.g. cyclohexane, at higher conversions where carboxylic acids are formed as oxidation products.

## 9.2 ZEOLITE-ENCAPSULATED REDOX METAL COMPLEXES

Large pore zeolites possess intersections that are large enough to accommodate metal complexes of ligands such as phthalocyanines, porphyrins, etc. The large pore faujasite zeolite, for example, contains supercages of 13 Å diameter, which are intersected by channels of 7.4 Å. In the ship-in-a-bottle approach to encapsulation [83, 84] the metal complex is too large to access the pores and, therefore, needs to be assembled *in situ*. Since the complexes are physically entrapped in intrazeolite space they can be regarded as supramolecular catalysts. Provided that the complex is stable towards dissociation and/or oxidative destruction no leaching of the metal ion should occur. Encapsulation combines the advantages of homogeneous and heterogeneous catalysts and more closely resembles enzymes where a metal complex is encapsulated in a protein mantle.

Pioneering studies of oxidations catalyzed by faujasite (zeolite X and Y) - encapsulated iron phthalocyanines (FePc) were performed by Herron and colleagues [85]. The oxidation of linear and cycloalkanes with iodosylbenzene (PhIO) were catalyzed by NaX- and NaY-encapsulated FePc. Although rather

interesting shape selectivities were observed, reminiscent of heme-containing oxygenases, activities were poor (ca. 6 turnovers). More recently, Jacobs and coworkers found that FePc-Y, containing 1 FePc per 77 supercages, gave turnovers as high as 6000 in the oxidation of n-octane with TBHP [86]. Turnover frequencies were rather low ( $12 \text{ h}^{-1}$ ), however. The presence of free iron ions in the zeolite leads to nonproductive TBHP decomposition and synthesis methods were optimized to minimize this effect: the use of ferrocene as the iron source was found to be essential [86]. Apparently, site-isolation of active Fe-centres not only precludes the formation of unreactive  $\mu$ -oxoiron dimers (see earlier) but also protects the phthalocyanine ligands from oxidative degradation, suggesting that the latter is an intermolecular process.

A further improvement to this system was achieved by embedding the zeolite in a hydrophobic polydimethylsiloxane (PDMS) membrane [87]. The latter mimics the hydrophobic phospholipid membrane in which cytochrome P450 resides, acting as an interface between the two immiscible phases (aqueous TBHP and alkane substrate). The catalyst exhibited a 20-fold increase in activity compared to the membrane-free FePc and the turnover frequency of cyclohexane oxidation at room temperature ( $3.3 \text{ min}^{-1}$ ) is comparable to that of enzymes. However, reactivity orders of primary, secondary and tertiary C-H bonds (e.g.  $\text{C}^2/\text{C}^3 = 0.26$  in adamantane) are indicative of the intermediacy of tert-butoxy radicals.

Balkus and coworkers [89] synthesized a NaX-encapsulated ruthenium perfluorophthalocyanine complex ( $\text{RuF}_{16}\text{Pc-X}$ ), containing 1 Ru per 125 supercages by the template method (using the metallophthalocyanine as a structure-directing agent in hydrothermal synthesis). It proved to be an active catalyst for the room temperature oxidation of cyclohexane with TBHP (Table 2). There were no signs of deactivation in 8 days, in contrast to the analogous iron complex which deactivated.

*Table 2. Ru-Phthalocyanine catalyzed oxidation of cyclohexane with TBHP [89]*

Catalyst	Time (h)	Conv. (%)	Selectivity (%)		TBHP efficiency (%)	TOF ( $\text{h}^{-1}$ )
			ketone	alcohol		
RuPc	5	47	72	27	30	7.5
$\text{RuF}_{16}\text{Pc}$	24	83	78	22	48	15
$\text{RuF}_{16}\text{Pc-X}$	192	86	98	1	97	125



More recently, Jacobs and coworkers [90] have described the encapsulation of iron(III) picolinate and 2-pyridinecarboxamide complexes in NaY. The resulting materials are of interest as ‘inorganic’ mimics of MMO and heterogeneous analogues of Gif systems (see earlier). They were shown to catalyze the oxidation of cyclic alkanes with  $\text{H}_2\text{O}_2$  or TBHP. The normalized  $\text{C}^3/\text{C}^2$  ratio of 3 observed in the oxidation of adamantane with TBHP is characteristic of attack of tert-butoxy radicals on the C-H bonds.

### 9.3 ZEOLITE-GRAFTED AND -TETHERED METAL COMPLEXES

Another approach to immobilizing redox metal centres in intrazeolite space is by grafting or tethering (via a spacer ligand) of organometallic or coordination complexes to the internal surface [91]. This approach creates new possibilities for the preparation of novel heterogeneous catalysts containing structurally well-defined active centres. Moreover, as noted by Thomas [91] the tethered complexes in particular contain a readily accessible active site which is “free to flutter in the molecular breeze during the process of catalytic conversion”. For example, Thomas and colleagues [91] mentioned that an oxo-centred tricobaltic acetate, tethered to the inner walls of the mesoporous MCM-41 molecular sieve, is an active catalyst for the selective oxidation of cyclohexane to cyclohexanone and cyclohexanol (the oxidant was not defined). However, bearing in mind the discussion of analogous framework-substituted systems (see earlier) it is highly likely that this system involves a classical free radical autoxidation pathway.

### 9.4 GAS PHASE OXIDATIONS WITH REDOX MOLECULAR SIEVES

As alluded to earlier there are two major problems associated with the use of redox molecular sieves as catalysts for liquid phase oxidations: (a) facile leaching of the metal ion under oxidizing conditions and (b) the ubiquitous free radical chain autoxidation pathway competes effectively with any Mars-van Krevelen type mechanism. Both effects are expected to be less serious in the gas phase owing to lower substrate concentrations and less facile solvolysis of M-O bonds. Hence, the use of hydrophobic redox molecular sieves in the gas phase, where the hydrophobic character of the molecular sieve would favour adsorption of the hydrocarbon substrate over the alcohol product, is expected to be more suitable for the partial oxidation of light alkanes.

There are few examples of the use of redox molecular sieve catalysts in gas phase oxidations. Iron-substituted ZSM-5 [92] and silicalite [93] have been synthesized but their use as a catalyst has been mainly limited to acid-catalyzed reactions. The former was used as a catalyst for methane oxidation, at room temperature, with  $\text{N}_2\text{O}$  as the primary oxidant [94]. A  $\mu$ -oxoiron(III) species was suggested as the active oxidant on the basis of Mössbauer spectra evidence



[94]. In this context it is worth pointing out that regeneration of the active oxidant via a bimolecular mechanism (see Figure 2) would seem to require immobilization of a dinuclear species. In another study [95] a copper(II) exchanged FeZSM-5 was found to give better methanol selectivities (up to 78% at very low conversions) than FeZSM-5 in methane oxidation with  $N_2O$ . It was suggested that the exceptional behaviour of Cu-FeZSM-5 results in some way from synergism between the copper and iron centres, possibly in a dinuclear complex.

Lyons and coworkers [96, 97] reported the gas phase oxidation of methane to methanol over manganese-substituted aluminophosphate molecular sieves. Apparently the methane conversions/methanol selectivities observed in these studies have not yet reached levels which are economically viable.

## 10. Concluding Remarks

Notwithstanding the plethora of investigations devoted to the subject an economically viable method for the partial oxidation of light alkanes to the corresponding alcohols and/or ketones (aldehydes) is not forthcoming. The quest for suprabiotic catalysis - of the Mars-van Krevelen type or otherwise - continues. Although it has not yet lived up to its 'great expectations' the redox molecular sieve approach is still worthy of further investigation because of the analogies to *in vivo* systems. Finally, a better understanding of the intricate mechanistic details of methane monooxygenase catalyzed oxidation of light alkanes could provide a sound basis for developing suprabiotic catalysts.

## 11. References

1. Sheldon, R.A. and Kochi, J.K. (1981) *Metal-Catalyzed Oxidations of Organic Compounds*, Academic Press, New York.
2. Sheldon, R.A. and van Santen, R.A. (eds.) (1995) *Catalytic Oxidation, Principles and Applications*, World Scientific, Singapore.
3. Bielanski, A. and Haber, J. (1991) *Oxygen in Catalysis*, Marcel Dekker, New York.
4. Franz, G. and Sheldon, R.A. (1991) Oxidation, in *Ullmann's Encyclopedia of Industrial Chemistry*, Vol. A18, VCH, Weinheim, pp. 261-311.
5. Anthony, C. (1982) *The Biochemistry of Methylotrophs*, Academic Press, New York.
6. Mars, P. and van Krevelen, D.W. (1954) Oxidations carried out by means of vanadium oxide catalysts, *Chem. Eng. Sci. Spec. Suppl.*, **3**, 41.

7. Coulston, G.W., Bare, S.R., Kung, H., Birkeland, K., Bethke, G.K., Harlow, R., Herron, N., and Lee, P.L. (1997) The kinetic significance of  $V^{5+}$  in n-butane oxidation catalyzed by vanadium phosphates, *Science* **275**, 191-193.
8. Hayaishi, O., Katagari, M., and Rothberg, S. (1955) Mechanism of the pyrocatechase reaction, *J. Am. Chem. Soc.*, **77**, 5450.
9. Mason, H.S., Fowlks, W.L., and Peterson, E. (1955) Oxygen transfer and electron transport by the phenolase complex, *J. Am. Chem. Soc.*, **77**, 2914.
10. Hayaishi, O. (1962) *Oxygenases*, Academic Press, New York.
11. Nguyen, H.H.T., Shiemka, A.K., Jacobs, S.J., Hales, B.J., Lidstrom, M.E., and Chan, S.I. (1994) The nature of the copper ions in the membranes containing the particular methane monooxygenase from *Methylococcus capsulatus* (Bath), *J. Biol. Chem.* **269**, 14995.
12. Sono, M., Roach, M.P., Coulter, E.D., and Dawson, J.H. (1996) Heme-containing oxygenases, *Chem. Rev.* **96**, 2841.
13. Mansuy, D. and Battioni, P. (1993) Dioxygen activation at heme centers in enzymes and synthetic analogs, in J. Reedijk (ed.), *Bioinorganic Catalysis*, Marcel Dekker, New York, p. 395.
14. Ortiz de Montellano, P.R. (ed.) (1995) *Cytochrome P450: Structure, Mechanism & Biochemistry*, 2nd ed., Plenum, New York.
15. Wallar, B.J. and Lipscomb, J.D. (1996) Dioxygen activation by enzymes containing binuclear non-heme iron clusters, *Chem. Rev.* **96**, 2625.
16. Que, L. (1993) Oxygen activation at non-heme iron centers, in J. Reedijk (ed.) *Bioinorganic Catalysis*, Marcel Dekker, New York, p. 347.
17. Feig, L. and Lippard, S.J. (1994) Reaction of non-heme iron(II) centers with dioxygen in biology and chemistry, *Chem. Rev.* **94**, 759.
18. Rosenzweig, A.C. and Lippard, S.J. (1994) Determining the structure of a hydroxylase enzyme that catalyzes the conversion of methane to methanol in methanotrophic bacteria, *Acc. Chem. Res.* **27**, 229.
19. George, A.R., Wilkins, P.C., and Dalton, H. (1996) A computational investigation of the possible substrate binding sites in the hydroxylase of soluble methane monooxygenase, *J. Mol. Catal. B: Enzymatic* **2**, 103.
20. Shu, L., Nesheim, J.C., Kaufmann, K., Munck, E., Lipscomb, J.D., and Que, L. (1997) An  $Fe_2^{IV}O_2$  diamond core structure for the key intermediate Q of methane monooxygenase, *Science* **275**, 515.
21. Nivorzhkin, A.L. and Girerd, J.J. (1996) Oxygen activation by mononuclear non-heme iron proteins, *Angew. Chem. Int. Ed. Engl.* **35**, 609.
22. Que, L. and Ho, R.Y.N. (1996) Dioxygen activation by enzymes with mononuclear non-heme iron active sites, *Chem. Rev.* **96**, 2607.
23. Rosenzweig, A.C., Frederick, C.A., Lippard, S.J., and Nordlund, P. (1993) Crystal structure of a bacterial non-heme hydroxylase that catalyzes the biological oxidation of methane, *Nature* **366**, 537.

24. Liu, K.E., Valentine, A.M., Qiu, D., Edmondson, D.E., Appelman, E.H., Spiro, T.G., and Lippard, S.J. (1995) Characterization of a diiron(III) peroxo intermediate in the reaction cycle of methane monooxygenase hydroxylase from *Methylococcus capsulatus* (Bath), *J. Am. Chem. Soc.* **117**, 4997.
25. Halfen, J.A., Mahapatra, S., Wilkinson, E.C., Kaderli, S., Young, V.G., Que, L., Zuberbühler, A.D., and Tolman, W.B. (1996) Reversible cleavage and formation of the dioxygen O-O bond within a dicopper complex, *Science* **271**, 1397.
26. Shteinman, A.A. (1995), The mechanism of methane and dioxygen activation in the catalytic cycle of methane monooxygenase, *FEBS Lett.*, **362**, 5.
27. Funabiki, T., (ed.) (1996) 'Oxygenases and Model Systems', Kluwer, Dordrecht.
28. Sheldon, R.A. (1993) A history of oxygen activation: 1773-1993, in D.H.R. Barton, A.E. Martell, and D.T. Sawyer (eds.), *The Activation of Dioxygen and Homogeneous Catalytic Oxidation*, Plenum, New York, p. 1.
29. Udenfriend, S., Clark, C.T., Axelrod, J., and Brodie, B.D. (1954) Ascorbic acid in aromatic hydroxylation. I. A model system for aromatic hydroxylation, *J. Biol. Chem.*, **208**, 731.
30. Mimoun, H. (1987) Metal complexes in oxidation, in G. Wilkinson, R.D. Gillard and J.A. McCleverty (eds.), 'Comprehensive Coordination Chemistry', Vol. 6, Pergamon, New York, p. 317.
31. Tabushi, I. (1988) Reductive dioxygen activation by use of artificial P450 systems, *Coord. Chem. Rev.*, **86**, 1.
32. Sheldon, R.A. (ed.) (1994) 'Metalloporphyrins in Catalytic Oxidations', Marcel Dekker, New York.
33. Montanari, F. and Casella, L. (eds.) (1994) 'Metalloporphyrin Catalyzed Oxidations', Kluwer, Dordrecht.
34. For key references see: Collman, J.P., Halpert, T.R., and Suslick, K.S. (1980) O<sub>2</sub> binding to heme proteins and their synthetic analogs, in T.G. Spiro (ed.), *Metal Ion Activation of Dioxygen*, Wiley, New York, p. 1.
35. Hrycay, E.G., Gustafsson, J.A., Ingelman-Sundberg, M., and Ernster, L. (1975) Sodium periodate, sodium chlorite, organic hydroperoxides and H<sub>2</sub>O<sub>2</sub> as hydroxylating agents in steroid hydroxylation reactions catalyzed by partially purified cytochrome P-450, *Biochem. Biophys. Res. Commun.* **66**, 209.
36. Groves, J.T., Nemo, T.E., and Myers, R.S. (1979) Hydroxylation and epoxidation catalyzed by iron-porphine complexes. Oxygen transfer from iodoxybenzene, *J. Am. Chem. Soc.*, **101**, 1032.

37. See for example: Murahashi, S.I., Oda, Y., and Naota, T. (1992) Iron and ruthenium-catalyzed oxidations of alkanes with molecular oxygen in the presence of aldehydes and acids, *J. Am. Chem. Soc.* **114**, 7913.
38. Ito, M., Fujisawa, K., Kitajima, N., and Moro-oka, Y. (1996) Model studies on nonheme monooxygenases - chemical models for nonheme iron and copper monooxygenases, in ref. 27, p. 345.
39. Kitajima, N., Fukui, H., and Moro-oka, Y. (1988) A model for methane monooxygenase: dioxygen oxidation of alkanes by use of a  $\mu$ -oxo binuclear iron complex, *J. Chem. Soc., Chem. Commun.*, 485.
40. Kitajima, N., Ito, M., Fukui, H., and Moro-oka, Y. (1991) Hydroxylation of alkanes and arenes using molecular oxygen, *J. Chem. Soc., Chem. Commun.*, 102.
41. Que, L. and Dong, Y. (1996) Modeling the oxygen activation chemistry of methane monooxygenase and ribonucleotide reductase, *Acc. Chem. Res.*, **29**, 190.
42. Kim, K. and Lippard, S.J. (1996) Structure and Mössbauer-spectrum of a ( $\mu$ -1,2-peroxo)bis( $\mu$ -carboxylato)diiron(III) model for the peroxo intermediate in the methane monooxygenase hydroxylase reaction cycle, *J. Am. Chem. Soc.*, **118**, 4914.
43. Menage, S., Brennan, B.A., Juarez-Garcia, C., Münck, E., and Que, L. (1990) Models for iron-oxo proteins: dioxygen binding to a diferrous complex, *J. Am. Chem. Soc.*, **112**, 6423.
44. Barton, D.H.R. and Doller, D. (1992) The selective functionalization of saturated hydrocarbons: Gif chemistry, *Acc. Chem. Res.*, **25**, 504.
45. Barton, D.H.R. and Doller, D. (1991) The selective functionalization of saturated hydrocarbons: Gif and all that, *Pure Appl. Chem.*, **63**, 1567.
46. Barton, D.H.R., Gastiger, M.J., and Motherwell, W.B. (1983) Activation of the C-H bond in hydrocarbons: the isolation and catalytic activity of a trinuclear organoiron carboxylate cluster, *J. Chem. Soc., Chem. Commun.*, 731.
47. Barton, D.H.R. and Taylor, D.K. (1996) Models for non-heme oxidation enzymes, *Pure Appl. Chem.*, **68**, 497.
48. Barton, D.H.R. (1997) Oxygen and I, *J. Mol. Catal. A: Chemical*, **117**, 3.
49. Perkins, M.J. (1996) A radical reappraisal of Gif reactions, *Chem. Soc. Rev.*, 229.
50. Barton, D.H.R. (1996) The mechanism of Gif reactions, *Chem. Soc. Rev.*, 237.
51. Arends, I.W.C.E., Ingold, K.U., and Wayner, D.D.M. (1995) A mechanistic probe for oxygen activation by metal complexes and hydroperoxides and its application to alkane functionalization by  $[\text{Fe}^{\text{III}}\text{Cl}_2\text{tris}(2\text{-pyridinylmethyl})\text{-amine}]^+\text{BF}_4^-$ , *J. Am. Chem. Soc.*, **117**, 4710.

52. MacFaul, P.A., Arends, I.W.C.E., Ingold, K.U., and Wayner, D.D.M. (1997) Oxygen activation by metal complexes and alkyl hydroperoxides. Applications of mechanistic probes to explore the role of alkoxyl radicals in alkane functionalization, *J. Chem. Soc., Perkin Trans.*, **2**, 135.
53. Barton, D.H.R., Hu, B., Taylor, D.K., and Rojas Wahl, R.U. (1996) The selective functionalization of saturated hydrocarbons. Part 32. Distinction between the  $\text{Fe}^{\text{II}}/\text{Fe}^{\text{IV}}$  and  $\text{Fe}^{\text{III}}/\text{Fe}^{\text{V}}$  manifolds in Gif chemistry. The importance of carboxylic acids for alkane activation. Evidence for a dimeric iron species involved in Gif-type chemistry, *J. Chem. Soc., Perkin Trans.*, **2**, 1031.
54. Kodera, M., Kano, K., and Funabiki, T. (1997) Nonheme monooxygenases, in T. Funabiki (ed.), *Oxygenases and Model Systems*, Kluwer, Dordrecht, p. 283.
55. Tabushi, I., Nakajima, T., and Seto, K. (1980) The oxidation of an iron salen complex modelling  $\omega$ -hydroxylase, *Tetrahedron Lett.*, **21**, 2565.
56. Barton, D.H.R., Li, T., and MacKinnon, J. (1997) Synergistic oxidation of cyclohexane and hydrogen sulfide under Gif conditions, *J. Chem. Soc., Chem. Commun.*, accepted for publication.
57. Gardner, K.A. and Mayer, J.A. (1995) Understanding C-H bond oxidations:  $\text{H}\cdot$  and  $\text{H}^-$  transfer in the oxidation of toluene by permanganate, *Science*, **269**, 1849.
58. Arndtsen, B.A., Bergman, R.G., Mobley, T.A., and Peterson, T.H. (1995) Selective intermolecular carbon-hydrogen bond activation by synthetic metal complexes in homogeneous solution, *Acc. Chem. Res.*, **28**, 154.
59. Crabtree, R.H. (1995) Aspects of methane chemistry, *Chem. Rev.*, **95**, 987.
60. Shilov, A.E. (1984) *Activation of Saturated Hydrocarbons by Transition Metal Complexes*, Reidel, Dordrecht.
61. Vargaftik, M.N., Stolarov, I.P., and Moiseev, I.I. (1990) Highly selective partial oxidation of methane to methyl trifluoroacetate, *J. Chem. Soc. Chem. Commun.*, 1049.
62. Periana, R.A., Taube, D.J., Evitt, E.R., Löffler, D.G., Wentreck, P.R., Voss, G., and Masuda, T. (1993) A mercury-catalyzed, high-yield system for the oxidation of methane to methanol, *Science*, **259**, 340.
63. Sen, A. (1996) New approaches in C-H activation of alkanes, in *Applied Homogeneous Catalysis with Organometallic Compounds*, B. Cornils and W.A. Herrmann (eds.), Vol. 2, VCH, Weinheim, p. 1081.
64. Lin, M. and Sen, A. (1992) A highly catalytic system for the direct oxidation of lower alkanes by dioxygen in aqueous medium. A formal heterogeneous analog of alkane monooxygenases, *J. Am. Chem. Soc.*, **114**, 7307.
65. Lin, M. and Sen, A. (1995) Direct catalytic conversion of methane to acetic acid in an aqueous medium, *Nature*, **368**, 613.

66. Ellis, P.E. and Lyons, J.E. (1990) Selective air oxidation of light alkanes catalyzed by activated metalloporphyrins - the search for a suprabiotic system, *Coord. Chem. Rev.*, **105**, 181 and references cited therein.
67. Lyons, J.E. and Ellis, P.E. (1994) Reactions of alkanes with dioxygen: toward suprabiotic systems, in ref. 32, p. 297 and references cited therein.
68. Grinstaff, M.W., Hill, M.G., Labinger, J.A., and Gray, H.B. (1994) Mechanism of catalytic oxygenation of alkanes by halogenated iron porphyrins, *Science*, **264**, 1311.
69. Labinger, J.A. (1994) A simplified model for catalyzed isobutane oxidation: implications for the mechanism of catalysis by halogenated porphyrin complexes, *Catal. Lett.*, **26**, 95.
70. Böttcher, A., Birnbaum, E.R., Day, M.W., Gray, H.B., Grinstaff, M.W., and Labinger, J.A. (1997) How do electronegative substituents make metal complexes better catalysts for the oxidation of hydrocarbons by dioxygen, *J. Mol. Catal. A: Chemical*, **117**, 229.
71. Böttcher, A., Grinstaff, M.W., Labinger, J.A., and Gray, H.B. (1996) Aerobic oxidation of hydrocarbons catalyzed by electronegative iron salen complexes, *J. Mol. Catal. A: Chemical*, **113**, 191.
72. Goldstein, A.S. and Drago, R.S. (1991) Hydroxylation of methane by a sterically hindered ruthenium complex, *J. Chem. Soc., Chem. Commun.*, p. 21.
73. Rabion, A., Buchanan, R.M., Seris, J.L., and Fish, R.H. (1997) Biomimetic oxidation studies. 10. Cyclohexane oxidation reactions with active site methane monooxygenase enzyme models and tert-butyl hydroperoxide in aqueous micelles: mechanistic insights and the role of t-butoxy radicals in the C-H functionalization reaction, *J. Mol. Catal. A: Chemical*, **116**, 43.
74. Ishii, Y. (1997) A novel catalysis of N-hydroxyphthalimide (NHPI) combined with  $\text{Co}(\text{acac})_n$  ( $n = 2$  or  $3$ ) in the oxidation of organic substrates with molecular oxygen, *J. Mol. Catal. A: Chemical*, **117**, 123 and references cited therein.
75. Ishii, Y., Iwahama, T., Sakaguchi, S., Nakayama, K., and Nishiyama, Y. (1996) Alkane oxidation with molecular oxygen using a new efficient catalytic system: N-hydroxyphthalimide (NHPI) combined with  $\text{Co}(\text{acac})_n$  ( $n = 2$  or  $3$ ), *J. Org. Chem.*, **61**, 4520.
76. Arends, I.W.C.E., Sheldon, R.A., Wallau, M., and Schuchardt, U. (1997) Oxidative transformations of organic compounds mediated by redox molecular sieves, *Angew. Chem. Int. Ed. Engl.*, **109**, in press.
77. Sheldon, R.A., Arends, I.W.C.E., and Lempers, H.E.B. (1997) Liquid phase oxidation at metal ions in constrained environments, *Catalysis Today*, in press.
78. Williams, R.J.P. (1986) Metallo-enzyme catalysis: the entactic state, *J. Mol. Catal., Review Issue*, p. 1.



79. Dewar, M.J.S. (1986) New ideas about enzyme reactions, *Enzyme*, **36**, 8.
80. Parton, R., De Vos, D., and Jacobs, P.A. (1992) Enzyme mimicking with zeolites, in *Zeolites and Microporous Solids. Synthesis, Structure and Reactivity*, E.G. Derouane et al. (eds.), Kluwer, Dordrecht, p. 555.
81. Vanoppen, D.L., De Vos, D.E., Genet, M.J., Rouxhet, P.G., and Jacobs, P.A. (1995) Cobalt-containing molecular sieves as catalysts for the low conversion autoxidation of pure cyclohexane, *Angew. Chem. Int. Ed. Engl.*, **34**, 560.
82. Chen, J.D. and Sheldon, R.A. (1995) Selective oxidation of hydrocarbons with O<sub>2</sub> over chromium aluminophosphate-5 molecular sieve, *J. Catal.*, **153**, 1.
83. Balkus, K.J. and Gabrielov, A.G. (1995) Zeolite encapsulated metal complexes, *J. Incl. Phen. Mol. Recogn. Chem.*, **21**, 159.
84. De Vos, D.E., Thibault-Starzyk, F., Knops-Gerrits, P.P., Parton, R.F., and Jacobs, P.A. (1994) A critical overview of the catalytic potential of zeolite supported metal complexes, *Macromol. Symp.*, **80**, 157.
85. Herron, N., Stucky, G.D., and Tolman, C.A. (1986) Shape selectivity in hydrocarbon oxidation using zeolite encapsulated iron phthalocyanine catalysts, *J. Chem. Soc., Chem. Commun.*, 1521.
86. Parton, R.F., Uytterhoeven, L., and Jacobs, P.A. (1991) Iron-phthalocyanines encaged in zeolite Y and VPI-5 molecular sieve as catalysts for the oxyfunctionalization of n-alkanes, *Stud. Surf. Sci. Catal.*, **59**, 395.
87. Parton, R.F., Vankelecom, I.F.J., Casselman, M.J.A., Bezoukhanova, C.P., Uytterhoeven, J.B., and Jacobs, P.A. (1994) An efficient mimic of cytochrome P-450 from a zeolite-encaged iron complex in a polymer membrane, *Nature*, **370**, 541.
88. Parton, R.F., Vankelecom, I.F.J., Tas, D., Janssen, K.B.M., Knops-Gerrits, P.P., and Jacobs, P.A. (1996) Membrane occluded catalysts: a higher order mimic with improved performance, *J. Mol. Catal. A: Chemical*, **113**, 283.
89. Balkus, K.J., Eissa, M., and Lavado, R. (1995) Cyclohexane oxidation catalyzed by zeolite encapsulated ruthenium perfluorophthalocyanines, *Stud. Surf. Sci. Catal.*, **94**, 713.
90. Knops-Gerrits, P.P., L'abbé, M., Leung, W.H., Van Bavel, A.M., Langouche, G., Bruynseraede, I., and Jacobs, P.A. (1996) Alkane partial oxidation with iron N,N'-bis(2-pyridinecarboxamide) complexes encaged in zeolite Y, *Stud. Surf. Sci. Catal.*, **101**, 811.
91. Thomas, J.M. (1997) Designing new inorganic catalysts, *J. Mol. Catal. A: Chemical*, **115**, 371.
92. Lin, D.H., Coudurier, G., and Vedrine, J.C. (1989) Fe-ZSM-5: Physicochemical and catalytic properties, in *Zeolites: Facts, Figures*,

- Future*, P.A. Jacobs and R.A. van Santen (eds.), Elsevier, Amsterdam, p. 1431.
93. Ratnasamy, P. and Kumar, R. (1991) Ferrisilicate analogs of zeolites, *Catalysis Today*, **9**, 329.
  94. Ovanesyan, N.S., Sobolev, V.I., Dubkov, K.A., Panov, G.I., and Shteinman, A.A. (1996) The nature of the active oxidant in biomimetic methane oxidation on Fe-ZSM-5 zeolite, *Izv. Akad. Nauk, Ser. Khim.*, **6**, 1583; *CA*, **125**, 247051u.
  95. Anderson, J.R. and Tsai, P. (1987) Methanol from oxidation of methane by nitrous oxide over FeZSM-5 catalysts, *J. Chem. Soc., Chem. Commun.*, p. 1435.
  96. Durante, V.A., Lyons, J.E., Walker, D.W., and Marcus, B.K. (1994) New manganese catalyst for light alkane oxidation, *US Pat.* 5345011 to Sun Co.; *CA*, **122**, 186943a.
  97. See also: Lyons, J.E., Ellis, P., and Durante, V. (1991) Active iron oxo centres for the selective catalytic oxidation of alkanes, *Stud. Surf. Sci. Catal.*, **67**, 99.



# HIGH YIELD, LOW TEMPERATURE OXIDATION OF METHANE TO METHANOL

ROY A. PERIANA\*, DOUGLAS J. TAUBE, SCOTT GAMBLE,  
HENRY TAUBE, HIROSHI FUJI  
*Catalytica Advanced Technologies, Inc.*  
*430 Ferguson Drive*  
*Mountain View, CA 94043*

## 1. Abstract

Developing methods for the direct oxidation of alkanes to fuel and chemicals will lead to a paradigm shift in the manufacture of chemicals and fuels in the 21<sup>st</sup> century. We wish to report the development of novel catalysts that allow the direct, low temperature, oxidative conversion of methane to a methanol equivalent product in 70% one-pass yield. To our knowledge, this is the highest one-pass yield ever reported for methane oxidation to a methyl product. The keys to achieving this high yield are : A) the development of novel catalysts that are stable and active for the oxidation of the CH bonds of methane at temperatures as low as 100°C and B) the chemical “protection” of the methanol product from over-oxidation by esterification. The catalysts utilized are novel ligated Pt complexes based on the bidiazine ligand family. A particularly effective oxidation system is based on 20mM solutions of (bipyrimidine)PtCl<sub>2</sub> in concentrated sulfuric acid. Reaction of methane at 500 psig at 250°C with this solution results in 90% conversion of methane to methyl bisulfate in 80% selectivity (70% one-pass yield) based on added methane.

Mechanistic studies show that Pt(II) is the most active oxidation state of the platinum species for reaction with methane. The reaction proceeds via CH activation of methane to generate a platinum-methyl species that is oxidized to generate the product, methyl bisulfate. Isotopic labeling studies suggest that a platinum-methane complex may be involved as an intermediate before CH activation. The bipyrimidine ligand plays a key role in minimizing platinum black formation. The generation of platinum black has been shown to lead to unselective combustion of methane and catalyst death. Control reactions show that the high selectivity and yield is possible because the methyl bisulfate is at

least 10 - 100 times *less reactive* than methane. This suggests that the reaction of the ligated Pt(II) with a CH bond proceeds via an electrophilic process and is retarded by the presence of electron withdrawing groups such as bisulfate.

## 2. Introduction

Developing methods for direct <sup>(1)</sup>, oxidation of low value, light alkane feedstocks to the corresponding alcohols will lead to a paradigm shift in energy and commodity chemical production in the 21<sup>st</sup> century. Currently light alkanes are underutilized, as in the case of abundantly available natural gas, or processed in inefficient multistep processes as in the case of conversion of ethane, propane or butane to the corresponding diols. Several major oil companies have recently announced new technologies for natural gas conversion to refinery feedstock [1] While this represent significant progress toward the goal of more efficient natural gas utilization these technologies still utilize high-temperature, energy intensive, expensive, indirect <sup>(1)</sup> processes based on intermediate syn-gas production. In the cases of the other light alkanes, no significant progress has been made in reducing the number of steps in the existing, multi-step processes. Lower temperature, selective, direct oxidation technology, the focus of this article, can be expected to allow dramatic reductions in cost and waste as less expensive equipment and fewer steps will be required. Our projections show that low temperature, direct oxidation processes have the potential to lower the capital cost for methane to methanol production by 50%. Such a reduction could lead to process for the conversion of methane to gasoline at costs that are competitive with gasoline today. In the case of the direct conversion of ethane, propane or butane to the corresponding diols, our calculations show the possibility "shut-down" <sup>(2)</sup> economics with direct, conversion processes.

Given the high payoff the goal of selective alkane oxidation has been the focus of substantial effort since the 1970's [2]. Indeed, the two most important areas for technology improvements identified in the *Catalyst Technology*

- 
- 1 In the field of hydrocarbon oxidation the term "direct oxidation" generally refers to oxidative processes that avoid the generation of syn-gas (CO/H<sub>2</sub> mixtures). In this report we also use "direct" to describe the oxidation of a CH bond directly to a functionalized bond. "Indirect" processes refer to alkane conversions that proceed via syn-gas as an intermediate step.
  - 2 An economic scenario characterized by manufacturing costs for a material from a new plant (that include material, operating and capital costs) that are lower than that from a depreciated plant (that only include operating and material costs).

*Roadmap Report* <sup>(3)</sup> aimed at addressing the needs identified in the *TECHNOLOGY VISION 2020: The U.S. Chemical Industry* <sup>(3)</sup> are Hydrocarbon oxidation and Alkane CH activation, the latter being the topic of this article. In spite of the obvious need and extensive efforts, very few selective alkane oxidation processes exist today. The primary reasons for this is because, except in a few special cases <sup>(4)</sup>, the basic chemistry for the selective, low-temperature, direct, oxidative conversion of alkane C-H bonds to useful functional groups in high yields has not yet been developed.

The development of such basic chemistry is challenging because; a) alkanes C-H bonds are among the least reactive known and b) the desired products of oxidation are typically more reactive than the starting alkanes. Consequently, only uneconomically low, one-pass yields <sup>(5)</sup> can be obtained with direct, oxidation chemistries available today without prohibitively expensive separations and recycle. We have developed chemistry that address these challenges and we now wish to report a novel, catalytic system for the low temperature, selective oxidation of methane to generate an ester of methanol in 73% one-pass yield and 81% selectivity <sup>(5)</sup> based on methane. To our knowledge, this is the highest one-pass yield known to date for the oxidative conversion of a light alkane. Recently, we reported a system based on catalytic mercuric salts for the selective oxidation of methane that is the only other known example of a high, one-pass yield (~43%) system for the selective oxidation of methane to a methyl product [3]. The current report deals with novel, platinum-based complexes that are more effective catalysts and that

---

3 “Catalyst Technology Roadmap Report” available at internet address <http://www.chem.purdue.edu/ccr/v2020/cat.html> based on the report entitled “TECHNOLOGY VISION 2020: The U.S. Chemical Industry” available at internet address <http://www.chem.purdue.edu/ccr/v2020>.

4 The oxidation of butane to maleic anhydride or acetic acid, propane to acrylonitrile or isobutane to t-butyl hydroperoxide are unique reactions that proceed in reasonable selectivities because either the products are uniquely stable as in the case of maleic anhydride, acetic acid and acrylonitrile or the starting alkane has a uniquely reactive CH bond as in the case of the tertiary CH bond of isobutane.

5 The phrase “one-pass yield” is used to describe the yield of product generated without separation and recycle of the starting materials. This is analogous to the yield from a batch process. Conversion, Selectivity and Yield are defined as:

% conversion =  $\{([\text{CH}_4]_{\text{initial}} - [\text{CH}_4]_{\text{final}}) \div [\text{CH}_4]_{\text{initial}}\} \times 100$

% selectivity to  $\text{CH}_3\text{OH} = ([\text{CH}_3\text{OH}] \div \{[\text{CH}_4]_{\text{initial}} - [\text{CH}_4]_{\text{final}}\}) \times 100$

% yield = (% conversion)  $\times$  (% selectivity)

operate via C-H activation <sup>(6)</sup> of methane. The keys to these unprecedented high-yields are: a) development of novel C-H activation catalysts that are long lived and that allow the selective oxidation of alkanes at temperatures below 250°C and b) the use of “product protection” to stabilize the desired product from over-oxidation as shown in Figure 1.

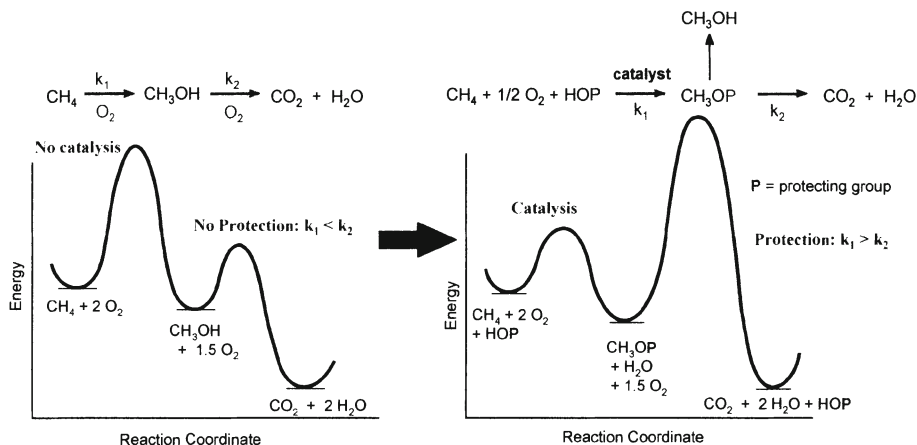


Figure 1. Schematic showing catalysis and “protection” strategy

We reported in our earlier work [3], that along with mercuric salts, the inorganic salts of thallium, gold, palladium and platinum were also shown to promote the oxidation of methane in strong oxidizing acids such as concentrated sulfuric acid. Only stoichiometric oxidations were observed with gold and thallium salts as these systems could not be made catalytic by reoxidation with suitable oxidants. Catalysis is observed with the more environmentally desirable salts of palladium and platinum, with platinum being the more active. However, catalyst life, as well as reaction selectivities were poor due to the well-known issue with irreversible bulk metal formation that occurs with the use of noble metals in redox reactions. The poor selectivity arises because the bulk noble metals catalyze the complete combustion of the desired products. This is a well-established issue that has been documented in the Shilov system and other alkane oxidation system employing noble metal.

The best documented solution to minimizing irreversible reduction of the group VIII noble metals is the use of chloride ligands to stabilize Pd(II) catalysts in the Wacker process [5]. Unfortunately, the addition of chloride are well as other well established solutions to metal reduction, such as the use of

6 "Activation" is used to describe a process where substitution of a stronger CH bond (375 - 440 kJ/mol) occurs to produce a weaker metal-carbon bond (210 - 335 kJ/mol). "Functionalization" is used to refer to a process where the metal-carbon bond is replaced by any bond except a CH bond

heteropoly acids, were not useful for methane oxidation system in strong acids. This work showed that a key challenge to developing low-temperature, active platinum-based oxidation catalysts was to stabilize the homogeneous platinum species with respect to irreversible catalyst decomposition reactions such as reduction to bulk platinum metal or formation of other insoluble species, without inhibiting CH activation and oxidation.

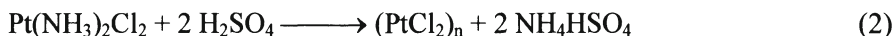
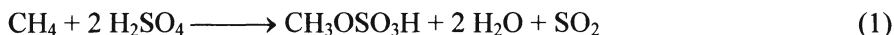
To address this issue, we focused our efforts on the use of ligands that could be expected to stabilize cationic platinum species in hot, concentrated, sulfuric acid solution. Given the strongly acidic, oxidizing environment, the primary issues considered in ligand design were the stability of the ligand-platinum bond to protolytic cleavage and the oxidative stability of the ligand itself. On the basis of the high kinetic lability of oxygen-based ligands and the poor oxidative and thermal stability of phosphorous-based ligands, we focused our efforts on nitrogen ligands.

Initial reactions with simple, sigma-donor, ammine platinum complexes quickly confirmed the validity of the approach. *Cis* or *trans* Pt(NH<sub>3</sub>)Cl<sub>2</sub>, was found to be soluble and stable in concentrated sulfuric acid at 180°C with a half live of approximately 15 minutes. During this time, this material is an active catalyst (Turn-Over-Frequency (TOF) = 10<sup>-3</sup> sec<sup>-1</sup>)<sup>(7)</sup> for the oxidation of methane with hot concentrated sulfuric acid to methyl bisulfate at >90% selectivity as shown in Eq 1<sup>(8)</sup>. The short life of the catalyst in concentrated sulfuric acid solutions were shown to be due to the expected irreversible protonation of the ammonia ligands to generate insoluble platinum chloride and

7 Turn-Over-Frequency = [(Mols of Product Produced) / (Mols of added Catalysts)] per sec and Turn-over-number = [(Mols of Product Produced) / (Mols of added Catalysts)] when reaction stopped.

8 Reactions were carried out under 34.5 bar methane (containing 3% Ne as internal standard), at 180 °C for 3 h with 10 mL of triflic acid containing 2.0 mmols of mercury(II) triflate in a 50-mL high-pressure Autoclave Engineers Hastaloy-C reactor equipped with Desperi-Max gas liquid mixer. Quantitative analysis of the samples was challenging; GC analysis of the crude reaction mixtures was inadequate. Routine analyses were carried out using HPLC to quantify the methanol produced by hydrolysis of a reaction aliquot. In selected cases, qualitative and quantitative <sup>13</sup>C NMR analyses of the crude reaction mixtures with acetic acid as an internal standard (added after reaction) were used to confirm the results. In reported cases, the mass balance on methane was >90%. This mass balance was obtained by accounting for unreacted methane, methyl bisulphate (as methanol after hydrolysis) and carbon dioxide. To obtain good mass balance, the methane/Ne mixture was dispensed from a known-volume, known-pressure reservoir. This procedure allowed the total moles of methane delivered to the reactor to be determined. The moles of methane remaining after reaction and carbon dioxide produced were determined by GC analysis of the gas phase using Ne as an internal standard.

ammonium bisulfate as shown in Eq 2. The stability of this simple di-ammine complex dissolved in hot, concentrated, sulfuric acid for even a limited time illustrates the hoped-for kinetic stability of N-ligands to protolysis, thermolysis and oxidation.



To develop more stable catalysts,  $\pi$ -acidic, nitrogen-based ligands were examined with the expectation that  $\pi$ -acid ligands could be expected to have both lower proton affinity as well as higher affinity for Pt(II), a  $\pi$ -donor metal, than sigma-donor ligands such as ammonia. This reasoning proved to be correct and eventually several complexes were identified that were both less susceptible to protolytic ligand loss as well to irreversible reduction to platinum metal. Among the most effective catalyst is platinum 2,2'-bipyrimidine dichloride, **2**, (bpym)PtCl<sub>2</sub>, Figure 2. Control experiments show that a 50 mM solution of this material is stable in oleum even after 200°C for 50 hours! No ligand decomposition was evident by NMR spectroscopy and the oleum solutions remained homogeneous.

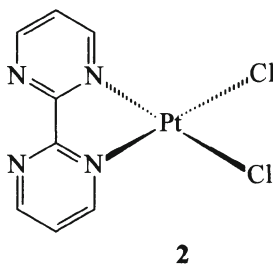


Figure 2. (bpym)PtCl<sub>2</sub> catalyst

Consistent with this unique stability, reaction of methane with catalytic amounts of **2** in 102% sulfuric acid at 220 °C results in >90% methane conversion and formation of ~1M solutions of methyl bisulfate at >81% selectivity <sup>(9)</sup>. Platinum turn-over-frequencies of 10<sup>-3</sup> sec<sup>-1</sup>, volumetric productivities of 10<sup>-6</sup> mol/cc.sec and platinum turn-over-numbers <sup>(7)</sup> of ~300 have been observed with this catalyst. Consistent with the high yield and

---

9 Exp procedure fr Pt(bpym) system.

selectivity, the catalysts remains active and homogeneous after reaction with methane; no visible formation of platinum black is observed.  $^{13}\text{C}$  NMR analyses of the crude reaction mixtures from oxidation of  $^{13}\text{C}$ -enriched methane confirm that the only liquid phase product is methyl bisulfate (and some free methanol) and that it is produced from the added methane, Figure 3. Significantly, unlike the  $\text{Hg(II)}$  system reported earlier [3] no methane sulfonic acid ( $\text{CH}_3\text{SO}_3\text{H}$ ) is produced in the presence of excess  $\text{SO}_3$ . Greater than 95% of the carbon has been accounted for in the reaction and the only observable side product is gas phase  $\text{CO}_2$ .

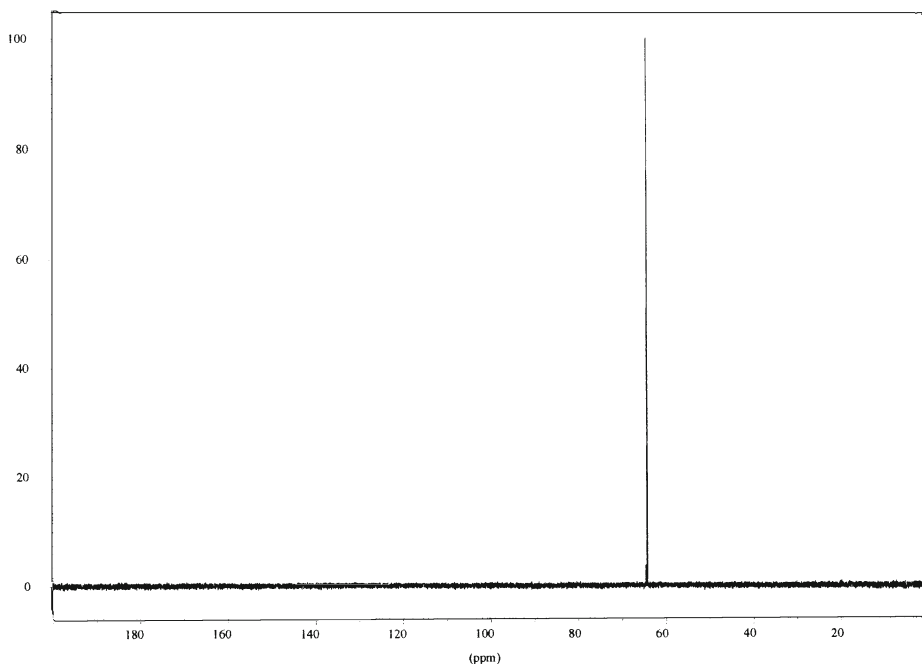


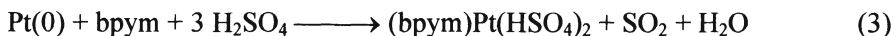
Figure 3.  $^{13}\text{C}$  NMR spectrum of a crude reaction mixture from methane oxidation in 102% sulfuric acid catalyzed by 2.

Analyses of the reaction profiles show that rate of methyl bisulfate formation drops during reaction. This has been shown to be due to the reduction in methane pressure as well as the reduction in acid concentration as water is generated during reaction, Eq 1. The reaction rate is sensitive to the acid concentration and reactions can only be usefully carried to ~80% sulfuric acid. Below this acid concentration, and in weaker acids such as trifluoroacetic or phosphoric acids, reaction of methane still occurs but the rates are low. In addition to sulfuric acid, other strong acids, such as Triflic acid or  $\text{HB}(\text{HSO}_4)_4$

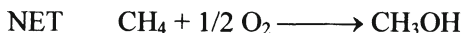
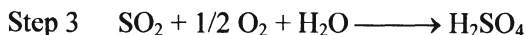


can be utilized as solvent and protecting group for the catalytic oxidation of methane oxidation with **2** if oxidants other than SO<sub>3</sub> or sulfuric acid are utilized.

The high acid stability of complex **2** to strong acid, oxidizing conditions has been traced to the high affinity of the bipyrimidine ligand for Pt(II). Unlike the simple NH<sub>3</sub> ligands that are irreversibly lost by protonation (Eq 1), remarkably, loss of the bipyrimidine ligand is *reversible*. This is dramatically demonstrated by the "self-assembling" characteristics of **2**. Thus, treatment of insoluble (PtCl<sub>2</sub>)<sub>n</sub> with one equivalent of bpym in hot, concentrated sulfuric acid leads to complete dissolution of (PtCl<sub>2</sub>)<sub>n</sub> and formation of a 50 mM homogeneous solution of **2**. By comparison, treatment of (PtCl<sub>2</sub>)<sub>n</sub> in hot, concentrated, sulfuric acid with >100 equivalents of ammonia (added in the form of NH<sub>4</sub>HSO<sub>4</sub>) does not lead to platinum dissolution. Perhaps, the most dramatic illustration of the affinity of bipyrimidine for Pt(II) is the observation that a solution of bpym ligand (20 mM) in hot, 96% sulfuric acid results in oxidative dissolution of equimolar amounts of platinum metal (added as platinum black) to produce a homogeneous solution of (bpym)Pt(HSO<sub>4</sub>)<sub>2</sub> as shown in Eq 3. Control experiments show that these dissolutions do not occur in the absence of the bpym ligand. These experiments show the effectiveness of the bpym ligand for maintaining the homogeneity of platinum cations in strong acids even under redox conditions.



In addition to the high yield and selectivities noted above, a key characteristic of this methane oxidation system is that a potentially practical scheme, Scheme I, can be developed based on known, facile, hydrolysis of the methyl bisulfate and reoxidation of SO<sub>2</sub>. Other systems that catalyze the oxidation of methane to methyl species [2] have been reported. However, the highest yields of methyl products claimed for these processes are < 3% based on added methane. Additionally, none of the reported systems utilize efficiently recyclable oxidants or afford efficient catalysis.



*Scheme I.* Process scheme for the net oxidation methane to methanol.



### 3. Reaction Mechanism

The N-ligated Pt oxidation systems are mechanistically related to our earlier reported system based on mercury [3] as well as to the Shilov aqueous Pt(II)/(IV) system [4] in that the same three key steps, CH activation, Oxidation and Functionalization are proposed for the catalytic sequence as shown in Figure 4. Sufficient mechanistic work has been carried out to support the proposal of these key steps for the reaction mechanism.

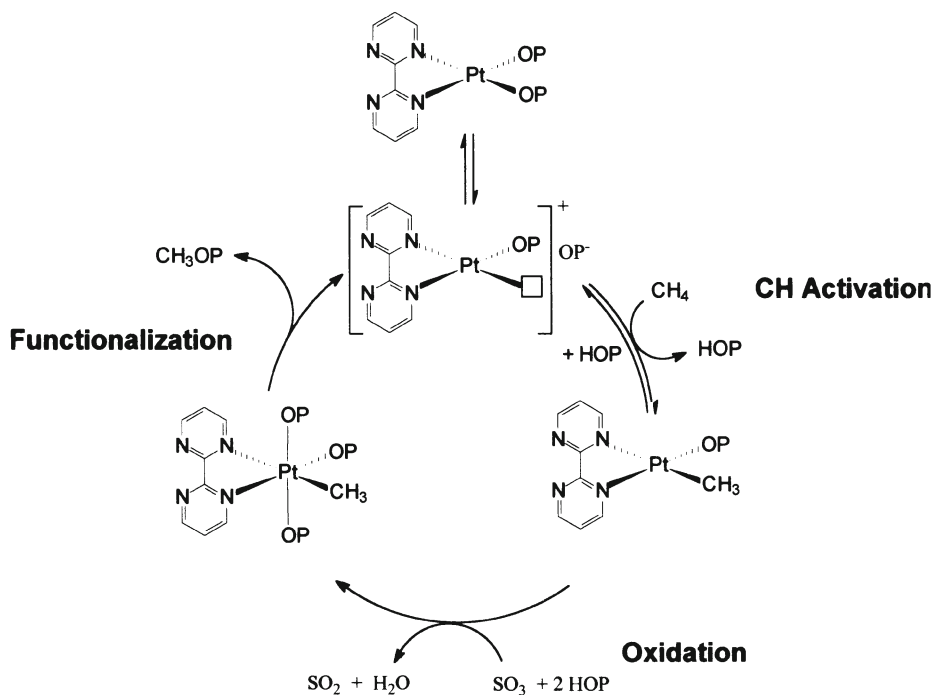


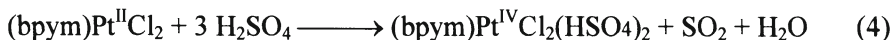
Figure 4. Proposed reaction mechanism for the oxidation of methane.

In the case of the CH activation step, the data is consistent with this step proceeding via the Pt(II) oxidation state rather than bulk metal, homogeneous Pt(0) or the Pt(IV) oxidation states. The proposed CH activation step can be conveniently monitored in isolation from the remaining two steps by carrying out the reaction of methane with **2** in a non-oxidizing, deuterated acid solvent such as CF<sub>3</sub>SO<sub>3</sub><sup>2</sup>H or in deuterated sulfuric acid at temperatures below 150°C. Under these conditions, the rate of CH activation (and the microscopic reverse) can be measured (without complications from net oxidation reactions from S(VI)) by the rate of deuterium exchange between methane and the solvent.

This is conveniently monitored by measuring the free, gas-phase methane containing deuterium. Extensive CH activation ( $\text{TOF} \sim 10^{-1} \text{ sec}^{-1}$ ) is observed with added Pt(II) (in the form of  $(\text{bpym})\text{PtSO}_4$ ) without any reduction (as evidenced by lack of oxidation products  $\text{CO}_2$  or methyl bisulfate) or oxidation (as evidenced by lack of reduction products such as  $\text{SO}_2$ ) of the Pt(II) occurring. However, if  $(\text{bpym})\text{PtSO}_4$  is replaced with Pt(IV) (added in the form of  $\text{H}_2\text{Pt}(\text{OH})_6$ ) or Pt(0) (added as high surface area Pt black) the rate of CH activation is not measurable under the reaction conditions<sup>(10)</sup>. Additional evidence that this reaction does not occur via reduced Pt metal can be obtained from the observations that adding Pt black to a methane oxidation reaction catalyzed by **2** leads to substantial over-oxidation of methyl bisulfate and substantially poorer selectivity than without added Pt black. Ruling out soluble Pt(0) is more difficult as stable, homogeneous Pt(0) species of bpym were not examined. However, the observation that added Pt(II) catalyze H/D exchange without any reduction to Pt(0) would tend to rule out this possibility.

An interesting question is whether the CH activation reaction occurs by an oxidative addition reaction mechanism or whether it occurs by electrophilic substitution as with the Hg(II) system. Recent work by Labinger [4] has shown this possibility must be considered for the Shilov system. We do not have sufficient data to differentiate between these closely related possibilities. However, we favor an electrophilic process that occurs by the cationic, highly electrophilic, coordinatively unsaturated,  $\pi$ -complex, as shown in Figure 4, because the rate of CH activation of  $\text{CH}_4$  with **2** is at least a hundred times higher than  $\text{CH}_3\text{OSO}_3\text{H}$ . While alternative explanations can be advanced, such as increased sterics with methyl bisulfate, we prefer the simple explanation that the substitution of a hydrogen atom of methane with the electron withdrawing bisulfate group inhibits electrophilic substitution of the CH bonds of methyl bisulfate.

Significantly, as for the Hg(II) system [3], the Oxidation step is the rate determining step in the catalytic sequence. At  $150^\circ\text{C}$ , while CH activation occurs, the oxidation of **2** to Pt(IV) species by concentrated sulfuric acid does not occur at a measurable rate. This is consistent with the lack of net methane oxidation to methyl bisulfate under these conditions. At higher temperatures both the oxidation of **2** by Eq 4, as well as the net oxidation of methane is observed.




---

10 If H/D exchange is occurring with these oxidation states the rates must be at least three orders of magnitude slower than with Pt(II)

These observations show that the Oxidation step can occur and that the CH activation step (that occurs under these low temperature conditions) is faster than either the Oxidation step or the Functionalization step or both. To examine the feasibility of the Functionalization step as well as establish the relative rates of the steps, the reaction with methane were carried out at the low temperature conditions (where S(VI) is not at all or poorly oxidative) in the presence of both **2** and Pt(IV) (added as  $\text{H}_2\text{Pt}(\text{OH})_6$ ). Under these conditions, in addition to rapid H/D exchange, now rapid and quantitative formation of methyl bisulfate (relative to added Pt(IV)) is observed. These results are consistent with the CH activation and Functionalization steps occurring faster than the Oxidation step. Consistent with the proposal that the Oxidation step is the rate determining step, Pt(II) complexes that undergo faster oxidation to Pt(IV) also lead to faster methyl bisulfate formation. Thus, the  $(\text{NH}_3)_2\text{PtCl}_2$  complex which is oxidized much more rapidly to Pt(IV) species than the (bpym)PtCl<sub>2</sub> catalyst (by analogous reaction to Eq. 4) also oxidizes methane at faster rate to methyl bisulfate (albeit with a shorter lifetime). Similar correlations are found with **2** and the Pt(bpym)SO<sub>4</sub>.

Unlike the Hg(II) system reported earlier, the key intermediate in the reaction mechanism, the proposed  $\text{Pt}^{\text{II}}\text{-CH}_3$  species obtained from the CH activation step, was not observed in the crude reaction mixtures. This is believed to be due to the substantially lower acid stability of  $\text{Pt}^{\text{II}}\text{-CH}_3$  species compared to  $\text{CH}_3\text{-Hg-OSO}_3\text{H}$  species. Methyl mercury bisulfate was shown to be stable in 96% sulfuric acid for days at room temperature (it eventually decomposes by methane loss) and could be quantitatively generated by treatment of methyl mercury hydroxide and sulfuric acid at room temperature. However, treatment of synthesized (bpym)Pt(CH<sub>3</sub>)(Cl) with sulfuric acid at room temperature leads to rapid evolution of methane with the stoichiometry shown in Eq 5.



Fortunately, decomposition to methane is sufficiently slow at room temperature to enable a methyl platinum species to be observed by <sup>1</sup>H NMR spectroscopy. This observation confirms that a methyl-platinum species in sulfuric acid is a plausible intermediate. However, at typical reaction temperatures for methane oxidation, 180 – 220°C, loss of methane from the added methyl platinum species is immediate and complete. The primarily product (>95%) is methane but methyl bisulfate (<1% yield based on added methyl-platinum) is also produced. These observations are consistent with the lack of observable methyl-platinum species as only a very low steady-state level of such species would be expected. The formation of low levels of methyl bisulfate also provides evidence for the conversion of **3** to product as proposed. As expected on the basis of experiments with added Pt(IV) as discussed above,

the addition of **3** to solutions of sulfuric acid containing Pt(IV) (as  $\text{H}_2\text{Pt}(\text{OH})_6$ ) leads to larger amounts of product along with methane. This is consistent with Shilov's and Labinger's proposal that Pt(IV) can be the oxidant for conversion of methyl-platinum species into product [4].

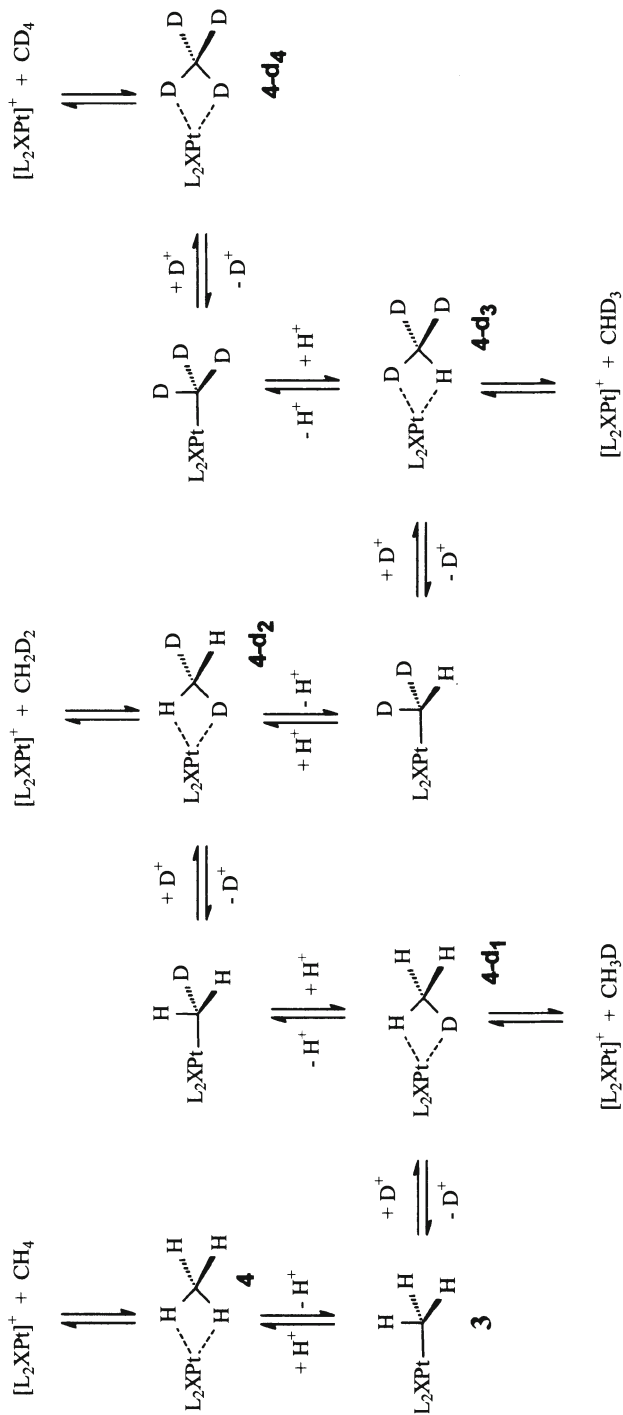
Other important piece of evidence that **3** is a key intermediate is based on the observations of none statistical multiple deuterium incorporation into the free, gas-phase methane observed from reaction of synthesized **3** with deuterated strong acids as well as from by CH activation reactions of methane with deuterated strong acids containing **2**. A plausible explanation for this non-statistical deuterium incorporations is the intermediacy of both **3** and a methane complex as shown in Scheme II<sup>(11)</sup>.

As discussed above a key role of the bpym ligand is maintaining the solubility of the Pt species. This coupled with the observations that simple, non-ligated platinum salts also catalyze methane oxidation (albeit at lower selectivities and rate, *vide infra*) and that bpym binding is reversible (*vide infra*) raise the important question of whether the bpym ligand is attached to the platinum center in the transition state for CH activation. This is useful information because the presence of the ligand in the transition state for CH activation could enable the selectivity of the CH activation reaction to be controlled. Initial experiments showing that the rates of CH activation of two substrates (methane and ethyl phosphonic acid) depend on the type of ligated catalyst strongly implicate that the ligands are attached to the metal during CH activation.

In summary, we have shown that 2,2'-bipyrimidine platinum dichloride is a remarkably stable and active catalyst for the selective, oxidation of methane to methyl bisulfate in sulfuric acid. This system allows the highest one-pass yields reported to date for direct, methane oxidation. The work confirms the utility of CH activation reactions, when combined with product protection, in the development of high selectivity, high yield alkane oxidations reactions.

---

11 Methane complexes are generally accepted intermediates proposed to be involved in CH activation reactions. To date, extensive indirect data have been obtained to support the intermediacy of such species. However, none have been isolated and characterized. Similar scrambling had been observed by Shilov [4] who proposed a carbene-hydride intermediate to explain the results.



*Scheme II.* Proposed mechanism that accounts for multiple exchanges on a single CH activation event via methane complexes

#### 4. References

1. Oil and Gas Journal, 16, 1997; U.S. Patents 4,833,170; 4,973,453; 4,686,238; 5,628,931; 5,658,497; 5,653,916; 5,639,401; 5,645,613; 5,621,155; 5,620,670; 5,543,437; 5,506,272; 5,504,118; 5,500,449; 5,324,335.
2. B. A. Arndtsen, R. G. Bergman, T. A. Mobley, T. H. Peterson, *Acc. Chem. Res.* 28, 154 (1995); J. A. Davies, P. L. Watson, J. F. Liebman, A. Greenberg. Eds., *Selective Hydrocarbon Activation* (Wiley-VCH, New York, 1990); C. L. Hill, *Activation and Functionalization of Alkanes* (Wiley-Interscience, New York, 1989); A. E. Shilov, *Activation of Saturated Hydrocarbons by Transition Metal Complexes* (D. Reidel Publishing Co., Dordrecht, 1984); A. Sen, *Acc. Chem. Res.* 21, 421 (1988); A. E. Shilov, E. I. Karasevich, *Catal. Met. Complexes.*, 17, 87, (1994); J. Sommer, J. Bukala, *Acc. Chem. Res.*, 26(7), 370, (1993); M. Ephritikhine, *Ind. Appl. Homogeneous Catal.* 257-75. (Reidel, Dordrecht, Neth. 1988); C. Hall, R. N. Perutz, *Chem. Rev.* 96(8), 3125, (1996); J. J. Schneider, *Angew. Chem., Int. Ed. Engl.* 35(10), 1068, (1996).
3. R. A. Periana, et. Al. *Science.*, 259, 340 (1993)
4. A. E. Shilov, *Activation of Saturated Hydrocarbons by Transition Metal Complexes* (D. Reidel Publishing Co., Dordrecht, 1984); M. W. Holtcamp, J. A. Labinger, J. E. Bercaw, *J. A. C. S.*, 119, 848 (1997) and references therein.
5. P. M. Henry, *Palladium Catalyzed oxidation of Hydrocarbons*, (D. Reidel, Dordrecht. Neth. 1980).

# FUNCTIONALIZATION OF LIGHT ALKANES CATALYZED BY HETEROPOLY COMPOUNDS

NORITAKA MIZUNO AND MAKOTO MISONO

*Department of Applied Chemistry, Graduate School of Engineering, The University of Tokyo, Hongo, Bunkyo-ku, Tokyo 113, Japan*

## 1. Introduction

Among hydrocarbons, the activation and functionalization of light alkanes such as methane, ethane, propane, and butanes are of great interests, because they are abundant in the natural gas, but the reactivities are very low [1-4]. It has been reported that the light alkanes were activated by (i) superacids [1,2], (ii) soft electrophiles such as  $\text{Pt}^{2+}$  and  $\text{Hg}^{2+}$  [3,5], (iii) solid bases like  $\gamma\text{-Al}_2\text{O}_3$  [6,7], and (iv)  $\text{O}_2$ , halides, and lights [8-11], to form carbonium and then carbenium ions,  $\sigma$ -bond complexes, carbanions, and alkyl radicals, respectively. Biological or biomimetic way is also interesting [4]. It was also reported that alkyl cations or alcohols were stabilized by the reaction with sulfate or trifluoroacetate anion to form the corresponding esters [5,12].

Polyanions are polymeric oxoanions formed by condensation of more than two different mononuclear oxoanions. Acidic elements such as Mo, W, V, Nb and Ta are present as oxoanions in aqueous solution and tend to polymerize by dehydration at low pH and form polyanions and water [13,14].

Catalytic function of heteropoly compounds in the solid state as well as in solution has attracted much attention because their acidic and redox properties can be controlled at atomic/molecular levels [15,16]. The strong acidity or oxidizing properties of heteropoly compounds induce a lot of studies on the heterogeneous and homogeneous catalysis [17]. Soft basicity of the polyanion sometimes plays an important role for high catalytic activity [16]. The additional attractive and important aspects are the oxidative stability and the possibility of the introduction of various elements into polyanions and the counteranions. These properties are suitable for the activation and functionalization of light alkanes as described above ((i) - (iv)).

Here, we wish to describe heterogeneous and homogeneous functionalization of light alkanes by utilizing heteropoly compounds of W and Mo as well as the catalysis of them in model reactions, mainly based on our recent work.

## 2. Characteristic Properties of Heteropoly Compounds Relevant to Activation of Light Alkanes

### 2.1 STRUCTURES

#### 2.1.1 Primary and Secondary Structure

The primary and the secondary structures of  $\text{H}_3\text{PW}_{12}\text{O}_{40}$  in the solid state are shown in figure 1.

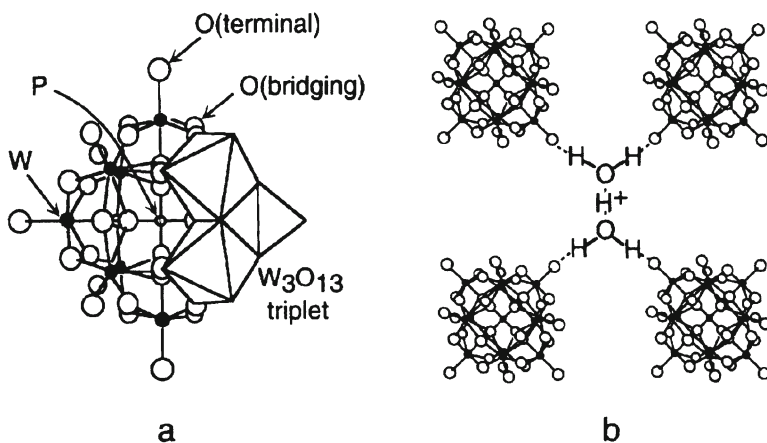


Figure 1. Primary and the secondary structures of  $\text{H}_3\text{PW}_{12}\text{O}_{40}$  in the solid state. (a) Primary structure ( $\text{PW}_{12}\text{O}_{40}^{3-}$ ), and (b) Secondary structure ( $\text{H}_3\text{PW}_{12}\text{O}_{40} \cdot 6\text{H}_2\text{O}$ ).

The primary structure in this case is the polyanion with Keggin structure as shown in Fig. 1a [18]. Four edge-shared octahedral,  $\text{W}_3\text{O}_{13}$ , are linked by shared corners to each other and to the central  $\text{PO}_4$  (W, poly- or addenda atom; P, central or hetero-atom). As an example of the secondary structure,  $\text{H}_3\text{PW}_{12}\text{O}_{40} \cdot 6\text{H}_2\text{O}$  is shown in Fig. 1b [19]. Here, the polyanions are packed in a bcc structure, in which the protonated water dimer,  $(\text{H}_2\text{O})_2\text{H}^+$ , connects to four polyanions by hydrogen bonding. The primary structure (Keggin anion) is stable in general, but the secondary structure is often variable upon the



interactions with polar molecules such as water, ethanol, and dimethylether, metal ions, etc. [15].

Among the polyanions having various compositions and structures, the Keggin anions are in general thermally stable.

### 2.1.2 Lacunary Polyanion as Unique Ligands

Lacunary polyanions which are formed at relatively high pH are widely used as ligands to 3d or 4d metal ions. For example, Fig. 2 shows the structure of  $PW_{11}CoO_{39}^{5-}$ . The vacancy represents a binding site, for example,  $PW_{11}O_{39}^{7-}$  acts as a pentadentate and tetradentate ligand to Co and Cu, respectively [14]. Complexes of anions such as  $XW_{11}O_{39}^{n-}$  ( $X = P, Si$ ) with metal ions have been used as inorganic analogues of metalloporphyrins and have important advantages as catalysts, i.e., high resistance to oxidative degradation and thermal stability [20].

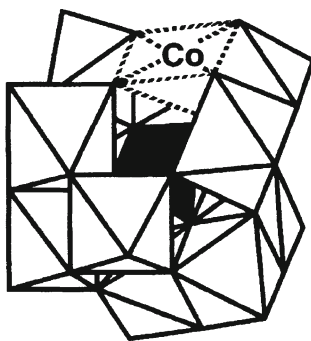


Figure 2. Structure of  $PW_{11}CoO_{39}^{5-}$ .

## 2.2 ACID AND REDOX PROPERTIES

### 2.2.1 Acidic Properties

Keggin-type polyanions such as  $H_3PW_{12}O_{40}$  and  $H_4SiW_{12}O_{40}$  are completely dissociated in an aqueous solution. The dissociation is often partial and stepwise in organic media. They are stronger acids than  $H_2SO_4$ ,  $HBr$ ,  $HCl$ ,  $HNO_3$ , and  $HClO_4$ . The acid strength has been measured by various methods and the general trends of the acid strength are  $W^{6+} > Mo^{6+} > V^{5+}$  (for polyatom) [21] and  $P^{5+} > Si^{4+}$ ,  $Ge^{4+} > B^{3+}$ ,  $Fe^{3+} > Co^{2+}$  (for heteroatom or the charge of polyanion) [22]. For example, in acetone the  $pK_1$  values (in parentheses) increased in the following order,  $PW_{12}^{3-}$  (1.6)  $>$   $PVW_{11}^{4-}$  (1.8)  $>$   $SiW_{12}^{4-}$  (2.0) =

$\text{PMo}_{12}^{3-}$  (2.0) >  $\text{SiMo}_{12}^{4-}$  (2.1) [21,23], where  $\text{PW}_{12}^{3-}$ , etc. denote the acidic  $\text{H}_3\text{PW}_{12}\text{O}_{40}$ , etc.

In the solid state, the strength and the number of acid centers of heteropoly compounds can be controlled by the structure and composition of polyanions, the extent of hydration, the type of support, the thermal pretreatment, etc. It was shown that heteropolyacids such as  $\text{H}_3\text{PW}_{12}\text{O}_{40}$  and  $\text{H}_3\text{PMo}_{12}\text{O}_{40}$  in the solid are pure Brönsted acids [24] and stronger acids than conventional acids such as  $\text{SiO}_2\text{-Al}_2\text{O}_3$ ,  $\text{H}_3\text{PO}_4/\text{SiO}_2$ , and H-X and H-Y zeolites [25].

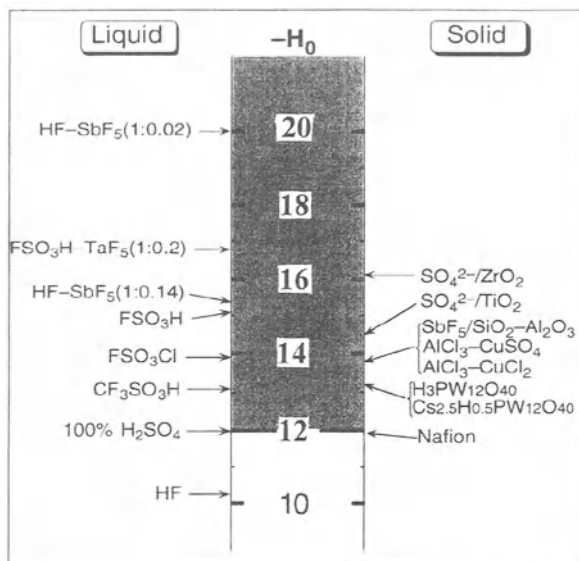


Figure 3. Acid strengths of liquid and solid superacids.

According to an indicator test,  $\text{H}_3\text{PW}_{12}\text{O}_{40}$  and  $\text{Cs}_{2.5}\text{H}_{0.5}\text{PW}_{12}\text{O}_{40}$  have a Hammett acidity function less than -8.2 [25a], and it has been suggested to be a superacid [26], of which the value of  $H_0$  is less than -12 (Fig. 3) [27]. It was confirmed by the temperature programmed desorption of  $\text{NH}_3$  that the acid strength of  $\text{Cs}_{2.5}\text{H}_{0.5}\text{PW}_{12}\text{O}_{40}$  is similar to that of  $\text{H}_3\text{PW}_{12}\text{O}_{40}$  [26a]. Solid-state  $^{31}\text{P}$  NMR spectroscopy was used to demonstrate that all protons of  $\text{Cs}_{2.5}\text{H}_{0.5}\text{PW}_{12}\text{O}_{40}$  are distributed nearly randomly through the solid bulk [28], so that the number of protons on the surface can be estimated by multiplying the formal concentration of protons per polyanion by the number of polyanions on the surface calculated from the surface area.

The change of the number of surface protons with Cs content is shown in Fig. 4a [28,29]. As the Cs content increases, the number of surface protons decreases at first, but increases when the Cs content exceeds 2. The increase in the number of surface protons is mainly due to the sharp increase in the surface

area (Fig. 4b, [30]). When  $x$  approaches from 2.5 to 3.0, the number of surface protons decreases in parallel with the decrease in the formal concentrations of proton.

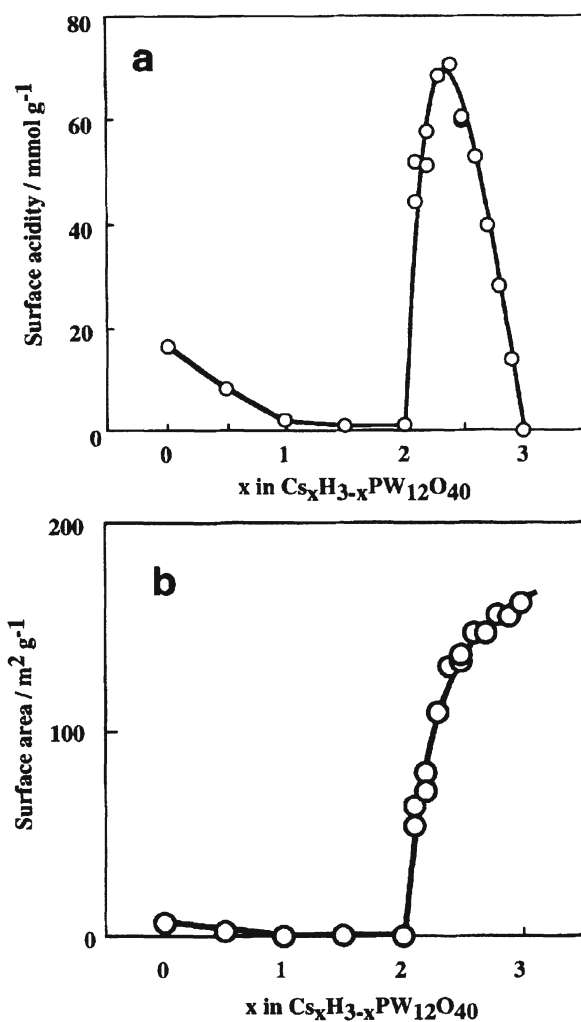


Figure 4. Amounts of surface protons (surface acidity) and surface areas as a function of Cs content for  $\text{Cs}_x\text{H}_{3-x}\text{PW}_{12}\text{O}_{40}$ . (a) Surface protons (surface acidity) and (b) surface areas.

### 2.2.2 Redox Properties

In solutions, the reduction potentials of polyanions containing Mo and V are high. Oxidative ability decreases in general in the order  $V^- > Mo^- > W^-$ -containing polyanions [31, 32]. The reduction potential (or oxidizing ability) decreased linearly with decreasing valency of the central atom or decreasing negative charge of the polyanions,  $PW_{12}^{3-} > GeW_{12}^{4-} > SiW_{12}^{4-} > FeW_{12}^{5-} > BW_{12}^{5-} > CoW_{12}^{6-} > CuW_{12}^{7-}$  [31]. For polyanions with mixed addenda atoms, the reduction potentials have been reported to be  $PMo_{10}V_2^{5-} > PMo_{11}V^{4-} > PMo_{12}^{3-}$  and  $PMo_6W_6^{3-} > PMo_{12}^{3-}$  [14].

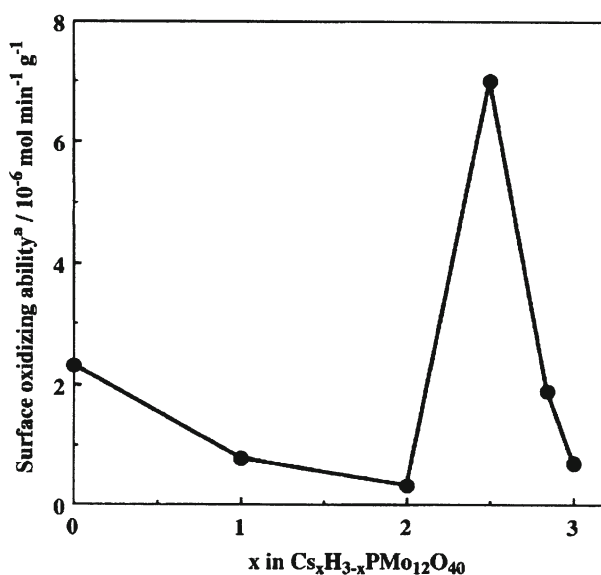


Figure 5. Change in the surface oxidizing ability with Cs content for  $Cs_xH_{3-x}PW_{12}O_{40}$ . a) The surface oxidizing ability can be evaluated by the rates of reduction by CO per weight of catalysts.

In the solid state, the redox properties of 12-heteropoly compounds depend on both the constituent elements of polyanions and counteranions. The oxidizing ability has been estimated from the rate of reduction of heteropoly compounds by  $H_2$ , CO, and organic compounds. However, the data are sometimes inconsistent, due to the difference in the kind of the reductants, inhomogeneity, nonstoichiometry, decomposition, etc. of the catalysts. Another important reason for the inconsistency is the ignorance of the presence of surface- and bulk-type reactions [15]. The rate of reduction of these heteropoly compounds by CO reflects the oxidizing ability of the surface [33a]. The change

in the surface oxidizing ability with Cs content is shown in Fig. 5 [33]. As the Cs content increases, the surface oxidizing ability decreases at first, but increases when the Cs content is 2.5. The increase is mainly due to the sharp increase in the surface area as described in the previous section.

The introduction of mixed-addenda atoms is an important way to control the redox properties. In fact, mixed-addenda heteropolyacids are widely utilized as industrial oxidation catalysts. However, the redox mechanism and its relation to oxidation catalysis remain unclarified. For example, the rate of reduction by  $H_2$  is slower and less reversible for solid  $PMo_{12-x}V_xO_{40}^{(3+x)-}$  than for solid  $PMo_{12}O_{40}^{3-}$  although in solution the formers are stronger oxidants than the latter [34]. The effects of substitution by V for Mo on the catalytic activity are controversial [35-40].

### 2.3 SOFT BASICITY. STABILIZATION OF ALKYL GROUP BY POLYANION

Soft basicity of the polyanion sometimes plays a very important role in catalysis. The order of softness estimated by the equilibrium constant in aqueous solution of the reaction,  $Ag_nX + nNaI \rightleftharpoons nAgI + Na_nX$  (X, polyanion), was  $SiW_{12}O_{40}^{4-} > GeW_{12}O_{40}^{4-} > PW_{12}O_{40}^{3-} > PMo_{12}O_{40}^{3-} > SiMo_{12}O_{40}^{4-} > SO_4^{2-}$  [41].

Ethyl and methyl groups are stabilized by the  $PW_{12}O_{40}^{3-}$  polyanion [42-47]. The  $^{13}C$  NMR data demonstrate the formation of ethoxide and methoxide with the absorption of ethanol and methanol, respectively. For example, the  $^{13}C$  NMR spectra of ethanol absorbed in  $H_3PW_{12}O_{40}$  is shown in Fig. 6. Three different species were observed. The resonances at 61.9 and 17.2 ppm; 65.0 and 16.8 ppm; and 82.1 ppm were assigned to  $(C_2H_5OH)_2H^+$ ,  $C_2H_5OH_2^+$ , and ethoxide in  $H_3PW_{12}O_{40}$ , respectively. Similarly the methoxide signal was observed at 79.3 ppm for the absorption of methanol. Thus, the basicity of the  $PW_{12}O_{40}^{3-}$  polyanion plays an important role for the stabilization of the alkoxides, which would be formed by the oxygenation of light alkanes.

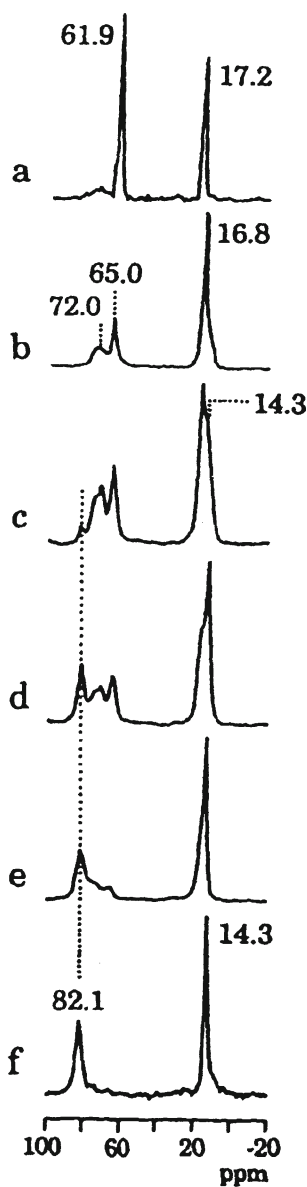


Figure 6.  $^{13}\text{C}$  NMR spectra of ethanol absorbed in  $\text{H}_3\text{PW}_{12}\text{O}_{40}$ . Transformation of protonated ethanol dimer in  $\text{H}_3\text{PW}_{12}\text{O}_{40}$  by heat treatment. Solid-state  $^{13}\text{C}$  CP/MAS NMR spectra were obtained by using high purity  $^{13}\text{C}$  ethanol: (a) dimer, (b) 333 K, (c) 343 K, (d) 363 K, (e) 373 K, (f) 423 K.

### 3. Functionalization of Light Alkanes Catalyzed by $\text{Cs}_x\text{H}_{3-x}\text{PMo}_{12}\text{O}_{40}$ (M = Mo, W)

#### 3.1 OXYGENATION OF ALKANES

##### 3.1.1 Gas-Solid Phase Oxygenation with Molecular Oxygen

There have been several attempts to obtain oxygenated products from light alkanes ( $\text{C}_1 - \text{C}_5$ ) by using heteropoly catalysts. It has been reported that the hydrogen form of  $\text{H}_3\text{PMo}_{12}\text{O}_{40}$  catalyzes the oxidation of light alkanes to aldehydes and carboxylic acids [48] and that the substitution of  $\text{V}^{5+}$  for  $\text{Mo}^{6+}$  modified the catalytic activity and selectivity [49-52].

By optimizing the quantity and type of constituent elements of polyanions and counter cations, fairly good yields were obtained for the oxidation of isobutane [53-57]. Recently, it was found that acidic cesium salts of Keggin-type heteropolymolybdates efficiently catalyzed the oxidation of isobutane to methacrylic acid with molecular oxygen. Mizuno et al. attempted to stabilize the polyanions by forming their cesium salts. The high yields were obtained for the conversion of isobutane to methacrylic acid (MAA) as shown in Table 1 [56]. The highest conversion was observed around  $x = 2.5$ . The main products were methacrylic acid, methacrolein (MAL) and acetic acid (AcOH). The substitution of Cs for H in  $\text{H}_3\text{PMo}_{12}\text{O}_{40}$  resulted in a great enhancement of the MAA production and the yield reached a maximum at  $x = 2.5$ . The sum of the yields of MAA and MAL on  $\text{Cs}_{2.5}\text{H}_{0.5}\text{PMo}_{12}\text{O}_{40}$  reached 5.1%.

Table 1. Oxidation of isobutane over  $\text{Cs}_x\text{H}_{3-x}\text{PMo}_{12}\text{O}_{40}$  at 613 K<sup>a</sup>

x	Surface area / $\text{m}^2 \cdot \text{g}^{-1}$	Conv. / %	Rate / $10^{-5} \text{ mol} \cdot \text{min}^{-1} \cdot \text{m}^{-2}$	Selectivity <sup>b</sup> / %					Sum of yields of
				MAA	MAL	AcOH	CO	CO <sub>2</sub>	
0	1.1	7	1.34	4	18	8	44	26	1.5
1	2.1	6	0.60	23	17	10	32	18	2.4
2	5.9	11	0.39	34	10	7	29	21	4.8
2.5	9.5	16	0.36	24	7	7	41	21	5.1
2.85	46.0	17	0.08	5	10	5	44	37	2.4
3 <sup>c</sup>	46.0	8	0.04	0	10	6	32	35	0.8

a) Isobutane, 17 vol%; O<sub>2</sub>, 33 vol%; N<sub>2</sub>, balance; catalyst, 1.0 g; total flow rate, ca. 30 cm<sup>3</sup> min<sup>-1</sup>.

b) Calculated on the C<sub>4</sub> (isobutane)-basis.

c) The selectivity to acetone was 17%.

Figure 7 shows a good correlation between the rates of oxidation of isobutane and non-catalytic reduction of catalysts by CO. The correlation noted in Fig. 7 indicates that the catalytic activity is controlled by the oxidizing ability of catalysts. The protonic acidity is also a factor controlling the catalytic activity [56].

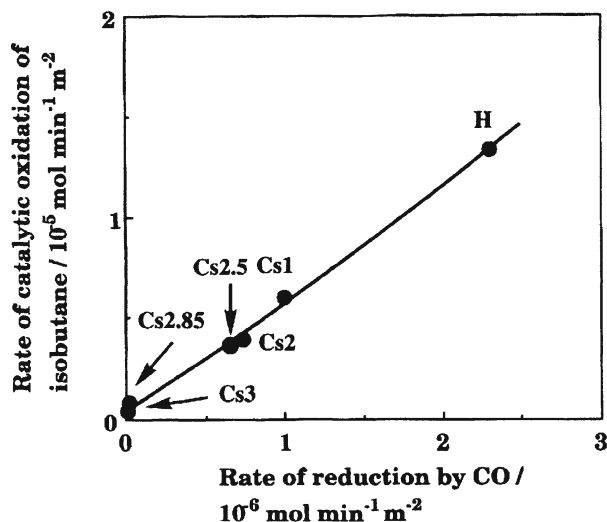


Figure 7. Correlation between rates of oxidation of isobutane and those of non-catalytic reduction of catalysts by CO.  $\text{Cs}_x$  and H show  $\text{Cs}_x\text{H}_{3-x}\text{PMo}_{12}\text{O}_{40}$  and  $\text{H}_3\text{PMo}_{12}\text{O}_{40}$ , respectively.

### 3.1.2 Liquid Phase Oxygenation of Alkanes

Scarcely is known of the liquid-phase oxygenation of light alkanes catalyzed by polyanions. Therefore, in this section oxidation reactions of not only light alkanes but also higher alkanes are described.

Polyanions having multiple active sites have been synthesized and applied to oxidation reactions of light alkanes with molecular oxygen. It was reported that propane, ethane, and methane were oxidized to the corresponding alcohols and ketones over *tri*-transition-metal-ion( $\text{Fe}_2\text{Ni}$ )-substituted  $\text{PW}_{12}\text{O}_{40}^{3-}$ , although the composition and structure of the catalyst are still to be examined [58]. Mizuno et al. characterized its structure [59], and confirmed that it catalyzed the oxygenation of adamantane, ethylbenzene, and cyclohexane with molecular oxygen alone [60].

For example, adamantane was catalytically oxidized mainly to 1-adamantanol with small amount of 2-adamantanol and 2-adamantanone. The total turnover number was 25 based on bulk polyanion or 3750 per surface



polyanion. This turnover number is of the highest level for the oxidation of adamantane with molecular oxygen on  $\mu$ -oxo *di*- or *tri*-iron and Ru complexes with or without reductants [61,62].

Recently, Neumann et al. reported that  $[\text{WZnRu}^{\text{III}}_2(\text{OH})(\text{H}_2\text{O})(\text{ZnW}_9\text{O}_{34})_2]^{11-}$  polyanion with a  $\text{WZnRu}_2$  ring between two  $\text{B-ZnW}_9\text{O}_{34}$  units promoted the oxygenation of adamantane with molecular oxygen [63]. It is suggested that Ru-O-O-W is an active oxygen species.

Hydrogen peroxide and alkyl hydroperoxides are important oxidants in organic synthesis, but they usually need to be activated by catalysts such as tungsten, molybdenum, and titanium oxides.

The selective oxidation of methane with hydrogen peroxide was efficiently catalyzed by  $\text{H}_4\text{PVMo}_{11}\text{O}_{40}$  catalyst precursor in  $(\text{CF}_3\text{CO})_2\text{O}$  solvent at 353 K. A conversion to the oxygenates such as methylformate and formic acid of 33.0% was achieved. Table 2 shows effects of solvents [64]. In  $\text{H}_2\text{O}$  and  $(\text{CH}_3)_2\text{SO}$  solvents, no reaction proceeded. On the other hand, the selective oxygenation of methane proceeded in  $\text{CH}_3\text{CN}$  and  $(\text{CF}_3\text{CO})_2\text{O}$ . Among the solvents used,  $(\text{CF}_3\text{CO})_2\text{O}$  gave the highest conversion of methane, 33.0%, and the TON reached 260. The conversions and TON reported so far were in the range of 0.03 - 8% and 5 - 513, respectively. The values obtained in our work are among the highest reported in refs. [65,66]. In  $(\text{CF}_3\text{CO})_2\text{O}$ , methylformate, formic acid, methyltrifluoroacetate, methanol, and carbon dioxide were produced, methylformate being the main product. It has been reported that  $(\text{CF}_3\text{CO})_2\text{O}$  reacts with  $\text{CH}_3\text{OH}$  and  $\text{H}_2\text{O}_2$  to form a stable ester, methylformate, and trifluoroperacetic acid, respectively [65]. In addition, among the solvents used,  $(\text{CF}_3\text{CO})_2\text{O}$  showed the highest solubility of methane. These are the reasons why the high conversion was obtained in  $(\text{CF}_3\text{CO})_2\text{O}$ .

Table 2. Effect of solvents at 353 K<sup>a</sup>

Solvent	Conv. / %	Turnover number	Yield / mmol				
			$\text{CH}_3\text{OH}$	$\text{HCOOH}$	$\text{HCOOCH}_3$	$\text{CF}_3\text{COOCR}_3$	$\text{CO}_x$
$(\text{CF}_3\text{CO})_2\text{O}^b$	33.0	260	0.04	1.06	2.40	0.39	0.16
$\text{CH}_3\text{CN}^b$	2.3	19	0.06	0.41	0	-	0
$\text{H}_2\text{O}$	0.0	0	0	0	0	-	0
$(\text{CH}_3)_2\text{SO}$	0.0	0	0	0	0	-	0

a) Reaction time, 24 h; catalyst,  $\text{H}_4\text{PVMo}_{11}\text{O}_{40}$  (0.025 mmol).

b) The conversions in the blank experiments were 4.6 and 2.0 %, respectively.

Co- or Mn-substituted  $\text{PW}_{12}\text{O}_{40}^{3-}$  and  $\text{SiW}_{11}\text{O}_{39}\text{Ru}(\text{OH}_2)^{5-}$  are also effective catalysts for oxygenation of alkanes with alkyl hydroperoxides. The compounds catalyze the oxidation of alkanes such as cyclohexane and adamantane [67-69], and epoxidation of cyclohexene by with *t*-butyl hydroperoxide, iodosylbenzene potassium persulfate, and sodium periodate [68,70]. The reactivity depends on the kind of the transition metals. In the case of epoxidation of cyclohexene with iodosylbenzene, the order of catalytic activity of  $\text{PW}_{11}(\text{M})\text{O}_{39}^{5-}$  is  $\text{M} = \text{Co} > \text{Mn} > \text{Cu} > \text{Fe}, \text{Cr}$ .

A Ni-containing sandwich complex,  $\text{Ni}_3(\alpha\text{-PW}_9\text{O}_{39})_2$ , is a better catalyst than  $\text{PW}_{11}(\text{M})\text{O}_{39}^{5-}$  ( $\text{M} = \text{Co}, \text{Mn}$ ) for the formation of *N*-alkylacetamide from adamantane and isobutane by using *t*-butylhydroperoxide [71].

As for the mechanism of oxygenation of alkanes with oxygen donors such as iodosylbenzene and potassium persulfate, a mechanism in which oxygenation of metal centers by oxygen donor is followed by oxo transfer from transition metal to C-H bonds of alkanes has been proposed [16,67].

### 3.2 SKELETAL ISOMERIZATION OF *n*-BUTANE

Although the skeletal isomerization of straight-chain alkanes which is important for the enhancement of the octane number of gasoline is not the functionalization, this will be briefly mentioned, since the reaction contains the activation of C-H bond.

Table 3. Activity and selectivity for skeletal isomerization of *n*-butane at 573 K<sup>a</sup>

Catalyst	Rate <sup>b</sup>	Selectivity / mol% <sup>c</sup>					
		$\text{CH}_4$	$\text{C}_2\text{H}_6 + \text{C}_2\text{H}_4$	$\text{C}_3\text{H}_8 + \text{C}_3\text{H}_6$	Isobutane	$\text{C}_4\text{H}_8$	$\text{C}_5(+)$
$\text{Cs}_{2.5}\text{H}_{0.5}\text{PW}_{12}\text{O}_{40}$	2.0	1.1	2.0	8.5	83.1	0.8	4.2
$\text{H}_3\text{PW}_{12}\text{O}_{40}$	0.4	1.1	2.4	11.7	80.9	0	3.9
$\text{SO}_4^{2-}/\text{ZrO}_2$	0.4	3.1	9.1	23.0	60.8	0	4.0
H-ZSM-5	2.9	0.7	2.3	74.5	14.1	0.4	8.0
H-Y <sup>d</sup>	0.03	15.8	33.3	18.1	11.1	18.1	2.9

a) Reaction conditions: *n*-Butane 5 % ( $\text{N}_2$  balance), catalyst; 1 g, total flow rate; 10 ml min<sup>-1</sup>, W/F = 40 g h mol<sup>-1</sup>.

b) Rate of isobutane formation; 10<sup>-8</sup> mol g<sup>-1</sup> s<sup>-1</sup>.

c) C5(+); hydrocarbons containing more than 5 carbons.

d) 673 K.

$\text{Cs}_{2.5}\text{H}_{0.5}\text{PW}_{12}\text{O}_{40}$  catalyzes the isomerization of *n*-butane at 573 K, and the rate of isobutane formation and the selectivity was much higher than those of

$\text{SO}_4^{2-}/\text{ZrO}_2$ , as shown in Table 3 [72]. The initial activity of  $\text{SO}_4^{2-}/\text{ZrO}_2$  is very high, but the conversion decreases considerably during the initial stage of reaction. In contrast, the deactivation is relatively small for  $\text{Cs}_{2.5}\text{H}_{0.5}\text{PW}_{12}\text{O}_{40}$ . Deactivation was observed at 473–573 K, but not at 423 K. At temperatures below 473 K,  $\text{SO}_4^{2-}/\text{ZrO}_2$  is more active than  $\text{Cs}_{2.5}\text{H}_{0.5}\text{PW}_{12}\text{O}_{40}$ . The skeletal isomerization of alkanes catalyzed by metal-promoted heteropoly compounds is described in the later section.

#### 4. Metal-Heteropoly Bifunctional Catalysis. Enhancement of Catalytic Performance by Metal Additives

##### 4.1 OXIDATION OF LIGHT ALKANES

###### 4.1.1 Oxygenation

Table 4 summarizes the oxygenation and oxidative dehydrogenation of light alkanes with molecular oxygen catalyzed by various metal-added heteropoly compounds. The catalytic properties of  $\text{Cs}_{2.5}\text{H}_{0.5}\text{PMo}_{12}\text{O}_{40}$  changed by the addition of transition metal ions [56]. The addition of Ni, Mn, or Fe increased the yields of MAA and MAL. In the case of Ni, the yields of MAA and MAL reached 6.5 and 1.5%, respectively. In contrast, Co, Cu, Hg, Pt, and Pd decreased the yields.

*Table 4.* Heterogeneous oxidation of light alkanes with molecular oxygen catalyzed by molybdovanadophosphates combined with transition metal cations

Reactant	Product	Catalyst	Yield / %	Yield and catalyst in the literature / %
Isobutane	Methacrylic acid	Ni / $\text{Cs}_{2.5}\text{H}_{1.5}\text{PVMo}_{11}\text{O}_{40}$	9	6 (Mo-P-As-Cs-Cu-O)
Propane	Acrylic acid	Fe / $\text{Cs}_{2.5}\text{H}_{1.5}\text{PVMo}_{11}\text{O}_{40}$	13	11 (V-Te-O)
Methane	Formic Acid	Pd / $\text{Cs}_{2.5}\text{H}_{1.5}\text{PVMo}_{11}\text{O}_{40}$	0.05	$\approx 0$ (Fe-P-O)
Propane	Propene	Cu / $\text{Cs}_{2.5}\text{H}_{3.5}\text{PV3Mo}_9\text{O}_{40}$	10	4 (V-Nb-Mo-O)
Ethane	Ethene	Mn / $\text{Cs}_{2.5}\text{H}_{1.5}\text{PV3Mo}_9\text{O}_{40}$	5	4 (Mo-Nb-O)

a) In the presence of hydrogen; 573 K.

b) 653 K.

Keggin-type V-substituted heteropolymolybdates,  $\text{Cs}_{2.5}\text{Ni}_{0.08}\text{H}_{1.34}\text{PVMo}_{11}\text{O}_{40}$ , more selectively catalyzed the oxidation of isobutane into methacrolein and

methacrylic acid. At 613 K the yield of methacrylic acid reached 9.0%. This yield was greater than the highest value of 6.2% reported at likely steady-state in the patent literature [48,50,51]. Here, the role of vanadium is of interest.

It is also interesting that the reduced heteropoly compounds showed higher selectivities to methacrylic acid for the oxidation of isobutane [50,53,56]. Ueda et al. applied reduced 12-molybdophosphoric acid to the oxidation of propane and obtained 50% selectivity to acrylic acid plus acrolein at 12% conversion [73,74].

The direct oxidation of propane into acrylic acid was also attempted with the heteropoly compounds. Among the catalysts tested,  $\text{Cs}_{2.5}\text{Fe}_{0.08}\text{H}_{1.26}\text{PVMo}_{11}\text{O}_{40}$  gave the highest yield of acrylic acid of 13% [75,76]. It is noteworthy that the 13% yield is higher than 10.5% reported on  $\text{V}_2\text{O}_5\text{-P}_2\text{O}_5\text{-TeO}_2$  catalyst [77].

As for the oxidation of ethane, no selectively oxygenated products were observed [78]. Selective oxidation of methane did not proceed with molecular oxygen alone, either. However, when hydrogen was added in the feed as in the case of  $\text{FePO}_4$  catalyst [79], the oxidation of methane into formic acid was observed for  $\text{Cs}_{2.5}\text{Pd}_{0.08}\text{H}_{1.26}\text{PVMo}_{11}\text{O}_{40}$  catalyst (Table 4) [80]. It is noted that the reaction proceeded even at 423 K. The conversion of methane monotonously increased with an increase in the reaction temperature and reached a maximum at 573 K. The rate for the methane conversion at 573 K was  $1.2 \times 10^{-4}$ , ca.  $3 \times 10^2$  greater than that of the  $\text{FePO}_4$  catalyst [79]. The selectivity to formic acid was more than 67%. Such a high selectivity of formic acid formation has not been reported so far in heterogeneous oxidation of methane [81]. The highest yield of formic acid was obtained at 573 K.  $\text{Pd}_{0.08}\text{Cs}_{2.5}\text{H}_{1.34}\text{PVMo}_{11}\text{O}_{40}$  also catalyzed the oxidation of ethane into acetic acid under similar conditions.

#### 4.1.2 Oxidative Dehydrogenation

With respect to the equilibrium, the oxidative dehydrogenation is favorable, since it can achieve complete conversion of alkanes at low temperatures and high pressures in comparison with simple dehydrogenation [82].

The oxidative dehydrogenation of propane was efficiently catalyzed by the  $\text{Cs}_{2.5}\text{Cu}_{0.08}\text{H}_{3.34}\text{PV}_3\text{Mo}_9\text{O}_{40}$  catalyst precursor, which showed 10% yield of propene (the conversion and selectivity to propene were 40 and 25%, respectively) at the reaction temperature as low as 653 K [83]. The 10% yield of propene is higher than 3 - 6% obtained for various catalysts at the reaction temperature of 673 K [82,83]. The yield of propene was greatly influenced by the content of V and partial pressure of oxygen.

The oxidative dehydrogenation of ethane was also catalyzed by heteropoly compounds. The yield of ethene for  $\text{Cs}_{2.5}\text{Mn}_{0.08}\text{H}_{1.34}\text{PVMo}_{11}\text{O}_{40}$  catalyst was 2.0% at 623 K and reached 4.3% at 698 K. The space time yield of ethene for  $\text{Cs}_{2.5}\text{Mn}_{0.08}\text{H}_{1.34}\text{PVMo}_{11}\text{O}_{40}$  was  $1.2 \times 10^{-5} \text{ mol min}^{-1} \text{ g}^{-1}$  at the  $\text{C}_2\text{H}_6/\text{O}_2$  ratio of

9/1. The value is in the range of  $1 - 7 \times 10^{-5} \text{ mol min}^{-1} \text{ g}^{-1}$  reported for the most active Mo-V-Nb-O catalysts for the oxidative dehydrogenation of ethane [82].

Cavani et al. reported that Dawson-type mono-iron-substituted heteropolytungstates and Keggin-type heteropolymolybdates were active for the oxidative dehydrogenation of isobutane [84,85] and ethane [86], respectively. According to the authors, the rate per specific surface area of  $\text{K}_7\text{P}_2\text{W}_{17}\text{FeO}_{61}$  for the oxidative dehydrogenation of isobutane was higher than those of active catalysts which had been reported.

#### 4.2 SKELETAL ISOMERIZATION OF N-BUTANE

The combination of Pt or Pd with  $\text{Cs}_{2.5}\text{H}_{0.5}\text{PW}_{12}\text{O}_{40}$  is effective for skeletal isomerization of n-butane to isobutane as shown in Fig. 8 [87-89]. The reaction was accelerated by a factor of about four by the addition of 0.1 wt% Pt. The rate and selectivity were nearly independent of the loading level of Pt above 0.1 wt%. The activity in the presence of  $\text{H}_2$  little changed with time. Pt- and Pd- $\text{Cs}_{2.5}\text{H}_{0.5}\text{PW}_{12}\text{O}_{40}$  show very high selectivities (94-96%) as compared with Pt- $\text{SO}_4^{2-}/\text{ZrO}_2$  (47%) and Pt-H-ZSM-5 (34%), while the activities of Pt- and Pd- $\text{Cs}_{2.5}\text{H}_{0.5}\text{PW}_{12}\text{O}_{40}$  for the formation of isobutane are comparable to those of Pt-H-ZSM-5 and Pt- $\text{SO}_4^{2-}/\text{ZrO}_2$ . Pt- $\text{Cs}_{2.5}\text{H}_{0.5}\text{PW}_{12}\text{O}_{40}$  efficiently catalyzes the reaction even at 473 K if the partial pressure of  $\text{H}_2$  is as low as 0.05 atm.  $\text{H}_2$  suppresses the catalyst deactivation by hydrogenating coke or precursor of the coke.

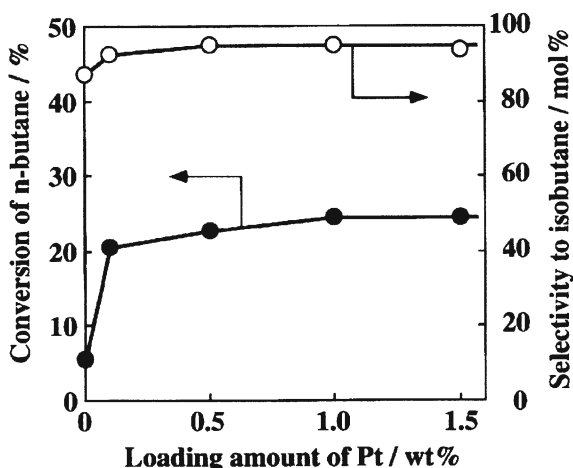


Figure 8. Effect of loading amount of Pt on n-butane isomerization over Pt- $\text{Cs}_{2.5}\text{H}_{0.5}\text{PW}_{12}\text{O}_{40}$ . (I); conversion of n-butane, (m); selectivity to isobutane. Feed gas; n-butane:  $\text{H}_2 : \text{N}_2 = 0.05 : 0.50 : 0.45$ , catalyst; 1 g, W/F = 40 g h (n-butane-mol) $^{-1}$ . Catalysts were pretreated with  $\text{O}_2$  at 573 K.

It was indicated that the high selectivity to isobutane for Pt-Cs<sub>2.5</sub>H<sub>0.5</sub>PW<sub>12</sub>O<sub>40</sub> is brought about by an unique role of protons which suppresses dramatically the hydrogenolysis and enhance the isomerization. In the absence of proton, the butenes or butyl group formed on Pt react with hydrogen to result in hydrogenolysis, while in the presence of proton, the butenes or butyl group interact with protons probably at the interface of Pt and Cs<sub>2.5</sub>H<sub>0.5</sub>PW<sub>12</sub>O<sub>40</sub> to form a butyl carbenium ion which is the intermediate for the skeletal isomerization.

## 5. Conclusion

The present results demonstrate that (1) the efficient oxidation and isomerization of light alkanes are possible by utilizing heteropoly compounds, (2) the catalytic performance is enhanced by selecting the countercations and addenda atoms, and (3) the oxidizing ability, acidity, and the soft basicity of polyanion are the key factors controlling the catalytic functions.

## 6. Future Opportunities

(1) The catalysis of *di*- or *tri*-metal-substituted polyoxometalates [90] is interesting not only to understand the action of iron- or copper-containing biomolecules but also to design an active catalyst for the alkane oxidation. (2) Enhancement of acid strength as well as the control of the soft basicity facilitate the alkane activation and the stabilization of products. (3) Further development of micro/meso porous materials containing polyanions or related to heteropoly compounds is expected. These materials will concentrate light alkanes in the pores and promote the selective catalysis.

## 7. Acknowledgment

This work was supported by the Grant-in-aid in priory area from the Ministry of Education, Culture, Sports and Science.

## 8. References

1. Olah, G., Prakash, G. K. S., and Summer, J. (1985) *Superacids*, Wiley, New York.
2. Olah, G., Prakash, G. K. S., William, R. E., Field, L. D., and Wade, K. (1987) *Hydrocarbon Chemistry*, Wiley, New York.

3. Shilov, A. E. (1984) *Activation of Saturated Hydrocarbons by Transition Metal Complexes*, Dordrecht, D. Reidel Pub.
4. Mansuy, D. (1987) *Pure Appl. Chem.* **59**, 759; Crabtree, R. H. (1995) *Chem. Rev.* **95**, 987; Kurtz, Jr. D. M. (1990) *Chem. Rev.* **90**, 585; Vincent, J. B., O-Lilley, G. L., and Averill, B. A. (1990) *Chem. Rev.* **90**, 1447.
5. Periana, R. A., Taube, D. J., Evitt, E. R., Loffler, D. G., Wentrcek, P. R., Voss, G., and Masuda, T. (1993) *Science* **259**, 340.
6. Larson, L. G., and Hall, W. K. (1965) *J. Phys. Chem.* **69**, 3080.
7. Robertson, P. J.; Scurrall, M. S., and Kemball, C. (1974) *J. Chem. Soc., Faraday Trans. I* 903.
8. Russel, G. A. (1992) *The Chemistry of Alkanes and Cycloalkanes* Wiley, New York.
9. Billups, W. E., Konarski, M. M., Hauge, R. H., and Margrave, J. L. (1980) *J. Am. Chem. Soc.* **102**, 7393.
10. Ozin, G. A., and MacCaffrey, J. G. (1982) *J. Am. Chem. Soc.* **104**, 7351; Ozin, G. A., McIntosh, D. F., and Mitchell, S. A. (1981) *J. Am. Chem. Soc.* **103**, 1574.
11. Parnis, J. M., and Ozin, G. A. (1986) *J. Am. Chem. Soc.* **108**, 1699; (1988) *J. Phys. Chem.* **92** 3959.
12. Kao, L. C., Huston, A. C., and Sen, A. (1991) *J. Am. Chem. Soc.* **113**, 700; Basicakes, N., Hogan, T. E., and Sen, A. (1996) *J. Am. Chem. Soc.* **118**, 13111.
13. Tsigdinos, G. A. (1978) *Topics Curr. Chem.* **76**, 1.
14. Pope, M. T. (1983) *Heteropoly and Isopoly Oxometalates*, Springer Verlag, Berlin; Pope, M. T., and Müller, A. (1991) *Angew. Chem. Int. Ed. Engl.* **30**, 34; (1994) *Polyoxometalates: From Platonic Solids to Anti-Retroviral Activity*, Kluwer, Dordrecht.
15. Mizuno N., and Misono M. (1997) *Chem. Rev.* submitted; Okuhara, T., Mizuno, N., and Misono, M. (1996) *Adv. Catal.* **41**, 113; Mizuno N., and Misono M. (1994) *J. Mol. Catal.* **86**, 319; Misono, M., (1993) *Proc. 10th Int. Congr. Catal., Budapest, 1992*, Elsevier, Amsterdam, p. 69; Misono, M. (1987) *Catal. Rev.-Sci. Eng.* **29**, 269; (1988) **30**, 339.
16. Reviews of oxidation of alkanes catalyzed by heteropoly compounds: Hill, C. L. (1989) *Activation and Functionalization of Alkanes*, Wiley, New York, p 243; Moffat, J. B. (1996) *Appl. Catal. A: General* **146**, 65.
17. Baraza, L., and Pope, M. T. (1975) *J. Phys. Chem.* **79**, 92; Izumi, Y., Matsuo, K., and Urabe, K. (1983) *J. Mol. Catal.* **18**, 299.
18. Keggin J. F. (1934) *Proc. Roy. Soc. A* **144**, 75.
19. Brown, G. M., Noe-Spirlet, M. R., Busing, W. R., and Levy, H. A. (1977) *Acta Crystallogr., Ser. B* **33**, 1038.
20. Baker, L. C. W. (1973) *Proc. XV Int. Conf. Coord. Chem.*, Moscow.
21. Kozhevnikov, I. V. (1987) *Russ. Chem. Rev.* **56**, 811.



22. Hu, C., Hashimoto, M., Okuhara, T., and Misono, M. (1993) *J. Catal.* **143**, 437; Okuhara, T., Hu, C., Hashimoto, M., and Misono, M. (1994) *Bull. Chem. Soc. Jpn.* **67**, 1186.
23. Polotebnova, N. A., Kozlenko, A. A., and Furtune, L. A. (1976) *Russ. Inorg. J. Chem.* **21**, 1511; Kozhevnikov, I. V., Kulikov, S. M., and Matveev, K. I. (1980) *Izv. Akad. Nauk SSSR, Ser Khim.*, 2213; Kulikov, S. M., and Kozhevnikov, I. V. (1981) *Izv. Akad. Nauk SSSR, Ser Khim.*, 498.
24. Furuta, M., Sakata, K., Misono, M., and Yoneda, Y. (1979) *Chem. Lett.*, 31.
25. (a) Otake, M., and Onoda, T. (1975) *Catalysts and Catalysis* **7**, 13. (b) Kapustin, G. I., Brueva, T. R., Klyachko, A. L., Timofeeva, M. N., Kulikov, S. M., and Kizhevnikov, I. V. (1990) *Kinet. Katal.* **31**, 1017.
26. (a) Okuhara, T., Nishimura, T., Watanabe, H., and Misono, M. (1992) *J. Mol. Catal.* **74**, 247. (b) Misono, M., and Okuhara, T. (1993) *CHEMTECH* **23**, 23.
27. Gillespie, R. J. (1968) *Acc. Chem. Res.* **1**, 202; Olah, G. A., Prakash, G. K. S., Sommer, J. (1985) *Superacids*, John Wiley & Sons, New York.
28. Okuhara, T., Nishimura, T., Watanabe, H., Na, K., and Misono, M. *Acid-Base Catalysis II*, Kodansha, Tokyo-Elsevier, Amsterdam, 1994; p. 419; Na, K., Iizaki, T., Okuhara, T., and Misono, M. (1997) *J. Mol. Catal.* **115**, 449.
29. Nishimura, T., Watanabe, H., Okuhara, T., and Misono, M. (1991) *Catalysts and Catalysis* **33**, 420
30. Nishimura, T., Okuhara, T., and Misono, M. (1995) *Chem. Lett.* 155.
31. Alternau, S. L., Pope, M. T., Prados, R. A., and So, H. (1975) *Inorg. Chem.* **2**, 417.
32. Kozhevnikov, I. V., and Matveev, K. I. (1983) *Appl. Catal.* **5**, 135.
33. (a) Mizuno, N., Watanabe, T., and Misono, M. (1985) *J. Phys. Chem.* **89**, 80. (b) Mizuno, N. unpublished results.
34. Matsumoto, H., Lee, K. Y., and Misono, M. (1991) *61st National Meeting of The Chemical Society of Japan*. Tokyo.
35. Cadot, E., Marchal-Roch, C., Fournier, M., Tézé, A., and Hervé, G. (1994) *Polyoxometalates: From Platonic Solids to Anti-Retroviral Activity*, Kluwer, Dordrecht, p. 315.
36. Bayer, R., Marchal, C., Liu, F. X., Tézé, A., and Hervé, G. (1996) *J. Mol. Catal. A: Chemical* **110**, 65; Marchal-Roch, C., Bayer, R., Moisan, J. F., Tézé, A., and Hervé, G. (1996) *Top. Catal.* **3**, 407.
37. Zuremcki, S. B. (1988) *Proc. 9th Int. Congr. Catal.* vol. 4, p. 1798.
38. Serwicka, E. M., Bruckman, K., Haber, J., Paukshtis, E. A., and Yurchenko, E. N. (1991) *Appl. Catal.* **73**, 153.
39. Bruckman, K., Haber, J., and Serwicka, E. M. (1988) *Faraday Disc. Chem. Soc.* **87**, 173.



40. Taouk, T., Ghoussoub, D., Bennani, A., Crusson, E., Rigole, M., Aboukais, A., Decressain, R., Fournier, M., and Guelton, M. (1992) *J. Chim. Phys.* **89**, 435.
41. Baraza, L., and Pope, M. T. (1975) *J. Phys. Chem.* **79**, 92; Izumi, Y., Matsuo, K., and Urabe, K. (1983) *J. Mol. Catal.* **18**, 299.
42. Knoth, W. H., and Harlow, R. L. (1984) *Inorg. Chem.* **23**, 4765.
43. Lee, K. Y., Mizuno, N., Okuhara, T., and Misono, M. (1989) *Bull. Chem. Soc. Jpn.* **62**, 1731.
44. Lee, K. Y., Arai, T., Nakata, S., Asaoka, S., Okuhara, T., and Misono, M. (1992) *J. Am. Chem. Soc.* **114**, 2836.
45. Lee, K. Y., Kanda, Y., Mizuno, N., Okuhara, T., Misono, M., Nakata, S., and Asaoka, S. (1988) *Chem. Lett.* 1175.
46. Hirano, Y., Inumaru, K., Okuhara, T., and Misono, M. (1996) *Chem Lett.* 1111.
47. Kanda, K., Lee, K. Y., Nakata, S., Asaoka, S., and Misono, M. (1988) *Chem. Lett.* 139.
48. Krieger, H., and Kirch, L. S. (1979) Rhom and Haas Co., *Eur. Patent* No. 0010902.
49. Centi, G., Burtini, M., and Trifiro, F. (1987) *Appl. Catal.* **32**, 353; J. B. Moffat (1996) *Appl. Catal.* **146**, 65.
50. Imai, H., Yamaguchi, T., and Sugiyama, M. (1988) Asahi Chemical Industry Co., *JP* 145249.
51. Nagai, K., Nagaoka, Y., Sato, H., and Osu, M. (1991) Sumitomo Chemical Co., *JP* 106839.
52. Centi, G., Nieto, J. L., Iapalucci, C., Bruckman, K., and Serwicka, E. M. (1989) *Appl. Catal.* **46**, 197; Cavani, F., Etienne, E., Favaro, M., Galli, A., Trifiro, F., and Hecquet, G. (1995) *Catal. Lett.* **32**, 215.
53. Mizuno, N., Tateishi, M., and Iwamoto, M. (1994) *J. Chem. Soc. Chem. Commun.* 1411.
54. Mizuno, N., Tateishi, M., and Iwamoto, M. (1994) *Appl. Catal. A: General* **118**, L1.
55. Mizuno, N., Han, W., Kudo, T., and Iwamoto, M. (1996) *Stud. Surf. Sci. Catal.* **101**, 1001.
56. Mizuno, N., Tateishi, M., and Iwamoto, M. (1996) *J. Catal.* **163**, 87.
57. Cavani, F., Etienne, E., Favaro, M., Galli, A., Trifiro, F., and Hecquet, G. (1995) *Catal. Lett.* **32**, 215.
58. Lyons, J. E., Ellis, P. E., and Durante, V. A. (1991) *Structure-Activity and Selectivity Relationships in Heterogeneous Catalysis*, Elsevier, Amsterdam, p. 99.
59. Mizuno, N., Tateishi, M., Hirose, T., and Iwamoto, M. (1994) *J. Mol. Catal.* **88**, L125.

60. Mizuno, N., Tateishi, M., Hirose, T., and Iwamoto, M. (1993) *Chem. Lett.* 2137.
61. Kitajima, N., Fukui, H., and Moro-oka, Y. (1988) *J. Chem. Soc., Chem. Commun.* 485; Kitajima, N., Itoh, M., Fukui, H., and Moro-oka, Y. (1991) *J. Chem. Soc., Chem. Commun.* 102; Murahashi, S., Oda, Y., and Naota, T. (1992) *J. Am. Chem. Soc.* **114**, 7913; Barton, D. H. R., Gastiger, M. J., and Motherwell, W. B. (1983) *J. Chem. Soc., Chem. Commun.* 731.
62. Lau, T.-C., and Mak, C.-K. (1993) *J. Chem. Soc., Chem. Commun.* 766; Khan, M. M. T., Chatterjee, D., Kumar S, S., Rao, A. P., and Khan, N. H. (1992) *J. Mol. Catal.* **75**, L49.
63. Neumann R., Khenkin, A. M., and Dahan, M. (1995) *Angew. Chem. Int. Ed. Engl.* **34**, 1587.
64. Seki, Y., Mizuno, N., and Misono, M., *Appl. Catal.* (1997) in press.
65. Kao, L. C., Huston, A. C., and Sen, A. (1991) *J. Am. Chem. Soc.* **113**, 700.
66. Lin, M., and Sen, A. (1994) *Nature*, **368**, 613; Nelson, K. T., and Foger, K. (1994) *Natural Gas Conversion II*, Elsevier, New York, p. 545; Kurioka, M., Nakata, K., Teturo, J., Taniguchi, Y., Takai, K., and Fujiwara, Y. (1995) *Chem. Lett.* 244; Nakata, K., Miyata, T., Yamaoka, Y., Taniguchi, Y., Takai, K. and Fujiwara, Y. (1994) *Natural Gas Conversion II*, Elsevier, New York, p. 521; Nishiguchi, T., Nakata, K., Takai, K., and Fujiwara, Y. (1992) *Chem. Lett.* 1141.
67. Faraj, M., and Hill, C. L. (1987) *J. Chem. Soc., Chem. Commun.* 1487.
68. Neumann, R. and A.-Gnim, C. (1989) *J. Chem. Soc., Chem. Commun.* 1324.
69. Matsumoto, Y., Asami, M., Hashimoto, M., and Misono, M. (1996) *J. Mol. Catal. A:Chemical* **114**, 161.
70. Hill, C. L., and Brown, R. B., Jr. (1986) *J. Am. Chem. Soc.* **108**, 536; Neumann, R., and A.-Gnim, C. (1990) *J. Am. Chem. Soc.* **112**, 6025.
71. Faraj, M., Lin, C. -H., and Hill, C. L. (1988) *New J. Chem.* **12**, 745.
72. Na, K., Nakata, S., Okuhara, T., and Misono, M. (1995) *J. Chem. Soc. Faraday Trans.* **91**, 367.
73. Ueda, W., Suzuki, Y., Lee, W., and Imaoka, S. (1996) *Stud. Surf. Sci. Catal.* **101**, 1065.
74. Ueda, W., and Suzuki, Y. (1995) *Chem. Lett.* 541.
75. Mizuno, N.; Tateishi, M., and Iwamoto, M. *Appl. Catal. A: General* **1995**, 128, L165.
76. Mizuno, N., Han, W., and Kudo, T. *J. Mol. Catal. A:Chemical* **1996**, 114, 309.
77. Ai, M. (1986) *J. Catal.* **101**, 389.
78. Mizuno, N., Han, W., and Kudo, T. (1996) *Chem. Lett.* 1121.
79. Wang Y. and Otsuka, K. (1995) *J. Catal.* **155**, 256.
80. Mizuno, N., Ishige, T. Seki, Y., Misono, M., Suh, D.-J., Han, W., and Kudo, T. (1997) *Chem. Commun.*, in press.

81. Pitchai, R., and Klier, K. (1986) *Catal. Rev.-Sci. Eng.* **28**, 13; Gesser, H. D. Hunter, N. R., and Prakash, C. B. (1985) *Chem. Rev.* **85**, 235; Hutchings, G. J. Scurrrell, M. S. and Woodhouse, J. R. (1989) *Chem. Soc. Rev.* **18**, 251; Srivastava, R. D., Zhou, P., Stiegel, G. J., Rao, V. U. S., and Cinquegrane, G. (1992) *Catalysis* (London) **9**, 1993; Fierro, J. L. G. (1993) *Catal. Lett.* **22**, 67; Crabtree, R. H. (1995) *Chem. Rev.* **95**, 987; Axelrod, M. G., Gaffney, A. M., Pitchai, R., and Sofranko, J. A. (1994) *Natural Gas Conversion II*, Elsevier, New York, p. 93; Srivastava, R. D., Gollakota, S. V., Stiegel, G. J., and Bose, A. C. (1995) *Methane and Alkane Conversion Chemistry*, Plenum, New York, p. 291.
82. Kung, H. H. (1994) *Adv. Catal.* **40**, 1; Mamedov, E. A., and Corberan, V. C. (1995) *Appl. Catal., A: General* **127**, 1.
83. Mizuno, N., and Suh, D.-J. (1996) *Appl. Catal.* **146**, L249.
84. Cavani, F., Comuzzi, C., Dolcetti, G., Etienne, E., Finke, R. G., Selleri, G., Trifiro, F., and Trovarelli, A. (1996) *J. Catal.* **160**, 317.
85. Comuzzi, C., Dolcetti, G., Trovarelli, A., Cavani, F., Trifiro, F., Llorca, J., and Finke, R. G. (1996) *Catal. Lett.* **36**, 75.
86. Albonetti, S., Cavani, F., Trifiro, F., and Koutyrev, M. (1995) *Catal. Lett.* **30**, 253.
87. Na, K., Iizaki, T., Okuhara, T., and Misono, M. (1997) *J. Mol. Catal.* **115**, 449.
88. Na, K., Okuhara, T., and Misono, M. (1993) *J. Chem. Soc., Chem. Commun.* 1422.
89. Na, K., Okuhara, T., and Misono, M. (1995) *Catalytic Science and Technology II*, Kodansha Tokyo Elsevier, Amsterdam, p. 245.
90. Zhang, X.-Y., O'Connor, C. J., Jameson, G. B., and Pope, M. T. (1996) *Inorg. Chem.* **35**, 30.

## ALKANE ACTIVATION BY PSEUDO-METALS

G. DJÉGA-MARIADASSOU

*Université Pierre et Marie Curie, CNRS URA 1106,*

*Laboratoire Réactivité de Surface, Case 178*

*4, Place Jussieu, 75252 Paris Cedex 05, France*

### 1. Introduction

Early transition metals (groups 4 to 6) do not catalyze hydrocarbon conversion reactions but their nitrides and carbides are found to behave like precious metals. In the case of *clean tungsten carbide surfaces* (i.e. free of surface oxygen and polymeric carbon) prepared at high temperature (HT) (870 to 1070 K), catalytic dehydrogenation and hydrogenolysis reactions of alkanes and hydrogenation of alkenes are observed [1, 2]. More generally, early transition metal carbides and nitrides are good catalysts for reactions characteristic of noble metals. *Chemisorption of oxygen* modifies the surface properties of carbides or nitrides [1-4.] Chemisorbed oxygen inhibits hydrogenolysis [1, 2] and introduces acidic isomerization function on tungsten carbide surfaces [1, 2]. It appears that oxygen-exposed tungsten carbides possess a *bifunctional* surface that catalyzes both dehydrogenation and carbenium ion reactions typically occurring on reforming catalysts [3]. These findings are not unique to tungsten carbides and depend on the preparation of materials.

Carbides and Nitrides (HT) containing oxygen *in the bulk* can be prepared at high temperature [5-7]. These compounds are called "oxy"nitrides and "oxy"carbides. They clearly present a bifunctional surface that catalyzes both (de)hydrogenation, isomerization of hydrocarbons, hydrodenitrogenation and hydrodesulfurization (removal of nitrogen and sulfur from nitrogen-or-sulfur-containing molecules, respectively). A new class of bifunctional bulk "oxy"-catalysts has appeared whose reactivity depends upon their chemical composition.

In contrast, a finely divided molybdenum oxide treated at low temperature (LT) (620 K) by flowing  $H_2/n$ -alkane mixture was found to introduce carbon atoms in vacancies of the oxide and to lead to "oxycarbides" of molybdenum able to catalyze *n*-alkanes reactions according to a monofunctional pathway [8].

As clean carbides or nitrides of early transition metals behave in catalysis similarly to noble metals, *catalysis by metal remains a general guideline* for developing systematic studies on these new catalytic materials.

Bulk materials prepared at high temperature can be considered as interstitial alloys obtained by *insertion* of nitrogen and/or carbon in the lattice of the transition metal. Special features such as *interchangeability* between surface carbon, nitrogen, sulfur and oxygen make these materials still more interesting for reforming and hydrotreating reactions such as HDN and HDS.

Carbon seems to confer a more noble metal behaviour ([de]hydrogenation function) to the transition metal, and *oxycarbonitrides* can be prepared, leading to a wide range of chemically controlled compounds. Bimetallic materials are also studied [9].

*Bifunctional* properties open a new field of application of (oxy)carbides and (oxy)nitrides which can be considered as a new class of acidic (may be basic) compounds. They can be also supported on oxides, zeolites or carbon.

The concept of "*dual sites*" linked to the proximity of acidic and metallic sites have been proposed for bulk nitrides or carbides [7, 10]. The classification of these acidic sites in a quantitative scale of solid acidity strength remains to be done. The chemical structure of both metallic and acidic sites, the oxidation state of the transition metal, the metallic character of nitrides and carbides, the structure sensitivity of reactions on these materials, the activation of dihydrogen and basic reactants are still in progress.

The evolution of the main catalytic properties with the metallic and/or "acidic" character of the transition metal (for instance the acidic niobium behaviour compared to that of molybdenum or tungsten) also remains to be studied.

This paper will shortly review some of the preceding topics and mainly discuss about activation of alkanes on fresh or oxygen-exposed pseudo-metals prepared at low or high temperature.

## **2. Crystal structure of (oxy)nitrides and (oxy)carbides of early transition metals**

Table 1 presents for molybdenum, tungsten and niobium, some crystallographic data which will help us to understand the evolution of their metallic properties. Once N or C is introduced into the body-centered cubic (*bcc*) lattice of the transition metal, an hexagonal closed packed (*hcp*) or face-centered cubic (*fcc*) structure occurs where N or C atoms are located in the octahedral interstitial sites of the *hcp* or *fcc* structure.

Table 1. Crystal structure of Mo, W and Nb high temperature phases

Metal	Carbide or oxycarbide			Nitride or oxynitride	
	<i>bcc</i>	<i>hcp</i>	<i>hex</i>	<i>fcc</i>	<i>hex</i>
Mo		$\beta\text{-Mo}_2\text{C}$	MoC	$\alpha\text{-MoC}_{1-x}$ [a]	$\gamma\text{-Mo}_2\text{N}$ $\text{MoN}_x\text{O}_y$ $\text{MoC}_x\text{O}_y$
W		$\beta\text{-W}_2\text{C}$	$\alpha\text{-WC}$	$\beta\text{-WC}_{1-x}$ [a]	$\beta\text{-W}_2\text{N}$ $\delta\text{-WN}$
Nb				NbC <i>NaCl</i> - type [b]	$\delta\text{-NbN}$ <i>NaCl</i> - type [b]

[a] With  $x$  near from 0.5 and defined as *fcc*  $\beta\text{-W}_2\text{C}$  by Ribeiro *et al.* [11]

[b] This structure is based on the *fcc* lattice with both the metal atoms and carbon atoms forming *fcc* sub-lattices

Figure 1 reports the NaCl-like structure for a bifunctional oxycarbonitride of molybdenum-type where both metal and C (or N or O) atoms are ordered according to a *fcc* lattice. Gouin *et al.* [12] have shown that these structures are non-stoichiometric ones, vacancies being considered in the metal sub-lattice. Furthermore, chemical analysis of oxynitride shows that stoichiometry can be near from 0.8 molybdenum atom for 1 (N or C) atom. These products lack molybdenum atoms and preserve the X-ray diffraction pattern of the *fcc*  $\gamma\text{-Mo}_2\text{N}$ . A review of these structures have been made by Oyama [39].

Fresh carbides (HT) powders were also found to have stoichiometric surfaces that lack W metallic sites [1].

Table 2 shows, for niobium compounds, the evolution of the lattice parameter  $a_0$  which is rising according to the following order : metal < nitride < carbide.

Table 2. Lattice parameter for cubic niobium compounds [7, 13]

Compound		Lattice parameter $a_0$ (pm)
Nb	<i>bcc</i>	330.6
NbN	<i>fcc</i>	439.2
NbC	<i>fcc</i>	447.0

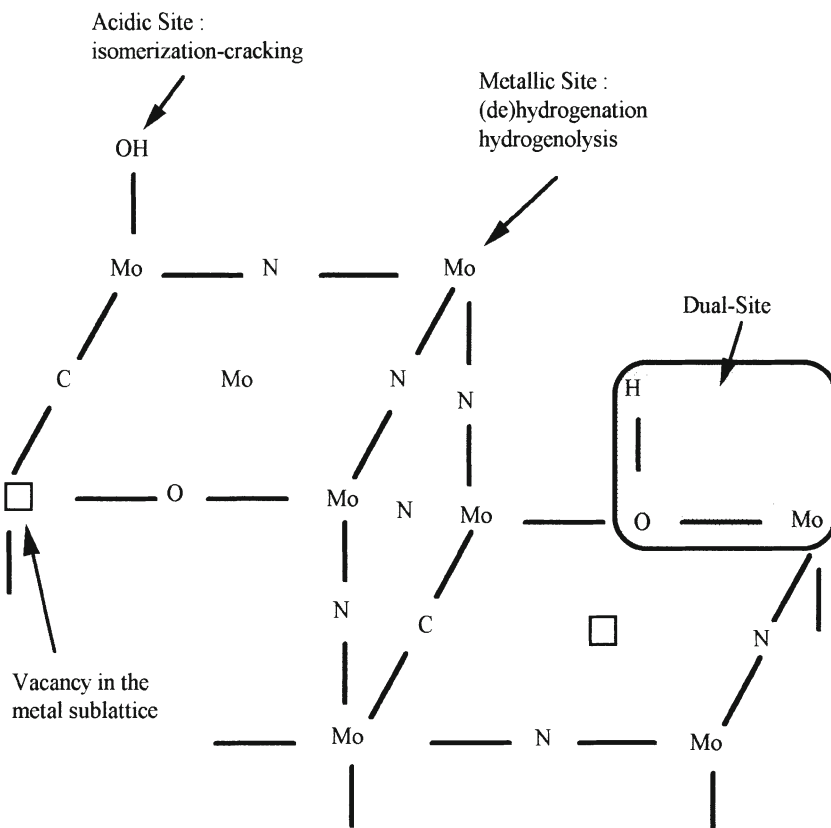


Figure 1. The bifunctional *fcc* model for an oxycarbonitride of molybdenum where C, N, O are located in the octahedral sites of the *fcc* structure (Non-stoichiometric oxycarbonitride)

Why nitrides or carbides catalyze reactions characteristic of precious metal catalysts can be first explained qualitatively. The introduction of C or N atoms in the lattice of an early transition metal leads to an increase of its lattice parameter  $a_0$  (Table 2). Simultaneously, according to the quantum-mechanical theory, the width of the d band of the transition metal decreases as  $1/a_0^5$  [14]. Hence the d electron density of the transition metal after carburization or nitridation becomes higher at the Fermi level and properties shift towards those of metals on the right of the Periodic Table, that is towards precious metals as shown in Table 3.

Table 3. Groups 4 to 10 transition metals in the Periodic Table

Group	4	5	6	7	8	9	10
	<b>Ti</b>	<b>V</b>	Cr	Mn	Fe	Co	Ni
	Zr	<b>Nb</b>	<b>Mo</b>	Tc	<b>Ru</b>	<b>Rh</b>	<b>Pd</b>
	Hf	<b>Ta</b>	<b>W</b>	Re	<b>Os</b>	<b>Ir</b>	<b>Pt</b>

Eberhart and MacLauren [14] recently reported the results of full-potential-linear-augmented-slater-type-orbital (FLASTO) band calculations on the early transition metal monocarbides. They demonstrated that the origin of the compounds properties is due to the hybridization of carbon p-orbitals with metal d-orbitals. One carbon p-electron participates in s-bonding and two carbon p-electron in  $\pi$ -bonding, the result of this hybridization being an electronic structure near the Fermi level energy which is similar to that of a *fcc* metal three or four elements to the right of the Periodic Table. As all electrons are involved in bonding, the band near the Fermi energy is metallic in character. It is this band which is responsible for the catalytic properties of the monocarbides. Table 4 reports from reference [14] the results of full quantum mechanical calculations to place the Fermi energy with respect to the metal d-band.

Table 4. Fermi energy with respect of the metal d-band. Expected metal-like behaviour.

	Fermi Energy	Metal-like Density of State (DOS)
TiC	below the d-band	Tc or Re
WC	near the center of the d-band	Ru, Rh
NbC	similarly placed relative to the d-band	Ru, Rh
WC	Top of the d-band	Pd, Pt

### 3. Preparation of nitrides, carbides, oxynitrides and oxycarbides of early transition metals

#### 3.1 HIGH TEMPERATURE PHASES

The first preparation of nitride powders, starting from metal oxides, followed Volpe and Boudart's work [15]. A general method for preparing *high surface area* nitrides and carbides is reported in a patent by Boudart *et al.* [16]. Most of



the preparations presented in this section are derived from this general method [11, 15, 17-20].

Nitridation is proceeded by flowing ammonia, and carburization by flowing a  $\text{CH}_4/\text{H}_2$  mixture. As reactivity of carbides and nitrides strongly depend on their preparation, oxygen treatment and surface composition, emphasis will be given here on the materials whose activity in alkane activation will be discussed in the next sections.

### 3.1.1 Preparation of high surface area nitrides

High specific surface area nitrides can be prepared by nitridation of oxide precursors. Temperature-programmed reaction between  $\text{MoO}_3$ ,  $\text{WO}_3$ ,  $\text{Nb}_2\text{O}_5$ ,  $\text{TiO}_2$  with  $\text{H}_3\text{N}$  provides a way to prepare  $\text{Mo}_2\text{N}$ ,  $\text{W}_2\text{N}$  [15],  $\text{NbN}$  [6] and  $\text{TiN}$  [5] powders, with specific surface areas as high as  $220 \text{ m}^2\text{g}^{-1}$  for  $\text{Mo}_2\text{N}$ . The transformation of the oxide to the nitride can be topotactic as in the case of  $\text{Mo}_2\text{N}$ . Bulk oxynitride intermediates exist. Details are reported in the above references.

### 3.1.2 High surface area carbides : $\alpha\text{-WC}$ and $\beta\text{-W}_2\text{C}$ (or $\beta\text{-WC}_{1-x}$ fcc) "fresh" powders.

Two procedures can be used leading to these two different materials.

*Carburization of a nitride* [17].  $\beta\text{-W}_2\text{C}$  can be prepared by converting first  $\text{WO}_3$  to  $\beta\text{-W}_2\text{N}$  by exposing the oxide to  $\text{NH}_3$  ( $60 \text{ mmol s}^{-1}$ ) at 700K and increasing the temperature from 700K to 1000K.  $\beta\text{-W}_2\text{C}$  is then prepared by carburizing  $\beta\text{-W}_2\text{N}$  with an 80%  $\text{CH}_4$ /20%  $\text{H}_2$  (Pd-diffused) mixture ( $100 \text{ mmol s}^{-1}$ ) as the sample is heated from 700 to 1050K at  $8.3 \text{ K s}^{-1}$ . To remove polymeric carbon, a treatment is applied consisting of flowing  $\text{H}_2$  over the samples at 973K during 2h. As a result, the polymeric carbon reacts with  $\text{H}_2$  to form  $\text{CH}_4$ . Following this procedure, these samples free of oxygen and of polymeric carbon will be called "Fresh samples".

*Direct carburization of the oxide.* Ribeiro *et al.* [1] have reported a new procedure for the preparation of high surface area stoichiometric  $\alpha\text{-WC}$ .  $\text{WO}_3$  is heated in helium to 1100K and then exposed to an 80%  $\text{CH}_4$ /20%  $\text{H}_2$  mixture ( $100 \text{ mmol s}^{-1}$ ) at 1100K for 6h. Polymeric carbon is removed by flowing hydrogen at 973K for 1 h. In these conditions  $\alpha\text{-WC}$  formed reproducibly. Following this procedure, the samples will be called "fresh samples". A well documented study on  $\text{WO}_3$  carburization has been published recently [20].

Keller [10] prepared equivalent fresh samples called "In Situ Samples" (ISS). The precursor is the ammonium paratungstate  $(\text{NH}_4)_6\text{H}_2\text{W}_{12}\text{O}_{40}$ . The carburization is done by flowing pure methane during a temperature

programmed reaction ( $2.5 \text{ K min}^{-1}$ ) to 1123K, remaining at 1123K for 30 min. This material is protected by an amorphous carbon layer [18]. It is then pretreated before catalytic run by flowing pure hydrogen at 1023K for 15 min.

### ***3.1.3 Carbides exposed to oxygen at room temperature (RT) or at $T < 800\text{K}$ for a short time (0.25 h)***

These materials will be identified as WC/O-T or  $\beta\text{-W}_2\text{C/O-T}$  for WC or  $\beta\text{-W}_2\text{C}$  phases exposed to oxygen, where T is the exposure temperature.

The effect of chemisorbed oxygen on catalytic and chemisorptive properties can be studied by exposing fresh carbides first to oxygen at RT (see "passivation" section) then at higher temperatures such as 700, 800K. A treatment in flowing hydrogen at 673K for 1h is necessary before any chemisorption or catalytic run measurement. Depending on the time of treatment, carbides may retain only chemisorbed oxygen or suffer a bulk oxidation.

### ***3.1.4 Carbides exposed to oxygen at higher temperatures for a short time (a few minutes)***

Keller [10] also studied WC samples exposed to oxygen at 973K for a few minutes. This sample will be noted WC/O-973K(few min). It still corresponds to a surface "chemisorbed" oxygen species.

### ***3.1.5 Carbides exposed to oxygen at 973K for 4-5 h.***

Powders denoted WC/O-973K,5h were studied [10]: they correspond to a deeper oxidation of the carbides and will behave differently as it will be seen later.

### ***3.1.6 Other high temperature carbide preparations***

Niobium nitride can be carburized according to the same procedure [21]

Niobium carbide was also prepared by direct carburization of  $\text{Nb}_2\text{O}_5$  mixed with beads of a commercial  $\text{NiMo/Al}_2\text{O}_3$  catalyst [13] to lower the temperature of carburization.

Titanium carbide TiC was prepared by direct carburization of  $\text{TiO}_2$  (Degussa P25) by a 4vol% $\text{CH}_4/\text{H}_2$  at 1220 K [5].

Sellem *et al.* [22] started from two polyanionic compounds  $(\text{NH}_4)_6\text{H}_2\text{W}_{12}\text{O}_{40}$  and  $(\text{NH}_4)_6\text{P}_2\text{W}_{18}\text{O}_{62}$  as precursors in the standard procedure of Volpe and Boudart. The last compound permitted to investigate the effect of phosphorus on reactivity.

Typical specific surface areas are given in Table 5. Oxycompounds generally present a lower surface area than compounds with no oxygen in the bulk.

Table 5. Specific surface areas ( $S_g$ ), determined by the BET method, for some high temperature materials

Compounds	$S_g/\text{m}^2\text{g}^{-1}$	References
1. $\text{Mo}_2\text{N}$	220	15
2. $\text{W}_2\text{N}$	91	15
3. $\alpha\text{-MoC}_{1-x}$	190	17
4. $\beta\text{-W}_2\text{C}$	100	1
5. $\beta\text{-WC}_{1-x}$	30	1
6. $\text{MoN}_x\text{O}_y$	200	23
7. $\text{MoN}_{0.7}\text{O}_{0.7}$	110	24
8. $\text{MoN}_{0.14}\text{C}_{0.27}\text{O}_{0.76}$	75	24
9. $\text{NbN}_{0.91}\text{O}_{0.98}$	80	6
10. $\text{NbC}_{1.0}\text{O}_{0.0}$	50	7
11. $\text{TiN}_x\text{O}_y$	46	5
	61 to 87	25
12. $\text{TiC}$	20	25

### 3.2 LOW TEMPERATURE PHASES : INSERTION OF CARBON ATOMS IN VACANCIES OF PARTIALLY REDUCED $\text{MoO}_3$ AT 623 K [8] LEADS TO NEW ACTIVE PHASES

#### 3.2.1 Carburation of an oxidized molybdenum carbide.

A molybdenum carbide ( $\text{Mo}_2\text{C}$ ) is first prepared at high 1500 K by reaction between  $\text{MoO}_3$  vapor and a high surface area carbon [26, 27]. Before catalytic run the carbide is oxidized under flowing air ( $15 \text{ cm}^3 \text{ min}^{-1}$ ) at 623 K for 14 h, to oxidize the surface of the carbide and form a " $\text{Mo}_2\text{C}$ -oxygen-modified-material". The X-Ray diffraction pattern of this material mainly presents the

Mo<sub>2</sub>C lines and a small contribution of MoO<sub>3</sub>, indicating that only a thin surface layer of Mo<sub>2</sub>C is oxidized to MoO<sub>3</sub>.

This material is then submitted to an activation by flowing an hydrogen-hydrocarbon (*n*-hexane or heptane or octane) mixture at 623 K for 7 h. This treatment leads to an *active oxycarbide phase*. This solid only shows peaks of Mo<sub>2</sub>C, probably due to the too thin oxycarbide phase deposited at the surface. The very high dispersion does not permit a detection by X-Ray diffraction. Nevertheless this oxycarbide presents a "chevron" structure to HRTEM.

### 3.2.2 Carburation of a molybdenum oxide

A "*MoO<sub>3</sub>-carbon-modified*" catalyst was also prepared directly by flowing the same hydrogen-hydrocarbon (*n*-hexane or heptane or octane) mixture at 623 K for 7 h. After 3h reaction all MoO<sub>3</sub> was transformed to MoO<sub>2</sub> mixed with another unidentified phase considered to be the active "oxycarbide".

High specific surface area carbides of silicon and transition metals were also prepared by Ledoux and Pham-Huu [28] by reaction of metal oxide vapors with solid carbon.

## 4. Passivation step and percentage of oxygen in bulk materials

The pyrophoric character of nitrides and carbides is quite similar to that of highly dispersed metals after reduction. For samples stored in air after preparation, passivation have to be done to avoid bulk oxidation.

Materials are passivated by flowing 1 vol.%O<sub>2</sub> in He. Pulses of oxygen can be used to control this passivation step [1, 10].

Bulk chemical formula such as MoN<sub>0.7</sub>O<sub>0.7</sub>[24] or NbN<sub>1.14</sub>O<sub>0.82</sub> [7] were obtained. Such powders containing substantial amounts of oxygen, (possibly as a result of the passivation), are called (oxy)nitrides. "Passivation" of carbides can be done by multilayers of polymeric carbon [18] [29].

The presence of oxygen in the bulk of solids during the preparation of nitrides when oxides are used as precursors have been documented [30]. The high oxygen content observed for the passivated sample 7 (Table 5) MoN<sub>0.7</sub>O<sub>0.7</sub> could suggest that an X-ray amorphous MoO<sub>2</sub> phase is present in spite of the fact that no MoO<sub>2</sub> XRD peaks were detected. Nevertheless, this material presents the X-ray pattern of  $\gamma$ -Mo<sub>2</sub>N face-centered cubic (*fcc*) structure, and calculation on stoichiometry led us to consider sample 7 as an homogeneous bulk oxynitride rather than a mixture of amorphous MoO<sub>2</sub> with  $\gamma$ -Mo<sub>2</sub>N. Such a conclusion has been done by Boudart and Oyama for Mo<sub>2</sub>C [31]. Samples 6 and 7 (Table 5) are both passivated samples whose compositions indicate the presence of oxygen in the bulk. But comparison of their respective specific surface area, - 200 and 110 m<sup>2</sup>g<sup>-1</sup> -, emphasizes the importance of controlling

the passivation : for sample 6 admittance of oxygen in the reactor after preparation was done very slowly with a low partial pressure of oxygen relatively to sample 7. Ribeiro *et al.* [2] exposed fresh tungsten carbides to oxygen at room temperature, leaking oxygen into the cell of  $0.1 \text{ mmol s}^{-1} \text{ g}^{-1}$  for a 0.1 - 0.3 g sample and a  $70 \text{ cm}^3$  cell volume. In this case oxygen uptake was only about one monolayer at room temperature.

## 5. Determination of site density by hydrogen, oxygen, CO and nitrogen chemisorption.

Metallic site density can be measured by hydrogen, CO, oxygen or nitrogen specific chemisorption. Table 6 reports equivalent data from different authors, for *in situ* powders.

Table 6. Number density for irreversibly chemisorbed species at RT /  $10^{15} \text{ cm}^{-2}$

	Clean WC <sup>[a]</sup>	In Situ Sample <sup>[b]</sup>
CO	0.39	0.53
H	0.37	0.56
N <sup>[c]</sup>	0.34	0.05 <sup>[d]</sup>
O	1.39	1.30

<sup>[a]</sup> Ribeiro et al.[1] Fresh WC

<sup>[b]</sup> Keller [10]

<sup>[c]</sup> Temperature Programmed Desorption of  $\text{NH}_3$  adsorbed at RT

<sup>[d]</sup> using  $\text{N}_2$

$10^{15} \text{ cm}^{-2}$  is equivalent to 1 monolayer

## 6. Metallic function: Interchangeability between C, N and O atoms in the lattice of nitrides and carbides

As previously discussed on the origin of the metallic behaviour of nitrides and carbides compared to that of precious metals, the exchange of nitrogen atoms by carbon ones, in the lattice of a nitride, is expected to bring it a stronger metallic function. This partial "carburization" of the nitride can occur during a catalytic reaction. Let us consider first the effect on the hydrogenating function.

## 6.1 HYDROGENATING FUNCTION

The enhancement of propylbenzene hydrogenation to propylcyclohexane, over  $\text{MoN}_{0.75}\text{O}_{0.55}$  at 540K, is a nice example of the process [24]. Without any previous carburization, Figure 2 shows the strong deactivation of  $\text{MoN}_{0.75}\text{O}_{0.55}$  during its first run at 540K. This deactivation is due to a very strong chemisorption of propylbenzene on the oxynitride surface [24]. Carburization of the catalyst by the reactive mixture (1wt% propylbenzene in cyclohexane) during the reaction under 50 bars of hydrogen, at 720K for 10 h, completely suppressed the deactivation process : a drastic modification of propylbenzene chemisorption on the surface of this carburized nitride has occurred, leading to 100% conversion at 540K. This modification of catalytic behaviour by partial carburization was checked over the same nitride after its direct carburization by flowing  $\text{CH}_4/\text{H}_2$  in the already defined standard conditions. Fig. 2 reports the corresponding plot obtained during its first run over what can then be considered as an "oxycarbonitride of molybdenum" ( $\text{MoN}_x\text{C}_y\text{O}_z$ ).

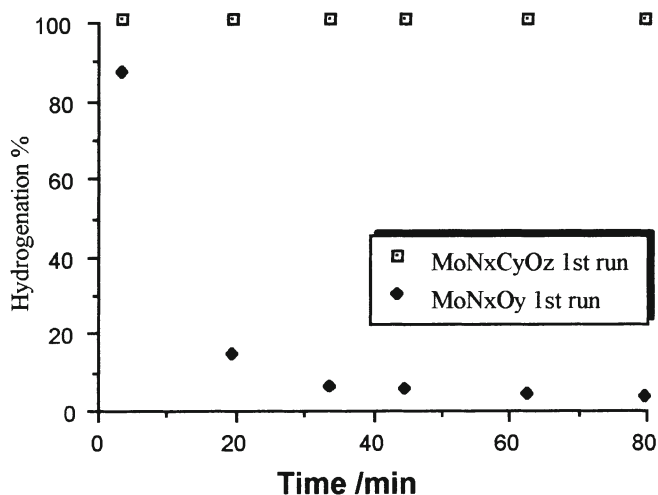


Figure 2. Hydrogenation of 1 wt% propylbenzene /cyclohexane ; T = 540 K ; 5 MPa hydrogen

The effect of substituting nitrogen atoms by carbon ones is thus clearly shown. It probably corresponds to a drastic change in the chemisorptive properties of the solid, leading to a not too much stable surface intermediate (adsorbed propylbenzene) as required by Sabatier's Principle. A stronger

hydrogenating function of the catalyst is thus induced. This carbon effect also agrees with the data from catalytic reactions on  $\beta$ -W<sub>2</sub>C,  $\beta$ -W<sub>2</sub>N, and WC [1] as it will be seen in the next section.

## 6.2 NEOPENTANE HYDROGENOLYSIS

Neopentane hydrogenolysis is a molecular probe reaction of metallic property of carbides. Ribeiro *et al.* [1] have shown that tungsten carbides with WC and  $\beta$ -W<sub>2</sub>C structures catalyze neopentane hydrogenolysis with turnover rates  $v_t$  similar to those on Ru catalysts. Table 7 shows that "fresh" WC is quite active compared to Ru/Al<sub>2</sub>O<sub>3</sub>. Furthermore, WC (stoichiometry : 1/1) compared to  $\beta$ -W<sub>2</sub>C (stoichiometry: 2/1) presents a stronger metallic activity in hydrogenolysis which can be linked to its higher content in carbon. This tendency confirms the data obtained with other molecular probe reactions.

Table 7. Steady-state turnover rates for neopentane hydrogenolysis on "fresh" tungsten carbides (9.8 kPa neopentane, 95 kPa H<sub>2</sub>)

Catalysts	$v_t^a / 10^{-4} \text{ s}^{-1}$
	Fresh carbides <sup>b</sup> (490K)
$\beta$ -W <sub>2</sub> C	10
WC	300
0.5%Ru/Al <sub>2</sub> O <sub>3</sub> c	85

<sup>a</sup> Turnover rates ( $v_t$ ) based on site densities measured by irreversible CO chemisorption at RT.

<sup>b</sup> "Fresh" carbides are materials treated by H<sub>2</sub> at 973K to remove polymeric carbon produced during carburization of the precursor.

<sup>c</sup> Supported Ru catalyst was used in catalytic comparison with tungsten carbides. Data from Reference [1].

## 7. *n*-Alkane activation on high temperature carbides and nitrides

### 7.1 *n* - HEXANE HYDROGENOLYSIS WITH HIGH SELECTIVITY OVER FRESH WC AND $\beta$ -W<sub>2</sub>C FREE OF POLYMERIC CARBON AND RESIDUAL SURFACE OXYGEN

No isomers were detected (Table 8) suggesting that these materials have no isomerization surface function. Ribeiro *et al.* [2] have shown that hydrogenolysis products desorb readily without re-adsorption and secondary hydrogenolysis steps after desorption. Muller *et al.* [32] found that on a clean tungsten carbide the products of hydrogenolysis of 2-methylpentane, *n*-hexane and methylcyclopentane can be accounted for by successive C-C bond breaking. For 2-methylpentane a single C-C bond breaking leads to *n*-pentane which can undergo other cleavage to give *n*-butane etc... The same activities are observed over both WC and  $\beta$ -W<sub>2</sub>C.

Table 8. *n*-Hexane reaction on fresh tungsten carbides (6.1 kPa *n*-hexane, 94.9 kPa H<sub>2</sub>) [2]

Initial products	WC	$\beta$ -W <sub>2</sub> C
C <sub>1</sub>	27	23
C <sub>2</sub>	17	18
C <sub>3</sub>	15	18
<i>n</i> C <sub>4</sub>	18	18
<i>n</i> C <sub>5</sub>	23	23

Conversion % were 3.6 and 3.5 at 428 and 425 K respectively for WC and  $\beta$ -W<sub>2</sub>C.

C<sub>1</sub> : methane, C<sub>2</sub> : ethane, C<sub>3</sub> : propane, *n*-C<sub>4</sub> : *n*-butane, *n*-C<sub>5</sub> : *n*-pentane.

### 7.2 CHEMISORBED OXYGEN INHIBITS NEOPENTANE HYDROGENOLYSIS AND INTRODUCES ISOMERIZATION FUNCTION ON TUNGSTEN CARBIDE SURFACES

Hydrogenolysis of neopentane is drastically inhibited by chemisorbed oxygen at room temperature (RT) as can be seen Table 9, but an isomerization function on tungsten carbide surface is introduced.

It is quite remarkable that the fresh WC catalyzes hydrogenolysis with a turnover rate similar to that on Ru, one of the most active metals in hydrogenolysis of hydrocarbons.



Table 9. Turnover rates  $v_t / s^{-1}$  [33]

	WC fresh,	0.5%/Ru/Al <sub>2</sub> O <sub>3</sub>	WC/O-RT <sup>(a)</sup>
Temperature	490K	490K	580K
Hydrogenolysis	0.03	0.0085	0.0004
Isomerization	0	0	0.00005 <sup>(b)</sup>

<sup>(a)</sup> O<sub>2</sub>-exposed at room temperature (RT)<sup>(b)</sup>  $v_t$  based upon CO chemisorption

Detailed product distribution for neopentane reaction over tungsten carbide exposed to controlled pulses of oxygen are given in Table 10 [10]

Table 10. Product distribution for neopentane reaction at 623 K (1.3 kPa neopentane, 99 kPa hydrogen)

	Total conversion %	Isomerization %	Hydrogenolysis %				
			C <sub>1</sub>	C <sub>2</sub>	C <sub>3</sub>	iC <sub>4</sub>	iC <sub>5</sub>
In situ sample without oxygen	100	0	100	0	0	0	0
O <sub>2</sub> first pulse	19.8	0	52.4	39.8	3.9	3.8	-
O <sub>2</sub> 2 <sup>nd</sup> pulse	3.57	1	63.9	19.1	0.8	14.9	1.1

These results are in quite good agreement with those of Ribeiro [33] as hydrogenolysis remains predominant at 623 K. Oxygen drastically lowers the total conversion of neopentane, even if it does not need acidic sites to isomerize. These results mean that metallic sites disappear by oxygen exposure.

### 7.3 SURFACE OXYGEN ALSO INHIBITS CO AND HYDROGEN CHEMISORPTION, AND HYDROGENOLYSIS OF *n*-HEXANE

Table 11 shows that when a fresh carbide sample is exposed to oxygen at different temperatures, hydrogenolysis drastically diminishes, with a simultaneous rising of the residual oxygen content. As CO and hydrogen titrate metallic sites (WC<sub>x</sub>), WC<sub>x</sub> surface concentration is drastically lowered when fresh carbides are exposed to oxygen. As will be shown later, WC<sub>x</sub> species

transform to  $\text{WO}_x$  acidic sites. Table 10 shows that isomerization is simultaneously rising in the case of *n*-hexane.

Table 11. Hydrogenolysis of *n*-hexane(520 K, 6.1 kPa  $n\text{-C}_6$ , 95 kPa  $\text{H}_2$ ) [33]

	WC fresh	WC/O-RT	WC/O-700 K
Site-time yield / $10^{-3} \text{ s}^{-1}$			
Hydrogenolysis	340	1.7	0.9
Isomerization	0	10.4	102
Residual oxygen / $10^{15} \text{ cm}^{-2}$	0.12	0.61	2.67
Site density/ $10^{15} \text{ cm}^{-2}$	0.39	0.11	0.045
$\text{Sg/m}^2 \text{ g}^{-1}$	31	32	26

#### 7.4 EFFECT OF OXYGEN ON HYDROGEN DISSOCIATIVE CHEMISORPTION [10]

In situ WC samples, without oxygen, were found to dissociate  $\text{H}_2$  at 77K. Keller has evidenced that chemisorbed oxygen highly enhances the temperature of dihydrogen dissociation, as shown by  $\text{H}_2/\text{D}_2$  exchange. It was found that the temperature of dissociation of  $\text{H}_2$  depends on the amount of chemisorbed oxygen ; furthermore, the oxygen-modified WC does not hydrogenate butene.

Iglesia *et al* [34] showed that *n*-hexane hydrogenolysis rates increase linearly with increasing  $\text{WC}_x$  site density titrated by CO and hydrogen chemisorption.

### 8. Depending on the preparation and the nature of materials, is alkane isomerization over oxygen-modified carbides a monofunctional or a bifunctional catalysis ?

As the main objective of the chapter concerns light alkane activation, the section will gather data for a given alkane. These alkanes can also be used as molecular probes for testing the surface properties of materials.

The main conclusion of this section will be that on the surface of tungsten carbides,  $\text{WC}_x$  and  $\text{WO}_x$  can be considered as metallic and acidic sites respectively [34].

8.1 *n*-HEPTANE REACTION

Two monofunctional pathways can be considered via C<sub>5</sub>-ring and metallacyclobutane intermediates. In order to decide which route is mainly followed by the reactant-catalyst system, it is necessary to detail the product distribution for each pathway.

8.1.1 *Monofunctional isomerization.*

Let us consider first if C<sub>5</sub>-ring hydrogenolysis pathways occurs for *n*-heptane isomerization over tungsten carbides. Hydrogenolysis C<sub>5</sub>-ring intermediate is characteristic of monofunctional highly dispersed platinum.

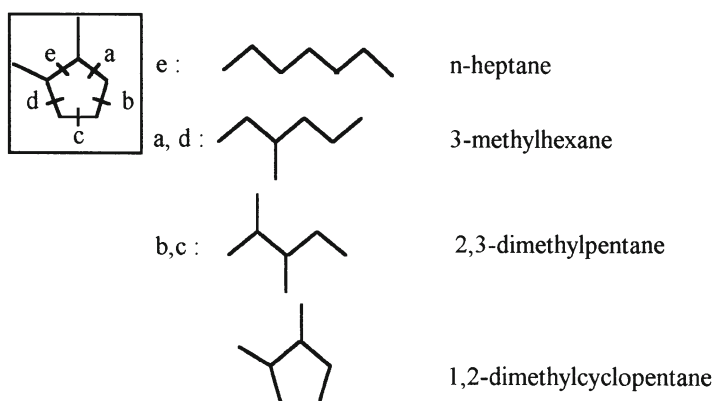


Figure 3: C-5 ring (1,2-dimethylcyclopentane) intermediate pathways for *n*-heptane reaction

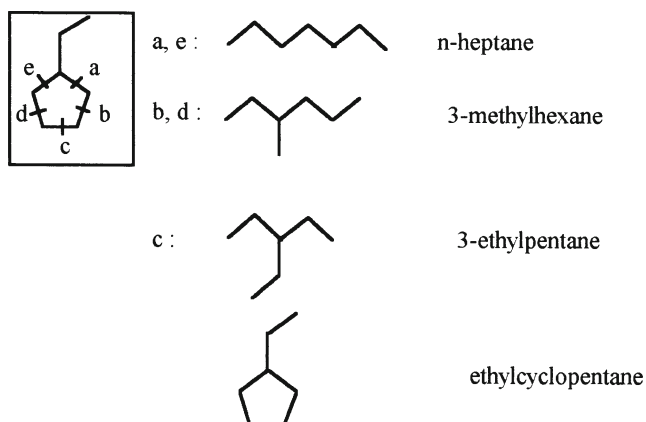


Figure 4 : C<sub>5</sub> ring (ethylcyclopentane) intermediate pathways for *n*-heptane reaction

Figures 3 and 4 shows that ring closure of *n*-heptane leads to C<sub>5</sub>-ring intermediate on the metallic site. No carbenium ion is formed and characteristic products of these pathways are: 3-methylhexane, predominant product; 2,3-dimethylpentane (which does not exist in bifunctional pathways) ; 1,2-dimethyl cyclopentane or ethylcyclopentane can be predicted. No 2-methylhexane can be formed.

A good example for C<sub>5</sub>-ring hydrogenolysis is given by *n*-heptane reaction over Pt/SiO<sub>2</sub> [2] (Table 12) where the characteristic products can be well identified. Pt/SiO<sub>2</sub> is often used as reference for well-dispersed noble metal on non-acidic support, that is as a monofunctional catalyst.

Table 12. *n*-heptane reaction over 0.78% Pt/SiO<sub>2</sub> at 623 K. (4.4 kPa *n*-heptane, 96 kPa H<sub>2</sub>. Total conversion : 10.5%).

C1	0.78	Bz	1.1
C2	1.1	2-MH	0.75
C3	8.2	3-MH	6.5
iC4	0.65	2,3-DMP	3.3
nC4	3.6	DMP	0.45
iC5	0.0	EP	2.2
nC5	3.5	ECP	19.2
iC6	0.4	1,2-DMCP	23.7
nC6	2.0	MCH	0.8
		TOL	23.7
		Heptene	3.8

C1: methane; C2: ethane; C3: propane; iC4: isobutane; nC4: *n*-butane; iC5: isopentane; nC5: *n*-pentane; iC6: isohexane; nC6: *n*-hexane; Bz: benzene; MH: methylhexane; DMP: dimethylpentane; EP: ethylpentane; ECP: ethylcyclopentane; DMCP: dimethylcyclopentane; MCH: methylcyclohexane; TOL: toluene.

As can be seen the main characteristic products described in Figures 3 and 4 are predominant : 3-methylhexane, 2,3-dimethylpentane. Cyclic compounds corresponding to the C<sub>5</sub>-ring intermediates are observed : ethylcyclopentane, 1,2-dimethylcyclopentane and also toluene. 2-Methylhexane remains at a very low concentration.

### 8.1.2 Pathway for bifunctional isomerization : carbenium ion and methyl shift process

The passivation step, as well as oxygen treatment at higher temperatures, induces acidic properties [1,2]. The traditional molecular probe reaction for testing the bifunctionality of catalysts is the isomerization of *n*-pentane [35].

The classical sequence of elementary steps over noble metals supported on acidic oxides is shown on Fig. 5. In the present case, the same scheme can apply, the "metallic site" being the transition metal promoted by nitrogen or carbon atoms, and the acidic sites being probably Brönsted sites as shown on Fig. 1.

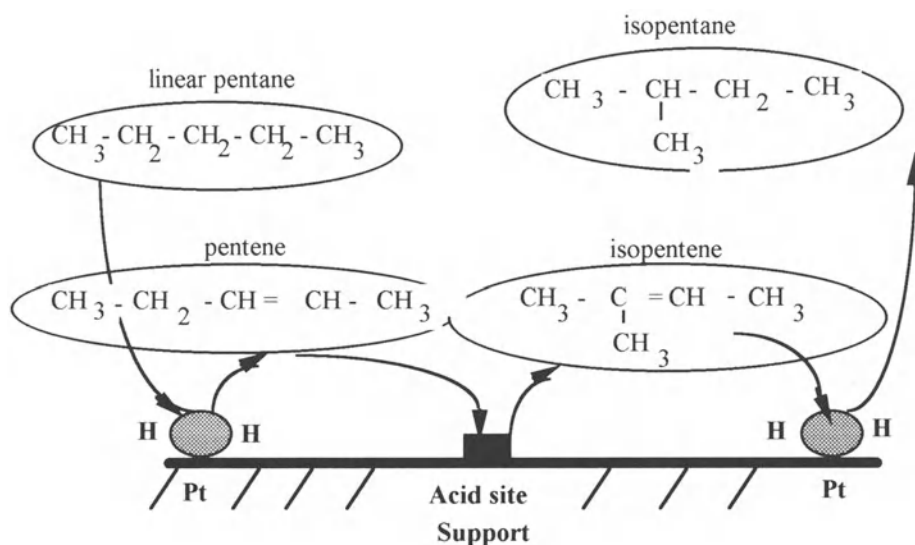


Figure 5. Bifunctional reaction over precious metal supported catalyst : elementary steps for *n*-pentane isomerization to isopentane

The main differences between, for instance, Pt supported on  $\text{SiO}_2\text{-Al}_2\text{O}_3$  (or Zeolite) and oxynitrides or oxycarbides, remain in the strength of the hydrogenating and acidic functions and in the atomic distance between the two kinds of sites. In the case of precious metal supported catalysts, the intermediate *alkene* (Fig. 5) has to migrate from the metallic site to the acidic one through the gas phase.

In the case of oxynitride or oxycarbide, a concept of "dual site" can be considered as shown on Fig. 1 where metallic and acidic sites are side by side.

As for precious metal supported catalysts the following functions can be envisaged for each kind of sites:

$\text{WC}_x$  can be considered as the metallic sites.  $\text{WO}_x$  are metal-oxo sites but can be potential Brönsted sites.

## Metallic site

- (De) hydrogenation
- Hydrogenolysis

## Acid site

- Isomerization
- Cracking

A methyl-shift mechanism associated with the formation of carbenium ion (as will be shown later for *n*-hexane (Fig.8 ), will produce the following main products for the *n*-heptane reaction on a bifunctional surface .

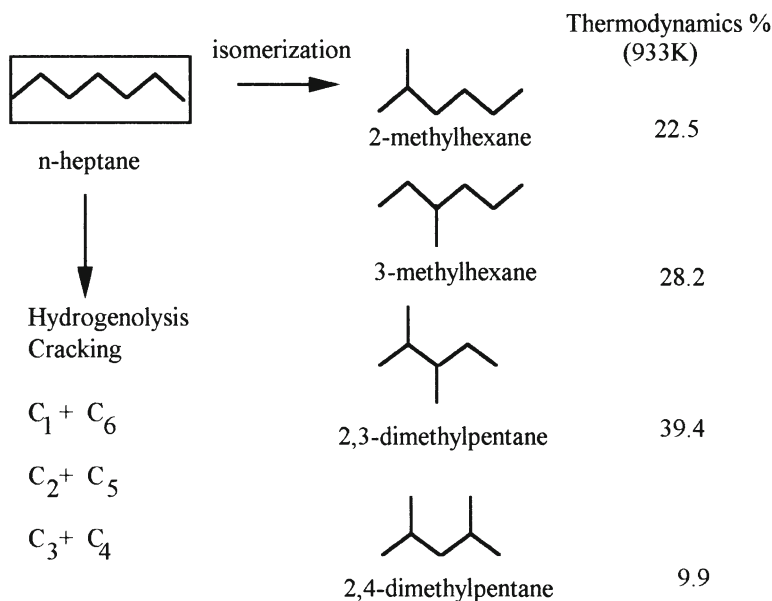


Figure 6. Product distribution for *n*-heptane bifunctional isomerization pathways

### 8.1.3 Results and discussion

Table 13 reports the product distribution for *n*-heptane reactions over three different oxygen-exposed tungsten carbides. WC/O-973 K (few min) (chemisorbed oxygen species) and WC/O-973 k (4h)(bulk oxygen) are both samples treated at high temperature, the first one for a short time, the second for 4 h.  $\beta$ -W<sub>2</sub>C/O-700 K for 0.25 h.

Comparison between Ribeiro *et al* data [1], and Keller's ones [10] shows that oxygen-exposed carbides do not follow the C<sub>5</sub>-ring mechanism.

As can be seen WC/O-973 K (few min) behaves like fresh carbide of Ribeiro *et al.*, (Table 8) producing mainly hydrogenolysis. For the two other carbides, these two works show that hydrogenolysis and isomerization are the

predominant *n*-heptane reactions over oxygen-modified tungsten carbides. Toluene selectivities are only about 0.37 % and other cyclization products : alkylcyclopentanes, methylcyclohexane account for less than 1 % of the converted *n*-heptane. 2-Methylhexane and 3-methylhexane are also produced at similar rates on WC/0-800 K. Therefore *n*-heptane isomerization does not occur via C<sub>5</sub>-ring hydrogenolysis because such reaction pathways are unable to form 2-methylhexane isomers as initial products. Furthermore, the 2-methylhexane/3methylhexane ratio is equal to 0.92-0.94, independent of contact time and conversion. All heptenes (1-heptene, *cis*,*trans*-2-heptene and 3-heptene) quickly reach steady-state concentrations suggesting their potential role as reactive intermediate in *n*-heptane isomerization. Ribeiro *et al.* showed that the heptene/heptane ratio presents its equilibrium values at 623 K. Thus it appears that hydrocarbon dehydrogenation-hydrogenation reactions are fast and do not limit overall reaction rates in the bifunctional dehydrogenation / isomerization sequence.

Table 13. Main products distribution for *n*-heptane reactions over WC/0-973 K, few min [10], WC/0-973 K, 4h [10], and  $\beta$ -W<sub>2</sub>C /0-700 K, 0.25 h [2]

	WC/0-973 K few min [a]	WC/0-973 K, 4h [a]	$\beta$ -W <sub>2</sub> C/0-700 K [b]
	Products %	Products %	Products %
2-MH		28.0	33.3
3-MH		27.9	35.2
C <sub>1</sub>	9.7	1.0	2.9
C <sub>2</sub>	28.2	1.9	2.3
C <sub>3</sub>	25.3	1.3	2.8
<i>n</i> -C <sub>4</sub>	16.0	8.6	2.9
<i>n</i> -C <sub>5</sub>	13.2	4.7	3.8
<i>n</i> -heptenes	-	-	3.7
toluene			0.37

[a] 623 K, 0.7 kPa *n*-heptane, 100.3 kPa H<sub>2</sub>

[b] 623 K, 4.4 kPa *n*-heptane, 96 kPa H<sub>2</sub>.

*n*-Heptane data over oxygen-exposed tungsten carbides finally show [2] that alkane dehydrogenation on WC<sub>x</sub> sites is quasi equilibrated whereas isomerization rates are limited by subsequent "WO<sub>x</sub>" catalyzed rearrangement of alkene intermediates. The absence of methylcyclopentane intermediates

suggests that isomerization pathways do not involve cyclic intermediates and, in contrast with Pt, these materials lack a catalytic cyclization functionality.

*n*-Hexane reactions on a fresh or on a tungsten carbide exposed to oxygen at low temperature for a short time, will confirm these results obtained on the *n*-heptane for carbides prepared at high temperature.

## 8.2 *n*-HEXANE REACTION

*n*-Hexane is a molecular probe which presents some differences with *n*-heptane product distribution. C<sub>5</sub>-ring and bifunctional mechanism will be first presented.

### 8.2.1 *n* - Hexane isomerization via C<sub>5</sub>-ring intermediate hydrogenolysis pathway

*n*-Hexane is a less interesting molecular probe because the predicted products for *n*-hexane isomerization are the same for both the bifunctional route with methyl bond shift and C<sub>5</sub>-ring hydrogenolysis pathways (monofunctional characteristic of well-dispersed platinum).

C<sub>5</sub>-ring hydrogenolysis can be considered to occur according to the following scheme:

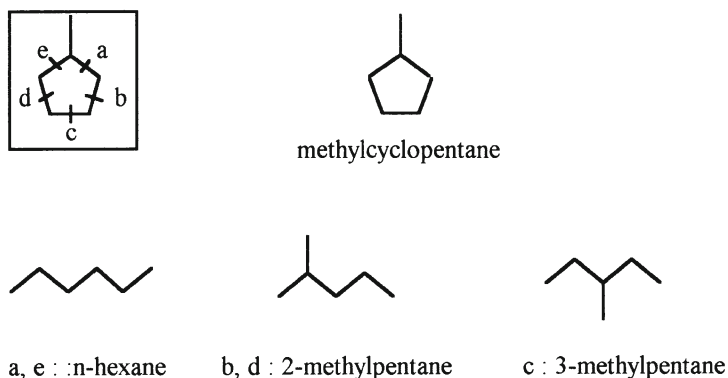


Figure 7. C<sub>5</sub>- ring intermediate pathways for *n*-hexane reaction

The model predicts a thermodynamic 2-methylpentane/3-methylpentane ratio of 2:1.

Table 14 [10] reports data on a fresh clean WC prepared *in situ*. Data are in good agreement with the predicted products previously presented.



Table 14. Product distribution for methylcyclopentane hydrogenolysis over a "clean WC in situ sample" of WC without oxygen at 523 K. (0.46 kPa methylcyclopentane)[10]

cyclopentane	0.25
n-hexane	0.08
2-methylpentane	0.39
3-methylpentane	0.28

No cycle enlargement

A good example is given by the *n*-hexane isomerization over 0.5 Pt/SiO<sub>2</sub> [33], as well as over an "in situ clean sample" prepared by Keller [10], (even if the methylcyclopentane is not found to be an intermediate for the *n*-hexane reaction). For the same conversion, Table 15 clearly permits to observe the 2/1 ratio for 2-methylpentane/3-methylpentane over both catalysts, but methylcyclopentane does not form over  $\beta$ -W<sub>2</sub>C.

Table 15. Product distribution for n-hexane isomerization over 0.5 wt % Pt/SiO<sub>2</sub>, at 622 K, compared to that over  $\beta$ -W<sub>2</sub>C/0-700 K [2].

	0.5 % Pt/SiO <sub>2</sub>	$\beta$ -W <sub>2</sub> C/0-700 K
Dimethylbutane	-	1.4
2-methylpentane	34.0	55.2
3-methylpentane	13.5	26.8
methylcyclopentane	33.1	-
Total conversion % (Isomerization Hydrogenolysis )	+ 6.8	5.4

As no methylcyclopentane is observed (as it is the case with Pt/SiO<sub>2</sub>, 33.1 %) it can be considered that the isomerization route does not involve cyclic C<sub>5</sub> intermediates characteristic of the monofunctional mechanism.

These data show the different behaviour of  $\beta$ -W<sub>2</sub>C which behaves like a bifunctional material, whose reaction intermediates are carbenium ions, unable to give methylcyclopentane.

### 8.2.2 The bond shift mechanism for a bifunctional pathway

Figure 8 reports the main steps for the bond shift mechanism for *n*-hexane isomerization over bifunctional tungsten carbides. It is equivalent to the scheme on Figure 5. In this model, the isomerization of the carbenium ion adsorbed on an acid site is the rate determining step. If it is the case over oxygen-exposed carbides, the rate of isomerization can be predicted to increase with the acid site

concentration. Table 15b shows that the isomerization Site-Time-Yield increase, in agreement with the predicted behaviour.

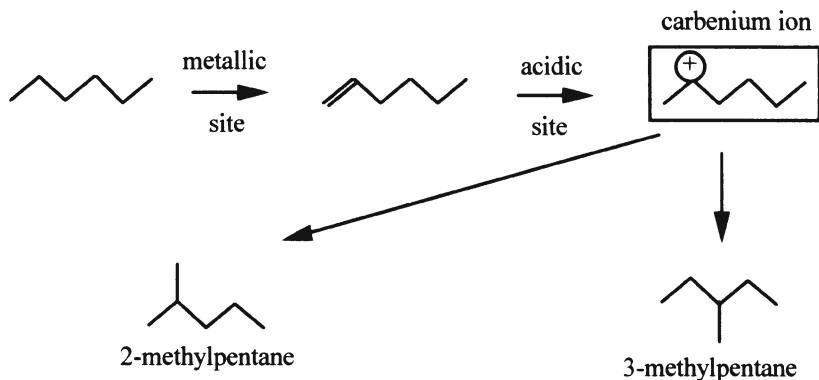


Figure 8. *n*-hexane isomerization over a bifunctional tungsten carbide

The rate determining step is the isomerization of the carbenium ion.

Table 15b. Site-Time Yields (STYs) at steady-state for the *n*-hexane reactions at 630 K (6.1 kPa *n*-hexane ; 94.9 kPa H<sub>2</sub>) [2]

	STY/10 <sup>-3</sup> s <sup>-1</sup>	
	2-methylpentane	3-methylpentane
WC/0-RT	5.1	2.2
WC/0-573 K	56	30
WC/0-700 K	160	84
β-W <sub>2</sub> C/0-700 K	83	42

STY are based on the number of site measured by irreversible CO chemisorption at RT after reaction. Clearly these STY have to be obtained only by measuring the density of WO<sub>x</sub> unavailable data at that time.

Conclusion on *n*-hexane reactions over tungsten carbides exposed to oxygen at relatively low temperature, for a short contact time can now be drawn.

2- and 3-Methylpentane are the predominant products as predicted either by the C<sub>5</sub>-ring or methyl bond-shift in carbenium-ion pathways. But as no methylcyclopentane was detected (from C<sub>5</sub>-ring intermediate), assumption can be made that isomerization is bifunctional in agreement with the evolution of the STY vs oxygen concentration (WO<sub>x</sub> species). As alkane dehydrogenation on WC<sub>x</sub> sites is quasi-equilibrated, isomerization rates on WO<sub>x</sub> sites is the rate-determining -step.

Iglesia et al. [34] considered that chemisorbed oxygen titrates  $WC_x$  sites and forms  $WO_x$  ones at the surface on fresh then oxygen-exposed WC.

*Are acidic sites Brönsted Sites?* The presence of acid sites on oxygen-modified carbide surfaces was demonstrated by  $NH_3$  temperature programmed desorption (TPD) studies [1, 36].

Oxygen passivates reactive sites ( $WC_x$  metal-like) subsequently able to chemisorb ammonia irreversibly without dissociation. Thus temperature-programmed desorption of ammonia permitted to titrate acid-like sites on tungsten carbide surfaces. Iglesia *et al.* [34] also established the bifunctional character of the *n*-heptane isomerization by demonstrating that *n*-heptane isomers reach equilibrium values, and that dehydrogenation steps are quasi-equilibrated on WC/0-800 K, the rate determining step involving isomerization and cracking of alkene intermediates. Furthermore, they studied the isotopomer distribution in *n*-heptane-1- $^{13}C$  reaction products. They found that the products of the isomerization on WC/0-800 K contain  $^{13}C$  only in terminal carbon positions, consistent with methyl-shift rearrangement, without incorporation of  $^{13}C$  into non terminal carbon atoms. Consequently isomerization definitively does not involve  $C_5$ -ring intermediate.

### 8.3 NEOPENTANE REACTION

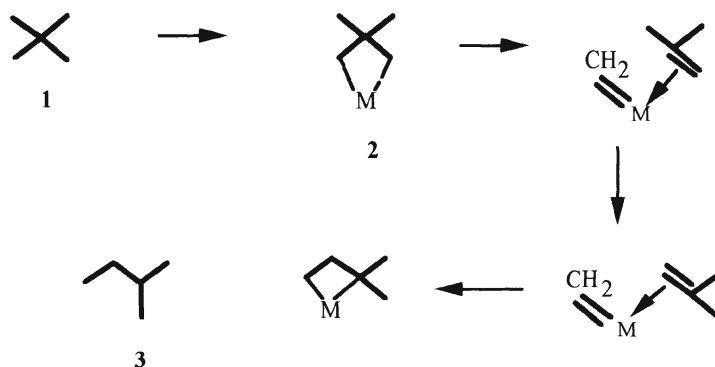
#### ***8.3.1 Isomerization to isopentane via a metallacyclobutane intermediate.***

In the case of platinum, according to Gault [37] the direct formation of the metallacyclobutane, without the  $\pi$ -alkylic intermediate, can explain the high activity of Pt to catalyze the isomerization of neopentane to isopentane.

As clean carbide surfaces do not catalyse neopentane isomerization, chemisorbed oxygen must introduce new catalytic sites such as  $WO_x$  species. As a consequence, "WO" must substitute "M" in the proposed pathway in Figure 9.

Neopentane isomerization to isopentane occurs only on Pt, Ir and Au surfaces. Neopentane is an interesting molecular probe as it is unable to produce carbenium ion.

Oxygen-exposed carbides are very active in neopentane hydrogenolysis, a reaction characteristic of precious metal. This reaction must be monofunctional, and oxygen atoms must act only as spectators.



- 1 : neopentane  
 2 : metallacyclobutane  
 3 : isopentane

Figure 9. Neopentane isomerization to isopentane via metallacyclobutane intermediate.

#### 8.4 3,3-DIMETHYLPENTANE ISOMERIZATION [1] – ON OXYGEN-EXPOSED TUNGSTEN CARBIDES (WC/0-800 K)

Secondary carbon atoms increase the isomerization rate of 3,3-dimethylpentane, and allow alkene intermediates and secondary carbenium ion intermediates characteristic of a bifunctional pathway with methyl bond shifts.

3,3-dimethylpentane is a much more sensitive molecular probe of isomerization pathways, as shown by the following turnover rates over WC/0-800 K.

Table 16. Turnover rates of neopentane and 3,3-dimethylpentane isomerization over WC/0-800 K.

Reactant	Vt/s <sup>-1</sup>
Neopentane	5.0 x 10 <sup>-5</sup>
3,3-dimethylpentane	0.275

The isomer distribution greatly differs among three pathways : (i) carbenium ion pathway corresponding to a bifunctional surface, and rearrangement of an olefin intermediate ; (ii) C<sub>5</sub>-ring hydrogenolysis, and (iii) metallacyclobutane bond-shift mechanism.

The first pathway mainly leads to 2,3-dimethylpentane and 2,4-dimethylpentane as seen on Figure 10.

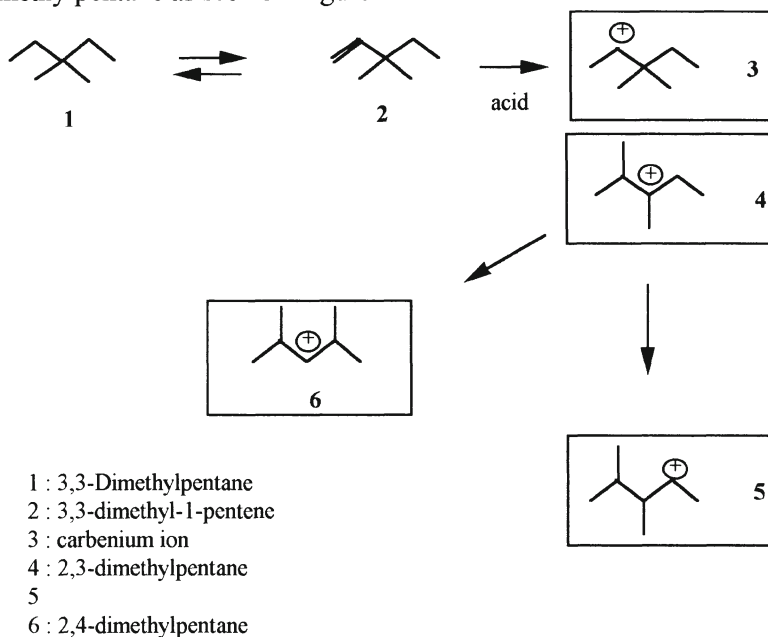


Figure 10. Bifunctional-carbenium ion-methyl shift reactions for 3,3-dimethylpentane.

The second route, via  $C_5$ -ring hydrogenolysis pathways, leads to 2-methylhexane and 2,2-dimethylpentane ; the dimethylcyclopentane is expected as seen on Figure 11. Ethylcyclopentane should be expected. It is a monofunctional catalysis ; typical of highly dispersed platinum.

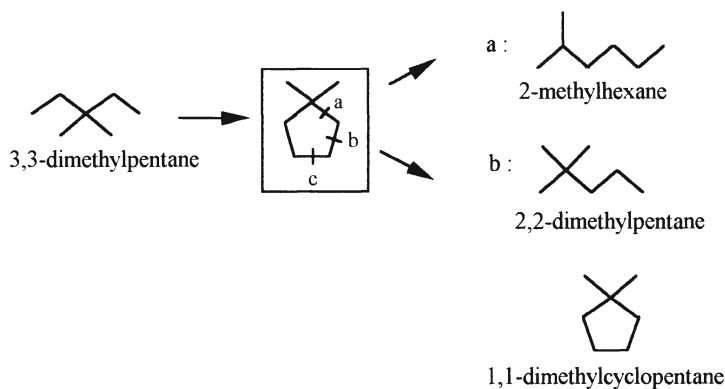


Figure 11. C-5 ring intermediate pathways for 3,3-dimethylpentane reaction.

The last pathway involves two metallacyclobutane intermediates and mainly produces 2,3-dimethylpentane (Figure 12).

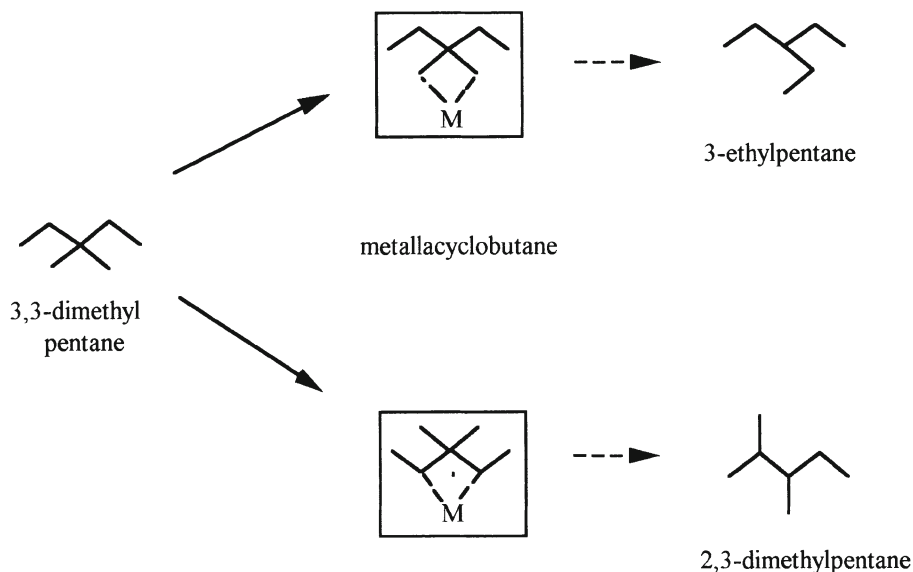


Figure 12. Metallacyclobutane intermediates for 3,3-dimethylpentane reaction

*Results and discussion.* The predominant reaction product over WC/0-800 K (Table 17) is 2,3-dimethylpentane ; 2,3 and 2,4 - dimethylpentane approach equilibrium values, but not 2,2-dimethylpentane. These data are characteristic of a carbenium ion rearrangement.

The primary formation of 2,3 and 2,4-dimethyl pentane (52 % and 15 % respectively) as well as the detection of 3,3-dimethyl-1-pentene suggest that 3,3-dimethylpentane isomerization follows an acid-catalyzed carbenium ion rearrangement of olefin intermediates.

Table 17. Initial selectivities for 3,3-dimethylpentane reaction over WC/0-800 K (623 K, 4.5 kPa 3,3-dimethylpentane, 96 kPa H<sub>2</sub>) [34]

	Selectivity %
2,3-dimethylpentane	52
2,4-dimethylpentane	15
2-methylhexane	4
2,2-dimethylpentane	12
3-ethylpentane	0.4

## 8.5 ISOMERIZATION OF *n*-HEXANE VIA A METALLACYCLOBUTANE INTERMEDIATE

Ribeiro [3] proposed that the bond shift mechanism for the isomerization of neopentane could be used in principle for *n*-hexane. He then demonstrated that the data lead to the existence of the bifunctionality of all oxygen-exposed tungsten carbides prepared at high temperature. Hereafter is presented the corresponding scheme.

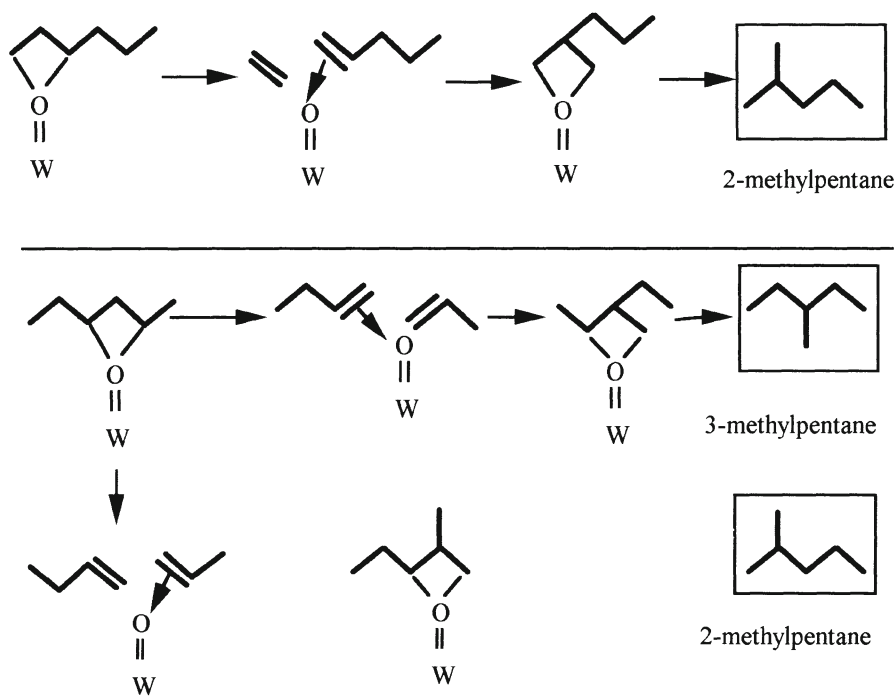


Figure 13. Isomerization pathways for *n*-hexane via metallacyclobutane intermediates

It must be noted that 2 moles of 2-methylpentane are formed for 1 mole of 3-methylpentane, this ratio corresponding also to the experimental data.

## 9. Isomerization of *n*-hexane and *n*-heptane over bulk or supported tungsten nitrides

### 9.1 COMPARISON BETWEEN OXYNITRIDES AND OXYCARBIDES

Table 18 reports the data on *n*-hexane reactions over both  $\beta$ -W<sub>2</sub>C and  $\beta$ -W<sub>2</sub>N *exposed to air*.

*Table 18.* A comparison of *n*-hexane reactions over  $\beta$ -W<sub>2</sub>C and  $\beta$ -W<sub>2</sub>N (samples exposed to air)

	Specific rate/10 <sup>-2</sup> $\mu\text{mol s}^{-1}\text{g}^{-1}$ (630 K, P <i>n</i> -hexane/P hydrogen = 0.06)		
	After 100 min run		
$\beta$ -W <sub>2</sub> C <sup>a,b</sup>	63	36	44
$\beta$ -W <sub>2</sub> N <sup>c</sup>	0.52	0.25	0.33

<sup>a</sup> sample reduced in H<sub>2</sub> at 673 K for 2 h before reaction

<sup>b</sup> data obtained at 670 K and extrapolated to 630 K

<sup>c</sup> data obtained at 670 K and extrapolated to 630 K assuming an activation energy of 100 kJ mol<sup>-1</sup>

*Table 19.* Product distribution for the *n*-heptane reactions over tungsten oxynitrides (623 K, H<sub>2</sub> : *n*-heptane = 18:1, 70 mg catalyst, total pressure 101 kPa)

	Fraction of 100 moles of n-heptane converted				Pt/SiO <sub>2</sub>
	WN <sub>1.34</sub> O <sub>0.42</sub>		WN <sub>1.34</sub> O <sub>0.60</sub> P <sub>0.12</sub>		
	Non-passivated	Passivated	Non-passivated	Passivated	
ECP	0	0	0	0	21.1
1,2-DMCP	0	5.8	0	2.76	17.9
2-MH + 3-MH	76	87.9	35.5	83.4	14.9
HEP	12.1	1.3	5.8	6.5	10.1
TOL	0	0	0	0	18.6
Hydrogenolysis <sup>a</sup>	4.2	1.2	43.9	2.6	3.9
Isomerization <sup>a</sup>	79.0	96.2	48.2	88.2	61.9
Dehydrogenation <sup>a</sup>	12.6	1.3	7.9	6.6	30.3

<sup>a</sup> reaction for 100 mol of *n*-heptane converted

ECP : ethylcyclopentane ; DMCP : dimethylcyclopentane ; MH : methylhexane ; HEP : heptenes ; TOL : toluene



$\beta$ -W<sub>2</sub>N catalyzes *n*-hexane isomerization and hydrogenolysis similarly to  $\beta$ -W<sub>2</sub>C, but its specific rates is lower by a factor of about 130. The 2-methylpentane/3 - methylpentane ratio is near from 2 as expected. As previously seen tungsten nitride has a quite lower metallic behaviour than oxycarbides and therefore is less bifunctional than  $\beta$ -W<sub>2</sub>C.

## 9.2 OXYNITRIDES ALSO CATALYZE THE ISOMERIZATION OF ALKANES

Product distribution of *n*-heptane, reported by Sellem et al. (22) over two tungsten oxynitrides WN<sub>1.34</sub> O<sub>0.42</sub> and WN<sub>1.34</sub> O<sub>0.60</sub> P<sub>0.12</sub>, also confirms (Table 19) that nitrides exhibit bifunctional properties. 2- and 3-methylhexane are the predominant products. No ethylcyclopentane was detected and *n*-heptene evolving during the reaction show that isomerization is bifunctional. Furthermore, the tungsten oxynitrides are active in hydrogenation of propene and Figure 14 shows the efficient promoting effect of phosphorous to avoid the deactivation of the oxynitride.

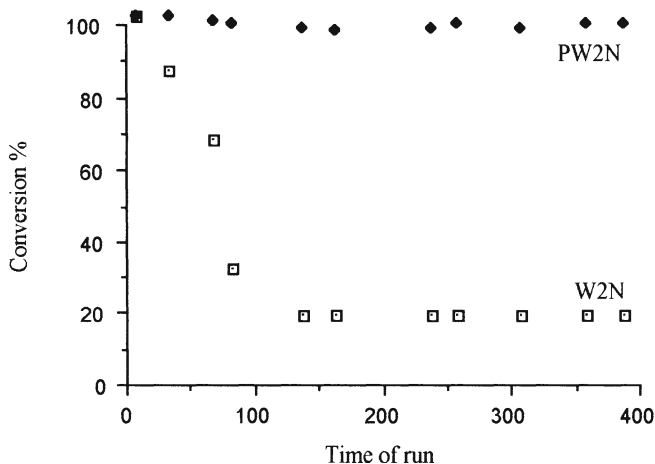


Figure 14. Propene hydrogenation over W<sub>2</sub>N and PW<sub>2</sub>N at 423 K [36]

### 9.3 MOLYBDENUM NITRIDE AND CARBIDE SUPPORTED ON EMT ZEOLITE [38]

Nitride and carbide can be supported on zeolite. Becue (38) found for passivated samples at RT, pretreated by flowing hydrogen at 773 K for 5 h prior to *n*-heptane reaction, that Mo nitride/NaEMT and Mo carbide/NaEMT behave like bulk material due to the non-acidic NaEMT zeolite. Table 20 shows that a bifunctional behaviour can be deduced from the 86.1 % and 77.6 % 2- and 3-methylhexane, 22.1 and 18.6 heptenes, whereas hydrogenolysis/cracking reactions occur, 22.3 % and 3.8 % for the supported nitride and carbide respectively.

Table 20. Product distribution for *n*-heptane reactions on supported molybdenum nitride and carbide.

	Conversion	Isomerization	Heptenes	Hydrogenolysis/ cracking
MoN/NaEMT	1.3	55.6 (86.1 % 2- and 3- methylhexane)	22.1	22.3
MoC/NaEMT	1.0	77.6 (85.1 % 2- and 3- methylhexane)	18.6	3.8

Temperature of reaction: 623 K,  $H_2/n$ -heptane = 17

### 10. Molybdenum oxycarbides prepared at low temperature (623 K) by the reaction mixture

The preparation of these materials is described in Section 3.2 of this chapter. Both alkane (*n*-hexane, *n*-heptane) reactions lead to the same product distribution (Tables 21, 22). Pt/ $\beta$ -zeolite is a typical bifunctional catalyst. In both cases, no cyclic intermediate form during the reaction. For *n*-heptane the 2-MP/3MP ratio is 2, the predicted value for both mechanisms. Similarly, the same ratio is 1 for *n*-hexane.

From this data analysis, no difference appears compared to high temperature materials.

In contrast, at high conversion, Ledoux's materials do not deactivate (no coking), data which leads the authors to consider these oxycarbides as monofunctional, without any acidity capable of cracking : with time of run the mid-molecule cleavage characteristic of a bifunctional catalyst decreases.

The second reason to differentiate the products synthesized at low and high temperature, is the behaviour of Ledoux oxycarbides when passing from

*n*-heptane to *n*-octane, which does not increase the isomerization rate, as it is the case for a bifunctional mechanism. The demethylation of reactant becoming predominant with time of run, Ledoux proposed a metallacyclobutane isomerization mechanism for his monofunctional oxycarbides.

*Table 21.* Main product distribution for *n*-hexane reaction over Ledoux's materials [8]

	Mo metal	Mo <sub>2</sub> C-oxygen modified	MoO <sub>3</sub> -carbon modified	Pt/ $\beta$ -zeolite <sup>[a]</sup>
Sg / m <sup>2</sup> g <sup>-1</sup>	16	45	145	-
Conversion %	24	23	35	40.4
Isom selectivity %	95	93	96	99.2
2-MP	63.0	63.6	62.0	53.6
3-MP	35.2	34.4	35.0	34.3
Cyclic	0.8	0.8	0.7	0.3

0.66 kPa *n*-hexane ; 100 kPa H<sub>2</sub> ; 623 K

[a] T = 543 K

2-Mp = 2-methylpentane ; 3-MP = 3-methylpentane

*Table 22.* Main product distribution for *n*-heptane reaction over Ledoux's materials [8]

	Mo <sub>2</sub> C-oxygen modified	MoO <sub>3</sub> -carbon modified	Pt/ $\beta$ -zeolite
Time of run	25 h	43 h	-
T reaction/K	623	573	503
Conversion %	14.0	29.8	29
Isom selectivity %	86	82	97
DMP	11.0	17.5	12.6
2-MH	41.1	40/9	43.7
3-MH	39.9	38.3	41.1
Cyclic	4.8	0.6	0.3

## 11. Conclusion

This chapter is related to the catalytic properties of (oxy)nitrides and (oxy)carbides of early transition metals. Clean materials appear to produce

mainly hydrogenolysis of light alkanes. This reaction is characteristic of the metallic properties of these substitutes of precious metals.

Powders prepared at high temperature and subsequently exposed to oxygen at relatively low temperature (less than 800 K) present an acidic character. These materials are therefore bifunctional. They are able to isomerize alkanes via the formation of a carbenium ion. The isomerization of this carbocation occurs on the acidic center and follows a bond-shift pathway : it is the rate determining step of the overall reaction.

Carbides treated in oxygen at high temperature for several hours are capable of isomerization via metallacyclobutane or  $\pi$ -allyl intermediates.

(Oxy)nitrides are also found to follow the same tendency. Nevertheless they are less metallic than (oxy)carbides.

Instead of adsorbing oxygen or introducing oxygen into the lattice or carbides, carbon can be introduced into oxygen vacancies of an oxide. A well dispersed molybdenum oxide submitted to the reaction mixture (alkane + hydrogen) at 620 K, is able to transform to an oxycarbide after several hours. This material is not bifunctional and isomerization of light alkanes was found to proceed via a metallocyclobutane intermediate, with a high selectivity and no deactivation at high conversion.

As can be seen a large variety of compounds can be prepared in a controlled way.

## 12. References

1. Ribeiro, F.H., Dalla Betta, R.A., Boudart, M., Baumgartner, J.E., and Iglesia, E.I. (1991) *J. Catal.* 130, 86.
2. Ribeiro, F.H., Boudart, M., Dalla Betta, R.A., and Iglesia, E.I. (1991) *J. Catal.* 130, 498.
3. Iglesia, E., Ribeiro, F.H., Boudart M., and Baumgartner, J.E. (1992) *Catal. Today*, 15, 455.
4. Keller, V., Cheval, M., Vayer, M., Ducros R., and Maire G. (1991) *Catal. Lett.*, 10, 137.
5. Shin, C.H., Bugli, G., and Djéga-Mariadassou, G. (1991) *J. Solid State Chem.*, 95, 145.
6. Kim, H.S., Shin, C.H., Bugli, G., Bureau-Tardy, M., and Djéga-Mariadassou G. (1994) *Appl. Catal. A*. 119, 223.
7. Kim, H.S., Sayag, C., Bugli, G., Djéga-Mariadassou, G., and Boudart, M. (1995) *Mat. Res. Science Symp. Proc. series* 368, 3.
8. Ledoux, J.M., Pham-Huu, C., York, A.P.E., Blekkan, E.A., Delporte, P., and Del Gallo, P. (1996) *The Chemistry of Transition Metal Carbides and*

- Nitrides*, S.T. Oyama (ed.) Blackie Academic & Professional, Publishers, p.373.
9. Charles Yu, C., Ramanathan, S., Fawzy Sherif, and Oyama, S.T. (1994) *J. Phys. Chem.* 98, 13038.
  10. Keller, V. (1993) *University Louis Pasteur, Strasbourg, Thesis*.
  11. Ribeiro, F.H., Dalla Betta, R.A., Guskey, G.J., and Boudart, M. (1991) 3, 805.
  12. Gouin, X., Marchand, R., L'Haridon, P., and Laurent, Y., (1994) *J. Solid State Chem.* 109, 175.
  13. Kim, H.S. (1993) *University Pierre et Marie Curie, Paris, Thesis*.
  14. Eberhart M.E. and MacLauren J.M. (1996) in "The chemistry of Transition Metal Carbides and Nitrides" S.T. Oyama Ed., Blackie Academic and Professional, Glasgow, p. 107
  15. Volpe, L., and Boudart, M. (1985) *J. Solid State Chem.* 59, 332.
  16. Boudart, M., Oyama, S.T, and Volpe, L. (1985) US Patent 4,515,763. Volpe and Boudart
  17. Volpe, L., and Boudart, M. (1985) *J. Solid State Chem.* 59, 348.
  18. Leclercq, L., Imura, K., Yoshida, S., Barbee, T. and Boudart, M. (1978) *Preparation of Catalysts II*, B. Delmon, P. Grange, and G. Poncelet, (eds.), p. 627.
  19. Leclercq, L. (1983) *Surface properties and Catalysis by Non metals*, J.P. Bonnelle, B. Delmon and Derouane, eds (Reidel, Dordrecht), p. 433.
  20. Leclercq, G., Kamal, M., Giraudon, J.M., Devassine, P., Feigenbaum, L., Leclercq, L., Frennet, A., Bastin, J.M., Löfberg, A., and Dufour, M. (1996) *J. Catal.*, 158, 142.
  21. Teixeira da Silva, V.L.S., Schmal, M., and Oyama, S.T. (1996) *J. Solid. State Chem.* 123, 168.
  22. Sellem, S., Potvin, C., Manoli, J.M., Contant, R. and Djéga-Mariadassou, G. (1995) *J. Chem. Soc., Chem. Commun.*, 359.
  23. Rodrigues J.A.J. (1996) *University Pierre et Marie Curie, Paris, Thesis*.
  24. Djéga-Mariadassou, G., Boudart, M., Bugli, G., and Sayag, C. (1995) *Catal. Lett.* 31, 411.
  25. Sayag, C. (1993) *University Pierre et Marie Curie, Paris, Thesis*.
  26. Ledoux, M.J., Guille, J., Pham Huu, C., and Marin, S. (1989) *Eur. Pat. App.* N° 0 396 475 A1.
  27. Blekkan, E.A., Pham-Huu, C., Ledoux, M.J., and Guille, J. (1994) *Ind. Eng. Chem. Res.*, 33, 1657.
  28. Ledoux M.J., and Pham-Huu (1992) *Catal. Today*, 15, 263
  29. Muller, A., Keller, V., Ducrosq, R., and Maire, G. (1995) *Catal. Lett.*, 35, 65.
  30. Toth L.E. (1971) in "Transition Metal Carbides and Nitrides" Academic : New York, p. 22

31. Boudart, M., and Oyama, S.T. (1990) Proceed. 12th Iberoamerican Symposium on Catalysis, Rio de Janeiro
32. Muller, A., Keller, V., Ducrosq, R., and Maire, G. (1995) Catal. Lett., 25, 337.
33. Ribeiro, F. H. (1989), Ph. D. dissertation, Stanford University.
34. Iglesia, E., Baumgartner, J.E., Ribeiro, F.H., and Boudart, M.(1991) J. Catal., 131, 523.
35. Sinfelt, J.H., Hurwitz, H., and Rohrer, J.C. (1960) J. Phys. Chem., 64, 892.
36. Sellem, S. (1996) University Pierre et Marie Curie, Paris, Thesis.
37. Gault, F., (1981) Mechanisms of Skeletal Isomerization of Hydrocarbons on metals, Adv. in Catal., 30, p. 1, Academic Press.
38. Bécue, T. (1996) University Pierre et Marie Curie, Paris, Thesis.
39. Oyama, S.T. (1996) The Chemistry of Transition Metal Carbides and Nitrides, S.T. Oyama (ed.) Blackie Academic & Professional, Publishers, p.1.

# MOLECULAR CHEMISTRY OF ALKANE ACTIVATION

## *Formation and Reactions of $\text{CH}_x$ species on Metal Surfaces*

F. SOLYMOSI

*Institute of Solid State and Radiochemistry, A. József University  
and Reaction Kinetics Research Group of the Hungarian Academy  
of Sciences, P.O.Box 168, H-6701 Szeged, Hungary*

The results obtained on the formation, stability and reactions of  $\text{C}_x\text{H}_y$  hydrocarbon fragments ( $\text{CH}_2$ ,  $\text{CH}_3$ ,  $\text{C}_2\text{H}_5$  and  $\text{C}_3\text{H}_7$ ) on metal single crystal surfaces, particularly on Rh and Pd, are summarized and discussed.  $\text{C}_x\text{H}_y$  species are produced by thermal and photo-induced dissociation of corresponding iodo compounds. Methods used include X-ray and ultraviolet photoelectron spectroscopy, high resolution electron energy loss spectroscopy and temperature programmed desorption. Studies performed on supported metals on the chemistry of  $\text{C}_x\text{H}_y$  fragments and on the reaction of adsorbed  $\text{CH}_3$  and gaseous  $\text{CO}_2$  are also reported.

### 1. Introduction

Studies of the chemistry of hydrocarbon fragments ( $\text{C}_x\text{H}_y$ ) on metal surfaces are of fundamental interest in understanding mechanisms of Fischer-Tropsch synthesis, transformation of methane into higher hydrocarbons and other more valuable compounds [1-10]. Evaluation of the role, bonding and reactivity of  $\text{C}_x\text{H}_y$  species on catalyst surfaces is hampered by the fact that the catalytic reactions involving hydrocarbons occur at relatively high temperatures, where the lifetime of  $\text{C}_x\text{H}_y$  intermediates on the catalyst surface is very limited. Recently, several ways have been elaborated to produce these  $\text{C}_x\text{H}_y$  moieties in larger concentrations on solid surfaces even at low temperature, which made possible to investigate their reactions.

In the present paper an account is given on chemistry of hydrocarbon fragments on well oriented metals under UHV conditions, using several tools of surface science, and on supported metals. A particular attention is paid to the Rh and Pd, as both metals are very effective catalysts in the reactions involving hydrocarbons. Emphasis will be given (i) on the production at hydrocarbon

species of desired composition, (ii) on the thermal stability and couplings of these intermediates, and (iii) on their reactions with other adsorbed adatoms.

## 2. Methods for production of $\text{CH}_x$ fragments

One possibility for the production of hydrocarbon fragments,  $\text{C}_x\text{H}_y$ , at lower temperatures is the thermal dissociation of corresponding halogenated hydrocarbons. The characteristic features of the adsorption and dissociation of these compounds on metal surfaces have been discussed in recent reviews [12]. The gas phase carbon-halogen bond energies in alkyl halides are as follows: C-I, 55 kcal/mol, C-Br, 70 kcal/mol, C-Cl, 85 kcal/mol. In harmony with these data, the reactivity of alkyl halides with metals decreases in the order iodides > bromides > chlorides. As a result of this feature mostly iodide compounds are used to generate hydrocarbon fragments on solid surfaces. The sensitivity of these compounds to illumination provides a possibility to produce  $\text{C}_x\text{H}_y$  fragments on metal surfaces even at  $\sim 100$  K where the decomposition of  $\text{C}_x\text{H}_y$  can be excluded [12,13].

The dissociation of iodo compounds can be easily followed by X-ray photoelectron spectroscopy (XPS) via the binding energy (BE) of I(3d), as it differs by about 1.5-2.0 eV for molecularly adsorbed compounds and for atomically adsorbed iodine. The ultraviolet photoelectron spectroscopy (UPS) can be also used, but this method is less sensitive than the XPS. High resolution electron energy loss spectroscopy (HREELS) is also applied in this area, as the characteristic vibrations of  $\text{CH}_x\text{I}_y$  and  $\text{CH}_x$  are different. In this case the limited resolution of HREELS may cause a problem. To illustrate the use of XPS method, XPS spectra of I(3d) for adsorbed  $\text{CH}_2\text{I}_2$  on Pd(100) are presented as a function of annealing temperature in Fig. 1 [14]. The molecularly adsorbed  $\text{CH}_2\text{I}_2$  is characterized by a binding energy at 620.55 eV.

When a monolayer is annealed, a clear shift occurred in the binding energy for I(3d) from 620.55 to 619.5 eV in the temperature range of 160-233 K, indicating a change in its chemical state.

Recently Stair et al. [15,16] described a methyl radical source for use in high vacuum. Methyl radicals are generated through azomethane pyrolysis in a tubular reactor located inside an ultrahigh vacuum chamber. Methyl yields as high as 42% have been achieved. By means of this method almost pure adsorbed  $\text{CH}_3$  layer can be produced on the solid surfaces. Other gases formed during the pyrolysis or in the reaction of methyl radicals on the walls of the reactor include nitrogen, methane, ethane and hydrogen. From these gases hydrogen is the less desired product. In contrast to halogen atoms, it reacts readily with adsorbed methyl groups at relatively low temperature.



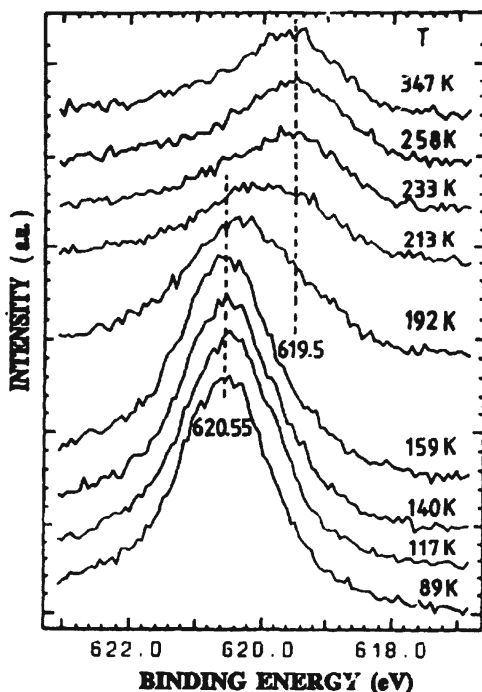


Figure 1. XPS of  $I(3d_{5/2})$  of adsorbed  $CH_2I_2$  after heating the adsorbed layer to different temperatures [14]

In the case of the generation of methylene ( $CH_2$ ),  $ClCH_2I$ ,  $CH_2CO$  [17] and  $CH_2N_2$  [18] are also used in addition to  $CH_2I_2$ . The advantage of  $ClCH_2I$  is that the temperature of its complete dissociation is only slightly higher than that of  $CH_2I_2$ , but almost 50% of adsorbed  $Cl$  will be removed around 200 K in the form of  $HCl$ . As a result the concentration of halogen adatoms will be lower. The best source of  $CH_2$  is probably the  $CH_2N_2$ , as  $N_2$  produced in the low-temperature dissociation of the compound desorbs at once leaving behind only  $CH_2$  species. The explosive nature of this compound, however, makes its application less attractive.

### 3. Chemistry of $CH_x$ fragments on metal single crystals

#### 3.1 FORMATION AND REACTIONS OF ADSORBED $CH_2$

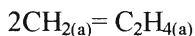
Monolayer adsorption of  $CH_2I_2$  on platinum metals resulted in a work function decrease of 0.75-0.85 eV [14,19-21]. The adsorption is dissociative at

submonolayer at 90-100 K and molecular at monolayer. The dissociation of the compound can be completed by illumination at 100 K, as indicated by the significant shift in the binding energy of I(3d) (Fig. 1). The primary products of the dissociation are CH<sub>2</sub> and I species. The photoemission signal of CH<sub>2</sub> species is located at 5.9-6.1 eV in UPS [14]. In the HREEL spectrum the dissociation of adsorbed CH<sub>2</sub>I<sub>2</sub> on Rh(111) was indicated by the appearance of vibration losses at 2940 cm<sup>-1</sup> (γ<sub>as</sub>(CH<sub>2</sub>)), 1190 cm<sup>-1</sup> (w(CH<sub>2</sub>)), 780 cm<sup>-1</sup> (γ<sub>s</sub>(M-C) [19]. These peaks differ from those characteristic for adsorbed CH<sub>2</sub>I<sub>2</sub> and agree well with the vibration of CH<sub>2</sub> species produced by the dissociation of various CH<sub>2</sub>-containing compounds on metal surfaces (Table 1.)

As regards the reactions of CH<sub>2</sub> on Pd(100) surface, the following features were established [14]. A fraction of adsorbed CH<sub>2</sub> is self-hydrogenated to methane



which desorbs immediately after its formation at 150-300 K. Parallel with this reaction a significant fraction of CH<sub>2</sub> is dimerized to yield adsorbed ethylene,



which desorbs in a broad peak between 140-250 K [14]. An increase in the surface concentration of CH<sub>2</sub> (by illumination of adsorbed CH<sub>2</sub>I<sub>2</sub>) markedly enhanced the formation of ethylene. In optimum case, the ratio C<sub>2</sub>H<sub>4</sub>/CH<sub>4</sub> was 3.0-3.5 [14]. These features are in harmony with the theoretical calculation, which showed that the activation energy of coupling of the species CH<sub>2</sub> on metal surfaces is only 6-9 kcal/mol [22].

*Table 1.* Vibrational frequencies (in cm<sup>-1</sup>) of adsorbed CH<sub>2</sub> produced by the dissociation of various compounds.

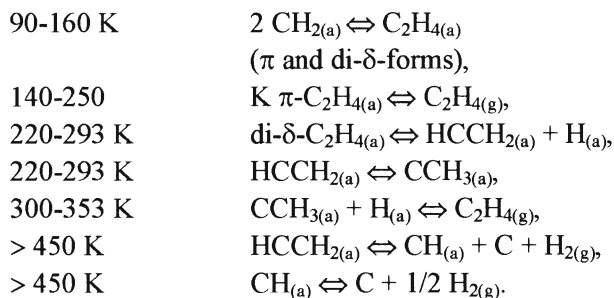
Assignment	CH <sub>2</sub> (CH <sub>2</sub> CO)	CH <sub>2</sub> (CH <sub>2</sub> N <sub>2</sub> )	CH <sub>2</sub> (CH <sub>2</sub> CO)	CH <sub>2</sub> (CH <sub>2</sub> I <sub>2</sub> )
$\nu_{\text{as}}(\text{CH}_2)$	2495	-	-	2940
$\nu_{\text{s}}(\text{CH}_2)$	2870	2965	2970	
$\delta(\text{CH}_2)$	1295	-	1430	
$\omega(\text{CH}_2)$	1065	1165	1020	1190
$\chi(\text{CH}_2)$	-	-	930	
$\rho(\text{CH}_2)$	890	785	790	780
$\nu_{\text{as}}(\text{M-C})$	-	-	-	
$\nu_{\text{s}}(\text{M-C})$	-	-	650	-650

Data were taken from Ref. 19.

In bracket we indicate the original compounds.

Taking into account the behaviour of adsorbed ethylene on metal surfaces, this desorbing ethylene very likely corresponds to the weakly held  $\pi$ -bonded form. The formation of ethylene was also manifested by the UP spectra. When the molecularly adsorbed CH<sub>2</sub>I<sub>2</sub> was heated up to 195 K, the photoemission lines (6.2, 8.8 and 12.8 eV) detected agree well with those observed following ethylene adsorption on Pt metals.

Analysis of UP and XP spectra suggests that adsorbed hydrocarbon fragments remain on the surface even above 250 K, and reactions occur in the adsorbed layer above this temperature, too. In UPS, photoemission signals at 5.2, 9.3, 11.7 and 13.0 eV were seen in the magnified difference spectra even at 278 K. In XPS, significant shifts occurred in the position of the C(1s) peak above 222 K, and at 293-452 K a peak at 285.0 eV became the dominant spectral feature. This behaviour was explained by formation of C<sub>2</sub>H<sub>y</sub> from the di- $\delta$ -bonded ethylene. The following scheme for the reactions of adsorbed ethylene formed in the dimerization of CH<sub>2</sub> species on Pd(100) was proposed:



On Rh(111) surface the dominant mode of the reactions of  $\text{CH}_2$  was its transformation to methane [19]. Ethylene formation was very limited: the  $\text{C}_2\text{H}_4/\text{CH}_4$  ratio varied between 0.01-0.03. When the surface concentration of adsorbed  $\text{CH}_2$  was increased by illumination of molecularly adsorbed  $\text{CH}_2\text{I}_2$ , the coupling reaction became more extensive: the  $\text{C}_2\text{H}_4/\text{CH}_4$  ratio attained a value of 0.08-0.1. Interestingly, the characteristic losses of strongly adsorbed  $\text{CH}_2$  on Rh(111) can be detected up to 350-400 K, when it decomposes to CH species. The high stability is very likely associated with the less tendency of  $\text{CH}_x$  for coupling on Rh(111), in contrast to Pd(100) surface. In Figure 2, HREEL spectra of adsorbed  $\text{CH}_2\text{I}_2$  on Rh(111) are displayed as a function of annealing temperature.

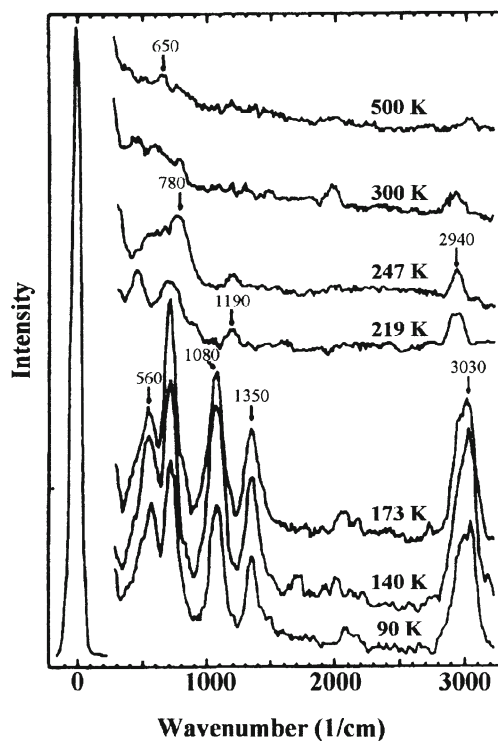


Figure 2. HREELS spectra of adsorbed  $\text{CH}_2\text{I}_2$  on Rh(111) annealed to different temperatures [19].

From the study of the adsorption of diazomethane on a clean Pt(111) it appeared that the C-N bond breaking occurs even at 110 K producing adsorbed  $\text{CH}_2$  and  $\text{N}_2(\text{g})$ . Most or all of the nitrogen was desorbed at 110 K [23]. Methylene species formed reacted to give  $\text{CH}_4$  (Tp=235 and 275 K),  $\text{C}_2\text{H}_4$

( $T_p=290, 525$  and  $660$  K). The  $C_2H_4/CH_4$  ratio at the highest exposure was nearly 0.5, which means that a significant fraction of  $CH_2$  has been transformed into ethylene. The carbonaceous species formed in the decomposition of  $CH_2(a)$  was established by Auger electron spectroscopy. On H-covered Pt(111) the gross features of the TPD profile were similar to those for a clean surface. But both the absolute and relative amounts of ethylene decreased.

Several interesting observations were made concerning the chemistry of adsorbed  $CH_2$  in the study of  $ClCH_2I$  adsorption on Pt(111) surface [21]. XPS results suggested that the C-I cleavage occurs even at 150 K, but the C-Cl bond remains intact. The activation of this bond requires higher temperature, at least 170 K. Methane desorption, as a result of the self-hydrogenation of adsorbed  $CH_2$  was observed above 180 K with a  $T_p=220$  K. It is important that no coupling of  $CH_2$  into  $C_2H_4$  was observed. After heating to 260 K, there was a HREELS evidence for the accumulation of  $CH(a)$  fragment, but unreacted  $CH_2(a)$  was still present. Its transformation into  $CH_4$  occurred in the range 355-360 K. In the explanation of the high stability of this  $CH_2(a)$ , the presence of coadsorbed halogens was considered. As  $CH_4$  desorption around 400 K was registered following  $CH_2N_2$  adsorption on Pt(111), other factors, e.g. local adsorbate structural organization are probably also important.

The analysis of HREEL spectra of annealed layer revealed the presence of other hydrocarbon species above 450 K. Loss features emerged at 830 and  $3035\text{ cm}^{-1}$  were attributed to the vibration of  $CCH_{(a)}$  species: its coverage was calculated to be only 0.04 ML. This surface compound decomposed above 500 K. The lack of ethylene formation indicated that Pt, which is an effective catalysts for C-H and C-C bond breaking, is not effective for C-C bond formation. However, taking into account that after adsorption of  $CH_2N_2$  on Pt(111) surface, a significant amount of  $C_2H_4$  production was observed [23], it appears that the accumulation of halogens may prevent a higher surface coverage of  $CH_2$  species, or their migration on the surface.

The behaviour of Ru [24,25] is very similar to that of Pd. A completely different picture was obtained for Cu(100) and Cu(110) surfaces:  $CH_2$  species generated by the thermal dissociation of  $CH_2I_2$ , recombined easily to give ethylene with a peak temperature of 290-300 K [26-28]. There was no or only very slight indication for the formation of methane. Interestingly, a reaction between adsorbed  $CH_2$  and  $CH_3$  to give  $C_2H_5$  was also observed on Cu(110) [26,27], which was never experienced for Pd(100) and Rh(111) surfaces.

The chemistry of  $CH_2$ , produced by thermal dissociation of  $ClCH_2I$ , was also studied on Ag(111) surface [29]. It was found that the first monolayer of  $ClCH_2I$  adsorbed on Ag(111) at 100 K undergoes mainly dissociation to give surface methylene fragments and halogen atoms.  $CH_2$  species transformed into ethylene which desorbed at 190-220 and 260 K. Methane formation was not reported.

### 3.2 FORMATION AND REACTIONS OF ADSORBED CH<sub>3</sub>

Methyl iodide adsorbs on platinum metal surfaces with high sticking probability at  $\sim 100$  K, even up to multilayer coverages. The adsorption is accompanied by a significant work function decrease (at monolayer  $\Delta\phi = 1.1$ -1.6 eV) indicating a dipole with the positive end pointed away from the surface [30-32]. This is consistent with bonding of molecular CH<sub>3</sub>I through the iodine atom, since alkyl halide molecules all have permanent dipoles with the methyl group positive. UPS spectra of molecularly adsorbed CH<sub>3</sub>I suggest that the adsorption caused little distortion of the gas-phase molecular electronic structures of CH<sub>3</sub>I. At high exposures multilayers form which desorb at 129-136 K.

As regards the dissociation of the molecule, it is a general observation that CH<sub>3</sub>I adsorbs dissociatively at submonolayer coverage on most of the platinum metals even at 90-100 K yielding adsorbed CH<sub>3</sub> and I [30-35]. At higher coverages the adsorption is molecular: monolayer dissociates only at elevated temperatures (150-200 K), where the decomposition of CH<sub>3</sub> also proceeds.

UPS (He II) and XPS study for CH<sub>3</sub>I - Pd(100) system revealed the following characteristics [30,31]. At low coverage, only one photoemission peak appeared in the He II spectra at 8.5 eV, which is due to 1 e orbital of the pyramidal CH<sub>3</sub> radical formed in the dissociation of CH<sub>3</sub>I. At high exposures, photoemission peaks developed at 4.5, 7.0 and 9.2 eV, which are characteristic for molecularly adsorbed CH<sub>3</sub>I. In the XPS, the C(1s) signal appeared at 284.8 eV at low exposure. The C(1s) peak shape and position remained constant up to 2.0 L exposure. This binding energy is very probably associated with the same adsorbed species (CH<sub>3</sub>) which gave a photoemission peak at 8.5 eV in the UPS. With further increase of the CH<sub>3</sub>I exposure, the position of the C(1s) peak shifted to a higher binding energy, 285.3-285.4 eV, and became broader. This change in the C(1s) region is very likely the result of the formation of a multilayer.

The interaction of CH<sub>3</sub>I with clean Rh(111) was studied by HREELS measurements [32]. At submonolayer coverages vibrational losses appeared at 2920, 1350, 1185, 760 and 540 cm<sup>-1</sup> following CH<sub>3</sub>I adsorption at 90 K. On the basis of vibrational characteristics of CH<sub>3</sub>I and CH<sub>3</sub> (Table 2), these spectral features were attributed to the vibration of adsorbed CH<sub>3</sub> formed in the dissociation of CH<sub>3</sub>I. With the increase of the exposure, a new peak developed at 3044 cm<sup>-1</sup> and small shifts occurred in the positions of other peaks, as a result of the formation of undissociated CH<sub>3</sub>I. The HREELS annealing set of multilayer CH<sub>3</sub>I on Rh is shown in Figure 3A. The most important feature is the appearance of a loss peak at 2920 cm<sup>-1</sup> even at 148 K which is indicative of the dissociation of CH<sub>3</sub>I.

The complete dissociation of molecularly bonded CH<sub>3</sub>I on platinum metals can be achieved even at 90-100 K following the irradiation of the adsorbed

layer with full arc of mercury lamp for extended period of time [13,30,32]. This is demonstrated by HREEL spectra presented in Figure 3B. The advantage of the photo-induced dissociation compared to thermal dissociation is the absence of secondary reactions of hydrocarbon fragments, which occur easily during the thermal processes at higher temperatures.

Table 2. Vibrational frequencies of adsorbed  $\text{CH}_3$  group (in  $\text{cm}^{-1}$ ) produced by alkyl halide dissociation\*.

Assignment	Pt(111)	Pt(111)	Cu(111)	Cu(111)	Rh(111)
$\nu_a(\text{CH}_3)$	2925	2950	2950	2910	2920
$\nu_s(\text{CH}_3)$	2775	2770	2820	2781	
$\delta_a(\text{CH}_3)$	1425	1410	1370	1386	1350
$\delta_s(\text{CH}_3)$	1165	1180	1180	1185	1185
$\rho_s(\text{CH}_3)$	790	820	854	760	
$\nu(\text{M-C})$	520	495			

\*Data were taken from Ref. 32.

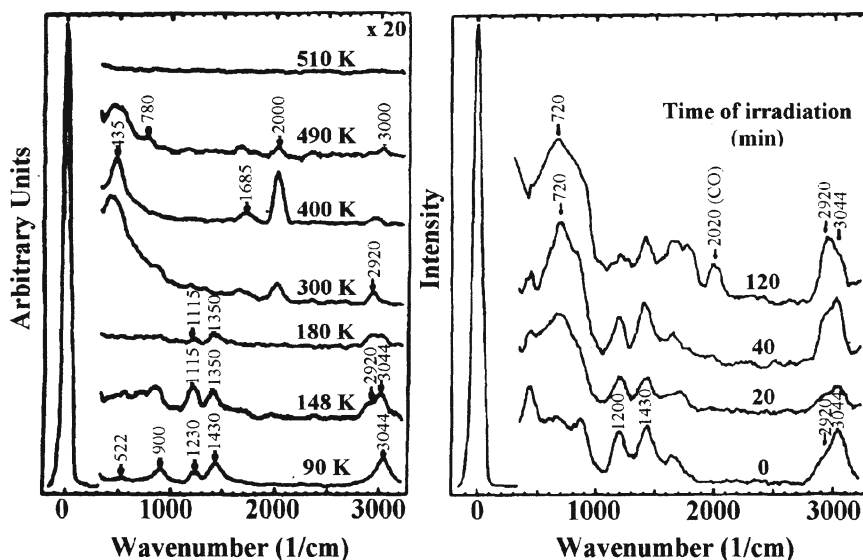
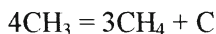


Figure 3. (A) HREEL spectra of a multilayer  $\text{CH}_3\text{I}$  on Rh(111) annealed to different temperature. (B) Effect of illumination time on the HREEL spectra of a multilayer  $\text{CH}_3\text{I}$  at 90-95 K [32].

The reactivity of adsorbed  $\text{CH}_3$  sensitively depends on the nature of the metals. On  $\text{Pd}(100)$  surface the photoemission signal of  $\text{CH}_3$  at 8.5 eV disappeared at 225-250 K [30,31]. The dominant mode of the reactions of  $\text{CH}_3$  species is its decomposition to carbon and self-hydrogenation into  $\text{CH}_4$



The peak temperature of methane formation was 160 - 170 K for other Pt metals. Coupling of  $\text{CH}_3$  on these metals occurred to a very limited extent (ethane was only 1-2% of that of methane formed).

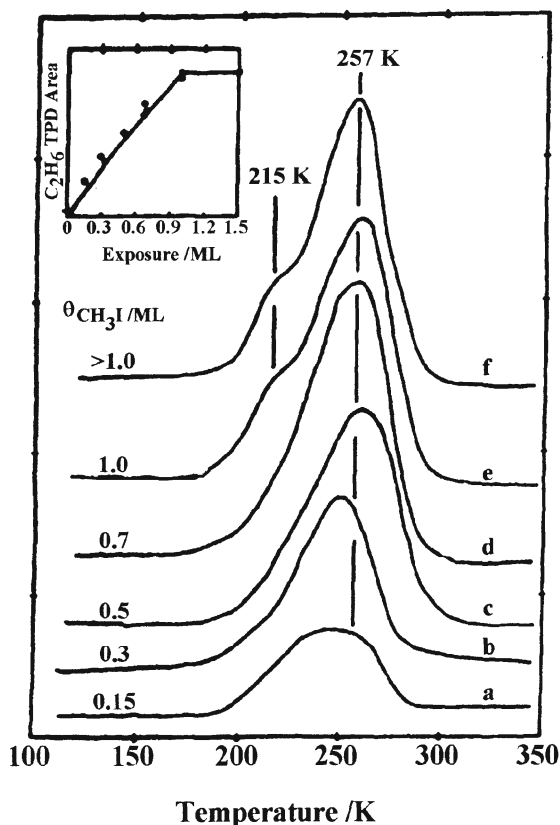
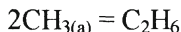


Figure 4. TPD of  $\text{C}_2\text{H}_6$  from  $\text{CH}_3\text{I}/\text{Ag}(111)$  as a function of  $\text{CH}_3\text{I}$  coverage [36].

Adsorbed  $\text{CH}_3$  group exhibits a completely different behaviour on  $\text{Ag}(111)$  surface [36]. Methane and hydrogen, the major products of the decomposition



and self-hydrogenation of  $\text{CH}_3$  species on Pt metals, are absent in the desorbing products.  $\text{CH}_3$  groups recombine into ethane



which desorbs with  $T_p = 257$  K. TPD curves for ethane formation are depicted in Figure 4. The ethane formation is a reaction limited process, as ethane adsorbs very weakly on the Ag(111) surface: no uptake of ethane was observed at 90-100 K.

Adsorbed  $\text{CH}_3$  at high coverages behaves similarly on Cu(110) and Cu(111) surfaces where methyl coupling to form ethane is favored over dehydrogenation reaction [26,27,37,38]. The peak temperature of ethane desorption from Cu(110) varied between 400-450 K. However, at low coverages the primary products are methane and ethylene which are evolved simultaneously at 400-500 K. The differences between the two Cu surfaces are that on Cu(111) propylene is also formed and the  $\text{CH}_4/\text{C}_2\text{H}_4$  ratio for Cu(110) is 2.1, whereas that for Cu(111) is 4.1.

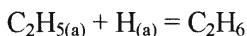
### 3.3 FORMATION AND REACTIONS OF $\text{C}_2\text{H}_5$

The adsorption of  $\text{C}_2\text{H}_5\text{I}$  on Pt metals is characterized by a work function decrease between 1.8-2.0 eV at monolayer [39,40]. It is assumed that, similarly to the other iodo-compounds,  $\text{C}_2\text{H}_5\text{I}$  bonds through I atom.  $\text{C}_2\text{H}_5\text{I}$  adsorbs mostly molecularly even at submonolayer coverage [39-42]. Its thermal dissociation occurs at 150-210 K, or following extended irradiation even at 90 K. Photoemission lines for adsorbed  $\text{C}_2\text{H}_5$  in UPS were registered at 6.4, 8.3 and 12.5 eV [39]. Vibrational frequencies of various modes of adsorbed  $\text{C}_2\text{H}_5$  are listed in Table 3, which are only slightly different from those of molecularly adsorbed  $\text{C}_2\text{H}_5\text{I}$ .

Ethyl moiety is relatively stable species on Pt metals. TPD spectra registered for Pd(100) suggest that  $\text{C}_2\text{H}_5$  dehydrogenates to yield  $\text{C}_2\text{H}_4$  on one hand



and hydrogenates to  $\text{C}_2\text{H}_6$



on the other hand. A fraction of the ethylene ( $\Pi$ -bonded form) desorbs between 150-250 K, and another fraction (di- $\sigma$ -form) is transformed into a vinyl species,

which decomposes only above 450 K. The desorption of ethane is characterized with  $T_p = 180$  K. As ethane does not adsorb on Pd(100) surface above 120 K, the release of ethane is a reaction limited process. The ratio of  $C_2H_4/C_2H_6$  is 0.5. It is important to mention that no recombination of  $C_2H_5$  to  $C_4H_{10}$  was observed.

Similar features were established for Rh(111) surface [40]. The main products of  $C_2H_5$  reactions were again  $C_2H_4$  and  $C_2H_6$  with  $C_2H_4/C_2H_6$  ratio of 0.3-0.5. XPS studies revealed that  $C_2H_5I$  adsorbs dissociatively at submonolayer coverage at 90 K. [40]. The dissociation of a monolayer starts above 170 K and completes below 250 K.

Illumination of adsorbed  $C_2H_5I$  induced the dissociation even at  $\sim 90$  K. No thermal and photoinduced cleavage of C-C bond in  $C_2H_5$  species was observed. Bol and Friend [43] also stated that  $C_2H_5I$  is cleaved upon adsorption at 100 K on clean Rh(111) yielding adsorbed  $C_2H_5$  and I. This conclusion was based on the absence of the  $\delta(C-C-I)$  and  $\nu(C-I)$  modes and the presence of modes at  $220\text{ cm}^{-1}$   $\nu(Rh-I)$  and  $430\text{ cm}^{-1}$   $\nu(Rh-C)$  in the corresponding spectrum. As regards the decomposition of  $C_2H_5$  they report that  $C_2H_5$  decomposes to  $H_2$  and adsorbed C via the formation of ethylene. No TPD spectra were presented.

Table 3. Vibrational frequencies (in  $\text{cm}^{-1}$ ) of adsorbed  $C_2H_5$  species produced by dissociation of various compounds.

	$C_2H_5/Pt(111)$ ( $C_2H_5Cl$ )	$C_2H_5/Cu(001)$ ( $C_2H_5Br$ )	$C_2H_5/Si(111)$ ( $(C_2H_5)_2Zn$ )	$C_2H_5/Rh(111)$ ( $C_2H_5I$ )	$C_2H_5/Rh(111)$ ( $(C_2H_5)_2Zn$ )
$\nu(M-C)$	484	370	630	420	510
$\rho(CH_3)$	941	855	900	810	860
$\nu(C-C)$	1022	-	-	nr.	nr.
$\omega(CH_2)$	1173	1140	1230	1180	1140
$\delta(CH_3)$	1376-1430	1420	1430	1410	1430
$\nu(CH_3)$	2918	2730,2900	2920	2900	2900

Data were taken from Ref. 40.

In bracket we indicate the original compounds.

On Pt(111), besides ethylene and ethane, the formation of methane was also identified which indicates the rupture of C-C bond and the decomposition of hydrocarbon fragments formed [11,41,42]. On Ag(111) surface C-H or C-C bond cleavage was not observed [44], and  $C_2H_5$  formed in the dissociation of  $C_2H_5I$  recombined into gas-phase butane around 190 K.

The product distribution of ethyl species both on Pd(100) and Rh(111) is dramatically influenced by the presence of Zn adatoms [45,46]. The  $C_2H_5$  and Zn coadsorbed system was produced by thermal and photodissociation of  $(C_2H_5)_2Zn$ .

Whereas on I-covered Pd surface no coupling of  $C_2H_5$  was observed, in the presence of Zn adatoms significant amounts of butene ( $T_p = 183$  K) and butane ( $T_p = 186$  K) were produced (Figure 5). At the highest surface concentration of  $C_2H_5$  on Zn/Pd(100), the following ratios were measured: 1.0:4.6:6.3:8.5 for butane:ethane:butene. On Rh(111), the coupling of  $C_2H_4$  into  $C_4H_8$  was the dominant reaction, butane formation was much less [46].

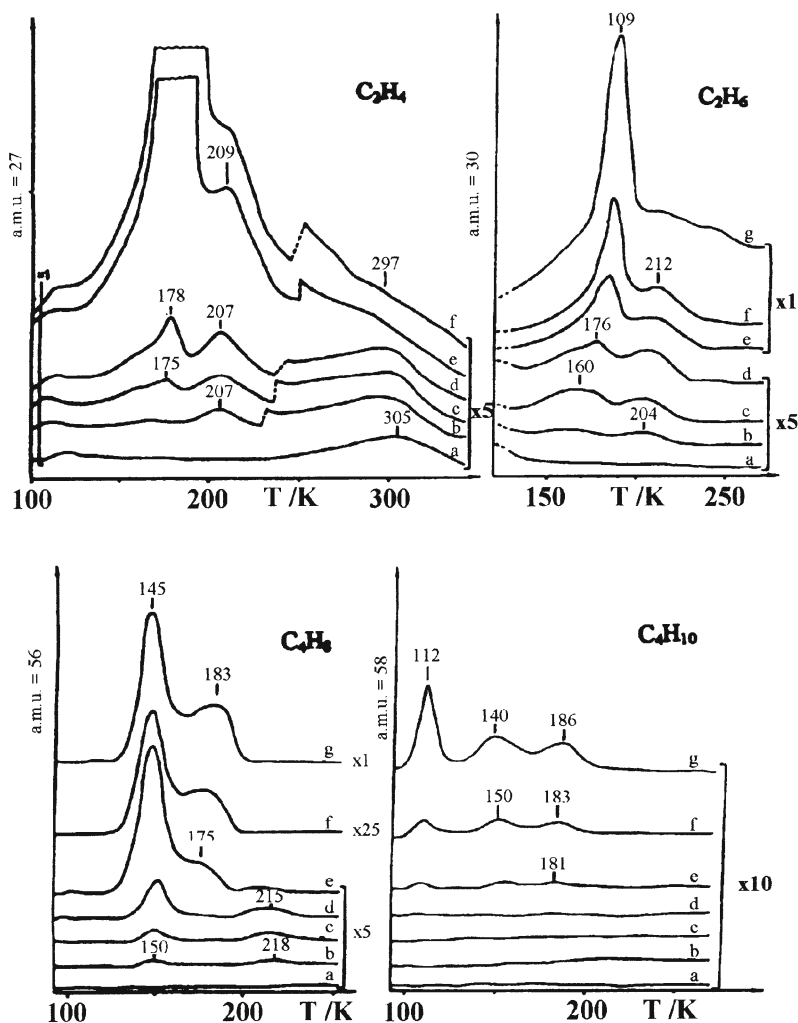


Figure 5. Thermal desorption spectra of  $C_2H_4$ ,  $C_2H_6$ ,  $C_4H_8$ , and  $C_4H_{10}$  following the adsorption of  $(C_2H_5)_2Zn$  on Pd(100) at 90 K [45].

### 3.4 FORMATION AND REACTION OF 2-C<sub>3</sub>H<sub>7</sub>

There are very few observations concerning the chemistry of propyl on metal single crystal surfaces. Bol and Friend [43] studied the interaction of 2-propyl iodide with Rh(111). By means of HREELS measurements they found that the C-I bond ruptures upon adsorption even at 100 K. The absence of the modes associated with intact C-I bonds,  $\delta(\text{C-C-I})$  at 260 cm<sup>-1</sup> and  $\nu(\text{C-I})$  at 295 cm<sup>-1</sup>, and the presence of modes at 220 cm<sup>-1</sup>,  $\nu(\text{Rh-I})$ , and 430 cm<sup>-1</sup>,  $\nu(\text{Rh-C})$ , were considered as a clear indication of C-I bond cleavage affording adsorbed 2-propyl and iodine. TPD studies showed that annealing the adsorbed 2-propyl iodide on Rh(111), the formation of gaseous H<sub>2</sub> and surface carbon predominated: some propene and trace amounts of propane were also identified. The T<sub>p</sub> values for the desorption of these products were not given.

## 4. Chemistry of CH<sub>x</sub> fragments on supported metals

Relatively few attempts have been made to generate CH<sub>x</sub> fragments on supported metals and to study their reaction pathways. The main difficulty is that the halogenated hydrocarbons also adsorb on the support of high surface area and it is not easy to differentiate between reactions occurring on metals and oxidic supports.

The adsorption and dissociation of CH<sub>2</sub>Cl<sub>2</sub> on Pd/SiO<sub>2</sub> have been investigated by means of infrared spectroscopy combined with mass spectrometry [47]. CH<sub>2</sub>Cl<sub>2</sub> adsorbs molecularly at low temperature (193-213 K) and interacts strongly with the OH groups of silica to form H-bridge-bonded methylene halide. This is exhibited by a significant attenuation of the 3744 cm<sup>-1</sup> band exhibited by silica and by the development of a broad spectral feature at 3662 cm<sup>-1</sup>. The dissociation of CH<sub>2</sub>Cl<sub>2</sub> was observed at 233-243 K. The primary product of dissociation, CH<sub>2</sub>, was characterized by adsorption bands at 2984 and 2907 cm<sup>-1</sup>. The CH<sub>2</sub> species dimerized into C<sub>2</sub>H<sub>4</sub> above 263 K. A fraction of ethylene desorbed, while another fraction was transformed into ethylidyne. The latter compound is characterized by absorption bands at 2922 and 2857 cm<sup>-1</sup>. By means of mass spectrometry, C<sub>2</sub>H<sub>4</sub> and HCl were identified in the desorbing gases at 250-330 K. Decomposition of CH<sub>2</sub>Cl<sub>2</sub> occurred above 350 K yielding C<sub>2</sub>H<sub>4</sub>, CH<sub>4</sub>, HCl, and H<sub>2</sub>O.

The adsorption and dissociation of CH<sub>3</sub>Cl and CH<sub>3</sub>I on Pd/SiO<sub>2</sub> have been also investigated by the same methods [48]. Both compounds adsorb molecularly at 193 K and interact strongly with the OH groups of silica to form H-bridge-bonded alkyl halides, which was accompanied by the same spectral changes as observed for the adsorption of CH<sub>2</sub>Cl<sub>2</sub>. The absorption band at 2920 cm<sup>-1</sup> due to adsorbed CH<sub>3</sub> species, was detected first at 263 K and was

eliminated above 373 K. Preadsorbed CO and O exerted no observable influence on the adsorption and dissociation  $\text{CH}_3\text{Cl}$ . However, potassium additive promoted the dissociation and somewhat stabilized the  $\text{CH}_3$  group on the surface. The dissociation of  $\text{CH}_3\text{I}$  occurred at lower temperature and to a greater extent than that of  $\text{CH}_3\text{Cl}$ . In this case very weak absorption bands were also produced at 2945, 2850 and  $1394\text{ cm}^{-1}$ , which were assigned to the stretching and deformation modes of CH in methoxy species.

The open question is the location of methoxy species. It is important to point out that the presence of adsorbed oxygen on Pd can be excluded as the sample was reduced at 673 K. In addition, it was found by several groups [49] that methoxy is rather unstable on Pd metals: it decomposes below 200 K. As methoxy is not formed following the adsorption of  $\text{CH}_3\text{I}$  on pure silica under same conditions, the obvious explanation of the production of methoxy is that  $\text{CH}_3$  species formed on Pd migrates onto silica where it reacts with OH groups to yield methoxy. We observed similar phenomena in the  $\text{NO}+\text{CO}$  reaction and after the adsorption of HNCO on supported metals: NCO species formed on metal crystallites spilt over onto the support where it was stabilized and accumulated [50].

The adsorption of methyl halides has been recently studied by means of FTIR spectroscopy on reduced  $\text{Cu/SiO}_2$  containing a relatively large amount, 15 wt%, of Cu [51]. The generation of  $\text{CH}_3$  species, indicated by the absorption band at  $2924\text{ cm}^{-1}$ , has been identified at 298 K. It was concluded that  $\text{CH}_3$  is bonded to Cu particles. The  $2924\text{ cm}^{-1}$  band was eliminated above 423 K. However, more stable bands at 2985, 2954 and  $2852\text{ cm}^{-1}$  were also detected, and were assigned to  $\text{Si-OCH}_3$ . The formation of later compound was described by the migration of  $\text{CH}_3$  from Cu on the support, where it reacted with  $\text{Si-OH}$  to give  $\text{Si-OCH}_3$ . Using a larger amount of catalyst sample, gas phase methane was observed after  $\text{CH}_3\text{I}$  adsorption on  $\text{Cu/SiO}_2$  at 298 K. The formation of ethane was not reported. As noted before, in the case of Cu single crystal the dominant pathway of the reaction of  $\text{CH}_3$  is its coupling into  $\text{C}_2\text{H}_6$ . It would be interesting to analyze the gas phase under different conditions. If the absence of ethane formation is confirmed, it would indicate that the transformation of  $\text{CH}_3$  into  $\text{CH}_3\text{O}$  on silica is more favourable than its coupling into ethane.

## 5. Oxidation of $\text{CH}_x$ on metal

Recently several studies have been performed concerning the selective addition of oxygen atoms to  $\text{C}_x\text{H}_y$  fragments and their oxidation. We point out only the main features of the reactions. In the case of  $\text{CH}_2$  species the formation of formaldehyde was observed at 170-330 K on  $\text{Rh}(111)$  [19,20,52],  $\text{Pt}(111)$  [21] and  $\text{Pd}(100)$  [53]. The coupling of O atoms with  $\text{CH}_3$  species to give  $\text{CH}_3\text{O}$

was also registered for Rh(111) [54,55] and Pd(100) [53]. The oxidation of  $C_2H_5$  on Rh(111) and Pd(100) gave acetaldehyde possibly via the transient formation of  $C_2H_5O$  [43,55,56]. In all cases the complete oxidation of  $C_xH_y$  fragments were also established.

## 6. Reaction of adsorbed $CH_3$ with $CO_2$

Several recent studies showed that supported platinum metals, particularly Rh, are efficient catalysts for the  $CH_4+CO_2$  reaction to produce synthesis gas,  $CO+H_2$  [7,8,57]. Its advantage, compared to the Ni catalyst, is its less sensitivity to coking, which is probably responsible for the deactivation of the Ni catalyst. In the explanation of this feature we proposed that  $CH_x$  fragments formed in the decomposition of  $CH_4$  react with  $CO_2$ , without their complete decomposition to surface carbon [7,8].

Recently we made an attempt to examine the reactivity of adsorbed  $CH_3$  on Rh/SiO<sub>2</sub> catalyst towards  $CO_2$ . Method used was Fourier transform infrared (FTIR) spectroscopy combined with mass spectrometry [58]. Methyl radicals have been produced by the pyrolysis of azomethane. The adsorption of  $CH_3$  on Rh/SiO<sub>2</sub> at 300 K resulted in the appearance of the bands at 2960, 2922 and 2854  $cm^{-1}$ . The positions of these bands are basically different from those observed following the adsorption of molecular azomethane. On the basis of the previous vibration studies, the band at 2922  $cm^{-1}$  is assigned to the C - H stretching vibration of adsorbed  $CH_{3(a)}$ , while the doublet at 2960 and 2858  $cm^{-1}$  to the C - H stretchings in  $CH_3O_{(a)}$ . In the low frequency region we detected weaker bands at 1350 and 1457  $cm^{-1}$ . The first one can be attributed to the  $\delta_a$  ( $CH_3$ ) of adsorbed  $CH_3$  and the second one to the  $\delta_a$  ( $CH_3$ ) of adsorbed  $CH_3O$ .

Annealing the adsorbed layer under constant evacuation led to a gradual attenuation of the above bands, but the relatively more intense CH stretching frequencies were detectable even after heating up the sample to 573 K. In the presence of  $CO_2$ , the 2922  $cm^{-1}$  band disappeared at significantly lower temperature (523 K) than on the effect of evacuation. Similar effect was observed under isotherm conditions. This can be seen clearly from the data presented in Figure 6, where we plotted the values of R (ratio of  $I_T/I_0$ ) against temperature ( $I_T$  = integrated absorbance defined at t time of annealing and  $I_0$  = integrated absorbance measured after adsorption of  $CH_3$ ). While the  $CH_3$  band remained practically unchanged at 373 K in vacuum, it markedly declined in the presence of  $CO_2$ . This effect of  $CO_2$  was also exhibited at 423 K, when the 2922  $cm^{-1}$  band completely vanished in 30 min (Fig 6).

In the analysis of the IR spectra of Rh/SiO<sub>2</sub> in other region we found the development of an absorption band at 2024  $cm^{-1}$  which we attribute to adsorbed CO. This band was detected first at 373 K slightly growing with the increase of

the reaction time. At 423 K, almost four times more intense CO band was registered following the CO<sub>2</sub> adsorption on CH<sub>3</sub>-covered catalyst. Parallel with the IR measurements, mass spectrometric analysis of the gas phase was also performed. The most striking feature of MS data is the appearance of  $m/e=16$  (CH<sub>4</sub>) and 28 (CO) mass numbers, when the annealing was made in the presence of CO<sub>2</sub>. Note that the adsorption of CH<sub>3</sub> radicals on pure silica produced the same adsorption bands (2960, 2927 and 2858 cm<sup>-1</sup>) in the CH stretching region as observed for Rh/SiO<sub>2</sub> sample, the admission of CO<sub>2</sub> on CH<sub>3</sub>-covered silica, however, exerted very little influence on the stability of these spectral features.

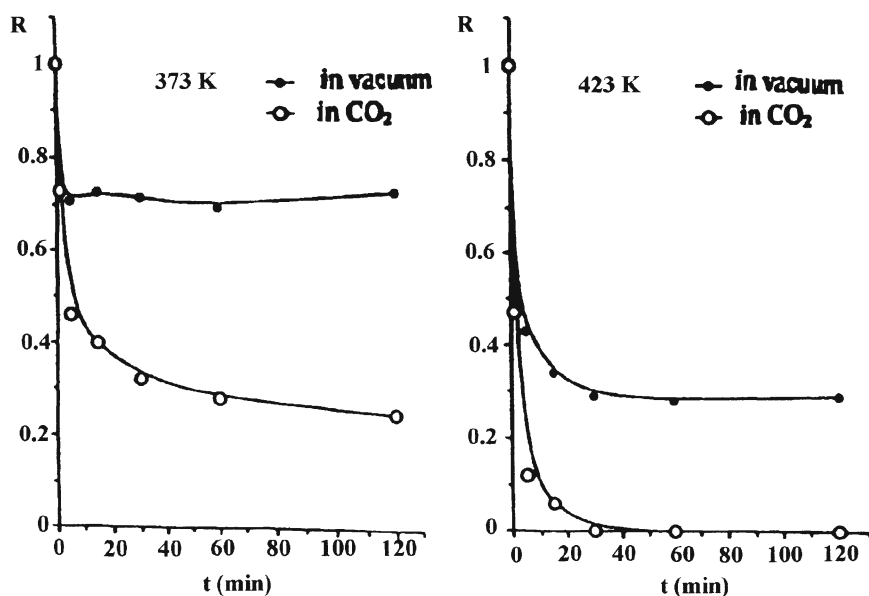
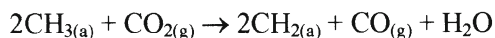


Figure 6. Changes in the ratio of integrated absorbances (R) of the band at 2922 cm<sup>-1</sup> due to CH<sub>3(a)</sub> in vacuum and in the presence of 1 Torr of CO<sub>2</sub> at 373 K and 423 K [58].

The appearance of CO in gas phase for Rh/SiO<sub>2</sub> and the concomitant decrease in the integral absorbance of the CH<sub>3(a)</sub> band strongly suggest the occurrence of a reaction between CH<sub>3(a)</sub> and CO<sub>2(g)</sub> leading to the formation of CO:





which would be a key step in the reforming of  $\text{CH}_4$ . It seems very likely that  $\text{CH}_2$  may also react with  $\text{CO}_2$ , which needs experimental confirmation. Alternatively,  $\text{CH}_2$  may undergo self-hydrogenation to give methane, and/or to a much less extent, dimerizes to ethylene, as was observed for Rh(111) under UHV conditions [19].

Although the large majority of surface species formed during the adsorption of  $\text{CH}_3$  are located on silica of high surface area, the different behaviour of Rh-free and Rh-containing silica in the presence of  $\text{CO}_2$  suggests the involvement of Rh in the reaction. It appears that the reaction between gaseous  $\text{CO}_2$  and adsorbed  $\text{CH}_3$  occurs on or at the periphery of Rh crystallites. The area of this interface should not be great, however, we may count with the migration of  $\text{CH}_3$  species from the silica to the neighborhood of Rh, where the reaction may take place. Further investigations are progress to disclose more details on this process.

## 7. Conclusions

Organic iodo compounds are suitable to produce hydrocarbon fragments ( $\text{CH}_2$ ,  $\text{CH}_3$ ,  $\text{C}_2\text{H}_5$  etc.) on metals surfaces of known composition. The formation and reactions of  $\text{C}_x\text{H}_y$  surface intermediates can be easily followed by spectroscopic methods of surface science. Depending on the nature of the metals,  $\text{C}_x\text{H}_y$  species react in different pathways. Whereas on platinum metals,  $\text{CH}_2$  and  $\text{CH}_3$  species are mainly selfhydrogenated into methane, on Cu and Ag surfaces their coupling is the dominant reaction.  $\text{C}_2\text{H}_5$  undergoes dehydrogenation into ethylene on one hand, and hydrogenation into ethane on other hand. Recombination of  $\text{C}_2\text{H}_5$  occurred only in the presence of Zn adatoms. Hydrocarbon fragments are combined with the adsorbed oxygen atoms even below 250-300 K to give different oxygenated compounds.

## 8. References

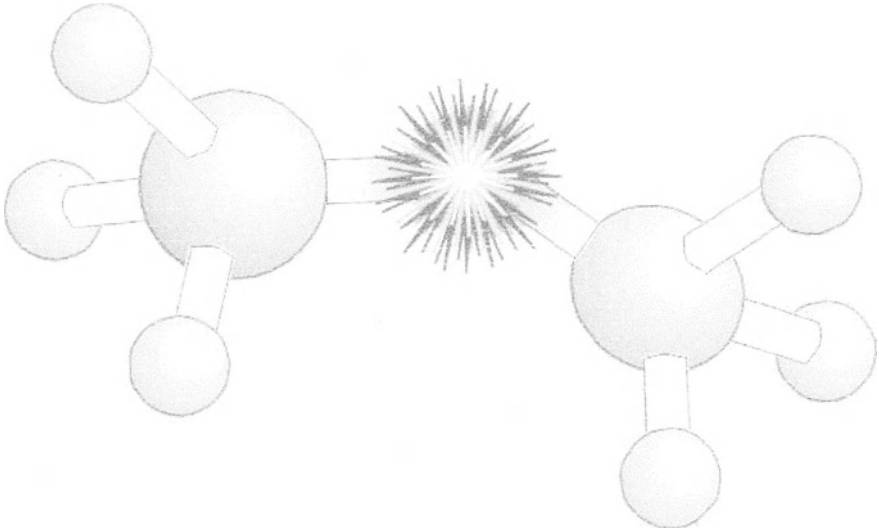
1. Bibby, D.M., Chang, C.D., Howe, R.F. and Yurchak, S. (eds.) (1988) *Methane Conversion, Studies on Surface Science and Catalysis*, Vol. 36 Elsevier, Amsterdam.
2. Lunsford, J.H., on Guczi, L., Solymosi F. and Tétényi P. (eds.) (1993) *Proc. of 10th Intern. Congress in Catalysis*, Akadémiai Kiadó, Budapest, p. 103
3. Ono, Y. (1992) *Catal. Rev. Sci. Eng.* **34**, 179.
4. van Santen, R.A., de Koster A. and Koerts, T. (1990) *Catal. Lett.* **7**, 1;
5. Koerts, T., Deelen, M.J.A.G. and van Santen, R.A. (1992) *J. Catal.* **138**, 101.



6. Rostrup-Nielsen, J.R. (1988) *Stud. Surf. Sci. Catal.* **36**, 73.
7. Solymosi, F., Erdöhelyi, A. and Cserényi, J. (1992) *Catal. Lett.* **16**, 399.
8. Erdöhelyi, A., Cserényi, J. and Solymosi, F. (1993) *J. Catal.* **141**, 287.
9. Solymosi, F., Erdöhelyi, A., Cserényi, J. and Felvégi, A. (1994) *J. Catal.* **147**, 272.
10. Solymosi, F. and Cserényi, J. (1994) *Catal. Today* **21**, 561.
11. Zaera, F. (1994) *J. Mol. Catal.* **86**, 221; Zaera, F. (1992) *Acc. Chem. Res.* **25**, 260; Bent, B.E. (1996) *Chem. Rev.* **96**, 1361.
12. Berkó A. and Solymosi, F. (1989) *J. Phys. Chem.* **93**, 12; Solymosi, F., Berkó, A. and Révész, K. (1990) *Surf. Sci.* **240**, 50; Kiss, J., Berkó, A., Révész, K. and Solymosi, F. (1990) *Surf. Sci.* **240**, 59; Solymosi, F., Kiss, J. and Revesz, K. (1991) *J. Chem. Phys.* **94**, 8510.
13. Zhou, X.-L., Zhou, X.-Y. and White, J.M. (1991) *Surf. Sci. Rep.* **13**, 73.
14. Solymosi, F. and Kovács, I. (1993) *Surf. Sci.* **296**, 171.
15. Peng, X.D., Wiswanathan, R., Smudde, G.H. and Stair, P.C. (1963) *Sci. Instrum.* **63**, 3930.
16. Jenz, D., Trenary, M., Peng X.D. and Stair, P. (1995) *Surf. Sci.* **341**, 282.
17. McBreen, P.H., Erley, W. and Ilach, H. (1984) *Surf. Sci.* **148**, 292.
18. Hills, M.M., Parmeter, J.E., Mullins, C.B. and Weinberg, W.H. (1986) *J. Am. Chem. Soc.* **108**, 3554.
19. Klivényi G. and Solymosi, F. (1995) *Surf. Sci.* **342**, 168.
20. Solymosi, F. and Klivényi G. (1995) *J. Phys. Chem.* **99**, 8950.
21. Zhou, X.-L., Lin, Z.-M., Kiss, J., Sloan, D.W. and White, J.M. (1995) *J. Am. Chem. Soc.* **117**, 3565.
22. Shustovich, E. and Bell, A.T. (1988) **205**, 492.
23. Berlowitz, P., Yang, B.L., Butt, J.B. and Kung, H.H. (1985) **159**, 540.
24. Hills, M.M., Parmeter, J.E., Mullins, C.B. and Weinberg, W.H. (1986) *J. Am. Chem. Soc.* **108**, 3554.
25. Henderson, M.A., Radloff, P.L., White, J.M. and Mims, C.A. (1988) *J. Phys. Chem.* **92**, 4111.
26. Liu, J.-L. and Bent, B.E. (1992) *J. Phys. Chem.* **96**, 8529.
27. Chiang, Ch.-M., Wentzlaff, T.H. and B.E. Bent (1992) *J. Phys. Chem.* **96**, 1836.
28. Kovács, I. and Solymosi, F. *J. Phys. Chem. in press.*
29. Zhou, X.-L. and White, J.M. (1991) *J. Phys. Chem.* **95**, 5575.
30. Solymosi, F. and Révész, K. (1993) *Surf. Sci.* **280**, 38.
31. Solymosi, F. and Révész, K. (1991) *J. Am. Chem. Soc.* **113**, 9145.
32. Solymosi, F. and Klivényi, G. (1993) *J. Elect. Spect. and Rel. Phen.* **64/65**, 499.
33. Henderson, M.A., Mitchell, G.E. and White, J.M. (1987) *Surf. Sci.* **184**, L325.
34. Chan, J.J. and Winograd, N. (1994) *Surf. Sci.* **314**, 188.

35. Zaera, F. (1991) *Langmuir* **7**, 1998; Zaera, F. and Hoffmann, H. (1991) *J. Phys. Chem.* **95**, 6797.
36. Zhou, X.L., Solymosi, F., Blass, P.M., Cannon, K.C. and White, J.M. (1989) *Surf.Sci.* **219**, 294.
37. Liu, J.-L., and Bent, B.E, (1992) *J. Vac. Soc. Technol. A.* **10**, 2202; Chiang, C.-M. and Bent, B.F. (1992) *Surf. Sci.* **279**, 79.
38. Lin, J.-L., Chiang, Ch.-M., Jenks, C.J., Yang, M.X., Yang, M.X., Wentzlaff, T.H. and Bent, B.E. (1994) *J. Catal.* **147**, 250.
39. Kovács, I. and Solymosi, F. (1993) *J. Phys. Chem.* **97**, 11056; Solymosi, F., Kovács, I. and Révész, K. (1994) *Catal. Letts.* **27**, 53.
40. Bugyi, L., Oszkó, A. and Solymosi, F. (1996) *Langmuir* **12**, 4145.
41. Zaera, F. (1990) *J. Am. Chem. Soc.* **111**, 4240.
42. Zaera, F. (1990) *J. Phys. Chem.* **94**, 8350.
43. Bol, C.W.Y. and Friend, C.M. (1995) *J. Phys. Chem.* **99**, 11930.
44. Zhou, X.-L. and White, J.M. (1989) *Catal. Lett.* **2**, 375.
45. Kovács, I., Iost, N. and Solymosi, F. (1994) *J. Chem. Phys.* **101**, 4236.
46. Klivényi, G. and Solymosi, F. *to be published*.
47. Solymosi, F. and Raskó, J. (1995) *J. Catal.* **155**, 74.
48. Raskó, J., Bontovics, I. and Solymosi, F. (1993) *J. Catal.* **143**, 138.
49. Solymosi, F., Berkó, A. and Tóth, Z. (1993) *Surf. Sci.* **285**, 197; Davis, J.L. and Barteau, M.A. (1980) *Surf. Sci.* **235**, 235; Guo, X., Hanley, L. and Yates, J.T. Jr. (1989) *J. Am. Chem. Soc.* **111**, 4605.
50. Solymosi, F., Völgyesi, L. and Sárkány, J. (1978) *J. Catal.* **54**, 336; Solymosi, F., Völgyesi, L. and Raskó, J. (1980) *Z. Phys. Chem.* **120**, 79; Solymosi, F. and Bánsági, T. (1979) *J. Phys. Chem.* **83**, 552.
51. Driessen, M.D. and Grassian, V.H. (1996) *J. Catal.* **161**, 810.
52. Bol, C.W.J. and Friend (1995) *J. Am. Chem. Soc.* **117**, 11572; *Surf. Sci.* **331**, L800.
53. Solymosi, F., Kovács, I. and Révész, K. (1996) *Surf. Sci.* **356**, 121.
54. Bol, C.W.J. and Friend (1995) *J. Am. Chem. Soc.* **117**, 8053.
55. Bugyi, L., Oszkó, A. and Solymosi, F. (1997) **159**, 305.
56. Bugyi, L. and Solymosi, F. *to be published*.
57. Richardson, J.T. and Paripatyadar (1991) *J. Catal.* **61**, 293.
58. Raskó, J. and Solymosi, F. *Catal Letts. in press*.

## **SECTION 2**



## **COMMUNICATIONS**

# THE EFFECT OF ACID SITES IN SKELETAL ISOMERIZATION OF N-BUTENES OVER FERRIERITES AND COALPO-11

JIRÍ CEJKA, NADEZDA ZILKOVÁ, ZDENA TVAROZOVÁ  
AND BLANKA WICHTERLOVÁ

*J. Heyrovský Institute of Physical Chemistry, Academy of Sciences  
of the Czech Republic, Dolejškova 3, CZ - 182 23 Prague 8*

## 1. Abstract

Acid sites of H-, NaH-ferrierites and those partly or fully dehydroxylated, and CoAlPO-11 were characterized by TPD of ammonia, UV-VIS spectroscopy, IR spectroscopy of D<sub>3</sub>-acetonitrile and by transformation of n-butenes. It has been shown that the high density of strong bridging OH groups or their simultaneous presence with strong Lewis sites support oligomerization reactions to higher olefins, leading via cracking to C<sub>3</sub>-C<sub>5</sub> olefins, C<sub>4</sub> paraffins and some coking. Thus, a low density of strong OH groups and absence of Lewis sites led to the selective performance of ferrierite. Under the same reaction conditions CoAlPO-11 with very low number of acid sites exhibited the highest and moreover stable activity to isobutene (yield 45 % at 620 K) for at least 48 hrs. This is a result, besides very narrow channels, of cooperative effect of weakly acidic both P-OH groups and Co<sup>2+</sup> Lewis sites. When P-OH groups were completely removed by calcination, skeletal isomerization selectively proceeds only on Co<sup>2+</sup> sites.

## 2. Introduction

While aluminas modified by fluorination or phosphoric acid were not able to reach sufficient selectivity to isobutene in n-butene isomerization, molecular sieve based catalysts are providing new approach in solving this problem. Since the discovery of Shell and Mobil Oil Co. in 1990 that molecular sieves with rather narrow channels can act as selective catalysts for skeletal isomerization of n-butenes to isobutene different opinions on the mechanism of isobutene formation were suggested. At first Mooiweer et al. [1] assumed a bimolecular

mechanism consisting of dimerization of butenes to  $C_8$  olefins with their subsequent isomerization and selective cracking to isobutene. Monomolecular reaction pathway was suggested by Meriaudeau et al. [2] using  $^{13}C$ -labelled 1-butene over ferrierite and by Gielgens et al. [3] on crystalline aluminophosphates. On the other hand, Guisnet et al. [4] believe that selective skeletal isomerization over ferrierite takes place by alkylation of adsorbed hydrocarbon residues. However, without any doubt the most important factor controlling the selective skeletal isomerization of linear butenes has appeared to be the geometry and architecture of the molecular sieve channels, i.e. shape selective effect. With this respect aluminosilicates of ferrierite structure and MeAlPO-11 provide the highest catalyst life-time, selectivity and yields to isobutene.

This contribution evaluates the effect of acid sites nature, number and strength by using molecular sieves with inner channel geometry most suitable for the butenes skeletal isomerization. A role of the density of  $H^+$  sites and presence of Lewis sites in ferrierites and low acidic both P-OH and Lewis sites represented by  $Co^{2+}$  ions in CoAlPO-11 is discussed.

### 3. Experimental

$NH_4$ -ferrierite with  $Si/Al = 8.4$  (TOSOH, Japan) and  $NaNH_4$ -ferrierites prepared by ion exchange with  $NaNO_3$  solution, and CoAlPO-11s with different concentrations of cobalt (up to 1.2 wt. %), synthesized from pseudoboehmite, orthophosphoric acid and di-*n*-propylamine as a template [5], were used. XRD, SEM and FTIR of skeletal vibrations confirm good crystallinity of the samples. The nature, acid strength and number of acid sites in ferrierites and CoAlPOs were determined by TPD of ammonia and FTIR spectra of adsorbed  $D_3$ -acetonitrile provided quantitative information on the number (and estimated strength) of Brönsted and Lewis sites. UV-VIS spectroscopy was used to follow coordination of cobalt.

Molecular sieves were activated at 670, 720 or 990 K in oxygen (ferrierite, CoAlPO-11) or hydrogen (CoAlPO-11). *n*-Butene skeletal isomerization was tested in a through-flow glass microreactor with 10 vol. % of 1-butene in nitrogen at WHSV  $4.5\ h^{-1}$  at 620 K with "on-line" connected GC-FID-MSD analysis of reaction products employing a high resolution capillary column ( $KCl/Al_2O_3$ ).

#### 4. Results and Discussion

D<sub>3</sub>-acetonitrile was used and its extinction coefficients with respect to Brönsted and Lewis sites were established, enabling thus to determine a total number of both acid sites. According to TPD of ammonia ferrierite exhibits very strongly acidic protonic sites (slightly higher compared to H-ZSM-5), while CoAlPO-11 shows acid sites of low acid strength. Calcination of ferrierite already above 670 K revealed the zeolite dehydroxylation proceeds (in contrast to a higher stability of OH groups in e.g. H-ZSM-5) leading to the increase in concentration of Lewis sites (Fig. 1). CoAlPO-11 exhibits very low number and strength of both P-OH groups and Co<sup>2+</sup> ions electron acceptor sites. By calcination of CoAlPO-11 at 970 K all P-OH groups were removed and only Co<sup>2+</sup> Lewis sites were present. Tetrahedral coordination of cobalt, observed by UV-VIS spectra, was found up to about 1.0 wt. % of cobalt in the aluminophosphate (Fig. 2a). At higher Co loadings in the synthesis mixture substantial increase in the concentration of highly distorted and octahedrally coordinated cobalt species was found (Fig. 2b).

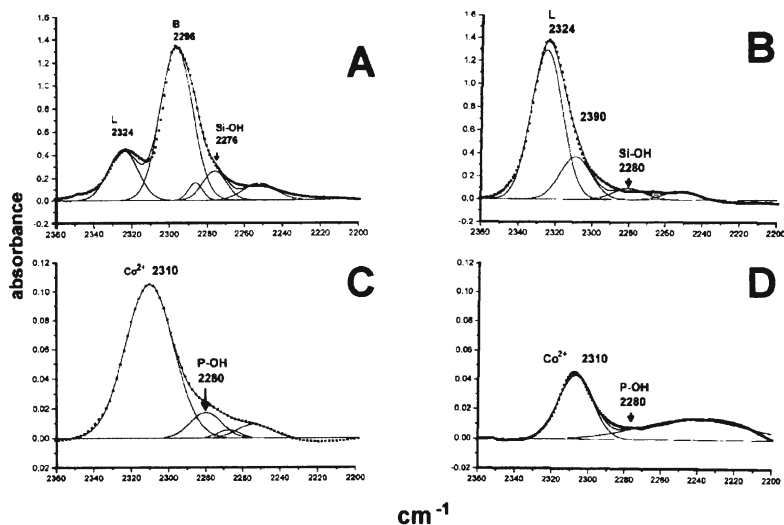


Figure 1. IR spectra of adsorbed D3 acetonitrile on ferrierite activated at 720 K (A) and 990 K (B), and CoAlPO-11 activated at 720 K (C) and 990 K (D).

The results of catalytic tests are given in the Table. With decreasing number of Brönsted sites and increasing number of strong Lewis sites in ferrierites formed by dehydroxylation at increasing activation temperature, total n-butene conversion, selectivity, and yield to isobutene decrease. For all these samples a

slight increase in isobutene yield and deactivation by coke with T-O-S was found. With increasing Na ion exchange by protonic sites, the NaH-ferrierites exhibit higher yield to isobutene and the deactivation is dramatically suppressed. These results indicate that the Lewis sites enhance the oligomerization reactions of butenes and following non-selective cracking to C<sub>3</sub>-C<sub>5</sub> olefins and formation of C<sub>4</sub> paraffins. However, even presence of exclusively of strong Lewis sites catalyzes these reactions. Partial Na exchange results in both lower density of Brönsted sites, but also in lowering the amount of Lewis sites. In connection with the above results, suppression of the number of Lewis sites seems to play a dominant role in increasing in the isobutene yield and resistance of the zeolite to deactivation by coking.

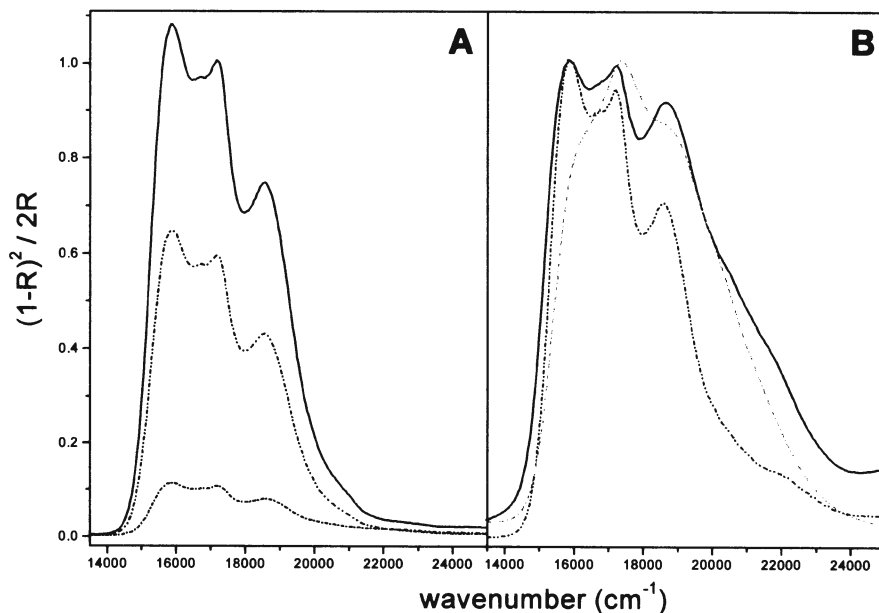


Figure 2. UV-VIS spectra of CoAlPO-11 with preferential T<sub>d</sub> coordination of Co (A) and large amount of octahedrally coordinated Co (B).

CoAlPO-11s with cobalt in T<sub>d</sub> coordination exhibit high and stable conversion and yield to isobutene being about 45 % and reaching almost the thermodynamic concentration. This can be ascribed to very narrow channels and low acidity of P-OH groups which probably cooperate with low acidic Lewis sites (Co<sup>2+</sup>) next to the P-OH groups. However, CoAlPO-11s with cobalt possessing distorted or octahedral coordination yield much lower selectivity to isobutene, thus indicating that highly crystalline samples with defined Co<sup>2+</sup>....P-OH site are required. However, if CoAlPO-11 was calcined at 990 K all the P-

OH groups were removed and it exhibited only low number of  $\text{Co}^{2+}$  Lewis sites, the reaction still proceeds rather selectively to isobutene and without fast deactivation. It indicates that weak acid Lewis sites can be the active sites for skeletal isomerization.

*Table* n-Butene skeletal isomerization to isobutene over H-ferrierite and CoAlPO-11

Zeolite	Activation temp. (K)	B/L* (mmol/g)	T-O-S (min.)	Conversion (%)	Selectivity (wt.%)	Yield (%)
H-ferrierite	670	1.7/0.12	5	60.0	51.2	30.7
			180	55.7	66.3	37.0
H-ferrierite	720	1.7/0.15	5	59.8	51.2	30.7
			180	49.5	66.3	37.0
H-ferrierite	990	trace/0.5	5	38.5	24.4	9.4
			180	22.2	36.3	8.1
Na,H-ferrierite	720	1.1/0.09	5	56.2	51.5	28.9
			180	49.1	70.5	34.6
Na,H-ferrierite	720	0.3/0.03	5	46.6	75.5	35.0
			180	49.6	70.0	34.7
CoAlPO-11	720	0.02/0.06	5	47.3	97.0	45.9
			180	46.0	97.6	44.9
CoAlPO-11	990	0/0.02	5	37.5	86.0	32.3
			180	30.6	97.2	29.8

\* Concentration of Brönsted and Lewis sites,

The results of butene isomerization over ferrierites clearly indicate that strong Lewis sites support bimolecular transformation of n-butenes to  $\text{C}_3$ - $\text{C}_5$  olefins and  $\text{C}_4$  paraffins. On the other hand, n-butene transformation on CoAlPO-11 with nearly 100 % selectivity to isobutene and thermodynamic yields of isobutene lead us to conclusion that monomolecular mechanism of n-butenes to isobutene proceeds on weak acidic sites in cooperation of Brönsted and Lewis ( $\text{P-OH} \dots \text{Co}^{2+}$ ) or on weak Lewis  $\text{Co}^{2+}$  sites. However, it should be considered that in addition to these effects for both molecular sieves the monomolecular or bimolecular reaction pathway is affected by geometry of inner channels (*restricted transition state selectivity*). All this implies that low strength of the both Brönsted and Lewis sites and suppression of the presence of strong Lewis sites result in high yields of isobutene.



## 5. Acknowledgement

Financial support from EC - Copernicus project (CIPA - CT94 - 0184) and Grant Agency of Academy of Sciences of the Czech Republic (No. A4040707) is highly acknowledged.

## 6. References

1. Mooiweer, H.H.de Jong K.P., Kraushaar-Czarnetzki B., Stork W.H.J. Krutzen B.C.H.: *Stud. Surf. Sci. Catal.*, 84 (1994) 2327.
2. Meriaudeau P., Bacaud R., Ngoc Hung L., Vu A.T.: *J. Mol. Catal. A* 110 (1996) L177.
3. Gielgens L.H., Veenstra I.H.E., Ponec V., Haanepen M.J., van Hooff J.H.C.: *Catal. Lett.* 32 (1995) 195.
4. Guisnet M., Andy P., Gnep N.S., Travers C., Benazzi E.: *Stud. Surf. Sci. Catal.* 105 (1996) 1365.
5. Corma A.: Private communication.

## OXIDATIVE DEHYDROGENATION OF PROPANE ON LARGE-PORE ZEOLITES

MIROSLAW DEREWINSKI,<sup>(1)</sup> JOANNA KRYSCIAK,<sup>(1)</sup>  
ZBIGNIEW OLEJNICZAK,<sup>(2)</sup> BOGDAN SULIKOWSKI,<sup>(1)</sup>  
GEMA BUENO<sup>(3)</sup>, VICENTE CORTÉS CORBERÁN,<sup>(3)</sup> RITA  
XIMENA VALENZUELA<sup>(3)</sup>

<sup>(1)</sup> *Institute of Catalysis and Surface Chemistry, Polish Academy of Sciences, Niezapominajek 1, 30-239 Kraków, Poland*

<sup>(2)</sup> *Institute of Nuclear Physics, Radzikowskiego 152, 31-342 Kraków, Poland*

<sup>(3)</sup> *Instituto de Catálisis y Petroleoquímica, Campus Universidad Autónoma Cantoblanco, 28-049 Madrid, Spain*

### 1. Introduction

Transformation of low molecular weight alkanes to alkenes and aromatics *via* oxidative and non-oxidative routes presents a major challenge since the implementation of the "Cyclar" process. Catalysts containing ZSM-5 zeolite modified with Ga or Zn species were investigated widely for this purpose [1]. Recently other zeolites (faujasite, ferrierite, Beta) were studied in the title reaction [2,3]. We showed that the already few gallium ions accommodated by the faujasite matrix significantly increase the selectivity to propene [2]. Preliminary results on zeolite Beta modified with Ga- and B-species [3] have also shown that this structure possesses promising activity and selectivity in the oxidative dehydrogenation (ODH) of propane.

In this communication we explore in details the catalytic and physico-chemical properties of zeolite Beta substituted with boron and aluminium. Beta is a high-silica, large-pore crystalline material. It possesses the interconnected 12-membered ring channels with 5.5 x 5.5 and 7.6 x 6.4 Å dimensions [4].

## 2. Experimental

Beta zeolites with different amounts of B and/or Al in the framework were synthesized hydrothermally at 423 K for 2-3 days. The gels were stirred during synthesis at 300-400 rpm. The samples were calcined at 773 K to remove tetraethylammonium hydroxide (TEAOH) used as an organic template and ion-exchanged with 1 M ammonium nitrate solution for 24 h at 365 K. The distribution of T atoms (T = Al, B) in the framework/extraframework positions was studied by FT IR,  $^{11}\text{B}$ ,  $^{27}\text{Al}$  and  $^{29}\text{Si}$  MAS NMR.

## 3. Results and Discussion

The as-prepared and ion-exchanged samples of zeolite Beta were, according to XRD, highly crystalline. Scanning electron microscopy (SEM) revealed that neither amorphous phase nor another crystalline phase were present in the samples. Despite the composition, uniform in size (0.5-1  $\mu\text{m}$ ) crystals displayed the almond-like morphology.

Calcination of Beta samples affects differently the status of framework B and Al.  $^{11}\text{B}$  MAS NMR confirmed the presence of only tetrahedrally coordinated framework boron in the as-prepared samples (Fig. 1a). After calcination at 773 K to remove organic template (TEAOH) both four- and three-coordinated boron species are seen (Fig. 1b). Thus, boron is readily expelled into extraframework positions with the formation of vacancies [1,5], but remains within crystals. The following ion exchange procedure washed out these extraframework boron species, leaving behind only the four-coordinated framework boron (Fig. 1c). The amount of extracted boron removed in this way is about 80% [5].

The process of boron removal, which emerges from NMR studies, is fully confirmed by IR studies in the framework vibration region of zeolite. An absorption band of Si-O-B vibrations is seen at  $898\text{ cm}^{-1}$  in the as-prepared material [B,Al]-BEA (Fig. 2a). Upon calcination the band of framework boron disappears nearly completely leaving a shoulder at about  $900\text{ cm}^{-1}$ . Simultaneously, a new band at  $944\text{ cm}^{-1}$  appears in the spectrum (Fig. 2b). This is assigned to silanol groups formed at the boron vacancies in the zeolite framework. As amount of boron displaced from framework sites is relatively high, the bands of the zeolite Beta framework at  $500\text{-}655\text{ cm}^{-1}$  are decreased in intensity. A subsequent ion exchange procedure restores the original spectrum of ordered zeolitic framework. The residual tetrahedrally coordinated framework boron is seen as a shoulder at  $900\text{ cm}^{-1}$ .

$^{27}\text{Al}$  MAS NMR studies of the samples showed that the state of aluminium is not affected by calcination and ion-exchange. In all the NMR spectra the only

observed signal is due to tetrahedrally coordinated framework aluminium, which confirms that Al is stable at the zeolite Beta framework sites.

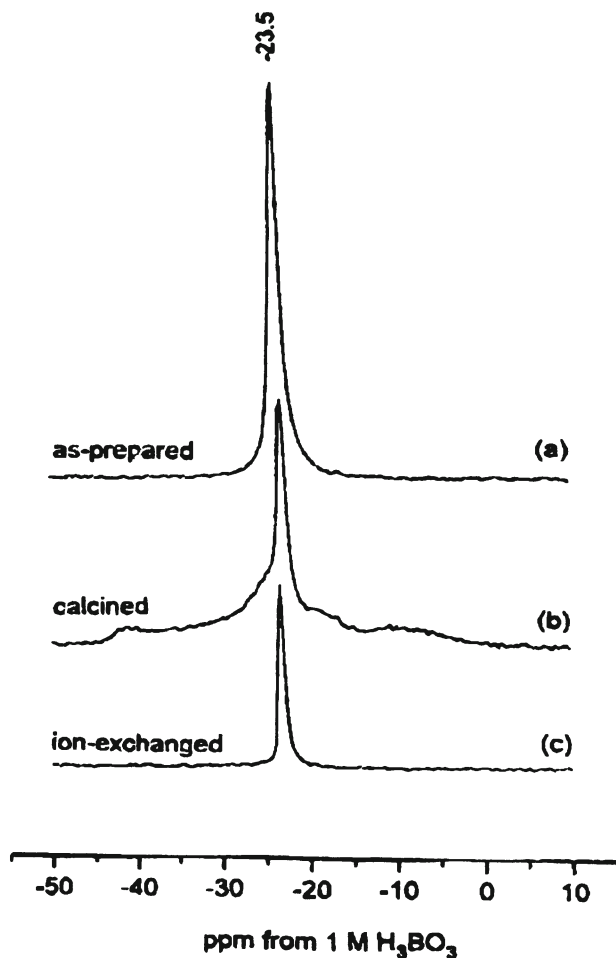


Figure 1.  $^{11}\text{B}$  MAS NMR spectra of [B, Al]-Beta on the absolute intensity scale. Chemical shifts given in ppm from external 1 M  $\text{H}_3\text{BO}_3$  in water [1].

The conversion of propane was elucidated at 673-873 K ( $\text{C}_3\text{H}_8:\text{O}_2=2:1$ , 1 atm). The overall  $\text{C}_3\text{H}_8$  conversion is a function of catalyst composition (Table). Below 800 K the [B, Al]-Beta sample is less active, whereas at higher temperatures its activity is higher or equal to [Al]-Beta. It is seen that when the sample contains only aluminium, selectivity to propene is low. However, if the sample contains two heteroatoms, the selectivity to olefin increases significantly to 51%, while combustion to  $\text{CO}_2$  was considerably suppressed.

Similar selectivities were found for a sample containing more boron, however the overall conversion of propane was lower. Both effects will be dwelled on within the frame of isomorphous substitution by boron and/or aluminium in zeolite Beta.

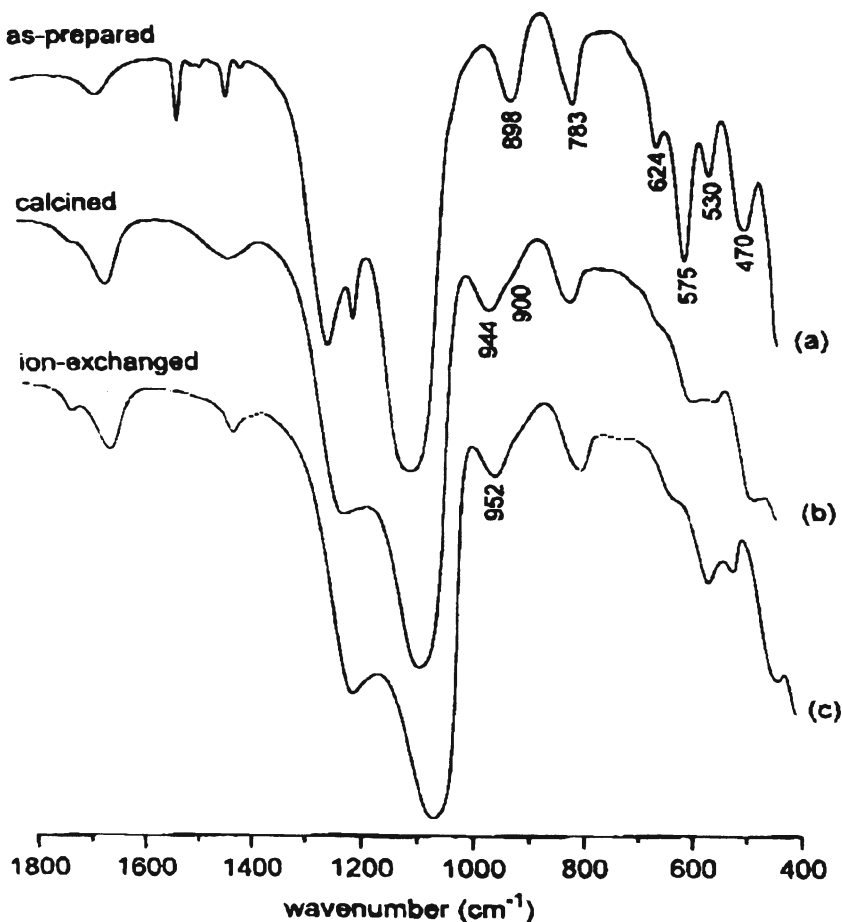


Figure 2. FT IR spectra of [B, Al]-BEA in the framework vibration region.

*Table.* Conversion and selectivity of propane ODH on zeolite Beta (BEA) containing aluminium [Al]-BEA or boron and aluminium [B, Al]-BEA

Sample	Temp. (K)	Conv. (mol %)	Selectivity (%)				
			Propene	CO <sub>2</sub>	CO	CH <sub>4</sub>	C <sub>2</sub> H <sub>4</sub>
[Al]-BEA	723	2.73	33.3	44.3	22.4	0	0
Si/Al=31.4	773	7.55	23.9	34.3	38.2	0.2	3.3
	823	16.38	25.5	20.6	47.5	1.3	5.0
[B, Al]-BEA	723	0.65	0	57.9	42.1	0	0
Si/B=77.1	773	4.52	50.6	17.7	26.1	0.5	5.1
	823	13.11	42.3	11.4	34.1	2.2	10.0

#### 4. Acknowledgement

Support from the Polish Academy of Sciences/C.S.I.C. Interchange Agreement is gratefully acknowledged.

#### 5. References

1. B. Sulikowski, *Heterogeneous Chemistry Reviews*, 3, (3), 203-268 (1996).
2. B. Sulikowski, Z. Olejniczak, V. Cortés Corberán, *J. Phys. Chem.*, 100, (24), 10323-30 (1996).
3. V. Cortés Corberán, R. X. Valenzuela, B. Sulikowski, M. Derewinski, Z. Olejniczak, J. Kryciak, *Catalysis Today*, 32, (1-4), 193-204 (1996).
4. W.M. Meier, D.H. Olson, Ch. Baerlocher, "Atlas of Zeolite Structure Types", 4th edition, Elsevier, London, 1996, p. 62.
5. M. Derewinski, F. Fajula, *Appl. Catal. A*, 108, 53-61 (1994).

# OXIDATIVE COUPLING OF METHANE OVER SODIUM-MANGANESE CATALYSTS IN THE PRESENCE OF HCl

E.V. SHISCHAK, M.S. KAZI, I.P. DZIKH, S.S. ABADJEV AND V.U. SHEVCHUK

*Petroleum Refinery Engineering Department, State University "Lvivska Polytechnica", S. Bandery St., 12, 290646 Lviv-13, Ukraine*

## 1. Abstract

The oxidative coupling of methane (OCM) has been studied over sodium-manganese catalysts under a wide range of operating conditions. The effect of temperature and oxygen concentration were examined. Relatively high methane conversion (28-30 %) and high selectivity to C<sub>2</sub> formation (60-70 %) is achieved. Time-on-stream of these catalysts does not exceed 18-20 h. Effect of HCl partial pressure on the CH<sub>4</sub> conversion and selectivities to principal products and on the time-on-stream has been studied. Addition of HCl into initial methane-oxygen mixture can increase selectivity to C<sub>2</sub> and decrease selectivity to carbon oxide's formation. In the presence of HCl the time-on-stream increases to 35-40 h. On the basis of these results the mechanism of OCM reaction is also discussed.

## 2. Introduction

Catalytic natural gas transformation by oxidative coupling of methane (OCM) is one of the most perspective alternative ways of valuable multi-tonnage petrochemical products such as ethene, arenes, vinyl chloride, *etc.* production [1-3]. The OCM reaction, which involves the catalytic transformation of methane and oxygen to ethane and water with furthering ethane conversion into ethene [4], has been studied intensively for the last 15 years. The reason for such a high interest in this reaction is that these very important petrochemical products can be utilized as feedstock for the chemical and petrochemical industry for producing chemicals.

Reaction of direct methane conversion to higher hydrocarbons has serious thermodynamic limitations. At same time such reactions are quite possible because of using oxygen as oxidant. The main problem in such a case, however, is selective formation of main reaction products (ethane, ethene and higher hydrocarbons) which may be oxidized to carbon oxides  $\text{CO}_x$  ( $\text{CO}$  and  $\text{CO}_2$ ) and water under the reaction conditions. This may be achieved by the selection of effective catalysts.

The OCM reaction has attracted much attention since the report by Keller and Bhasin [5], who showed the possibility of higher hydrocarbon's ( $\text{C}_{2+}$ ) formation from methane while they contacted with some systems, which were catalysts-reactants, at 700-800 °C. After that many reports appeared in the literature about studies of OCM, which were generalized in a series of reviews [1-4, 6-13]. The search for effective catalysts for direct methane transformation into ethane, ethene, benzene, formaldehyde, *etc.*, is carried out in many laboratories.

In earlier studies the goal of the applied research was often to maximize  $\text{C}_2$  yield by varying catalyst composition and reaction conditions; economical evaluations have shown that  $\text{C}_2$  selectivity is more important than yield, provided, of course, one can obtain a modest level of  $\text{CH}_4$  conversion.

Many alkali metal catalysts [14], alkaline earth catalysts [15, 16] and rare earth catalysts [17] are claimed to be effective catalysts for such process. The addition of chloride ions to an oxidative coupling catalyst can have a marked effect on its properties, particularly with respect to the  $\text{C}_2\text{H}_4/\text{C}_2\text{H}_6$  ratio [4]. Typically, the properly chlorided catalysts give  $\text{C}_2\text{H}_4/\text{C}_2\text{H}_6$  ratios between 3 and 5 [4]. It has been reported, however, that the highest selectivity to ethene is achieved when chloride ions are in the oxide catalysts [18-20], or if a chlorine-containing compound is introduced into the gas stream during the reaction [21-23]. However, these chlorine-containing catalysts generally lost activity within a few hours, which is a common problem with many of the chlorine-containing catalysts. Most of the chlorine is lost as  $\text{HCl}$  in the reaction of water with the catalyst. The rate of chlorine loss can be minimized by operating a catalyst at lower temperatures [4]. It was found, however, that the presence of  $\text{HCl}$  into initial methane-oxygen mixtures may increase considerably time-on-stream of these catalysts [24-26]. In addition,  $\text{HCl}$  may have significant effect on the OCM reaction [26].

In this work we have investigated the catalytic performance of sodium-manganese catalysts for OCM reaction under a wide of operating conditions, *i.e.* temperature, oxygen concentration and time-on-stream. Moreover, the influence of  $\text{HCl}$  partial pressure on activity, selectivity and time-on-stream has also been studied. On the basis of these results the mechanism of OCM reaction in the presence of  $\text{HCl}$  is also discussed.



### 3. Experimental

MgO, aerosil and H-ZSM-5 type zeolite ( $\text{SiO}_2:\text{Al}_2\text{O}_3=34$ ) were used as supports for the preparation of catalyst samples for the OCM reaction. Sodium chloride and manganese acetate were deposited on these supports by the incipient wetness impregnation.

The active component to carrier molar ratio was 0.14:1 for all catalysts. This ratio was chosen on the basis of literature data and preliminary experiments.

Catalyst's preparations were carried out by mixing of aqueous salt solutions with aqueous suspensions of the corresponding supports. Mixtures obtained were evaporated at constant stirring, dried and calcined in air stream at 550-600 °C for 3 h. The catalysts were tabletted, ground and the fraction of 0.25-0.5 mm was screened.

Natural gas with nearly 1.0 vol. % of ethane was used as a source of methane.  $\text{CH}_4\text{-O}_2$  and  $\text{CH}_4\text{-O}_2\text{-HCl}$  mixtures were prepared in separate vessels made from stainless steel. Purity of oxygen and hydrogen chloride was 99.7 and 99.6 vol. % respectively (main impurity - nitrogen).

Experiments were carried out in a flow reactor within the temperature range of 710-900 °C, weight hourly space velocity (WHSV)=1.0-20.0  $\text{h}^{-1}$  at atmospheric pressure. The catalyst volume was 0.375  $\text{cm}^3$  (0.55-0.65 g). Some experiments were carried out in a pulse reactor of the same volume.

The carbon-containing products of OCM were  $\text{C}_2\text{H}_6$ ,  $\text{C}_2\text{H}_4$ , CO and  $\text{CO}_2$ , which were analyzed by gas chromatography. Selectivity to separate reaction products formation was calculated as % of reacted methane, which was converted completely into corresponding reaction product. Amount of ethane was calculated as the difference between ethane content in gases after reactor and ethane content in the initial mixture.

### 4. Results and Discussion

In a few studies [24-28] recently we have examined the catalytic properties of different alkaline and earth-alkaline metal-containing catalysts. MgO, aerogel and H-ZSM-5 zeolite are active carrier for catalysts of OCM reaction. Carrier modification by used inorganic salts lead to a considerable increase of catalyst activities and selectivities. The most effective catalysts were chlorine-containing systems such as NaCl-MnO/MgO, NaCl-MnO/aerosil and NaCl-MnO/H-ZSM-5 [28]. A preliminary study of OCM over these sodium-manganese systems shows that the high methane conversions (16-25 %), concentrations of ethene and selectivities to  $\text{C}_2$  formation (40-60 %) were achieved.

#### 4.1 EFFECT OF REACTION CONDITIONS OVER DIFFERENT SODIUM-MANGANESE CATALYSTS

The effect of temperature and oxygen concentration on the reaction (Table 1) were examined. With the increase of oxygen concentration in the initial gas mixtures, the ethane concentration does not change significantly, the ethene concentration increases and the selectivity to  $C_2$  formation decrease. This fact reveals that the initial reaction product is ethane; ethene is formed by  $C_2H_6$  dehydrogenation.

Dependence of selectivity to  $C_2$  formation upon the temperature for initial mixture alone has an extremal character and achieves maximum at about 750 °C. Probably, the increase of selectivity with temperature increase is connected with the lower energy of activation of methane deep oxidation to CO and  $CO_2$  as compared with ethane formation.

*Table 1.* Oxidative coupling of methane over sodium-manganese catalysts (WHSV=8.9 h<sup>-1</sup>, pulse reactor)

Catalyst	T °C	[O <sub>2</sub> ] <sub>0</sub> (vol. %)	Concentration in gases after reactor (vol. %)		Selectivity (%)	
			C <sub>2</sub> H <sub>6</sub>	C <sub>2</sub> H <sub>4</sub>	C <sub>2</sub> H <sub>6</sub> +C <sub>2</sub> H <sub>4</sub>	C <sub>2</sub> H <sub>4</sub>
NaCl-MnO/MgO	730	3.6	1.52	0.80	50.9	42.3
		5.6	1.52	1.00	44.3	38.1
		10.4	1.26	1.29	35.3	32.8
		19.9	0.91	1.71	28.4	25.8
NaCl-MnO/aerogel	780	7.5	1.66	2.82	73.5	65.9
		10.4	1.70	3.24	61.3	57.8
		20.0	1.59	3.84	47.9	43.3
NaCl-MnO/H-ZSM-5	630	19.8	0.87	0.60	29.0	12.2
	680	19.8	1.35	1.95	38.4	23.6
	740	19.8	2.03	5.25	58.4	42.1
	770	19.8	1.02	4.68	52.8	43.3
	800	19.8	0.98	0.60	32.9	12.5
	845	8.6	2.07	1.90	58.3	42.5
		11.0	1.98	2.15	52.1	40.4
		14.8	1.85	2.60	41.2	31.6

Table 1 shows that with oxygen content of nearly 20 vol. % sufficiently high selectivity to  $C_2$  formation (58.4 %) is achieved over the NaCl-MnO/H-ZSM-5 catalyst at 740 °C. Relatively high methane conversion (28-30 %) and high selectivity to  $C_{2+}$  formation (60-70 %) are achieved over sodium-manganese catalysts. Analysis of results obtained shows that the selectivity to  $C_2$  formation decreases with the increase of oxygen concentration in initial mixture and

concentrations of these hydrocarbons increase at all temperature except for 800 °C.

It was established that methane conversion and selectivity to C<sub>2</sub> formation decrease with the increase of catalyst time-on-stream at constant temperature and WHSV [28]. The decrease of catalytic activity and selectivity may arise as a consequence of irreversible removal of catalyst active component, change of nature of active centres or catalyst surface, *etc.* From this point of view it was necessary to determine the catalyst time-on-stream during which catalytic activity and selectivity practically did not change. Results obtained showed that sodium-manganese catalysts studied have the relatively long time-on-stream (18-20 h), in comparison with other systems (LiF-MnO/aerogel, LiCl/MgO, K<sub>2</sub>CO<sub>3</sub>/MgO, Na<sub>3</sub>PO<sub>4</sub>-MnO/aerogel) in which time-on-stream does not exceed 3-4 h [28]. The increase of catalyst time-on-stream to more than 20 h leads to a sharp decrease of both methane conversion and selectivity to C<sub>2</sub> formation.

The possible reason for the deactivation of sodium-manganese catalysts may be NaCl hydrolysis:



because chlorine-containing catalysts are unstable under methane coupling reaction conditions and slowly release chlorine into the gas phase [22].

One of the possible ways of enhancement of the stability work of chlorine-containing catalysts and consequently the reducing NaCl hydrolysis rate is to accent equilibrium of this reaction to the left. It was reported by us previously [24-26], and also our preliminary studies showed that HCl presence into initial methane-oxygen mixtures may increase considerably the stability of sodium-manganese catalysts. From this point the aim of following part of this work was to examine HCl effect on the OCM reaction proceeding.

## 4.2 OCM REACTION IN THE PRESENCE OF HCl

A study of OCM reaction in the presence of HCl was carried in a flow reactor out under the following conditions:  $T=750$  °C,  $WHSV=1.0-14.9$  h<sup>-1</sup> at atmospheric pressure. Partial pressure of HCl ( $P_{\text{HCl}}$ ) in initial mixtures was varied within the range from 0 to 78 Torr at constant  $P(\text{O}_2)=68$  Torr. NaCl-MnO/H-ZSM-5 was used as catalyst.

The principal products selectivities for CH<sub>4</sub>-O<sub>2</sub>-HCl mixture's transformations over NaCl-MnO/H-ZSM-5 catalyst are listed in Table 2. Data obtained under similar conditions but without using HCl [28] are presented also for comparison. The selectivity to C<sub>2+</sub> formation does not exceed 52.4% at methane-oxygen mixture conversion without HCl. The increase of  $P_{\text{HCl}}$  in initial

mixtures at constant WHSV leads to insignificant decrease of  $\text{CH}_4$  conversion and increase of selectivity to  $\text{C}_{2+}$  formation, ethene particularly. The extremal behaviour of selectivity to  $\text{C}_2\text{H}_6$  formation as a function of the  $P_{\text{HCl}}$  is observed. At the same time, in this HCl pressure range, the amount of  $\text{C}_2$  hydrocarbons increased while the amount of  $\text{CO}+\text{CO}_2$  decreased. It should be noted that the selectivities to  $\text{CO}_x$  formation decrease sharply (nearly twice - for CO and by more than 4 times - for  $\text{CO}_2$ ) to compare with experiments without HCl. The selectivity to ethene formation achieves 73.7 % and selectivity to  $\text{C}_{2+}$  - nearly 80 % at  $P_{\text{HCl}}=78$  Torr. Results obtained are in good agreement with mechanism, proposed by Otsuka and co-workers [23].

Moreover, as it was established above, sodium-manganese catalysts did not reduce their activity till 20 working hours. The increase of catalyst time-on-stream over 20 h leads to the sharp decrease of both methane conversion (by 70-80 rel. %) and selectivity to  $\text{C}_{2+}$  formation (by 50 rel. %).

*Table 2.* Activity and selectivities to principal products formation over NaCl-MnO/H-ZSM-5 catalyst ( $T=750^\circ\text{C}$ ,  $P(\text{O}_2)=68$  Torr, time-on-stream – 30 min., flow reactor)

WHSV ( $\text{h}^{-1}$ )	$P_{\text{HCl}}$ (Torr)	$\text{CH}_4$ conversion (%)	Selectivity (vol. %)				
			$\text{C}_2\text{H}_6$	$\text{C}_2\text{H}_4$	$\text{C}_{2+}$	CO	$\text{CO}_2$
8.9	0	20.3	10.4	42.0	52.4	24.8	22.8
8.9	15	19.6	13.6	51.9	65.5	18.9	15.7
8.9	32	17.3	11.8	61.8	73.6	15.3	11.1
8.9	51	15.8	8.2	70.8	79.0	15.9	6.1
8.9	78	17.5	6.5	73.7	80.2	12.6	5.4
1.0	42	14.8	13.2	65.3	78.5	15.8	5.7
1.7	42	15.6	17.3	63.9	81.2	13.1	5.7
4.8	42	16.6	20.5	60.8	81.3	11.3	7.3
8.9	42	15.7	8.2	72.2	80.4	13.4	6.2
14.9	42	13.6	7.7	67.1	74.8	11.9	13.4

It must be underlined that in the presence of HCl in initial mixtures the time-on-stream of the catalyst increases to 35-40 h. During this time its catalytic activity and selectivity practically do not change. Probably, there should be related to the positive influence of HCl on the catalyst by stabilization of its composition [22].

### 4.3 HOMOGENEOUS AND HETEROGENEOUS REACTIONS OF OCM IN PRESENCE OF HCl

A model based on the original scheme of OCM proposed by Ito *et al.* [29] for C<sub>2</sub> hydrocarbon's formation is:



(the symbol  $\square$  denotes an oxide ion vacancy, and the subscript *s* an adsorbed species).

A coupling of two methyl radicals in the gas phase but near the surface produces C<sub>2</sub>H<sub>6</sub>:



Ethane reacts with surface O<sub>s</sub><sup>-</sup> ions to produce ethene:



Product distribution as a function of residence time shows that ethane appears as primary product while C<sub>2</sub>H<sub>4</sub>, CO and CO<sub>2</sub> are secondary. This suggests that ethane is formed by the coupling of CH<sub>3</sub><sup>•</sup> radicals.

The participation of reaction (5) has been demonstrated by Mims *et al.* [30] for the OCM over a Li/MgO catalyst by using labeled methane (<sup>13</sup>CH<sub>4</sub> or CD<sub>4</sub>). The study of recombination of methyl radicals in the gas phase [31] show that over a Li/MgO catalyst more than 40-45 % of C<sub>2</sub>H<sub>6</sub> was derived from the reaction (5). Similarly, Feng and Gutman [32] concluded that greater than 75 % of the ethane resulted from the coupling of CH<sub>3</sub><sup>•</sup> radicals in the gas phase when the catalyst was Sr/La<sub>2</sub>O<sub>3</sub>. These results show the importance of gas-phase reactions in OCM.

The main pathway of CO and CO<sub>2</sub> formation is heterogeneous and gas-phase oxidation of methyl radicals:



In the presence of HCl, this scheme can be extended to include HCl as a reactant by adding the gas-phase reactions (12)-(14). Similar reactions has been used to explain of the effect CH<sub>3</sub>Cl addition [23] to initial methane-oxygen mixtures over Li/MnO<sub>2</sub> catalyst.



The possible way for chlorine radical's formation is the reaction:



HCl efficiently scavenges the H<sup>•</sup> radicals via the fast reaction (14) and contribute to the inhibition of the gas-phase oxidation reactions.

Results obtained suggest that selectivity to C<sub>2+</sub> formation and ethene in particular, increases, time-on-stream of the catalyst increases also. From our point of view, the role of HCl in OCM reaction is to increase the rate of hydrocarbons C<sub>2+</sub> formation, similar to chlorine-containing catalysts [33], and proceeding of reversible reaction (12) is possible. Coincidence of selectivity to ethene formation increase and ethane decrease at P<sub>HCl</sub> > 32 Torr (Table 2) is explained by the fact that the reaction (13) of C<sub>2</sub>H<sub>6</sub> with chlorine radical proceeds together with reaction of oxidative ethane dehydrogenation [34, 35]. These facts confirmed the important positive role of HCl in its homogeneous reactions under methane-coupling conditions.

In addition, HCl may inhibit the general methane oxidation and carbon-containing reaction products to CO<sub>x</sub>. The presence of HCl in initial methane-oxygen mixtures accelerates the concentration of Cl<sup>•</sup> radicals [36], according to the reactions:



It must be emphasized that reactions (15) and (16) are very important, both of which remove the  $O^{\bullet\bullet}$  and  $OH^{\bullet}$  radicals from the system [36]. Obviously, these reactions are responsible for the increasing of selectivity to  $C_2$  hydrocarbon's formation and the inhibition of gas-phase oxidation at high HCl concentration.

Finally, HCl also increases the time-on-stream of the catalyst by stabilization of its composition and modification of its surface [22] with new active centre's formation.

## 5. Acknowledgement

This work was supported by the Ukrainian Ministry of Education.

## 6. References

1. N.D. Parkyns, C.I. Warburton, J.D. Wilson: *Catal. Today*, **18**, 385 (1993).
2. J.M. Fox III: *Catal. Rev. - Sci. Eng.*, **35**, 169 (1993).
3. P. Chaumette: *Rev. Inst. Fr. Petr.*, **20**, 711 (1996).
4. J.H. Lunsford: *Angew. Chem. Int. Ed. Engl.*, **34**, 970 (1995).
5. G.E. Keller, M.M. Bhasin: *J. Catal.*, **73**, 9 (1982).
6. M.G. Poirier, A.R. Sanger, K.J. Smith: *Can. J. Chem. Eng.*, **69**, 1027 (1991).
7. J.R. Anderson: *Appl. Catal.*, **47**, 177 (1989).
8. J.S. Lee, S.T. Oyama: *Catal. Rev. - Sci. Eng.*, **30**, 249 (1988).
9. J.H. Lunsford: *Catal. Today*, **6**, 235 (1990).
10. O.V. Krylov: *Catal. Today*, **18**, 209 (1993).
11. A.M. Maitra: *Appl. Catal. A*, **104**, 11 (1993).
12. A.M. Maitra: *Appl. Catal. A*, **114**, 65 (1994).
13. Y. Amenomiya, V.I. Birss, M. Golezdzinowski, J. Galuszka, A.R. Sanger: *Catal. Rev. - Sci. Eng.*, **32**, 163 (1990).
14. S.J. Korf, J.A. Roos, L.I. Veltman, J.G. van Ommen, J.R.H. Roos: *Appl. Catal.*, **56**, 119 (1989).
15. A.M. Maitra, I. Campbell, R.I. Tyler: *Appl. Catal.*, **85**, 27 (1992).
16. J.A.S.P. Carreiro, M. Baerns: *J. Catal.*, **117**, 258 (1989).
17. K. Otsuka, K. Jinno, A. Morikawa: *J. Catal.*, **100**, 353 (1986).
18. J.M. Thomas, W. Ueda, J. Williams, K.D.M. Harris: *J. Chem. Soc. Faraday Discuss. I*, **87**, 33 (1989).
19. S. Ahmed, J.B. Moffat: *Appl. Catal.*, **58**, 83 (1990).
20. B.K. Warren: *Catal. Today*, **13**, 311 (1992).
21. R. Burch, E.M. Crabb, G.D. Squire, S.C. Tsang: *Catal. Lett.*, **2**, 249 (1989).

22. R. Burch, S. Chalker, S.J. Hibble: *Appl. Catal. A*, **96**, 289 (1993).
23. K. Otsuka, M. Hatano, T. Komatsu: *Catal. Today*, **4**, 409 (1989).
24. V.U. Shevchuk, I.P. Dzikh, S.S. Abadjev, M.S. Kazi: in Proceeding 14th North American Meeting of the Catalysis Society, Snowbird, 92 (1995).
25. I.P. Dzikh, E.V. Shischak, S.S. Abadjev, V.U. Shevchuk: in Proceeding 2nd European Congress on Catalysis (EuropaCat-2), Maastricht, 146 (1995).
26. E.V. Shischak, M.S. Kazi, I.P. Dzikh, S.S. Abadjev, V.U. Shevchuk: *React. Kinet. Catal. Lett.* (in press).
27. I.P. Dzikh, E.V. Shischak, S.S. Abadjev, V.U. Shevchuk: in Proceeding 8th International Symposium on Relations between Homogeneous and Heterogeneous Catalysis, Balatonfüred, 102 (1995).
28. E.V. Shischak, M.S. Kazi, I.P. Dzikh, S.S. Abadjev, V.U. Shevchuk: *React. Kinet. Catal. Lett.*, **61**, 83 (1997).
29. T. Ito, J.-X. Wang, C.-H. Lin, J.H. Lunsford: *J. Am. Chem. Soc.*, **107**, 5062 (1985).
30. C.A. Mims, R.B. Hall, K.D. Rose, G.R. Myers: *Catal. Lett.*, **2**, 361 (1989).
31. K.D. Campbell, E. Morales, J.H. Lunsford: *J. Am. Chem. Soc.*, **109**, 7900 (1987).
32. Y. Feng, D. Gutman: *J. Phys. Chem.*, **95**, 6556 (1991).
33. R. Burch, S. Chalker, P. Loader, D.A. Rice: *Appl. Catal. A*, **79**, 265 (1991).
34. S. Sugiyama, K. Sogabe, T. Miyamoto, H. Hiyashi, J.B. Moffat: *Catal. Lett.*, **42**, 127 (1996).
35. S. Sugiyama, N. Kondo, K. Satomi, H. Hiyashi, J.B. Moffat: *J. Mol. Catal. A*, **95**, 35 (1995).
36. S.B. Karra, S.M. Senkan: *Ind. Eng. Chem. Res.*, **27**, 1163 (1988).



# MONO- AND BINUCLEAR IRON COMPLEXES IN ZEOLITES, CLAYS AND MESOPOROUS OXIDES AS BIOMIMETIC CATALYSTS

P.P. KNOPS-GERRITS AND P.A. JACOBS  
*Centrum voor Oppervlaktechemie en Katalyse,  
Katholieke Universiteit Leuven,  
Kardinaal Mercierlaan 92,  
B-3001 Heverlee, Belgium.*

## 1. Biomimetic Catalysts

Many metallo-proteins that catalyse the incorporation of oxygen atoms derived from dioxygen into organic substrates usually contain iron in mono- or polynuclear form. The “Ship-in-a-Bottle” approach proves an interesting approach to synthesise such metal complexes in zeolites and microporous materials [1]. The mechanistic understanding of the iron-containing heme-oxygenases has been substantially advanced (high-valent iron porphyrin oxo-complexes) [2]. In case of iron-containing non-heme-oxygenases such as methane mono-oxygenase [3] our understanding is more limited as only a few suitable models are known.

The choice of the ligand to coordinate the  $\text{Fe}^{2+}$  in the lattice (faujasite, mesoporous oxides HMS and MCM-41 or montmorillonite clays) affects the stability of the resulting complexes and the relative coordination of these with the lattice. Lattices in general coordinate in a polydentate fashion. The ligands chosen in this work coordinate in a mono-, bi-, tri-, tetra- or hepta-dentate fashion. The strength of complexation of the ligand, described by their position in the spectro-chemical series, affects the degree of iron complexation and thus its competition with lattice coordination. Aromatic ligands were selected due to their stability towards oxidation, diimines such as 2,2'-bipyridine, 2,6,2',6'-bipyrimidine and 1,10-phenanthroline are the most stable and allow a wide variety of coordinative geometries. Whereas for catalytic purposes coordinatively unsaturated environments, with bis complexation are preferred, for optical purposes coordinatively saturated environments, with tris complexation are preferred.

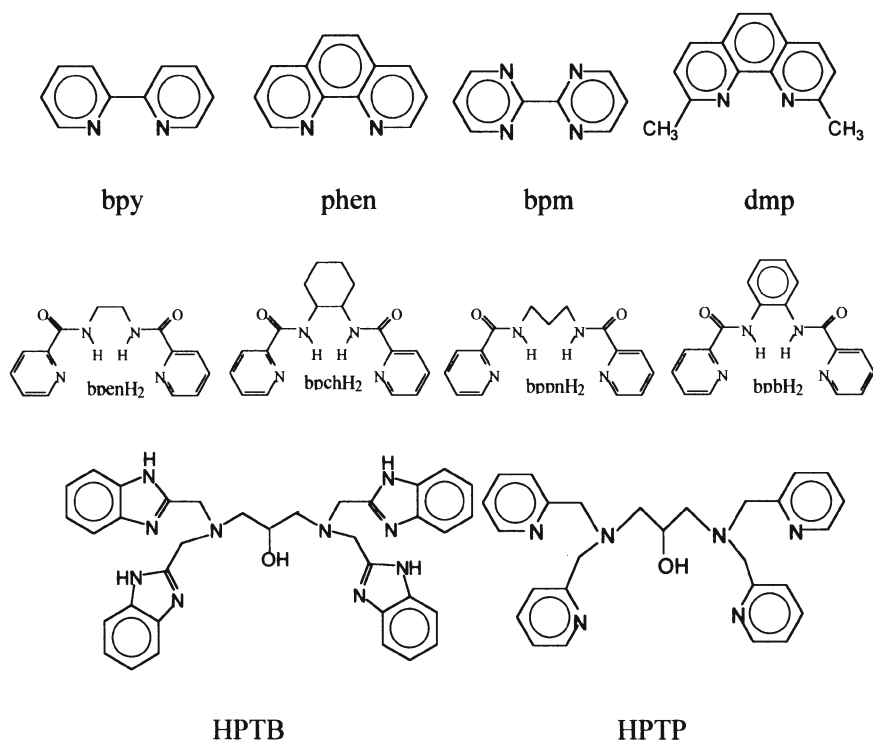


Figure 1. Organic ligands used for the iron complexation in oxides.

The deprotonation of carboxylic acids or amide groups on aromatic ligands in the presence of iron ions in zeolites affects their complex coordination geometry. For the tetradentate *N,N'*-bis-(2-pyridinecarboxamide)-1,2-alkane ligand deprotonation is complete for zeolite occluded iron complexes. The stoichiometry of ligand coordination is influenced by the high crystal field stabilisation energy for iron. Coordinative effects are observed in Mössbauer, DRS and EPR spectroscopy for the different complexes in faujasite zeolites. An Fe(bpR)-Y with one Fe<sup>2+</sup> ion per supercage is made by exchange of NaY with FeSO<sub>4</sub> · 7 H<sub>2</sub>O in water for 4 h under a N<sub>2</sub>-flow at pH 4, to circumvent oxidation to Fe<sup>3+</sup>. The light-blue Fe<sup>II</sup>-NaY is washed and dried for 16h at 473 K under N<sub>2</sub>-flow at a temperature increase of 1° / minute. bpR is added in a 1:1 metal to ligand ratio. After complexation for 4 days at 10-20 K above the ligand melting point the sample is obtained and soxhlet-extracted to remove excess ligand.

The heptapodate *N,N,N',N'*-tetrakis(2-*R*-methyl)-2-hydroxy-1,3-diaminopropane ligands with *R* = benzimidazolyl (HPTB) and *R* = pyridyl (HPTP), allow the coordination of two iron molecules to generate a dinuclear reaction center that can selectively bind peroxides in case of Fe<sup>III</sup> coordination. [Fe<sub>2</sub>(HPTP)(μ-OH)]<sup>4+</sup> and [Fe<sub>2</sub>(HPTB)(μ-OH)]<sup>4+</sup> complex cores show no accessibility to 12 MR pores of faujasite zeolites and need larger mesoporous supports for their inclusion. They can be retained in the mesoporous oxides, MCM-41 and HMS and in the MMT clay. The difference with the salts [Fe<sub>2</sub>(HPTP)(μ-OH)(NO<sub>3</sub>)<sub>2</sub>](ClO<sub>4</sub>)<sub>2</sub> and [Fe<sub>2</sub>(HPTB)(μ-OH)(NO<sub>3</sub>)<sub>2</sub>](NO<sub>3</sub>)<sub>2</sub> are the changes in the coordination geometry due to substitution or removal of the charge compensating anions, the variation in the extent of H-bridging of hydroxo- or oxo- groups of complexes to support oxo- or hydroxo-groups, the stabilisation of the complex guest by a better fit in the mesoporous oxide support host, the selective binding of peroxides on the diferric sites and the

stable association of organic peroxides on supports and the stabilisation of the complexes against self-oxidation. The synthesis, characterization and proposed mechanism of formation of the HPTP/B complexes in mesoporous materials e.g. MCM-41 [5] and HMS [6] is described. The Mössbauer, DRS, EPR, FT-IR & Raman and SEM characterisation of the pure and heterogenised complexes are discussed.

Montmorillonite (MMT, bentonite, linden/ bavaria) was purified and made homoionic with Na<sup>+</sup> by standard methods. Complexes are introduced into the interlayer region of MMT by ion exchange from CH<sub>3</sub>CN and water [4].

Hexagonal MCM-41 is used for complex impregnation (0.3% Fe on MCM-41 from XPS) in refluxing MeCN. An HMS structure is used for complex impregnation (0.3% Fe on HMS

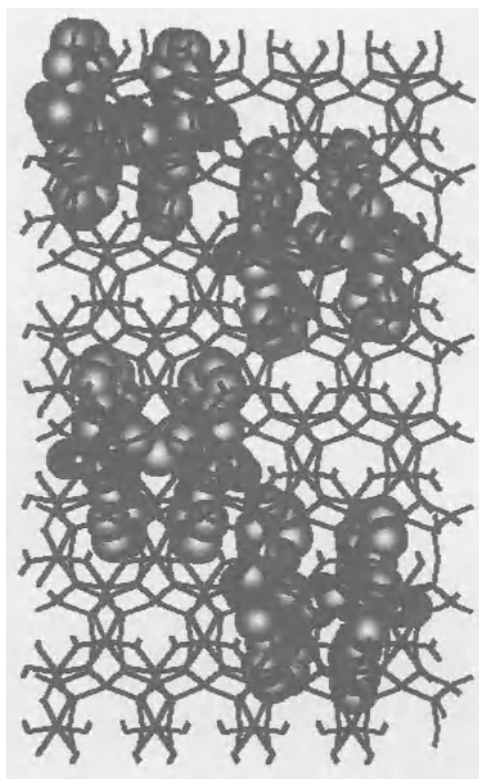


Figure 2. [Fe<sub>2</sub>(HPTP)(OH)(NO<sub>3</sub>)<sub>2</sub>] between montmorillonite layers.

from XPS) in refluxing MeCN. HMS has thicker framework walls and improved textural mesoporosities compared to MCM-41.

The cyclohexane and adamantane oxidation and the cyclohexylhydroperoxide deperoxidation chemistry are described and compared for all these systems. Mechanistic aspects on alkane activation may vary from radicalar Fenton chemistry to "Groves"-type oxo catalysis. Radicalar  $\text{Fe}^{\text{III}}$ -OOH decomposition is encountered for the bidentate diimine complexes, whereas an  $\text{Fe}^{\text{IV}}=\text{O}$  species is active in  $\text{N,N}'$ -bis-(2-pyridine-carboxamide)-1,2-alkane complexes. Still another intermediate is seen for the  $[\text{Fe}_2(\text{HPTP})(\mu\text{-OH})]^{4+}$  methane monooxygenase mimics for which  $\text{Fe-O}^\circ\text{-Fe}$  radicals are formed out of an  $\text{Fe-OO-Fe}$  intermediate, whereas singlet oxygen can also be directly liberated from the active site, and be responsible for the observed product distribution. Catalytic results after appropriate heterogenisation more closely match this observed for the enzymatic activity.

## 2. Acknowledgements

PPKG thanks the FWO for a grant as research-assistant and the IUAP-PAI sponsoring from the Belgian Federal Government in the frame of a programme on "Supramolecular Chemistry and Catalysis".

## 3. References

1. P.P.Knops-Gerrits, D.E.De Vos, F.Thibault-Starzyk and P.A.Jacobs, *Nature*, 369, 543-546, (1994); P.P.Knops-Gerrits, F.De Schryver, H.Van Mingroot, M.Van der Auweraer, P.A.Jacobs; *Chem.Eur.J.*, 2, 1996, 592-597.
2. Meunier, B., *Bull.Soc.Chim.France*, 1986, 4, 578; P.P.Knops-Gerrits, M.L'abbé, W.H.Leung, A.-M.Van Bavel, G.Langouche, Y.Bruynseraede, P.A.Jacobs; *Stud.Surf. Sci.Catal.*, 101, 1996, 811-820; P.P.Knops-Gerrits, A.M.Van Bavel, G.Langouche, M.L'abbé, P.A.Jacobs, *ECME* 96, 1996, 193-196.
3. Fish, R.H., et al., *Inorg.Chem.*, 1991, 30, 3002; P.P.Knops-Gerrits, S.Dick, A. Weiss, G.Langouche, M.Genet, P.Rouxhet, P.A.Jacobs; *Stud.Surf.Sci.Catal.*, submitted.(1997).
4. Nishida, Y., Nasu, M., Akamatsu, T., *Z.Naturforsch* 47b, 1992, 115.
5. Weiss, A., Dick, S., *Z.Naturforsch* 49b, 1994, 1051.
6. Beck, J.S. et al., *J. Am. Chem. Soc.*, 1992, 114, 10834.
7. Monnier, A. et al., *Science*, 1993, 261, 1299.

# MIXED $M_2O_3 \cdot ZrO_2 \cdot SO_4^{2-}$ (M=GA, IN, TL) CATALYSTS: PREPARATION, CHARACTERISATION AND CATALYTIC BEHAVIOUR IN DEHYDROISOMERISATION OF N-HEXANE

V. PARVULESCU<sup>a</sup>, S. COMAN<sup>b</sup>, P. GRANGE<sup>c</sup> AND V.I. PARVULESCU<sup>b</sup>

<sup>a</sup>- *Institute of Physical Chemistry of the Romanian Academy, Splaiul Independentei 202, Bucharest 77208, Romania.*

<sup>b</sup>- *University of Bucharest, Faculty of Chemistry, Department of Chemical Technology and Catalysis, B-dul Republicii 13, Bucharest 70346, Romania.*

<sup>c</sup>- *Université Catholique de Louvain, Unite de Catalyse et Chimie des Materiaux Divises, Place Croix du Sud 2/17, 1348 Louvain-la-Neuve, Belgium*

## 1. Introduction

Activation of alkanes on strong acid sulfate oxides catalysts elicited a large interest in the last decade mainly because of the possibility to isomerize n-butane at low temperatures with good selectivities [1].

A common feature of all the preparation procedures of mentioned catalysts is the adsorption on solid  $ZrO_2$  of an undetermined amount of sulfate from the excess it was exposed to. According to this, in a first step a zirconium salt is hydrolyzed with aqueous ammonia to produce zirconium hydroxide. Experiments performed using different kind of zirconium salts showed the importance of the precursors [2]. The sulfur content in these catalysts depends both on the nature of the zirconia hydroxide and on the calcination temperature. The use of the sol-gel technique to prepare  $Zr(OH)_4$  was also achieved. Catalysts prepared via this route exhibit higher surface areas and homogeneity. A new innovative methodology for the single-stage preparation of  $ZrO_2 \cdot SO_4^{2-}$  catalysts was recently proposed [3-5]. According to this procedure zirconium alkoxide is mixed with an alcohol and an inorganic acid. To hydrolyze the catalysts, a mixture of alcohol/water is slowly added dropwise with stirring.

Here we present the results obtained by modified one-step procedure using the colloidal sol gel technique. Sulfated  $\text{ZrO}_2$  and  $15\text{wt}\%\text{M}_2\text{O}_3\cdot\text{ZrO}_2$  ( $\text{M}=\text{Ga}, \text{In}, \text{Ti}$ ) were prepared. The catalysts were investigated in the dehydroisomerisation of n-hexane. Previous studies made by Valyon et al. [6] reported isomerization of n-hexane on titania modified  $\text{ZrO}_2$ .

## 2. Experimental

The catalysts were prepared via colloidal sol-gel technique as following.  $\text{ZrOCl}_2\cdot 8\text{H}_2\text{O}$  was dissolved in water and precipitated with  $\text{NH}_3$  solution till a  $\text{pH} = 9.0$ . The precipitate was washed in distilled water up to elimination of  $\text{Cl}^-$  and then peptized with  $\text{H}_2\text{SO}_4$  1N solution. Gelification was carried out at  $60^\circ\text{C}$  for 3 weeks. In the case of samples II the gelification was performed in the presence of template - tetrabutyl ammonium hydroxide. In this case, Ga, In or Ti was added during the gelification step as nitrate.

Samples were characterised by elemental analysis, measurements of the acidity using the Hammett's indicator technique, adsorption of  $\text{N}_2$  at 77 K, XPS, XRD, Laser Raman and Laser FT-IR spectroscopy,. Elemental analysis was performed by atomic emission spectroscopy with inductively coupled plasma atomization (ICP-AES). For determination of the acidity, the indicator (p-dimethylamino-azobenzene,  $H_0 = 3.3$ , crystal violet,  $H_0 = 0.8$ , anthraquinone,  $H_0 = 8.2$  or 2,4-dinitrofluoro-benzene,  $H_0 = -14.52$ ) was placed into a small ampoule and evacuated by a freeze-pump-thaw procedure. After samples were outgassed at  $500^\circ\text{C}$  for 1 h, these were cooled down to room temperature and then contacted with the above indicator by breaking the ampoule in situ. Distribution of the acid site strength was then determined by titration with propylamine.

Catalytic tests were performed in a fixed-bed quartz microreactor using 0.4 g catalyst. n-Hexane in a ratio 1 :1 with argon was preheated at  $150^\circ\text{C}$  and then passed over the catalyst bed with space velocities between 6 and  $30\text{ h}^{-1}$ . The experiments were carried out in the temperature range  $120 - 140^\circ\text{C}$ . The composition of the product stream was one-line chromatographically analysed. Rates of the reactions were determined by extrapolating the declining conversions to zero time of the stream. The apparent activation energies were determined from the temperature dependence of each rate.

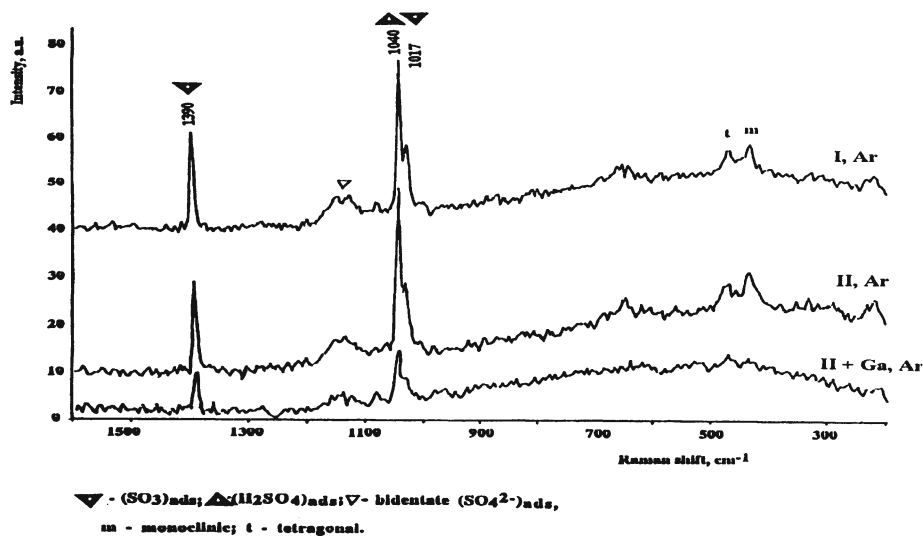


Figure 1. Raman spectra recorded for sulfated ZrO<sub>2</sub> and Ga<sub>2</sub>O<sub>3</sub>.ZrO<sub>2</sub> activated in Ar.

### 3. Results and Discussion

ZrO<sub>2</sub> and M<sub>2</sub>O<sub>3</sub>.ZrO<sub>2</sub>.SO<sub>4</sub><sup>2-</sup> (M=Ga, In, Tl) catalysts prepared using the above procedure exhibit an amorphous structure. Activation in air at 873 K induces a crystallisation process a XRD analysis indicates both the presence of sulfated and tetragonal ZrO<sub>2</sub> phases. These measurements are in total agreement with Raman spectra (Figure 1). The surface area of the samples is between 70 and 90 m<sup>2</sup>.g<sup>-1</sup>, depending on the chemical composition. In these conditions it was calculated a surface density of the sulfate groups corresponding to 3.6 — 14 groups.nm<sup>2</sup>. Titration experiments indicated that only 3-4 percents of the acid sites exhibit "superacid strength".

XPS spectra of the investigated samples indicated a large shift in the Zr<sub>3d</sub> band compared with pure ZrO<sub>2</sub> oxide, whereas no modification in the position of the energy bands was determined for Ga, In and Tl respectively. The band assigned to S<sub>2s</sub> (Figure 3) exhibit two components, one located at 169 eV and another at 170 eV.

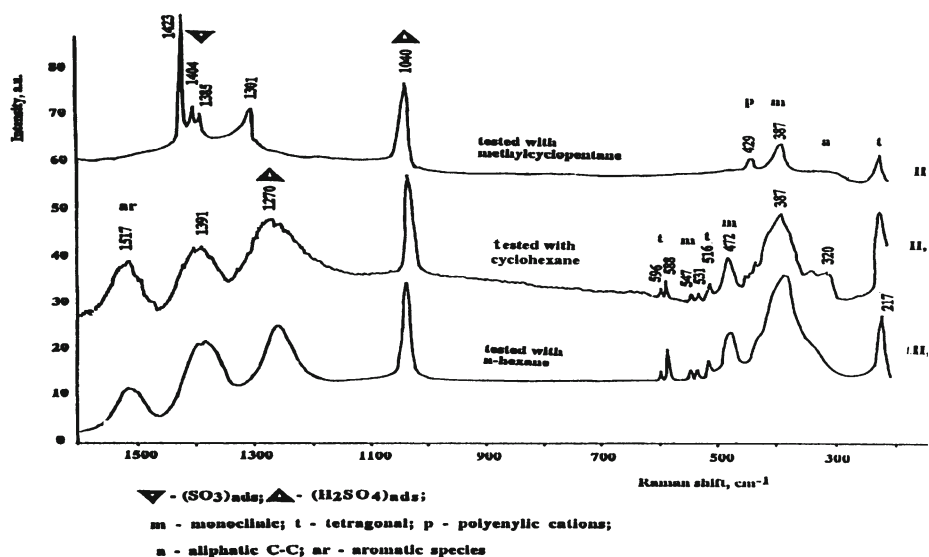


Figure 2. Raman spectra recorded for ZrO<sub>2</sub>.SO<sub>4</sub>2- (II) after reaction in the presence of n-hexane, methylcyclopentane or cyclohexane at 200 °C.

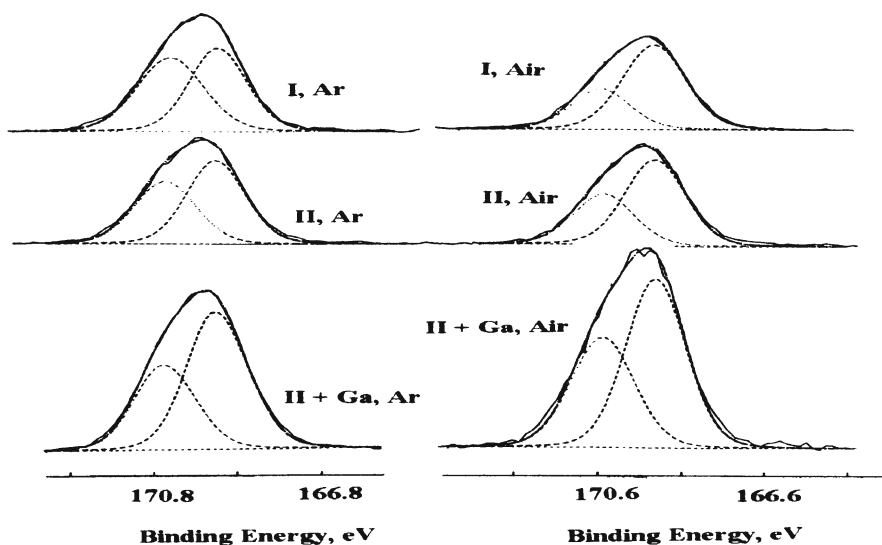


Figure 3. XPS spectra in the range of S2p binding energy

Variation of the reaction rate as well as of the reaction selectivity seems to be related on the ratio of these bands intensity (Figure 4). This ratio could also



be correlated with the Brönsted to Lewis ratio in these catalysts. The dehydroisomerisation occurs according to the bimolecular reaction proposed by Sommers [7], and the formation of methylcyclopentane could offer some arguments. However, in the investigated conditions the catalysts quickly deactivate and the Raman spectra recorded after reaction indicate the existence of aliphatic, polyenylic and aromatic species (Figure 2). Hydrogen released during the reaction is retained on the catalyst surface and the band assigned to  $\text{H}_2\text{SO}_4$  species is strongly increased after reaction.

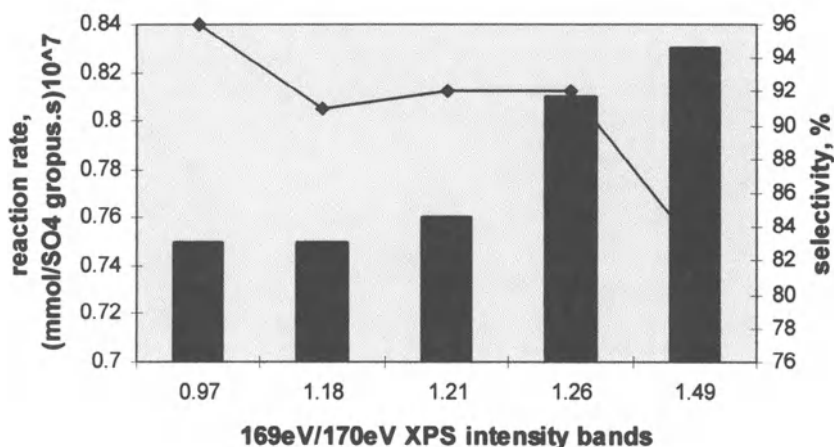


Figure 4. Variation of the reaction rate and selectivity to methylcyclopentane (◆); 473 K

#### 4. References

1. X.Song and A. Sayari, Catal.Rev.-Sci.eng. 38, 329 (1996).
2. B.H.Davis, R.A.Keogh and R.Srinivasan, Catal.Today 20, 219 (1994).
3. D.A.Ward and E.I.Ko, J.Catal. 150, 18 (1994).
4. M.Signoretto, F.Pinna, G.Strukul, G.Cerrato and C.Morterra, Catal.Lett. 36, 129 (1996).
5. D.Tichit, B.Coq, H.Armendanz and F.Figueras, Catal.Lett. 38, 109 (1996).
6. F.Lonyi, J.Valyon, J.Engelhardt and F.Mizukami, J.Catal. 160, 279 (1996).
7. F.Sommers, Catal.Today, to be published.

# THE SELECTIVE OXIDATION OF *N*-BUTANE TO MALEIC ANHYDRIDE; DEVELOPMENT OF SILICA-AND TITANIA SUPPORTED V-P-O CATALYSTS

MATTHIJS RUITENBEEK, R.A. OVERBEEK, D.C.  
KONINGSBERGER AND J.W. GEUS

*Utrecht University, Debye Institute,  
Department of Inorganic Chemistry  
PO Box 80083, 3508 TB Utrecht, The Netherlands  
tel. +31.30.253.6765 fax +31.30.251.1027  
m.ruitenbeek@anorg.chem.ruu.nl*

## 1. Introduction

The selective oxidation of *n*-butane to maleic anhydride (Eq. 1) over catalysts based on V-P-O (Vanadium Phosphorus Oxide) is a commercially attractive route in view of the availability of *n*-butane and the carbon efficiency of the reaction. However, the *n*-butane content in the gas flow, containing oxygen, being passed over the catalyst, is restricted due to explosion danger (1,2). The major part of the *bulk* V-P-O catalyst is formed by vanadylpyrophosphate,  $(VO)_2P_2O_7$ , but evidence has been found that other (amorphous) V-P-O phases on the surface play an important role too (3).

Of great interest from an industrial point of view is the development of supported V-P-O catalysts and therefore we developed a method to prepare supported V-P-O catalysts on various supports. These catalysts have extensively been characterized and tested (4,5). The new supported V-P-O catalysts show interesting properties like *i*) a well controlled and reproducible preparation procedure; *ii*) a large surface area to make more active sites available; *iii*) a very short activation period; *iv*) a high attrition resistance, which makes them suitable for fluidized bed processes.



(1)

The mechanism mostly assumed to be operative for selective catalytic oxidation over solid oxides is the Mars-Van-Krevelen mechanism, in which the catalyst is alternatively reduced by the compound to be oxidized and oxidized by gaseous molecular oxygen. It is important to assess whether the oxidation of *n*-butane over the selective V-P-O catalyst also proceeds via a Mars-Van-Krevelen mechanism. When this mechanism is operative with the V-P-O catalyst, recirculation of the catalyst between a gas flow in which the catalyst is exposed exclusively to *n*-butane and one in which the catalyst is re-oxidized by gaseous oxygen, is viable. Recovery of the more concentrated maleic anhydride from the gas flow can be performed more easily and the risk of explosions is lower. Moreover, Gleaves *et al.* (6) have shown that passing a flow of  $^{18}\text{O}_2$  and *n*-butane over the catalyst resulted in  $\text{C}^{18}\text{O}^{18}\text{O}$ , which indicates that oxygen that is chemisorbed from the gas phase leads to a rapid non-selective oxidation. The authors used TAP (Temporal Analysis of Products) in their investigations. This rapid oxidation to carbon dioxide by oxygen, chemisorbed from the gas phase, suggests that, in the absence of gaseous oxygen, a higher selectivity can be achieved.

It is desirable that catalysts, to be used in assessing the mechanism of the oxidation of *n*-butane, exhibit a high surface-to-volume ratio of the active component, since the reduction of the catalyst may involve only (part of) the surface layer. Furthermore, the catalyst should preferably be active at low temperatures. Centi *et al.* (7) have observed that exposure of the usual bulk V-P-O catalyst to *n*-butane at more elevated temperatures leads exclusively to desorption of carbon oxides. Reaction of *n*-butane with the surface in the absence of oxygen, or with an oxygen content too low to achieve oxidation of *n*-butane, causes carbon-containing species to be deposited on the surface of the catalyst. Exposure of the thus covered catalyst surface to molecular oxygen at temperatures of 400 to 450°C, results in gaseous carbon oxides only. To investigate whether the adsorbed carbon-containing species can react with molecular oxygen to maleic anhydride calls for operation at lower temperature and, hence, for a catalyst being active at lower temperatures.

In this project, we investigated the mechanism of *n*-butane oxidation using a titania-supported V-P-O catalyst. A new procedure for the application of hydrated vanadia on the surface of supports involving  $\text{V}^{\text{III}}$  was used to prepare titania-supported V-P-O catalysts of high activity (4).  $\text{V}^{\text{III}}$  was produced via a scaled-up electrochemical reduction procedure of  $\text{V}^{\text{V}}$  salts.

Using on-line mass spectrometry, the composition of effluent gas from the catalysts after reaction with consecutive pulses of *n*-butane and oxygen was analyzed. To establish the reduction of the active component, XANES (X-ray Absorption Near-Edge Structure) spectroscopy can be used (8). This technique provides information about the oxidation state of the vanadium (9-12). Furthermore, the characterization can be performed *in-situ*, and under well-

defined reaction conditions. Since the titania-supported catalysts are well-dispersed, the contribution of the (active) surface to the total spectrum is large. Therefore, the surface reactivity of the titania-supported V-P-O catalyst can be assessed with this technique.

Because of the high activity of the titania-supported catalysts, it was possible to use these in a separate reduction-oxidation process in which *n*-butane was adsorbed in absence of molecular oxygen at relatively low temperatures ( $\pm 280^\circ\text{C}$ ). In a second step, the catalyst was reoxidized in absence of *n*-butane leading to the selective formation MA. The selectivity to maleic anhydride was remarkably better in the oxidation-reduction process than under steady state conditions (13). A special titania-supported V-P-O catalyst has been prepared and characterized *in-situ* in the separate oxidation-reduction process with X-ray Absorption Spectroscopy (8).

XANES revealed that after a few reaction cycles, no more change in the valence state of vanadium occurs after reduction or reoxidation of the sample. This indicates that the generally assumed Mars-Van-Krevelen mechanism is not operative for this catalyst.

Recently, we started the analysis of the EXAFS (Extended X-ray Absorption Fine Structure) part of the X-ray absorption data. Figure 1 shows the Fourier transform of the raw data of a typical equilibrated bulk catalyst and a titania-supported catalyst.

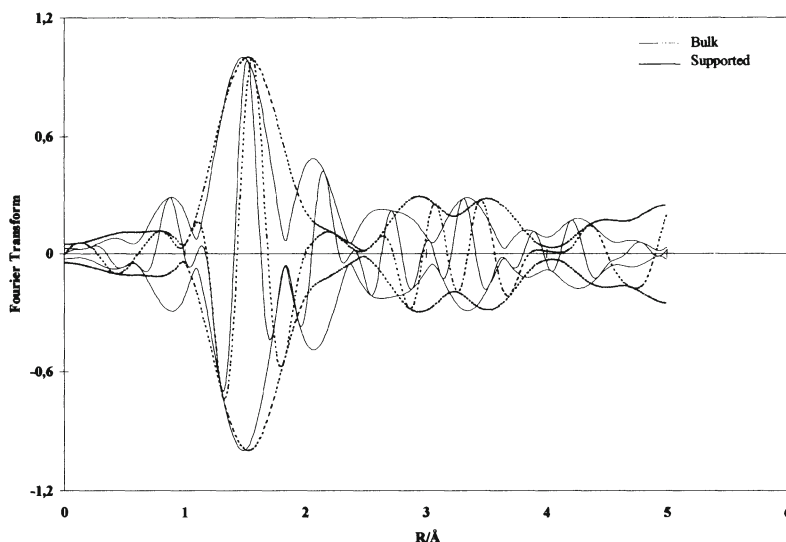


Figure 1. Fourier Transformation ( $k^2$ ,  $\Delta k=3-11\text{\AA}^{-1}$ ) of an equilibrated (organic preparation) bulk catalyst (dotted line) and a titania-supported catalyst (solid line). Spectra were recorded in He at  $-196^\circ\text{C}$  at the SRS in Daresbury (UK), station 8.1

It is obvious that the structure of the titania-supported catalysts is completely different from the structure of a bulk V-P-O catalysts. Furthermore, large differences in the local environment of vanadium were observed during the sequential steps in the earlier described reduction-reoxidation process.

Data were fitted in *R*-space by means of the difference-file technique with an in-house developed computer program, XDAP (14,15). Results of the fits of two bulk V-P-O catalysts, prepared in organic and in aqueous media are in good agreements with crystallographic data (16). In Table 1, the EXAFS results of an organic bulk catalysts as well as the results of a titania-supported V-P-O catalysts (8.2 wt.% V) are represented.

*Table 1.* Atomic distances, coordination numbers and Debye-Waller factors of an equilibrated bulk catalyst (organic preparation) and a titania-supported catalyst. Input data for the bulk catalyst were fixed and taken from (16).

	<i>Bulk</i>			<i>Supported</i>		
	R (Å)	N	$\Delta\sigma^2$	R (Å)	N	$\Delta\sigma^2$
V-O <sub>1</sub>	1.59	1	0.00347	1.59	1.11	0.00165
V-O <sub>2</sub>	1.94	2	-0.00199	1.92	1.92	-0.00504
V-O <sub>3</sub>	2.07	2	0.00465	-		
V-O <sub>4</sub>	2.36	1	0.00330	-		
V-O <sub>5</sub>				2.58	2.01	-0.00313
V-V	3.23	1	0.01592	-		
V-P	3.33	4	0.00400	3.42	3.23	0.00944

The experimental data for the titania-supported catalyst gave a satisfactory fit for all spectra. A comparison between the structure of bulk V-P-O and the titania-supported V-P-O catalyst under reaction conditions in the different steps of the reduction-oxidation process will be discussed. Furthermore, it will be shown that EXAFS gives important information about the type of oxygen that is consumed during the oxidation/reduction process.

## 2. References

1. G. Centi, F. Trifiro, J.R. Ebner, and V.M. Franchetti, *Chem. Rev.* **88** (1988), 55.
2. *Vanadylpyrophosphate Catalysts*, ed. G. Centi, *Catal. Today* **16** (1993), 1.
3. R.A. Overbeek, M. Ruitenbeek, R.T. Wegh, M. Versluijs-Helder, A.J. van Dillen, and J.W. Geus, submitted to *J. Catal.*
4. R.A. Overbeek, P.A. Warringa, M.J.D. Crombag, L.M. Visser, A.J. van Dillen, and J.W. Geus, *Appl. Catal. A: General* **135** (1996), 209-230.

5. R.A. Overbeek, A.R.C.J. Pekelharing, A.J. van Dillen, and J.W. Geus, *Appl. Catal. A: General* **135** (1996), 231-248.
6. J.T. Gleaves, J.R. Ebner, T.C. Kuechler, *Catal. Rev. Sc. Eng.* **30**(1) (1988), 49.
7. G. Centi, F. Trifiro, G. Busca, J. Ebner, J. Gleaves, *Disc. Faraday Soc.* **87** (1989), 215.
8. M. Ruitenbeek, R.A. Overbeek, A.J. van Dillen, D.C. Koningsberger, J.W. Geus, *Recl. Trav. Chim. Pays-Bas* **115** (1996), 519.
9. J. Wong, F.W. Lytle, R.P. Mesmer, D.H. Maylotte, *Phys. Rev. B.* **30** (1984), 5596.
10. J. Wong, D.H. Maylotte, F.W. Lytle, R.B. Gregor, R.L. St. Peeters, in "EXAFS and Near Edge Structure", A. Bianconi, L. Inoccia and S. Stipcich, eds., Springer Verlag, Berlin, 1983, p. 206.
11. J. Wong, R.P. Mesmer, D.H. Maylotte, in "EXAFS and Near Edge Structure", A. Bianconi, L. Inoccia and S. Stipcich, eds., Springer Verlag, Berlin, 1983, p. 130.
12. I. Davoli, S. Stizza, M. Benfatto, O. Gzowski, L. Murawski, A. Bianconi, in "EXAFS and Near Edge Structure", A. Bianconi, L. Inoccia and S. Stipcich, eds., Springer Verlag, Berlin, 1983, p. 162.
13. M. Ruitenbeek, R.A. Overbeek, L.M. Visser, A.J. van Dillen, D.C. Koningsberger, J.W. Geus, *to be published in Catal. Letters*.
14. M. Vaarkamp, J.C. Linders, D.C. Koningsberger, *Physica B* (1995), 208.
15. M. Vaarkamp, J.C. Linders, D.C. Koningsberger, *Proc. XAFS VIII*, Berlin, 159.
16. P.T. Nguyen, R.D. Hoffman, A.W. Sleight, *Mat. Res. Bull.* **30** (1995), 1055.

# THE EFFECT OF COBALT DOPING ON THE STRUCTURAL TRANSFORMATION SEQUENCES OCCURRING DURING THE ACTIVATION OF VANADIUM PHOSPHORUS OXIDE CATALYSTS

S. SAJIP<sup>a</sup>, C. RHODES<sup>b</sup>, J.K. BARTLEY<sup>b</sup>, A. BURROWS<sup>a</sup>, C.J. KIELY<sup>a,b</sup>, AND G.J. HUTCHINGS<sup>b</sup>.

<sup>a</sup> *Department of Materials Science and Engineering, University of Liverpool, Liverpool L69 3BX, United Kingdom.*

<sup>b</sup> *Leverhulme Centre for Innovative Catalysis, Department of Chemistry, University of Liverpool, Liverpool, L69 3BX, United Kingdom.*

## 1. Introduction

Vanadium phosphorus oxide (VPO) is commercially used to catalyse the oxidation of *n*-butane to maleic anhydride (MA). The catalyst itself is formed by activating the hemihydrate precursor  $\text{VOHPO}_4 \cdot 0.5\text{H}_2\text{O}$  in an *n*-butane/air mixture at about 400°C for at least 100 hours [1]. Although many authors believe that this reaction is dependent solely on the presence of the crystalline  $(\text{VO})_2\text{P}_2\text{O}_7$  phase [2], Hutchings *et al* have argued that the initial reaction step requires a  $\text{V}^{5+}$  phase and that selectivity and activity improve if a significant amount of a disordered  $\text{V}^{4+}$ - $\text{V}^{5+}$  phase is present [3].

Kiely *et al* [4] have recently examined a series of activated VPO catalysts prepared in an organic medium in which the activation time was systematically varied. Detailed microstructural characterisation showed a direct topotactic transformation from [001]  $\text{VOHPO}_4 \cdot 0.5\text{H}_2\text{O}$  to [100]  $(\text{VO})_2\text{P}_2\text{O}_7$  at the periphery of the hemihydrate platelet. The  $\text{VOHPO}_4 \cdot 0.5\text{H}_2\text{O}$  in the interior of the platelet initially transformed epitaxially into [100]  $\delta\text{-VOPO}_4$  which was embedded in a disordered matrix. The domains of  $\delta\text{-VOPO}_4$  were shown to shrink and further transform into the final  $(\text{VO})_2\text{P}_2\text{O}_7$  phase as the activation procedure continued. Catalyst performance data showed an increase in activity and selectivity to MA production with increasing activation time.

The role of promoter elements in this system has only been considered to any appreciable extent in the patent literature. A wide range of transition metals including Co, Cd and Ni [5] have been found to have a beneficial effect on



activity and MA selectivity. In particular, Ben Abdelouahab *et al* [6] have demonstrated that doping the bulk structure of the hemihydrate precursor with cobalt favours the nucleation of  $\text{VOPO}_4$  phases at a lower temperature. Sananes-Schulz *et al* [7] found that both the *n*-butane conversion and selectivity to MA increase when a small amount of Co is incorporated in the VPO precursor.  $^{31}\text{P}$  NMR by spin echo mapping also suggested that the activated cobalt doped VPO catalyst consists of a mixture of crystalline  $(\text{VO})_2\text{P}_2\text{O}_7$  and a disordered  $\text{V}^{4+}\text{-V}^{5+}$  phase, which are responsible for the improved catalytic performance.

In the present study we have used a combination of XRD and electron microscopical analysis to follow the structural transformations which occur when a 1wt% Co doped  $\text{VOHPO}_4 \cdot 0.5\text{H}_2\text{O}$  sample is activated for varying time periods. In this way, we hope to gain an insight into the role of the promoter element in facilitating the oxidation of *n*-butane to maleic anhydride.

## 2. Experimental

### 2.1 CATALYST PREPARATION

The 1wt% Co doped precursor, denoted VPOCo1, was prepared by firstly dissolving cobalt acetylacetonate (0.166g) in 125ml isobutanol.  $\text{V}_2\text{O}_5$  (5.9g) and  $\text{H}_3\text{PO}_4$  (8.245g, 85%) were introduced into the mixture which was then refluxed for 16h. The light blue suspension was subsequently separated from the organic solution by filtration and washed with isobutanol (200ml) and ethanol (150ml, 100%). Finally, the resulting solid was refluxed in water (9ml  $\text{H}_2\text{O/g}$  solid), filtered hot and dried in air (110°C, 16h). Four separate activation experiments were then carried out subjecting the VPOCo1 precursor to identical reaction conditions (1.5% *n*-butane/air, GHSV=12000 $\text{h}^{-1}$ ). All the samples were ramped up from room temperature to 400°C at a rate of 0.5°Cmin $^{-1}$  in a standard laboratory reactor. The time on stream at 400°C was then systematically varied; namely 0.1h, 8h, 84h and 132h. Following the activation period, the samples were cooled down under the flowing gas mixture. The four 'activated' catalysts are denoted VPOCo-0.1, VPOCo-8, VPOCo-84 and VPOCo-132 respectively.

### 2.2 CATALYST CHARACTERISATION

The catalysts were analysed using a Hiltonbrooks modified Philips 1050 XRD diffractometer employing a  $\text{CuK}_\alpha$  source. Samples appropriate for transmission electron microscopy analysis were prepared by dispersing the catalyst powder onto a lacey carbon film supported on a copper mesh grid. TEM observations



were made in a JEOL 2000FX electron microscope (operating at 200kV) equipped with a LINK systems EDX detector.

### 3. Results and Discussion

The XRD pattern of the VPOCo1 precursor was characteristic of the  $\text{VOHPO}_4 \cdot 0.5\text{H}_2\text{O}$  phase. Individual hemihydrate crystallites exhibit a rhomboid platelet morphology (Figure 1), and EDX analysis confirmed that the cobalt dopant is homogeneously distributed throughout the bulk of the platelets. Analysis of fringe spacings and intersection angles in HREM images confirmed that the platelet normal was [001].

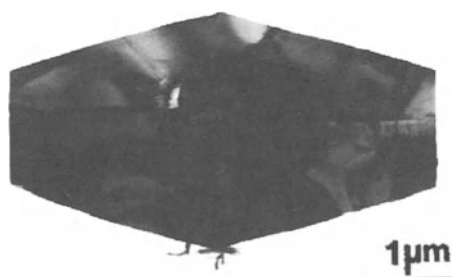


*Figure 1.* Bright field image of the hemihydrate precursor VPOCo1

The XRD pattern of the VPOCo-0.1 sample exhibited three distinct peaks, two of which could be identified as  $\delta\text{-VOPO}_4$ , whilst the third corresponded to the (040) plane of  $\text{VOHPO}_4 \cdot 0.5\text{H}_2\text{O}$ . The XRD patterns of VPOCo-x (where x = 8, 84, 132h) were very similar to each other. The strongest peak in these samples could be indexed to the (020) plane of  $\delta\text{-VOPO}_4$ . In addition, the (200) plane of  $(\text{VO})_2\text{P}_2\text{O}_7$  appeared strongly in all the longer activated samples. An increase in crystallinity from VPOCo-84 to VPOCo-132 was evident however, and the (200) reflection of  $(\text{VO})_2\text{P}_2\text{O}_7$  gradually became stronger with increasing activation time. No characteristic  $\text{VOHPO}_4 \cdot 0.5\text{H}_2\text{O}$  peaks were found in any of the samples activated for more than 0.1 h.

TEM indicated that the rhomboid platelet morphology is retained in all the activated samples. The VPOCo-0.1 sample exhibits circular voids of up to 20nm in diameter, throughout the platelets (which incidentally are particularly beam sensitive). Fissures which appear to be aligned along the minor axis of the rhomboid platelets are also occasionally encountered.

We believe these latter features to be characteristic of the presence of a domain of crystalline  $\delta\text{-VOPO}_4$  [4]. After 8 hours of activation two further changes are apparent. Firstly, the average diameter of the circular features in the

platelet interior have now increased to 50-70nm. More significantly, a 25nm thick rim of crystalline material has formed at the platelet edges as shown in Figure 2(a). Figure 2(b) shows a high resolution electron micrograph from this region which shows a typical rim made up of a string of blocky crystallites approximately 50-100nm in size. Analysis of fringe spacings and intersection angles has allowed us to index this image as the [100] projection of the  $(\text{VO})_2\text{P}_2\text{O}_7$  phase. The VPOCo1-84 and VPOCo1-132 specimens look rather similar to the sample activated for 8 hours. Characteristic fissures were present in all the samples and this was confirmed by dark field imaging experiments. The main differences observed as the activation time was increased are the expansion of the voids which reach a maximum of 100nm in diameter and a slight increase in crystallinity and thickness of the  $(\text{VO})_2\text{P}_2\text{O}_7$  phase at the platelet edges. In addition, EDX analyses were carried out on the interior of the platelets and the crystalline crust at the edge of the platelet as shown in Figures 2(c) and 2(d) respectively. It is clear that the  $(\text{VO})_2\text{P}_2\text{O}_7$  crystallites do not contain Co (at least at the 0.1% detectability limit of the technique), which suggests that the dopant is effectively insoluble in the  $(\text{VO})_2\text{P}_2\text{O}_7$  phase and is preferentially segregated into the disordered phase in the platelet interior.

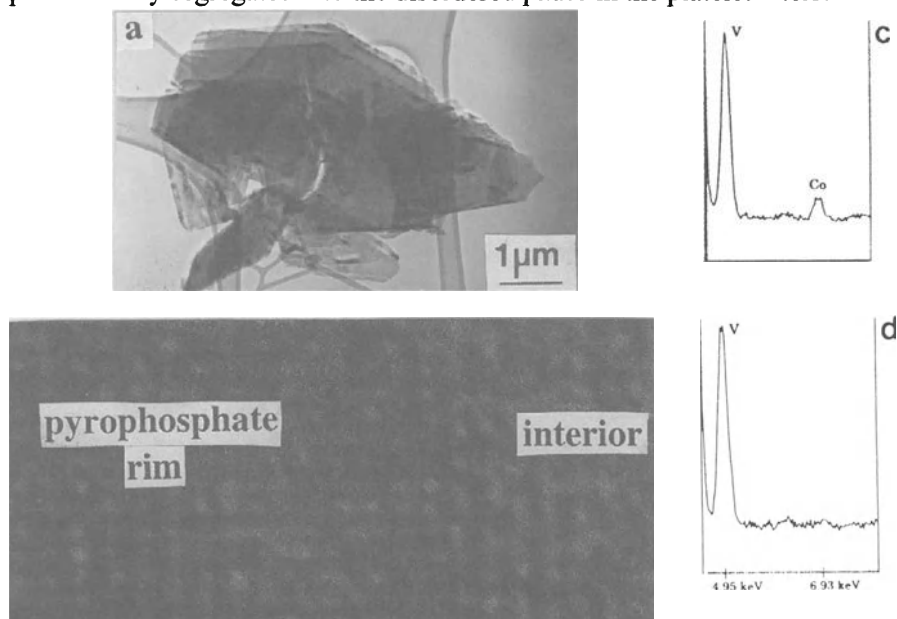


**Figure 2.** (a) Bright field image of VPOCo-8 and (b) High Resolution Electron image showing [100] projection of crystalline  $(\text{VO})_2\text{P}_2\text{O}_7$  at periphery of platelet in VPOCo-8. EDX spectra obtained from the disordered interior material (c) and  $(\text{VO})_2\text{P}_2\text{O}_7$  crust at platelet edge (d).

Comparison of our results to those of an identical set of undoped samples [4] which were activated under similar conditions confirms that the Co doped samples are more disordered than the undoped samples in all cases. The undoped series showed the  $\delta$ -VOPO<sub>4</sub> phase initially, which then transformed almost exclusively to crystalline (VO)<sub>2</sub>P<sub>2</sub>O<sub>7</sub> after 132 hours of activation. However all the cobalt doped activated samples exhibited significant diffraction signals which could be assigned to the  $\delta$ -VOPO<sub>4</sub> phase. Electron microscopy also showed that the platelet interior consisted primarily of disordered material incorporating small domains of crystalline  $\delta$ -VOPO<sub>4</sub>. In addition, crystalline (VO)<sub>2</sub>P<sub>2</sub>O<sub>7</sub> was found at the platelet peripheries in all the samples activated for more than 0.1h. Our results suggest that the presence of Co stabilises a disordered matrix containing mixed V<sup>4+</sup>-V<sup>5+</sup> centres and also encourages the retainment of the  $\delta$ -VOPO<sub>4</sub> phase, even after an extended activation period.

## References

1. G. Centi, *Cat. Today*, 16, 5, (1993).
2. F. Trifiro, *Cat. Today*, 16, 91, (1993).
3. G.J. Hutchings, A. Desmartin-Chomel, R. Olier and J.C. Volta, *Nature*, 368, 41, (1994).
4. C.J. Kiely, A. Burrows, G.J. Hutchings, K. Bere, M. Abon, A. Tuel and J.C. Volta, *Faraday Discussions*, 105, (1997) in press.
5. R. Lemal, J. Vekemans, U.S. Patent 3987063 (1976) assigned to U.C.B.
6. F. Ben Abdelouahab, M. Ziyad, C. Leclercq, J.M. Millet, R. Olier and J.C. Volta, *J.Chim.Phys.* 92, 1320, (1995).
7. M.T. Sananes-Schulz, A. Tuel, G.J. Hutchings, J.C. Volta, *J. Catal*, 166 (2), 388, (1997).

# ON THE ACTIVE SITES FOR SELECTIVE AMMOXIDATION OF PROPANE ON VANADIUM CONTAINING OXIDE CATALYSTS

HORST ZANTHOFF

*Lehrstuhl für Technische Chemie, Ruhr-Universität Bochum,  
D-44780 Bochum, Germany*

## 1. Background

The development of effective catalysts for the oxidative functionalization of alkanes is one of the challenges in the research on mixed-oxide catalysts. One example reaction is the formation of acrylonitrile (ACN) by direct catalytic ammoxidation of propane. This conversion represents a technically interesting alternative route to the presently used SOHIO process [1], which bases on the reaction of propene with ammonia and oxygen. However, the obtainable yields to acrylonitrile are still low. Using modified V-Sb-oxide catalysts ACN yields of  $Y_{\text{ACN}} = 40\%$  are reported in literature [2]. Understanding the key factors of the surface properties of these catalysts and their relationship with the elementary steps of ammoxidation of propane is thus an important step towards the controlled design of mixed-oxides in oxidative functionalization reactions in order to achieve more appropriate catalysts of industrial interest. In consequence considerable effort was put on the investigation of the characterization of V-Sb-oxide catalysts (e.g. [3,4]) and the mechanism of ammoxidation of propane on these catalysts (e.g. [5,6,7]). However, the nature of the active sites is still a matter of discussion [3-6]. In the present work a relationship between several physico-chemical properties and the catalytic performance under stationary and transient conditions is set up. On the basis of these results the nature of the active sites in ammoxidation of propane on modified V-Sb-Al-oxides is elucidated.

## 2. Experimental

$\text{VSb}_y\text{O}_x$  ( $y = 1, 2, 5$ ) and  $\text{VSb}_5\text{MeO}_x$  (30 wt-%)/ $\text{Al}_2\text{O}_3$  catalysts ( $\text{Me} = \text{W}, \text{Nb}, \text{Mg}, \text{Te}, \text{Ga}, \text{Sm}, \text{Pb}$ ) were prepared by redox reaction of  $\text{NH}_4\text{VO}_3$ ,  $\text{Sb}_2\text{O}_3$ ,

$\text{Al}(\text{OH})_3$  and soluble salts of the promotor metals in a slurry after a method described by Catani et al. [8]. Physico-chemical properties of the catalysts were characterized applying various methods: XRD, TEM/EDX, FTIR, in-situ ESR, vanadium average redox state titration, TPR (bulk properties); DRIFTS of pyridine, BET (surface properties). The physico-chemical properties were determined before and after the catalytic tests. Catalytic performance was determined using a micro-catalytic fixed bed reactor with an inlet gas mixture of  $\text{C}_3\text{H}_8/\text{NH}_3/\text{O}_2/\text{Ne} = 1:2:2:2.5$  ( $m_{\text{cat}}/V = 1.08 \text{ gsm}^{-1}$ ;  $P_{\text{tot}} = 0.1 \text{ MPa}$ ;  $T_{\text{R}} = 720\text{--}960 \text{ K}$ ) and a vacuum transient technique in the Temporal-Analysis-of-Products reactor (TAP) [9]. Prior to the experiments the catalysts were kept under reaction conditions for 5 h at 923 K to obtain a stable catalytic performance.

### 3. Results

#### 3.1 PHYSICO-CHEMICAL PROPERTIES

The results of the different characterization methods applied reveal the existence of several phases in the catalysts. In pure V-Sb-oxides crystalline  $\alpha\text{-Sb}_2\text{O}_4$ ,  $\approx\text{SbVO}_4$  and  $\text{V}_2\text{O}_5$  (only visible by EDX) were determined. The modified V-Sb-Al-oxide catalysts additionally contain  $\gamma\text{-Al}_2\text{O}_3$  and mixed Al-rich Al-(V/Sb/Me)-regions, most probably  $\text{Al}_2\text{O}_3$  covered with  $\text{MeO}_x/\approx\text{SbVO}_4$ . Also  $\text{SbO}_x$  particles grown on  $\text{Al}_2\text{O}_3$  was observed. The properties of the catalysts change significantly after the catalytic tests. The amount of crystalline  $\text{Sb}_2\text{O}_4$  is strongly decreased. Using TEM/EDX analysis uniformly Al-rich Al-(V/Sb/Me) particles could be detected. The  $\text{SbO}_x$  particles grown on  $\text{Al}_2\text{O}_3$  completely disappeared.

Pyridine adsorption DRIFT spectra as well as  $\text{NH}_3$ -TPD experiments reveal that the fresh catalysts possess moderate acidity (Lewis- and Brönsted sites;  $1\text{--}2\cdot 10^{17} \text{ sites/m}^2$ ), located on alumina and antimony oxide. For the used catalyst the acidity is decreased ( $1\text{--}7\cdot 10^{16} \text{ sites/m}^2$ ) increasing in the order of the promotor metals:  $\text{Sm} < \text{Pb} < \text{Ga}$ , unpromoted  $< \text{Te} < \text{Mg} < \text{Nb} < \text{W}$ . The Brönsted acidic sites have disappeared as well as the Lewis sites located on/at alumina.

The average vanadium oxidation state amounted to  $4.39\pm 0.07$  for the fresh Al-containing catalysts, as determined by potentiometric titration. During reaction, however, the catalysts became reduced to average V-oxidation state values between 3.89 and 4.29, decreasing in the order of dopants:  $\text{Sm} > \text{unpromoted} > \text{Nb} > \text{W}$ . Nb and W modified V-Sb-Al-oxides only contain the vanadium redox pair  $\text{V}^{4+}/\text{V}^{3+}$ .

ESR investigations on the W promoted V-Sb-Al-oxide catalyst showed that different kinds of  $\text{V}^{4+}$  species exist, i.e. clustered (isotropic signal) and isolated

$V^{4+}$  sites (hyperfine structure, cf. Figure 1). During reaction the number of both kinds of species increases. However, in-situ ESR investigations using flows of  $C_3H_8/NH_3/O_2/N_2$ ,  $C_3H_8/O_2/N_2$  and  $C_3H_8/N_2$  at temperatures up to 793 K reveal that only the clustered species participate in the redox cycle (cf. Figure 2), since only the isotropic signal changes upon interaction with the reaction gases while the hyperfine structure remained unchanged.

### 3.2 CATALYTIC PERFORMANCE

The catalysts exhibited a 5 h formation period in which the selectivities to ACN increased ( $SC_{3H_6}$  decreased), while conversion of  $NH_3$  and formation of  $N_2$  decreased. The promoted V-Sb-Al-oxides showed significant differences in their catalytic performance in the ammoxidation of propane. ACN yields between 5 and 13.2 % were achieved under the reaction conditions applied. The maximum ACN-yield increased in the promotor order: Pb, Sm < unpromoted, Ga < Te < Nb, Mg < W.

Transient vacuum experiments with  $^{18}O_2$  showed that only lattice oxygen participates in selective as well as in non-selective reaction pathways. In the initial stages only  $^{16}O$  containing products (acrolein, CO,  $CO_2$ ) were observed. Under the reduced pressure conditions applied, the oxygen partial pressure was not sufficient to fully reoxidize the catalysts. The amount of excess oxygen in the products, stemming from lattice oxygen not being replaced by gas phase oxygen, could be correlated with the amount of vanadium in the  $VSb_yO_x$  catalysts ( $y = 1, 2, 5$ ).

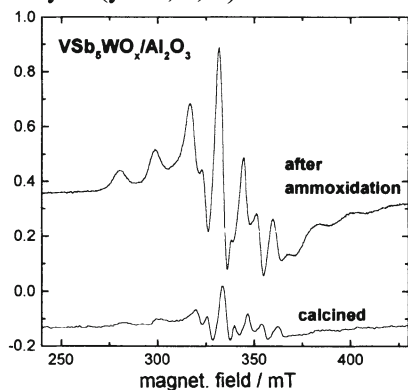


Figure 1 ESR signals for  $V^{4+}$  species (a) before and (b) after ammoxidation of propane

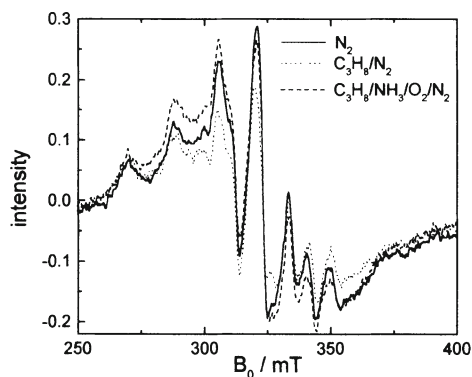


Figure 2 Changes in the ESR signal of  $V^{4+}$  species upon interaction with (i)  $C_3H_8$  and (ii)  $C_3H_8/NH_3/O_2$

#### 4. Conclusions

The presented results clearly indicate that vanadium is the active key element for ammoxidation of propane in modified V-Sb-oxide catalysts. The changes in the physico-chemical properties (especially vanadium valence state, ESR) and catalytic performance during the first hours on-stream indicate that  $V^{4+}$  sites are the active sites for propane activation and ACN production. According to recent investigations of Nilsson et al. [3] these sites are structurally isolated V-centers on the surface of the Sb-rich  $SbVO_4$  phase. Such sites were also observed in the present work (ESR) but do not participate in the reaction. In-situ ESR investigation clearly showed that clustered  $V^{4+}$  centers only participate in the redox cycle reaction. The location of these sites is yet not fully clear. The  $SbVO_4$  phase itself, or clustered  $V^{4+}$ -O- $V^{4+}$  centers on alumina could be possible positions. Furthermore, the TEM/EDX analyses and DRIFTS investigations reveal that antimony is spreading over the alumina under reaction conditions removing strong acid sites responsible for total oxidation and cracking.

#### 5. Acknowledgement

The author likes to thank Dr. A. Brückner (Institut für Angewandte Chemie, Berlin-Adlershof e.V.) and S.A. Buchholz (RUB Bochum) for experimental support.

#### 6. References

1. Moro-oka, Y.; Ueda, W.; in: *Catalysis Vol. 11*, Royal Soc. Chem., Athenaeum Press Ltd., Newcastle, GB, 1994.
2. Grasselli, R.K.; Centi, G.; Trifiro, F.; *Appl. Catal.* 57, 149 (1990).
3. Nilsson, J.; Landa-Canovas, A.; Hansen, S.; Andersson, A.; *Catal. Today* 33, 97 (1997).
4. Centi, G.; Mazzoli, P.; *Catal. Today* 28, 351 (1996).
5. Nilsson, J.; Landa-Canovas, A.; Hansen, S.; Andersson, A.; *J. Catal.* 160, 244 (1996).
6. Centi, G.; Marchi, F.; Perathoner, S.; *J. Chem. Soc., Faraday Trans.* 92(24), 5141 (1996); *ibid.* 92(24), 5141 (1996).
7. Buchholz, S.A.; Zanthoff, H.W.; *ACS Symp. Ser.* 638, e.d. B.Warren and T.Oyama, Chap. 19, 259 (1996).
8. Catani, R.; Centi, G.; Trifiro, F.; Grasselli, R.K.; *Ind. Eng. Chem. Res.* 31, 107 (1992).
9. Gleaves, J.T.; Ebner, J.R.; Kuechler, T.C.; *Catal. Rev.-Sci. Eng.* 30(1), 49 (1988).



# THEORETICAL MODELLING OF PROPANE PARTIAL OXIDATION OVER TITANIUM SILICALITES

GEORGI N. VAYSSILOV

*University of Sofia, Faculty of Chemistry, Sofia 1126, Bulgaria*

*e-mail: gnv@chem.uni-sofia.bg*

## 1. Introduction

The selective catalytic oxidation of saturated hydrocarbons with hydrogen peroxide using titanium silicalite (TS-1) as catalyst is one of the most interesting catalytic processes developed recently [1,2]. The growing number of studies on the coordination state of titanium and formation, characterisation and oxidation activity of titanium-peroxo complexes, carried out recently, gave much useful information and interesting speculations about the processes occurring during the catalytic reaction [3]. The particular catalytic properties of titanium silicalites in partial oxidation are usually explained by decrease of the positive charge on peroxide oxygens after coordination to Ti(IV) centers and hydrophobicity of the silicate framework [4-6].

Alkane oxidation with  $\text{H}_2\text{O}_2$ /TS-1 catalytic system is interesting not only from practical point of view but also in connection with the mechanism of the catalytic transformation because of the peculiarities of process [1,4-6]:

- oxidation occurs at mild conditions;
- alkanes are oxidized even in presence of alcoholic solvents;
- C-H bonds at primary carbon atoms are not activated under the reaction conditions;
- alkylhydroperoxides do not oxidize alkanes over TS-1.

There are different suggestions about the mechanism of alkane oxidation over TS-1 — Huybrechts [5] proposed radical mechanism, while Clerici [1] found the reaction behaviour similar to electrophilic processes. Both homolytic and heterolytic processes can proceed in different ways - via inner-sphere (Ti-C bonding) or outer-sphere oxidation [1,4-6]. A comparative study of Davis and co-workers [6] suggested two alternative mechanistic schemes for inner-sphere radical and non-radical oxidation.



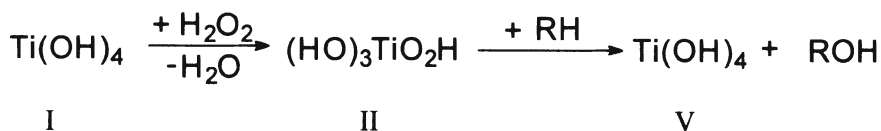
In this situation theoretical calculations are essential for understanding the reaction mechanism. Recent DFT studies of the electrophilic epoxidation of alkenes with hydrogen peroxide over TS-1 gave useful information about the structure of different Ti-H<sub>2</sub>O<sub>2</sub> complexes and the reaction energetics [7,8]. The aim of the present work is to give the initial impression of the reaction path for alkane oxidation based on the proposal for outer-sphere electrophilic reaction mechanism. Propane and methane are used as model molecules.

## 2. Method

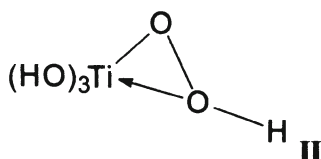
All quantum chemical calculations are performed at ab initio RHF level with STO-3G basis set using Gaussian program [9]. The atomic charges are calculated using Mulliken population analysis. Titanium centers are modelled as surrounded by OH groups. Full geometry optimisation is performed for initial, intermediate and final structures.

## 3. Results

The quantum chemical calculations performed concern the following catalytic processes:



where RH is propane or methane and ROH is the corresponding alcohol. The structure (both geometric and electronic) of the adsorption complex formed after interaction of hydrogen peroxide with Ti centers in the framework is very important when the mechanism of catalytic oxidation is discussed. These calculations showed complete hydrolysis of one Ti-OH bond after hydrogen peroxide adsorption to Ti(OH)<sub>4</sub> (I), with peroxide adsorption energy -56 kJ/mol. The adsorption geometry corresponds to cyclic side-bonded Ti-hydroperoxo complex (TiHPC) - structure II:



Similarly to our recent DFT calculations for a bigger cluster, the charge on Ti after adsorption remains almost the same as in the initial structure while the charge on both peroxide oxygens has higher negative values, compared to the single molecule due to the stronger polarization of O-H bonds in peroxide part. This observation disagrees with the intuitive explanation of hydrogen peroxide activation with a decrease of the negative charge on oxygen atoms after adsorption at titanium site due to the electron withdrawing from oxygens to titanium via the coordination bond.

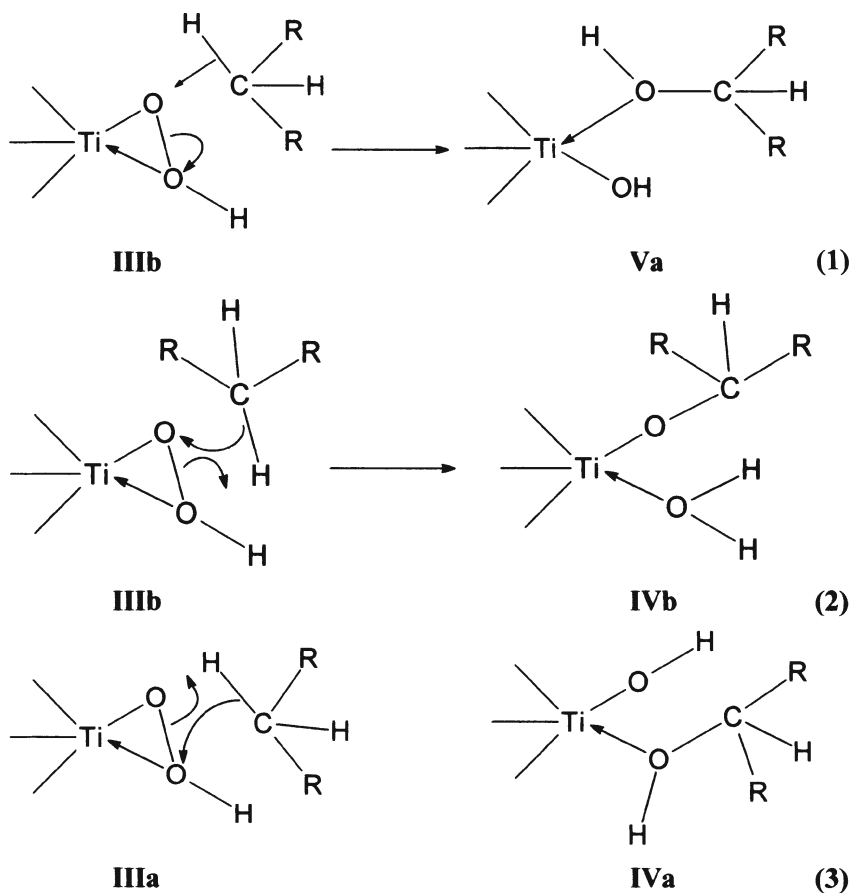
The outer-sphere mechanism of alkane oxidation requires electrophilic attack from a peroxide oxygen to a carbon atom in the organic molecule. In this connection the situation in the area of the lowest unoccupied molecular orbitals (LUMOs) of TiHPC is important. As lower the energy of an unoccupied orbital with contribution from the peroxide oxygen AOs is, as easier the acceptance of the electrons from the organic substratum will be. The results show that the LUMO energy in TiHPC is indeed with 2.2 eV lower than in the single peroxide molecule. So, the catalytic activity of titanium silicalites can be explained by the lowering the unoccupied orbitals' energy of peroxide oxygens after adsorption at Ti site. In this way the energy barrier of the electrophilic reaction is reduced.

On the other hand the energy and orbital coefficients of HOMOs area in propane are important for the position selectivity of the oxidation reaction (table 1) As seen the HOMO is responsible for C-C bonds mainly, which are hardly accessible for the reaction. Next occupied MO corresponds to C-H bonds of the central CH<sub>2</sub> group in propane, which suggests that the reaction proceeds preferentially with breaking of this C-H bond. This is in agreement with the experimentally observed selectivity to oxidation of secondary carbon atoms in alkane molecules with respect to the primary ones [1,6].

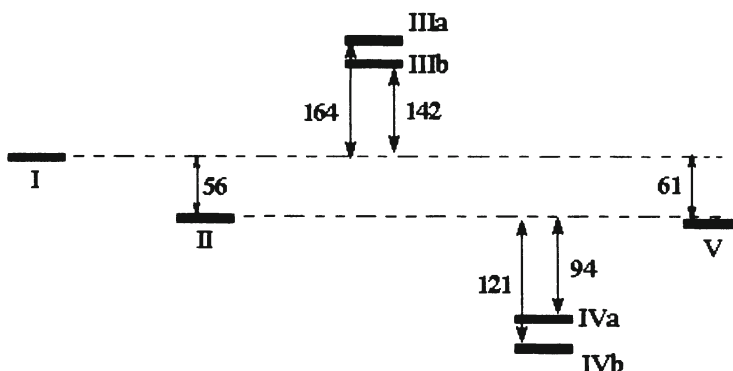
*Table 1.* Relative orbital energies (with respect to HOMO energy) and coefficients in the HOMOs area of propane.

Energy eV	CH <sub>2</sub> group		CH <sub>3</sub> groups	
	C	H	C	H
0	0.22	0.36	0.36	0.18
-0.11	0.21			
-0.15	0.21		0.22	

Three reaction schemes for the outer-sphere electrophilic oxidation of propane or methane with TiHPC can be considered:



In the former two cases, the carbon atom undergoing oxidation, should approach the single oxygen atom  $\text{O}_a$  (structure **IIIb**), while in the later one, the oxidant is the hydroxylic part of the cycle (structure **IIIa**). The attempts to find at least weakly bonded alkane for both initial complexes were not successful because of the repulsive interaction between propane or methane and  $\text{TiHPC}$ . The influence of the poor basis set in these calculations on this result should also be mentioned. However, two pseudo-initial structures were simulated with fixing the distance between one of the peroxide oxygens and the central carbon atom in the alkane. Substantial orbital interactions were not observed in these structures, but some weak alteration of the charge on peroxide oxygens occurs. As expected, the structure **IIIa** was found to be more unstable due to the sterical hindrance from the peroxide hydrogen.



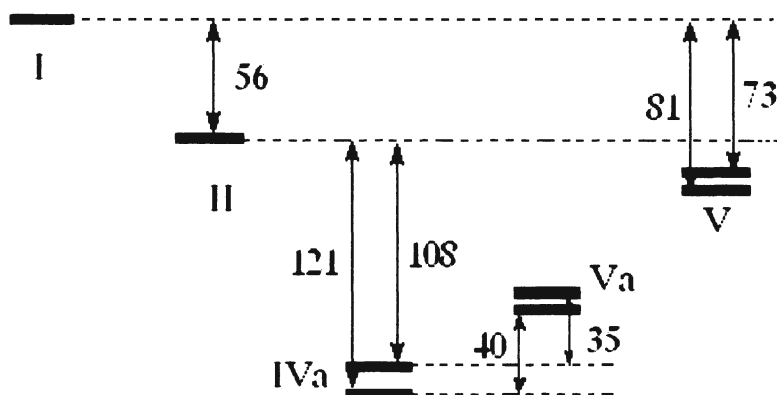
*Scheme 1.* Relative energies of the proposed intermediates during methane oxidation over the cyclic Ti-hydroperoxo complexes. The structure of the complexes **III** and **IV** is shown in eqs. (1)-(3). The state **V** corresponds to final products.

Both for propane and methane the whole reaction is exothermic but the most stable structures are the complexes formed after oxidation to corresponding alcohols (schemes 1, 2). Two types of such adsorption complexes are considered - bonded alkoxy-group and coordinated water (**IVb**) and bonded additional hydroxyl group and coordinated alcohol molecule (**IVa**). Complexes **IVa** can be formed via oxygen insertion into C-H bond according to eq.(1) or by electrophilic attack of the Ob peroxide oxygen to the reactive carbon atom, breaking the O-O bond and formation of a hydroxyl group with the remaining hydrogen - eq.(3). When the reacting carbon atom is near to the single peroxide oxygen, in the latter way the complex **IVb** should be formed. Although **IVb** is more stable, formation of alcohol molecule (as in **IVa**) is a necessary step before its desorption from the catalytic site.

The calculations show similar reaction energies for propane oxidation to 1- and 2-propanol -73 kJ/mol and -81 kJ/mol, respectively. The energies of the reaction intermediates **IV** are similar to the case for methane and the intermediates for oxidation at the secondary C atom have 13 kJ/mol lower energy (scheme 2).

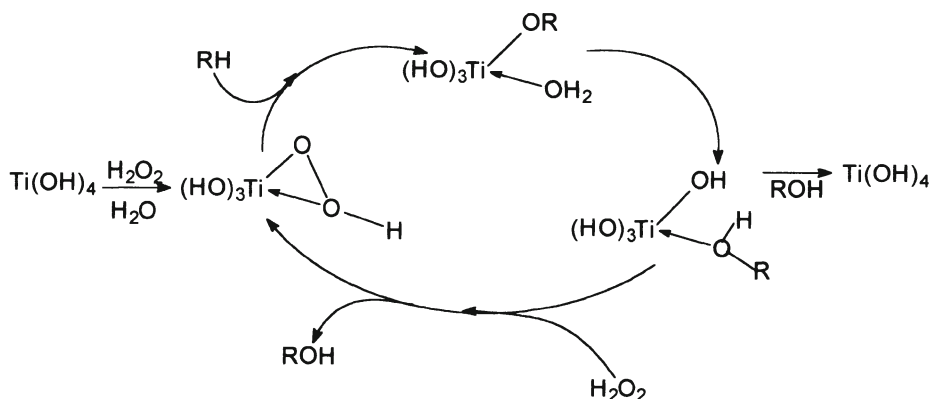
The almost equal energy of the initial TiHPC (**II**) and the products **V** suggests very small driving force of the catalytic reaction. A reasonable possibility for decrease of the energy at the end of the catalytic cycle is restoration of the TiHPC via interaction of the complexes **IV** with new H<sub>2</sub>O<sub>2</sub> molecule during desorption of alcohol. The destruction of the stable complexes **IV** will be easier due to the lower energy difference - from ca. 90 kJ/mol it is reduced to ca. 40 kJ/mol (scheme 2). In this way the catalytic transformation

can continue without intermediate regeneration of the starting  $\text{Ti}(\text{OH})_4$  clusters (scheme 3). The reaction energy of each catalytic cycle is, of course, the same as for the complete reaction.



*Scheme 2.* Relative energies of the intermediates during propane oxidation over the cyclic Ti-hydroperoxo complexes. The complex  $\text{IVa}$  is shown in eqs. (1),(3),  $\text{V}$  is the final state and  $\text{Va}$  corresponds to the restoration of the TiHPC during desorption of the product (see scheme 3). Lower levels correspond to oxidation at the secondary C atom.

Although the structure and energy of the transition states for the step from  $\text{II}$  into  $\text{IV}$  were not found, the energy barrier for the process should be above 200 kJ/mol (scheme 1). Desorption step is also difficult but with lower desorption energy.



*Scheme 3.* Proposed cyclic scheme for catalytic oxidation of alkanes with  $\text{H}_2\text{O}_2$  over titanium silicalites.

#### 4. Concluding Remarks

The calculations performed give a general information about the reaction scheme for heterolytic alkane oxidation with  $\text{H}_2\text{O}_2/\text{TS-1}$  catalytic system. The structures and energies of the reaction intermediates are found and suggestions about the mechanism of peroxide activation and cyclic model of the catalytic transformation are presented. However, this is just beginning of the exploration of problem - the main question about the reaction mechanism has to be solved by following the reaction path between structures **II-III-IV**. It is worth performing such calculations with extended basis set and unrestricted method in order to catch weaker interactions and eventual radical formation. Of course, this is connected with much more computer time and power.

#### 5. References

1. M.G.Clerici, *Appl.Catal.* 68 (1991) 249.
2. B.Notari, *Adv.Catal.* 41 (1996) 253.
3. G.N.Vayssilov, *Catal.Rev.* (1997), in press.
4. G.Bellussi and M.Rigurro, *Stud.Surf.Sci.Catal.* 85 (1994) 177.
5. D.R.C.Huybrechts, L.de Bruycker, and P.A.Jacobs, *J.Mol.Catal.* 71 (1992) 184.
6. C.B.Khouw, C.B.Dartt, J.A.Labinger, M.E.Davis, *J.Catal.* 149 (1994) 195.
7. M.Neurock and L.E.Manzer, *J.Chem.Soc.,Chem.Comm.* (1996) 1133.
8. G.N.Vayssilov and R.A.van Santen, submitted.
9. Gaussian 92, Revision E.1, M. J. Frisch, G. W. Trucks, M. Head-Gordon, P. M. W. Gill, M. W. Wong, J. B. Foresman, B. G. Johnson, H. B. Schlegel, M. A. Robb, E. S. Replogle, R. Gomperts, J. L. Andres, K. Raghavachari, J. S. Binkley, C. Gonzalez, R. L. Martin, D. J. Fox, D. J. Defrees, J. Baker, J. J. P. Stewart, and J. A.Pople, Gaussian, Inc., Pittsburgh PA, 1992.

# CHLORINATED ALUMINA CATALYST FOR ISOBUTANE / 2-BUTENE ALKYLATION :INFLUENCE OF ADDED NOBLE METALS

J.M. GOUPIL, G. CLET, F. HEMMING-MAIRE AND  
D. CORNET

*Laboratoire « Catalyse et Spectrochimie »  
ISMRA - Université de Caen  
14050 Caen Cedex*

G. SZABO, P. NASCIMENTO AND R. LOUTATY

*Centre Européen de Recherches et Techniques.  
TOTAL  
76700 Harfleur*

## 1. Introduction

Many solids with a high surface acidity have been tested as catalysts for alkylation of isobutane with butene [1]. All of them suffer a rapid deactivation, which is generally ascribed to secondary reactions leading to carbonaceous deposit. Rejuvenation has been attempted through hydrogenation of the deposit, catalyzed by a small amount of a noble metal [2]. We found that chlorinated alumina when prepared in a proper way, was an effective catalyst when alkylation was performed at 0°C and olefin dilution  $\alpha = 20$  [3]. Accordingly, a fast deactivation occurs, although carbon deposition is rather limited. Furthermore, the lifetime of the catalyst is markedly improved upon doping with alkaline cation. This points to a different mechanism of deactivation. Indeed, when chlorinated alumina doped with platinum is used in alkane isomerization, its chlorine content is permanently renewed by adding chloroalkanes to the feed. Therefore, in the alkylation catalyzed by  $\text{Al}_2\text{O}_3\text{-Cl}$  some loss of HCl may be a further cause of deactivation, and addition of a metallic phase (Pt or Pd) was expected to assist the rejuvenation of the acidic surface, either through hydrogenation of the adsorbed carbonaceous species, or through decomposition of a chloroalkane yielding HCl.

## 2. Experimental Part

### 2.1 CATALYSTS

The starting  $\gamma$ -alumina (Ketjen CK 300), was impregnated with an aqueous solution of  $\text{PtH}_2\text{Cl}_6$  or  $\text{PdCl}_2$  also containing  $\text{HCl}$ . The solids were further contacted with a  $\text{LiCl}$  solution. Calcined Li-Pt-A (0.32 % Pt , 0.09 % Li by weight) and Li-Pd-A (0.14 % Pd , 0.07 % Li) precursors were chlorinated immediately before the alkylation test. The activation involved four successive steps.

- 1° reduction under hydrogen at 400°C,
- 2° further dehydroxylation under  $\text{N}_2$  at 540°C,
- 3° chlorination at 670°C with a  $\text{HCl}$  (80) +  $\text{H}_2$  (20) mixture,
- 4° cooling to 40°C under  $\text{N}_2$  /  $\text{HCl}$  /  $\text{H}_2$ .

The chlorine content of these Me-A-Cl catalysts was about 4% per weight.

### 2.2 CATALYTIC EXPERIMENTS

The reaction of isobutane with *trans*-but-2-ene (molar ratio  $i\text{C}_4/\text{C}_{4=}$  = 20) was carried out in a fixed-bed reactor.  $\text{H}_2$  could be added to the feed. Space velocity was fixed at 0.35 g(butene)/g(cat)/h. Temperature was set at 0°C, pressure at 40 bars so that the catalyst was swept by a liquid phase. At the reactor outlet, reactants and products were depressurized, and the exit gas was analyzed every thirty minutes in a gas chromatograph fitted with a CP Sil 5B capillary column.

### 2.3 REJUVENATION

After reaction, the liquid phase was swept from the reactor by hydrogen, then a hydrogen flow of 16 mL(STP)  $\text{min}^{-1}$  was maintained for three hours at 40 bars and 155°C. Then the reactor was fed with carbon tetrachloride dissolved in isobutane (4  $\mu\text{mol min}^{-1}$ ). Decomposition of  $\text{CCl}_4$  yielded nascent  $\text{HCl}$ . After one hour, the catalyst was cooled down in isobutane and a further run was started.



### 3. Results and discussion :

#### 3.1 EVALUATION OF THE ALKYLATION ABILITY.

To evaluate the alkylation ability of these catalysts, the reaction products were lumped into "light products"  $C_5-C_7$ , octanes  $C_8$  and "heavy products"  $C_{9+}$ . Altogether they form the alkylate which was virtually olefin free. Normal butane also appeared, it was assigned to hydrogenation of butene. Consumption of butene allowed calculation of its total conversion ( $x_{tot}$ ). This was the sum of the conversions into butane ( $x_{hyd}$ ) and into alkylate ( $x_{alk}$ ). The conversion into trimethylpentanes ( $x_{TMP}$ ) reflects the efficiency of the catalyst towards the aimed reaction. In Table 1, activities of various catalysts are compared at zero time on stream. In the case of Pd-A-Cl used with addition of  $H_2$  the fractional conversions are plotted on Figure 1 as a function of time on stream.

Table 1 : Activities of catalytic systems at zero time on stream.

Catalyst	Conversion of butene				Distribution of the alkylate			
	$x_{tot}$	$x_{hyd}$	$x_{alk}$	$x_{TMP}$	$C_{5-7}$	$C_8$	TMP*	$C_{9+}$
Without addition of hydrogen								
A-Cl	0.81	0	0.81	0.51	24	73	87	4
Pt-A-Cl	0.86	0	0.86	0.57	19	75	88	5
Pd-A-Cl	0.92	0	0.92	0.56	24	70	85	5
With addition of hydrogen								
A-Cl	0.93	0	0.93	0.60	20	75	87	5
Pt-A-Cl	0.96	0.49	0.47	0.41	24	73	88	3
Pd-A-Cl	0.81	0.13	0.68	0.44	11	84	88	4

\* TMP is the content of trimethyl-pentanes amongst the octanes.

When the alkylation is carried out without hydrogen, all catalysts give a very similar alkylate composition. Activity is lost after about 5 hours. Whatever the time on stream, TMP's are the main isomers among the octanes. 224-TMP that is the likely isomer produced in this way is the most abundant. Thus, alkylation proceeds always much faster than dimerization. Light products amount to about 25% of the alkylate, then decline with time on stream. They result from

cracking of primary  $C_8$  products. All the products are alkanes; balance in carbon and hydrogen implies that consumption of isobutane occurs through self-alkylation.

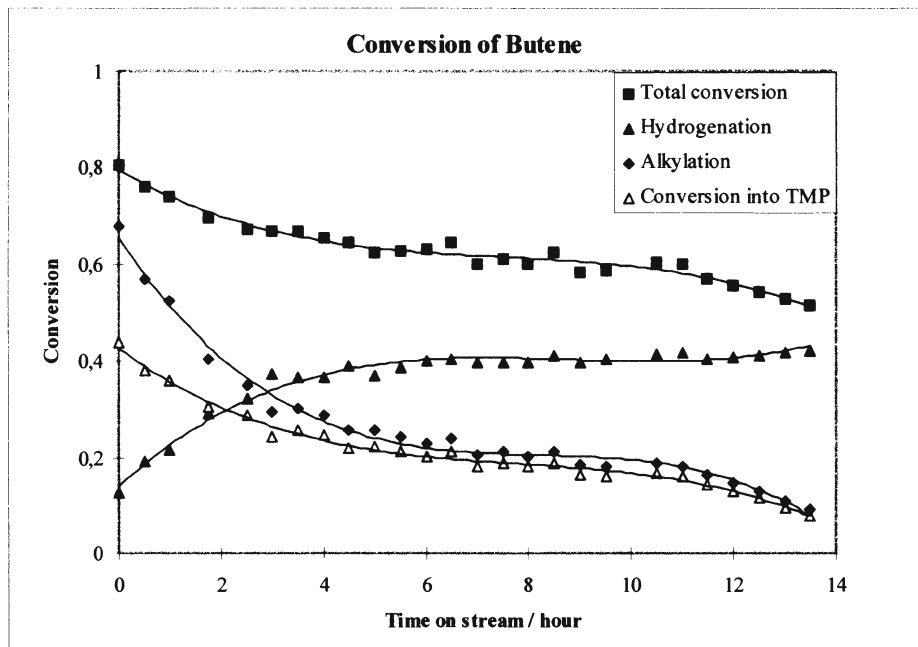


Figure 1. Conversion of butene observed over Pd-A-Cl catalyst with addition of  $H_2$ .

When hydrogen is admitted at a flow rate of  $1.2 \text{ mL (STP) min}^{-1}$ , i.e. at a molar ratio butene/hydrogen = 2, no change occurs in the case of chlorinated alumina. However, in presence of a metal hydrogenation and alkylation compete. Over a Pt-A-Cl catalyst, hydrogenation takes place at the very beginning of reaction and ensures nearly complete consumption of hydrogen. Over Pd-A-Cl catalyst full hydrogenation starts with some delay, alkylation being faster than hydrogenation in the early time. However catalysts remain active for hydrogenation while the yield of alkylate steadily decreases.

### 3.2 ASSISTANCE TO REJUVENATION.

Preliminary experiments showed that hydrocarbons were evolved when the spent catalysts were heated under hydrogen pressure. A maximum rate of evolution was noted at  $150^\circ\text{C}$ . Such a treatment with  $H_2$  alone is unable to rejuvenate the chlorinated alumina, but operates in the case of the catalysts containing Pt or Pd. In experiments shown on Figure 2, catalysts were submitted

to H<sub>2</sub>-rejuvenation followed by HCl treatment to restore acidic sites. Alkylation and hydrogenation conversions after successive cycles (reaction then rejuvenation) are plotted. Regeneration of the catalyst was less and less effective and after a few cycles the activity decreased irreversibly.

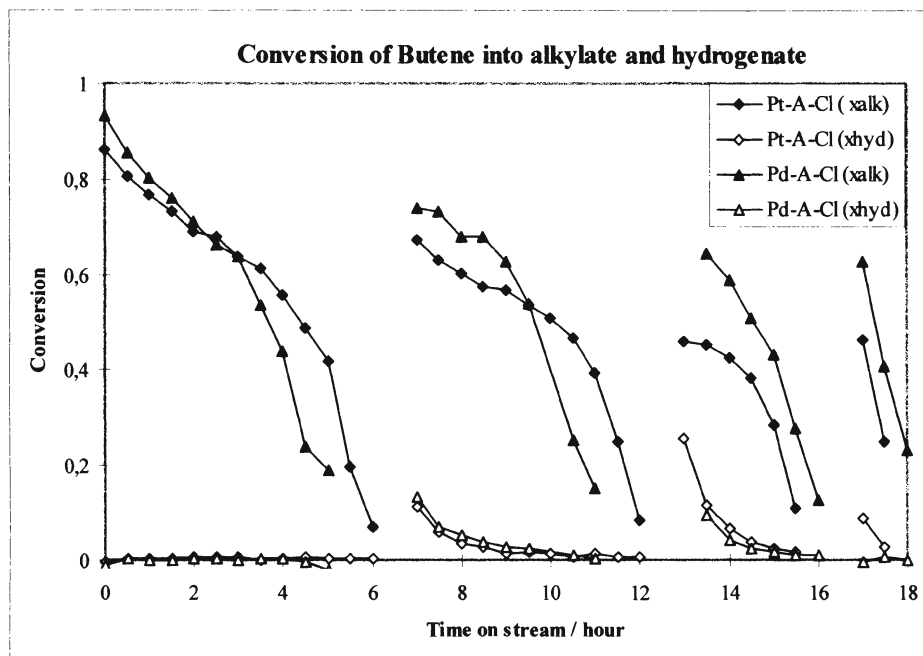


Figure 2. Successive reactions performed after rejuvenation by treatment with H<sub>2</sub>.

### 3.3 DISCUSSION.

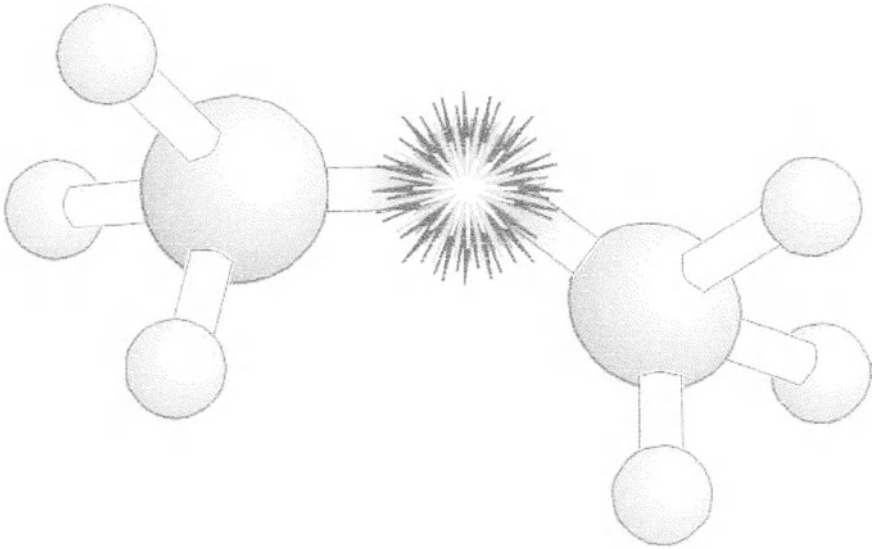
The primary effect of the noble metal phase added onto chlorinated alumina is to catalyze the hydrogenation of butene, when hydrogenation is present. Platinum is more active than palladium in this respect. The noble metal seems to improve the selectivity into TMP. However, the distribution of alkylate, when compared at isoconversion, is not significantly affected by the presence of the metal. Then, the effects on secondary reactions, cracking, poisoning, may be ascribed to the local enhancement of the dilution of butene due to its consumption by hydrogenation. In any case, deactivation still occurs so that the hydrogenating function does not efficiently maintain the alkylation activity. Growing of adsorbed species is not slowed down. Therefore, the presence of a metallic phase does not modify the acidic behaviour of the chlorinated alumina.

Nevertheless, it allows elimination of the carbonaceous deposit and readjustment of the chlorine content of these catalysts when rejuvenating treatment is carried out with H<sub>2</sub> and HCl at 150°C, 40 bars. Hence, the presence of a noble metal phase is required to design an easily regenerable catalyst.

#### **4. References**

1. A.Corma and A. Martinez, *Catal. Rev. Sci. Eng.* **35**(4), 483, (1993)
2. G. Clet, Thesis, University of Caen (1997)
3. C.M.A.M. Mesters, D. Peferoen, J.P. Gilson, C. de Groot, P.T.M. de Brugge and K.P. de Jong; *Appl. Catal. A* (In press).

## **SECTION 3**



**EC WORKSHOP**

## REPORT OF THE WORKSHOP ON CHALLENGES AND OPPORTUNITIES IN LIGHT ALKANE ACTIVATION

JAY A. LABINGER<sup>a</sup> AND GRAHAM J. HUTCHINGS<sup>b</sup>

<sup>a</sup> *Beckman Institute, California Institute of Technology, 139-74, Pasadena, CA 91125, USA.*

<sup>b</sup> *Leverhulme Centre for Innovative Catalysis, Department of Chemistry, University of Liverpool, Liverpool, L69 3BX, UK.*

### 1. Abstract

The main conclusions and discussions of an EC workshop on the challenges and opportunities in light alkane activation are presented. The workshop took the form of a series of discussion sessions, each addressing a specific question. A number of viable research targets for the utilization of alkanes were identified particularly in the area of the replacement of olefin feedstocks. These targets include the oxidation of alkanes to alcohols and/or aldehydes, the synthesis of acrolein and acrylonitrile from propane and the conversion of butane to methacrylates. The replacement of other feedstocks, e.g. synthesis gas, was also considered and a viable target was identified to be the conversion of ethane to acetic acid. The selective activation of methane was viewed separately from higher alkanes and the conversion of methane to benzene and the co-conversion of methane and alkenes were considered to be suitable targets. Potential novel reactions were discussed and the conversion of butane to furan and/or 1,4-butane diol was concluded to be a viable target. If these target reactions are to be addressed it was a main conclusion of the workshop that multidisciplinary teams are required to minimize the research timescale. Teams should comprise expertise drawn from both industry and academe in the fields of catalytic chemistry, materials science, theoretical methodology and chemical engineering. In addition, heterogeneous catalysis should not be viewed as the automatic choice for an optimized process, and either homogeneous catalysis or biomimetic alkane activation should be incorporated into the initial project design considerations.

## 2. Introduction

In conjunction with the NATO Advanced Study Institute on “*Advances and Challenges in the Catalytic Activation and Functionalization of Light Alkanes*”, which took place during the period 25 May-7 June, 1997, a workshop was held to discuss the demanding topic of the *Challenges and Opportunities in Light Alkane Activation*. Participants and lecturers of the ASI convened in several informal discussion sessions, to expand upon and "brainstorm" some of the topics introduced during the more formal lectures that characterized the ASI. For each session a general topic was identified, in the form of a question whose answer seemed crucial to identifying the main challenges and opportunities in the field of alkane activation. Each session was opened by one or more discussion leaders, who briefly introduced the issues that seemed most important to them; but most of the time was devoted to open discussion. There was little or no attempt to reach any unanimous conclusions; rather the emphasis was on stimulating new ideas that might serve as the stimulus for further research. This paper consists of a summary of these workshop discussions (along with some relevant issues that arose or were discussed during the ASI), organized according to the topics that served as the bases for the individual sessions as posed in a series of questions, followed by some general recommendations on how future research in this field might best be carried out. The overall approach adopted was along the lines of “what do we want to make” and “how can we achieve this”.

## 3. What products of alkane conversion offer opportunities?

It is pointless to investigate the possibility of developing novel transformations without as clear as possible a prior understanding of which such transformations are of potential utility, as well as which make sense in terms of chemistry and engineering considerations. A number of opportunities were identified, that can be conveniently broken down into a few basic types:

### 3.1 REPLACEMENT OF OLEFINIC FEEDSTOCKS BY ALKANES

There are clear economic opportunities here, as alkanes are considerably cheaper than olefins as raw materials. In addition, raw materials costs are typically of the order of 70% of the total production costs of commodity chemicals. A new, alkane-based process could be economically advantageous if the yield were sufficiently good, and if the additional costs of process, capital, etc. did not overcome the advantage. Therefore, it is essential that in the first instance, process conditions for utilizing alkanes should

match those of the olefin based process being replaced, so that existing plant can be utilized effectively.

Some potential transformations that fall into this class were targeted by simply comparing the relative cost of alkane to olefin, and then assuming that the feedstock replacement could be made with no changes at all to the process. In this model, making suitable allowances for risks associated with development of new technology, it is calculated that ethane would compete as a feedstock for ethanol if the process could be run at a yield of about 55%, vs. 97% (recycle yield) for the present process from ethylene. Corresponding target yields are 53% for acetaldehyde (vs. 94%), 53% for vinyl chloride (vs. 94%), and 45% for ethylene oxide (vs. 80%). Similar calculations for higher alkanes point to replacing propylene with propane for isopropanol, acrylic acid, acrylonitrile, propylene oxide; and using isobutane as a precursor to methacrylates as being all viable targets.

Of course, this simple economic calculation is not realistic. In the first place, it is very unlikely that such a feedstock change could be accomplished without major process changes, whose effects may operate in either direction (see section 3.1., below). Furthermore, some of the apparent opportunities, such as direct conversion of alkane to epoxide, appear unrealistic based on any known chemistry.

A related substitution would be the direct oxidation of linear alkanes to terminal alcohols, important in detergents and other industries. Currently these are made by hydroformylation of terminal alkenes, so one would have not only a cheaper feedstock but no need for syngas as co-reagent.

A separate but relevant approach is the use of oxidative dehydrogenation as an alternative technology for converting alkanes to olefins. Thermal dehydrogenation is both thermodynamically and kinetically limited: it does not become favorable until 800 C for ethane (somewhat lower for higher alkanes), resulting in expensive endothermic processes. Oxidative dehydrogenation would avoid this problem; but catalysts to date have been insufficiently selective for dehydrogenation relative to non-selective deep oxidation.

### 3.2 METHANE UTILIZATION

Alternatives to the indirect, energy-intensive conversion of methane via synthesis gas continue to be of interest. The direct oxidation to methanol and/or formaldehyde, or the oxidative coupling to C2 hydrocarbons have received the most attention; the key issue is whether the limitations on yield that have characterized all work to date can be overcome via new approaches. Recent reports on conversion of methane to benzene (by Mo/zeolite catalyst), or on the co-conversion of methane plus olefins to aromatics (by Ga/zeolite catalyst) suggest other possibilities for consideration.



There are also opportunities for improvement in the indirect routes, especially considering that syngas production by steam reforming accounts for such a large fraction of the total cost. Catalytic partial oxidation is an intriguing case, especially in conjunction with the possibility of a low-temperature, high-conversion process for methanol synthesis, which could allow operation of partial oxidation by air (rather than oxygen) and direct use of the resulting nitrogen-diluted syngas stream.

### 3.3 OPPORTUNITIES IN FUELS PROCESSING

There are a number of areas in refinery processes where improvements in catalytic technology could have a major impact. These include isomerizations and alkylations, with the main goal of converting linear or lightly branched, low-octane alkanes to more branched high-octane isomers. The main opportunities here appear to be in the realm of strong acid catalysts. Aromatization of alkanes is also of interest here, especially with recent developments in the field (the Cyclar process), but increasingly stringent restrictions on benzene and other aromatics in fuels may severely limit such routes.

### 3.4 OPPORTUNITIES FOR NEW, MORE EFFICIENT TRANSFORMATIONS

General methods for highly selective alkane oxidations could lead to completely new routes for manufacture of complex products. The inspiration in this area is the oxidation of butane to maleic anhydride, a complex process involving multiple dehydrogenations and oxygen insertions that nonetheless is commercially practiced at high selectivity. Transformations of potential value include the analogous oxidation of higher alkanes to phthalic anhydride, and the oxidation of butane to 1,4-butanediol.

## 4. What are the issues and new approaches in the area of chemical engineering?

Besides the challenges of coming up with new catalysts for the new transformations targeted above, there are additional constraints presented by process considerations. These include:

*Separations.* Processes that require separations of light hydrocarbons are particularly demanding, as they will generally require cryogenic methods that may severely constrain allowable pressure ranges and cause difficulties in

overall process schemes that involve one or more steps at much higher temperatures. For example, the cost of separating propane from propylene is about a third of the total cost of propane dehydrogenation. Such factors need to be taken into account in considering new approaches. There are also possible advantages here, though; one might imagine carrying out reactions on mixed feedstocks if the products are easier to separate than the reactants, and if suitable catalysts can be found.

*Temperature control.* Particularly when dealing with oxidation of alkanes, it must be recalled that exothermicity correlates inversely with selectivity. The usual conversion-selectivity curves suggest that a reaction might be run at a given desired yield at different points along such a curve; but these conditions are not equivalent at all from the point of view of heat evolution, which can be a major problem in designing such processes. This could be an important consideration in the replacement of olefins with alkanes as feedstocks: the possibility of running at lower yield because of the cheaper raw materials cost needs to be balanced against the accompanying increased heat evolution.

*Environmental and safety considerations.* Processes that are accompanied by almost any waste stream, or that present potential hazards (e.g., HF leaks, or oxidations operating near explosion limits), will be increasingly unacceptable. Such considerations need to be taken into account at the earliest stages of conceptualization.

All the above limitations also imply opportunities for novel reactor and process design. Examples include the use of short contact time reactors (where sufficiently active catalysts are applicable), membrane reactors for separations and/or to drive otherwise thermodynamically unfavorable reactions, or distributed feed fixed bed reactors, to improve heat control or selectivity in cases that depend strongly on local reactant composition. There is also the possibility of integrating separate concepts into a single reaction or group of reactions. An example of the latter is autothermal dehydrogenation, carried out by combining the output stream of a methane oxidative coupling (which by itself is insufficiently selective for economic application) with an ethane feed; the heat and steam produced in the first step bring about the second. Integration of separation and reaction steps in a single operation, as in reactive columns, may also have applications to alkane transformation.

## **5. What new materials and methodologies are needed in the area of heterogeneous catalysis?**

### **5.1 ADVANCES IN MATERIALS**

In light of the various goals that might be achieved in the activation of light alkanes, a number of areas became obvious where improvement is needed in the performance of catalysts, as well as the means available for their preparation and study. In the realm of known classes of catalytic materials, opportunities were identified in several areas.

Major advances in the synthesis and understanding of microporous materials, zeolites and zeotypes, as well as mesoporous materials, have been achieved recently and are ongoing. The use of molecular modeling promises to allow tailoring of microstructure to desired transformations. Synthesis of the envisioned structure presents at least as big a challenge, but there have been recent advances here as well, such as the design-by-modeling of a template for a particular structure. Catalysts in this class are particularly intriguing because they combine well-defined structural features with the possibility of multifunctional catalysis: acid-base as well as oxidation. Of particular interest are those materials that incorporate redox-active sites into the framework, either at low levels (transition-metal substituted zeolites and zeotypes) or completely, with a number of examples of mesoporous transition metal oxide structures being reported.

With oxide catalysts, there are always a variety of functions that can occur, including dehydrogenation and oxygen insertion. Catalysts that can select for one over another, for processes such as oxidative dehydrogenation, or that can perform all with sufficient facility, for oxygenations, are needed. A key requirement for such developments is better mechanistic understanding of how these reactions proceed and what properties (e.g., oxygen mobility, basicity, bond strengths) control their relative rates. Improvements are needed in both activity and selectivity; these are not necessarily antithetical (although they often are), as for some processes an increase in activity will permit operation at lower temperature which may automatically lead to better selectivity in itself. Also higher activity can permit operation at short contact times, which helps when selectivity is impaired by secondary reactions.

For solid acid catalysts, the problem is often one of stability. New materials are needed that can stably catalyze reactions that require strong acid sites, such as isomerizations and alkylations. Heteropolyacids are a particularly interesting subclass, since (like zeolites) they can be synthesized with a high degree of structural control and can exhibit dual acid/oxidation functionality, but stability and regenerability has been a major problem. Solid base catalysts are much less

well studied, but may be applicable to alkane transformations as well, such as isomerizations or, perhaps, oxidations.

Non-oxidic catalysts, such as metal carbides, nitrides, etc. deserve much more attention than they have received. In general, catalysis chemists will profit from paying more attention to developments in the area of materials science. Techniques for making "intelligent" ceramics with good structural control and desirable properties such as oxidation-resistance may be applicable; a limitation is the usually very low surface area, but perhaps that may be overcome with developments in new synthesis methodologies, such as sol-gel processing.

## 5.2 ADVANCES IN METHODOLOGY

New techniques are needed in the areas of both preparation and characterization of catalytic materials. The main recommendations for characterization are to make use of combinations of methods, and to emphasize *in situ* examination wherever possible. Of particular interest in this context are the various spectroscopies and diffraction methods that make use of high-intensity synchrotron radiation and of neutron sources. Of great value would be a reliable data base, consisting of characterization and reactivity data, collected under very well-defined conditions, for a group of standard catalysts and reactions. New approaches to catalyst preparation include methods for generating metastable structures, which require mild and controlled conditions, such as electrochemical deposition of active materials on supports.

An intriguing approach is the possibility of applying methodology for rapid synthesis and screening of libraries of materials, that has been so successfully applied lately in drug design and related fields. Both the synthetic and (especially) screening techniques will be much more difficult problems for heterogeneous catalytic materials, but if they can be solved these would provide powerful new tools.

Computationally based theoretical techniques (including both forcefield and electronic structure methods) have had a substantial impact on catalytic science during the last ten years. Most work has, however, concentrated on the modeling of bulk and surface structures (both long-range and local) and the physical chemistry of catalytic materials, especially sorption and diffusion. The emphasis of this field is now changing and future work should be oriented towards:

(i) *Materials design*. The design of new microporous structures with specific architectures is increasingly realizable. The ability of computational techniques to design the structures and surfaces of materials for specific applications should be increasingly exploited in the field of catalysis.

(ii) *Reaction mechanism*. Electronic structure techniques are now able to perform accurate calculations on mechanisms (including transition state

identification) of the elementary steps of catalytic reactions. This ability can be exploited to improve our knowledge of the fundamentals of alkane activation. It is important that theoretical studies be closely tied to available experimental results, including detailed kinetics and other mechanistic investigations, to maximize the reliability and interpretability of theoretical conclusions.

## **6. What alternatives to heterogeneous catalysis are available?**

Homogeneous catalysis offers advantages in a number of areas, such as uniformity of active sites, detailed understanding of mechanism, etc.; but the (real or perceived) disadvantages in process engineering have kept it from receiving as much attention as it deserves. Nonetheless there are some clear indications that desired types of alkane reactivity may be more readily accessible in some homogeneous systems. These may be classified as follows:

### **6.1 ORGANOMETALLIC ACTIVATION**

In the last 15 years organometallic complexes have been shown to exhibit remarkable reactivity towards alkanes, activating C-H bonds by a variety of mechanisms under very mild conditions, even sub-ambient temperatures. The main limitation to date has been to find overall practicable transformations compatible with the properties of organometallics. The most promising routes currently available appear to be oxidations based on the so-called electrophilic mode of activation, exhibited by complexes of metals such as Pt, Hg and Rh. Oxidations with unusual selectivities have been achieved; examples include ethane to ethanol to ethylene glycol, by Pt; methane (plus CO) to methanol and acetic acid, by Rh; and methane to methyl bisulfate, by Hg or Pt. These are generally limited by low activity, only moderate selectivity, and in some cases inability to use oxygen as terminal oxidant. The last example demonstrates one approach to solving these problems, by protecting the oxidation product as a sulfate ester, and using sulfuric acid as the oxidant, as it can separately be regenerated with oxygen; but there are costs associated with the subsequent deprotection and separation steps.

For non-oxidative processes the problem is of finding transformations compatible with thermodynamics under the mild conditions at which these species activate alkanes. Reactions such as dehydrogenation or carbonylation are not thermodynamically favorable; they have been driven by photocatalytic methods, but it is questionable whether that approach could ever be economically favorable. The addition of alkanes to olefins, to form higher alkanes, is generally thermodynamically allowed; this may present an opportunity. Another may be found in nearly thermoneutral isomerizations and

rearrangements, such as the recently reported alkane metathesis and hydrogenolysis catalyzed by oxide-supported metal complexes. The general issue of heterogenizing homogeneous catalysts has long been of interest, as a method for having both the reactivity of homogeneous systems and the process advantages of heterogeneous catalysts, and these latest results may provide new impetus for further advances.

## 6.2 BIOLOGICAL AND BIOMIMETIC ACTIVATION

Biological alkane activation proceeds with remarkable activity and selectivity: methane monooxygenases (MMO) oxidize methane, the least reactive alkane, to methanol under ambient conditions; while cytochromes P-450 carry out a variety of highly selective alkane hydroxylations. The mechanism of the latter is reasonably well understood, although details of the actual hydroxylation are still somewhat unclear; that of the former, especially why it is able to activate methane better than any other substrate, are not well understood at all. A particular question, relevant to the possibility of constructing biomimetic catalysts to carry out the same or similar transformations, is to what extent the various special properties of proteins, such as cooperativity, organization of multiple sites, controlled access to the active site, maintenance of hydrophobic environments, binding and/or activation of substrate by distal functions, and reactivity enhancement through imposition of distorted structures (the "entatic" state), are essential.

Prospects for direct application of biological catalysts to light alkane transformations do not appear too promising, as intact organisms will generally convert the majority of substrate for production of biomass rather than the desired product, while cell extracts are generally quite unstable and usually require sacrificial co-reactants which are much too expensive if not produced metabolically. There may be opportunities with genetically modified cells that divert a much larger fraction of their output to target products.

Although a number of biomimetic catalysts have been developed that closely reproduce known structures of the biological catalysts, and reproduced the chemistry to a more limited degree, it appears that most or perhaps all of these operate via a radical-chain autoxidation mechanism for alkane oxidation. Successful applications will require both accelerating the non-chain mechanisms employed by enzymatic catalysts, and repressing the chain mechanism. One approach, which is inspired by the role of the hydrophobic environment of the enzyme active sites, is to carry out biomimetic reactions in two-phase systems, where the phase where catalysis actually takes place might be the interior of a redox molecular sieve, or a fluoruous phase.



## 6.3 SUPERACID CHEMISTRY

Superacids are capable of activating alkanes under quite mild conditions, generating carbenium ions; but again the difficulty lies in finding favorable overall transformations. Net transformations have been achieved by reactions such as hydride transfer, or oxidation (e.g., by sulfuric acid), but the resulting carbenium ions typically have a number of accessible pathways and selectivity is difficult to control. Combination of superacid activation with oxidation by oxygen is possible, but separation becomes a problem: co-products such as water reduce the acidity while desired products can undergo further transformations. New approaches for exploiting the activating powers of superacids in practical processes are needed.

## 7. Conclusions and General Recommendations

### 7.1 IMPLICATIONS FOR OPTIMIZING RESEARCH EFFORTS

It was the strong sense of the workshop, that advances in catalysis could be strongly promoted by greater integration of efforts and expertise. Catalysts and processes cannot be addressed separately, but must be developed in parallel with continuing interactions between groups. Better connections between academic and industrial efforts are also needed. Academic programs often study reactions and catalysts under conditions that are convenient, such as low pressure, but not necessarily relevant to potential applications; while industrial labs rarely devote much effort to mechanistic study, which is often central to progress. To combat this the research programmes aimed at addressing the proposed research targets, as set out below, should involve multidisciplinary teams comprising catalytic chemists, materials scientists, theoretical scientists and chemical engineers. In addition, it is essential that these should be drawn from both academe and industry. These consortia need to be established at the project design stage to ensure that both viable targets and timescales are established and achieved.

### 7.2 PROMISING AREAS AND TIME-FRAME CONSIDERATIONS

As indicated above, the workshop considered that targeted research requires a multidisciplinary approach that adopts the recent innovations in the fields of process engineering, materials science and theoretical methodologies in addition to new approaches from chemistry. Heterogeneous catalysis should not be considered as the automatic choice for an optimized process and the need to

consider and/or pursue alternative approaches should be incorporated into the initial thoughts of the project design team. Against this background, the viable targets that emerged from the workshop are:

(i) Replacement of olefin feedstocks. The conversion of alkanes to alcohols and/or aldehydes is considered to be of general interest for both short and long chain alkanes. It is considered to be the best target for ethane replacement of ethylene. Specific targets for higher alkanes include the production of acrolein and acrylonitrile from propane and methacrylates from butane.

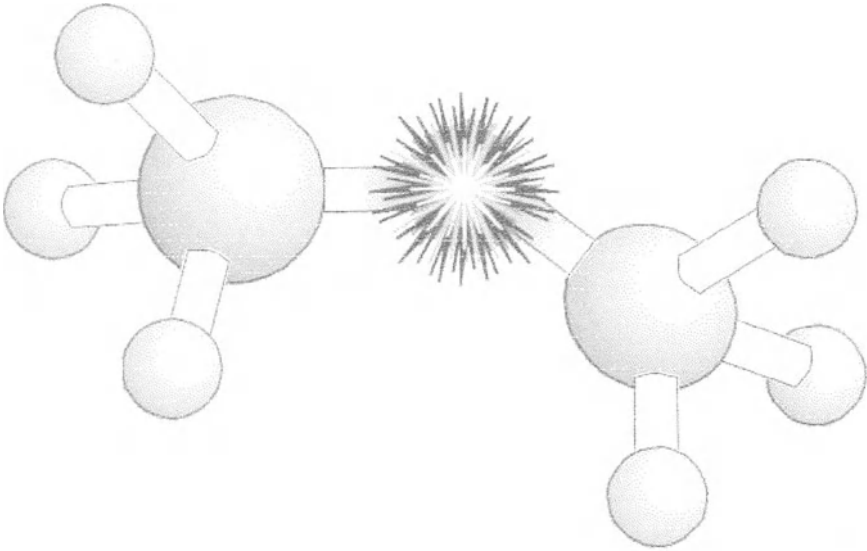
(ii) Replacement of other feedstocks. In this case one specific target was identified, this being the replacement of synthesis gas with ethane for the selective synthesis of acetic acid.

(iii) Methane utilization. In view of the considerable effort expended in the last decade on the selective activation of methane via coupling or partial oxidation, it was concluded that only new directions should be pursued at this stage. Two such targets were identified, these being the direct conversion of methane to benzene and the co-conversion of methane and olefins to higher hydrocarbons.

(iv) New reactions. While many transformations of alkanes to higher value products can be envisaged this was not an area where it was thought that research should be undertaken in the absence of clear indications from experimental observations that the novel chemistry may be viable. On this basis the conversion of butane to furan and/or butane diol were considered to be useful and achievable targets.

It was considered that with the application of a multidisciplinary approach the above targets should be successfully addressed at the catalysts design stage (i.e. microreactor scale) in the next 4-6 years. Other targets which are equally desirable, e.g. alkane conversion to epoxides or alkane conversion to alkyl halide, were not considered viable targets at this stage, since innovation in the basic chemistry is required prior to further extensive studies being initiated at this stage.





## **PARTICIPANTS**

**DIRECTORS:**

- Prof. Eric Derouane  
Leverhulme Centre for Innovative Catalysis  
University of Liverpool  
PO Box 147  
Liverpool L69 3BX  
United Kingdom
- Prof. Jerzy Haber  
Institute of Catalysis and Surface Chemistry  
Polish Academy of Sciences  
ul. Niezapominajek  
PL-30239 Krakow  
Poland

**ORGANISING COMITEE:**

- Prof. Francisco Lemos  
Instituto Superior Técnico  
Departamento de Engenharia Química  
Av. Rovisco Pais 1  
1096 Lisboa Codex  
Portugal
- Prof. Michel Guisnet  
URA CNRS 350  
Laboratoire de Chimie 7  
40 avenue du Recteur Pineau  
86022 Poitiers Cedex  
France
- Prof. Fernando Ramôa Ribeiro  
Instituto Superior Técnico  
Departamento de Engenharia Química  
Av. Rovisco Pais 1  
1096 Lisboa Codex  
Portugal

## LOCAL COMITEE:

- Prof. Filipe Freire  
Instituto Superior Técnico  
Departamento de Engenharia Química  
Av. Rovisco Pais 1  
1096 Lisboa Codex  
Portugal
- Prof. Maria Amélia Lemos  
Instituto Superior Técnico  
Departamento de Engenharia Química  
Av. Rovisco Pais 1  
1096 Lisboa Codex  
Portugal
- Prof. Isabel Santos Silva  
Faculdade de Ciências e Tecnologia  
Universidade Nova de Lisboa  
Quinta da Torre  
2825 Monte da Caparica  
Portugal
- Prof. José Manuel Lopes  
Instituto Superior Técnico  
Departamento de Engenharia Química  
Av. Rovisco Pais 1  
1096 Lisboa Codex  
Portugal
- Dr<sup>a</sup>. Maria da Mercês Marques  
Instituto Superior Técnico  
Departamento de Engenharia Química  
Av. Rovisco Pais 1  
1096 Lisboa Codex  
Portugal
- Prof. Carla Pinheiro  
Instituto Superior Técnico  
Departamento de Engenharia Química  
Av. Rovisco Pais 1  
1096 Lisboa Codex  
Portugal

## LECTURERS:

- Prof. Jean-Marie Basset  
Laboratoire COMS  
CPE Lyon - UMR CNRS 9986  
43, Bd du 11 Novembre 1918  
F-69616 Villeurbanne Cedex  
France
- Prof. C.Richard A. Catlow  
Royal Institution of Great Britain  
Davy Faraday Research Laboratory  
21 Albermarle Street  
London W1X 4BS  
United Kingdom
- Prof. Avelino Corma  
Instituto de Tecnológica Química  
UPV-CSIC  
Camino de Vera s/n  
E-46071  
Spain
- Prof. Graham Hutchings  
Leverhulme Centre for Innovative Catalysis  
University of Liverpool  
PO Box 147  
Liverpool L69 3BX  
United Kingdom
- Prof. Pierre A. Jacobs  
Centrum voor Oppervlaktechemie en Katalyse  
Katholieke Universiteit Leuven - KUL  
Kardinaal Mercierlaan, 92  
B-3001 Heverlee  
Belgium
- Prof. Ivan Kozhevnikov  
Leverhulme Centre for Innovative Catalysis  
University of Liverpool  
PO Box 147  
Liverpool L69 3BX  
United Kingdom

- Prof. Jay Labinger  
Beckman Institute  
California Institute of Technology  
139-74, Pasadena  
CA 91125  
USA
- Prof. Djega Mariadassou  
Laboratoire de Réactivité de Surface et de Structure  
4 Place Jussieu, Tour 54-55, 2e étage  
Université Pierre et Marie Curie  
F-75252 Paris Cedex 05  
France
- Prof. Noritaka Mizuno  
Department of Applied Chemistry  
University of Tokyo  
Bunkyo-ku  
Tokyo 113  
Japan
- Dr. Roy A. Periana  
Catalytica Inc.  
430 Ferguson Drive, Building 3  
Mountain View, CA. 94043  
USA
- Prof. Roger Sheldon  
Laboratory of Organic Chemistry and Catalysis  
Delft University of Technology  
136, Julianalaan  
NL-2628 BL Delft  
The Netherlands
- Prof. Frigyes Solymosi  
Institute of Solid State and Radiochemistry  
University of Szeged  
Dóm tér 7  
6701-Szeged  
Hungary

- Prof. Jean Sommer  
Institut de Chimie  
Université Louis Pasteur  
4, rue Blaise Pascal  
F-67000 Strasbourg  
France
- Prof. Pierluigi Villa  
Dipartimento di Chimica  
Universita di L'Aquila  
Monteluco di Roio  
I-67100 L'Aquila  
Italy

#### PARTICIPANTS:

- Dr. Sharifah Bee Abd Hamid-Derouane  
Leverhulme Centre for Innovative Catalysis  
University of Liverpool  
PO Box 147  
Liverpool L69 3BX  
United Kingdom
- Dr. A. Nilgün Akin  
Kocaeli University  
Kactaltepe Filiz St N° 47/10  
Bakirkoy Istanbul 34730  
Turkey
- Dr. Ahmet E. Aksoylu  
Bogazici University  
Dept.Chemical Engineering  
80815 Bebek, Istanbul  
Turkey
- Dr. Saeed M. Al-Wahabi  
Sabic R&D  
P.O. BOX 42503  
Riyadh 11551  
Kingdom of Saudi Arabia

- Dr. Bruce G. Anderson  
Schuit Institute of Catalysis  
Eindhoven Univ. of Technology  
P.O. Box 513  
5600 MB Eindhoven  
The Netherlands
- Dr. Claudia Letizia Bianchi  
University of Milan  
Department of Physical Chemistry  
Via Golgi 19  
20133 Milano  
Italy
- Dr. James F. Brazdil  
BP. Chemicals Inc.  
4440 Warrensville Center Road  
Cleveland, OH 44128-2837  
USA
- Prof. Fernanda Carvalho  
Instituto Superior Técnico  
Av. Rovisco Pais, 1  
1096 Lisboa Codex  
Portugal
- Dr. Jiri Cejka  
J. Heyrovsky Institute of Physical Chemistry  
Academy of Sciences of the Czech Republic  
Dolejskova 3  
CZ-18223 Prague 8  
Czech Republic
- Dr. Qianjun Chen  
UOP  
50 E. Algonquin Road  
Des Plaines  
IL 60017  
USA
- Dr Vicente Cortes Corberan  
CSIC  
Instituto de Catalisis y Petroleoquimica, CSIC  
Campus UAM Cantoblanco  
28049 Madrid  
Spain

- Dr. Carla Costa  
Instituto Superior Técnico  
Departamento de Engenharia Química  
Av. Rovisco Pais 1  
1096 Lisboa Codex  
Portugal
- Prof. Igor P. Dzikh  
Lvivska Polytechnica State Univ.  
P.O. Box 1103  
290045 Lviv-45  
Ukraine
- Ms. Suzanne Ellis  
Johnson Matthey  
Blount's Court  
Sonning Common  
Reading RG4 9NH, Berkshire  
United Kingdom
- Dr. Marcus Fathi  
Dep. of Industrial Chemistry, NTNV  
Sem Saelanos Vei 4  
N-7034 Trondheim  
Norway
- Prof. José Luís Figueiredo  
Fac.Engenharia  
Rua dos Bragas  
4099 Porto Codex  
Portugal
- Dr. Mark R. Flid  
Sci-Res.Inst."Sintez"  
2 Ugreshskaya str.  
PO Box 56  
109432 Moscow  
Russia
- Dr. Ngi Suor Gnep  
Université de Poitiers - UFR Sciences  
URA CNRS 350  
40, Av. Du Recteur Pineau  
86022 Poitiers Cedex  
France



- Dr. Jean-Michel Goupil  
Universite de Caen  
Laboratoire Catalyse & Spectrochimie  
ISMRA  
14050 Caen cedex  
France
- Dr. Alberto Guercio  
Snamprogetti S.p.A.  
via Maritano 26  
20097 S. Donato Milanese  
Milan  
Italy
- Dr. Andrea Gusso  
ENIRICERCHE S.p.A.  
Via Maritano,26  
20037-San Donato Milanese  
Milan  
Italy
- Dr. Arja Hakuli  
Microchemistry Ltd.  
P.O. Box 45  
02151 Espoo  
Finland
- Dr. Tamotsu Imai  
UOP  
50E Algonquin Road  
Des Plaines P.O. Box 5016  
Illinois 60017  
USA
- Dr. Irina I. Ivanova  
Laboratory of kinetics and catalysis  
Moscow State University  
Vorob'evy Gory  
117234 Moscow  
Russia

- Dr. Staale Forre Jensen  
Statoil  
Statoil Research Center  
Postuttak  
N-7005 Trondheim  
Norway
- Prof. George W. Keulks  
University of Wisconsin-Milwaukee  
P.O. Box 340  
Milwaukee  
WI 53201  
USA
- Prof. A. Kharlamov  
Problems of Materials  
3, Krjijanivskoho Str.  
252680 Kuiv  
Ukraine
- Dr Peter-Paul H.J.M. Knops-Gerrits  
Catholic University of Leuven  
Center for Surface Sci. and Catalysis  
Kardinaal Mercierlaan 92  
B-3001 Heverlee  
Belgium
- Dr. Joseph A. Kocal  
UOP  
50 East Algonquin Road  
Des Plaines  
60017 Illinois  
USA
- Dr. Leiv Laate  
Dep. of Industrial Chemistry, NTNV  
Sem Saelanos Vei 4  
N-7034 Trondheim  
Norway
- Dr Andrzej Machocki  
University of Marie Curie-Sklodowska  
Dept. of Chemical Technology  
3, Marie Curie-Sklodowska Square  
20-031 Lublin  
Poland

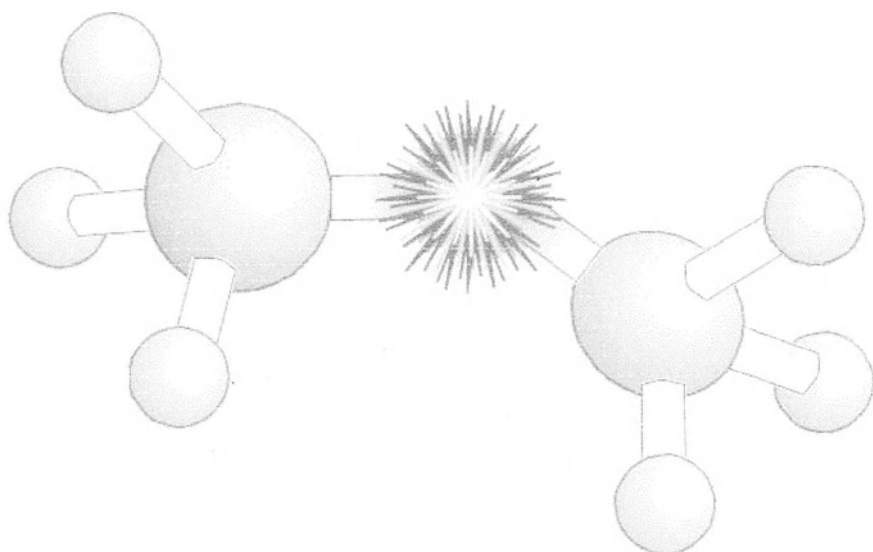
- Dr. Luís Miguel Palma Madeira  
Instituto Superior Técnico  
Av. Rovisco Pais 1  
1096 Lisboa Codex  
Portugal
- Dr. Cezar Ion Marcu  
University of Bucharest  
Dept. of Chem.Tech.& Catalysis  
P.O. Box 12-241  
Bucharest  
Romania
- MSc. Américo Martins  
I.N.E.T.I./D.T.I.Q.  
Estrado do Paço do Lumiar  
1699 Lisboa Codex
- Dr. Luísa Margarida Dias Ribeiro de Sousa Martins  
Instituto Superior de Engenharia de Lisboa  
Secção de Química Inorgânica  
Rua Conselheiro Emídio Navarro  
1900 Lisboa  
Portugal
- Dr. Marisa Alejandra Marturano  
Centro de Inv. y Des. en Procesos Cataliticos  
68 N: 612. Piso:1  
Depto: C.  
La Plata (1900) Buenos Aires  
Argentina
- Dr. Jean-Marc M. Millet  
Institut de Recherches sur la Catalyse  
2 av. A. Einstein  
69626 Villeurbanne Cedex 5  
France
- Prof. Claude Naccache  
Institut de Recherche sur la Catalyse  
2 Av. A. Einstein  
69626 Villeurbanne Cedex 5  
France

- Dr. Laszlo Nemeth  
UOP  
50E Algonquin Road  
Des Plaines IL 60017-5016  
USA
- Dr. Gerald P. Niccolai  
Centre Nationale de Recherche Scientifique  
Laboratoire COMS, CPE Lyon  
43, boulevard du 11 novembre 1918  
R-69616 Villeurbanne cedex  
France
- Prof. Zeynep İlsen Önsan  
Bogazici University  
Dept. Chemical Engineering  
80815 Bebek-Istanbul  
Turkey
- Dr. Marc T. Garriga Oostenbrink  
Utrecht University, Debye Institute  
Department of Inorganic Chemistry  
Sorbonnelaan 16  
3585 CA Utrecht  
The Netherlands
- Dr. Kevin C. Ott  
MS J514 Los Alamos National Laboratory  
Chemical Sciences and Technology Division  
Los Alamos  
NM 87545  
USA
- Prof. Carlos Paliteiro  
Universidade de Coimbra  
Faculdade de Ciências e Tecnologia  
3000 Coimbra  
Portugal
- Prof. Vasile I. Parvulescu  
University of Bucharest  
Faculty of Chemistry, Dept. of Catalysis  
B-dul Republicii 13  
Bucharest 70346  
Romania

- Dr. Jens Perregaard  
Haldortopsoe A/S  
Haldortopsoe A/S  
NYMOLLEVEJ 55  
DK-2800  
Denmark
- Dr. J.A.Z. Pieterse  
Dollardstraat 90  
7523 GS Enschede  
The Netherlands
- Eng. Artur Álvaro Pimenta  
Instituto Superior Técnico  
Departamento de Engenharia Química  
Av. Rovisco Pais 1  
1096 Lisboa Codex  
Portugal
- Dr. Andrzej Rokicki  
United Catalysts Inc.  
PO Box 32370  
Louisville Ky. 40232-2370  
USA
- Dr. Matthijs Ruitenbeek  
Utrecht University, Debye Institute  
Department of Inorganic Chemistry  
Sorbonnelaan 16  
3585 CA Utrecht  
The Netherlands
- Dr Janusz Ryczkowski  
University of Maria Curie - Skłodowska  
Faculty of Chemistry, Dept. of Chem. Technology  
3 M.Curie-Skłodowska Square  
20-031 Lublin  
Poland
- Miss Sujata Sajip  
University of Liverpool, Dept. of Materials Sci.  
21 Hartington Road  
Liverpool L80SD  
United Kingdom

- Dr. George A. Shafeev  
General Phys. Inst. of Russian Academy of Sciences  
Wave Phenomena Department  
38, Vavilov str.  
117942, Moscow  
Russia
- Dr. Michela Signoretto  
Facoltà di Scienze  
Dip. di Chimica  
Calle Larga S. Marta, 2137  
30123 Venice  
Italy
- Dr. João Miguel Silva  
Instituto Superior de Engenharia de Lisboa  
Secção de Engenharia Química  
Rua Conselheiro Emídio Navarro  
1900 Lisboa  
Portugal
- Dr. Oleg V. Sokolov  
Institute of Chemical Physics  
Kosygin St 4  
Moscow 117334  
Russia
- Dr. Sadesh H. Sookraj  
Sastech  
P.O. Box 1  
Sasolburg  
9570  
South Africa
- Dr. Bogdan Sulikowski  
Institute of Catalysis and Surface Chemistry  
Niezapominajek 1  
PL 30-239 Krakow  
Poland
- Dr. Erl M. Thorsteinson  
Union Carbide Corporation  
P.O. Box 8361, Bldg. 770-148  
South Charleston, WV 25303  
USA

- Dr. Marina A. Trushechkina  
Sci-Res.Inst."Sintez"  
2 Ugreshskaya str.  
PO Box 56  
109432 Moscow  
Russia
- Dr. Rita Ximena Valenzuela Balderrama  
Instituto de Catalisis y Petroleoquimica - CSIC  
Campus UAM - Cantoblanco  
28049 Madrid  
Spain
- Dr. Jeroen A. van Bokhoven  
Utrecht University, Debye Institute  
Department of Inorganic Chemistry  
Sorbonnelaan 16  
3585 CA Utrecht  
The Netherlands
- Dr. Georgi Vayssilov  
University of Sofia  
Faculty of Chemistry  
1, J.Bourchier avenue  
Sofia 1126  
Bulgaria
- Prof. Joaquim Vital  
Faculdade de Ciências e Tecnologia  
Universidade Nova de Lisboa  
Quinta da Torre  
2825 Monte da Caparica  
Portugal
- Dr. Horst-Werner Zanthoff  
Ruhr-Universitaet Bochum  
Lehrstuhl für Technische Chemie  
D-44780 Bochum  
Germany



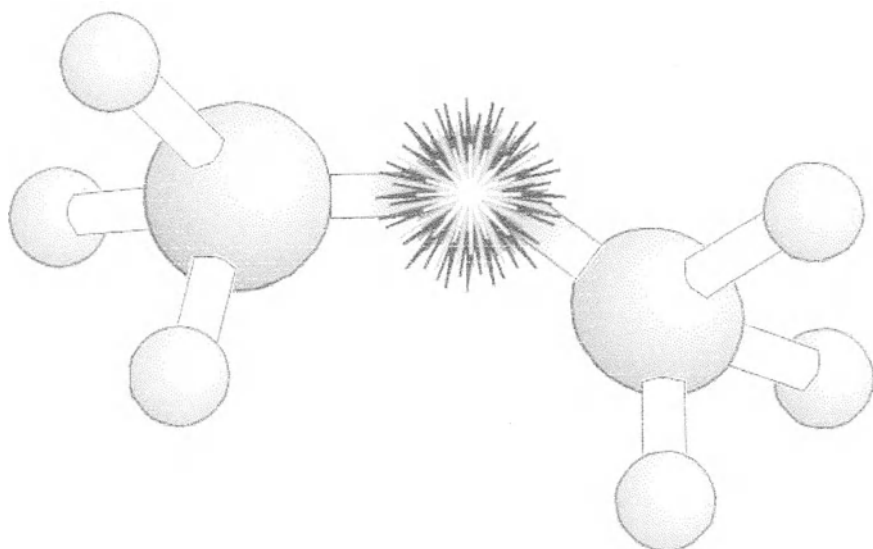
## **SUBJECT INDEX**



Acetic Acid .....	19, 260
Acetylene .....	10
Acrolein .....	260
Acrylonitrile .....	260
Adamantane .....	246, 250, 251
Alkane .....	75, 77, 79, 82, 86, 89, 112, 118, 119, 186, 215, 241, 247, 257, 270, 273, 278, 284, 293, 294, 299, 310, 312, 319, 320, 327, 331, 333, 369, 439, 456
Alkylation .....	51, 57, 451
ALPOs .....	202, 284
Ammoxidation .....	435
Andrussov Process .....	8
Aromatization .....	39, 458
Bioinorganic .....	289
Biomimetic .....	215, 273, 293, 413
Brönsted .....	41, 46, 47, 48, 49, 54, 58, 59, 63, 64, 65, 79, 99, 128, 159, 203, 204, 207, 245, 314, 350, 356, 392, 393, 395, 421, 436
Butene .....	179
Calcination .....	393, 398, 448
Carbon Disulphide .....	9
Carburization .....	338, 343
Chemisorbed .....	333
Chemisorption .....	211, 333
Chlorofluorocarbon .....	7
Chloroform .....	7
Chloromethane .....	19, 20
Cumene .....	260
Cyclar Process .....	39, 43, 397, 458
Cycloalkanes .....	327
Cyclohexane .....	79, 91, 244, 247, 248, 249, 260, 293, 294
Cyclohexanone .....	250, 260
Cytochrome P450 .....	268, 289
Desorption .....	52, 342, 444
Desulphurisation .....	14
Deuteration .....	94
Ethene .....	323
Ethylbenzene .....	27, 29
Ethylene Dichloride .....	27
Ethylene Oxide .....	27, 28, 260
Ferrierite .....	70
Flavin .....	265

Formaldehyde .....	19, 260
Friedel-Crafts .....	29
Functionalisation.....	75, 86, 257
Gasoline .....	20
Hammett .....	48, 49, 59, 314
Hartree-Fock .....	174, 208
Heptene .....	349, 363
Heteropolyacids .....	460
Huels Process .....	10
Hydroformylation .....	21
Hydrogen Cyanide .....	7, 8, 9, 186
Hydrogenolysis .....	112, 114, 344, 345, 346, 347, 348, 351, 354, 363
Hydroisomerisation.....	117
Hydroxylation .....	290, 291, 293
Ionization .....	93
Isobutane .....	46, 50, 97, 103, 105, 319, 322, 323
Isobutene .....	182, 260
Isodewaxing .....	69, 70
Isomerisation .....	46, 47, 51, 63, 68, 69, 71, 112, 346, 347, 351, 354, 356, 360, 361, 363, 367
Keggin Structures .....	83, 312, 313, 327
Ketone .....	249
Ligands .....	222, 229, 275, 313, 414
Liquid Petroleum Gas (LPG) .....	25, 36, 39, 43, 125
Mesoporous .....	215, 413
Metalloporphyrin .....	290
Metalloporphyrins .....	290
Methanation .....	14
Methane .....	6, 7, 10, 31, 32, 33, 34, 37, 38, 75, 76, 151, 154, 165, 241, 297, 303, 304, 305, 308, 309, 323, 331, 375, 378, 386, 465
Methyl Chloride.....	7
Methylamines .....	19
Methylene Chloride .....	7
Methylmethacrylate .....	19
Methylterbutylether.....	19, 20, 39, 43, 90, 182
MFI-Type Zeolite .....	39, 40, 41, 42, 202
Microcalorimetry .....	49
Micropores .....	195, 211, 212, 294
Montmorillonite.....	415
Mössbauer .....	220, 224, 225, 226, 227, 228, 230, 231, 232, 238, 239, 240, 241, 253, 256, 272, 287, 414, 415
Natural Gas .....	6, 14, 15, 31, 33, 405

Neopentane .....	344, 356, 357
Nitridation .....	338
Nucleophilic .....	158
Octene .....	61
Organometallic .....	111, 123, 292
Oxidative Coupling of Methane .....	11, 12, 37, 403, 404, 405, 407, 409, 410
Oxycompounds .....	339
Oxygen .....	216, 263, 288, 289, 290, 291, 292, 319, 346, 356
Oxygenase .....	264, 265, 267, 289, 290, 292
Paraffins .....	34, 119, 183, 187
Petrochemistry .....	25
Polyethylene .....	27, 28
Polymerisation .....	27, 28
Polyoxometalates .....	82, 327, 328
Polytetrafluoroethylene .....	7
Propene .....	182, 323, 362, 401
Propylene .....	260
Protonation .....	50
Redox .....	284, 316
Rhodium .....	21, 165
Sachsse-Bartholomé Process .....	10
SAPO .....	67, 69, 70, 71, 202, 285
SbF .....	89, 92, 96, 97, 98, 100, 102, 105, 106, 107
Schultz-Flory .....	17
Singlet .....	242
Steam Reforming .....	13, 14
Styrene .....	186
Sulfated Zirconia .....	49
Suprabiotic .....	281
Syngas .....	13, 15, 16, 22, 39
Terephthalic Acid .....	260
Triflic Acid .....	303
Vanadylpyrophosphate .....	426
Wacker Process .....	79, 262, 300
XPS .....	221, 222, 224, 229, 233, 234, 370, 371, 373, 375, 376, 380, 415, 418, 419, 420
X-Ray Diffraction ....	147, 194, 221, 235, 341, 392, 398, 418, 419, 430, 431, 436
Zeolites .....	21, 46, 54, 57, 67, 203, 207, 209, 211, 212, 213, 214, 215, 256, 284, 294, 350, 395, 401, 413
Zeolitic .....	193, 194
Ziegler-Natta .....	27, 28, 75, 83, 84, 114, 115
ZSM-5 .....	21, 38, 39, 40, 41, 43, 49, 68, 69, 70, 287, 397



## **AUTHOR INDEX**

	491
S.S. Abadjev	403
J.K. Bartley	429
Jean-Marie Basset	111
R.G. Bell	189
J. Bukala	89
Gema Bueno	397
A. Burrows	429
C.R.A. Catlow	189
Jiri Cejka	391
G. Clet	447
S. Coman	417
Avelino Corma	35
D. Cornet	447
Vicente Cortés Corberán	397
Mirosław Derewinski	397
G. Djéga-Mariadassou	333
I.P. Dzikh	403
Hiroshi Fuji	297
J.D. Gale	189
Scott Gamble	297
J.W. Geus	423
J.M. Goupil	447
P.Grange	417
Jerzy Haber	157
M. Hachoumy	89
F. Hemming-Maire	447
Graham J. Hutchings	125, 429, 455
P.A. Jacobs	215, 413
R. Jost	89
M.S. Kazi	403
C.J. Kiely	429
P.P. Knops-Gerrits	215, 413
D.C. Koningsbergen	423
Ivan V. Kozhevnikov	75
Joanna Krysciak	397
Jay A. Labinger	455
G. Langouche	215
D.W. Lewis	189
R. Loutaty	447
Agustín Martínez	35
Makoto Misono	311
Noritaka Mizuno	311

P. Nascimento	447
Gerald P. Niccolai	111
Zbigniew Olejniczak	397
R.A. Overbeek	423
V. Parvulescu	417
V.I. Parvulescu	417
Roy A. Periana	297
S. Rapagnà	1
C. Rhodes	429
Matthijs Ruitenbeek	423
S. Sajip	429
D.C. Sayle	189
R.A. Sheldon	259
V.U. Shevchuk	403
E.V. Shischak	403
P.E. Sinclair	189
F. Solymosi	369
J. Sommer	89
Bogdan Sulikowski	397
G. Szabo	447
Douglas J. Taube	297
Henry Taube	297
Zdena Tvarozová	391
Rita Ximena Valenzuela	397
A.-M. Van Bavel	215
Georgi N. Vayssilov	439
P.L. Villa	1
Blanka Wichterlová	391
Horst Zanthoff	435
Nadezda Zilková	391